MOLECULAR MECHANISMS OF PATHOGEN-DRIVEN INFECTIOUS AND NEOPLASTIC DISEASES

EDITED BY: Giulia De Falco, Davide Gibellini, Pier Paolo Piccaluga, Paul Gerard Murray and Sam Mbulaiteye

PUBLISHED IN: Frontiers in Cell and Developmental Biology

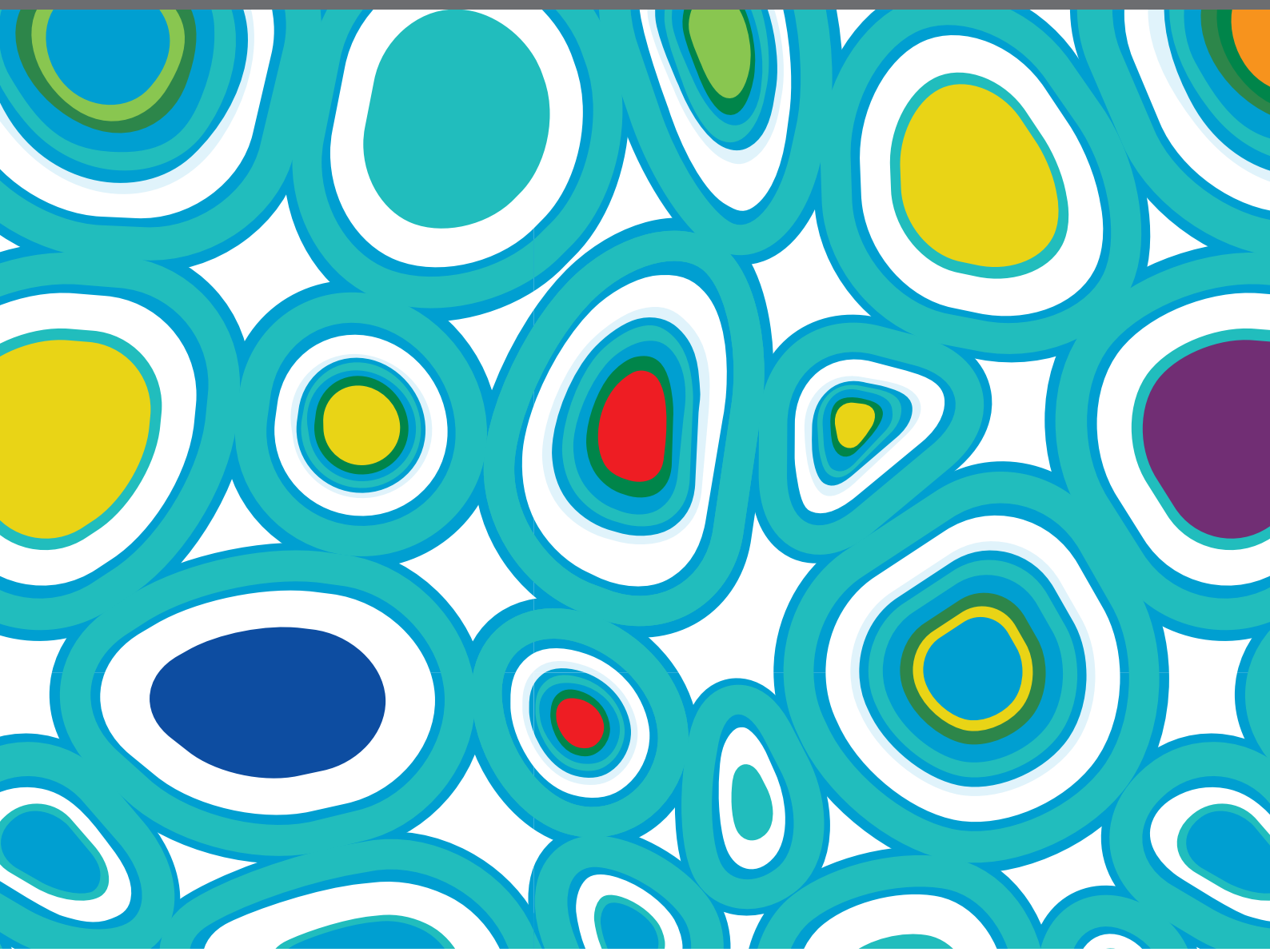

frontiers Research Topics

frontiers

ISSN 1664-8714
ISBN 978-2-88971-066-9
DOI 10.3389/978-2-88971-066-9

About Frontiers

Frontiers is more than just an open-access publisher of scholarly articles: it is a pioneering approach to the world of academia, radically improving the way scholarly research is managed. The grand vision of Frontiers is a world where all people have an equal opportunity to seek, share and generate knowledge. Frontiers provides immediate and permanent online open access to all its publications, but this alone is not enough to realize our grand goals.

Frontiers Journal Series

The Frontiers Journal Series is a multi-tier and interdisciplinary set of open-access, online journals, promising a paradigm shift from the current review, selection and dissemination processes in academic publishing. All Frontiers journals are driven by researchers for researchers; therefore, they constitute a service to the scholarly community. At the same time, the Frontiers Journal Series operates on a revolutionary invention, the tiered publishing system, initially addressing specific communities of scholars, and gradually climbing up to broader public understanding, thus serving the interests of the lay society, too.

Dedication to Quality

Each Frontiers article is a landmark of the highest quality, thanks to genuinely collaborative interactions between authors and review editors, who include some of the world's best academicians. Research must be certified by peers before entering a stream of knowledge that may eventually reach the public - and shape society; therefore, Frontiers only applies the most rigorous and unbiased reviews.
Frontiers revolutionizes research publishing by freely delivering the most outstanding research, evaluated with no bias from both the academic and social point of view. By applying the most advanced information technologies, Frontiers is catapulting scholarly publishing into a new generation.

What are Frontiers Research Topics?

Frontiers Research Topics are very popular trademarks of the Frontiers Journals Series: they are collections of at least ten articles, all centered on a particular subject. With their unique mix of varied contributions from Original Research to Review Articles, Frontiers Research Topics unify the most influential researchers, the latest key findings and historical advances in a hot research area! Find out more on how to host your own Frontiers Research Topic or contribute to one as an author by contacting the Frontiers Editorial Office: frontiersin.org/about/contact

MOLECULAR MECHANISMS OF PATHOGEN-DRIVEN INFECTIOUS AND NEOPLASTIC DISEASES

Topic Editors:
Giulia De Falco, Queen Mary University of London, United Kingdom
Davide Gibellini, University of Bologna, Italy
Pier Paolo Piccaluga, University of Bologna, Italy
Paul Gerard Murray, University of Birmingham, United Kingdom
Sam Mbulaiteye, National Cancer Institute (NCI), United States

Citation: De Falco, G., Gibellini, D., Piccaluga, P. P., Murray, P. G., Mbulaiteye, S., eds. (2021). Molecular Mechanisms of Pathogen-Driven Infectious and Neoplastic Diseases. Lausanne: Frontiers Media SA. doi: 10.3389/978-2-88971-066-9

Table of Contents

frontiers in Cell and Developmental Biology

EDITORIAL
published: 31 May 2021
doi: 10.3389/fcell.2021.696152

Editorial: Molecular Mechanisms of Pathogen-Driven Infectious and Neoplastic Diseases

Giulia De Falco[1], Davide Gibellini[2], Pier Paolo Piccaluga[3], Paul G. Murray[4] and Sam Mbulaiteye[5]*

[1] Nanchang Joint Programme, School of Biological and Chemical Sciences, Queen Mary University of London, London, United Kingdom, [2] Microbiology Section, Department of Diagnostics and Public Health, University of Verona, Verona, Italy, [3] Department of Experimental Diagnostic and Specialty Medicine, University of Bologna, Bologna, Italy, [4] Institute of Immunology and Immunotherapy, University of Birmingham, Birmingham, United Kingdom, [5] Division of Cancer Epidemiology & Genetics Infections and Immunoepidemiology Branch, National Cancer Institute, Bethesda, MD, United States

Keywords: pathogens, infectious diseases, cancer, molecular mechanisms, viruses

Editorial on the Research Topic:

Molecular Mechanisms of Pathogen-Driven Infectious and Neoplastic Diseases

I would like to start this Editorial by quoting a couple of sentences from the article "Multiple Network-Based Approaches to Identify a Key Regulator of Non-lethal Infections" by Mitchell et al. published in this Research Topic. *"Viruses that are newly introduced to the human population have the potential to be highly pathogenic. While the pathogenicity of these new strains tends to wane as adaptation progresses, emerging viruses are an ever-present threat to human health and the global economy because it is difficult to predict when a new pathogenic strain will appear."*

When we started discussing about editing a special issue to highlight how pathogens may not only cause infectious diseases, but also contribute to cancer, we would have never imagined that, shortly after, a new pathogen, COVID-19, would emerge, causing a pandemic of biblical proportion and resulting in so many deaths and much grief. COVID-19 quickly became the most intensively studied pathogen as the scientific community worldwide raced to discover effective preventive and therapeutic measures. Three articles published in this Research Topic focus on this new coronavirus and highlight its mechanism of infection ("The mechanisms and animal models of SARS-CoV-2 infection," by Jia et al.), neurological complications observed in infected patients ("Severe Acute Respiratory Syndrome Coronavirus 2-Induced Neurological Complications," by Yu and Yu), and explore the possible use of curcumin to counteract the cytokine storm induced by this virus, which seems to contribute to the severity of signs and symptoms experienced by infected individuals ("The Inhibitory Effect of Curcumin on Virus-Induced Cytokine Storm and Its Potential Use in the Associated Severe Pneumonia," by Liu and Ying). However, inflammation is a key response to all pathogens and, if aberrantly activated, can be harmful and predispose to severe diseases. This crucial aspect is investigated in "Microbes as Master Immunomodulators: Immunopathology, Cancer and Personalized Immunotherapies," by Lérias et al. in which the association of certain human leukocyte antigen (HLA) alleles with a strong pro-inflammatory response and increased susceptibility to development of specific cancer types in the settings of a pathogenic infection is nicely unraveled. The role of an excessive inflammatory response is further investigated in "LncRNA MALAT1 Affects Mycoplasma pneumoniae Pneumonia *via* NF-κB Regulation," by Gu et al. in which the Authors illustrate how down-regulation of the lncRNA MALAT-1, which is linked with an excessive inflammatory response, may reduce pulmonary inflammation caused by *Mycoplasma pneumoniae*.

OPEN ACCESS

Edited and reviewed by:
Masaru Katoh,
National Cancer Centre, Japan

****Correspondence:***
Giulia De Falco
giulia.defalco@qmul.ac.uk

Specialty section:
This article was submitted to Molecular Medicine, a section of the journal Frontiers in Cell and Developmental Biology

Received: *16 April 2021*
Accepted: *29 April 2021*
Published: *31 May 2021*

Citation:
De Falco G, Gibellini D, Piccaluga PP, Murray PG and Mbulaiteye S (2021) Editorial: Molecular Mechanisms of Pathogen-Driven Infectious and Neoplastic Diseases. Front. Cell Dev. Biol. 9:696152. doi: 10.3389/fcell.2021.696152

Two articles of this Research Topic focus on Hepatitis B virus and its link with liver dysfunction and hepatocellular carcinoma. In "Hepatitis B e Antigen Induces NKG2A+ Natural Killer Cell Dysfunction *via* Regulatory T Cell-Derived Interleukin 10 in Chronic Hepatitis B Virus Infection," by Ma et al. the Authors illustrate how the virus increases production of IL-10, which in turn determines an increased expression of NKG2A on NK cells, which is responsible for NK cell dysfunction during chronic hepatitis B infection. Based on their findings, the Authors conclude that HBeAg-IL-10-NKG2A+ NK cell axis is a potential therapeutic target in HBV chronically-infected patients. The link between cytokine release and chronic hepatitis B infection is further unraveled in "IL-35: A Novel Immunomodulator in Hepatitis B Virus-Related Liver Diseases," by Li et al. In this article the Authors give an overview about how this recently discovered cytokine is key to determine progression from a chronic hepatitis B infection to development of hepatocellular carcinoma and metastatisation. In particular, the Authors illustrate how IL-35 can contribute to this process by inhibiting proliferation and cytotoxicity of HBV-specific cytotoxic T lymphocyte (CTL), deactivating the immature effector T-cells (Teffs), and delaying the proliferation of dendritic cells.

In "Genome-Scale Metabolic Modeling for Unraveling Molecular Mechanisms of High Threat Pathogens," by Sertbas and Ulgen, the Authors provide an overview about how genome-scale metabolic models are useful to unravel pathogenetic mechanisms used by specific pathogens to infect a host, and how the subsequent interplay develops. Understanding the mechanisms that are involved in this cross-talk and what pathways become unbalanced following an infection may be crucial to design promising therapeutic applications against pathogens for global preventative healthcare.

The application of these sophisticated techniques is further explored in two other articles of this Research Topic, "The Role of EGFR in Influenza Pathogenicity: Multiple Network-Based Approaches to Identify a Key Regulator of Non-lethal Infections," by Mitchell et al. in which the Authors focus on how the expression of specific genes can be unraveled by network clustering and topology. In this study the Authors highlight that signaling downstream of EGFR, coagulation pathways, and B-cell down-regulation in the lung are tied to infection severity in highly pathogenic influenza strains.

In "Chlorogenic Acid Promotes Autophagy and Alleviates *Salmonella Typhimurium* Infection Through the lncRNAGAS5/miR-23a/PTEN Axis and the p38 MAPK Pathway," by Tan et al. RNA Seq profiling was used to investigate how lncRNAs are regulated upon immune cell stimulation or pathogen invasion, focusing in particular on lncRNA GAS5. The Authors explore the mechanisms underlying the therapeutic effects of chlorogenic acid in *Salmonella typhimurium* infection, and demonstrate that this treatment up-regulates lncRNA GAS5 in epithelial cells, thus leading to autophagy *via* the miR-23a/PTEN/p38MAPK axis.

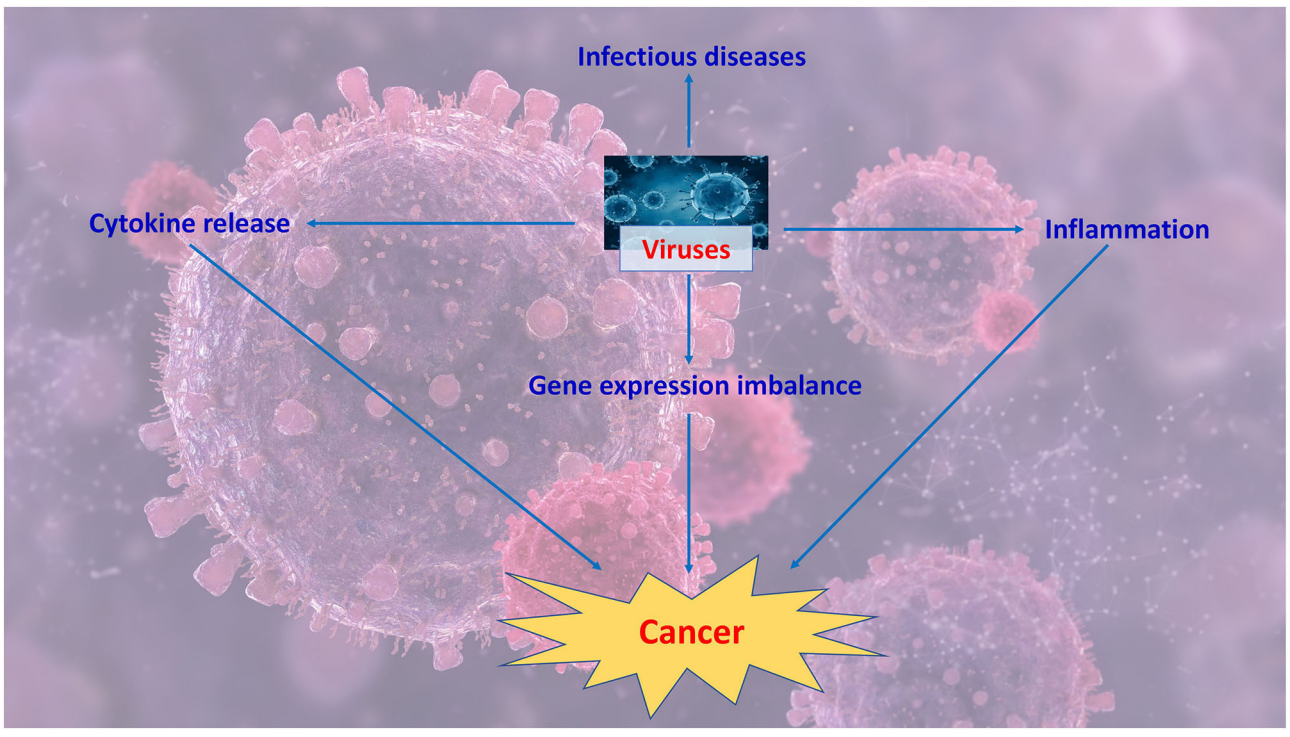

FIGURE 1 | Viruses might contribute to cancer by inducing a prolonged inflammation, dysregulating immune response and unbalancing gene expression.

The link between Human Papillomavirus infection and cancer is explored in "The Role of RNA Splicing Factors in Cancer: Regulation of Viral and Human Gene Expression in Human Papillomavirus-Related Cervical Cancer," by Cerasuolo et al. in which the Authors highlight how HPV contributes to the dysregulation of splicing regulation thus leading to the aberrant production of oncogenes. They focus in particular on the role of hnRNP and SR splicing factors in the production of viral oncoprotein isoforms involved in viral life cycle and in cell transformation. **Figure 1** summarizes key events that might contribute to virally-driven cancers.

The article "Advances in CMV Management: A Single Center Real-Life Experience," by Malagola et al. provides an overview of how the introduction of a recently approved drug improved prognosis of allogenic transplant recipients, which is often compromised by CMV infections in a prolonged immunosuppression setting.

In "The good the bad and the tick," by Cabezas-Cruz et al. the Authors provide an overview about a large variety of tick-borne parasites, which cause several types of infection, focusing in particular on the Protozoon *Theileria* spp. and the bacterium *Anaplasma phagocitophylum*. The Authors illustrate that these pathogens contribute to malignant transformation by unbalancing epigenetic regulation in the host cells, which is in contrast with DNA genetic modifications often observed in virally-driven cancers, thus suggesting that a plethora of different mechanisms can be used by different types of pathogens to dysregulate the host cells and lead to cancer.

However, microbes are not always pathogenic and "good" microbes are crucial for our well-being. This important aspect is highlighted by two articles of this Research Topic. In "The Recombinant Protein Based on *Trypanosoma cruzi* P21 interacts with CXCR4 receptor and abrogates the invasive phenotype of human breast cancer cells," by Borges et al. it is illustrated how the recombinant p21 protein of *Trypanosoma cruzi* may play a protective role against breast cancer, by downregulating CXCR4 gene expression, and leading to its internalization, thus preventing migration, invasion, and progression in MDA-MB-231 cells. This article is a very good example of how, despite many pathogens' products playing a role in driving malignant transformation, pathogens' proteins can also be used to our own advantage to fight cancer.

"Fine Particulate Matter Exposure Alters Pulmonary Microbiota Composition and Aggravates *Pneumococcus*-Induced Lung Pathogenesis," by Chen et al. provides an example of how microbiota play a protective role for us as their dysregulation is associated with diseases as pneumonia. In this study, the Authors highlight how exposure to fine particulate matter (PM) with aerodynamic diameter $\leq 2.5\,\mu m$ ($PM_{2.5}$) is closely correlated with respiratory diseases, which seems to be linked to microbiota dysbiosis, thus promoting disease progression.

On behalf of all topic-Editors, I would like to thank all the Authors for their invaluable contribution to this Research Topic, which has broadened our knowledge and understanding of the Molecular mechanisms of pathogen-driven infectious and neoplastic diseases.

AUTHOR CONTRIBUTIONS

GDF wrote the editorial and embedded comments of other topic Editors. All authors contributed to the article and approved the submitted version.

Conflict of Interest: The authors declare that the research was conducted in the absence of any commercial or financial relationships that could be construed as a potential conflict of interest.

frontiers in Cell and Developmental Biology

OPINION
published: 15 May 2019
doi: 10.3389/fcell.2019.00079

The Good, the Bad and the Tick

Alejandro Cabezas-Cruz[1]*, *Agustin Estrada-Peña*[2] *and Jose de la Fuente*[3,4]

[1] UMR BIPAR, INRA, ANSES, Ecole Nationale Vétérinaire d'Alfort, Université Paris-Est, Maisons-Alfort, France, [2] Faculty of Veterinary Medicine, University of Zaragoza, Zaragoza, Spain, [3] SaBio, Instituto de Investigación en Recursos Cinegéticos IREC-CSIC-UCLM-JCCM, Ciudad Real, Spain, [4] Department of Veterinary Pathobiology, Center for Veterinary Health Sciences, Oklahoma State University, Stillwater, OK, United States

Keywords: ticks, *Theileria* spp., *Anaplasma phagocytophilum*, cancer, networks, malignant transformation

How tick-borne pathogens (TBPs) could help us understand cancer? The diversity of pathogens transmitted by ticks is higher than that of any other known arthropod vector and includes protozoa (e.g., *Babesia* spp. and *Theileria* spp.), bacteria (e.g., intracellular *Rickettsia* spp. and extracellular *Borrelia* spp.), viruses (e.g., Tick-borne encephalitis (TBE) and Crimean-Congo hemorrhagic fever (CCHF) virus), helminths (e.g., *Cercopithifilaria*) and, although less known, fungi (e.g., *Dermatophilus*) (Otranto et al., 2013; Brites-Neto et al., 2015; de la Fuente et al., 2017). TBPs have complex life cycles that involve vertebrate hosts and the ticks. Intracellular TBP infection triggers cellular and molecular responses that change host cell physiology in fundamental ways. Within vertebrate host cells, the apicomplexan parasites *Theileria parva* and *Theileria annulata* activate molecular pathways that result in increased production of reactive oxygen species (ROS), cell immortalization, cancer and host death. In contrast, infection by the rickettsia *Anaplasma phagocytophilum* inhibits apoptosis, block the production of ROS and results in a self-limiting infection that rarely is lethal for the host. *Theileria* spp. and *A. phagocytophilum* modulates host cell response by inducing transcriptional reprogramming of their vertebrate host cells, leukocytes. Transcriptional reprogramming is induced by pathogen-encoded effector proteins that modify host epigenetic pathways that affect not only gene transcription but also protein levels. The complexity of molecular pathways modulated by TBP infection in vertebrate host cells parallel that of cancer which offers a unique opportunity for comparative studies to understand complex health problems such as cancer. Identification of differences between the molecular pathways hijacked by *Theileria* spp. and *A. phagocytophilum* with those leading to non-infectious cancer will provide insights into proteins, pathways and biological processes (BP) associated with malignant transformation.

This hypothesis is based in the following rationality: (i) *Theileria* spp. (Cheeseman and Weitzman, 2015), *A. phagocytophilum* (Sinclair et al., 2014) and oncogenic factors (González-Herrero et al., 2018) behave as "epigenators" (Berger et al., 2009; Cheeseman and Weitzman, 2015) because they have the potential to trigger intracellular signaling pathways that lead to changes in chromatin status and gene expression, (ii) transcriptional reprograming and proteome modulation are hallmarks of infection by *Theileria* spp. (Kinnaird et al., 2013) and *A. phagocytophilum* (de la Fuente et al., 2005; Lee et al., 2008), and oncogenesis (González-Herrero et al., 2018), (iii) transcriptional reprograming and proteome modulation in *Theileria* spp. and *A. phagocytophilum* infections and oncogenesis are associated with similar molecular and cellular processes including apoptosis (Borjesson et al., 2005; Brown and Attardi, 2005; Hayashida et al., 2010; Ayllón et al., 2015), metabolic reprograming (Medjkane and Weitzman, 2013; Yu et al., 2018; Cabezas-Cruz et al., 2019; Masui et al., 2019), oxidative stress and ROS production (IJdo and Mueller, 2004; Medjkane et al., 2014; Takaki et al., 2019) among others. To compare the cell response to

OPEN ACCESS

Edited by:
Pier Paolo Piccaluga, University of Bologna, Italy

Reviewed by:
Fabrice Caudron, Queen Mary University of London, United Kingdom

***Correspondence:**
Alejandro Cabezas-Cruz
cabezasalejandrocruz@gmail.com

Specialty section:
This article was submitted to Molecular Medicine, a section of the journal Frontiers in Cell and Developmental Biology

Received: *11 March 2019*
Accepted: *30 April 2019*
Published: *15 May 2019*

Citation:
Cabezas-Cruz A, Estrada-Peña A and de la Fuente J (2019) The Good, the Bad and the Tick. Front. Cell Dev. Biol. 7:79. doi: 10.3389/fcell.2019.00079

Theileria spp. and *A. phagocytophilum* infections and carcinogens we propose the combination of quantitative proteomics and network analysis (**Figure 1**). Networks of proteins and BPs clustered in *Emerging Biological Pathways* (i.e. network modules resulting from the clustering of proteins and BPs in response to different stimuli) can represent the topology of the specific cell response to *Theileria* spp. and *A. phagocytophilum* infection and exposure to carcinogens. The significance of proteins and processes can be then ranked and hierarchized by indexes representing the centrality of proteins and processes in the networks.

TICK-BORNE PATHOGENS AS MODELS IN CANCER RESEARCH

Infection-induced malignant transformation accounted for 17.8% (1.9 million cases) of the global cancer burden in the year 2002 (Parkin, 2006). The contribution of infectious diseases to cancer epidemiology increased in 2008 to ∼2 million new cancer cases attributable to infection with viruses, platyhelminthes, and bacteria (Oh and Weiderpass, 2014). The loss of cellular identity and the transformation of normal into tumor cells is a central and challenging problem in cellular biology. Major advances have been made in understanding the genetic basis and phenotypic changes underlining the continuum from normal cell to tumor cell to malignant transformation (Hanahan and Weinberg, 2000, 2011; Vogelstein et al., 2013). DNA mutations are observed in all types of cancer (Vogelstein et al., 2013). A significant proportion of cancer patients, however, do not have known coding driver mutations and several non-coding mutations affecting not gene function but gene transcription have been identified in cancer (Fredriksson et al., 2014; Zhang et al., 2018; Reyna et al., 2019). In consequence, the attention has been shifted to phenotypic changes induced by aberrant gene expression that also drive tumor and malignant transformation (Guo et al., 2017; Karki et al., 2017; Parfett and Desaulniers, 2017).

In contrast to virus-induced tumorigenesis that include DNA mutations in somatic cells (Ji et al., 2014), *Theileria*-induced tumorigenesis in bovines does not involve changes in DNA sequence (Cheeseman and Weitzman, 2015; Tretina et al., 2015). Instead, epigenetic mechanisms underlie phenotypic changes associated with *Theileria*-induced malignant transformation (Cheeseman and Weitzman, 2015). *Theileria* is consider as a good model to study the molecular basis of phenotypic changes associated with transformation (Cheeseman and Weitzman, 2015; Marsolier et al., 2015). Comparing the *T. annulata* genome with that of *Toxoplasma gondii* (as a control of intracellular and non-transforming apicomplexan parasite), Marsolier et al. (2015) identified 33 *Theileria*-specific proteins among which they found a homolog of mammalian Pin1, a Peptidyl Prolyl Isomerase that regulates cell proliferation, pluripotency, and survival (Marsolier et al., 2015). The human homolog of Pin1 is overexpressed in breast cancer, increases the transcriptional activity of c-Jun and promotes tumor growth (Wulf et al., 2001). It turned out that by interacting and inducing the degradation of FBW7 protein, which degrades c-Jun, *Theileria*'s Pin1 induces c-Jun accumulation and activates the oncogenic c-Jun pathway which in turn promote transformation (Marsolier et al., 2015; Fernandes et al., 2018).

Thus, comparing the genomes of transforming (i.e., *Theileria*) and non-transforming (i.e., *Toxoplasma*) parasites proved a valid strategy for the identification of Pin1 as a protein relevant in cell transformation and tumor growth (Wulf et al., 2001; Marsolier et al., 2015). Oncogenic viruses such as Kaposi's Sarcoma Herpesvirus also activates c-Jun activity in host cells via virus-encoded proteins (An et al., 2004; Hamza et al., 2004; Xie et al., 2005). However, the complexity of the mechanisms leading tumor transformation is revealed by the fact that infections by non-transforming pathogens (e.g., Reovirus and *Staphylococcus aureus*) also induce and activate c-Jun transcriptional activity (Clarke et al., 2001; Borjesson et al., 2005). *Staphylococcus aureus* infection induces *JUN* (the gene encoding for c-Jun) expression in neutrophils (Borjesson et al., 2005), and staphylococcal α-Toxin activates c-Jun by inducing phosphorylation of its serine 73 (Moyano et al., 2018). Reoviruses can also activate c-Jun activity (Clarke et al., 2001) and were even proposed as cancer therapy (Harrington et al., 2010). Another more general example is that in both *Theileria*-induced and non-infectious neoplastic transformation, apoptosis is inhibited (Fernald and Kurokawa, 2013; Dasgupta et al., 2016). Apoptosis inhibition is therefore considered a hallmark of cancer (Hanahan and Weinberg, 2000, 2011). However, *A. phagocytophilum* infection also inhibits apoptosis but, as mentioned above, it does not result in malignant cell immortalization. One conclusion can be reached from these simple comparisons; c-Jun activation, or apoptosis inhibition, alone do not suffice to transform normal cells in tumor cells. What other pathway or pathways have to be modified in a cell to become a tumor cell? A comprehensive comparison between the timing and totality of cell molecular pathways modulated by *Theileria* spp., *A. phagocytophilum* and carcinogens may provide an integrative view of the molecular pathways leading to malignant transformation.

SEMANTIC NETWORKS TO FIND THE KEYWORDS

In graph theory, a network is a set of nodes that are connected by edges (also known as links). In networks representing food webs (Dunne et al., 2013) or host-parasite interactions (Lafferty et al., 2006; Estrada-Peña et al., 2015), nodes are the organisms and the links represent interactions between them. The directionality and strength of the interactions can be measured as the "weight of interaction" (e.g., the number of times a parasite has been found on a host). We proposed to build "semantic networks" (Estrada-Peña et al., 2018) to capture the changes in cell response induced by different stimuli, *Theileria* spp., *A. phagocytophilum* and carcinogens (**Figure 1**). In such framework, two type of nodes can be distinguished [i.e., proteins with Gene Ontology (GO) annotation (Villar et al., 2014) and BPs], and the links between them would be the participation of proteins in one or more BPs (Estrada-Peña et al., 2018). In this regard, semantic networks are directed because a 'source' (i.e., the protein) is

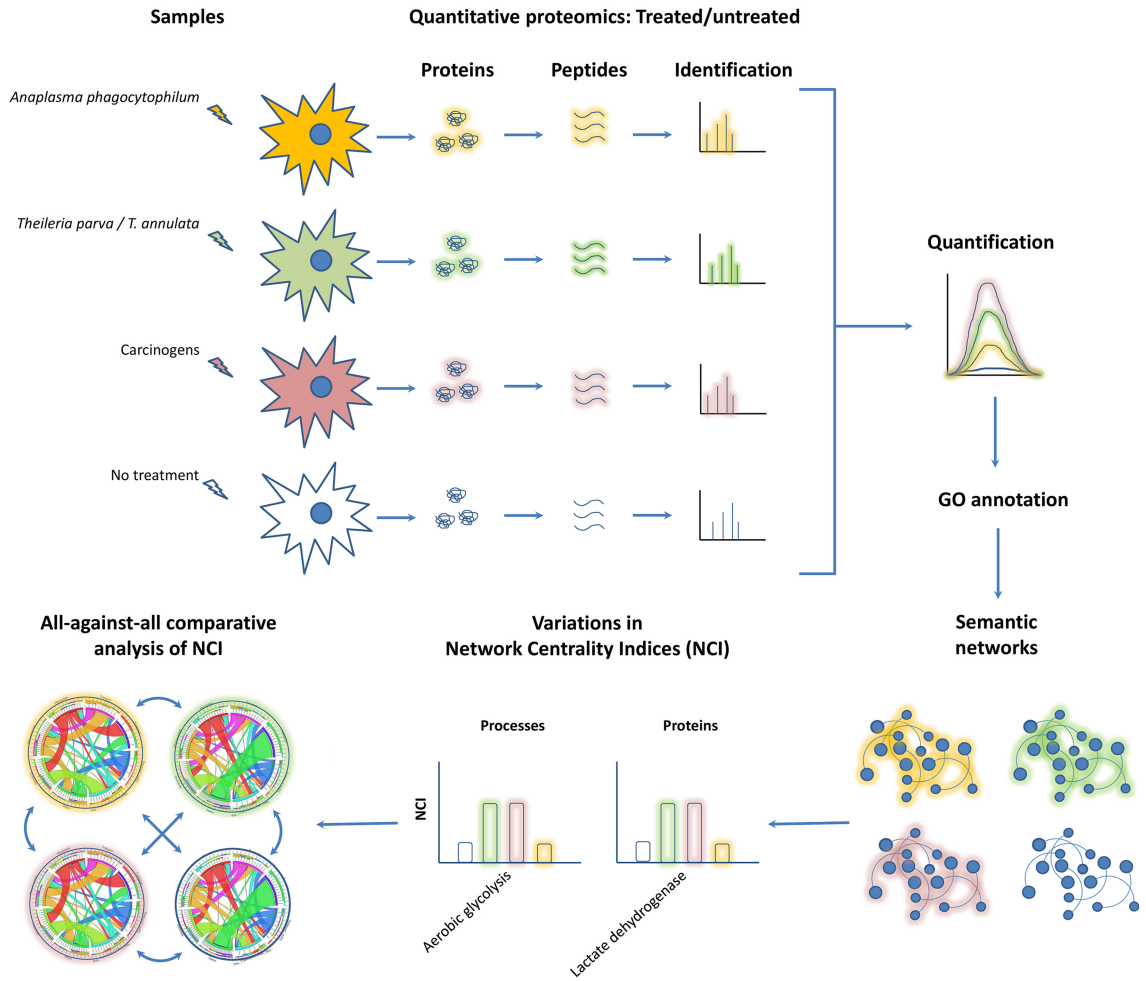

FIGURE 1 | Integration of quantitative proteomics with network analysis to elucidate proteins and BPs key to malignant transformation. The figure displays a workflow previously proposed for the characterization of cell response to *A. phagocytophilum* infection (Estrada-Peña et al., 2018). Samples can be prepared using different stimuli, in this case, a non-transforming bacterium (i.e., *A. phagocytophilum*, colored in orange), a transforming apicomplexan parasite (i.e., *T. parva* and/or *T. annulata*, colored in green) and carcinogens (i.e., know chemical compounds capable of causing cancer, colored in brown). Following standard quantitative proteomics and GO annotation, the names of proteins (nodes type 1) are linked to the biological process (BP) (nodes type 2) in which that protein participates using bipartite networks. The links between nodes type 1 and 2 have strength equivalent to protein expression levels (expressed as normalized Peptide-Spectrum Matches) in treated and untreated cells (no colored). In these networks, BPs with many proteins connected to it and proteins with high relative expression will play a key role in keeping the structure of the network. After comparing with untreated cells, three types of phenotypic changes would be uncovered, those related with infectious transformation (in networks resulting from *Theileria* spp. infection), non-infectious transformation (in networks resulting from cells exposed to carcinogens), and non-transforming infection (in networks resulting from *A. phagocytophilum* infection). Finally, comparing the centrality indices of proteins and BPs in cells treated with carcinogens and those infected with *Theileria* spp and *A. phagocytophilum* will reveal key players in non-infectious transformation. Likewise, comparing the centrality indices of proteins and BPs in cells infected with *Theileria* spp. and *A. phagocytophilum* will provide proteins and BPs critical to infectious transformation. Other comparisons following this logic can provide further insights on infection and cancer.

linked to a "destination" (i.e., the BP). In addition, the links have weight equivalent to the protein levels measured by quantitative proteomics and the Degree of each node is proportional to either the protein level or the sum of links reaching a BP.

Initially, semantic networks were used to describe the global cell transformation in response to *A. phagocytophilum* infection (Estrada-Peña et al., 2018). The results demonstrated that the resulting interactions between proteins and BP can be used to calculate the centrality indices of each node of the network (Estrada-Peña et al., 2018). Centrality indices are fundamental measures of the structure of a network and account for intimate changes in the relative importance of key functions. In addition, centrality indices can be used to identify both proteins and BP that are "central" and therefore occupy prominent positions in the cellular response to different stimuli. The argument here is that centrality indices (e.g., Degree centrality, Weighted Degree, and Betweenness Centrality) are powerful indicators of subtle changes in the proteome, which could be missed when standard protein representation analysis is used. Comparison of centrality indices between *A. phagocytophilum*-infected and

non-infected human and tick cells revealed (i) that infection by this pathogen rewires the network of cell processes and changes the relative importance of biological pathways and (ii) that tick and human cells respond differently to *A. phagocytophilum* infection (Estrada-Peña et al., 2018). More importantly, the ras-related protein Rab14, with a high centrality in infected tick cells, was selected for functional validation by gene knockdown. Rab14 knockdown resulted in a significant decrease in *A. phagocytophilum* infection levels, suggesting that *A. phagocytophilum* increases the relative importance of Rab14 in the proteome to facilitate infection (Estrada-Peña et al., 2018). The identification of Rab14 as a key protein in *A. phagocytophilum* infection shows that in addition to reveal the global cell response to stimuli, semantic networks can be also used to identify individual proteins that change the relative importance of different BPs and can be validated in further laboratory experiments (Estrada-Peña et al., 2018).

Network analysis has been used previously to study cancer progression and reversal (Parikh et al., 2014), to prioritize rare mutations in protein-coding and non-coding genomic regions (Fredriksson et al., 2014; Zhang et al., 2018; Reyna et al., 2019), to study how *PIK3CA* mutations interact with others components of luminal-breast cancer cell signaling network and predict clinical outcomes (McGee et al., 2017) among others. Most network approaches to study cancer use protein-protein interactions where the nodes are proteins and the links between them represent physical protein-protein interactions (Ozturk et al., 2018). In signaling networks, nodes are also proteins but the links represent signaling relations between them (McGee et al., 2017). Other approaches explicitly violate or relax rules of gene and/or protein interactions and allows for biological noise and uncertainty that are expected to occur in tumor cells (Creixell et al., 2015). Our approach is different to those previously reported in two fundamental ways: (i) semantic networks (Estrada-Peña et al., 2018) connect nodes using GO terms which are broader in scope than pathways (Creixell et al., 2015) or protein-protein interactions, and (ii) the links between nodes are weighted based in experimentally-determined protein levels. Thus, semantic networks have the potential to identify not only key BPs, but also those proteins with the higher contribution to that BP in response to the selected stimuli. These two properties, protein-BP connectivity and weighted contribution of proteins result in Emerging Biological Pathways unique to the stimuli in question (e.g., *Theileria* spp., *A. phagocytophilum* and carcinogens). The characterization of key proteins and BPs may lead to the identification of fundamental processes involved in carcinogenesis, with possible implication in disease prevention and control.

AUTHOR CONTRIBUTIONS

AC-C, AE-P, and JdF: conceived the idea, drafted the manuscript, reviewed and accepted the manuscript in its current form.

ACKNOWLEDGMENTS

We thank members of our labs for insightful discussions on this topic.

REFERENCES

An, J., Sun, Y., and Rettig, M. B. (2004). Transcriptional coactivation of c-Jun by the KSHV-encoded LANA. *Blood* 103, 222–228. doi: 10.1182/blood-2003-05-1538

Ayllón, N., Villar, V., Galindo, R. C., Kocan, K. M., Šíma, R., López, J. A., et al. (2015). Systems biology of tissue-specific response to *Anaplasma phagocytophilum* reveals differentiated apoptosis in the tick vector *Ixodes scapularis*. *PLoS Genet*. 11:e10 05120. doi: 10.1371/journal.pgen.1005120

Berger, S. L., Kouzarides, T., Shiekhattar, R., and Shilatifard, A. (2009). An operational definition of epigenetics. *Genes. Dev*. 23, 781–783. doi: 10.1101/gad.1787609

Borjesson, D. L., Kobayashi, S. D., Whitney, A. R., Voyich, J. M., Argue, C. M., and Deleo, F. R. (2005). Insights into pathogen immune evasion mechanisms: *Anaplasma phagocytophilum* fails to induce an apoptosis differentiation program in human neutrophils. *J. Immunol*. 174, 6364–6372. doi: 10.4049/jimmunol.174.10.6364

Brites-Neto, J., Duarte, K. M., and Martins, T. F. (2015). Tick-borne infections in human and animal population worldwide. *Vet. World*. 8, 301–315. doi: 10.14202/vetworld.2015.301-315

Brown, J. M., and Attardi, L. D. (2005). The role of apoptosis in cancer development and treatment response. *Nat. Rev. Cancer*. 5, 231–237. doi: 10.1038/nrc1560

Cabezas-Cruz, A., Espinosa, P., Alberdi, P., and de la Fuente, J. (2019). Tick-pathogen interactions: the metabolic perspective. *Trends Parasitol*. 35, 316–328. doi: 10.1016/j.pt.2019.01.006

Cheeseman, K., and Weitzman, J. B. (2015). Host-parasite interactions: an intimate epigenetic relationship. *Cell Microbiol*. 17, 1121–1132. doi: 10.1111/cmi.12471

Clarke, P., Meintzer, S. M., Widmann, C., Johnson, G. L., and Tyler, K. L. (2001). Reovirus infection activates JNK and the JNK-dependent transcription factor c-Jun. *J. Virol*. 75, 11275–11283. doi: 10.1128/JVI.75.23.11275-11283.2001

Creixell, P., Reimand, J., Haider, S., Wu, G., Shibata, T., Vazquez, M., et al. (2015). Pathway and network analysis of cancer genomes. *Nat. Methods* 12, 615–621. doi: 10.1038/nmeth.3440

Dasgupta, A., Nomura, M., Shuck, R., and Yustein, J. (2016). Cancer's Achilles' Heel: Apoptosis and Necroptosis to the Rescue. *Int. J. Mol. Sci*. 18:E23. doi: 10.3390/ijms18010023

de la Fuente, J., Antunes, S., Bonnet, S., Cabezas-Cruz, A., Domingos, A. G., Estrada-Peña, A., et al. (2017). Tick-pathogen interactions and vector competence: identification of molecular drivers for tick-borne diseases. *Front. Cell. Infect. Microbiol*. 7:114. doi: 10.3389/fcimb.2017.00114

de la Fuente, J., Ayoubi, P., Blouin, E. F., Almazán, C., Naranjo, V., and Kocan, K. M. (2005). Gene expression profiling of human promyelocytic cells in response to infection with *Anaplasma phagocytophilum*. *Cell. Microbiol*. 7, 549–559. doi: 10.1111/j.1462-5822.2004.00485.x

Dunne, J. A., Lafferty, K. D., Dobson, A. P., Hechinger, R. F., Kuris, A. M., Martinez, N. D., et al. (2013). Parasites affect food web structure primarily through increased diversity and complexity. *PLoS Biol*. 11:e1001579. doi: 10.1371/journal.pbio.1001579

Estrada-Peña, A., de la Fuente, J., Ostfeld, R. S., and Cabezas-Cruz, A. (2015). Interactions between tick and transmitted pathogens evolved to minimise competition through nested and coherent networks. *Sci. Rep*. 5:10361. doi: 10.1038/srep10361

Estrada-Peña, A., Villar, M., Artigas-Jerónimo, S., López, V., Alberdi, P., Cabezas-Cruz, A., et al. (2018). Use of graph theory to characterize human and arthropod vector cell protein response to infection with *Anaplasma phagocytophilum*. *Front. Cell. Infect. Microbiol*. 8:265. doi: 10.3389/fcimb.2018.00265

Fernald, K., and Kurokawa, M. (2013). Evading apoptosis in cancer. *Trends Cell Biol*. 23, 620–633. doi: 10.1016/j.tcb.2013.07.006

Fernandes, R., Ferreira, S., and Botelho, M. C. (2018). Commentary: theileria parasites secrete a prolyl isomerase to maintain host leukocyte transformation. *Front. Med*. 5:120. doi: 10.3389/fmed.2018.00120

Fredriksson, N. J., Ny, L., Nilsson, J. A., and Larsson, E. (2014). Systematic analysis of non-coding somatic mutations and gene expression alterations across 14 tumor types. *Nat. Genet*. 46, 1258–1263. doi: 10.1038/ng.3141

González-Herrero, I., Rodríguez-Hernández, G., Luengas-Martínez, A., Isidro-Hernández, M., Jiménez, R., García-Cenador, M. B., et al. (2018). The making of leukemia. *Int. J. Mol. Sci.* 19:E1494. doi: 10.3390/ijms19051494

Guo, Y., Nie, Q., MacLean, A. L., Li, Y., Lei, J., and Li, S. (2017). Multiscale modeling of inflammation-induced tumorigenesis reveals competing oncogenic and oncoprotective roles for inflammation. *Cancer Res.* 77, 6429–6441. doi: 10.1158/0008-5472.CAN-17-1662

Hamza, M. S., Reyes, R. A., Izumiya, Y., Wisdom, R., Kung, H. J., and Luciw, P. A. (2004). ORF36 protein kinase of Kaposi's sarcoma herpesvirus activates the c-Jun N-terminal kinase signaling pathway. *J. Biol. Chem*. 279, 38325–38330. doi: 10.1074/jbc.M400964200

Hanahan, D., and Weinberg, R. A. (2000). The hallmarks of cancer. *Cell* 100, 57–70. doi: 10.1016/S0092-8674(00)81683-9

Hanahan, D., and Weinberg, R. A. (2011). Hallmarks of cancer: the next generation. *Cell* 144, 646–674 doi: 10.1016/j.cell.2011.02.013

Harrington, K. J., Vile, R. G., Melcher, A., Chester, J., and Pandha, H. S. (2010). Clinical trials with oncolytic reovirus: moving beyond phase I into combinations with standard therapeutics. *Cytokine Growth Factor Rev*. 21, 91–98. doi: 10.1016/j.cytogfr.2010.02.006

Hayashida, K., Hattori, M., Nakao, R., Tanaka, Y., Kim, J. Y., Inoue, N., et al. (2010). A schizont-derived protein, TpSCOP, is involved in the activation of NF-kappaB in Theileria parva-infected lymphocytes. *Mol. Biochem. Parasitol*. 174, 8–17. doi: 10.1016/j.molbiopara.2010.06.005

IJdo, J. W., and Mueller, A. C. (2004). Neutrophil NADPH oxidase is reduced at the *Anaplasma phagocytophilum* phagosome. *Infect Immun.* 72, 5392–5401. doi: 10.1128/IAI.72.9.5392-5401.2004

Ji, X., Zhang, Q., Du, Y., Liu, W., Li, Z., Hou, X., et al. (2014). Somatic mutations, viral integration and epigenetic modification in the evolution of hepatitis B virus-induced hepatocellular carcinoma. *Curr. Genomic* 15, 469–480. doi: 10.2174/1389202915666141114213833

Karki, R., Man, S. M., and Kanneganti, T. D. (2017). Inflammasomes and Cancer. *Cancer Immunol. Res*. 5, 94–99. doi: 10.1158/2326-6066.CIR-16-0269

Kinnaird, J. H., Weir, W., Durrani, Z., Pillai, S. S., Baird, M., and Shiels, B. R. (2013). A bovine lymphosarcoma cell line infected with theileria annulata exhibits an irreversible reconfiguration of host cell gene expression. *PLoS ONE*. 8:e66833. doi: 10.1371/journal.pone.0066833

Lafferty, K. D., Dobson, A. P., and Kuris, A. M. (2006). Parasites dominate food web links. *Proc. Natl. Acad. Sci. U.S.A*. 103, 11211–11216. doi: 10.1073/pnas.0604755103

Lee, H. C., Kioi, M., Han, J., Puri, R. K., and Goodman, J. L. (2008). *Anaplasma phagocytophilum*-induced gene expression in both human neutrophils and HL-60 cells. *Genomics* 92, 144–151. doi: 10.1016/j.ygeno.2008.05.005

Marsolier, J., Perichon, M., DeBarry, J. D., Villoutreix, B. O., Chluba, J., Lopez, T., et al. (2015). *Theileria* parasites secrete a prolyl isomerase to maintain host leukocyte transformation. *Nature* 520, 378–382. doi: 10.1038/nature14044

Masui, K., Onizuka, H., Cavenee, W. K., Mischel, P. S., and Shibata, N. (2019). Metabolic reprogramming in the pathogenesis of glioma: update. *Neuropathology* 39, 3–13. doi: 10.1111/neup.12535

McGee, S. R., Tibiche, C., Trifiro, M., and Wang, E. (2017). Network analysis reveals a signaling regulatory loop in the PIK3CA-mutated breast cancer predicting survival outcome. *Genom. Proteom. Bioinforma*. 15, 121–129. doi: 10.1016/j.gpb.2017.02.002

Medjkane, S., Perichon, M., Marsolier, J., Dairou, J., and Weitzman, J. B. (2014). *Theileria* induces oxidative stress and HIF1α activation that are essential for host leukocyte transformation. *Oncogene* 33, 1809–1817. doi: 10.1038/onc.2013.134

Medjkane, S., and Weitzman, J. B. (2013). A reversible Warburg effect is induced by Theileria parasites to transform host leukocytes. *Cell Cycle*. 12, 2167–2168. doi: 10.4161/cc.25540

Moyano, A. J., Racca, A. C., Soria, G., Saka, H. A., Andreoli, V., Smania, A. M., et al. (2018). c-Jun Proto-oncoprotein plays a protective role in lung epithelial cells exposed to staphylococcal α- and Toxin. *Front. Cell. Infect. Microbiol*. 8:170. doi: 10.3389/fcimb.2018.00170

Oh, J. K., and Weiderpass, E. (2014). Infection and cancer: global distribution and burden of diseases. *Ann. Glob. Health* 80, 384–392. doi: 10.1016/j.aogh.2014.09.013

Otranto, D., Dantas-Torres, F., Brianti, E., Traversa, D., Petrić, D., Genchi, C., et al. (2013). Vector-borne helminths of dogs and humans in Europe. *Parasit Vectors* 6:16. doi: 10.1186/1756-3305-6-16

Ozturk, K., Dow, M., Carlin, D. E., Bejar, R., and Carter, H. (2018). The emerging potential for network analysis to inform precision cancer medicine. *J. Mol. Biol*. 430, 2875–2899. doi: 10.1016/j.jmb.2018.06.016

Parfett, C. L., and Desaulniers, D. (2017). A Tox21 approach to altered epigenetic landscapes: assessing epigenetic toxicity pathways leading to altered gene expression and oncogenic transformation *in vitro*. *Int. J. Mol. Sci.* 18:E1179. doi: 10.3390/ijms18061179

Parikh, A. P., Curtis, R. E., Kuhn, I., Becker-Weimann, S., Bissell, M., Xing, E. P., et al. (2014). Network analysis of breast cancer progression and reversal using a tree-evolving network algorithm. *PLoS Comput. Biol*. 10:e1003713. doi: 10.1371/journal.pcbi.1003713

Parkin, D. M. (2006). The global health burden of infection-associated cancers in the year 2002. *Int. J. Cancer* 118, 3030–3044. doi: 10.1002/ijc.21731

Reyna, M. A., Haan, D., Paczkowska, M., Verbeke, L. P. C., Vazquez, M., Kahraman, A., et al. (2019). PCAWG drivers and functional annotation group, ICGC/TCGA pan-cancer analysis of whole genomes. pathway and network analysis of more than 2,500 whole cancer genomes. *bioRxiv* 2019:385294. doi: 10.1101/385294

Sinclair, S. H., Rennoll-Bankert, K. E., and Dumler, J. S. (2014). Effector bottleneck: microbial reprogramming of parasitized host cell transcription by epigenetic remodeling of chromatin structure. *Front. Genet*. 5:274. doi: 10.3389/fgene.2014.00274

Takaki, A., Kawano, S., Uchida, D., Takahara, M., Hiraoka, S., and Okada, H. (2019). Paradoxical roles of oxidative stress response in the digestive system before and after carcinogenesis. *Cancers* 11:E213. doi: 10.3390/cancers11020213

Tretina, K., Gotia, H. T., Mann, D. J., and Silva, J. C. (2015). *Theileria*-transformed bovine leukocytes have cancer hallmarks. *Trends Parasitol*. 31, 306–314. doi: 10.1016/j.pt.2015.04.001

Villar, M., Popara, M., Ayllón, N., Fernández de Mera, I. G., Mateos-Hernández, L., Galindo, R. C., et al. (2014). A systems biology approach to the characterization of stress response in *Dermacentor reticulatus* tick unfed larvae. *PLoS ONE* 9:e89564. doi: 10.1371/journal.pone.0089564

Vogelstein, B., Papadopoulos, N., Velculescu, V. E., Zhou, S., Diaz, L. A., and Kinzler, K. W. (2013). Cancer genome landscapes. *Science* 339, 1546–1558 doi: 10.1126/science.1235122

Wulf, G. M., Ryo, A., Wulf, G. G., Lee, S. W., Niu, T., Petkova, V., et al. (2001). Pin1 is overexpressed in breast cancer and cooperates with Ras signaling in increasing the transcriptional activity of c-Jun towards cyclin D1. *EMBO J*. 20, 3459–3472. doi: 10.1093/emboj/20.13.3459

Xie, J., Pan, H., Yoo, S., and Gao, S. J. (2005). Kaposi's sarcoma-associated herpesvirus induction of AP-1 and interleukin 6 during primary infection mediated by multiple mitogen-activated protein kinase pathways. *J. Virol*. 79, 15027–15037. doi: 10.1128/JVI.79.24.15027-15037.2005

Yu, X., Ma, R., Wu, Y., Zhai, Y., and Li, S. (2018). Reciprocal regulation of metabolic reprogramming and epigenetic modifications in cancer. *Front. Genet*. 9:394. doi: 10.3389/fgene.2018.00394

Zhang, W., Bojorquez-Gomez, A., Velez, D. O., Xu, G., Sanchez, K. S., Shen, J. P., et al. (2018). A global transcriptional network connecting non-coding mutations to changes in tumor gene expression. *Nat. Genet*. 50, 613–620. doi: 10.1038/s41588-018-0091-2

Conflict of Interest Statement: The authors declare that the research was conducted in the absence of any commercial or financial relationships that could be construed as a potential conflict of interest.

frontiers in Cell and Developmental Biology

ORIGINAL RESEARCH
published: 20 September 2019
doi: 10.3389/fcell.2019.00200

The Role of EGFR in Influenza Pathogenicity: Multiple Network-Based Approaches to Identify a Key Regulator of Non-lethal Infections

Hugh D. Mitchell[1], Amie J. Eisfeld[2], Kelly G. Stratton[1], Natalie C. Heller[1], Lisa M. Bramer[1], Ji Wen[1], Jason E. McDermott[1], Lisa E. Gralinski[3], Amy C. Sims[3], Mai Q. Le[4], Ralph S. Baric[3], Yoshihiro Kawaoka[2,5,6] and Katrina M. Waters[1]**

[1] Pacific Northwest National Laboratory, Richland, WA, United States, [2] Department of Pathobiological Sciences, University of Wisconsin–Madison, Madison, WI, United States, [3] Department of Microbiology and Epidemiology, The University of North Carolina at Chapel Hill, Chapel Hill, NC, United States, [4] National Institute of Hygiene and Epidemiology, Hanoi, Vietnam, [5] Division of Virology, Department of Microbiology and Immunology, Institute of Medical Sciences, The University of Tokyo, Tokyo, Japan, [6] International Research Center for Infectious Diseases, Institute of Medical Sciences, The University of Tokyo, Tokyo, Japan

OPEN ACCESS

Edited by:
Davide Gibellini,
University of Bologna, Italy

Reviewed by:
Yoo-Ah Kim,
National Institutes of Health, United States
Gualtiero Alvisi,
University of Padua, Italy

***Correspondence:**
Hugh D. Mitchell
hugh.mitchell@pnnl.gov
Katrina M. Waters
katrina.waters@pnnl.gov

Specialty section:
This article was submitted to Molecular Medicine, a section of the journal Frontiers in Cell and Developmental Biology

Received: 19 March 2019
Accepted: 05 September 2019
Published: 20 September 2019

Citation:
Mitchell HD, Eisfeld AJ, Stratton KG, Heller NC, Bramer LM, Wen J, McDermott JE, Gralinski LE, Sims AC, Le MQ, Baric RS, Kawaoka Y and Waters KM (2019) The Role of EGFR in Influenza Pathogenicity: Multiple Network-Based Approaches to Identify a Key Regulator of Non-lethal Infections. Front. Cell Dev. Biol. 7:200. doi: 10.3389/fcell.2019.00200

Despite high sequence similarity between pandemic and seasonal influenza viruses, there is extreme variation in host pathogenicity from one viral strain to the next. Identifying the underlying mechanisms of variability in pathogenicity is a critical task for understanding influenza virus infection and effective management of highly pathogenic influenza virus disease. We applied a network-based modeling approach to identify critical functions related to influenza virus pathogenicity using large transcriptomic and proteomic datasets from mice infected with six influenza virus strains or mutants. Our analysis revealed two pathogenicity-related gene expression clusters; these results were corroborated by matching proteomics data. We also identified parallel downstream processes that were altered during influenza pathogenesis. We found that network bottlenecks (nodes that bridge different network regions) were highly enriched in pathogenicity-related genes, while network hubs (highly connected network nodes) were significantly depleted in these genes. We confirmed that this trend persisted in a distinct virus: Severe Acute Respiratory Syndrome Coronavirus (SARS). The role of epidermal growth factor receptor (EGFR) in influenza pathogenesis, one of the bottleneck regulators with corroborating signals across transcript and protein expression data, was tested and validated in additional mouse infection experiments. We demonstrate that EGFR is important during influenza infection, but the role it plays changes for lethal versus non-lethal infections. Our results show that by using association networks, bottleneck genes that lack hub characteristics can be used to predict a gene's involvement in influenza virus pathogenicity. We also demonstrate the utility of employing multiple network approaches for analyzing host response data from viral infections.

Keywords: systems biology, network topology, influenza, SARS-CoV, data integration

INTRODUCTION

Viruses that are newly introduced to the human population have the potential to be highly pathogenic. While the pathogenicity of these new strains tends to wane as adaptation progresses, emerging viruses, such as highly pathogenic avian influenza strains, are an ever-present threat to human health and the global economy because it is difficult to predict when a new pathogenic strain will appear. The 1918 influenza A virus pandemic claimed 20–100 million lives worldwide (Peiris et al., 2004). Multiple influenza pandemics have emerged since. Most recently, human infections of H7N9 influenza, which first emerged in the spring of 2013, have resulted in 1568 infections including 616 deaths (Food and Agriculture Organization [FAO], 2019). Since 2003, H5N1 avian influenza has caused 860 human infections with a mortality rate of 53% (World Health Organization [WHO], 2018). The 2009 H1N1 pandemic caused less severe disease in humans but spread to nearly 200 countries (Michaelis et al., 2009) and may have contributed to the deaths of an estimated 284,000 people (Dawood et al., 2012). The fact that influenza strains vary greatly in pathogenicity underscores the need to understand the underlying host mechanisms that contribute to the severity of infection so that we are better prepared to alleviate the effects of highly pathogenic strains. Despite the potential for pandemic infection with a highly virulent, highly transmissible new strain of influenza, the current understanding of these mechanisms remains limited.

A major advantage of a systems biology approach to pathobiology is the ability to identify novel, key elements of a biological process, such what regulators are involved in critical processes. High-throughput profiling methods (e.g., transcriptomics) provide powerful tools for examining how entire systems respond to different perturbations such as acute disease. Network reconstruction provides the opportunity to utilize all available data and is a critically important tool for representing complex sets of interactions. For biological systems, network analysis has proven useful for analyzing genetic interactions among genes, as well as protein–protein, protein–DNA, and kinase–substrate interactions (Ideker and Krogan, 2012). In addition, network approaches have attempted to identify regulatory associations between genes and proteins by comparing expression patterns across multiple conditions (Faith et al., 2007; McDermott et al., 2009, 2012). These approaches may capture physical interactions but can also identify more subtle, though equally important, regulatory relationships between gene pairs or within gene clusters. Previous work has shown that prioritization of key regulators based on network topology is superior to simple ranking of differentially expressed genes (McDermott et al., 2011). Our group and others have demonstrated that genes occupying certain topological positions in association networks play important regulatory roles in the biological process being studied (Yu et al., 2007; McDermott et al., 2009, 2016; Mitchell et al., 2013). Network hubs are identified by the degree centrality metric, which is the number of edges associated with any given node. Network bottlenecks are identified by the betweenness centrality metric, which is the number of shortest paths between all pairs of nodes that pass through a given node. These are two of the most studied topological features, yet it is unclear from the literature which of these is the most effective predictor of regulatory function for any given network construction approach or biological context. It is also unclear what distinct regulatory roles each has; such information is important to discern as it may be used to identify targets for therapeutic intervention.

Typically, studies that attempt to uncover the underlying mechanisms of pathogenicity simply compare a single high- and low-pathogenicity strain or dose (Hatta et al., 2001; Kobasa et al., 2007; Cilloniz et al., 2009; Safronetz et al., 2011; Tisoncik-Go et al., 2016). While this approach may allow pathogenicity-related host responses to be identified, it can be difficult to distinguish between responses that are truly tied to pathogenicity and those that are strain-specific. For this study, we use network clustering and topology to compare six influenza strains and mutants of varying pathogenicity (referred to herein as the pathogenicity gradient) at multiple doses and four time points in the context of a murine infection model. This allows us to identify pathogenicity-related traits with greater certainty than in previous studies. We utilize global transcriptomic and proteomic data from these experiments, thus providing a more complete view of the layered interaction between host and virus. We demonstrate a network-based approach for identifying critical factors in influenza pathogenesis and test our findings with a pharmacological inhibitor during lethal and non-lethal infections.

MATERIALS AND METHODS

Data Deposition

Microarray data was deposited previously in the gene expression omnibus (GEO) under the following accession numbers: GSE33263: Influenza A/VN/1203/04 infection in mice with three viral doses at 1, 2, 4, and 7 days (IM001); GSE37572: HA avirulent mutation in A/Vietnam/1203/2004(H5N1) infection in mice at 10^4 PFU at 1, 2, 4, and 7 days (IM004); GSE43301: Influenza A/VN/1203/04 PB2-627E mutant infection in mice with 10^4 PFU at 1, 2, 4, and 7 days (IM005); GSE43302: Influenza A/VN/1203/04 PB2-627E mutant infection in mice with 10^3 PFU at 1, 2, 4, and 7 days (IM005); GSE44441: Influenza A/VN/1203/04 PB1-F2 mutant infection in mice with 10^4 PFU at 1, 2, 4, and 7 days (IM006); GSE44445: Influenza A/VN/1203/04 NS1trunc124 mutant infection in mice with two doses at 1, 2, 4, and 7 days (IM007); GSE37569: Influenza A/CA04/2009 infection in mice with four doses at 1, 2, 4, and 7 days (CA04M001); GSE33266: SARS-CoV MA15 infection in mice with four viral doses at 1, 2, 4, and 7 days (SM001); GSE50000: SARS-CoV MA15, icSARS-CoV, or SARS BatSRBD infection in mice with two viral doses at 1, 2, 4, and 7 days (SM003); GSE49262: SARS-CoV MA15 or SARS deltaORF6 infection in mice with 1O5 PFU at 1, 2, 4, and 7 days (SM012); GSE49263: SARS-CoV MA15 or SARS nsp16 infection in mice with 10^5 PFU at 1, 2, 4, and 7 days (SM014). Proteomics data for IM001, IM004, IM005, IM006, and IM007 (described above) can be found at https://omics.pnl.gov/project-data/systems-virology-contract-data.

Construction of Pathogenicity Profile

We set out to build a synthetic pathogenicity profile that represents the severity of the infection for each experimental condition. The viruses used to construct the pathogenicity gradient include the H1N1 strain, A/California/04/2009 (CA04), from the 2009 pandemic,; the highly pathogenic H5N1 avian strain, A/Vietnam/1203/2004 (VN1203); and four mutants of VN1203: VN1203-HAavir (which lacks the multi-basic cleavage site in the viral hemagglutinin protein that is critical for extra-pulmonary viral spread), VN1203-PB2-627E (which lacks a mammalian-adapting mutation that substantially increases the replicative ability of the viral polymerase complex in mammalian cells), VN1203-NS1trunc (which encodes a C-terminal truncation in the effector domain of the NS1 host response antagonist protein), and VN1203-PB1F2del (which lacks expression of the PB1-F2 protein). Genes that mirror this profile are hypothesized to be related to pathogenicity in some way, a proposition similar to that given by Taylor et al. (2016). To construct the profile, we scaled all six strains/mutants proportional to their median lethal dose (MLD_{50}) value, or the amount of viral particles at which 50% of infected mice succumb to infection (**Figure 1A**). We therefore assigned a score for each strain corresponding to the log of the MLD_{50} and then adjusted the scores to account for differences in administered doses across studies. Since infection conditions for each strain included a dose at 10^4 PFU, the corresponding strain's log MLD_{50} was assigned to all infection conditions at this dose. To make the score more intuitive (high score = high pathogenicity), each log MLD_{50} was subtracted from the maximum observed log MLD_{50}. The intent was to quantitatively relate the experimental conditions to each other, with the expectation that genes related to pathogenicity would manifest expression patterns similar to the pathogenicity profile. To avoid negative values, an additional unit was added to each score. Therefore, the pathogenicity level for a given infection condition *i,* with dose d_i and the particular viral strain's MLD_{50} m_i, is given by:

$$P_i = 1 + \log\left(\frac{m_{max}}{m_i}\right) + \log\left(\frac{d_i}{d_{com}}\right)$$

where m_{max} is the maximum observed MLD_{50}, and d_{com} is the dose common to all strains/mutants, i.e., the experimental conditions for all infections included at least this dose, if not others. Applying this calculation across all conditions yielded the profile (**Figure 1B**). Since the array of conditions differed somewhat between the transcripts and protein data, profiles unique to each of these datasets were generated.

Data Pre-processing

Sample collection and microarray processing are described for this dataset in Tchitchek et al. (2013). For our analysis, we selected the probes that were (1) present on all arrays after quality control filtering, (2) previously identified as significantly changed from mock expression (q-value < 0.05), and (3) had a simultaneous log2 fold change of at least 1.5 in at least one experimental condition (Li et al., 2011). This resulted in the selection of 7471 probes for analysis. The results for proteomic data, sample processing, capillary LC-MS/MS analysis, spectral matching, and peptide-to-protein rollup are described in Tchitchek et al. (2013). Missing value imputation was performed using a regularized expectation maximization algorithm (Webb-Robertson et al., 2015). Selected proteins were only those that were (Peiris et al., 2004) detected in every experiment before imputation (experiment = set of infections with one given strain), and (Food and Agriculture Organization [FAO], 2019) significantly changed from mock ($p < 0.05$) in at least one experimental condition; this resulted in 1476 proteins that were used in our analysis.

For the correlation calculations (below), expression data from selected time points were extracted and then mean-summarized for each strain and dose. Some viruses received heavier experimental coverage than others; we therefore expanded the data compendium to equalize the influence each virus strain in the pathogenicity gradient has on the correlation calculations by duplicating the data from under-represented conditions so that every strain was equally represented in the compendium.

Correlation

We calculated Pearson's correlation using the expanded expression profile for each gene/protein and the appropriately expanded pathogenicity profile. Day 1, day 2, day 4, and day 7 designations were used to refer to the top 5% of pathogenicity-correlated genes (both positive and negative correlation) using individual time point data for correlation calculations.

Association Network Topology

Network inference was performed using the Context Likelihood of Relatedness software tool as described (Mitchell et al., 2013). The network centrality measures of betweenness and degree were determined using the R igraph package.

Interactor Enrichment Analysis

To identify regulators of interest, we used the "Interactions By Protein Function" and "Significant Interactions Within Set(s)" tools in the MetaCore software package (Clarivate Analytics, Philadelphia PA) to identify genes/proteins whose interactors were enriched among pathogenicity-related proteins. A similar approach was used for pathogenicity-related genes.

Cluster Analysis

We used the R weighted gene correlation network analysis (WGCNA) package to identify clusters of genes or proteins with behavioral similarity (Langfelder and Horvath, 2008). Cluster identification was performed using the blockwiseModules function with the following parameter values for transcript cluster analysis: power = 12, minModuleSize = 30, maxBlockSize = 8000, reassignThreshold = 0, mergeCutHeight = 0.25, and pamRespectsDendro = F.

Ethics Statement

All animal experiments and procedures were approved by the University of Wisconsin (UW)-Madison School of Veterinary Medicine Animal Care and Use Committee under relevant institutional and American Veterinary Association guidelines.

Biosafety

All experiments using replication competent H1N1 viruses were performed in biosafety level 2 (BSL-2) or animal enhanced biosafety level 2 (ABSL-2) containment laboratories at UW-Madison. Experiments using replication competent H5N1 virus were performed in an ABSL-3+ containment laboratory at UW-Madison. UW-Madison BSL-2, ABSL-2, and ABSL-3+ laboratories are approved for use by the United States (US) Centers for Disease Control and Prevention (CDC) and the US Department of Agriculture. Experiments using replication competent SARS-CoV were performed in an ABSL-3+ containment laboratory at the University of North Carolina at Chapel Hill (UNC). UNC BSL-2, ABSL-2, and ABSL-3+ laboratories are approved for use by the US CDC.

Cells

Madin-Darby canine kidney (MDCK) cells were propagated in a minimum essential medium (MEM) containing 5% newborn calf serum and were maintained at 37°C in an atmosphere of 5% CO_2. Cell stocks are periodically restarted from early passage aliquots and routinely monitored for mycoplasma contamination.

Viruses

The A/California/04/09 H1N1 virus (CA04) was provided by the US CDC. The A/chicken/Vietnam/TY167/2011 (H5N1) virus (TY167) was obtained through surveillance activities in Vietnam. Stock viruses were generated by passaging an aliquot of the original virus once in MDCK cells containing 0.6% bovine serum albumin (BSA) fraction V (Sigma-Aldrich) and 1 μg/ml tosyl phenylalanyl chloromethyl ketone (TPCK)-treated trypsin (CA04) or in embryonated chicken eggs (TY167), as previously described (Eisfeld et al., 2014). Stock virus titers were quantified by plaque assay in MDCK cells using standard methods. SARS-CoV was propagated and assayed for titer levels, as published previously (Gralinski et al., 2013).

Mouse Infections

Nine- to ten-week-old female C57BL/6J mice (The Jackson Laboratory) were administered 0 or 100 mg/kg of Gefitinib (Tocris Bioscience) in 1% Tween-80 in phosphate-buffered saline (PBS) by oral gavage 1 day prior to infection and each subsequent day until the end of the experiment. Four mice were used for each drug and viral dose combination. For infection, mice were anesthetized by intraperitoneal (i.p.) injection of ketamine and dexmedetomidine (45–75 mg/kg ketamine + 0.25–1 mg/kg dexmedetomidine) and were intranasally inoculated with 50 μl of PBS-containing viruses, as indicated in **Figure 6** and the corresponding text in the "Effect of EGFR Inhibition on Influenza Pathogenesis in Mice" section. Following inoculation, dexmedetomidine was reversed by i.p. injection of atipamezole (0.1–1 mg/kg). Subsequent to infection, individual body weights and survival were monitored for up to 17 days, and mice were humanely euthanized when exhibiting severe clinical symptoms or at the end of the observation period. SARS-CoV infections in mice were performed as previously published (Gralinski et al., 2013).

Statistical Analysis

To model the trend in mice weight over time, we used linear mixed effects models with a normal conditional distribution and identity link on each time course. Fixed effects were day, gefitinib level, and the interaction between day and gefitinib level, while random effects for each mouse were included to account for variability in the mice and for the non-independent nature of the data over time. A second model that did not include the gefitinib level and day interaction terms was also fit; a likelihood ratio test was then conducted to determine if the group slopes were significantly different.

Due to the patterns of mouse weight over time, a single linear model was not always sufficient to model the data; this was determined by using linear splines to estimate change points where separate linear models should be used to represent the trend for different time ranges. Specifically, knot points were identified by determining if adding an additional time point to the linear model of an existing segment changed the model. If the new point changed the model significantly, then a new knot point was identified; otherwise, the time point was added to the segment. After all knot points were found, a single random mixed effect model was fit to each segment of data. TY167 at 10^3 PFU was modeled as a single segment, CA04 at 10^2 PFU and 10^3 PFU in three segments, and TY167 at 10^2 PFU in four segments. Separate *p*-values were determined for each segment (as identified from the knot points as boundaries), which are provided in **Table 2**.

RESULTS

Experimental Overview

Our overall strategy is depicted in **Figure 2**. We used transcriptomics and proteomics data in conjunction with pathogenicity data from the different virus strains/mutants (**Figures 2A,B**) to identify pathways and individual genes/proteins that were important for influenza pathogenicity. Correlated gene modules in the transcriptomics were first detected (**Figure 2C**) and compared with the pathogenicity profile (**Figure 2A**) to identify gene modules whose behavior linked them to pathogenicity. Individual proteins whose behavior correlated with pathogenicity were incorporated into interaction enrichment analysis, which identified genes whose interaction neighbors from curated networks were enriched among pathogenicity-correlated proteins (**Figure 2D**). These results could be connected to host responses evident in the gene clusters depicted in **Figure 2C**. An association network built from mutual information of perturbed gene pairs (**Figure 2E**) was used for topology analysis, which yielded network hubs and bottlenecks. Lists of pathogenicity-correlated genes from early and late time points (**Figure 2F**) were combined and compared to network nodes with high hub and bottleneck scores. Comparison of genes correlated with pathogenicity to network hubs and bottlenecks showed significant overlap with network bottlenecks (**Figure 2G**), but hubs were strikingly excluded (**Figure 2H**). Examination of results from interaction enrichment (**Figure 2D**) and network topology (**Figures 2E–G**) revealed epidermal

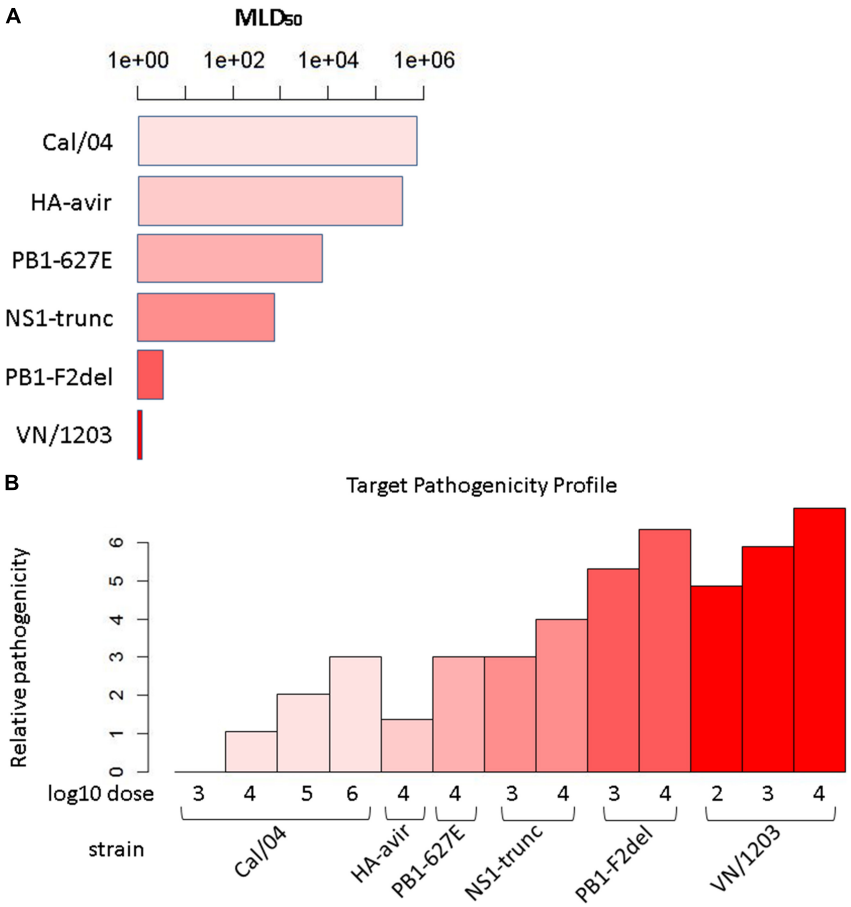

FIGURE 1 | Target pathogenicity profile. **(A)** Median lethal dose 50 (MLD50) values for the six strains/mutants in the influenza virus pathogenicity gradient. Mouse MLD_{50} data was previously published in Tchitchek et al. (2013). **(B)** Target pathogenicity profile based on MLD50 values.

growth factor receptor (EGFR) as a candidate for follow-up experiments (**Figure 2I**).

Correlation With Pathogenicity

We utilized transcriptomic and proteomic datasets (represented by **Figure 2B**) of mouse infection with six strains/mutants of influenza at varying doses and times, as described in Tchitchek et al. (2013). These viruses display varying degrees of virulence, as assessed by the minimal dose that is lethal to 50% of animals to which it is administered (MLD_{50}, **Figure 1A**, see section "Materials and Methods" for details). Samples were collected at 1, 2, 4, and 7 days post-infection for global transcriptomics and proteomics analysis of lung tissues relative to time-matched mock-infected controls.

Clustering of Expression Data

To identify transcripts correlated with pathogenicity, we used the WGCNA network clustering approach (Langfelder and Horvath, 2008) to cluster gene expression profiles across all experiments into expression modules that represent groups of genes with similar expression behaviors (**Figure 2C**). This approach further affirms that the overall gene expression pattern of each module has true biological meaning because each identified pattern is manifested by many genes. The representative expression profile of each module, or eigengene, can be correlated with clinical measures or other metadata to identify modules of interest (Langfelder and Horvath, 2008; Saris et al., 2009; Levine et al., 2013). We thus applied WGCNA to our transcript dataset to identify network modules related to influenza pathogenicity. **Figure 3A** shows the correlations of all eigengene profiles to pathogenicity. Two of the modules, pink and black, showed much higher correlations than the others and were selected for further analysis. The pink module is strongly *positively* correlated with pathogenicity (**Figure 3B**). We found statistical enrichment in plasminogen activation among the genes in this module, particularly KLKB1 and coagulation factor X1; this suggests that pathogenic influenza infection involves a perturbed coagulation cascade. The black module (**Figure 3C**) is strongly *negatively* correlated with pathogenicity and was strikingly enriched for B-cell activation, implying that a diminished presence of B-cell activity is related to pathogenesis in influenza. Interestingly, a previous report showed that influenza caused apoptotic loss of bone marrow B-cells in mice despite the complete lack of viral particles detected in the bones (Sedger et al., 2002). Since

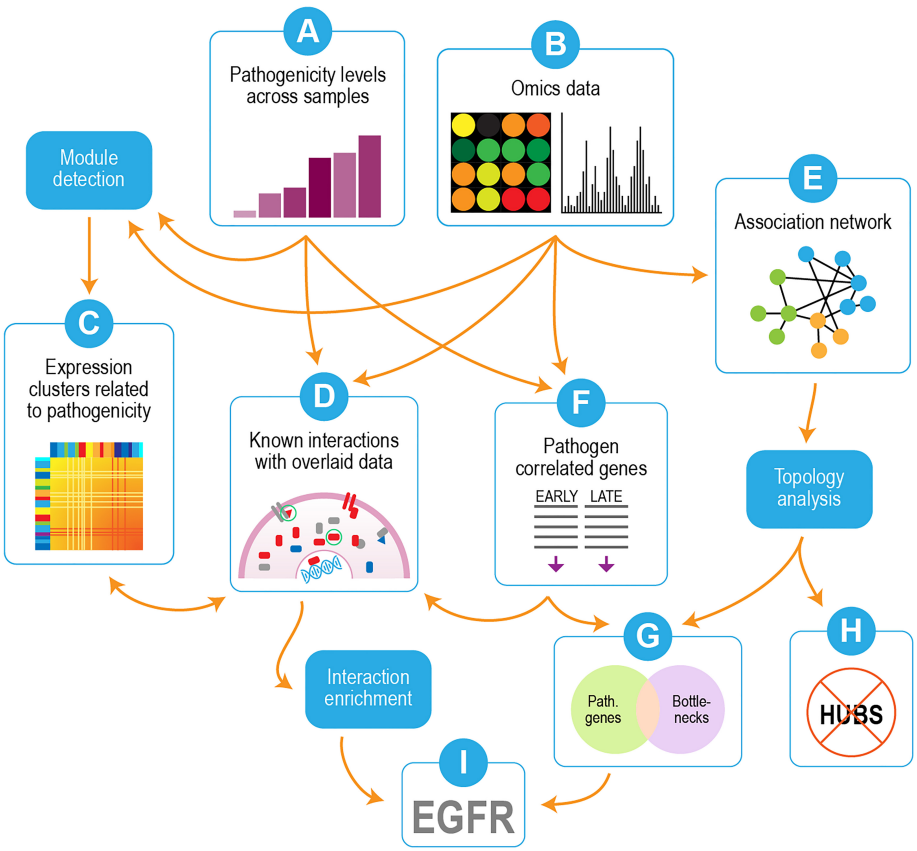

FIGURE 2 | Overview of analysis strategy. Omics data (transcriptomics and proteomics) were used in conjunction with pathogenicity data from the different virus strains/mutants **(A,B)**. Correlated modules in the transcriptomics were detected **(C)** and compared with the pathogenicity profile **(A)** to identify gene modules whose behavior linked them to pathogenicity. Individual proteins whose behavior correlated with pathogenicity were submitted to interaction enrichment analysis, which looked for genes whose interaction neighbors from curated networks were enriched among pathogenicity-correlated proteins **(D)**. An association network built from mutual information of perturbed gene pairs **(E)** was used for topology analysis, which yielded network hubs and bottlenecks. Lists of pathogenicity-correlated genes from early and late time points **(F)** were combined and compared to network nodes with high hub and bottleneck scores. Overlap was seen with network bottlenecks **(G)** but not hubs **(H)**. EGFR was identified as a candidate for follow-up experiments based on overlaps between interaction enrichment and pathogenicity-related bottlenecks **(I)**.

B-cells are known to both reside in and travel through the lungs (Polverino et al., 2016), high-path flu may trigger death of lung B-cells, resulting in previously unappreciated effects on host response during these infections.

Transcriptome/Proteome Integration

To determine the extent to which proteome data validated our transcriptomics findings, we used the matching protein expression data to evaluate downstream pathway regulation related to infection severity at different time points (**Figure 2D**). We reasoned that correlation with pathogenicity could have different meanings depending on which time points are used for the correlation calculation. Correlated genes identified early in the infection could be filling regulatory roles, while those from later points are expected to be the downstream effects of earlier events. Accordingly, we identified genes and proteins whose expression profiles correlated with pathogenicity at individual time points and designated the resulting lists as day 1, day 2, day 4, and day 7. We then integrated the gene and protein data using target enrichment to identify the regulatory targets of protein pathway expression (**Supplementary Tables S1**, **S2**). We found that Syk, Prkcb, and Ebf1 were day 1 genes and that each of these is a regulator of B-cell activation/maturation. Proteins known to be regulated by and/or bind to these regulators were significantly enriched among day 1 (Syk) proteins, while transcripts of genes regulated by Ebf1 and Prkcb were enriched among day 1 and day 7 (Ebf1) or day 4 (Prkcb) genes. Like the B-cell-related module from the cluster analysis, the expression profiles of all three of these B-cell regulators showed strong negative correlation to pathogenicity, thus reinforcing the concept of decreased B-cell presence in the mouse lung during severe influenza infection. Thus, our observation that the presence of B-cell-related functions is tied to pathogenicity is borne out by comparing results across time points and data types. Similarly, we observed enrichment in proteins regulated by coagulation factor XIII A1 (F13a1) in day 4 proteins, with the F13a1 transcript also among day 4 genes. Transcripts for coagulation regulators Plat and Serpine1 as

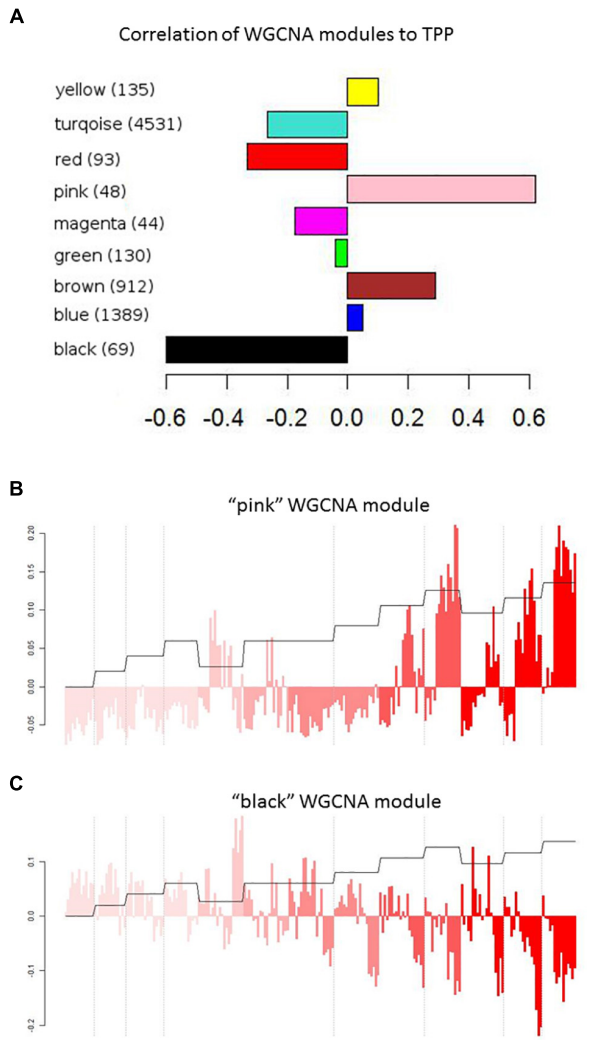

FIGURE 3 | WGCNA modules. **(A)** Pearson's correlation values of WGCNA modules with the pathogenicity profile. **(B,C)** Correlation of the "pink" **(B)** or "black" **(C)** WGNCA module eigengene with the pathogenicity profile. Module eigengenes are the principle component of the expression levels of modules that contains similarly behaving genes, and therefore represent the expression patterns across all genes in a module. Each bar represents the expression of the module's genes in an individual mouse infected with a particular strain of influenza at a certain dose for a set number of days (1, 2, 4, or 7). Color intensity represents strains/mutants with increasing pathogenicity, as in **Figure 2**. Dashed lines indicate dose separations for a single strain. Orange trace shows the pathogenicity profile.

well as their downstream targets were found among day 7 genes. These latter results validated our findings from transcript expression that coagulation-related pathways are linked to pathogenicity. In addition to findings related to regulation of B-cell activity and coagulation, we also observed that direct protein targets of EGFR activity are significantly enriched among day 1 and day 4 proteins. In this way, integration of transcriptomic and proteomic data enhances our analysis and identifies the pathways most likely to be important for infection severity.

From this analysis we constructed three lists of genes that were identified as being correlated to pathogenicity in early infection (**Supplementary Table S3**), late infection (**Supplementary Table S4**), or both (**Figure 2F** and **Supplementary Table S5**). We focused on genes that are correlated with pathogenicity both early and late in the infection, for two reasons: (Peiris et al., 2004) high correlations from two separate groups of data points for the same gene means it is likely that these genes truly correlate with pathogenicity, and (Food and Agriculture Organization [FAO], 2019) the overlap of the two groups helps yield the identity of genes important both early and throughout the infection process. Because influenza viral titers reach maximal levels by day 2, regulatory responses are likely to occur in the first 24 h of infection. We thus designated the day 1 results as "early" and other time points as "late." To identify genes with both early and late infection correlation to pathogenicity, genes were identified from the top 5% of pathogenicity-correlated genes at early time points. The same procedure was used for late time points, and the intersection of these two resulted in a list of early/late correlated genes. The overlap between day 1 genes and the set of combined day 2, day 4, and day 7 genes resulting in 54 genes (we refer to these as early/late correlated genes). The overlap between early and late was highly significant (p = 6.4e-13, Fisher test).

Association Network Topology Analysis

The clustering analysis provided a way to determine what kinds of genes manifested expression behaviors connected to pathogenicity. However, we were interested in identifying regulatory mechanisms of influenza infection in the context of pathogenicity. As a means of identifying key regulators, we turned to an approach based on network topology. A growing body of work has shown that network topology, or the placement of nodes in the network structure, can be used to identify entities with key regulatory roles (Yu et al., 2007; Zhou and Liu, 2014; Narang et al., 2015; McDermott et al., 2016). Of particular interest are network bottlenecks and hubs, both of which have been shown to be enriched for regulators under various circumstances (Yu et al., 2007; McDermott et al., 2009, 2012, 2016; Zhou and Liu, 2014; Narang et al., 2015). We built a mutual information-based association network with transcript data (McDermott et al., 2009, 2016; Mitchell et al., 2013) using 7471 genes deemed significantly changed in at least one experimental condition (strain, dose, or time; see section "Materials and Methods") as input; we also identified network hubs and bottlenecks, which were defined as the top 5% of betweenness scores and degree scores, respectively (**Figure 2E**).

Since network hub nodes are known to have critical systemic functions, we hypothesized that pathogenicity-related genes may be enriched in bottleneck or hub genes. To test this hypothesis, we examined the statistical enrichment of the identified pathogenesis sets with bottlenecks and hubs identified from the network analysis. Interestingly, no overlap was discovered between network hubs and early/late correlated genes (p = 0.11, two-sided Fisher test). In contrast, we found these genes to be significantly enriched in network bottlenecks (10 of the 54, p = 2.9e-4, two-sided Fisher test), suggesting bottlenecks are

TABLE 1 | Pathogenicity-related bottleneck genes.

Gene symbol	Entrez	Description	Comment
EGFR	13649	Epidermal growth factor receptor	Receptor tyrosine kinase
TBC1D10C	108995	TBC1 domain family, member 10c	Inhibits Ras and calcineurin
CD22	12483	CD22 antigen	B-cell/B-cell interactions
FCRL1	229499	Fc receptor-like 1	Ig receptor, promotes B-cell activation and differentiation
ELOVL1	54325	Elongation of very long chain fatty acids	Associated diseases include peroxisomal disease and adrenoleukodystrophy
IKZF3	22780	IKAROS family zinc finger 3	B-cell activation and differentiation
MBD1	17190	Methyl-CpG binding domain protein 1	Transcriptional repressor of methylated DNA
TSPAN32	27027	Tetraspanin 32	Involved with hematopoietic cell function, associated with some cancers
KIF21B	16565	Kinesin family member 21B	ATP-dependent microtubule-based motor protein, associated with inflammatory bowel disease and multiple sclerosis
SLC10A6	75750	Solute carrier family 10 (sodium/bile acid cotransporter family), member 6	Lung sulfonated steroid importer

important early regulators of pathogenesis (**Figures 2G,H**; names and descriptions of the genes are found in **Table 1**). Notably, three of these ten, CD22, FCRL1, and IKZF3, are closely related to B-cell activation and overlapped with members of the black WGCNA module. Another of these 10 genes is EGFR (**Figure 2I**), which we found to have protein targets enriched among correlated proteins at day 1 and day 4. To determine if these results were biased by the selection of arbitrary thresholds, we generated rankings for the degree, betweenness, and correlation to pathogenicity of all genes, then produced matrices of upper percentile thresholds by applying a Fisher enrichment test for each threshold pairing. Remarkably, we observed a dramatic exclusion (blue cells in **Figure 4**, upper right) of hubs from correlated genes across a wide range of thresholds. In contrast, bottlenecks showed a strong enrichment trend (red cells in **Figure 4**, upper left). These results show that for influenza infection, network hubs and bottlenecks have strikingly opposite roles regarding pathogenicity of the virus.

Given that network bottlenecks have a unique relationship with genes related to pathogenicity, we hypothesized that network hubs might be enriched in genes involved in more general aspects of infection. To test this, we identified the most highly perturbed genes across the transcriptome by ranking genes by their maximum fold change value across all data sets and then built matrices that compared the maximum expression to betweenness and degree, as before. As shown in the lower panels of **Figure 4**, genes with high maximum expression overlapped dramatically with network hubs but showed minimal enrichment for bottlenecks. Thus, highly connected genes (hubs) are strongly related to high expression and are strongly segregated from pathogenicity-related genes, while network bottlenecks show a strikingly different strong relationship to pathogenicity.

To determine if similar relationships exist in a distinct infection system, we applied a similar analysis to a compendium of four datasets obtained from mice infected with the SARS coronavirus (SARS-CoV), one of which was previously published by Gralinski et al. (2013). Mice were infected with WT SARS-CoV and three attenuated mutants at varying doses and analyzed for lung gene expression at one, two, four, and seven days post-infection. Since lethality is not readily observed in attenuated SARS-CoV mutants, we used animal weight loss at each time point to represent pathogenicity at each infection condition. Also, since viral replication kinetics are slower for SARS-CoV infection compared to that of influenza virus, we used days 1 and 2 to represent early infection and days 4 and 7 for late infection when ranking genes for pathogenicity. When applying the approach outlined above, we observed very similar results with SARS-CoV to those seen with influenza virus (**Figure 5**). The same patterns of exclusion and enrichment of hubs and bottlenecks in regard to pathogenesis-correlated genes and high-expression genes was shown to be even more dramatic in SARS-CoV. Thus, the enrichment of pathogenicity-related genes in network bottlenecks and their exclusion from network hubs appears to be a widespread phenomenon characteristic of respiratory viral infections in mice.

This finding is significant because the network betweenness measurement we applied was in no way informed by our pathogenicity results, yet it is able to significantly enrich for pathogenicity-related genes. Thus, network bottlenecks but not hubs facilitate the identification of critical regulators as intervention targets. Further studies will determine whether this approach is applicable in other infection systems as well.

Interestingly, no overlap was found between pathogenicity-related genes in influenza and SARS-CoV, but significant overlap in bottlenecks (39 genes, p-value $< 10^{-6}$) and hubs (203 genes, p-value $<< 10^{-6}$) was found between the two viruses.

Effect of EGFR Inhibition on Influenza Pathogenesis in Mice

Epidermal growth factor receptor has previously been shown to play a role in influenza infection (Eierhoff et al., 2010; Ueki et al., 2013) but has not been tied to pathogenicity. Because we identified EGFR as a pathogenicity-correlated bottleneck gene with apparent signaling effects evident in proteomics and transcriptomics, we investigated the role of EGFR in pathogenesis further with a mouse model. We treated mice for 14 days with the EGFR inhibitor gefitinib and monitored infection-related weight loss of treated and untreated animals to determine if EGFR inhibition affected the course of infection. After one day of treatment, mice were infected with one of two strains of influenza virus at various doses: CA04 (10^2, 10^3, and 10^4 PFU) or the highly pathogenic H5N1 avian strain, A/chicken/Vietnam/TY167/2011 (TY167) (10^1, 10^2, 10^3, and 10^4 PFU). The alternative H5N1

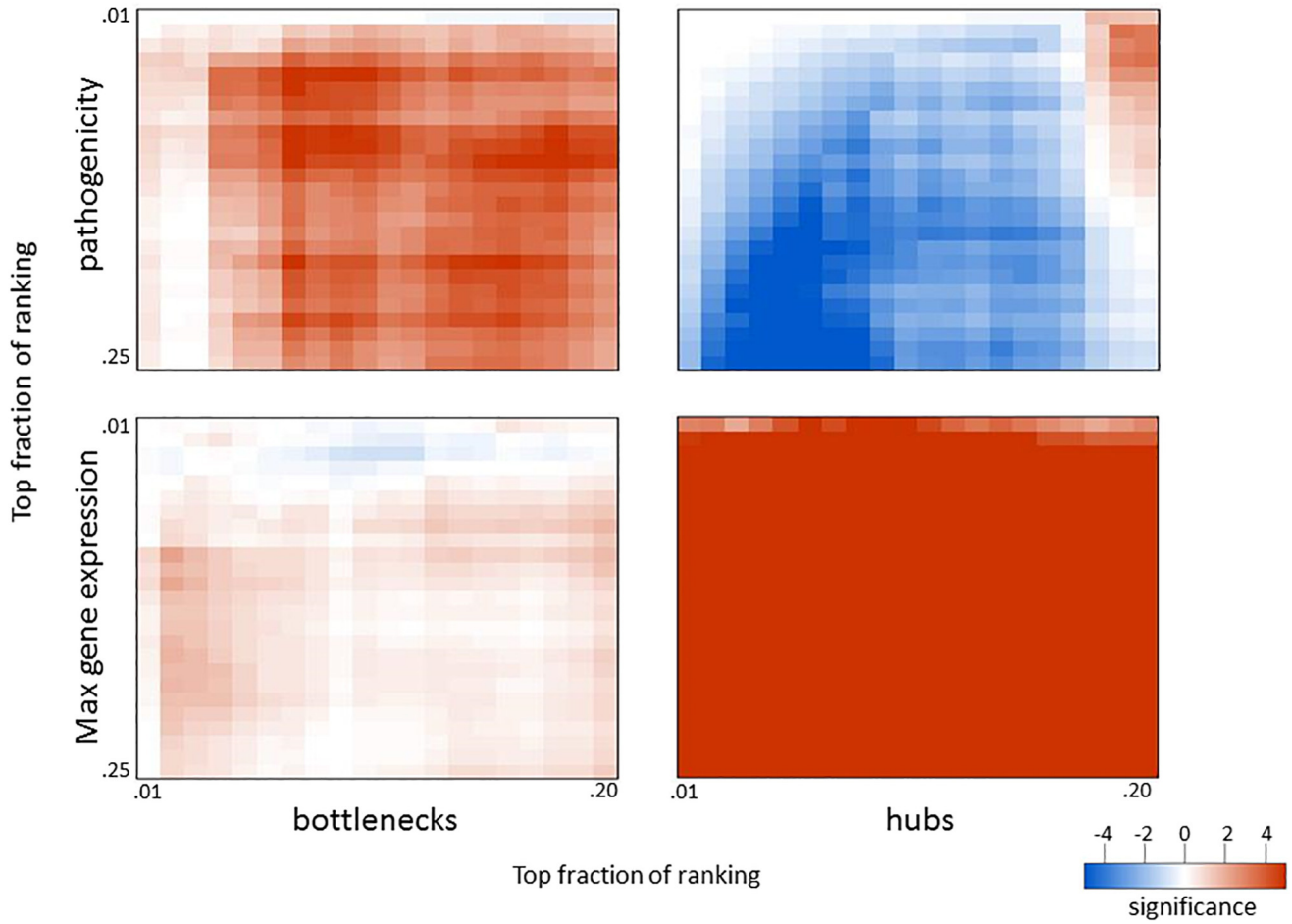

FIGURE 4 | Overlap in biological measures and graph topology for influenza infection. Genes were ranked according to their correlation with the pathogenicity profile (**top** panels), maximum fold change across all infection conditions (**bottom** panels), network betweenness (**left** panels), and network degree (**right** panels). The top fraction from one ranking was compared to the top fraction in the other ranking using a two-tailed Fisher's exact test as indicated. Numerical scale represents the absolute value of the log10 *p*-value. For negative enrichment, these values were multiplied by –1.

strain was used since the MLD50 for VN-1203 is very low and makes identification of drug effects difficult. Linear mixed effects models were used to model the weight loss trajectories from different infection conditions and to determine if the weight loss slope differed between treatments (**Table 2** and **Figure 6**). Red lines represent segments of the data that could be modeled with a single linear model; segments are separated by knot points. For all doses of Cal/04 and the two lower doses of TY167, drug treatment significantly increased infection severity in some segments. However, higher doses of TY167 erased this trend and possibly partially reversed it. While all animals died by day 13, weight loss was less rapid by a small but significant margin in drug-treated animals at the highest viral dose. Thus, EGFR appears to play a significant role in the severity of non-lethal infections such that when it is inhibited, the infection is more severe. However, when the threshold is crossed to the highly lethal pathogenesis of H5N1, other mechanisms potentially take over and supersede or override the role of EGFR.

DISCUSSION

We used a multi-faceted approach to uncover critical components of pathogenicity in an attempt to take full advantage of the pathogenicity gradient in our study's influenza viruses and mutants. We compared the expression behavior of genes and proteins to the pathogenicity measurements of viruses in our study; this allowed us to identify which pathways and features are most closely associated with pathogenicity. The results provide clues to the underlying causes of the severity of highly pathogenic strains.

Our group previously used this dataset to determine that host responses to various infection conditions involve similar pathways but are characterized by distinct kinetic expression profiles (Tchitchek et al., 2013). In the current study, we use a complementary approach to identify the genes and pathways that are most closely associated with more pathogenic viruses instead of identifying elements common to all. We show that the network topology of association networks can be used to

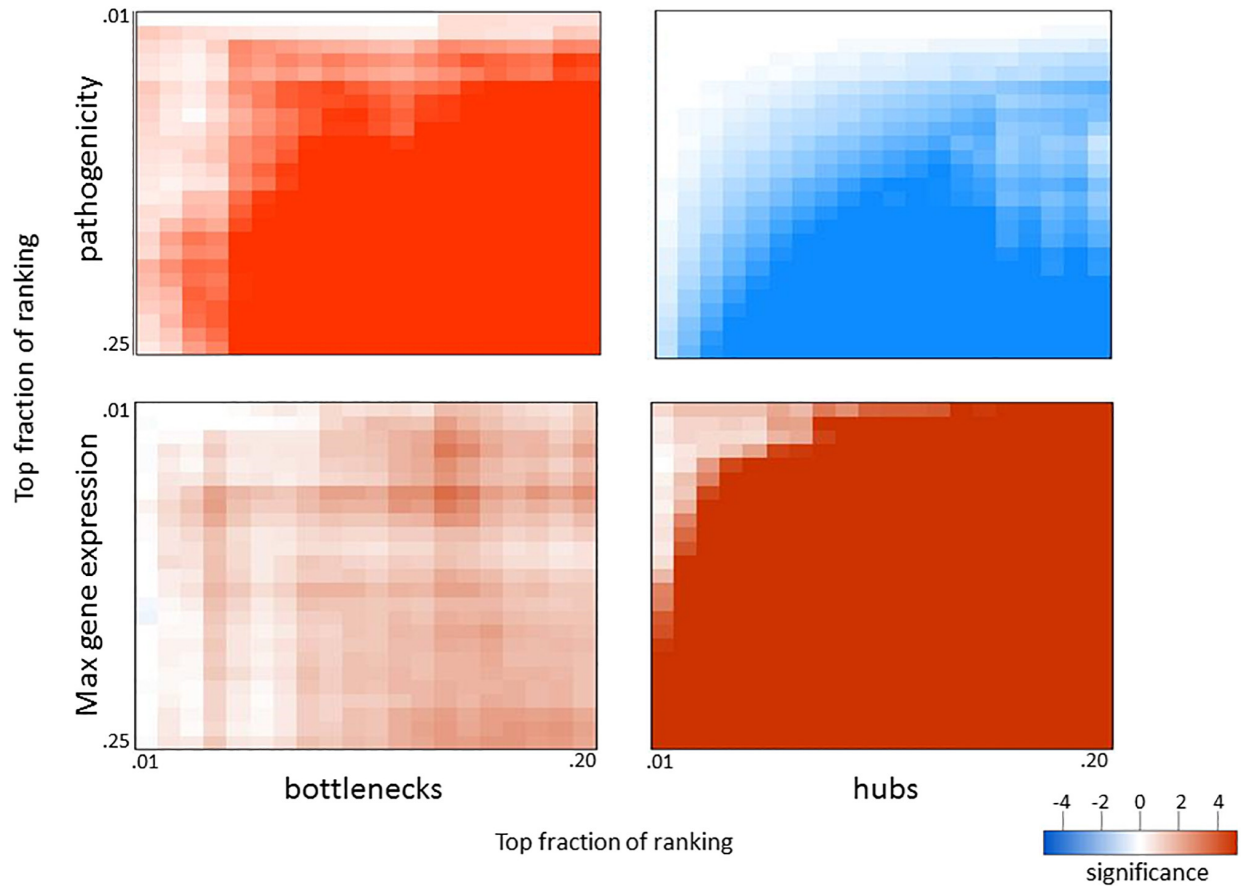

FIGURE 5 | Overlap in biological measures and graph topology for SARS-CoV infection. Significance matrices were generated for SARS-CoV infection experiments as in **Figure 4**; however, weight loss values at each infection condition were used as a pathogenicity measurement. Weight loss correlations for early (days 1 and 2) and late (days 4 and 7) were combined to obtain the pathogenicity ranking.

predict genes' involvement in pathogenicity-related processes. We used this knowledge in conjunction with other network methods to identify genes and pathways associated with disease severity. Our results show that signaling downstream of EGFR, coagulation pathways, and B-cell down-regulation in the lung are tied to infection severity in highly pathogenic influenza. A follow-up validation study in mice confirms the role of EGFR in influenza pathogenicity.

We first asked what broad trends in pathogenicity could be identified using a network clustering approach. One of the detected network clusters was strongly enriched for functions related to B-cells and was negatively correlated with the pathogenicity profile. This could be caused by either a general down-regulation of gene expression in lung B-cells or a general loss of B-cells from the lung. Although influenza may infect B-cells expressing flu-specific B-cell receptors (Dougan et al., 2013), initially naïve mice from our experiment are not likely to have expanded virus-specific B-cells during the time frame of our OMICs experiments. Thus, the effect is not likely a result of gene regulation within infected B-cells and is more likely due to a diminished B-cell lung population in highly pathogenic infections. A previous report demonstrated apoptotic death of bone marrow B-cells in flu-infected mice despite failing to show that the virus was present in the bone marrow (Sedger et al., 2002). Therefore, a systemic signal appears to target remote B-cells and may target lung B-cells as well. While the adaptive immune response is not likely to play a direct role during the time frame of these experiments, a lower B-cell population, for whatever reason, may signal important immune response dynamics not previously understood. Histological or other studies would be necessary to confirm the relationship between severe infection and diminished B-cell numbers. The second cluster was related to coagulation/fibrinolysis, which has shown a precedent in previous work for an involvement in influenza infection (Berri et al., 2013). Plasminogen (which opposes clot formation) appears to promote destructive inflammation during influenza infection. While we observed both pro- and anti-coagulation factors that were positively correlated with pathogenicity, these responses may represent a mixture of virus-induced responses and host responses to a pathogenic state.

We then corroborated these results by identifying links between pathogenicity-correlated genes and pathogenicity-correlated targets of these genes. Since a dataset of this kind deals strictly with the expression of genes and proteins, other

TABLE 2 | Modeling strategy for weight loss results from EGFR inhibition study.

Experiment/ Viral load	Approach	Knot point	Results: *p*-value
CA04/10^2 PFU	Data modeled in 3 segments	Day 5	Segment 1: 0.01979
		Day 8	Segment 2: 0.7377
			Segment 3: 0.07305
CA04/10^3 PFU	Data modeled in 3 segments	Day 5	Segment 1: 0.01059
		Day 8	Segment 2: 0.7170
			Segment 3: 0.002228
CA04/10^4 PFU	Data modeled in 3 segments	Day 6	Segment 1: 0.3498
		Day 9	Segment 2: 0.9064
			Segment 3: 0.03589
TY167/10^1 PFU	Data modeled in 3 segments	Day 4	Segment 1: 0.09511
		Day 9	Segment 2: 0.2128
			Segment 3: 0.8031
TY167/10^2 PFU	Data modeled in 4 segments	Day 3	Segment 1: 0.4661
		Day 7	Segment 2: 0.6107
		Day 10	Segment 3: 0.2895
			Segment 4:.03364
TY167/10^3 PFU	Data modeled in 1 segment	NA	0.074
TY167/10^4 PFU	Data modeled in 4 segments	Day 6	Segment 1: 0.02235
			Segment 2: 0.0769

events such as protein–protein interactions, protein–mRNA interactions, and phosphorylation/dephosphorylation events are not directly monitored. Thus, a portion of the very early events that determine the severity of an infection is not observable with this dataset. By integrating transcript and protein data, however, we were able to reveal links between upstream and downstream effectors for EGFR signaling, coagulation regulation, and B-cell down-regulation that would not be possible without the availability of both data types. Since correlations between transcript and protein expression profiles are consistently observed to be low across biological systems (Vogel and Marcotte, 2012), validation of transcript expression using direct correlation of protein abundances is generally not successful. However, we believe that functional rather than direct correspondence of transcripts and proteins represents an effective integration of both data types. Hence, our study provides hypotheses for the involvement of a number of genes/pathways in the pathogenicity of influenza virus.

To learn more about regulatory mechanisms of influenza infection, we determined whether topological positions in association networks were related to pathogenicity. We found that genes correlated with pathogenesis overlapped significantly with bottlenecks but were dramatically excluded from hubs. This result may be explained by the fact that network hubs are highly connected to many other network nodes so that rather than being involved only in highly pathogenic conditions, they tend to be involved in *all* infection conditions. This is affirmed by the observation that genes with the largest changes in gene expression (therefore likely to exert the strongest influence on other genes) were very strongly enriched for hub genes. On the other hand, network bottlenecks represent nodes linking different areas of the network and may identify genes that have an influence on only a subset of the processes being monitored by the data. Interestingly, in a network built with data from infections of varying pathogenicity, the genes exerting these influences appear to be involved in pathogenicity-related processes. The same relationships between network topology, viral pathogenicity, and gene expression that were observed for influenza virus were also noted when we used a similar dataset of SARS-CoV infections, thus further validating our analysis and demonstrating that these relationships appear to apply to respiratory viruses in general. We observed remarkably high (77% of possible) overlap between hub genes in SARS-CoV and influenza virus networks; this is consistent with the tendency of these genes to have a universal influence during infectious disease. In contrast, bottlenecks and pathogenicity genes showed much lower or non-existent overlap between the two infection systems, suggesting that each virus maintains unique mechanisms of host interaction. This finding is important because it demonstrates that the identification of non-hub bottlenecks may represent a way to naively identify virus-specific pathogenicity-related genes when pathogenicity data is not available. Previous work has shown that network bottlenecks have important regulatory roles (Yu et al., 2007; McDermott et al., 2009, 2011, 2012, 2016; Mitchell et al., 2013), but this is the first time that an association has been seen between bottlenecks and pathogenesis, with network hubs being conspicuously excluded.

To validate our findings, we treated mice with the EGFR inhibitor gefitinib during infection with high- and low-path influenza. Weight loss was significantly worsened when EGFR was inhibited during low-path infection as well as during low dose infection treatment with a highly pathogenic strain, all of which were non-lethal infections. These results suggest that care should be taken when administering gefitinib to patients at risk of or currently infected with influenza. Interestingly, however, high-dose, high-pathogenicity conditions displayed a possible reversal of this trend, with gefitnib showing a significant slowing of the weight loss trend at the highest dose. Thus, the role of EGFR is dependent on the severity of the current infection, indicating a role in pathogenicity as predicted by our OMICS studies. EGFR stimulation has previously been shown to play a role in promoting influenza particle uptake, and EGFR inhibition diminished viral titer in infected mice (Eierhoff et al., 2010; Ueki et al., 2013). However, the effect of EGFR inhibition on pathogenicity was not determined in previous studies. Viral titer measurements made during this experiment would have allowed us to determine the effect of the drug on viral replication simultaneously with pathogenicity, allowing a clearer picture of the mechanisms at play during EGFR inhibition. While the specific mechanisms are unknown, our results point to a scenario where EGFR inhibition mainly exacerbates pathogenicity at low severity, likely because of the resulting blockage of host benefits such as wound-healing in the lungs (Puddicombe et al., 2000). Interestingly, SARS-CoV infection in the context of overactive EGFR results in pulmonary fibrosis (Venkataraman et al., 2017), supporting the idea that EGFR signaling supports tissue regrowth during respiratory

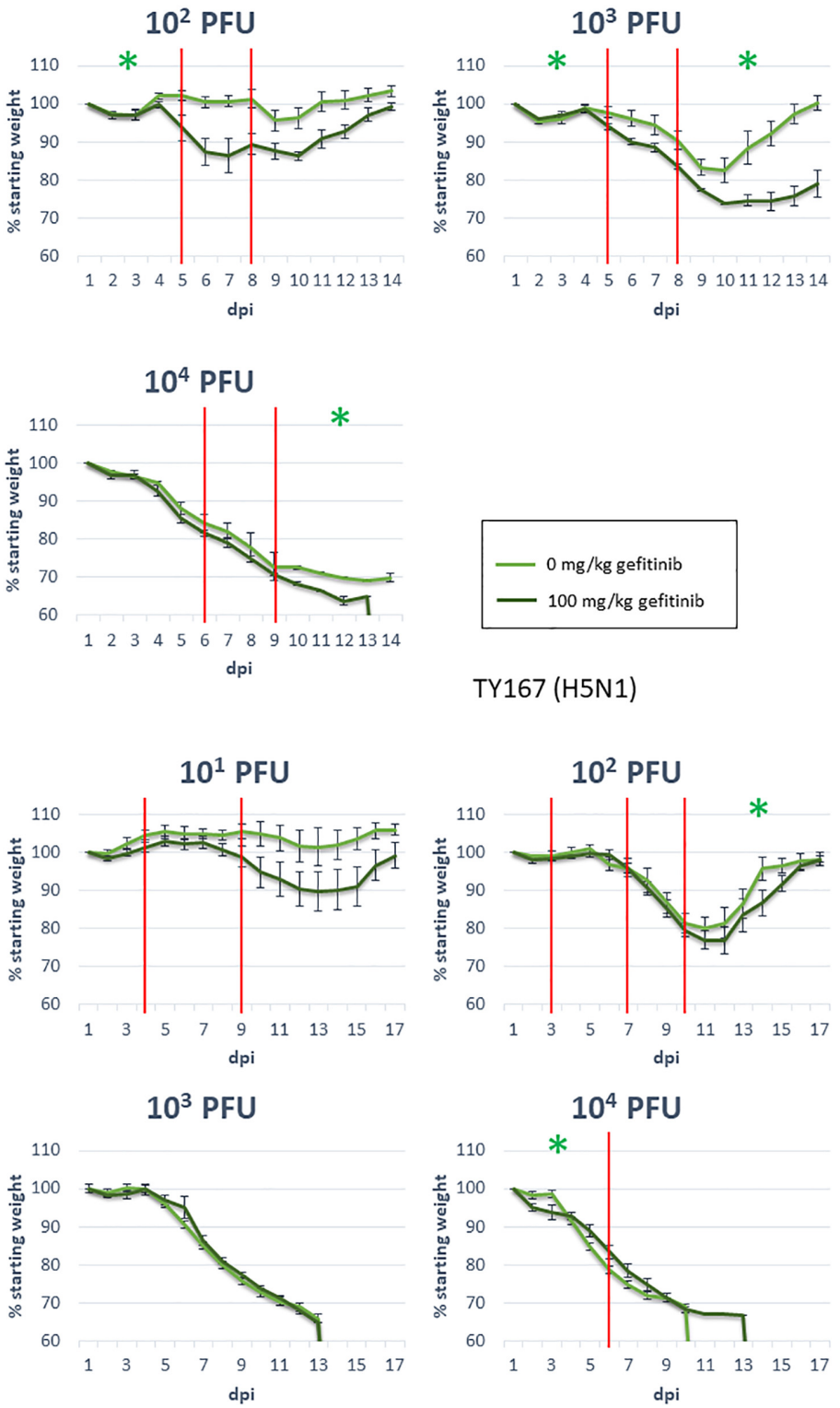

FIGURE 6 | EGFR inhibition during influenza infection. Mice were exposed to the indicated dosages of gefitinib and influenza virus strains, then monitored for body weight over the indicated days post-infection (dpi). Red vertical lines indicate knot points for linear modeling (see sections "Materials and Methods" and "Statistical Analysis"). Green star: significance below 0.05; see **Table 2** for segments with near-significant changes (segments with no significance indication had *p*-values above 0.1).

infection. The beneficial effect that comes from preventing viral particle uptake is only apparent under severe conditions when the host is largely unable to repair damaged tissue, as is likely the case in our high-dose, high-pathogenicity infection when mice are moribund. Thus, EGFR activation is a double-edged sword in influenza infection, promoting viral replication through increased virion uptake or suppression of cytokine production (Kalinowski et al., 2014) while simultaneously driving tissue maintenance. This shift in the effect of EGFR inhibition across pathogenicity provides new clues to the role of EGFR regulation during lethal and non-lethal influenza virus disease.

In summary, we have used a unique combination of network-based analyses of transcript and protein expression from our pathogenicity gradient dataset to (1) identify B-cell down-regulation and coagulation pathway up-regulation as being likely associated with pathogenicity in influenza; (2) show that identification of non-hub bottlenecks represents a way to use association networks to enrich prediction of pathogenicity-related genes and pathways; (3) validate the involvement of one of these pathways, EGFR signaling; and (4) show that EGFR inhibition appears to override a key host response mechanism involved in non-lethal viral infections.

DATA AVAILABILITY STATEMENT

The transcriptomics datasets generated for this study can be found in Gene Expression Omnibus, GSE50000, GSE49262, GSE33263, GSE37572, GSE43301, GSE43302, GSE44441, GSE44445, GSE37569, GSE33266, and GSE49263. Proteomics datasets can be found at https://omics.pnl.gov/project-data/systems-virology-contract-data.

ETHICS STATEMENT

All animal experiments and procedures were approved by the University of Wisconsin (UW)-Madison School of Veterinary Medicine Animal Care and Use Committee under relevant institutional and American Veterinary Association guidelines.

AUTHOR CONTRIBUTIONS

ML isolated a virus strain. AE, LG, RB, YK, and KW designed the experiments. AE, LG, and AS performed the experiments. HM, KS, JM, and KM conceived and designed the analysis. HM, KS, NH, and JW performed the analysis. HM and KW wrote the manuscript. All authors reviewed the manuscript.

FUNDING

This study was funded by grant U19AI106772, provided by the National Institute of Allergy and Infectious Diseases, National Institutes of Health. Pacific Northwest National Laboratory is a multi-program laboratory operated by Battelle for the United States Department of Energy (DOE) under Contract DE-AC05-76RL01830.

ACKNOWLEDGMENTS

The authors would like to thank Daniel Beechler for technical assistance, Catherine Himes for editorial services, and Nathan Johnson for graphic arts contributions.

SUPPLEMENTARY MATERIAL

The Supplementary Material for this article can be found online at: https://www.frontiersin.org/articles/10.3389/fcell.2019.00200/full#supplementary-material

REFERENCES

Berri, F., Rimmelzwaan, G. F., Hanss, M., Albina, E., Foucault-Grunenwald, M. L., Le, V. B., et al. (2013). Plasminogen controls inflammation and pathogenesis of influenza virus infections via fibrinolysis. *PLoS Pathog.* 9:e1003229. doi: 10.1371/journal.ppat.1003229

Cilloniz, C., Shinya, K., Peng, X., Korth, M. J., Proll, S. C., Aicher, L. D., et al. (2009). Lethal influenza virus infection in macaques is associated with early dysregulation of inflammatory related genes. *PLoS Pathog.* 5:e1000604. doi: 10.1371/journal.ppat.1000604

Dawood, F. S., Iuliano, A. D., Reed, C., Meltzer, M. I., Shay, D. K., Cheng, P. Y., et al. (2012). Estimated global mortality associated with the first 12 months of 2009 pandemic influenza A H1N1 virus circulation: a modelling study. *Lancet Infect. Dis.* 12, 687–695. doi: 10.1016/S1473-3099(12)70121-4

Dougan, S. K., Ashour, J., Karssemeijer, R. A., Popp, M. W., Avalos, A. M., Barisa, M., et al. (2013). Antigen-specific B-cell receptor sensitizes B cells to infection by influenza virus. *Nature* 503, 406–409. doi: 10.1038/nature12637

Eierhoff, T., Hrincius, E. R., Rescher, U., Ludwig, S., and Ehrhardt, C. (2010). The epidermal growth factor receptor (EGFR) promotes uptake of influenza A viruses (IAV) into host cells. *PLoS Pathog.* 6:e1001099. doi: 10.1371/journal.ppat.1001099

Eisfeld, A. J., Neumann, G., and Kawaoka, Y. (2014). Influenza A virus isolation, culture and identification. *Nat. Protoc.* 9, 2663–2681. doi: 10.1038/nprot.2014.180

Faith, J. J., Hayete, B., Thaden, J. T., Mogno, I., Wierzbowski, J., Cottarel, G., et al. (2007). Large-scale mapping and validation of *Escherichia coli* transcriptional regulation from a compendium of expression profiles. *PLoS Biol.* 5:e8. doi: 10.1371/journal.pbio.0050008

Food and Agriculture Organization [FAO] (2019). *H7N9 Situation Update*. Available at: http://www.fao.org/ag/againfo/programmes/en/empres/H7N9/situation_update.html (accessed September 13, 2019).

Gralinski, L. E., Bankhead, A. III, Jeng, S., Menachery, V. D., Proll, S., Belisle, S. E., et al. (2013). Mechanisms of severe acute respiratory syndrome coronavirus-induced acute lung injury. *mBio* 4:e00271-13. doi: 10.1128/mBio.00271-13

Hatta, M., Gao, P., Halfmann, P., and Kawaoka, Y. (2001). Molecular basis for high virulence of Hong Kong H5N1 influenza A viruses. *Science* 293, 1840–1842. doi: 10.1126/science.1062882

Ideker, T., and Krogan, N. J. (2012). Differential network biology. *Mol. Syst. Biol.* 8:565. doi: 10.1038/msb.2011.99

Kalinowski, A., Ueki, I., Min-Oo, G., Ballon-Landa, E., Knoff, D., Galen, B., et al. (2014). EGFR activation suppresses respiratory virus-induced IRF1-dependent CXCL10 production. *Am. J. Physiol. Lung Cell. Mol. Physiol.* 307, L186–L196. doi: 10.1152/ajplung.00368.2013

Kobasa, D., Jones, S. M., Shinya, K., Kash, J. C., Copps, J., Ebihara, H., et al. (2007). Aberrant innate immune response in lethal infection of macaques with the 1918 influenza virus. *Nature* 445, 319–323. doi: 10.1038/nature05495

Langfelder, P., and Horvath, S. (2008). WGCNA: an R package for weighted correlation network analysis. *BMC Bioinform.* 9:559. doi: 10.1186/1471-2105-9-559

Levine, A. J., Horvath, S., Miller, E. N., Singer, E. J., Shapshak, P., Baldwin, G. C., et al. (2013). Transcriptome analysis of HIV-infected peripheral blood monocytes: gene transcripts and networks associated with neurocognitive functioning. *J. Neuroimmunol.* 265, 96–105. doi: 10.1016/j.jneuroim.2013.09.016

Li, C., Bankhead, A. III, Eisfeld, A. J., Hatta, Y., Jeng, S., Chang, J. H., et al. (2011). Host regulatory network response to infection with highly pathogenic H5N1 avian influenza virus. *J. Virol.* 85, 10955–10967. doi: 10.1128/JVI.05792-11

McDermott, J. E., Archuleta, M., Stevens, S. L., Stenzel-Poore, M. P., and Sanfilippo, A. (2011). Defining the players in higher-order networks: predictive modeling for reverse engineering functional influence networks. *Pac. Sympos. Biocomput.* 2011, 314–325. doi: 10.1142/9789814335058_0033

McDermott, J. E., Diamond, D. L., Corley, C., Rasmussen, A. L., Katze, M. G., and Waters, K. M. (2012). Topological analysis of protein co-abundance networks identifies novel host targets important for HCV infection and pathogenesis. *BMC Syst. Biol.* 6:28. doi: 10.1186/1752-0509-6-28

McDermott, J. E., Mitchell, H. D., Gralinski, L. E., Eisfeld, A. J., Josset, L., Bankhead, A. III, et al. (2016). The effect of inhibition of PP1 and TNFalpha signaling on pathogenesis of SARS coronavirus. *BMC Syst. Biol.* 10:93. doi: 10.1186/s12918-016-0336-6

McDermott, J. E., Taylor, R. C., Yoon, H., and Heffron, F. (2009). Bottlenecks and hubs in inferred networks are important for virulence in *Salmonella typhimurium*. *J. Comput. Biol.* 16, 169–180. doi: 10.1089/cmb.2008.04TT

Michaelis, M., Doerr, H. W., and Cinatl, J. Jr. (2009). Novel swine-origin influenza A virus in humans: another pandemic knocking at the door. *Med. Microbiol. Immunol.* 198, 175–183. doi: 10.1007/s00430-009-0118-5

Mitchell, H. D., Eisfeld, A. J., Sims, A. C., McDermott, J. E., Matzke, M. M., Webb-Robertson, B. J., et al. (2013). A network integration approach to predict conserved regulators related to pathogenicity of influenza and SARS-CoV respiratory viruses. *PLoS One* 8:e69374. doi: 10.1371/journal.pone.0069374

Narang, V., Ramli, M. A., Singhal, A., Kumar, P., de Libero, G., Poidinger, M., et al. (2015). Automated identification of core regulatory genes in human gene regulatory networks. *PLoS Comput. Biol.* 11:e1004504. doi: 10.1371/journal.pcbi.1004504

Peiris, J. S., Yu, W. C., Leung, C. W., Cheung, C. Y., Ng, W. F., Nicholls, J. M., et al. (2004). Re-emergence of fatal human influenza A subtype H5N1 disease. *Lancet* 363, 617–619. doi: 10.1016/S0140-6736(04)

Polverino, F., Seys, L. J., Bracke, K. R., and Owen, C. A. (2016). B cells in chronic obstructive pulmonary disease: moving to center stage. *Am. J. Physiol. Lung Cell. Mol. Physiol.* 311, L687–L695. doi: 10.1152/ajplung.00304.2016

Puddicombe, S. M., Polosa, R., Richter, A., Krishna, M. T., Howarth, P. H., Holgate, S. T., et al. (2000). Involvement of the epidermal growth factor receptor in epithelial repair in asthma. *FASEB J.* 14, 1362–1374. doi: 10.1096/fj.14.10.1362

Safronetz, D., Rockx, B., Feldmann, F., Belisle, S. E., Palermo, R. E., Brining, D., et al. (2011). Pandemic swine-origin H1N1 influenza A virus isolates show heterogeneous virulence in macaques. *J. Virol.* 85, 1214–1223. doi: 10.1128/JVI.01848-10

Saris, C. G., Horvath, S., van Vught, P. W., van Es, M. A., Blauw, H. M., Fuller, T. F., et al. (2009). Weighted gene co-expression network analysis of the peripheral blood from Amyotrophic Lateral Sclerosis patients. *BMC Genomics* 10:405. doi: 10.1186/1471-2164-10-405

Sedger, L. M., Hou, S., Osvath, S. R., Glaccum, M. B., Peschon, J. J., van Rooijen, N., et al. (2002). Bone marrow B cell apoptosis during in vivo influenza virus infection requires TNF-alpha and lymphotoxin-alpha. *J. Immunol.* 169, 6193–6201. doi: 10.4049/jimmunol.169.11.6193

Taylor, A., Vagany, V., Jackson, A. C., Harrison, R. J., Rainoni, A., and Clarkson, J. P. (2016). Identification of pathogenicity-related genes in *Fusarium oxysporum* f. sp. cepae. *Mol. Plant Pathol.* 17, 1032–1047. doi: 10.1111/mpp.12346

Tchitchek, N., Eisfeld, A. J., Tisoncik-Go, J., Josset, L., Gralinski, L. E., Becavin, C., et al. (2013). Specific mutations in H5N1 mainly impact the magnitude and velocity of the host response in mice. *BMC Syst. Biol.* 7:69. doi: 10.1186/1752-0509-7-69

Tisoncik-Go, J., Gasper, D. J., Kyle, J. E., Eisfeld, A. J., Selinger, C., Hatta, M., et al. (2016). Integrated omics analysis of pathogenic host responses during pandemic H1N1 influenza virus infection: the crucial role of lipid metabolism. *Cell Host Microbe* 19, 254–266. doi: 10.1016/j.chom.2016.01.002

Ueki, I. F., Min-Oo, G., Kalinowski, A., Ballon-Landa, E., Lanier, L. L., Nadel, J. A., et al. (2013). Respiratory virus-induced EGFR activation suppresses IRF1-dependent interferon lambda and antiviral defense in airway epithelium. *J. Exp. Med.* 210, 1929–1936. doi: 10.1084/jem.20121401

Venkataraman, T., Coleman, C. M., and Frieman, M. B. (2017). Overactive epidermal growth factor receptor signaling leads to increased fibrosis after severe acute respiratory syndrome coronavirus infection. *J. Virol.* 91:e00182-17. doi: 10.1128/JVI.00182-17

Vogel, C., and Marcotte, E. M. (2012). Insights into the regulation of protein abundance from proteomic and transcriptomic analyses. *Nat. Rev. Genet.* 13, 227–232. doi: 10.1038/nrg3185

Webb-Robertson, B. J., Wiberg, H. K., Matzke, M. M., Brown, J. N., Wang, J., McDermott, J. E., et al. (2015). Review, evaluation, and discussion of the challenges of missing value imputation for mass spectrometry-based label-free global proteomics. *J. Proteome Res.* 14, 1993–2001. doi: 10.1021/pr501138h

World Health Organization [WHO] (2018). *Cumulative Number of Confirmed Human Cases for Avian Influenza A(H5N1) Reported to WHO, 2003-2018*. Available at: https://www.who.int/influenza/human_animal_interface/2018_12_13_tableH5N1.pdf (accessed September 13, 2019).

Yu, H., Kim, P. M., Sprecher, E., Trifonov, V., and Gerstein, M. (2007). The importance of bottlenecks in protein networks: correlation with gene essentiality and expression dynamics. *PLoS Comput. Biol.* 3:e59. doi: 10.1371/journal.pcbi.0030059

Zhou, X., and Liu, J. (2014). A computational model to predict bone metastasis in breast cancer by integrating the dysregulated pathways. *BMC Cancer* 14:618. doi: 10.1186/1471-2407-14-618

Conflict of Interest: The authors declare that the research was conducted in the absence of any commercial or financial relationships that could be construed as a potential conflict of interest.

frontiers in Cell and Developmental Biology

REVIEW
published: 23 January 2020
doi: 10.3389/fcell.2019.00362

Microbes as Master Immunomodulators: Immunopathology, Cancer and Personalized Immunotherapies

Joana R. Lérias[1], Georgia Paraschoudi[1], Eric de Sousa[1], João Martins[1], Carolina Condeço[1], Nuno Figueiredo[2], Carlos Carvalho[2], Ernest Dodoo[3], Mireia Castillo-Martin[4], Antonio Beltrán[4], Dário Ligeiro[5], Martin Rao[1†], Alimuddin Zumla[6†] and Markus Maeurer[1†]*

[1] ImmunoSurgery Unit, Champalimaud Centre for the Unknown, Lisbon, Portugal, [2] Digestive Unit, Champalimaud Centre for the Unknown, Lisbon, Portugal, [3] University of Heidelberg, Heidelberg, Germany, [4] Department of Pathology, Champalimaud Centre for the Unknown, Lisbon, Portugal, [5] Lisbon Centre for Blood and Transplantation, Instituto Português do Sangue e Transplantação, Lisbon, Portugal, [6] Division of Infection and Immunity, NIHR Biomedical Research Centre, University College London Hospitals NHS Foundation Trust, University College London, London, United Kingdom

OPEN ACCESS

Edited by:
Giulia De Falco,
Queen Mary University of London,
United Kingdom

Reviewed by:
Deyin Xing,
School of Medicine, Johns Hopkins University, United States
Yoshiyuki Goto,
Chiba University, Japan

***Correspondence:**
Markus Maeurer
markus.maeurer@fundacaochampalimaud.pt

†These authors share senior authorship

Specialty section:
This article was submitted to Molecular Medicine, a section of the journal Frontiers in Cell and Developmental Biology

Received: 06 April 2019
Accepted: 12 December 2019
Published: 23 January 2020

Citation:
Lérias JR, Paraschoudi G, de Sousa E, Martins J, Condeço C, Figueiredo N, Carvalho C, Dodoo E, Castillo-Martin M, Beltrán A, Ligeiro D, Rao M, Zumla A and Maeurer M (2020) Microbes as Master Immunomodulators: Immunopathology, Cancer and Personalized Immunotherapies. Front. Cell Dev. Biol. 7:362. doi: 10.3389/fcell.2019.00362

The intricate interplay between the immune system and microbes is an essential part of the physiological homeostasis in health and disease. Immunological recognition of commensal microbes, such as bacterial species resident in the gut or lung as well as dormant viral species, i.e., cytomegalovirus (CMV) or Epstein-Barr virus (EBV), in combination with a balanced immune regulation, is central to achieve immune-protection. Emerging evidence suggests that immune responses primed to guard against commensal microbes may cause unexpected pathological outcomes, e.g., chronic inflammation and/or malignant transformation. Furthermore, translocation of immune cells from one anatomical compartment to another, i.e., the gut-lung axis via the lymphatics or blood has been identified as an important factor in perpetrating systemic inflammation, tissue destruction, as well as modulating host-protective immune responses. We present in this review immune response patterns to pathogenic as well as non-pathogenic microbes and how these immune-recognition profiles affect local immune responses or malignant transformation. We discuss personalized immunological therapies which, directly or indirectly, target host biological pathways modulated by antimicrobial immune responses.

Keywords: pathogens, microbiota, inflammation, neoplasia, immune responses, antibodies, cancer, immunotherapy

BACKGROUND

Our understanding of the immune system stems, in great part, from studying the host response to infection, which in most individuals leads to the absence of clinical disease and establishment of highly apt immunological memory. The host immune response in relation to opportunistic pathogens as well as to the endogenous microbiota is pivotal to deter not only infectious diseases, yet also central to providing general physiological health (Manfredo Vieira et al., 2018;

Mathieu et al., 2018a; Schachter et al., 2018). Chronic infections, particularly those which are primarily characterized by an asymptomatic intracellular life cycle, e.g., latent *Mycobacterium tuberculosis* infection (LTBI), hepatitis B virus (HBV) infection, *Chlamydia trachomatis* infection, cytomegalovirus (CMV) or Epstein-Barr virus (EBV) infections, present a unique premise to decipher the fine balance between protective host immune responses, immunopathology and full-fledged clinical disease. Nevertheless, while a chronic host immune response driven by pathogens may be protective against clinical disease, it may also elevate the risk of inflammation-induced dysplasia. The association of certain human leukocyte antigen (HLA) alleles which predispose individuals to a greater risk of harmful inflammation and disease (Mignot et al., 2001; De la Herran-Arita et al., 2013; Tafti et al., 2016; Matzaraki et al., 2017) play a central role in pro-inflammatory processes. We will first highlight some of the major neoplasia-associated infections of clinical relevance in the context of neoplasia and immune response modulation.

Although overt inflammatory responses play a major role in malignant transformation of host cells following an infection, it is a disbalanced immune responses, which contribute to drive malignant transformation. Thus, the local immunological milieu in tissue compartments forms the nature and magnitude of the host responses, i.e., frequencies of regulatory T cells (Tregs) vs. T-helper 17 (Th17) cells, amount of pro-inflammatory cytokines vs. anti-inflammatory cytokines, extent of neutrophilia and antigen-presenting-cell (APC) activation, among others. The second part of the review discusses potential host-directed interventional strategies based on existing translational and clinical knowledge of infection-induced inflammation, as well as cancer initiation/progression models.

PATHOGEN-DRIVEN INFLAMMATION AND NEOPLASIA: EXISTING KNOWLEDGE AND NEW INSIGHTS

Viral Pathogens and Immuno-Oncogenesis

Most infection-induced cancers worldwide are attributed to viral pathogens, possibly representing up to 80% of cases reported (Chang Y. et al., 2017). Although harbored by at least 90% of the world's population, EBV causes malignant transformation only in a handful of individuals, which has been in part linked to the genetic variations in the infecting strain (Tzellos and Farrell, 2012). EBV-induced cancers, such as nasopharyngeal carcinoma (NPC) and B-cell lymphomas in the form of severe lymphoproliferative disease (LPD) following stem cell transplantation, non-Hodgkin's lymphoma (NHL) as well as Hodgkin's lymphoma (HL) are well documented (comprehensively reviewed in Saha and Robertson, 2011; Farrell, 2019). LPDs can also involve some populations of T cells (thus, manifesting as a T-cell lymphoma) and natural killer (NK) cells (Kim et al., 2017). The fact that patients with some cancer histologies/molecular profiles respond to immune checkpoint inhibitors (ICI), such as anti-PD-1, anti-CTLA-4, and anti-PD-L1 allows the study their impact on non-target T-cell populations (those not directed specifically against cancer-associated mutations or neoantigens), i.e., on CMV or EBV-reactive T cells. A clinical study with anti-PD-1 blockade in patients with lung cancer showed that EBV-specific T cells were not expanded during lung cancer treatment (Kamphorst et al., 2017). There is also a clinical trial currently underway to treat patients with EBV-positive NHL or other LPDs with EBV-specific cytotoxic T cells activated using antigen-pulsed dendritic cells in combination with nivolumab (anti-PD-1 antibody) (ClinicalTrials.gov identifier: NCT02973113). EBV-specific tumour infiltrating lymphocytes (TILs)/T cells have also been shown to mediate tumor killing *in vitro* as well as disease remission in patients with NPC (He et al., 2012; Li et al., 2015). HLA-B35, along with HLA-B2, -A2 and -A11 have been shown to be associated with a higher risk of developing post-transplant lymphoproliferative disease (PTLD) post solid-organ transplantation (Pourfarziani et al., 2007), while another study in Denmark showed that HLA-B45 and HLA-DR13 pose an increased PTLD risk (Vase et al., 2015). Indeed, a HLAB35-restricted epitope from EBV BZLF1 protein was previously shown to elicit strong cytotoxic T-cell responses (Tynan et al., 2005), while circulating IFN-γ+ CD8+ T cells in patients with PTLD were dominantly reactive to a HLA-B35-restricted epitope from EBV Epstein-Barr nuclear antigen 1 (EBNA1) (Jones et al., 2010). Interestingly, EBNA1 is also involved in downregulation of the HLA class I molecule to avoid immune surveillance (Levitskaya et al., 1995), while, more recently, the late lytic cycle associated EBV protein BDLF3 (recombinant EBV probable membrane antigen GP85) was shown to downregulate HLA class I and class II, CD54 (ICAM-1, important for cell trafficking and adhesion) and CD71 (transferrin receptor, necessary for iron homeostasis) (Quinn et al., 2015). EBV-derived IL-10 has been shown to induce pro-inflammatory polarization in human monocytes by STAT3 (signal transducer and activator of transcription 3) downregulation (Jog et al., 2018) and is more efficient than human IL-10 at inducing B-cell proliferation along with a high density of IL-10R1 expression on the cell surface (Yoon et al., 2012). The Cancer Genome Atlas Research Network published a comprehensive molecular analysis of gastric cancer (GC) samples to identify possible mutational signatures and found that an EBV-associated gene expression profile, particularly in tumor tissue isolated from the gastric fundus (upper part of the stomach) in line with a DNA hypermethylation pattern, formed a distinct clinical subtype of GC (Cancer Genome Atlas Research, 2014).

Merkel cell polyomavirus (MCPyV) is associated with most cases of Merkel cell carcinoma (MCC), considered an aggressive, though relatively rare, neuroendocrine skin cancer (DeCaprio, 2017; Miller et al., 2018). Interestingly, both MCC "virus-positive" or "virus-negative" are very immunogenic and elicit not only a CD8+ and CD4+ T-cell response (Iyer et al., 2011), but also a B-cell response against MCPyV T-antigen proteins (Paulson et al., 2010, 2017). A striking feature concerning the MCPyV is the fact that it can cause a lifelong, but relatively innocuous infection, even in people at an early age (DeCaprio, 2017).

Merkel cell polyomavirus has two transcriptional units coding four splices mRNAs encoding four proteins, which includes a large T-antigen (LT), 57kT, small T-antigen (ST) and ALTO, and also two viral coat proteins (VP1 and VP2) (Carter et al., 2013; Theiss et al., 2015). It is described that approximately 80% of all MCC contains clonally integrated copies of these virus, leading in mutations resulting in LT truncation with deletion of its DNA binding and helicase domains and 57 kT growth suppressing domain at the carboxyl-terminus loss (Shuda et al., 2008; Li et al., 2013). Typically, virus-positive MCC tumors express ST and truncated LT, supporting their role in the initiation and maintenance of MCC. Besides the presence of viral DNA and protein expression, tumor genomes are significantly different between virus-positive and virus-negative MCC. Indeed, "virus-positive" MCC contains few somatic mutations and copy number alterations. On the other hand, "virus-negative" MCC have a high frequency of DNA mutations, since these MCC are usually associated to UV damage (Wong et al., 2015; DeCaprio, 2017; Starrett et al., 2017). Another difference is that most "virus-positive" MCC still contains a non-mutated retinoblastoma suppressor gene (RB1), contrarily to "virus-negative" MCC, in which RB1 is usually mutated (Harms et al., 2016). The protein coded by this gene can restrict cell-cycle progression by inhibiting the entrance to S phase due to E2F family repression. Therefore, MCPyV MCC will fail to stop in G1/S and increase the proliferation rate of such cells (Borchert et al., 2014; DeCaprio, 2017).

There is a close relationship between MCC and other malignancies associated to immune cells, such as chronic lymphatic leukemia, multiple myeloma or non-Hodgkin lymphoma. Indeed there is an increased incidence of MCC in patients that also have one of the diseases mentioned above (Tadmor et al., 2011), probably due to the compromised immune responses in lymphoid malignancies. Indeed, these patients will probably have a higher propensity for colonization with MCPyV, which would then increase the incidence of MCC. Besides, patients with lymphoid malignancies are also frequently subjected to T-cell-suppressive therapies, that would influence MCPyV infection and the course of MCC (Tadmor et al., 2011; Brewer et al., 2012; Triozzi and Fernandez, 2013).

Various *human papilloma virus (HPV)* genotypes are generally associated with oncogenesis, although HPV-16 and -18 are implicated in the pathogenesis of several cancers in addition to cervical cancer (also HPV-31, -33, -35, -39, -45, -51, -52, -56, -58, -59), such as cancers of the oral cavity, oropharynx, and tonsils (Cogliano et al., 2011; Bansal et al., 2016). HPV-38, which is associated with skin cancer (Kocjan et al., 2009), interacts with the eukaryotic elongation factor 1 A (eEF1A) via the viral E7 protein to remodel actin fibers in the cytoskeleton and thereafter promoting aberrant cell proliferation, as shown in human keratinocytes (Yue et al., 2011). The double methylation of eEF1A Lys55 by the human methyltransferase-like 13 (METTL13) protein was recently found to be a crucial facilitator of mutant KRAS-driven oncogenesis in the pancreas and lungs (Liu et al., 2019). METTL13, which is also annotated as FEAT has anti-apoptotic functions (Liang et al., 2015) and has been linked to cirrhotic lesions in the human liver adjacent to hepatocellular carcinoma (HCC) tissue, suggesting a role in inflammation (Takahashi et al., 2011). The only approved vaccine against HPV-associated cervical cancer, Gardasil®, targets the L1 protein from HPV-6, -16, -11, and -18 and offers remarkable immunological protection of up to 5 years against HPV-6/-11-driven genital warts, as well as HPV-16/-18-linked cervical intraepithelial neoplasia grade 2 (CIN-2+) lesions (Harper et al., 2010). Patients with HPV+ head and neck cancer have been shown to have a higher number of PD-1+ CD8+ tumor infiltrative lymphocytes (TIL) infiltrating their tumors, compared to HPV-naïve patients further to experiencing better clinical outcomes following standard therapy (Kansy et al., 2017). In a clinical study testing TIL efficacy against HPV+ cervical cancer, nine patients with metastatic cervical cancer were given TIL, which in four of the patients had specific T cell recognizing HPV E6 and E7 peptides that were also detected post-infusion. Two patients who exhibited complete responses lasting between 15 and 22 months after T-cell therapy showed shared CD4+ T-cell reactivity to HPV $E7_{5-19}$ (the first patient also has CD4+ T-cell responses to two other E7 peptides, including $E7_{9-19}$) (Stevanovic et al., 2015), indicating the potential of HPV-specific T cells in mediating clinically meaningful responses in HPV malignancies. In another study, thirty patients with vulvar intraepithelial neoplasia infected with HPV-16 who were treated with long peptides from the HPV-16 E6 and E7 proteins (two patients received three vaccinations, while the remaining 28 patients were given four vaccinations) showed very favorable clinical results (9/30 patients with complete response at 12 months post-vaccination, which last a further 12 months – thus a total of 24 months) (Kenter et al., 2009). A cervical cancer-derived CD8+ T cell specific for an HLA-A2-restricted HPV-16 E6 epitope has also been shown to be enriched in the tumor compared with peripheral blood (Draper et al., 2015). Furthermore, the corresponding TCR was transduced into naïve T cells and tested for anti-tumor activity against several HPV+ cancer cell lines, resulting in target-cell elimination. These clinically relevant results are indicative of the potential anti-tumor functionality of HPV-specific T cells either directly or by means of modulating the local immunological milieu by molecular mimicry to potentiate disease control.

A link between immune evasion in cervical cancer cells, perpetrated by HPV, has been shown in the context of HLA class II molecules. The effect of IFN-γ on HPC+ cervical cancer cells has been shown to mobilize class II-associated invariant chain peptide (CLIP) and HLA-DMA into the cytoplasm while HLA-DMA dynamics (HLA-DM being a "molecular editor" for loading peptides into the MHC class II binding cleft) was not affected, although HLA-DR expression at the cell surface was increased (Zehbe et al., 2005). In line with this, IFN-γ treatment of HPV+ ME180 cervical cancer cells promoted immune recognition by a HLA-DR4-restricted CD4+ T-cell clone CCA1 (which is specific for a peptide derived from the HPV E7 protein) (Zehbe et al., 2005). Nevertheless, CLIP expression was not affected by IFN-γ treatment, hinting at alternate strategies by which HLA class II immune surveillance may be increased in HPV-associated malignancies.

The involvement *of hepatitis B and C viruses (HBV/HCV)* in the pathogenesis of HCC is also well-established. A combination of natural selection of antagonistic HLA class I viral epitopes and upregulation of PD-1 on infected hepatocytes contributes to immune evasion of HBC/HCV in the liver (Bertoletti et al., 1994; Cox et al., 2005; Golden-Mason et al., 2007). Virus-mediated counter-regulation of cholesterol metabolism in host cells by manipulating the subtilisin Kexin Isozyme-1 (SKI-1)/Site-1 Protease (SKI-1/S1P) pathway has been implicated in the establishment of a successful infection (Olmstead et al., 2012). This was further strengthened by the finding that pharmacological inhibition of the SKI-1/S1P pathway limited viral particle generation by reducing the amount of intracellular lipid droplet formation. A similar scenario has been observed in the infection of liver cells with dengue virus, another highly clinically relevant flavivirus, and it's blockade with PF-429242, specific inhibitor of the SKI-1/S1P pathway (Hyrina et al., 2017). The HBV-encoded HBx protein has been previously shown to interact with the afore-mentioned eEF1A, which is a downstream target of the METTL13/FEAT enzyme and participates in remodeling of actin filaments in hepatoma cells by blocking eEF1A dimerization (Lin et al., 2012). Anti-PD-1 therapy with nivolumab induced strong anti-viral activity to the effect of reducing viral load by approximately 4-log, with the viral load reduced to undetectable levels in two patients (Gardiner et al., 2013). Similarly, anti-CTLA-4 blockade (tremelimumab) in patients with HCC and chronic HCV infection extended the time to disease progression, with almost 60 patients experiencing stable disease and in addition to dramatic reduction in HCV load (Sangro et al., 2013). IFN-γ-producing T cells, in response to HCV antigen exposure, were also detected in peripheral blood of some patients up to 300 days post tremelimumab treatment initiation (after at least three cycles had been completed). Apoptosis-inducing cytotoxic T cells with engineered with anti-HCV TCRs (directed against the non-structural proteins NS3 and NS5) as well as those targeting HBV are being developed (Balasiddaiah et al., 2017; Bertoletti et al., 2017; Kah et al., 2017).

Kaposi's sarcoma herpes virus (KSHV), presently known as human herpesvirus-8 (HPV-8), is the etiological agent of Kaposi's sarcoma, a form of endothelial cancer which can manifest in mucosal tissue surfaces, i.e., lymph nodes and skin as well as two other lymphoproliferative disorders, namely multicentric Castleman's disease (MCD) and primary effusion lymphoma (PEL) (Robey et al., 2011). Kaposi's sarcoma (KS) was, in the 1980s and early 1990s, identified as a major co-morbidity of HIV/AIDS-related immunosuppression (Chang et al., 1994; Strickler et al., 1999). KSHV can dampen innate immune responses via several strategies (reviewed in Lee et al., 2010), simultaneously producing viral interleukin (IL) 6 which promotes the pathogenesis of MCD and PEL (Sakakibara and Tosato, 2011). Importantly, latent KSHV has been reported to upregulate host IL-6 production (by infected cells) triggered by the KSHV latency-associated nuclear antigen (LANA), hinting at an ongoing inflammatory response despite absence of clinical disease as well as in MCD and PEL (An et al., 2002). Central memory T-cell responses (IFN-γ) to the virus has been observed to the crucial even in the presence of sirolimus therapy (rapamycin, immunosuppressant) following renal transplantation (Barozzi et al., 2008). In a recent clinical study investigating the therapeutic efficacy of anti-PD-1 (nivolumab or pembrolizumab, anti-PD-1 antibodies) blockade in HIV-associated KS, six out of nine patients who received the treatment showed objective responses (five patients = partial responses; one patient = complete remission) (Galanina et al., 2018). Interestingly, some of the patients who responded to anti-PD-1 therapy ($n = 4$) displayed low PD-L1 levels in their tumors, coupled with low CD4 counts and high HIV burden.

Although not related to cancer, influenza vaccine-mediated narcolepsy development in susceptible individuals presents a very clinically relevant human modality pertinent to antigen cross-reactivity influenced by the restricting HLA elements in an individual (Mignot et al., 2001; De la Herran-Arita et al., 2013; Tafti et al., 2016; Bomfim et al., 2017). HLA-DQB1*0602 confers protective immune responses against developing type 1 *diabetes mellitus* (T1DM), while the same individuals suffer a greater risk of contracting narcolepsy (Mignot et al., 1997, 2001; Siebold et al., 2004). Similarly, some HLA class I alleles, i.e., HLA-A11:01, HLA-C04:01, and HLA-B35:01, are implicated in the susceptibility of certain groups of individuals to develop narcolepsy (Tafti et al., 2016). HLA-DQB1*0602 in association with HLA-DRB1*1501/02/03 present a propensity to induce development of Th17 and Th1 cells, which is necessary for the control of bacterial infections at very early stages, but not later due to the effect it has on culminating in autoimmune pathology (more reflective of Th17 cells) (Mangalam et al., 2013). Asian populations have a higher frequency of the HLA-DQB1*0602 allele, while West African have at least twice as more polymorphisms in the HLA class II allele pools compared to White Caucasians, which may have evolved to provide superior protection against the former populations against infections agents such as *Mycobacterium tuberculosis*, *Klebsiella* sp., *Leishmania* sp. (Mangalam et al., 2013). In contrast, HLA-DQB*0601 is associated with resistance to developing autoimmune disease, based on studies in mice with experimental autoimmune encephalomyelitis (Mangalam et al., 2008), the murine model of multiple sclerosis (MS).

Bacterial Pathogens, Inflammation, and Oncogenesis

Helicobacter pylori is perhaps the best described and most known oncogenic bacterial pathogen in relation to gastric cancer (GC) thus classified as a group I carcinogen (Wroblewski et al., 2010). Proteins produced by *H. pylori*, comprising the vac and cag families, induce molecular changes in stomach epithelial cells leading to malignant transformation (Wroblewski et al., 2010). Bacterial urease, on the other hand, promotes apoptosis of epithelial cells by direct binding to the HLA class II molecules (Fan et al., 2000). Downregulation of HLA class II molecules by *H. pylori* strain N6 via enhanced expression of CD300E and miRNA-4270 suppression in human macrophages was recently found to be an immune evasion strategy employed by this pathogen (Pagliari et al., 2017). *H. pylori* VacA (from strain CCUG17874) was previously shown to interfere with the synthesis and presentation of nascent HLA class II molecules

(Molinari et al., 1998), as well as the interaction between B7-H2 and CD28 on CD4+ T cell to trigger immune activation marked by early IL-17 production to control infection (Lina et al., 2014). Thus, deterring CD4+ T-cell responses appears to play an important role in *H. pylori*-mediated immune evasion, but the same effect may play potentiate anti-cancer responses. An interesting example being the observation of IFN-γ+ CD4+ T cells responding to HLA-DRB1*1501-restricted *H. pylori* hemagglutinin ($HpaA_{88-100}$) in *H. pylori*-infected patients with GC who exhibited less severe disease (Chen et al., 2013).

The local immune responses in the stomach to *H. pylori* has also been shown to be strain-dependent, augmenting the release of a panel of pro-inflammatory cytokines, such as IL-6, TNF-α, IL-12, and IL-1β (Andres et al., 2011). Also, the suppression of microRNA Let-7b expression in gastric cells by *H. pylori* infection promotes TLR4 expression and downstream Myd88 activation to trigger NF-κB-mediated immune responses (Teng et al., 2013). The finding that *H. pylori* infection leads to upregulation of vitamin D receptor (VDR) expression in gastric epithelial cells and extracellular supply of vitamin D3 is able to improve intracellular bacterial killing (Guo et al., 2014) indicates that a subpopulation of patients may be able to control bacterial infection via vitamin D-associated mechanisms. A recent review of clinical trial data suggests that vitamin D may have a protective effect in cancer although further controlled real-world evidence is required to strengthen this stance (Grant, 2018).

Escherichia coli-derived colibactin and the risk of colon/colorectal cancer (CRC) has been proposed due to the DNA alkylating nature of the bacterial toxin. The strain of *E. coli* which produces colibactin is prevalent in the human gut, but not everyone with colibactin + *E. coli* develops malignancies. An earlier preclinical study showed that the colibactin gene is encoded in the *pks* genomic island of certain *E. coli* strains, which have also been recovered from some patients with CRC (Dalmasso et al., 2014). Furthermore, using cell culture and a mouse model of human CRC, pks + *E. coli* negatively affects p53 SUMOylation and, thereafter, the structural integrity of the p53 protein leading to DNA breaks. Infection of cells (as well as mice) with pks + *E. coli* also induced the production of growth factors, i.e., HGF, FGF, and GM-CSF associated with tumor outgrowth and poor outcome. Enteropathogenic *E. coli* (EPEC) which produces Shiga toxin, the causative agent of haemolytic uraemic syndrome (HUS), may also be involved in the pathogenesis of CRC based on the findings of a clinical study published in 2015 (Magdy et al., 2015). *Citrobacter rodentium* infection of the mouse colon, which represents similar pathological features to EPEC infection and intestinal inflammation in humans, has been shown to promote Th17 induction with the involvement of the resistin-like molecule alpha (RELMα) (Osborne et al., 2013).

In their meta-analysis of 22 clinical studies, Zhu and colleagues further strengthened the existing link between *C. trachomatis* infection and the occurrence of cervical cancer (Paavonen, 2001), while identifying co-infection with HPV to promote a higher risk of developing malignant disease. A 2019 clinical study showed that women with serum antibodies against the Pgp3 protein of *C. trachomatis* suffer a twofold risk of developing ovarian cancer (Trabert et al., 2019). Pgp3 is a plasmid-encoded virulence factor which can form a complex with human cathelicidin (also known as LL-37) to induce IL-6 and IL-8 production in neutrophils (Hou et al., 2019). Mechanistic studies using cell culture systems have provided empirical proof that infection with *C. trachomatis* induces DNA double-strand breaks (DSBs) in cells while impairing the repair process by inhibiting recruitment of ataxia telangiectasia mutated kinases (ATM) and p53-binding protein 1 (53BP1), further to inducing production of the epidermal growth factor (EGF), which is implicated in dysplasia (Chumduri et al., 2013; Patel et al., 2014).

To date, no direct link has been established between *Mycobacterium tuberculosis* (*Mtb*) infection and oncogenesis in the lungs. However, some existing clinical and translational evidence suggest that *Mtb* infection-induced fibrotic lesions in the lungs may contribute to malignant transformation, partly due to genetic aberrations caused by the local inflammatory response comprising an armament of IFN-γ, TNF-α, IL-12, IL-18, IL-17, and IL-6 to clear the pathogen (Kaufmann et al., 2014; Zumla et al., 2015; Nikitina et al., 2018). Mutations in the epidermal growth factor receptor (EGFR) gene, associated with lung adenocarcinoma pathogenesis, have been linked to the presence of old pulmonary tuberculosis (TB) lesions in patients with lung cancer (Luo et al., 2012). In agreement with this, the presence of old pulmonary TB lesions has been shown to be an independent predictor of shortened survival among patients with squamous cell carcinoma of the lung (SCC) (Zhou et al., 2013). A 2006 report showed that 25% of patients in a New York City study cohort with an underlying cancer diagnosis, i.e., lung cancer, Hodgkin's and NHL, head and neck cancer or leukemia, died within three months of being diagnosed with pulmonary TB (Kamboj and Sepkowitz, 2006). Taiwanese patients with various solid cancers (particularly lung cancer) and TB, compared to those who did not have cancer, exhibited a significantly lower anti-TB treatment success rate (43 vs. 75.8%) and almost four times the mortality rate (48.4 vs. 13.9%) (Chiang et al., 2009). *Mtb* infection has been shown to induce DSBs in host macrophages, reminiscent of pre-apoptotic DNA fragmentation (Castro-Garza et al., 2018), hinting at an added mechanism of promoting malignant transformation of host cells.

Some bacterial pathogens, such as *Salmonella*, *Klebsiella*, and *Yersinia* sp., which are etiological agents of enteric infection, have been associated with downregulation of the HLA-B27 allele in PBMCs of infected patients (Kirveskari et al., 1999). These pathogens have also been associated with the pathogenesis of ankylosing spondylitis (AS), particularly in HLA-B27+ individuals (Martínez et al., 2004). HLA-B27 expression is a risk factor for AS and patients with AS have an increased risk for developing hematological malignancies, colon, bone as well as prostate cancer (Chang C.C. et al., 2017). An association between HLA-B27 and immune responses against ovarian cancer – associated antigens has been reported (Szender et al., 2016). Taking these into consideration, it would be clinically relevant to investigate the relationship between bacterial infection at mucosal surfaces, local immune responses therein and the modulation of HLA alleles in relation to neoplasia. Although beyond the scope of this paper, a recent genome-wide association study (GWAS) in more than 200,000 individuals of European

ancestry provided evidence of susceptibility loci in the HLA class I and class II alleles (Tian et al., 2017) to various infections (bacterial, viral, and fungal), thus paving the way for future high-throughput large-scale studies to better understand the fine details of infection and immunomodulation.

Helminths in the Inflammation-Induced Oncogenesis

Besides the role of viral and bacterial pathogens as well as the microbiome discussed above, several helminth infections – mainly affecting the developing world – are an important cause of infection-induced inflammation and oncogenesis. *Schistosoma haematobium*, commonly known as the urinary blood fluke, is a parasitic flatworm prevalent in Sub-Saharan Africa and the Middle East and recognized by the IACR as a human carcinogen (Cogliano et al., 2011). Eggs deposited in the bladder wall has been shown to induce chronic inflammation following long-term interaction with the host's immune cells (Ishida and Hsieh, 2018). Furthermore, *S. haematobium*-induced inflammation can result in KRAS mutations leading to oncogenic transformation of bladder cells (Botelho et al., 2013), while parasite-derived antigen preparations can directly induce inflammation leading to dysplasia in otherwise normal and healthy mice (Botelho et al., 2011). Similarly, the Southeast Asian liver fluke *Opisthorchis viverrini* and Chinese blood fluke *Clonorchis sinensis* have also been shown to perpetrate liver and bile duct cancer by means of establishing chronic inflammation (Sripa et al., 2007, 2012; Kim et al., 2016). *O. viverrini* also secretes an important mitogenic factor, namely granulin-like *Ov*-GRN-1, which promotes aberrant growth of host cells in the bile duct further to activating Myd88-dependent NF-κB-driven inflammation (Sripa et al., 2012). During the chronic phase of *C. sinensis* infection, a disrupted balance between pro- and anti-inflammatory immune responses (Th1 suppression, Th2 increase) leads to DNA damage and neoplastic transformation of host cells (Kim et al., 2016). As such, the immunological axes involved in helminth-induced oncogenesis are akin to those observed in cancers with bacterial and viral pathogens.

THE MICROBIOME IN INFLAMMATION-INDUCED NEOPLASIA

The role of the microbiome, especially in the gut, play a quintessential role in maintaining physiological balance and homeostasis in health and disease (Roy and Trinchieri, 2017). Metabolites derived from gut bacteria, such as butyrate, are essential for maintaining gut barrier function (Zheng et al., 2017), which is necessary for deterring unwanted inflammation. The gut microbiota is also directly involved in drug metabolism and control of drug-associated toxicity (Zimmermann et al., 2019). Dysbiosis of the lung microbiota is implicated in the development of autoimmune pathology (O'Dwyer et al., 2016), while immune activation of gut fungal microbiota-specific T cells can influence and alter immune responses in the lung (Bacher et al., 2019). Among the constituents of the microbiome which often emerge in clinical studies are *Bacteroides* and *Prevotella* species which, in addition to the gut, are also members of the lung microbiome (Mathieu et al., 2018b; Pragman et al., 2018). The former has been associated with desirable clinical outcomes in patients with metastatic melanoma who undergo anti-CTLA-4 therapy (Chaput et al., 2017). Translational and clinical studies have linked an abundance of *Prevotella* sp. in the gut to improved protection to influenza infection (Lee et al., 2019), clinical TB (Maji et al., 2018), and general immunological homeostasis in the airways (Huffnagle et al., 2017), thus providing a link between this commensal and pulmonary immune equilibrium. *Prevotella* abundance has been reported in patients with ulcerative colitis (UC) who are also smokers (Pascal et al., 2017), in agreement with a previous study which also found an abundance of *Bacteroides* (Lucke et al., 2006). In contrast, pediatric patients with new-onset Crohn disease (CD) (thus, treatment-naive) do not have a link to *Prevotella* in the gut microbiota but, however, display a reduced abundance of *Bacteroidales* (Gevers et al., 2017). It is also relevant to refer to another recent finding of a megaphage that specifically targets *Prevotella* species in the human gut (Devoto et al., 2019), warranting further investigation in relation to induction of intestinal inflammation and neoplasia.

Mechanistic studies performed in preclinical models have shed light on some hitherto unknown immune-related mechanisms driving – potentially also contributing to neoplastic transformation of tissue – with a link to the local microbiota. IL-17B production by APCs following exposure to bacterial outer membrane vesicles (OMVs) has recently been shown to enhance the development pathogenesis of bleomycin-induced pulmonary fibrosis (PF) (Yang et al., 2019). Most strikingly, the OMV which appeared to be most prominently promoting fibrotic transformation in the alveoli of mice derived from *Bacteroides* and *Prevotella* species. The lung microbiome in mice – but not including *Bacteroides* and *Prevotella* – were shown to augment IL-1β and IL-23-driven (also involved in IL-17 production) T-cell pathology which promoted mutant KRAS and p53 lung adenocarcinoma development (Jin et al., 2019). This pathway was eventually mapped to the activation of Vγ6Vδ1+ T cells and their local production of IL-17 perpetrating malignant transformation. In another study that investigated the role of TCR γδ T cells in celiac disease, a specific population of intraepithelial lymphocytes (IEL) comprising cytolytic Vγ4Vδ1+ T cells recognizing butyrophilin (BTLN) 8/3 were shown to be decreased following gluten-induced inflammation concomitant with BTLN8 downregulation (Mayassi et al., 2019). Instead, a new subset of Vδ1+ T cells, which did not recognize BTLN8/3, occupied the same IEL niche. Provision of a gluten-free diet allowed for recuperation of BTLN8 expression, although the host-protective Vγ4Vδ1+ IEL populations could not be rejuvenated. Celiac disease has been linked to predisposing patients to a higher risk of developing esophageal cancer (Han et al., 2015), thus making it a relevant model to study early events in inflammation-induced neoplasia.

Commensal bacteria which trigger IL-17 and IL-22 production in the gut may in fact do so via Mincle-Syk kinase and C-type lectin 4e (Clec4e) signaling in dendritic cells (DCs), as recently shown in murine Peyer's patches (Martínez-López et al., 2019).

The signaling pathway, in response to sensing of microbiome-associated molecular patterns, produce IL-6 and IL-23p19, which in turn promote the development of Th17 and the production of IL-22 from type 3 innate lymphoid cells (ILC3) in the intestines. Aberrations in the Mincle-Syk pathway led to reduced gut barrier integrity, bacterial translocation to the liver and promotion of inflammation, in addition to compromised production of IgA by resident plasma cells. Adhesion-mediated endocytic uptake of antigenic cargo derived from the cell wall components of commensal gut bacteria by intestinal epithelial cells (IECs) appears to induce Th17 development in mice, requiring the activity of cell division control protein 42 homolog (CDC42) (Ladinsky et al., 2019). Thus, this system postulates one important mechanism by which microbiota-directed T-cell responses are primed in the gut and how this may play an induction of deleterious inflammation in disease.

Elevated levels of CD4+ T cells which produce IL-17 (Th17 subset) in peripheral blood of patients with type 2 *diabetes mellitus* (T2DM) has been recognized as a major contributor to chronic inflammation in these individuals (Jagannathan-Bogdan et al., 2011). Importantly, perturbation in the gut microbiome is very intimately linked to DM development (Harsch and Konturek, 2018), thus making the IL-17 axis a very relevant accomplice in this regard. More recently, a meta-analysis of 121 cohorts comprising 20 million individuals from across the globe confirmed that DM predisposes patients to developing various cancers, generally putting women more at risk than men (Ohkuma et al., 2018). A clinical study reported in 2016 showed that patients with T1DM and chronic periodontitis (oral bacterial infection) carry polymorphisms in the *IL17A* gene perpetrating exaggerated cytokine production and pathology (Borilova Linhartova et al., 2016). Patients with T2DM and pulmonary TB also exhibit high levels of serum IL-17A, in addition to TNF-α and IFN-γ, concomitant with disease severity in the lungs and reduced functionality of CD8+ cytotoxic T cells and NK cells (Kumar et al., 2013, 2015). These findings hint at a role for IL-17A in predisposing individuals with DM, particularly those harboring infections which trigger IL-17 responses, to neoplastic transformation.

Another interesting point was raised by Yoshimoto et al. (2013), that an obesity-associated distinct microbiome appears to be associated with higher incidence of liver cancer; the increase in deoxycholic acid (DCA) – associated to microbiome alterations, as a result of obesity – may provoke a senescence-associated secretory phenotype (SASP) in hepatic stellate cells, and subsequently increase the production of inflammatory molecules and tumor-promoting factors in the liver associated with an increase in HCC development after exposure to chemical carcinogens (Yoshimoto et al., 2013). Another study showed evidence of SASP signs in hepatic stellate cells in non-alcoholic steatohepatitis (Sun and Karin, 2012), demonstrating that a broad array of different factors may affect the microbiome and its complex impact on harmful or protective immune responses. Preferential colonization of mucosal tissues by certain microbiome-associated bacterial species – influenced by infections, drug intake, dietary changes and other lifestyle practices, e.g., smoking, breastfeeding (Victora et al., 2016) – can trigger unexpected immunological programs which can either promote neoplastic disease or offer protection. The microbiome does not only impact on the clinical outcome of patients with cancer treated with checkpoint inhibitors, yet also in long term survival of patients with pancreatic cancer. A high tumor microbiome diversity appears to be associated with immune activation; even a distinct intratumoral microbiome signature, defined by *Pseudoxanthomonas*, *Streptomyces*, *Saccaropolyspora,* and *Bacillus clausii*, has been shown to be associated with increased survival in patients with pancreatic cancer (Riquelme et al., 2019). In contrast to these beneficial microbiome signatures, bacterial or fungal species may drive harmful inflammation: *Saccaropolyspora rectivirgula* drives in general a pro-inflammatory environment, including hypersensitivity pneumonitis (Kim et al., 2010): the *mycobiome* (i.e., fungal commensals or pathogens) impacts on PDAC development mediated via (intratumoral) *Malassezia* that drives PDAC progression via complement activated inflammation (Aykut et al., 2019).

Among the currently discussed strategies to manipulate the microbiota, particularly in the gut and possibly also in the lung, is the use of CRISPR technology as well as the use of bacteriophages to select for preferential colonization of tissue with bacteria, fungi, perhaps in conjunction with certain bacteriophages, to promote host-beneficial immuno-physiology (Lee et al., 2018). Another use of CRISPR has also been to study the horizontal gene transfer between bacterial species comprising the microbiota and potentially pathogenic genetic islands that can perpetrate strong inflammatory responses and tissue transformation (Munck et al., 2018).

MOLECULAR MIMICRY OF PATHOGEN- AND HOST-DERIVED TARGETS: IMPLICATIONS IN ANTI-CANCER IMMUNE RESPONSES

Early work using T-cell lines specific for the melanoma-associated antigen Melan-A/MART-1_{27-35} HLA-A2 epitope (AAGIGILTV) showed cross-reactivity with an *E. coli* methionine synthase-derived peptide (AAGIGIIQI) and a peptide from the HSV-1 glycoprotein C (GIGIGVLAA), eliciting lysis and IL-2 production (Loftus et al., 1996; Carrabba et al., 2003). The binding of *Mtb*-derived epitopes with mimicry to host peptides to common HLA class I and class II molecules has also been shown using bioinformatic analysis (Chodisetti et al., 2012). This concept has now been reawakened in line with clinical biomarkers and immunotherapy in cancer, with a seminal article dissecting the immunological characteristics of long-term survivors of pancreatic cancer in whom polyclonal, neoantigen-specific CD8+ T-cell responses along with a high load of neoantigens emerged as the quintessential determinant of protection against disease progression (Balachandran et al., 2017). The authors also incorporated data linking the high quality of neoantigen-directed TCRs – which had not been negatively selected during disease pathogenesis due to their cross

reactivity to microbial peptides (Balachandran et al., 2017). These cross-reactive T cells were found in blood and tumor tissue. This appears to be biologically (and immunologically) plausible, as it is in the host's interest to fight pathogens and, therefore, not to remove these TCRs from the memory pool.

Another study, based on mathematical modeling of neoantigen characteristics and mimicry of pathogen-derived targets, showed that increased dissimilarity of neoantigens to (non mutant) target sequences increased the possibility to produce meaningful immuno-protective responses after immune checkpoint blockade therapy – designated as "neoantigen fitness" – further to binding to TCRs which also recognize infectious disease-related targets (Luksza et al., 2017). Thus, the concept of molecular mimicry which allows for pathogen- and host-reactive T cells to elicit immune responses may be crucial in mediating clinically relevant responses in cancer as well as infectious diseases.

INFECTION, INFLAMMATION, AND NEOPLASIA: IMPLICATIONS FOR PERSONALIZED IMMUNOTHERAPY

Targeting the immune system at early stages of infection may be detrimental, as the developing anti-pathogen response mounted by the host is crucial for augmenting innate and adaptive immune responses to control the pathogen's replication as well as to form long-term immunological memory. The window of opportunity for modulating the host immune responses lies in clinically intervening when the inflammatory milieu becomes overt and perpetrates unnecessary tissue pathology – potentially leading to oncogenesis. Particularly, this time point is almost impossible to capture in humans, with some exceptions, as tissue transformation in patients with *H. pylori* (Dore et al., 2018) or EBV infection (post-transplantation) (Shannon-Lowe et al., 2017), which can be monitored more closely using appropriate diagnostics and immunological testing, respectively. Primarily, the timing of intervention herein is of utmost importance. For instance, in patients with drug-sensitive pulmonary TB who undergo the standard 6-month antibiotic therapy, IL-6 overproduction at diagnosis (serum levels) can be predictive of individuals who will sustain severe lung damage at the end of treatment – albeit successfully clearing the pathogen from the lungs (Nagu, 2017). In contrast, patients who produce too little IL-6 are more likely to succumb to TB and die within the first 2 months post-diagnosis and after initiating treatment. Thus, and as previously shown, IL-6 is necessary to control *Mtb* infection in patients, but overt circulating amounts of the cytokine may be deleterious and can, therefore, be considered for therapeutic targeting. Therefore, aberrant inflammatory processes which do not result in optimal clinical outcomes offer the ideal Achilles heel for intervention. Along these lines, platforms such as spatial transcriptomics (ST) (Berglund et al., 2018) and immunohistology-based mathematical modeling (hyperspectral cell sociology) (Enfield et al., 2019) can be useful in determining areas in diseased tissue where inflammation occurs and how this affects neoplastic transformation at the gene expression level even before pathological features and clinical symptoms can be observed.

Another important fact is the existence of microbiome variations due to geographical and ethnical differences, which should also be considered in personalized therapy. Indeed, there are several studies reporting significant variations in microbiome composition in healthy individuals from different ethnicities (Nasidze et al., 2009; Nam et al., 2011; Yap et al., 2011; Yatsunenko et al., 2012; Gupta et al., 2017). These differences may also predispose individuals for some malignancies, such as inflammatory bowel disease (IBD), or increase the risk of a viral infection with oncogenic potential. An example is association between EBV and NPC, which is endemic in southern Chinese population, with special incidence in individuals of Cantonese origin. Most likely, genetic susceptibility and environmental factors, such as the consumption of dietary nitrosamines, play a role in EBV and NPC incidence (Tsao et al., 2017).

Using Immunological Effectors as Host-Directed Therapeutics

Recent evaluation of human T-cell responses to opportunistic pathogens has also revealed some interesting insights into immune priming and the risk of tissue pathology. Bacher et al. (2019) showed that CD4+ T cells which produce in response to *Candida albicans*, a commensal fungus which can cause opportunistic infections, readily cross-react with at least 30 other fungal species, based on assessment of peripheral blood-derived T-cell responses. Importantly, IL-17+ CD4+ T cells which recognize *C. albicans* antigens and cross-react with *Aspergillus fumigatus*, were identified to be specifically expanded in tissue samples from patients with airway disease (chronic obstructive pulmonary disease, asthma, and cystic fibrosis). The same cell subset was found to be increased in blood from patients with Crohn's disease, indicating their potential to travel to the lung and promote pulmonary inflammation. Effector memory CD4+ T cells which arise early in development and produce tumor necrosis factor (TNF-α) have also been shown to promote intestinal tissue growth, which is compromised in prematurely born infants (Schreurs et al., 2019).

For instance, influenza-specific tissue-resident memory (TRM) CD8+ T cells are indispensable for protection to full-fledged flu-associated pathology in the lung (Pizzolla et al., 2018). TRM cells are likely to be established in non-lymphoid tissue compartments and not even detected in blood, meaning that the highly specialized TCR repertoire in tissue differs from that seen in peripheral circulation. Indeed, TIL from human cancer tissue have an arsenal of TCRs which are specific for viral antigens, i.e., influenza CMV and EBV, but also react to cancer neoantigens (Simoni et al., 2018; Scheper et al., 2019). Thus, there is a high chance that a 'pre-wired' matrix of the tissue-resident TCR repertoire might participate in orchestrating pathology and disease due to molecular mimicry between immunogenic epitopes of microbes and host-associated antigens. One preclinical study showed that influenza-primed T-cell responses were able to recognize the overexpression of host proteins by the 3LL lung tumor cell line and confer protection

against lung cancer development in a murine model (Iheagwara et al., 2014). TRM CD8+ T-cells have been shown to express a similar gene program as compared to TIL (Milner et al., 2017). These TRMs, characterized by a specific transcription factors (Hobbit, Blimp-1, Notch, Runx3) (Milner et al., 2017) are believed to reside in non-lymphoid tissues in order to be able to rapidly respond to infectious pathogens – or to cancer (Kumar et al., 2017) TRMs require mitochondria dependent lipid oxidation (Pan et al., 2017), a pathway that is not properly functioning in chronic inflammation, chronic infection as well as in cancer lesions, due to the immune-suppressive environment and a "frozen," non-functional chromatin state (Philip et al., 2017), that appears to be at least in part be reversible (Li et al., 2019). The transcription factor Bhlhe40 maintains immune fitness in TRMs and in TIL, where a subpopulation of stem-cell like TCF1+ TIL have been shown to be responsive to checkpoint inhibition – and may indeed by responsible for clonal expansion in response to pathogens or cancer cells. Of note, checkpoint inhibitors are thought to revert dysfunctional *in situ* T-cell responses leading to clinically relevant anti-tumor responses (Pauken et al., 2016). However, clinically relevant immune responses were associated with recruitment of new T-cell clones accumulating into cancer lesions, since pre-existing (exhausted) *in situ* T-cell clones could not be reverted by checkpoint inhibitors, most likely due to "fixed" epigenetic imprints (Kurtulus et al., 2019; Yost et al., 2019). A "fixed" epigenetic landscape appears also to be associated with T-cell phenotypes (Ghoneim et al., 2017) that can be manipulated by affecting the transcriptional regulator Tcf7/Tcf1 (Kurtulus et al., 2019) or Bhlhe40 (Mehta et al., 2017) promoting and maintaining TRMs and tumor-infiltrating immune cells by increased mitochondrial metabolism (Li et al., 2019), a situation that can be also be achieved using the genetic modifier HDAC (histone deacetylase inhibitor tubastatin A) or fatty acid acetate by affecting (Bhlhe40-negative) T-cells leading to increased IFN-γ production (Li et al., 2019).

The pathogenesis of IBDs, such as CD and UC, have also been attributed to arise from dysregulated host responses to microbial products, i.e., increased prevalence of gut microbiota-derived sphingolipids such as ceramide and induction of pro-inflammatory responses locally (Bryan et al., 2016; Franzosa et al., 2019). Bacterial strains from the gut microbiota of a patient with UC have also been shown to induce Th17 cells in germ-free mice following oral inoculation (Atarashi et al., 2015). As IBDs pose a high risk for CRC development (Althumairi et al., 2016), therapeutic interventions manipulating the microbiome and inflammation may represent a viable option to prevent malignant transformation. Along these lines, α4β7 integrin-expressing regulatory T cells (Tregs) can be used a cellular product to neutralize deleterious local inflammation to improve disease outcomes (Goldberg et al., 2019). Since Tregs from patients with IBDs express low levels of α4β7, a combination of rapamycin (sirolimus) and all-trans retinoic acid (ATRA) can be used to generate α4β7-expressing Tregs *in vitro* for cellular therapy. Pertaining to resolution of intestinal inflammation and antimicrobial defense, administration of BT-11, a locally active immuno-modulatory drug which enhances oxidative phosphorylation in immune cells, was shown to potentiate Treg induction and suppression of Th1 as well as Th17 responses in the murine model of *C. rodentium*-driven intestinal inflammation without compromising anti-*C. rodentium* immunological memory and clearance (Leber et al., 2019). Importantly, BT-11 targets the lanthionine synthetase C-like 2 (LANCL2) pathway, which happens to be central to inducing IL-10 production and amelioration of overt inflammation during infection, as shown in the context of influenza virus (Leber et al., 2017) and *H. pylori* (Leber et al., 2016) infections. These findings highlight LANCL2 as a host-directed therapy (HDT) target, which is expressed in the cell membrane of immune cells. Whether this approach would concomitantly promote exacerbation of an underlying bacterial infection in humans has to be formally tested in a suitable preclinical setting prior to clinical evaluation in patients.

Killer receptor NKG2D-expressing immune effector cells such as Vγ9Vδ2 T cells, NK cells and some populations of TCR αβ CD8+ cytotoxic T cells which recognize the HLA class I-like molecules MICA/B, represent an essential component of the immune system's arsenal against targeted elimination of diseased tissue, i.e., transformed cells in cancer and infectious diseases (Huergo-Zapico et al., 2014). For example, the FAK/Src pathway has been shown to trigger downregulation of the MICA in cells, which is reversible with the use of focal adhesion kinase (FAK) inhibitors (Moncayo et al., 2017). Although MICA/B were recently described to be localized intracellularly in many tumor cell types (Ghadially et al., 2017), inhibition of FAK may be able to increase its expression on the cell surface to promote cell-mediated cytotoxicity. At the transcriptional level, miR-10b has been shown to downregulate MICB expression in tumor cells, which is also reversible (Tsukerman et al., 2012). HBV, via upregulation of the transcription factors GATA2 and GATA3 – which is also involved in Th2 and ILC2 development in humans (Wan, 2014), can force the downregulation of MICA/B in hepatoma cells to escape NK-cell surveillance (Guan et al., 2016). As mentioned in the first part of this review, pharmacological inhibition of FAK, with the clinical candidates GSK2256098, defactinib and BI-853520, which are already in several clinical trials involving patients with solid and hematological malignancies [Clinical Trials.gov identifiers NCT00787033, NCT01778803, NCT03727880, NCT01951690, NCT01943292, NCT01138033 (Doi et al., 2019)], may also augment NKG2D-mediated immunomodulation. **Figure 1** is a schematic representation of how these above-mentioned pathogen-directed immune responses may be used for HDT for timely intervention after host responses to infectious agent are detected.

Pharmacological Agents for Therapeutic Immunomodulation in Infection and Neoplasia

Small molecules, such as valproic acid (VPA), a histone deacetylase inhibitor (HDI) and hydralazine may be used as adjuvants to improve immune responses in HPV+ patients and therefore may be a viable option due to the drugs' capacity to

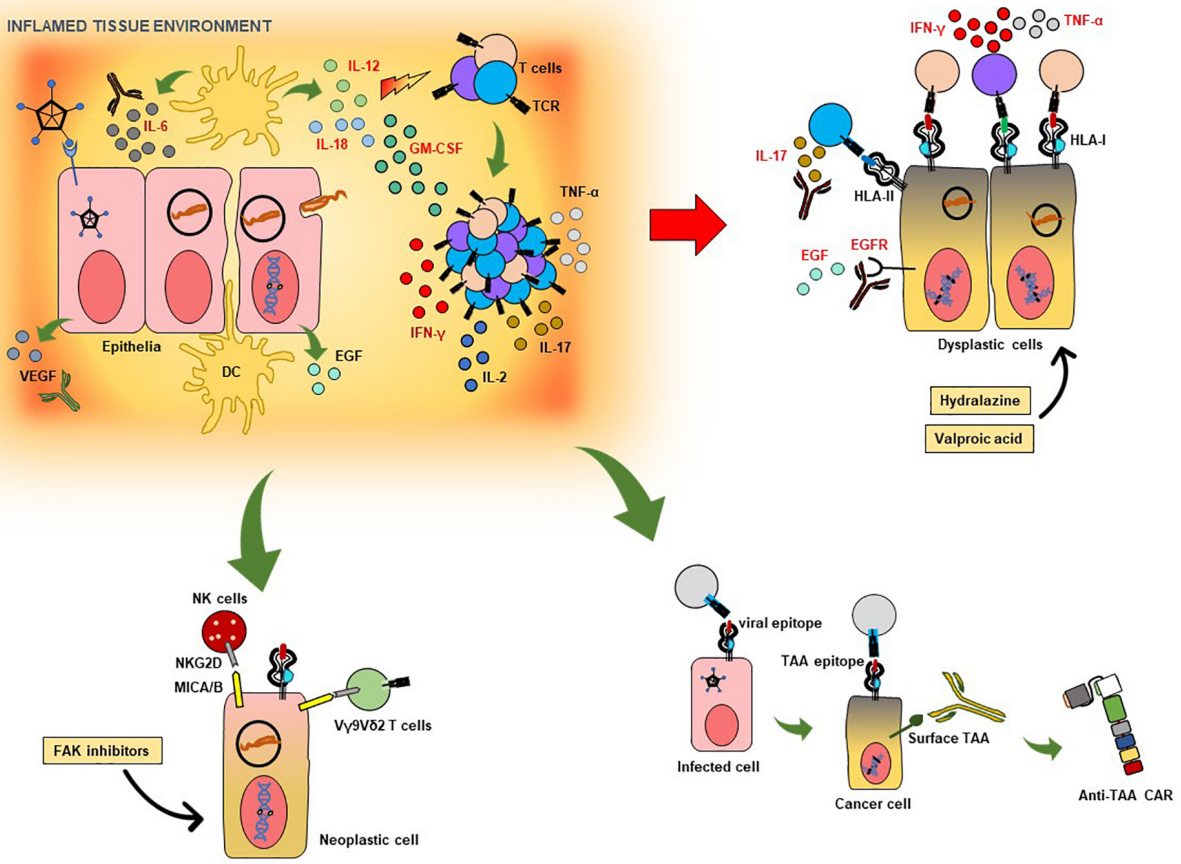

FIGURE 1 | Targeted immunotherapeutic strategies against infection- and inflammation-induced neoplasia. The schematic shows some of the possible strategies which can be pursued in developing targeted host-directed immunotherapies based on biomarkers in infection-induced inflammation and oncogenesis. Cells infected with viruses or bacteria may induce physiological and anatomical changes in tissue, leading to reduced barrier functions and tissue integrity. This contributes to the overall local immunological milieu associated with the production of pro-inflammatory cytokines, as IL-6, IL-18, IL-12, and GM-CSF. In some cases of viral infection, VEGF production is also observed, which leads to neovascularization and poses a risk for malignant transformation. The same is true for EGF release by host cells in some bacterial infections. The ensuing T-cell activation culminates in production of IFN-γ, TNF-α, IL-2 as well as IL-17 in several infections – which can be pathogenic and contribute to chronic inflammation and neoplasia. To the right of the schematic are dysplastic cells, which can present antigenic epitopes to T cells, some of which may be protective (HLA class I-restricted pathogen- or host cell-derived structures), while others may exacerbate the IL-17 response (HLA class-II-restricted Th17 epitopes). Excess IL-17 as well as IL-6 can be neutralized using therapeutic antibodies which are clinically licensed. VEGF neutralization, as well as EGFR blockade, may be clinically useful in halting disease progression due to aberrant inflammation induced by infection. Hydralazine and valproic acid, both of which are clinically approved medications, can increase HLA class I expression in host cells, thereby augmenting and enhancing CD8+ T cell-mediated immune control. FAK inhibitors may be able to increase MICA/B expression in neoplastic cells (as well dysplastic ones) to improve immune surveillance by TCR Vγ9Vδ2 T cells and NK cells expressing the killer receptor NKG2D. Virus-induced T-cell responses against certain host-cell epitopes may educate T cells to subsequently recognize tumor cells; such T-cell populations may be used in active cell therapies and the nominal (antigen-specific) TCR may be utilized for transfer into recipient surrogate immune cells. Host cell surface molecules associated with malignant transformation induced by infection and inflammation, if recognized by circulating as well as tissue-associated antibodies, may be used as as templates for inducing ADCC as well as viable targets for biologically and clinically relevant chimeric antigen receptors (CARs) transgenically expressed by immune effector cells.

upregulate HLA class expression in infected cells and CD8+ T-cell responses against them (Mora-Garcia Mde et al., 2006). Vorinostat, another HDI currently in clinical trials for cancer treatment (Bubna, 2015), along with VPA can actively inhibit *Mtb* growth in human cells and may shorten the treatment period with conventional first-line anti-TB drugs (Rao et al., 2018). Studies in mice suggest that carboplatin-derived cancer drugs exert their effects also via autophagy (Michaud et al., 2011), which facilitates anti-bacterial immune responses and clearance (Jo et al., 2013; Kaufmann et al., 2014). It may, therefore, be possible to investigate the immunological profile of cells isolated from platinum-treated patients with cancer for their responsiveness to pathogen-derived antigens and whether these cells can be used for therapeutic purposes. Rifampicin, which is a first-line anti-TB drug, has shown anti-angiogenic properties in preclinical studies, with inhibitory effects on human liver cancer cells and sarcoma cells (Shichiri and Tanaka, 2010), further to decreasing HCC to only a single occurrence in six patients who were HCV+ in

over 97 months (8 years) (Shichiri et al., 2009). Since rifampicin is used not only to treat mycobacterial infections, but also those caused by meningococci, staphylococci and enterococci (Forrest and Tamura, 2010), the immunomodulatory properties of this drug may apply across the gastrointestinal and pulmonary organ systems. Based on experience in cancer treatment, low-dose cyclophosphamide-induced immunological fine-tuning by modulating CD8+ T and regulatory T-cell activity may also be useful in changing the immune milieu in immunocompetent individuals (Sistigu et al., 2011).

With regard to helminth infections, praziquantel has shown very good efficacy particularly in women and children based on the WHO-recommended parasite egg reduction rate (ERR) to measure control of parasite burden (Sayasone et al., 2017; Kabuyaya et al., 2018). While *S. haematobium* and *O. viverrini* infections exhibit better treatment outcomes, the treatment efficacy is somewhat reduced in the context of *C. sinensis*, with repeated doses required (Hong et al., 2001). This also increases the chances of drug resistance while not addressing the existing chronic inflammation in patients. Furthermore, praziquantel on its own can induce neutrophil activity in the bladder after treatment of patients with *S. haematobium* infection (Stecher et al., 2017). Allicin, a sulfur-containing compound extracted from garlic and available over-the-counter, was able to reduce inflammation as well as parasite burden albeit to a lesser extent than praziquantel in a mouse model of schistosomiasis (Metwally et al., 2018). Interestingly, allicin was also shown to reduce the viability of human CRC, breast and lung cancer cell lines in a dose-dependent manner (Gruhlke et al., 2016) resonating with a preclinical study in mice reported in 1960 (DiPaolo and Carruthers, 1960), thus making it a good candidate for testing in patients with helminth-induced liver and bile duct cancers.

CONCLUSION

The chain of molecular and immunological events occurring between infection and neoplasia in humans is challenging to study. Nevertheless, biomarkers obtained via clinical and translational studies (the role of METTL13/FEAT in infection-driven neoplasia is a good example), as well as ongoing drug trials provide an avenue to examine fluctuations which reflect different stages of the immunopathological process. A combination of measurement of soluble biological mediators in blood, immunohistological methods, next-generation sequencing and existing clinical knowledge will be able to identify and design personalized therapies. Furthermore, constituents of the study cohorts in question, as inclusion of uninfected household contacts, unrelated healthy donors and geographical distribution play a remarkably important role to more accurately decipher the tenets of protective vs. pathological immune and genetic biomarkers which may have theranostic value.

AUTHOR CONTRIBUTIONS

MR, JL, AZ, and MM initiated, conceptualized, and wrote the first draft of the manuscript. All authors contributed with suggestions, revisions, and interpretation of different aspects in immune-interventions.

FUNDING

This work was supported by the Champalimaud Foundation.

REFERENCES

Althumairi, A. A., Lazarev, M. G., and Gearhart, S. L. (2016). Inflammatory bowel disease associated neoplasia: a surgeon's perspective. *World J. Gastroenterol.* 22, 961–973. doi: 10.3748/wjg.v22.i3.961

An, J., Lichtenstein, A. K., Brent, G., and Rettig, M. B. (2002). The Kaposi sarcoma–associated herpesvirus (KSHV) induces cellular interleukin 6 expression: role of the KSHV latency-associated nuclear antigen and the AP1 response element. *Blood* 99, 649–654. doi: 10.1182/blood.v99.2.649

Andres, S., Schmidt, H. M., Mitchell, H., Rhen, M., Maeurer, M., and Engstrand, L. (2011). *Helicobacter pylori* defines local immune response through interaction with dendritic cells. *FEMS Immunol. Med. Microbiol.* 61, 168–178. doi: 10.1111/j.1574-695X.2010.00761.x

Atarashi, K., Tanoue, T., Ando, M., Kamada, N., Nagano, Y., and Narushima, S. (2015). Th17 cell induction by adhesion of microbes to intestinal epithelial cells. *Cell* 163, 367–380. doi: 10.1016/j.cell.2015.08.058

Aykut, B., Pushalkar, S., Chen, R., Li, Q., Abengozar, R., and Kim, J. I. (2019). The fungal mycobiome promotes pancreatic oncogenesis via activation of MBL. *Nature* 574, 264–267. doi: 10.1038/s41586-019-1608-2

Bacher, P., Hohnstein, T., Beerbaum, E., Blango, M. G., Kaufmann, S., and Eschenhagen, P. (2019). Human anti-fungal Th17 immunity and pathology rely on cross-reactivity against *Candida albicans*. *Cell* 6, 1340–1355. doi: 10.1016/j.cell.2019.01.041

Balachandran, V. P., Luksza, M., Zhao, J. N., Makarov, V., Moral, J. A., and Remark, R. (2017). Identification of unique neoantigen qualities in long-term survivors of pancreatic cancer. *Nature* 551, 512–516. doi: 10.1038/nature24462

Balasiddaiah, A., Davanian, H., Aleman, S., Pasetto, A., Frelin, L., and Lohmann, V. (2017). Hepatitis C virus-specific T cell receptor mRNA-engineered human T cells: impact of antigen specificity on functional properties. *J. Virol.* 91:e00010-e17. doi: 10.1128/JVI.00010-17

Bansal, A., Singh, M. P., and Rai, B. (2016). Human papillomavirus-associated cancers: a growing global problem. *Int. J. Appl. Basic Med. Res.* 6, 84–89. doi: 10.4103/2229-516X.179027

Barozzi, P., Bonini, C., Potenza, L., Masetti, M., Cappelli, G., and Gruarin, P. (2008). Changes in the immune responses against human herpesvirus-8 in the disease course of posttransplant *Kaposi sarcoma*. *Transplantation* 86, 738–744. doi: 10.1097/TP.0b013e318184112c

Berglund, E., Maaskola, J., Schultz, N., Friedrich, S., Marklund, M., and Tarish, F. (2018). Spatial maps of prostate cancer transcriptomes reveal an unexplored landscape of heterogeneity. *Nat. Commun.* 9:2419. doi: 10.1038/s41467-018-04724-4725

Bertoletti, A., Sette, A., Chisari, F. V., Penna, A., Levrero, M., and Fiaccadori, F. (1994). Natural variants of cytotoxic epitopes are T-cell receptor antagonists for antiviral cytotoxic T cells. *Nature* 369, 407–410. doi: 10.1038/369407a0

Bertoletti, A., Tan, A. T., and Koh, S. (2017). T-cell therapy for chronic viral hepatitis. *Cytotherapy* 19, 1317–1324. doi: 10.1016/j.jcyt.2017.07.011

Bomfim, I. L., Lamb, F., Fink, K., Szakacs, A., Silveira, A., and Franzen, L. (2017). The immunogenetics of narcolepsy associated with A(H1N1)pdm09 vaccination (Pandemrix) supports a potent gene-environment interaction. *Genes Immun.* 18, 75–81. doi: 10.1038/gene.2017.1

Borchert, S., Neumann, F., Schmidt, C., Wimmer, P., Dobner, T., and Grundhoff, A. (2014). High-affinity Rb binding, p53 inhibition, subcellular localization, and transformation by wild-type or tumor-derived shortened Merkel cell

polyomavirus large T antigens. *J. Virol.* 88, 3144–3160. doi: 10.1128/JVI.02916-13

Borilova Linhartova, P., Kastovsky, J., Lucanova, S., Bartova, J., Poskerova, H., and Vokurka, J. (2016). Interleukin-17A gene variability in patients with type 1 diabetes mellitus and chronic Periodontitis: its correlation with IL-17 levels and the occurrence of periodontopathic bacteria. *Media. Inflamm.* 2016, 2979846–2979846. doi: 10.1155/2016/2979846

Botelho, M. C., Oliveira, P. A., Lopes, C., Correia da Costa, J. M., and Machado, J. C. (2011). Urothelial dysplasia and inflammation induced by *Schistosoma haematobium* total antigen instillation in mice normal urothelium. *Urol. Oncol.* 29, 809–814. doi: 10.1016/j.urolonc.2009.09.017

Botelho, M. C., Veiga, I., Oliveira, P. A., Lopes, C., Teixeira, M., and Machado, J. C. (2013). Carcinogenic ability of *Schistosoma haematobium* possibly through oncogenic mutation of KRAS gene. *Adv. Cancer Res. Treat.* 2013:876585.

Brewer, J. D., Shanafelt, T. D., Otley, C. C., Roenigk, R. K., Cerhan, J. R., and Kay, N. E. (2012). Chronic lymphocytic leukemia is associated with decreased survival of patients with malignant melanoma and merkel cell carcinoma in a SEER population-based study. *J. Clin. Oncol.* 30, 843–849. doi: 10.1200/JCO.2011.34.9605

Bryan, P. F., Karla, C., Edgar Alejandro, M. T., Sara Elva, E. P., Gemma, F., and Luz, C. (2016). Sphingolipids as mediators in the crosstalk between microbiota and intestinal cells: implications for inflammatory bowel disease. *Media. Inflamm.* 2016, 9890141–9890141.

Bubna, A. K. (2015). Vorinostat-an overview. *Indian J Dermatol.* 60:419. doi: 10.4103/0019-5154.160511

Cancer Genome Atlas Research (2014). Comprehensive molecular characterization of gastric adenocarcinoma. *Nature* 513, 202–209. doi: 10.1038/nature13480

Carrabba, M. G., Castelli, C., Maeurer, M. J., Squarcina, P., Cova, A., and Pilla, L. (2003). Suboptimal activation of CD8+ T cells by melanoma-derived altered peptide ligands. Role of Melan-A/MART-1 optimized analogues. *Cancer Res.* 63, 1560–1567.

Carter, J. J., Daugherty, M. D., Qi, X. J., Wipf, G. C., Robinson, K., and Roman, A. (2013). Identification of an overprinting gene in Merkel cell polyomavirus provides evolutionary insight into the birth of viral genes. *Proc. Natl. Acad. Sci. U.S.A.* 110, 12744–12749. doi: 10.1073/pnas.1303526110

Castro-Garza, J., Luevano-Martinez, M. L., Villarreal-Trevino, L., Gosalvez, J., Fernandez, J. L., and Davila-Rodriguez, M. I. (2018). Mycobacterium tuberculosis promotes genomic instability in macrophages. *Mem. Inst. Oswaldo Cruz* 113, 161–166. doi: 10.1590/0074-02760170281

Chang, C. C., Chang, C. W., Nguyen, P. A. A., Chang, T. H., Shih, Y. L., Chang, W. Y., et al. (2017). Ankylosing spondylitis and the risk of cancer. *Oncol. Lett.* 14, 1315–1322.

Chang, Y., Moore, P. S., and Weiss, R. A. (2017). Human oncogenic viruses: nature and discovery. *Philos. Trans. R. Soc. Lond. B Biol. Sci.* 372:20160264. doi: 10.1098/rstb.2016.0264

Chang, Y., Cesarman, E., Pessin, M. S., Lee, F., Culpepper, J., and Knowles, D. M. (1994). Identification of herpesvirus-like DNA sequences in AIDS-associated Kaposi's sarcoma. *Science* 266, 1865–1869. doi: 10.1126/science.7997879

Chaput, N., Lepage, P., Coutzac, C., Soularue, E., Monot, C., and Boselli, L. (2017). Baseline gut microbiota predicts clinical response and colitis in metastatic melanoma patients treated with ipilimumab. *Ann. Oncol.* 28, 1368–1379. doi: 10.1093/annonc/mdx108

Chen, L., Li, B., Yang, W. C., He, J. L., Li, N. Y., and Hu, J. (2013). A dominant CD4(+) T-cell response to *Helicobacter pylori* reduces risk for gastric disease in humans. *Gastroenterology* 144, 591–600. doi: 10.1053/j.gastro.2012.12.002

Chiang, C. Y., Lee, J. J., Yu, M. C., Enarson, D. A., Lin, T. P., and Luh, K. T. (2009). Tuberculosis outcomes in Taipei: factors associated with treatment interruption for 2 months and death. *Int. J. Tuberc. Lung Dis.* 13, 105–111.

Chodisetti, S. B., Rai, P. K., Gowthaman, U., Pahari, S., and Agrewala, J. N. (2012). Potential T cell epitopes of *Mycobacterium tuberculosis* that can instigate molecular mimicry against host: implications in autoimmune pathogenesis. *BMC Immunol.* 13:13. doi: 10.1186/1471-2172-13-13

Chumduri, C., Gurumurthy, R. K., Zadora, P. K., Mi, Y., and Meyer, T. F. (2013). Chlamydia infection promotes host DNA damage and proliferation but impairs the DNA damage response. *Cell Host Microbe* 13, 746–758. doi: 10.1016/j.chom.2013.05.010

Cogliano, V. J., Baan, R., Straif, K., Grosse, Y., Bouvard, V., and Guha, N. (2011). Preventable exposures associated with human cancers. *J. Natl. Cancer Inst.* 103, 1827–1839. doi: 10.1093/jnci/djr483

Cox, A. L., Mosbruger, T., Mao, Q., Liu, Z., Wang, X. H., and Yang, H. C. (2005). Cellular immune selection with hepatitis C virus persistence in humans. *J. Exp. Med.* 201, 1741–1752. doi: 10.1084/jem.20050121

Dalmasso, G., Cougnoux, A., Delmas, J., Darfeuille-Michaud, A., and Bonnet, R. (2014). The bacterial genotoxin colibactin promotes colon tumor growth by modifying the tumor microenvironment. *Gut Microb.* 5, 675–680. doi: 10.4161/19490976.2014.969989

De la Herran-Arita, A. K., Kornum, B. R., Mahlios, J., Jiang, W., Lin, L., and Hou, T. (2013). CD4+ T cell autoimmunity to hypocretin/orexin and cross-reactivity to a 2009 H1N1 influenza A epitope in narcolepsy. *Sci. Transl. Med.* 5:2013.

DeCaprio, J. A. (2017). Merkel cell polyomavirus and Merkel cell carcinoma. *Philos. Trans. R. Soc. Lond. B Biol. Sci.* 372:20160276. doi: 10.1098/rstb.2016.0276

Devoto, A. E., Santini, J. M., Olm, M. R., Anantharaman, K., Munk, P., and Tung, J. (2019). Megaphages infect *Prevotella* and variants are widespread in gut microbiomes. *Nat. Microbiol.* 4, 693–700. doi: 10.1038/s41564-018-0338-9

DiPaolo, J. A., and Carruthers, C. (1960). The effect of allicin from garlic on tumor growth. *Cancer Res.* 20, 431–434.

Doi, T., Yang, J. C., Shitara, K., Naito, Y., Cheng, A. L., and Sarashina, A. (2019). Phase I study of the focal adhesion kinase inhibitor BI 853520 in Japanese and Taiwanese patients with advanced or metastatic solid tumors. *Target Oncol.* 14, 57–65. doi: 10.1007/s11523-019-00620-0

Dore, M. P., Cipolli, A., Ruggiu, M. W., Manca, A., Bassotti, G., and Pes, G. M. (2018). *Helicobacter pylori* eradication may influence timing of endoscopic surveillance for gastric cancer in patients with gastric precancerous lesions: a retrospective study. *Medicine* 97:e9734. doi: 10.1097/MD.0000000000009734

Draper, L. M., Kwong, M. L. M., Gros, A., Tran, E., Kerkar, S., and Raffeld, M. (2015). Targeting of HPV-16+ epithelial cancer cells by TCR gene engineered T cells directed against E6. *Clin. Cancer Res.* 21, 4431–4439. doi: 10.1158/1078-0432.CCR-14-3341

Enfield, K. S. S., Martin, S. D., Marshall, E. A., Kung, S. H. Y., Gallagher, P., and Milne, K. (2019). Hyperspectral cell sociology reveals spatial tumor-immune cell interactions associated with lung cancer recurrence. *J. ImmunoTher. Cancer* 7:13. doi: 10.1186/s40425-018-0488-486

Fan, X., Gunasena, H., Cheng, Z., Espejo, R., Crowe, S. E., Ernst, P. B., et al. (2000). *Helicobacter pylori* urease binds to class II MHC on gastric epithelial cells and induces their apoptosis. *J. Immunol.* 165, 1918–1924. doi: 10.4049/jimmunol.165.4.1918

Farrell, P. J. (2019). Epstein–barr virus and cancer. *Ann. Rev. Pathol.* 14, 29–53.

Forrest, G. N., and Tamura, K. (2010). Rifampin combination therapy for nonmycobacterial infections. *Clin. Microbiol. Rev.* 23, 14–34. doi: 10.1128/CMR.00034-09

Franzosa, E. A., Fornelos, N., Haiser, H. J., Reinker, S., Vatanen, T., and Hall, A. B. (2019). Gut microbiome structure and metabolic activity in inflammatory bowel disease. *Nat. Microbiol.* 4, 293–305. doi: 10.1038/s41564-018-0306-4

Galanina, N., Goodman, A. M., Cohen, P. R., Frampton, G. M., and Kurzrock, R. (2018). Successful treatment of HIV-associated kaposi sarcoma with immune checkpoint blockade. *Cancer Immunol. Res.* 6, 1129–1135. doi: 10.1158/2326-6066.CIR-18-0121

Gardiner, D., Lalezari, J., Lawitz, E., DiMicco, M., Ghalib, R., and Reddy, K. R. (2013). A randomized, double-blind, placebo-controlled assessment of BMS-936558, a fully human monoclonal antibody to programmed death-1 (PD-1), in patients with chronic hepatitis C virus infection. *PLoS One* 8:e63818. doi: 10.1371/journal.pone.0063818

Gevers, D., Kugathasan, S., Knights, D., Kostic, A. D., Knight, R., and Xavier, R. J. (2017). A microbiome foundation for the Study of Crohn's disease. *Cell Host Microbe* 21, 301–304. doi: 10.1016/j.chom.2017.02.012

Ghadially, H., Brown, L., Lloyd, C., Lewis, L., Lewis, A., and Dillon, J. (2017). MHC class I chain-related protein A and B (MICA and MICB) are predominantly expressed intracellularly in tumour and normal tissue. *Br. J. Cancer* 116, 1208–1217. doi: 10.1038/bjc.2017.79

Ghoneim, H. E., Fan, Y., Moustaki, A., Abdelsamed, H. A., Dash, P., and Dogra, P. (2017). De Novo epigenetic programs inhibit PD-1 blockade-mediated T cell rejuvenation. *Cell* 170:e19. doi: 10.1016/j.cell.2017.06.007

Goldberg, R., Scotta, C., Cooper, D., Nir, E., Tasker, S., and Irving, P. M. (2019). Correction of defective T-regulatory cells from patients with Crohn's disease by ex vivo ligation of retinoic acid receptor alpha. *Gastroenterology* 156, 1775–1787. doi: 10.1053/j.gastro.2019.01.025

Golden-Mason, L., Palmer, B., Klarquist, J., Mengshol, J. A., Castelblanco, N., and Rosen, H. R. (2007). Upregulation of PD-1 expression on circulating and intrahepatic hepatitis C virus-specific CD8+ T cells associated with reversible immune dysfunction. *J. Virol.* 81, 9249–9258. doi: 10.1128/jvi.00409-07

Grant, W. B. (2018). A review of the evidence supporting the vitamin D-cancer prevention hypothesis in 2017. *Anticancer. Res.* 38, 1121–1136.

Gruhlke, M. C. H., Nicco, C., Batteux, F., and Slusarenko, A. J. (2016). The effects of allicin, a reactive Sulfur species from garlic, on a selection of mammalian cell lines. *Antioxidants* 6:1. doi: 10.3390/antiox6010001

Guan, Y., Li, W., Hou, Z., Han, Q., Lan, P., and Zhang, J. (2016). HBV suppresses expression of MICA/B on hepatoma cells through up-regulation of transcription factors GATA2 and GATA3 to escape from NK cell surveillance. *Oncotarget* 7, 56107–56119. doi: 10.18632/oncotarget.11271

Guo, L., Chen, W., Zhu, H., Chen, Y., Wan, X., and Yang, N. (2014). *Helicobacter pylori* induces increased expression of the vitamin d receptor in immune responses. *Helicobacter* 19, 37–47. doi: 10.1111/hel.12102

Gupta, V. K., Paul, S., and Dutta, C. (2017). Geography, ethnicity or subsistence-specific variations in human microbiome composition and diversity. *Front. Microbiol.* 8:1162. doi: 10.3389/fmicb.2017.01162

Han, Y., Chen, W., Li, P., and Ye, J. (2015). Association between Coeliac disease and risk of any malignancy and gastrointestinal malignancy: a meta-analysis. *Medicine* 94:e1612. doi: 10.1097/MD.0000000000001612

Harms, P. W., Collie, A. M., Hovelson, D. H., Cani, A. K., Verhaegen, M. E., and Patel, R. M. (2016). Next generation sequencing of Cytokeratin 20-negative Merkel cell carcinoma reveals ultraviolet-signature mutations and recurrent TP53 and RB1 inactivation. *Mod. Pathol.* 29, 240–248. doi: 10.1038/modpathol.2015.154

Harper, D. M., Vierthaler, S. L., and Santee, J. A. (2010). Review of gardasil. *J. Vaccines Vaccin.* 1:e1000107.

Harsch, I. A., and Konturek, P. C. (2018). The role of gut microbiota in obesity and type 2 and type 1 diabetes Mellitus: new insights into "Old". diseases. *Med. Sci.* 6:32. doi: 10.3390/medsci6020032

He, J., Tang, X. F., Chen, Q. Y., Mai, H. Q., Huang, Z. F., Li, J., et al. (2012). Ex vivo expansion of tumor-infiltrating lymphocytes from nasopharyngeal carcinoma patients for adoptive immunotherapy. *Chin. J. Cancer* 31, 287–294. doi: 10.5732/cjc.011.10376

Hong, S. T., Rim, H. J., Min, D. Y., Li, X., Xu, J., Feng, Z., et al. (2001). Control of clonorchiasis by repeated treatments with praziquantel. *Korean J. Parasitol.* 39, 285–292.

Hou, S., Sun, X., Dong, X., Lin, H., Tang, L., and Xue, M. (2019). Chlamydial plasmid-encoded virulence factor Pgp3 interacts with human cathelicidin peptide LL-37 to modulate immune response. *Microbes Infect.* 21, 50–55. doi: 10.1016/j.micinf.2018.06.003

Huergo-Zapico, L., Acebes-Huerta, A., López-Soto, A., Villa-Álvarez, M., Gonzalez-Rodriguez, A. P., and Gonzalez, S. (2014). Molecular bases for the regulation of NKG2D Ligands in cancer. *Front. Immunol.* 5:106. doi: 10.3389/fimmu.2014.00106

Huffnagle, G. B., Dickson, R. P., and Lukacs, N. W. (2017). The respiratory tract microbiome and lung inflammation: a two-way street. *Mucosal Immunol.* 10, 299–306. doi: 10.1038/mi.2016.108

Hyrina, A., Meng, F., McArthur, S. J., Eivemark, S., Nabi, I. R., and Jean, F. (2017). Human Subtilisin Kexin Isozyme-1 (SKI-1)/Site-1 Protease (S1P) regulates cytoplasmic lipid droplet abundance: a potential target for indirect-acting anti-dengue virus agents. *PLoS One* 12:e0174483. doi: 10.1371/journal.pone.0174483

Iheagwara, U. K., Beatty, P. L., Van, P. T., Ross, T. M., Minden, J. S., and Finn, O. J. (2014). Influenza virus infection elicits protective antibodies and T cells specific for host cell antigens also expressed as tumor-associated antigens: a new view of cancer immunosurveillance. *Cancer Immunol. Res.* 2, 263–273. doi: 10.1158/2326-6066.CIR-13-0125

Ishida, K., and Hsieh, M. H. (2018). Understanding urogenital schistosomiasis-related bladder cancer: an update. *Front. Med.* 5:223. doi: 10.3389/fmed.2018.00223

Iyer, J. G., Afanasiev, O. K., McClurkan, C., Paulson, K., Nagase, K., and Jing, L. (2011). Merkel cell polyomavirus-specific CD8(+) and CD4(+) T-cell responses identified in Merkel cell carcinomas and blood. *Clin. Cancer Res.* 17, 6671–6680. doi: 10.1158/1078-0432.CCR-11-1513

Jagannathan-Bogdan, M., McDonnell, M. E., Shin, H., Rehman, Q., Hasturk, H., Apovian, C. M., et al. (2011). Elevated proinflammatory cytokine production by a skewed T cell compartment requires monocytes and promotes inflammation in type 2 diabetes. *J. Immunol.* 186, 1162–1172. doi: 10.4049/jimmunol.1002615

Jin, C., Lagoudas, G. K., Zhao, C., Bullman, S., Bhutkar, A., and Hu, B. (2019). Commensal microbiota promote lung cancer development via gammadelta T cells. *Cell* 176:998-1013.e16. doi: 10.1016/j.cell.2018.12.040

Jo, E. K., Yuk, J. M., Shin, D. M., and Sasakawa, C. (2013). Roles of autophagy in elimination of intracellular bacterial pathogens. *Front. Immunol.* 4:97. doi: 10.3389/fimmu.2013.00097

Jog, N. R., Chakravarty, E. F., Guthridge, J. M., and James, J. A. (2018). Epstein barr virus interleukin 10 suppresses anti-inflammatory phenotype in human monocytes. *Front. Immunol.* 9:2198. doi: 10.3389/fimmu.2018.02198

Jones, K., Nourse, J. P., Morrison, L., Nguyen-Van, D., Moss, D. J., and Burrows, S. R. (2010). Expansion of EBNA1-specific effector T cells in posttransplantation lymphoproliferative disorders. *Blood* 116, 2245–2252. doi: 10.1182/blood-2010-03-274076

Kabuyaya, M., Chimbari, M. J., and Mukaratirwa, S. (2018). Efficacy of praziquantel treatment regimens in pre-school and school aged children infected with schistosomiasis in sub-Saharan Africa: a systematic review. *Infect. Dis. Povert.* 7:73. doi: 10.1186/s40249-018-0448

Kah, J., Koh, S., Volz, T., Ceccarello, E., Allweiss, L., and Bertoletti, A. (2017). Lymphocytes transiently expressing virus-specific T cell receptors reduce hepatitis B virus infection. *J. Clin. Invest.* 127, 3177–3188. doi: 10.1172/JCI93024

Kamboj, M., and Sepkowitz, K. A. (2006). The risk of tuberculosis in patients with cancer. *Clin. Infect. Dis* 42, 1592–1595.

Kamphorst, A. O., Pillai, R. N., Yang, S., Nasti, T. H., Akondy, R. S., and Wieland, A. (2017). Proliferation of PD-1+ CD8 T cells in peripheral blood after PD-1-targeted therapy in lung cancer patients. *Proc. Natl. Acad. Sci. U.S.A.* 114, 4993–4998. doi: 10.1073/pnas.1705327114

Kansy, B. A., Srivastava, R. M., Shayan, G., Lei, Y., Moskovitz, J., and Moy, J. (2017). PD-1 status in CD8+ T cells associates with survival and anti-PD-1 therapeutic outcomes in head and neck cancer. *Cancer Res.* 77, 6353–6364. doi: 10.1158/0008-5472.CAN-16-3167

Kaufmann, S. H., Lange, C., Rao, M., Balaji, K. N., Lotze, M., and Schito, M. (2014). Progress in tuberculosis vaccine development and host-directed therapies–a state of the art review. *Lancet Respir. Med.* 2, 301–320. doi: 10.1016/S2213-2600(14)70033-5

Kenter, G. G., Welters, M. J. P., Lowik, M. J. G., Vloon, A. P. G., Essahsah, F., and Fathers, L. M. (2009). Vaccination against HPV-16 oncoproteins for vulvar intraepithelial neoplasia. *New Eng. J. Med.* 361, 1838–1847. doi: 10.1056/nejmoa0810097

Kim, H. J., Ko, Y. H., Kim, J. E., Lee, S. S., Lee, H., and Park, G. (2017). Hematopathology study group of the Korean society of, epstein-barr virus-associated Lymphoproliferative disorders: review and update on 2016 WHO classification. *J. Pathol. Transl. Med.* 51, 352–358. doi: 10.4132/jptm.2017.03.15

Kim, T. S., Pak, J. H., Kim, J. B., and Bahk, Y. Y. (2016). Clonorchis sinensis, an oriental liver fluke, as a human biological agent of cholangiocarcinoma: a brief review. *BMB Rep.* 49, 590–597. doi: 10.5483/bmbrep.2016.49.11.109

Kim, Y. I., Park, J. E., Brand, D. D., Fitzpatrick, E. A., and Yi, A. K. (2010). Protein kinase D1 is essential for the proinflammatory response induced by hypersensitivity pneumonitis-causing thermophilic actinomycetes *Saccharopolyspora rectivirgula*. *J. Immunol.* 184, 3145–3156. doi: 10.4049/jimmunol.0903718

Kirveskari, J., He, Q., Leirisalo-Repo, M., Mäki-Ikola, O., Wuorela, M., Putto-Laurila, A., et al. (1999). Enterobacterial infection modulates major histocompatibility complex class I expression on mononuclear cells. *Immunology* 97, 420–428. doi: 10.1046/j.1365-2567.1999.00803.x

Kocjan, B. J., Seme, K., Cimerman, M., Kovanda, A., Potocnik, M., and Poljak, M. (2009). Genomic diversity of human papillomavirus (HPV) genotype 38. *J. Med. Virol.* 81, 288–295. doi: 10.1002/jmv.21392

Kumar, B. V., Ma, W., Miron, M., Granot, T., Guyer, R. S., and Carpenter, D. J. (2017). Human tissue-resident memory T cells are defined by core

transcriptional and functional signatures in lymphoid and mucosal sites. *Cell Rep.* 20, 2921–2934. doi: 10.1016/j.celrep.2017.08.078

Kumar, N. P., Sridhar, R., Banurekha, V. V., Jawahar, M. S., Fay, M. P., Nutman, T. B., et al. (2013). Type 2 diabetes mellitus coincident with pulmonary tuberculosis is associated with heightened systemic type 1, type 17, and other proinflammatory cytokines. *Ann. Am. Thoracic Soc.* 10, 441–449. doi: 10.1513/AnnalsATS.201305-112OC

Kumar, N. P., Sridhar, R., Nair, D., Banurekha, V. V., Nutman, T. B., and Babu, S. (2015). Type 2 diabetes mellitus is associated with altered CD8(+) T and natural killer cell function in pulmonary tuberculosis. *Immunology* 144, 677–686. doi: 10.1111/imm.12421

Kurtulus, S., Madi, A., Escobar, G., Klapholz, M., Nyman, J., and Christian, E. (2019). Checkpoint blockade immunotherapy induces dynamic changes in PD-1(-)CD8(+) tumor-infiltrating T cells. *Immunity* 50:e6. doi: 10.1016/j.immuni.2018.11.014

Ladinsky, M. S., Araujo, L. P., Zhang, X., Veltri, J., Soualhi, S., and Lee, C. (2019). Endocytosis of commensal antigens by intestinal epithelial cells regulates mucosal T cell homeostasis. *Science* 363:eaat4042. doi: 10.1126/science.aat4042

Leber, A., Bassaganya-Riera, J., Tubau-Juni, N., Zoccoli-Rodriguez, V., Lu, P., and Godfrey, V. (2017). Lanthionine synthetase C-Like 2 modulates immune responses to influenza virus infection. *Front. Immunol.* 8:178. doi: 10.3389/fimmu.2017.00178

Leber, A., Bassaganya-Riera, J., Tubau-Juni, N., Zoccoli-Rodriguez, V., Viladomiu, M., and Abedi, V. (2016). Modeling the role of lanthionine synthetase C-Like 2 (LANCL2) in the modulation of immune responses to *Helicobacter pylori* infection. *PLoS One* 11:e0167440. doi: 10.1371/journal.pone.0167440

Leber, A., Hontecillas, R., Zoccoli-Rodriguez, V., Chauhan, J., and Bassaganya-Riera, J. (2019). Oral treatment with BT-11 ameliorates inflammatory Bowel disease by enhancing regulatory T cell responses in the Gut. *J. Immunol.* 202, 2095–2104. doi: 10.4049/jimmunol.1801446

Lee, H. L., Shen, H., Hwang, I. Y., Ling, H., Yew, W. S., Lee, Y. S., et al. (2018). Targeted approaches for in situ gut microbiome manipulation. *Genes* 9:E351. doi: 10.3390/genes9070351

Lee, H. R., Lee, S., Chaudhary, P. M., Gill, P., and Jung, J. U. (2010). Immune evasion by Kaposi's sarcoma-associated herpesvirus. *Future Microbiol.* 5, 1349–1365. doi: 10.2217/fmb.10.105

Lee, K. H., Gordon, A., Shedden, K., Kuan, G., Ng, S., and Balmaseda, A. (2019). The respiratory microbiome and susceptibility to influenza virus infection. *PLoS One* 14:e0207898. doi: 10.1371/journal.pone.0207898

Levitskaya, J., Coram, M., Levitsky, V., Imreh, S., Klein, G., and Kurilla, M. G. (1995). Inhibition of antigen processing by the internal repeat region of the Epstein-Barr virus nuclear antigen-1. *Nature* 375, 685–688. doi: 10.1038/375685a0

Li, C., Zhu, B., Son, Y. M., Wang, Z., Jiang, L., and Xiang, M. (2019). The transcription factor Bhlhe40 programs mitochondrial regulation of resident CD8(+) T cell fitness and functionality. *Immunity* 51, 491–507e7. doi: 10.1016/j.immuni.2019.08.013

Li, J., Chen, Q. Y., He, J., Li, Z. L., Tang, X. F., and Chen, S. P. (2015). Phase I trial of adoptively transferred tumor-infiltrating lymphocyte immunotherapy following concurrent chemoradiotherapy in patients with locoregionally advanced nasopharyngeal carcinoma. *OncoImmunology* 4:e976507. doi: 10.4161/23723556.2014.976507

Li, J., Wang, X., Diaz, J., Tsang, S. H., Buck, C. B., and You, J. (2013). Merkel cell polyomavirus large T antigen disrupts host genomic integrity and inhibits cellular proliferation. *J. Virol.* 87, 9173–9188. doi: 10.1128/JVI.01216-13

Liang, H., Fu, Z., Jiang, X., Wang, N., Wang, F., and Wang, X. (2015). miR-16 promotes the apoptosis of human cancer cells by targeting FEAT. *BMC Cancer* 15:448. doi: 10.1186/s12885-015-1458-1458

Lin, W. S., Jiao, B. Y., Wu, Y. L., Chen, W. N., and Lin, X. (2012). Hepatitis B virus X protein blocks filamentous actin bundles by interaction with eukaryotic translation elongat ion factor 1 alpha 1. *J. Med. Virol.* 84, 871–877. doi: 10.1002/jmv.23283

Lina, T. T., Alzahrani, S., Gonzalez, J., Pinchuk, I. V., Beswick, E. J., and Reyes, V. E. (2014). Immune evasion strategies used by *Helicobacter pylori*. *World J. Gastroenterol.* 20, 12753–12766. doi: 10.3748/wjg.v20.i36.12753

Liu, S., Hausmann, S., Carlson, S. M., Fuentes, M. E., Francis, J. W., and Pillai, R. (2019). METTL13 methylation of eEF1A increases translational output to promote Tumorigenesis. *Cell* 176, 491.e–504.e. doi: 10.1016/j.cell.2018.11.038

Loftus, D. J., Castelli, C., Clay, T. M., Squarcina, P., Marincola, F. M., and Nishimura, M. I. (1996). Identification of epitope mimics recognized by CTL reactive to the melanoma/melanocyte-derived peptide MART-1(27-35). *J. Exp. Med.* 184, 647–657. doi: 10.1084/jem.184.2.647

Lucke, K., Miehlke, S., Jacobs, E., and Schuppler, M. (2006). Prevalence of *Bacteroides* and *Prevotella* spp. in ulcerative colitis. *J. Med. Microbiol.* 55, 617–624. doi: 10.1099/jmm.0.46198-0

Luksza, M., Riaz, N., Makarov, V., Balachandran, V. P., Hellmann, M. D., and Solovyov, A. (2017). A neoantigen fitness model predicts tumour response to checkpoint blockade immunotherapy. *Nature* 551, 517–520. doi: 10.1038/nature24473

Luo, Y. H., Wu, C. H., Wu, W. S., Huang, C. Y., Su, W. J., and Tsai, C. M. (2012). Association between tumor epidermal growth factor receptor mutation and pulmonary *tuberculosis* in patients with adenocarcinoma of the lungs. *J. Thorac. Oncol.* 7, 299–305. doi: 10.1097/JTO.0b013e31823c588d

Magdy, A., Elhadidy, M., Abdallah, E., Thabet, W., Youssef, M., and Khafagy, W. (2015). Enteropathogenic *Escherichia coli* (EPEC): does it have a role in colorectal tumourigenesis? A prospective Cohort study. *Int. J. Surg.* 18, 169–173. doi: 10.1016/j.ijsu.2015.04.077

Maji, A., Misra, R., Dhakan, D. B., Gupta, V., Mahato, N. K., and Saxena, R. (2018). Gut microbiome contributes to impairment of immunity in pulmonary tuberculosis patients by alteration of butyrate and propionate producers. *Environ. Microbiol.* 20, 402–419. doi: 10.1111/1462-2920.14015

Manfredo Vieira, S., Hiltensperger, M., Kumar, V., Dehner, C., Khan, N., and Costa, F. R. C. (2018). Translocation of a gut pathobiont drives autoimmunity in mice and humans. *Science* 359, 1156–1161. doi: 10.1126/science.aar7201

Mangalam, A., Luckey, D., Basal, E., Behrens, M., Rodriguez, M., and David, C. (2008). HLA-DQ6 (DQB1*0601)-restricted T cells protect against experimental autoimmune encephalomyelitis in HLA-DR3.DQ6 double-transgenic mice by generating anti-inflammatory IFN-gamma. *J. Immunol.* 180, 7747–7756. doi: 10.4049/jimmunol.180.11.7747

Mangalam, A. K., Taneja, V., and David, C. S. (2013). HLA class II molecules influence susceptibility versus protection in inflammatory diseases by determining the cytokine profile. *J. Immunol.* 190, 513–518. doi: 10.4049/jimmunol.1201891

Martínez, A., Pacheco-Tena, C., Vázquez-Mellado, J., and Burgos-Vargas, R. (2004). Relationship between disease activity and infection in patients with spondyloarthropathies. *Ann. Rheum. Dis.* 63, 1338–1340. doi: 10.1136/ard.2003.011882

Martínez-López, M., Iborra, S., Mastrangelo, A., Danne, C., Mann, E. R., and Reid, D. M. (2019). Microbiota sensing by Mincle-Syk Axis in Dendritic cells regulates interleukin-17 and -22 production and promotes intestinal barrier integrity. *Immunity* 50, 446.e–461.e. doi: 10.1016/j.immuni.2018.12.020

Mathieu, E., Descamps, D., Cherbuy, C., Langella, P., Riffault, S., Remot, A., et al. (2018a). Paradigms of lung microbiota functions in health and disease, particularly, in Asthma. *Front. Physiol.* 9:1168. doi: 10.3389/fphys.2018.01168

Mathieu, E., Escribano-Vazquez, U., Descamps, D., Cherbuy, C., Langella, P., and Riffault, S. (2018b). Paradigms of lung microbiota functions in health and disease, particularly, in Asthma. *Front. Physiol.* 9:1168. doi: 10.3389/fphys.2018.01168

Matzaraki, V., Kumar, V., Wijmenga, C., and Zhernakova, A. (2017). The MHC locus and genetic susceptibility to autoimmune and infectious diseases. *Genome Biol.* 18, 76–76. doi: 10.1186/s13059-017-1207-1

Mayassi, T., Ladell, K., Gudjonson, H., McLaren, J. E., Shaw, D. G., and Tran, M. T. (2019). Chronic inflammation permanently reshapes tissue-resident immunity in Celiac disease. *Cell* 176, 967.e–981.e. doi: 10.1016/j.cell.2018.12.039

Mehta, M. M., Weinberg, S. E., and Chandel, N. S. (2017). Mitochondrial control of immunity: beyond ATP. *Nat. Rev. Immunol.* 17, 608–620. doi: 10.1038/nri.2017.66

Metwally, D. M., Al-Olayan, E. M., Alanazi, M., Alzahrany, S. B., and Semlali, A. (2018). Antischistosomal and anti-inflammatory activity of garlic and allicin compared with that of praziquantel in vivo. *BMC Complement Altern. Med.* 18:135. doi: 10.1186/s12906-018-2191-z

Michaud, M., Martins, I., Sukkurwala, A. Q., Adjemian, S., Ma, Y., and Pellegatti, P. (2011). Autophagy-dependent anticancer immune responses induced by

chemotherapeutic agents in mice. *Science* 334, 1573–1577. doi: 10.1126/science.1208347

Mignot, E., Hayduk, R., Black, J., Grumet, F. C., and Guilleminault, C. (1997). HLA DQB1*0602 is associated with cataplexy in 509 narcoleptic patients. *Sleep* 20, 1012–1020.

Mignot, E., Lin, L., Rogers, W., Honda, Y., Qiu, X. H., and Lin, X. Y. (2001). Complex HLA-DR and -DQ interactions confer risk of narcolepsy-cataplexy in three ethnic groups. *Am. J. Hum. Genet.* 68, 686–699. doi: 10.1086/318799

Miller, N. J., Church, C. D., Fling, S. P., Kulikauskas, R., Ramchurren, N., and Shinohara, M. M. (2018). Merkel cell polyomavirus-specific immune responses in patients with Merkel cell carcinoma receiving anti-PD-1 therapy. *J. Immunother. Cancer* 6:131. doi: 10.1186/s40425-018-0450-457

Milner, J. J., Toma, C., Yu, B., Zhang, K., Omilusik, K., and Phan, A. T. (2017). Runx3 programs CD8(+) T cell residency in non-lymphoid tissues and tumours. *Nature* 552, 253–257. doi: 10.1038/nature24993

Molinari, M., Salio, M., Galli, C., Norais, N., Rappuoli, R., Lanzavecchia, A., et al. (1998). Selective inhibition of Ii-dependent antigen presentation by *Helicobacter pylori* toxin VacA. *J. Exp. Med.* 187, 135–140. doi: 10.1084/jem.187.1.135

Moncayo, G., Lin, D., McCarthy, M. T., Watson, A. A., and O'Callaghan, C. A. (2017). MICA expression is regulated by cell adhesion and contact in a FAK/Src-dependent manner. *Front. Immunol.* 7:687. doi: 10.3389/fimmu.2016.00687

Mora-Garcia Mde, L., Duenas-Gonzalez, A., Hernandez-Montes, J., De la Cruz-Hernandez, E., Perez-Cardenas, E., Weiss-Steider, B., et al. (2006). Up-regulation of HLA class-I antigen expression and antigen-specific CTL response in cervical cancer cells by the demethylating agent hydralazine and the histone deacetylase inhibitor valproic acid. *J. Transl. Med.* 4:55. doi: 10.1186/1479-5876-4-55

Munck, C., Sheth, R. U., Freedberg, D. E., and Wang, H. H. (2018). Real-time capture of horizontal gene transfers from gut microbiota by engineered CRISPR-Cas acquisition. *bioRxiv* doi: 10.1101/492751 [Preprint].

Nagu, T. (2017).). *Improving Treatment Outcomes for Patients With Pulmonary Tuberculosis in Tanzania: Host and Pathogen Factors*. 64. Thesis, Karolinska Institutet, Stockholm.

Nam, Y. D., Jung, M. J., Roh, S. W., Kim, M. S., and Bae, J. W. (2011). Comparative analysis of Korean human gut microbiota by barcoded pyrosequencing. *PLoS One* 6:e22109. doi: 10.1371/journal.pone.0022109

Nasidze, I., Li, J., Quinque, D., Tang, K., and Stoneking, M. (2009). Global diversity in the human salivary microbiome. *Genome Res.* 19, 636–643. doi: 10.1101/gr.084616.108

Nikitina, I. Y., Panteleev, A. V., Kosmiadi, G. A., Serdyuk, Y. V., Nenasheva, T. A., and Nikolaev, A. A. (2018). Th1, Th17, and Th1Th17 lymphocytes during *Tuberculosis*: Th1 lymphocytes predominate and appear as low-differentiated CXCR3(+)CCR6(+) cells in the blood and highly differentiated CXCR3(±)CCR6(-) cells in the lungs. *J. Immunol.* 200, 2090–2103. doi: 10.4049/jimmunol.1701424

O'Dwyer, D. N., Dickson, R. P., and Moore, B. B. (2016). The lung microbiome, immunity and the pathogenesis of chronic lung disease. *J. Immunol.* 196, 4839–4847. doi: 10.4049/jimmunol.1600279

Ohkuma, T., Peters, S. A. E., and Woodward, M. (2018). Sex differences in the association between diabetes and cancer: a systematic review and meta-analysis of 121 cohorts including 20 million individuals and one million events. *Diabetologia* 61, 2140–2154. doi: 10.1007/s00125-018-4664-5

Olmstead, A. D., Knecht, W., Lazarov, I., Dixit, S. B., and Jean, F. (2012). Human subtilase SKI-1/S1P is a master regulator of the HCV Lifecycle and a potential host cell target for developing indirect-acting antiviral agents. *PLoS Pathog.* 8:e1002468. doi: 10.1371/journal.ppat.1002468

Osborne, L. C., Joyce, K. L., Alenghat, T., Sonnenberg, G. F., Giacomin, P. R., and Du, Y. (2013). Resistin-like molecule alpha promotes pathogenic Th17 cell responses and bacterial-induced intestinal inflammation. *J. Immunol.* 190, 2292–2300. doi: 10.4049/jimmunol.1200706

Paavonen, J. (2001). Chlamydia trachomatis and cancer. *Sex Transm. Infect.* 77, 154–156. doi: 10.1136/sti.77.3.154

Pagliari, M., Munari, F., Toffoletto, M., Lonardi, S., Chemello, F., and Codolo, G. (2017). *Helicobacter pylori* affects the antigen presentation activity of macrophages modulating the expression of the immune receptor CD300E through miR-4270. *Front. Immunol.* 8:1288. doi: 10.3389/fimmu.2017.01288

Pan, Y., Tian, T., Park, C. O., Lofftus, S. Y., Mei, S., and Liu, X. (2017). Survival of tissue-resident memory T cells requires exogenous lipid uptake and metabolism. *Nature* 543, 252–256. doi: 10.1038/nature21379

Pascal, V., Pozuelo, M., Borruel, N., Casellas, F., Campos, D., and Santiago, A. (2017). A microbial signature for Crohn's disease. *Gut* 66, 813–822. doi: 10.1136/gutjnl-2016-313235

Patel, A. L., Chen, X., Wood, S. T., Stuart, E. S., Arcaro, K. F., and Molina, D. P. (2014). Activation of epidermal growth factor receptor is required for *Chlamydia trachomatis* development. *BMC Microbiol.* 14:277. doi: 10.1186/s12866-014-0277-274

Pauken, K. E., Sammons, M. A., Odorizzi, P. M., Manne, S., Godec, J., and Khan, O. (2016). Epigenetic stability of exhausted T cells limits durability of reinvigoration by PD-1 blockade. *Science* 354, 1160–1165. doi: 10.1126/science.aaf2807

Paulson, K. G., Carter, J. J., Johnson, L. G., Cahill, K. W., Iyer, J. G., and Schrama, D. (2010). Antibodies to merkel cell polyomavirus T antigen oncoproteins reflect tumor burden in merkel cell carcinoma patients. *Cancer Res.* 70, 8388–8397. doi: 10.1158/0008-5472.CAN-10-2128

Paulson, K. G., Lewis, C. W., Redman, M. W., Simonson, W. T., Lisberg, A., and Ritter, D. (2017). Viral oncoprotein antibodies as a marker for recurrence of Merkel cell carcinoma: a prospective validation study. *Cancer* 123, 1464–1474. doi: 10.1002/cncr.30475

Philip, M., Fairchild, L., Sun, L., Horste, E. L., Camara, S., and Shakiba, M. (2017). Chromatin states define tumour-specific T cell dysfunction and reprogramming. *Nature* 545, 452–456. doi: 10.1038/nature22367

Pizzolla, A., Nguyen, T. H., Sant, S., Jaffar, J., Loudovaris, T., and Mannering, S. I. (2018). Influenza-specific lung-resident memory T cells are proliferative and polyfunctional and maintain diverse TCR profiles. *J. Clin. Invest.* 128, 721–733. doi: 10.1172/JCI96957

Pourfarziani, V., Einollahi, B., Taheri, S., Nemati, E., Nafar, M., and Kalantar, E. (2007). Associations of Human Leukocyte Antigen (HLA) haplotypes with risk of developing lymphoproliferative disorders after renal transplantation. *Ann. Transplant.* 12, 16–22.

Pragman, A. A., Lyu, T., Baller, J. A., Gould, T. J., Kelly, R. F., and Reilly, C. S. (2018). The lung tissue microbiota of mild and moderate chronic obstructive pulmonary disease. *Microbiome* 6:7. doi: 10.1186/s40168-017-0381-384

Quinn, L. L., Williams, L. R., White, C., Forrest, C., Zuo, J., and Rowe, M. (2015). The missing link in epstein-barr virus immune evasion: the BDLF3 gene induces ubiquitination and downregulation of major histocompatibility complex class I (MHC-I) and MHC-II. *J. Virol.* 90, 356–367. doi: 10.1128/JVI.02183-15

Rao, M., Valentini, D., Zumla, A., and Maeurer, M. (2018). Evaluation of the efficacy of valproic acid and suberoylanilide hydroxamic acid (vorinostat) in enhancing the effects of first-line tuberculosis drugs against intracellular *Mycobacterium tuberculosis*. *Int. J. Infect. Dis.* 69, 78–84. doi: 10.1016/j.ijid.2018.02.021

Riquelme, E., Zhang, Y., Zhang, L., Montiel, M., Zoltan, M., and Dong, W. (2019). Tumor microbiome diversity and composition influence pancreatic cancer outcomes. *Cell* 178:e12. doi: 10.1016/j.cell.2019.07.008

Robey, R. C., Mletzko, S., and Gotch, F. M. (2011). The T-cell immune response against Kaposi's sarcoma-associated herpesvirus. *Adv. Virol.* 2010:e340356.

Roy, S., and Trinchieri, G. (2017). Microbiota: a key orchestrator of cancer therapy. *Nat. Rev. Cancer* 17, 271–285. doi: 10.1038/nrc.2017.13

Saha, A., and Robertson, E. S. (2011). Epstein-Barr virus-associated B-cell lymphomas: pathogenesis and clinical outcomes. *Clin. Cancer Res* 17, 3056–3063. doi: 10.1158/1078-0432.ccr-10-2578

Sakakibara, S., and Tosato, G. (2011). Viral interleukin-6: role in Kaposi's sarcoma-associated herpesvirus: associated malignancies. *J. Interf. Cytokine Res.* 31, 791–801. doi: 10.1089/jir.2011.0043

Sangro, B., Inarrairaegui, M., Garralda, E., Barrera, P., Larrea, E., and Alfaro, C. (2013). A clinical trial of CTLA-4 blockade with tremelimumab in patients with hepatocellular carcinoma and chronic hepatitis C. *J. Hepatol.* 59, 81–88. doi: 10.1016/j.jhep.2013.02.022

Sayasone, S., Meister, I., Andrews, J. R., Odermatt, P., Vonghachack, Y., and Xayavong, S. (2017). Efficacy and safety of praziquantel against light infections of *Opisthorchis viverrini*: a randomized parallel single-blind dose-ranging trial. *Clin. Infect. Dis.* 64, 451–458. doi: 10.1093/cid/ciw785

Schachter, J., Martel, J., Lin, C. S., Chang, C. J., Wu, T. R., Lu, C. C., et al. (2018). Effects of obesity on depression: a role for inflammation and the gut microbiota. *Brain Behav. Immun.* 69, 1–8. doi: 10.1016/j.bbi.2017.08.026

Scheper, W., Kelderman, S., Fanchi, L. F., Linnemann, C., Bendle, G., and Hirt, C. (2019). Low and variable tumor reactivity of the intratumoral TCR repertoire in human cancers. *Nat. Med.* 25, 89–94. doi: 10.1038/s41591-018-0266-5

Schreurs, R., Baumdick, M. E., Sagebiel, A. F., Kaufmann, M., Mokry, M., and Klarenbeek, P. L. (2019). Human fetal TNF-alpha-Cytokine-producing CD4(+) effector memory T cells promote intestinal development and mediate inflammation early in life. *Immunity* 50:e8. doi: 10.1016/j.immuni.2018.12.010

Shannon-Lowe, C., Rickinson, A. B., and Bell, A. I. (2017). Epstein-Barr virus-associated lymphomas. *Philos. Trans. R. Soc. Lond. B Biol. Sci.* 372:20160271. doi: 10.1098/rstb.2016.0271

Shichiri, M., Fukai, N., Kono, Y., and Tanaka, Y. (2009). Rifampicin as an oral angiogenesis inhibitor targeting Hepatic cancers. *Cancer Res.* 69, 4760–4768. doi: 10.1158/0008-5472.CAN-08-3417

Shichiri, M., and Tanaka, Y. (2010). Inhibition of cancer progression by rifampicin: involvement of antiangiogenic and anti-tumor effects. *Cell Cycle* 9, 64–68. doi: 10.4161/cc.9.1.10354

Shuda, M., Feng, H., Kwun, H. J., Rosen, S. T., Gjoerup, O., Moore, P. S., et al. (2008). T antigen mutations are a human tumor-specific signature for Merkel cell polyomavirus. *Proc. Natl. Acad. Sci. U.S.A.* 105, 16272–16277. doi: 10.1073/pnas.0806526105

Siebold, C., Hansen, B. E., Wyer, J. R., Harlos, K., Esnouf, R. E., and Svejgaard, A. (2004). Crystal structure of HLA-DQ0602 that protects against type 1 diabetes and confers strong susceptibility to narcolepsy. *Proc. Natl. Acad. Sci. U.S.A.* 101, 1999–2004. doi: 10.1073/pnas.0308458100

Simoni, Y., Becht, E., Fehlings, M., Loh, C. Y., Koo, S. L., and Teng, K. W. W. (2018). Bystander CD8(+) T cells are abundant and phenotypically distinct in human tumour infiltrates. *Nature* 557, 575–579. doi: 10.1038/s41586-018-0130-2

Sistigu, A., Viaud, S., Chaput, N., Bracci, L., Proietti, E., and Zitvogel, L. (2011). Immunomodulatory effects of cyclophosphamide and implementations for vaccine design. *Semin. Immunopathol.* 33, 369–383. doi: 10.1007/s00281-011-0245-0

Sripa, B., Brindley, P. J., Mulvenna, J., Laha, T., Smout, M. J., and Mairiang, E. (2012). The tumorigenic liver fluke *Opisthorchis viverrini*–multiple pathways to cancer. *Trends Parasitol.* 28, 395–407. doi: 10.1016/j.pt.2012.07.006

Sripa, B., Kaewkes, S., Sithithaworn, P., Mairiang, E., Laha, T., and Smout, M. (2007). Liver fluke induces cholangiocarcinoma. *PLoS Med.* 4:e201. doi: 10.1371/journal.pmed.0040201

Starrett, G. J., Marcelus, C., Cantalupo, P. G., Katz, J. P., Cheng, J., and Akagi, K. (2017). merkel cell polyomavirus exhibits dominant control of the tumor genome and transcriptome in virus-associated Merkel cell carcinoma. *mBio* 8:02079-2016. doi: 10.1128/mBio.02079-2016

Stecher, C. W., Fofana, H. K. M., Madsen, H., Wilson, S., Keita, A. D., and Landoure, A. (2017). Inflammation dynamics after praziquantel treatment of Schistosoma haematobium reflected by urinary eosinophil cationic protein. *Trans. R. Soc. Trop. Med. Hyg.* 111, 316–324. doi: 10.1093/trstmh/trx057

Stevanovic, S., Draper, L. M., Langhan, M. M., Campbell, T. E., Kwong, M. L., and Wunderlich, J. R. (2015). Complete regression of metastatic cervical cancer after treatment with human papillomavirus-targeted tumor-infiltrating T cells. *J. Clin. Oncol.* 33, 1543–1550. doi: 10.1200/JCO.2014.58.9093

Strickler, H. D., Goedert, J. J., Bethke, F. R., Trubey, C. M., Palefsky, J., and Whitman, J. E. (1999). Human herpesvirus 8 cellular immune responses in homosexual men. *J. Infect. Dis.* 180, 1682–1685. doi: 10.1086/315056

Sun, B., and Karin, M. (2012). Obesity, inflammation, and liver cancer. *J. Hepatol.* 56, 704–713. doi: 10.1016/j.jhep.2011.09.020

Szender, J. B., Eng, K. H., Matsuzaki, J., Miliotto, A., Gnjatic, S., and Tsuji, T. (2016). HLA superfamily assignment is a predictor of immune response to cancer testis antigens and survival in ovarian cancer. *Gynecol. Oncol.* 142, 158–162. doi: 10.1016/j.ygyno.2016.04.017

Tadmor, T., Aviv, A., and Polliack, A. (2011). Merkel cell carcinoma, chronic lymphocytic leukemia and other lymphoproliferative disorders: an old bond with possible new viral ties. *Ann. Oncol.* 22, 250–256. doi: 10.1093/annonc/mdq308

Tafti, M., Lammers, G. J., Dauvilliers, Y., Overeem, S., Mayer, G., and Nowak, J. (2016). Narcolepsy-associated HLA class i alleles implicate cell-mediated cytotoxicity. *Sleep* 39, 581–587. doi: 10.5665/sleep.5532

Takahashi, A., Tokita, H., Takahashi, K., Takeoka, T., Murayama, K., and Tomotsune, D. (2011). A novel potent tumour promoter aberrantly overexpressed in most human cancers. *Sci. Rep.* 1:15. doi: 10.1038/srep00015

Teng, G. G., Wang, W. H., Dai, Y., Wang, S. J., Chu, Y. X., and Li, J. (2013). Let-7b is involved in the inflammation and immune responses associated with *Helicobacter pylori* infection by targeting toll-like receptor 4. *PLoS One* 8:e56709. doi: 10.1371/journal.pone.0056709

Theiss, J. M., Gunther, T., Alawi, M., Neumann, F., Tessmer, U., and Fischer, N. (2015). A comprehensive analysis of replicating merkel cell Polyomavirus genomes delineates the viral transcription program and suggests a role for mcv-miR-M1 in episomal persistence. *PLoS Pathog.* 11:e1004974. doi: 10.1371/journal.ppat.1004974

Tian, C., Hromatka, B. S., Kiefer, A. K., Eriksson, N., Noble, S. M., and Tung, J. Y. (2017). Genome-wide association and HLA region fine-mapping studies identify susceptibility loci for multiple common infections. *Nat. Commun.* 8:599. doi: 10.1038/s41467-017-00257-255

Trabert, B., Waterboer, T., Idahl, A., Brenner, N., Brinton, L. A., and Butt, J. (2019). Antibodies against *Chlamydia trachomatis* and ovarian cancer risk in two independent populations. *J. Natl. Cancer Inst.* 111, 129–136. doi: 10.1093/jnci/djy084

Triozzi, P. L., and Fernandez, A. P. (2013). The role of the immune response in merkel cell carcinoma. *Cancers* 5, 234–254. doi: 10.3390/cancers5010234

Tsao, S. W., Tsang, C. M., and Lo, K. W. (2017). Epstein-Barr virus infection and nasopharyngeal carcinoma. *Philos. Trans. R. Soc. Lond. B Biol. Sci.* 372, 20160270. doi: 10.1098/rstb.2016.0270

Tsukerman, P., Stern-Ginossar, N., Gur, C., Glasner, A., Nachmani, D., and Bauman, Y. (2012). MiR-10b downregulates the stress-induced cell surface molecule MICB, a critical ligand for cancer cell recognition by natural killer cells. *Cancer Res.* 72, 5463–5472. doi: 10.1158/0008-5472.CAN-11-2671

Tynan, F. E., Elhassen, D., Purcell, A. W., Burrows, J. M., Borg, N. A., and Miles, J. J. (2005). The immunogenicity of a viral cytotoxic T cell epitope is controlled by its MHC-bound conformation. *J. Exp. Med.* 202, 1249–1260. doi: 10.1084/jem.20050864

Tzellos, S., and Farrell, P. J. (2012). Epstein-barr virus sequence variation-biology and disease. *Pathogens* 1, 156–174. doi: 10.3390/pathogens1020156

Vase, M. Ø, Maksten, E. F., Strandhave, C., Søndergaard, E., Bendix, K., and Hamilton-Dutoit, S. (2015). HLA associations and risk of posttransplant lymphoproliferative disorder in a Danish population-based cohort. *Transpl. Direct* 1:e25. doi: 10.1097/TXD.0000000000000534

Victora, C. G., Bahl, R., Barros, A. J. D., Horton, S., Krasevec, J., and Murch, S. (2016). Breastfeeding in the 21st century: epidemiology, mechanisms, and lifelong effect. *Lancet* 387, 475–490. doi: 10.1016/S0140-6736(15)01024-7

Wan, Y. Y. (2014). GATA3: a master of many trades in immune regulation. *Trends Immunol.* 35, 233–242. doi: 10.1016/j.it.2014.04.002

Wong, S. Q., Waldeck, K., Vergara, I. A., Schroder, J., Madore, J., and Wilmott, J. S. (2015). UV-associated mutations underlie the etiology of MCV-negative merkel cell carcinomas. *Cancer Res.* 75, 5228–5234. doi: 10.1158/0008-5472.CAN-15-1877

Wroblewski, L. E., Peek, R. M. Jr., and Wilson, K. T. (2010). *Helicobacter pylori* and gastric cancer: factors that modulate disease risk. *Clin. Microbiol. Rev.* 23, 713–739. doi: 10.1128/CMR.00011-10

Yang, D., Chen, X., Wang, J., Lou, Q., Lou, Y., and Li, L. (2019). Dysregulated lung commensal bacteria drive Interleukin-17B production to promote pulmonary Fibrosis through their outer membrane vesicles. *Immunity* 50, 692–706. doi: 10.1016/j.immuni.2019.02.001

Yap, G. C., Chee, K. K., Hong, P. Y., Lay, C., Satria, C. D., and Shek, L. P. C. (2011). Evaluation of stool microbiota signatures in two cohorts of Asian (Singapore and Indonesia) newborns at risk of atopy. *BMC Microbiol.* 11:193. doi: 10.1186/1471-2180-11-193

Yatsunenko, T., Rey, F. E., Manary, M. J., Trehan, I., Contreras, M., and Magris, M. (2012). Human gut microbiome viewed across age and geography. *Nature* 486, 222–227. doi: 10.1038/nature11053

Yoon, S. I., Jones, B. C., Logsdon, N. J., Harris, B. D., Kuruganti, S., and Walter, M. R. (2012). Epstein-Barr virus IL-10 engages IL-10R1 by a two-step

mechanism leading to altered signaling properties. *J. Biol. Chem.* 287, 26586–26595. doi: 10.1074/jbc.M112.376707

Yoshimoto, S., Loo, T. M., Atarashi, K., Kanda, H., Sato, S., and Oyadomari, S. (2013). Obesity-induced gut microbial metabolite promotes liver cancer through senescence secretome. *Nature* 499, 97–101. doi: 10.1038/nature12347

Yost, K. E., Satpathy, A. T., Wells, D. K., Qi, Y., Wang, C., and Kageyama, R. (2019). Clonal replacement of tumor-specific T cells following PD-1 blockade. *Nat. Med.* 25, 1251–1259. doi: 10.1038/s41591-019-0522-3

Yue, J., Shukla, R., Accardi, R., Siouda, M., Cros, M. P., and Krutovskikh, V. (2011). Cutaneous human papillomavirus type 38 E7 regulates actin cytoskeleton structure for increasing cell proliferation through CK2 and the eukaryotic elongation factor 1A. *J. Virol.* 85, 8477–8494. doi: 10.1128/JVI.02561-10

Zehbe, I., Hohn, H., Pilch, H., Neukirch, C., Freitag, K., and Maeurer, M. J. (2005). Differential MHC class II component expression in HPV-positive cervical cancer cells: implication for immune surveillance. *Int. J. Cancer* 117, 807–815. doi: 10.1002/ijc.21226

Zheng, L., Kelly, C. J., Battista, K. D., Schaefer, R., Lanis, J. M., and Alexeev, E. E. (2017). Microbial-derived butyrate promotes epithelial barrier function through IL-10 receptor-dependent repression of Claudin-2. *J. Immunol.* 199, 2976–2984. doi: 10.4049/jimmunol.1700105

Zhou, Y., Cui, Z., Zhou, X., Chen, C., Jiang, S., and Hu, Z. (2013). The presence of old pulmonary tuberculosis is an independent prognostic factor for squamous cell lung cancer survival. *J. Cardiothorac. Surg.* 8:123. doi: 10.1186/1749-8090-8-123

Zimmermann, M., Zimmermann-Kogadeeva, M., Wegmann, R., and Goodman, A. L. (2019). Separating host and microbiome contributions to drug pharmacokinetics and toxicity. *Science* 363:eaat9931. doi: 10.1126/science.aat9931

Zumla, A., Rao, M., Parida, S. K., Keshavjee, S., Cassell, G., and Wallis, R. (2015). Inflammation and tuberculosis: host-directed therapies. *J. Intern. Med.* 277, 373–387. doi: 10.1111/joim.12256

Conflict of Interest: The authors declare that the research was conducted in the absence of any commercial or financial relationships that could be construed as a potential conflict of interest.

frontiers in Cell and Developmental Biology

ORIGINAL RESEARCH
published: 03 June 2020
doi: 10.3389/fcell.2020.00421

Hepatitis B e Antigen Induces NKG2A$^+$ Natural Killer Cell Dysfunction via Regulatory T Cell-Derived Interleukin 10 in Chronic Hepatitis B Virus Infection

Qingqing Ma[1†], Xiaoyu Dong[2†], Siyu Liu[1], Tao Zhong[3], Dandan Sun[1], Lu Zong[1], Changcheng Zhao[4], Qiong Lu[1], Min Zhang[1], Yufeng Gao[5], Ying Ye[5], Jun Cheng[5], Yuanhong Xu[1] and Meijuan Zheng[1]**

[1] Department of Clinical Laboratory, The First Affiliated Hospital of Anhui Medical University, Hefei, China, [2] Department of Clinical Laboratory, Chaohu Hospital of Anhui Medical University, Chaohu, China, [3] Department of Blood Transfusion, The First Affiliated Hospital of Anhui Medical University, Hefei, China, [4] Department of Life Sciences and Medicine, The First Affiliated Hospital, University of Science and Technology of China, Hefei, China, [5] Department of Infectious Diseases, The First Affiliated Hospital, Anhui Medical University, Hefei, China

OPEN ACCESS

Edited by:
Giulia De Falco,
Queen Mary University of London,
United Kingdom

Reviewed by:
Taro Yamashita,
Kanazawa University, Japan
Ye Zhang,
Tangdu Hospital, China

***Correspondence:**
Yufeng Gao
aygyf@126.com
Meijuan Zheng
mjzheng@yahoo.com

† These authors have contributed equally to this work

Specialty section:
This article was submitted to Molecular Medicine, a section of the journal Frontiers in Cell and Developmental Biology

Received: 07 January 2020
Accepted: 06 May 2020
Published: 03 June 2020

Citation:
Ma Q, Dong X, Liu S, Zhong T, Sun D, Zong L, Zhao C, Lu Q, Zhang M, Gao Y, Ye Y, Cheng J, Xu Y and Zheng M (2020) Hepatitis B e Antigen Induces NKG2A$^+$ Natural Killer Cell Dysfunction via Regulatory T Cell-Derived Interleukin 10 in Chronic Hepatitis B Virus Infection. Front. Cell Dev. Biol. 8:421. doi: 10.3389/fcell.2020.00421

Although persistent hepatitis B virus (HBV) infection is associated with natural killer (NK) cell dysfunction, it remains obscure whether HBV viral antigens are responsible for NK cell dysfunction in patients with chronic hepatitis B (CHB) infection. In this study, we found that the percentage of NK cells expressing the inhibitory receptor, NKG2A, was increased in CHB patients, and NKG2A blockade restored NK cell function. Furthermore, in CHB patients, the frequency of NK cells expressing NKG2A positively correlated with the number of regulatory T cells (Tregs) and production of interleukin-10 (IL-10) in these Tregs. Moreover, exposure of peripheral blood mononuclear cells (PBMCs) isolated from healthy controls to sera from CHB patients resulted in increased proportion of NKG2A$^+$ NK cells; IL-10 blockade reduced the frequency of NKG2A$^+$ NK cells while increasing the percentage of IFN-γ^+ NK cells. In addition, stimulation of NK cells and Tregs from healthy controls with CHB sera together with anti-IL-10 antibody increased IFN-γ production in the culture supernatant. The frequencies of NKG2A$^+$ NK cells and IL-10$^+$ Tregs, along with serum levels of alanine transferase and HBV DNA, were significantly increased in CHB patients positive for the Hepatitis B e antigen (HBeAg, a marker of viral replication) when compared to HBeAg-negative CHB patients. Importantly, exposure of PBMCs from healthy controls to HBeAg resulted in increased IL-10 production but reduced levels of TNF and IFN-γ, and IL-10 blockade rescued the generation of TNF and IFN-γ in this assay. The reduced production of TNF and IFN-γ was also observed in NK cells and Tregs from healthy controls that were stimulated with HBeAg, while IL-10 blockade increased the secretion of these two cytokines. We conclude that HBeAg induces IL-10 production in Tregs, thereby leading to increased expression of NKG2A on NK cells, which contributes to NK cell dysfunction during CHB infection. These data suggest that HBeAg is associated with NK cell dysfunction in CHB.

Keywords: hepatitis B e antigen, HBV, NK cell, NKG2A, IL-10

INTRODUCTION

Hepatitis B virus (HBV) infection is a major public health problem worldwide and individuals with chronic HBV (CHB) infection are at high-risk for the development of cirrhosis and hepatocellular carcinoma (HCC) (Lozano et al., 2012; Maini and Peppa, 2013; Tian et al., 2013). CHB is associated with ineffective antiviral immune responses (Dienstag, 2008; Li et al., 2015), and accumulating evidence supports a relationship between CHB infection and impaired natural killer (NK) cell cytotoxicity and cytokine secretion (Martinet et al., 2012; Zheng et al., 2018). Despite this association, the mechanisms involved in NK cell dysfunction in CHB patients are yet to be clarified.

NK cells are the predominant lymphocyte subpopulation in the liver, constituting ∼31% of intrahepatic lymphocytes (Racanelli and Rehermann, 2006; Peng et al., 2016). NK cell activity is regulated by the combination of activating and inhibitory receptors they express (Long et al., 2013; Zheng et al., 2018; El-Deeb et al., 2019). The chronic viral infection is associated with increased expression of inhibitory receptors on NK cells, which correlates with a poor decline in viral titers after therapy (Golden-Mason et al., 2011; Rehermann, 2013). Recently, NKG2A has been reported as a marker of NK exhaustion in the hepatitis C virus infection and it contributes to viral persistence (Zhang et al., 2019). During HBV infection, the expression of NKG2A on NK cells is elevated in patients with active CHB, and blocking NKG2A signaling increases NK cell cytotoxicity *in vitro* (Li et al., 2013). Furthermore, high levels of NKG2A expression on NK cells leads to NK cell exhaustion and is associated with poor prognosis for patients with HCC (Sun et al., 2017). Anti-NKG2A treatment has been suggested to enhance NK cell activity in cancer vaccinations (Haanen and Cerundolo, 2018).

Increased regulatory T cells (Tregs) and interleukin 10 (IL-10) levels in the circulation are associated with weak T cell responses in patients with CHB (Park et al., 2016). Tregs can inhibit NK and $CD8^+$ T cell antiviral capacity through their secretion of IL-10 (Trehanpati and Vyas, 2017). Furthermore, high levels of IL-10 in patients with CHB inhibit IFN-γ production in NK cells (Peppa et al., 2010), and intrahepatic IL-10 contributes to the hyporesponsive state of $NKG2A^+Ly49^-$ NK cells in the liver (Lassen et al., 2010). Li et al. also found that hepatic Tregs contribute to NKG2A expression on murine NK cells, suggesting that reagents designed to block NKG2A signaling have considerable potential for application in the treatment of CHB infection (Li et al., 2013). Moreover, Hepatitis B e antigen (HBeAg, a marker of viral replication) has an important role in viral persistence, and is associated with dysfunctional T cell responses in patients with CHB infection (Tian et al., 2016; Yang et al., 2019), however, it is not clear whether viral factors are involved in the dysfunction of $NKG2A^+$ NK cells in patients with CHB.

In this study, we found that increased percentages of $NKG2A^+$ NK cells in peripheral blood correlated with HBV-DNA titers and that blocking NKG2A could restore the function of NK cells isolated from patients with CHB *in vitro*. We also observed a positive correlation between $NKG2A^+$ NK cells and $IL\text{-}10^+$ Tregs in patients with CHB. Moreover, exposure of peripheral blood mononuclear cells (PBMCs) or purified NK cells isolated from healthy controls to CHB sera resulted in impaired NK cell function. Meanwhile, HBeAg-positive patients had higher frequencies of $NKG2A^+$ NK cells and Tregs than those who were HBeAg-negative. Our data demonstrate that HBeAg can induce IL-10 secretion in Tregs and that blocking IL-10 enhances NK cell function. Overall, our findings delineate a possible mechanism underlying the dysfunction of $NKG2A^+$ NK cells in HBeAg-positive CHB patients and suggest that the HBeAg-IL-10-$NKG2A^+$ NK cell axis is a potential therapeutic target in CHB patients.

MATERIALS AND METHODS

Patients and Healthy Controls

The results reported in this study were generated from 69 patients with active CHB who had not received antiviral therapy, and 37 age- and sex-matched healthy controls (HCs). In addition, 15 patients with CHB post-therapy were recruited, and this group of patients were treated with entecavir (0.5 mg per day) for 6 months. All patients with CHB were characterized by serum alanine transferase (ALT) levels > 61 U/L and HBV-DNA levels > 2000 U/L, and none had overlapping infections with other hepatitis viruses, drug-induced hepatitis, alcoholic hepatitis, tumors, or autoimmune liver diseases. PBMCs were isolated from fresh blood using human peripheral blood lymphocyte isolation fluid (TBD Science, #LTS1077). The characteristics of enrolled patients with CHB and healthy controls, based on whole blood staining, are summarized in **Table 1**. All patients were diagnosed with CHB and all healthy donors were free from viral hepatitis, autoimmune hepatitis, and tumors. This study was approved by the local ethics committee of The First Affiliated Hospital of Anhui Medical University and the local ethics committee of Chaohu Hospital of Anhui Medical University.

Purification of Cells

NK cells were purified using a human NK cell Isolation Kit (Miltenyi Biotec, 130-092-957) and $CD4^+CD25^+$ Tregs were purified using a human $CD4^+CD25^+$ Regulatory T Cell Isolation

TABLE 1 | Clinical characteristics of enrolled subjects.

Clinical characteristics	CHB-actives	Healthy controls
Case	69	37
Sex (male)	50 (62.5%)	22 (59.5%)
Age, year [mean ± SEM]	39.4 ± 1.4	40.7 ± 1.9
ALT, U/L [mean ± SEM]	363.4 ± 56.5	23.2 ± 2.1
HBV DNA, U/m l [mean ± SEM]	(5.27 ± 1.02) E + 7	n.a.
HBsAg positive	69/69	n.a.
HBeAg positive	40/69	n.a.

SEM, standard error of mean; n.a., not applicable.

Kit (Miltenyi Biotec, 130-091-301). Cell purity was determined by flow cytometry and was > 90%.

Antibodies and Flow Cytometry

PBMCs isolated from fresh blood or cultured cells were stained with the following mouse anti-human antibodies: PerCP-Cy5.5-conjugated CD3, BV605 CD3, BV605 CD56, FITC CD56, PE TRAIL, PE NKP30, APC KIR3DL1, APC NKP46, APC CD244, FITC CD4, APC CD25, APC GranzymeB, FITC IFN-γ, PE TNF, and PE IL-10 (BD Biosciences); PE NKG2A, APC NKG2A, and FITC NKG2A (Miltenyi Biotec), and Alexa Flour 660 FoxP3 (eBioscience), and FITC Eomes (Thermo Fisher Scientific). A BD FACSCanto flow cytometer was used to assess stained cells and data were analyzed using Flowjo software VX (TreeStar, United States).

To analyze intracellular IFN-γ and IL-10 secretion, cells were stimulated with medium containing 10% fetal bovine serum (FBS; Gibco) with 50 ng/ml phorbol 12-myristate 13-acetate (Sigma-Aldrich), 50 ng/ml ionomycin (Merck Millipore), and 50 ng/ml monensin (Sigma-Aldrich), concurrently for 4 h. Then, cells were fixed and then permeabilized and stained with FITC mouse anti-human IFN-γ or PE mouse anti-human IL-10.

Cytometric Bead Array

Cytokines in serum and culture supernatant samples were analyzed by cytometric bead array (CBA) using a human Th1/Th2 Cytokine Kit II (BD Biosciences, 551809). Samples (50 μl) or standard recombinant protein dilutions were added to a mixture of cytokine beads (IL- 2, IL-4, IL-6, IL-10, TNF, and IFN-γ) and PE-conjugated detection reagent. After 3 h, capture beads were washed using CBA buffer and detected by flow cytometry (BD FACSCalibur), and cytokine concentrations quantified for each sample using recombinant standards and analysis software.

Serological Testing

Serum ALT was determined using an automatic biochemical analyzer (Cobas 8000, Roche Diagnostics GmbH, Switzerland). For the measurement of HBsAg and HBeAg, samples were analyzed using commercial enzyme immunoassay kits (Zhongshan Bio-Tech, China). The serum HBV DNA level was quantified using a real-time PCR machine (Roche LightCycler480, Switzerland). The above indicators were measured in The First Affiliated Hospital of Anhui Medical University.

In vitro Culture Systems

PBMC Culture System

A total of 2×10^5 PBMCs from patients with CHB were cultured in DMEM (HyClone SH30022.01) supplemented with 10% FBS and IL-2 (100 IU/ml), in the presence of an anti-human NKG2A blocking antibody (CloneZ199, Beckman Coulter, United States) or control IgG (BD Biosciences) at 37°C in 24-well plates. After 7 days, the phenotype and function of NK cells were analyzed by flow cytometry.

PBMCs (2×10^5) isolated from healthy donors were seeded into 24-well plates in DMEM in 20% serum from healthy controls containing 100 IU/ml IL-2, then 500 ng/ml HBeAg (Prospec, HBV272) was added into the wells and cells were cultured for 7 days at 37°C. In the presence of HBeAg, 50 ng/ml anti-human IL-10 neutralizing antibody (Clone25209, R&D, United States) or control IgG (BD Biosciences) was added. The intracellular cytokine in NK cells and the cytokine secreted in the supernatant were measured by flow cytometry.

Co-culture System

NK cells (5×10^4) and autologous $CD4^+CD25^+$ Tregs (5×10^4) purified from healthy donors were cultured with 20% serum from patients with CHB and 50 ng/ml anti-IL-10 neutralizing antibody or control IgG in DMEM containing 100 IU/ml IL-2 for 3 days at 37°C in 96-well plates. The cytokine in the supernatant was measured by flow cytometry after culture.

Purified NK cells (5×10^4) and autologous Tregs (5×10^4) from healthy controls at a 1:1 ratio were co-cultured in DMEM supplemented with 10% FBS and IL-2 (100 IU/ml), with or without 500 ng/ml HBeAg and 50 ng/ml anti-IL-10 or control IgG, in the presence of 50 ng/ml anti-CD3 and 50 ng/ml anti-CD28 (BD Bioscience) for 3 days. NK cells were stained for intracellular expression of IFN-γ and the expression of cytokines in culture supernatant measured by CBA analysis. Cells were cultured in 96-well plates.

Statistical Analysis

All data are expressed as the mean ± SEM and were analyzed using GraphPad Prism 5.0 software. The independent samples *t*-test was used to evaluate quantitative variables. Correlation analysis was by Pearson analysis. Significant differences were defined as $P < 0.05$.

RESULTS

Increased Expression of the Inhibitory Receptor, NKG2A, on Circulating NK Cells in Patients With CHB Infection

To investigate the NK cell phenotype, we analyzed the expression of activating (NKP30, NKP46, NKG2D, and CD244) and inhibitory (KIR3DL1, NKG2A) receptors on NK cells in the peripheral blood of patients with CHB and healthy controls, respectively. Gating strategies of lymphocytes and NK cells were showed in **Supplementary Figure S1**. Expression of inhibitory receptor, NKG2A, was significantly increased in patients with CHB compared with healthy donors, while there was no difference in the expression of other NK cell receptors, including KIR3DL1, NKP46, NKP30, CD244, and NKG2D (**Figures 1A,B**) between patients with CHB and healthy controls. Furthermore, both the mean fluorescence intensity and the absolute number of $NKG2A^+$ NK cells were higher in peripheral blood from patients with CHB relative to healthy controls (**Figures 1C,D**), however, there was no significant difference in NKG2A expression on $CD8^+$ T cells in patients with CHB compared with healthy controls (**Supplementary Figures S2A,B**). Moreover, in patients with CHB who had received effective antiviral treatment (entecavir, 0.5 mg per day for 6 months), NKG2A levels on NK cells were significantly reduced (**Figures 1E,F**), and serum

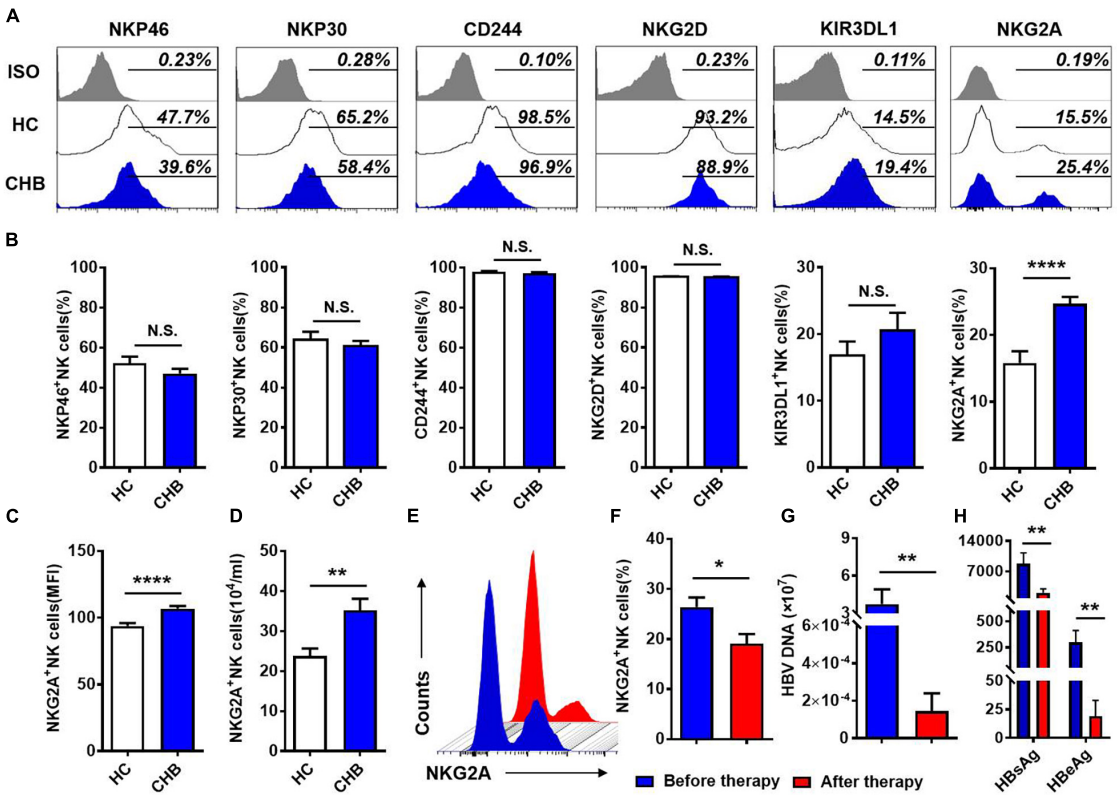

FIGURE 1 | NKG2A expression is increased on circulating NK cells in patients with CHB. **(A)** NKG2A expression is increased on circulating NK cells in patients with CHB. **(A)** Representative flow cytometry plots showing expression of NKG2A, KIR3DL1, NKP46, NKP30, CD244, NKG2D, and their isotype controls on peripheral NK cells from patients with CHB and healthy controls. **(B)** Comparison of the percentages of receptors in **(A)** expressed on peripheral NK cells in patients with CHB. **(C)** Mean fluorescence intensity (MFI) of NKG2A expression on peripheral NK cells in patients with CHB and healthy controls. **(D)** Absolute numbers of NKG2A + NK cells in peripheral blood samples from patients with CHB and healthy controls. z Representative flow cytometry plots showing NKG2A expression on peripheral NK cells from patients with CHB before and after antiviral therapy. **(F)** The percentage of NKG2A + NK cells in CHB patients before therapy and after therapy. **(G)** The HBV-DNA titers of CHB patients before therapy and after therapy. **(H)** The serum HBsAg and HBeAg levels of CHB patients before therapy and after therapy. Data are representative of more than three independent experiments. Results are presented as the mean ± SEM ($n \geq 3$ per group) and unpaired/paired two-tailed Student's *t*-tests were conducted; $^{*}p < 0.05$, $^{**}p < 0.01$, $^{****}p < 0.0001$; N.S., not significant.

levels of HBV-DNA, HBsAg, and HBeAg were also significantly reduced after therapy (**Figures 1G,H**).

NK cells can be divided into two subpopulations, $CD56^{dim}$ and $CD56^{bright}$, and we further investigated NKG2A expression on these two subsets in peripheral blood from patients with CHB. The gating strategies to separate $CD56^{dim}$ and $CD56^{bright}$ NK cells from PBMCs are detailed in **Figure 2A**. The frequency of $NKG2A^{+}$ cells among the $CD56^{bright}$ NK subpopulation did not differ significantly between these two groups (**Figures 2B,C**), while the. percentage of $NKG2A^{+}$ cells among the $CD56^{dim}$ NK subpopulation in patients with CHB was significantly higher than that in healthy controls (**Figures 2D,E**). Furthermore, serum HBV-DNA was found to positively correlate with the percentage of $NKG2A^{+}CD56^{dim}$ NK cells in CHB patients ($r = 0.45$, $p = 0.0001$, **Figure 2F**). In addition, serum levels of HBsAg and HBeAg were found to be positively associated with the percentage of $NKG2A^{+}CD56^{dim}$ NK cells ($r = 0.50$, $p = 0.0003$; $r = 0.49$, $p = 0.03$, **Figures 2G,H**), while there was no significant correlation between $NKG2A^{+}CD56^{dim}$ NK cells and the level of transaminases in patients with CHB (**Supplementary Figures S3A,B**).

TNF-related apoptosis-inducing ligand (TRAIL) is expressed by NK cell and it contributes to the elimination of HBV-specific $CD8^{+}$ T cells in CHB (Peppa et al., 2013). We found that expression of TRAIL was upregulated on NK cells in patients with CHB, however, the frequency of $TRAIL^{+}$ NK cells did not significantly correlate with HBV-DNA in patients with CHB infection (**Supplementary Figures S4A–C**). These results indicate that chronic HBV infection induces an increased expression of NKG2A on $CD56^{dim}$ NK cells, and that upregulation of NKG2A may be linked with the disease progression in CHB.

Blocking NKG2A Restores the Ability of NK Cells From Patients With CHB to Produce Cytokines

To evaluate the impact of increased NKG2A expression on NK cells in patients with CHB, we next assessed the function of NK cells from these patients. Gating strategies of lymphocytes,

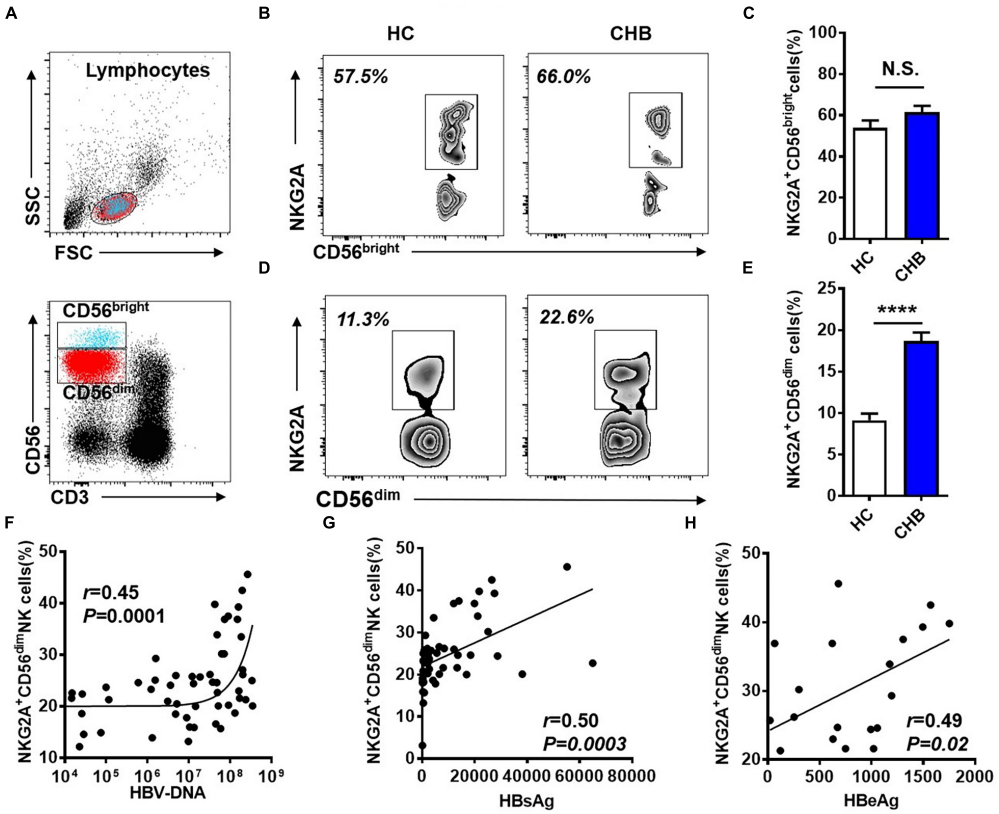

FIGURE 2 | Upregulation of NKG2A on CD56^{dim} NK cells and its positive correlation with HBV DNA levels. **(A)** Sequential strategy for gating CD56^{dim} and CD56^{bright} NK cells from lymphocytes with monitoring via flow cytometry. **(B,C)** Representative data plots show NKG2A expression on CD56^{dim} and CD56^{bright} NK cells in healthy controls and patients with CHB. **(D)** NKG2A^{+}CD56^{bright} NK cells and **(E)** NKG2A^{+}CD56^{dim} NK cells were detected in peripheral blood samples from patients with CHB and healthy controls. **(F)** Correlation between the percentage of NKG2A^{+}CD56^{dim} NK cells and serum HBV-DNA levels in patients with CHB. **(G)** Correlation between the percentage of NKG2A^{+}CD56^{dim} NK cells and serum HBsAg levels in patients with CHB. **(H)** Correlation between the percentage of NKG2A^{+}CD56^{dim} NK cells and serum HBeAg levels in patients with CHB. Data are representative of more than three independent experiments. Results are presented as the mean ± SEM ($n \geq 3$ per group) and unpaired two-tailed Student's *t*-tests or Spearman's correlation coefficients were used for analyses; $^{****}p < 0.0001$; N.S., not significant.

NK cells and CD56^{dim} NK cells were showed in **Supplementary Figure S5**. As shown in **Figure 3A**, the percentage and absolute numbers of IFN-γ^{+}CD56^{dim} NK cells were lower in patients with CHB than those in healthy controls (**Figures 3B,C**). Moreover, the frequency and absolute number of TNF^{+}CD56^{dim} NK cells were also significantly decreased in patients with CHB relative to controls (**Figures 3D,E**). These data demonstrate that cytokine production is impaired in NK cells from patients with CHB relative to healthy controls.

Next, to investigate the role of NKG2A in NK cell function, we purified NK cells from patients with CHB and incubated them with anti-human NKG2A blocking antibody *in vitro* (**Supplementary Figure S6B**). Gating information of CD56^{dim} NK cells was showed in **Supplementary Figure S6A**. Our results showed that blocking NKG2A significantly enhanced expression of the activating receptor, CD226, on CD56^{dim} NK cells isolated from patients with active CHB (**Figures 3F,G**), and significantly increased the expression of IFN-γ (**Figures 3H,I**) as well as TNF in CD56^{dim} NK cells (**Figures 3J,K**). Meanwhile, the frequency of Eomes^{+}CD56^{dim} NK cells was also significantly enhanced when NKG2A was blocked (**Figures 3L,M**). While the expression of CD226, IFN-γ, TNF and Eomes on NK cells were significantly increased in NKG2A blockade group compared with control, but there was no significant difference in the expression of these four markers on CD56^{bright} NK cells between these two groups (**Supplementary Figures S6C–F**). In addition, the expression of TRAIL and Granzyme-B did not change significantly in this assay ($P > 0.05$, **Supplementary Figures S6G,H**). These results suggest that the inhibitory receptor, NKG2A, expressed on NK cells, accounts for the impaired ability of NK cells to produce cytokines in patients with CHB infection, and that blocking NKG2A *in vitro* can restore the function of those NK cells.

IL-10^{+} Tregs Contribute to the Dysfunction of NKG2A^{+} NK Cells in Patients With CHB

We wondered which factors were responsible for the induction of NKG2A expression on NK cells. First, we examined

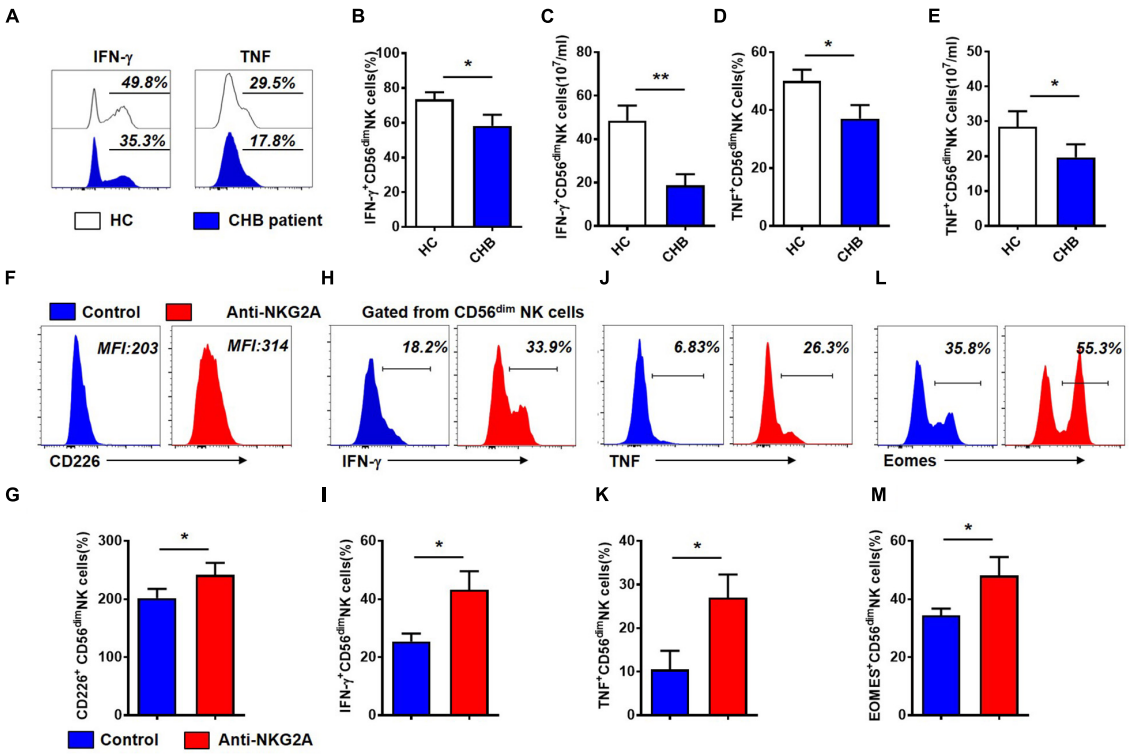

FIGURE 3 | Cytokine production by $CD56^{dim}$ NK cells is restored after blockade of NKG2A signaling in patients with CHB**. (A)** Representative flow cytometry plots showing IFN- γ and TNF expression in NK cells from patients with CHB and healthy controls. **(B)** Analysis of IFN- $\gamma^{+}CD56^{dim}$ NK cells in patients with CHB and healthy controls. **(C)** Comparison of absolute numbers of IFN - γ^{+} $CD56^{dim}$ NK cells in patients with CHB and healthy controls. **(D)** Analysis of $TNF^{+}CD56^{dim}$ NK cells in patients with CHB and healthy controls. **(E)** The absolute number of $TNF^{+}CD56^{dim}$ NK cells in patients with CHB and healthy controls. **(F–M)** NK cells isolated from patients with CHB were cultured in DMEM supplemented with 10% FBS and 100 IU/ml IL-2, with anti-human NKG2A antibody or control IgG. After 3 days, the phenotype and function of NK cells were analyzed by flow cytometry. **(F)** Representative plots of NKG2A and CD226 expressed in $CD56^{dim}$ NK cells after NK cells were cultured with anti-human NKG2A antibody or control IgG. **(G)** Expression of CD226 on total NK cells, $CD56^{bright}$ and $CD56^{dim}$ NK cells after isolated CHB NK cells were cultured with anti-human NKG2A antibody or control IgG. **(H)** Representative plots of IFN- γ expressed in $CD56^{dim}$ NK cells after NK cells were cultured with anti-human NKG2A antibody or control IgG. **(I)** Expression of IFN- γ on total NK cells, $CD56^{bright}$ and $CD56^{dim}$ NK cells after isolated CHB NK cells were cultured with anti-human NKG2A antibody or control IgG. **(J)** Representative plots of TNF expressed in $CD56^{dim}$ NK cells after NK cells were cultured with anti-human NKG2A antibody or control IgG. **(K)** Expression of TNF on total NK cells, CD56bright and $CD56^{dim}$ NK cells after isolated CHB NK cells were cultured with anti-human NKG2A antibody or control IgG. **(L)** Representative plots of Eomes expressed in $CD56^{dim}$ NK cells after NK cells were cultured with anti-human NKG2A antibody or control IgG. **(M)** Expression of Eomes on total NK cells, $CD56^{bright}$t and $CD56^{dim}$ NK cells after isolated CHB NK cells were cultured with anti-human NKG2A antibody or control IgG. Results are presented as the mean ± SEM ($n \geq 3$ per group) and unpaired/paired two-tailed Student's *t*-tests were conducted; $^{*}p < 0.05$, $^{**}p < 0.01$. N.S., not significant.

$CD4^{+}CD25^{+}Foxp3^{+}$ Tregs in patients with CHB and found that both the proportion and absolute number of Tregs in peripheral blood were significantly higher in patients with CHB than those in healthy controls (**Figures 4A–C**). Next, we measured cytokine production in Tregs and found that Tregs from CHB patients produced much higher levels than those from healthy controls (**Figures 4D,E**). Further, we assessed the level of serum IL-10 in healthy controls and CHB patients who had received effective antiviral therapy, and found that serum IL-10 level in treated CHB patients returned to a normal level, which was significantly lower than that in patients with CHB who had not received effective therapy (**Figure 4F**).

Interestingly, we detected a positive correlation between the percentage of Tregs and that of $NKG2A^{+}CD56^{dim}$ NK cells (**Figure 5A**). And both the percentage of IL-10^{+} Tregs and serum IL-10 level positively correlated with the percentage of $NKG2A^{+}CD56^{dim}$ NK cells (**Figures 5B,C**). To evaluate the effects of IL-10 on NKG2A expression, PBMCs were isolated from healthy donors and stimulated with 20% sera from CHB patients. We observed that the percentages of $NKG2A^{+}$ and $CD94^{+}$ NK cells were significantly increased by stimulation with CHB sera (**Figures 5D,E**). Interestingly, the percentage of $NKG2A^{+}$ NK cells was significantly reduced in PBMCs stimulated with CHB sera in the presence of anti-IL-10, relative to those stimulated with CHB sera only (**Figure 5F**). Furthermore, the percentage of $NKG2A^{+}$ NK cells was lower accompanied by a higher frequency of IFN-γ^{+} and TNF^{+} NK cells in the IL-10 blockade group when compared to that in the control group (**Figures 5G,H**). Accordingly, when NK cells and Tregs purified from healthy controls were stimulated with anti-CD3 and anti-CD28, and cultured with anti-human IL-10 neutralizing antibody or control IgG in the presence of CHB sera, we found that the

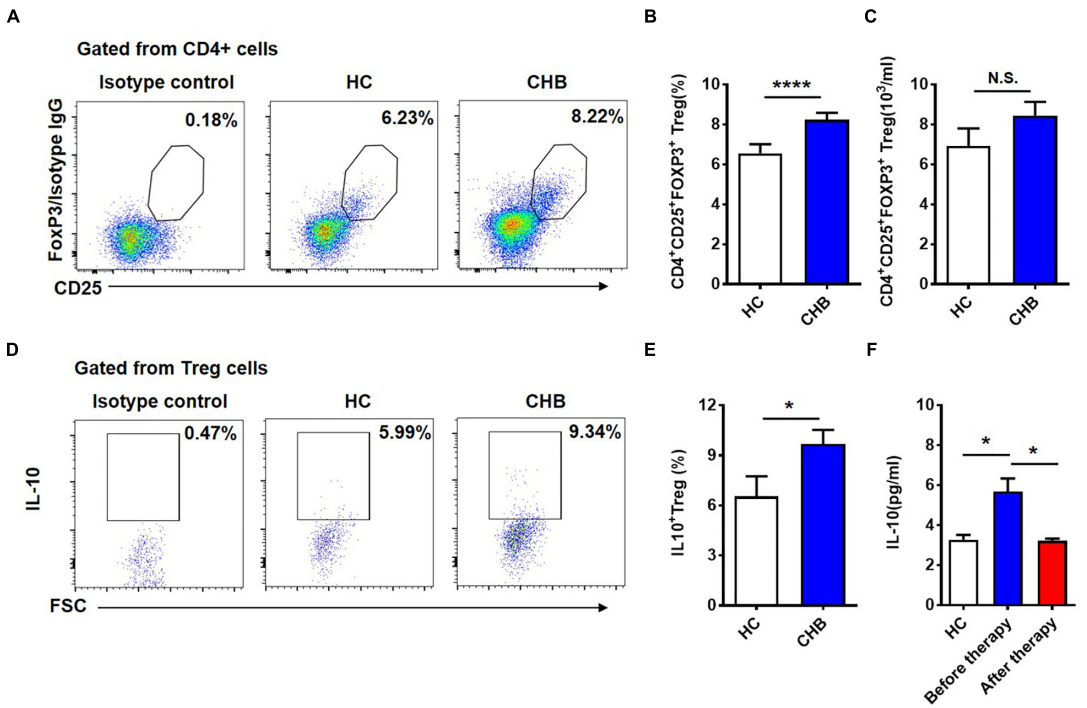

FIGURE 4 | Circulating Tregs and secreted IL-10 in patients with CHB infection. **(A)** Representative flow cytometry plots showing $CD4^+CD25^+FOXP3^+$ Tregs in peripheral blood samples from patients with CHB and healthy controls. **(B)** Data from **(A)** were compiled and analyzed for significance using the *t*-test. **(C)** Comparison of the absolutely numbers of $CD4^+CD25^+FOXP3^+$ Tregs in peripheral blood samples from patients with CHB and healthy controls. **(D)** Representative flow cytometry plots of $IL\text{-}10^+$ Tregs in peripheral blood samples from patients with CHB and healthy controls. **(E)** Data from **(D)** were compiled and analyzed for significance using the *t*-test. **(F)** Comparison of serum IL-10 levels detected using a CBA kit in healthy controls, and patients with CHB patients before and after antiviral treatment. Data are representative of more than three independent experiments. Results are presented as the mean ± SEM ($n \geq 3$ per group) and unpaired two-tailed Student's *t*-tests and one-way ANOVA were conducted; $^*p < 0.05$, $^{****}p < 0.0001$. N.S., not significant.

concentrations of IFN-γ and TNF in the culture supernatant were significantly increased after IL-10 blockade (**Figures 5I,J**). These findings suggest that Treg-derived IL-10 is involved in induction of $NKG2A^+$ NK cell and NK cell dysfunction.

HBeAg Induces NKG2A+ NK Cell Dysfunction Mediated by Treg-Derived IL-10

HBeAg has been suggested to play an important role in maintaining HBV persistence in patients with CHB. We next compared serum ALT and HBV-DNA between HBeAg-positive and -negative patients, and found that ALT and HBV-DNA levels were higher in HBeAg-positive patients than those that are HBeAg-negative (**Figures 6A,B**). Specifically, we observed that HBeAg-positive patients had significantly increased serum level of IL-10, as well as increased percentages of total Tregs, $IL\text{-}10^+$ Tregs and $NKG2A^+$ NK cells, respectively (**Figures 6C–F**). Together, these results suggest that HBeAg is associated with Treg-derived IL-10 production and NKG2A expression on NK cells in CHB patients.

To delineate the effect of HBeAg on $NKG2A^+$ NK cell dysfunction in patients with CHB, PBMCs were isolated from healthy controls and stimulated with HBeAg *in vitro*. We found that HBeAg induced human PBMCs to produce significantly more IL-10 upon stimulation with PMA, ionomycin, and monensin *in vitro* (**Figure 6G**). Moreover, levels of TNF and IFN-γ were decreased in PBMCs stimulated with HBeAg, while anti-IL-10 treatment increased the levels of these cytokines in the culture supernatant (**Figures 6H,I**). To test the direct effect of HBeAg on regulating NK cells, we added HBeAg directly to NK cells alone, but found that the frequency of $NKG2A^+$ NK cells did not alter significantly (**Supplementary Figure S7**). To directly investigate the possible role of HBeAg in regulating Treg and NK cells, these cells were purified from healthy controls and co-cultured *in vitro*. Addition of HBeAg to the culture system in the presence of anti-CD3 and anti-CD28 led to increased amounts of IL-10 in the supernatant (**Figure 6J**), accompanied by reduced levels of TNF and IFN-γ (**Figures 6K,L**); the defective production of these two cytokines was restored by addition of anti-IL-10 (**Figures 6K,L**). Together, these findings indicate that HBeAg promotes IL-10 production by Tregs, thereby inducing NKG2A expression on NK cells and contributing to the impaired cytokine-produced ability of NK cells.

DISCUSSION

CHB infection-induced immune tolerance is the biggest obstacle to the elimination of HBV in the host. As the vital effector

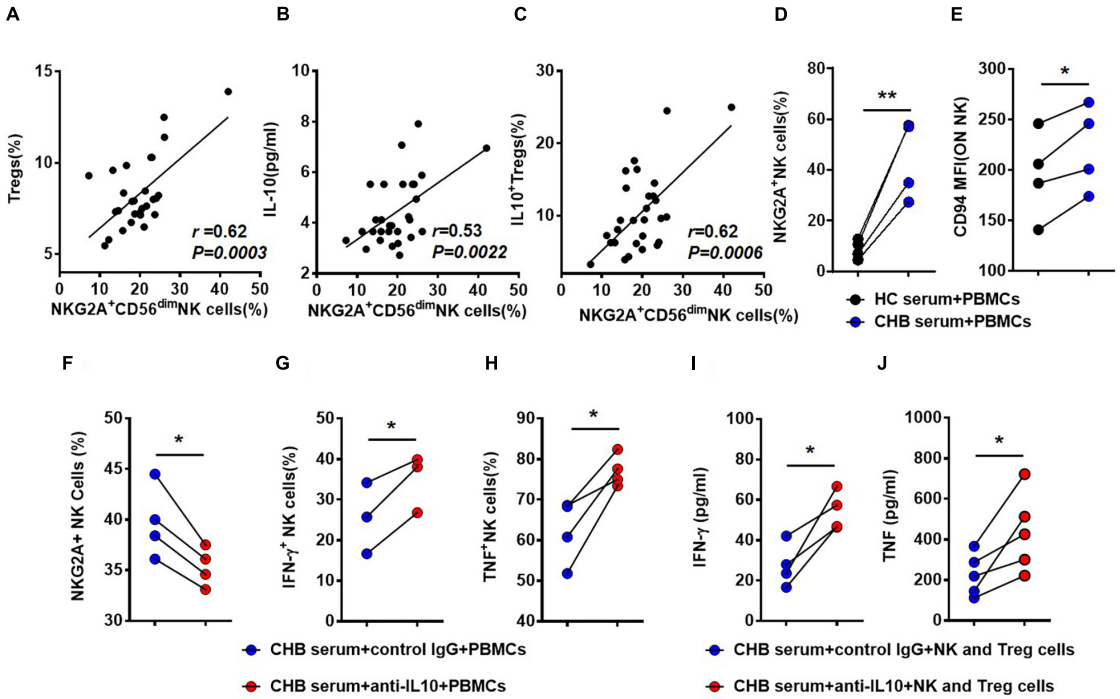

FIGURE 5 | Treg-derived IL-10 impairs NK cell function in patients with CHB. **(A)** Correlation between the percentage of NKG2A$^+$CD56^{dim} NK cells and Tregs in patients with CHB determined by flow cytometry. **(B)** Correlation between the percentage of NKG2A$^+$CD56^{dim} NK cells and serum IL-10 levels in serum samples from patients with CHB patients. **(C)** Correlation between the percentage of NKG2A$^+$CD56^{dim} NK cells and IL-10$^+$ Tregs in peripheral blood samples from patients with CHB. **(D,E)** PBMCs from healthy donors were cultured with 100 IU/ml IL-2 in the presence of 20% CHB or healthy control serum for 7 days. After 7 days of culture in the presence of 20% CHB or healthy control serum, expression of NKG2A and CD94 was monitored on NK cells by flow cytometry. **(F–H)** PBMCs from healthy donors were cultured with 20% CHB and 100 IU/ml IL-2 in the presence of 50 ng/ml anti-human IL-10 neutralizing antibody or control IgG. After 7 days, the percentages of NKG2A$^+$ NK cells, IFN- γ^+ NK cells and TNF$^+$ NK cells were detected after treatment of PBMCs with CHB serum and anti-IL-10 or control IgG *in vitro*. **(I,J)** NK cells (5 × 104) and Tregs (5 × 104) were purified from healthy donors and co-cultured in the presence of 20% CHB patient serum and 100 IU/ml IL-2, supplemented with anti-CD3 and-CD28 mAb, with 50 ng/ml anti-human IL-10 neutralizing antibody for 3 days. **(I)** The concentration of IFN-γ in the supernatant was measured using a CBA kit. **(J)** The concentration of TNF in the supernatant was measured using a CBA kit. Data are representative of more than three independent experiments. Results are presented as the mean ± SEM ($n \geq 3$ per group) and paired two-tailed Student's *t*-tests or Spearman's correlation coefficients were conducted; $^*p < 0.05$; $^{**}p < 0.01$.

lymphocytes of innate immune system, NK cells have an important role in defending against viruses and tumors, via rapid cytotoxic activity and cytokine production. In this study, we demonstrate that the percentage of NKG2A$^+$ NK cells increased in patients with CHB. We found that NKG2A$^+$CD56^{dim} NK cells correlated with HBV infection and NKG2A blockade could restore the function of NK cells *in vitro*. Furthermore, IL-10$^+$ Treg cells increased in patients with CHB and the frequency of NKG2A$^+$ NK cells was positively associated with Treg-derived IL-10, which is likely to contribute to the induction of NKG2A$^+$ NK cell dysfunction in CHB patients. Moreover, we found that the frequency of NKG2A$^+$ NK cell and level of Treg-derived IL-10 were elevated in HBeAg-positive patients relative to HBeAg-negative patients and that HBeAg promoted IL-10 production by Tregs, which further contributed to increased NKG2A expression on NK cells resulting in NK cell dysfunction (**Figure 7**).

NK cells are critical for HBV clearance in an HBV-transfected mouse model mimicking acute HBV infection in patients (Zheng et al., 2016). The expression pattern of various receptors on NK cells is abnormal, leading to their dysfunction during CHB infection (Sun et al., 2012; Peng and Tian, 2018). Down-regulation of activating receptors and up-regulation of inhibitory receptors on NK cells are associated with increased HBV viral load (Tjwa et al., 2011). NKG2A is also important for the maintenance of persistent hepatitis C virus infection (Golden-Mason et al., 2008). In patients with HCC, NKG2A, a checkpoint candidate, is expressed on NK cells and mediates NK cell dysfunction in intratumor tissues (Sun et al., 2017). Li et al. (2013) found that NKG2A expression is higher in patients with CHB and that, in a mouse model established by transfection of HBV plasmid, blocking NKG2A signaling promotes viral clearance. These data are consistent with our finding that up-regulation of NKG2A on CD56^{dim} NK is positively associated with the serum levels of HBV-DNA, HBsAg, and HBeAg in patients with CHB (**Figure 2**). We also demonstrated that NKG2A blockade restores the function of CD56^{dim} NK cells; specifically, this blockade enhances the IFN-γ and TNF production, and induces the expression of CD226 and Eomes in CD56^{dim} NK cells *in vitro* (**Figure 3**). Furthermore, NKG2A is expressed on CD8$^+$ T cells (Moser et al., 2002), however, no significant expression of NKG2A was detected on CD8$^+$ T cells in CHB patients in our study (**Supplementary Figure S1**). As NK cell dysfunction

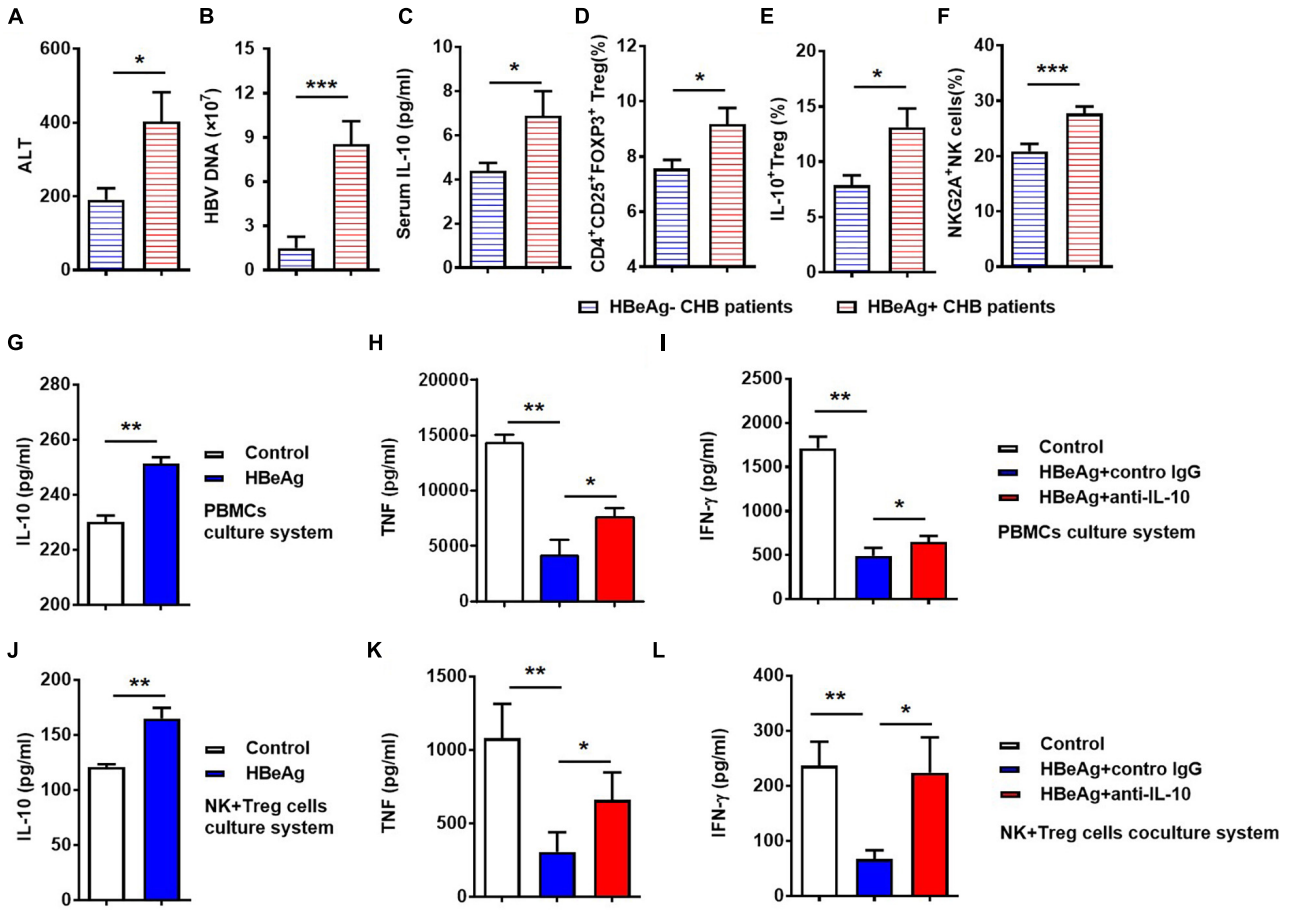

FIGURE 6 | HBeAg-induced IL-10 suppresses NK cell activation *in vitro*. **(A)** Serum ALT levels, **(B)** serum HBV DNA copy numbers, **(C)** serum IL-10 levels, **(D)** $CD56^{+}NKG2A^{+}$ NK expression, **(E)** percentages of Tregs, and **(F)** percentages of $IL\text{-}10^{+}$ Tregs were compared in HBeAg-positive and -negative patients with CHB. **(G–I)** For vitro experiments, PBMCs (2×10^5) isolated from healthy donors were cultured with or without 500 ng/ml HBeAg and 50 ng/ml anti-human IL-10 neutralizing antibody or control IgG in the presence of 100 IU/ml IL-2 for 7 days and the concentrations of cytokines in culture supernatant measured using a CBA kit. **(G)** IL-10 levels in supernatant after culture of PBMCs from healthy donors with or without HBeAg. **(H,I)** IFN-γ and TNF levels in supernatant after culture of PBMCs with HBeAg, in the presence of anti-IL-10 or control IgG. **(J–L)** In the co-culture system, 5×10^4 NK cells and 5×10^4 Tregs were purified from healthy donors and then co-cultured in the presence of 10% FBS, anti-CD3, and -CD28 mAb, with or without 500 ng/ml HBeAg and 50 ng/ml anti-IL-10 or control IgG in the presence of 100 IU/ml IL-2 for 3 days, then the concentration of cytokines in supernatant were measured using a CBA kit. **(J)** IL-10 in culture supernatants after co-culture of NK cells and Tregs with or without HBeAg for 3 days. **(K,L)** IFN-γ and TNF levels were detected in culture supernatant after co-culture of NK cells and Tregs with HBeAg in the presence of anti-IL-10 or control IgG. Data are representative of more than three independent experiments. Results are presented as the mean ± SEM ($n \geq 3$ per group) and unpaired/paired two-tailed Student's *t*-tests were conducted; $^{*}p < 0.05$, $^{**}p < 0.01$, $^{***}p < 0.001$.

is associated with impaired $CD8^{+}$ T cell responses in liver disease (Li et al., 2018; Zheng and Tian, 2019), it is possible that the elevated expression of NKG2A on NK cells is linked with dysfunctional $CD8^{+}$ T cells in patients with CHB.

In addition, after 24-week tenofovir treatment, the percentage of $NKG2A^{+}$ NK cells transiently decreased (Lv et al., 2012). Similarly, following treatment with PEG-interferon alpha-2a and adefovir for 48 weeks, the cytotoxic function of NK cells was restored and their IFN-γ secretion increased, while the number of $NKG2A^{+}$ NK cells was notably down-regulated (de Niet et al., 2017). In this study, we found that the frequency of $NKG2A^{+}$ NK cells, serum level of IL-10, and the levels of HBV-DNA, HBeAg, and HBsAg were significantly reduced after antiviral therapy (**Figures 1E–G**). IL-10 has an important role in sustaining the expression of $NKG2A^{+}Ly49^{-}$ on hepatic NK cells (Lassen et al., 2010). In an HBV-transfected mouse model, Li et al. demonstrated that Treg-derived IL-10 contributes to the upregulation of NKG2A expression on NK cells (Li et al., 2013). In liver diseases (e.g., CHB, cirrhosis and liver cancer), NK cell dysfunction is induced by elevated levels of IL-10 and TGF-β (Lunemann et al., 2014; Yang et al., 2017). The production of IL-10 is significantly enhanced by increased HBV titers, and IL-10 may suppress IFN- γ production in NK cells in patients with CHB (Li et al., 2010; Peppa et al., 2010; Tan et al., 2010). Our data show that Tregs increased the percentage of NKG2A cells in the presence of CHB serum supplemented with anti-CD3 and CD28, while secretion of IFN-γ and TNF from NK cells was up-regulated by IL-10 blockade in this co-culture system (**Figure 5**).

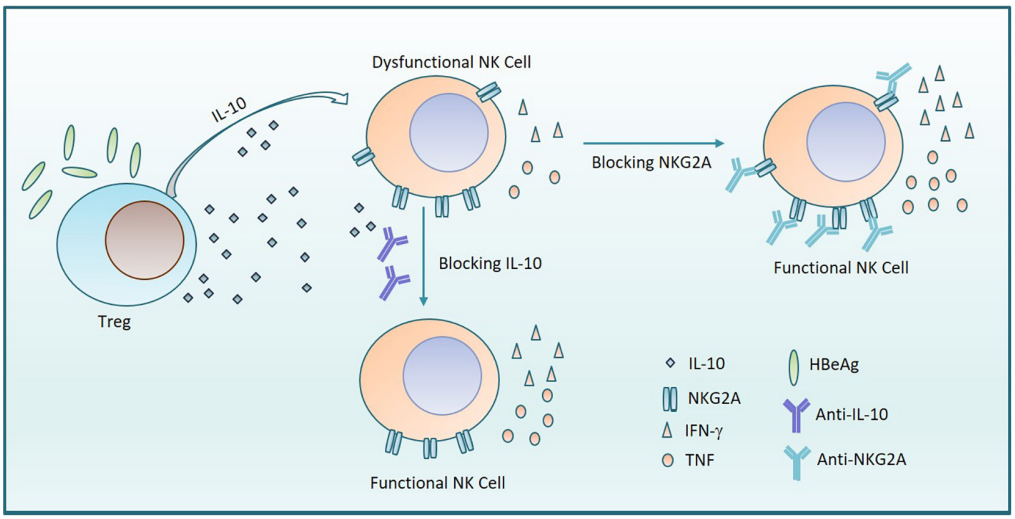

FIGURE 7 | HBeAg induces NKG2A$^+$ NK cell dysfunction via Tregs-derived IL-10. The diagram shows that HBeAg induces NK cell dysfunction with upregulated expression of NKG2A on NK cells and reduced secretion of TNF and IFN- γ, which is mediated by increased amounts of IL-10 secreted from Tregs. On the one hand, blocking NKG2A on NK cells leads to the recovery of NK cell function. On the other hand, the function of NK cells is also restored by addition of anti-IL-10.

HBeAg positivity is associated with viral replication and immunotolerance in CHB infection (European Association for the Study of The Liver, 2012). Moreover, CD4$^+$CD25$^+$ T cells are significantly elevated in HBeAg-positive patients when compared to HBeAg-negative patients, and their number is positively correlated with HBeAg levels (El-Badawy et al., 2012). HBeAg evades host immune responses by inhibiting lipopolysaccharide-induced NLRP3 inflammasome activation, which is critical for antiviral defense (Yu et al., 2017b). Loss of HBeAg is associated with short-term evolution, as it results in loss of HBeAg-mediated tolerance and reduced transmissibility of the HBeAg(-) virion (Kramvis et al., 2018). Furthermore, maternal-derived HBeAg was reported to contribute to the impaired function of hepatic macrophage cells (Tian et al., 2016). Consistently, HBeAg-induced expansion of monocytic myeloid-derived suppressor cells leads to impaired CD8$^+$ T cell responses in CHB infection (Yang et al., 2019). Moreover, the frequency and skewed T-cell receptor beta-chain variable patterns of peripheral Tregs correlate with HBeAg seroconversion (Yang et al., 2016), and CD3$^+$CD4$^+$Foxp3$^-$ cells can be induced to convert into CD3$^+$CD4$^+$Foxp3$^+$ Tregs in liver-draining lymph nodes (Yu et al., 2017a). There are also reports indicating that liver sinusoidal endothelial cells and B cells contribute to Treg induction (Carambia et al., 2014; Lu et al., 2015).

In our study, we demonstrate that HBeAg-positive patients had higher frequencies of NKG2A$^+$ NK cells than those who were HBeAg-negative. Tregs and IL-10 derived from these cells were significantly elevated in HBeAg-positive patients. When PBMCs or NK cells and Tregs purified from healthy controls were co-cultured with anti-CD3 and anti-CD28 *in vitro*, the addition of HBeAg led to increased production of IL-10 accompanied by reduced levels of TNF and IFN-γ, while the addition of HBeAg to NK cells alone did not have significant impact on the function of NK cells. Furthermore, the production of TNF and IFN-γ was restored by IL-10 blockade. These results indicate that HBeAg contributes to the up-regulation of IL-10$^+$ Tregs, then causing NK cell dysfunction (**Figure 6**).

In summary, during CHB infection, HBeAg is associated with HBV immune tolerance. We found that HBeAg induces IL-10 production in Tregs, which subsequently upregulates the expression of NKG2A on NK cells, leading to NK cell dysfunction, suggesting that HBeAg accounts for NK cell dysfunction in CHB patients. Together, our findings contribute to the understanding of the mechanisms underlying NK cell dysfunction in CHB patients and indicate that the HBeAg-IL-10-NKG2A$^+$ NK cell axis is a potential therapeutic target in these patients.

DATA AVAILABILITY STATEMENT

The datasets generated for this study are available on request to the corresponding author.

ETHICS STATEMENT

The studies involving human participants were reviewed and approved by the local ethics committee of The First Affiliated Hospital of Anhui Medical University and the local ethics committee of Chaohu Hospital of Anhui Medical University. The patients/participants provided their written informed consent to participate in this study.

AUTHOR CONTRIBUTIONS

QM and XD designed and wrote the manuscript. QM, XD, SL, and DS performed the experiments and analyses. TZ, CZ, QL,

MiZ, YY, and JC were involved in the collection of clinical samples. LZ and YX critically reviewed the manuscript. YG supplied and evaluated CHB patients. MeZ designed and supervised the experiments and wrote the manuscript.

FUNDING

This work was supported by the National Natural Science Foundation of China (Grant No. 81771685) and Anhui Medical University Basic and Clinical Cooperative Research Promotion Program (Grant No. 2019xkjT023).

SUPPLEMENTARY MATERIAL

The Supplementary Material for this article can be found online at: https://www.frontiersin.org/articles/10.3389/fcell.2020.00421/full#supplementary-material

REFERENCES

Carambia, A., Freund, B., Schwinge, D., Heine, M., Laschtowitz, A., Huber, S., et al. (2014). TGF-beta-dependent induction of CD4(+)CD25(+)Foxp3(+) Tregs by liver sinusoidal endothelial cells. *J. Hepatol.* 61, 594–599. doi: 10.1016/j.jhep.2014.04.027

de Niet, A., Jansen, L., Stelma, F., Willemse, S. B., Kuiken, S. D., Weijer, S., et al. (2017). Peg-interferon plus nucleotide analogue treatment versus no treatment in patients with chronic hepatitis B with a low viral load: a randomised controlled, open-label trial. *Lancet Gastroenterol. Hepatol.* 2, 576–584. doi: 10.1016/S2468-1253(17)30083-3

Dienstag, J. L. (2008). Hepatitis B virus infection. *N. Engl. J. Med.* 359, 1486–1500.

El-Badawy, O., Sayed, D., Badary, M. S., Abd-Alrahman, M. E., El-Feky, M. A., and Thabit, A. G. (2012). Relations of regulatory T cells with hepatitis markers in chronic hepatitis B virus infection. *Hum. Immunol.* 73, 335–341. doi: 10.1016/j.humimm.2012.01.014

El-Deeb, N. M., El-Adawi, H. I., El-Wahab, A. E. A., Haddad, A. M., El Enshasy, H. A., He, Y. W., et al. (2019). Modulation of NKG2D, KIR2DL and cytokine production by pleurotus ostreatus glucan enhances natural killer cell cytotoxicity toward cancer cells. *Front. Cell Dev. Biol.* 7:165. doi: 10.3389/fcell.2019.00165

European Association for the Study of The Liver, (2012). EASL clinical practice guidelines: management of chronic hepatitis B virus infection. *J. Hepatol.* 57, 167–185.

Golden-Mason, L., Bambha, K. M., Cheng, L., Howell, C. D., Taylor, M. W., Clark, P. J., et al. (2011). Natural killer inhibitory receptor expression associated with treatment failure and interleukin-28B genotype in patients with chronic hepatitis C. *Hepatology* 54, 1559–1569. doi: 10.1002/hep.24556

Golden-Mason, L., Madrigal-Estebas, L., Mcgrath, E., Conroy, M. J., Ryan, E. J., Hegarty, J. E., et al. (2008). Altered natural killer cell subset distributions in resolved and persistent hepatitis C virus infection following single source exposure. *Gut* 57, 1121–1128. doi: 10.1136/gut.2007.130963

Haanen, J. B., and Cerundolo, V. (2018). NKG2A, a new kid on the immune checkpoint block. *Cell* 175, 1720–1722. doi: 10.1016/j.cell.2018.11.048

Kramvis, A., Kostaki, E. G., Hatzakis, A., and Paraskevis, D. (2018). Immunomodulatory function of HBeAg related to short-sighted evolution, transmissibility, and clinical manifestation of hepatitis B virus. *Front. Microbiol.* 9:2521. doi: 10.3389/fmicb.2018.02521

Lassen, M. G., Lukens, J. R., Dolina, J. S., Brown, M. G., and Hahn, Y. S. (2010). Intrahepatic IL-10 maintains NKG2A+Ly49- liver NK cells in a functionally hyporesponsive state. *J. Immunol.* 184, 2693–2701. doi: 10.4049/jimmunol.0901362

Li, F., Wei, H., Wei, H., Gao, Y., Xu, L., Yin, W., et al. (2013). Blocking the natural killer cell inhibitory receptor NKG2A increases activity of human natural killer cells and clears hepatitis B virus infection in mice. *Gastroenterology* 144, 392–401. doi: 10.1053/j.gastro.2012.10.039

Li, H., Zhai, N., Wang, Z., Song, H., Yang, Y., Cui, A., et al. (2018). Regulatory NK cells mediated between immunosuppressive monocytes and dysfunctional T cells in chronic HBV infection. *Gut* 67, 2035–2044. doi: 10.1136/gutjnl-2017-314098

Li, H. J., Zhai, N. C., Song, H. X., Yang, Y., Cui, A., Li, T. Y., et al. (2015). The role of immune cells in chronic HBV infection. *J. Clin. Transl. Hepatol.* 3, 277–283. doi: 10.14218/JCTH.2015.00026

Li, J., Wu, W., Peng, G., Chen, F., Bai, M., Zheng, M., et al. (2010). HBcAg induces interleukin-10 production, inhibiting HBcAg-specific Th17 responses in chronic hepatitis B patients. *Immunol. Cell Biol.* 88, 834–841. doi: 10.1038/icb.2010.63

Long, E. O., Kim, H. S., Liu, D., Peterson, M. E., and Rajagopalan, S. (2013). Controlling natural killer cell responses: integration of signals for activation and inhibition. *Annu. Rev. Immunol.* 31, 227–258. doi: 10.1146/annurev-immunol-020711-075005

Lozano, R., Naghavi, M., Foreman, K., Lim, S., Shibuya, K., Aboyans, V., et al. (2012). Global and regional mortality from 235 causes of death for 20 age groups in 1990 and 2010: a systematic analysis for the Global Burden of Disease Study 2010. *Lancet* 380, 2095–2128. doi: 10.1016/S0140-6736(12)61728-0

Lu, F. T., Yang, W., Wang, Y. H., Ma, H. D., Tang, W., Yang, J. B., et al. (2015). Thymic B cells promote thymus-derived regulatory T cell development and proliferation. *J. Autoimmun.* 61, 62–72. doi: 10.1016/j.jaut.2015.05.008

Lunemann, S., Malone, D. F., Hengst, J., Port, K., Grabowski, J., Deterding, K., et al. (2014). Compromised function of natural killer cells in acute and chronic viral hepatitis. *J. Infect Dis.* 209, 1362–1373. doi: 10.1093/infdis/jit561

Lv, J., Jin, Q., Sun, H., Chi, X., Hu, X., Yan, H., et al. (2012). Antiviral treatment alters the frequency of activating and inhibitory receptor-expressing natural killer cells in chronic hepatitis B virus infected patients. *Mediators Inflamm.* 2012:804043. doi: 10.1155/2012/804043

Maini, M. K., and Peppa, D. (2013). NK cells: a double-edged sword in chronic hepatitis B virus infection. *Front. Immunol.* 4:57. doi: 10.3389/fimmu.2013.00057

Martinet, J., Dufeu-Duchesne, T., Bruder Costa, J., Larrat, S., Marlu, A., Leroy, V., et al. (2012). Altered functions of plasmacytoid dendritic cells and reduced cytolytic activity of natural killer cells in patients with chronic HBV infection. *Gastroenterology* 143, 1586.e8–1596.e8. doi: 10.1053/j.gastro.2012.08.046

Moser, J. M., Gibbs, J., Jensen, P. E., and Lukacher, A. E. (2002). CD94-NKG2A receptors regulate antiviral CD8(+) T cell responses. *Nat. Immunol.* 3, 189–195. doi: 10.1038/ni757

Park, J. J., Wong, D. K., Wahed, A. S., Lee, W. M., Feld, J. J., Terrault, N., et al. (2016). Hepatitis B virus–specific and global t-cell dysfunction in chronic hepatitis B. *Gastroenterology* 150, 684.e5–695.e5. doi: 10.1053/j.gastro.2015.11.050

Peng, H., and Tian, Z. (2018). NK cells in liver homeostasis and viral hepatitis. *Sci. China Life Sci.* 61, 1477–1485. doi: 10.1007/s11427-018-9407-2

Peng, H., Wisse, E., and Tian, Z. (2016). Liver natural killer cells: subsets and roles in liver immunity. *Cell Mol. Immunol.* 13, 328–336. doi: 10.1038/cmi.2015.96

Peppa, D., Gill, U. S., Reynolds, G., Easom, N. J., Pallett, L. J., Schurich, A., et al. (2013). Up-regulation of a death receptor renders antiviral T cells susceptible to NK cell-mediated deletion. *J. Exp. Med.* 210, 99–114. doi: 10.1084/jem.20121172

Peppa, D., Micco, L., Javaid, A., Kennedy, P. T., Schurich, A., Dunn, C., et al. (2010). Blockade of immunosuppressive cytokines restores NK cell antiviral function in chronic hepatitis B virus infection. *PLoS Pathog.* 6:e1001227. doi: 10.1371/journal.ppat.1001227

Racanelli, V., and Rehermann, B. (2006). The liver as an immunological organ. *Hepatology* 43, S54–S62.

Rehermann, B. (2013). Pathogenesis of chronic viral hepatitis: differential roles of T cells and NK cells. *Nat. Med.* 19, 859–868. doi: 10.1038/nm.3251

Sun, C., Fu, B., Gao, Y., Liao, X., Sun, R., Tian, Z., et al. (2012). TGF-beta1 down-regulation of NKG2D/DAP10 and 2B4/SAP expression on human NK cells

contributes to HBV persistence. *PLoS Pathog.* 8:e1002594. doi: 10.1371/journal.ppat.1002594

Sun, C., Xu, J., Huang, Q., Huang, M., Wen, H., Zhang, C., et al. (2017). High NKG2A expression contributes to NK cell exhaustion and predicts a poor prognosis of patients with liver cancer. *Oncoimmunology* 6:e1264562. doi: 10.1080/2162402X.2016.1264562

Tan, A. T., Koh, S., Goh, W., Zhe, H. Y., Gehring, A. J., Lim, S. G., et al. (2010). A longitudinal analysis of innate and adaptive immune profile during hepatic flares in chronic hepatitis B. *J. Hepatol.* 52, 330–339. doi: 10.1016/j.jhep.2009.12.015

Tian, Y., Kuo, C. F., Akbari, O., and Ou, J. H. (2016). Maternal-derived hepatitis B virus E antigen alters macrophage function in offspring to drive viral persistence after vertical transmission. *Immunity* 44, 1204–1214. doi: 10.1016/j.immuni.2016.04.008

Tian, Z., Chen, Y., and Gao, B. (2013). Natural killer cells in liver disease. *Hepatology* 57, 1654–1662.

Tjwa, E. T., Van Oord, G. W., Hegmans, J. P., Janssen, H. L., and Woltman, A. M. (2011). Viral load reduction improves activation and function of natural killer cells in patients with chronic hepatitis B. *J. Hepatol.* 54, 209–218. doi: 10.1016/j.jhep.2010.07.009

Trehanpati, N., and Vyas, A. K. (2017). Immune regulation by T regulatory cells in hepatitis B virus-related inflammation and cancer. *Scand. J. Immunol.* 85, 175–181. doi: 10.1111/sji.12524

Yang, F., Yu, X., Zhou, C., Mao, R., Zhu, M., Zhu, H., et al. (2019). Hepatitis B e antigen induces the expansion of monocytic myeloid-derived suppressor cells to dampen T-cell function in chronic hepatitis B virus infection. *PLoS Pathog.* 15:e1007690. doi: 10.1371/journal.ppat.1007690

Yang, H. L., Zhou, W. J., Chang, K. K., Mei, J., Huang, L. Q., Wang, M. Y., et al. (2017). The crosstalk between endometrial stromal cells and macrophages impairs cytotoxicity of NK cells in endometriosis by secreting IL-10 and TGF-beta. *Reproduction* 154, 815–825. doi: 10.1530/REP-17-0342

Yang, J., Sheng, G., Xiao, D., Shi, H., Wu, W., Lu, H., et al. (2016). The frequency and skewed T-cell receptor beta-chain variable patterns of peripheral CD4(+)CD25(+) regulatory T-cells are associated with hepatitis B e antigen seroconversion of chronic hepatitis B patients during antiviral treatment. *Cell Mol. Immunol.* 13, 678–687. doi: 10.1038/cmi.2015.100

Yu, J., Chen, Y., Wu, Y., Ye, L., Lian, Z., Wei, H., et al. (2017a). The differential organogenesis and functionality of two liver-draining lymph nodes in mice. *J. Autoimmun.* 84, 109–121. doi: 10.1016/j.jaut.2017.08.005

Yu, X., Lan, P., Hou, X., Han, Q., Lu, N., Li, T., et al. (2017b). HBV inhibits LPS-induced NLRP3 inflammasome activation and IL-1beta production via suppressing the NF-kappaB pathway and ROS production. *J. Hepatol.* 66, 693–702. doi: 10.1016/j.jhep.2016.12.018

Zhang, C., Wang, X. M., Li, S. R., Twelkmeyer, T., Wang, W. H., Zhang, S. Y., et al. (2019). NKG2A is a NK cell exhaustion checkpoint for HCV persistence. *Nat. Commun.* 10:1507. doi: 10.1038/s41467-019-09212-y

Zheng, M., Sun, H., and Tian, Z. (2018). Natural killer cells in liver diseases. *Front. Med.* 12, 269–279. doi: 10.1007/s11684-018-0621-4

Zheng, M., Sun, R., Wei, H., and Tian, Z. (2016). NK cells help induce anti-hepatitis B virus CD8+ T cell immunity in mice. *J. Immunol.* 196, 4122–4131. doi: 10.4049/jimmunol.1500846

Zheng, M., and Tian, Z. (2019). Liver-mediated adaptive immune tolerance. *Front. Immunol.* 10:2525. doi: 10.3389/fimmu.2019.02525

Conflict of Interest: The authors declare that the research was conducted in the absence of any commercial or financial relationships that could be construed as a potential conflict of interest.

frontiers in Cell and Developmental Biology

REVIEW
published: 12 June 2020
doi: 10.3389/fcell.2020.00479

The Inhibitory Effect of Curcumin on Virus-Induced Cytokine Storm and Its Potential Use in the Associated Severe Pneumonia

Ziteng Liu[1,2] *and Ying Ying*[1,3]*

[1] Jiangxi Province Key Laboratory of Tumor Pathogens and Molecular Pathology, School of Basic Medical Sciences, Nanchang University, Nanchang, China, [2] Nanchang Joint Program, Queen Mary School, Nanchang University, Nanchang, China, [3] Department of Pathophysiology, School of Basic Medical Sciences, Nanchang University, Nanchang, China

Coronavirus infection, including SARS-CoV, MERS-CoV, and SARS-CoV2, causes daunting diseases that can be fatal because of lung failure and systemic cytokine storm. The development of coronavirus-evoked pneumonia is associated with excessive inflammatory responses in the lung, known as "cytokine storms," which results in pulmonary edema, atelectasis, and acute lung injury (ALI) or fatal acute respiratory distress syndrome (ARDS). No drugs are available to suppress overly immune response-mediated lung injury effectively. In light of the low toxicity and its antioxidant, anti-inflammatory, and antiviral activity, it is plausible to speculate that curcumin could be used as a therapeutic drug for viral pneumonia and ALI/ARDS. Therefore, in this review, we summarize the mounting evidence obtained from preclinical studies using animal models of lethal pneumonia where curcumin exerts protective effects by regulating the expression of both pro- and anti-inflammatory factors such as IL-6, IL-8, IL-10, and COX-2, promoting the apoptosis of PMN cells, and scavenging the reactive oxygen species (ROS), which exacerbates the inflammatory response. These studies provide a rationale that curcumin can be used as a therapeutic agent against pneumonia and ALI/ARDS in humans resulting from coronaviral infection.

Keywords: curcumin, coronavirus, cytokine storm, pneumonia, lung injury

OPEN ACCESS

Edited by:
Giulia De Falco,
Queen Mary University of London, United Kingdom

Reviewed by:
Gabriele Margiotta,
Istituto Nazionale della Previdenza Sociale, Italy
Changyan Chen,
Northeastern University, United States

***Correspondence:**
Ying Ying
yingying@ncu.edu.cn

Specialty section:
This article was submitted to Molecular Medicine, a section of the journal Frontiers in Cell and Developmental Biology

Received: *25 April 2020*
Accepted: *22 May 2020*
Published: *12 June 2020*

Citation:
Liu Z and Ying Y (2020) The Inhibitory Effect of Curcumin on Virus-Induced Cytokine Storm and Its Potential Use in the Associated Severe Pneumonia. Front. Cell Dev. Biol. 8:479. doi: 10.3389/fcell.2020.00479

INTRODUCTION

During the Spanish influenza pandemic in 1917–1918, it was found that the deaths were not just seen in the elderly with weak immunity, but also young individuals with normal immunity. As part of a robust immune response in severe cases, the virus triggers overaction of immune systems, producing a large number of inflammatory factors, which causes severe damage to the lung and manifests acute respiratory distress syndrome (ARDS), resulting in high mortality. The same damaging effects of immune over-reaction were observed in outbreaks of severe acute respiratory syndrome coronavirus (SARS-CoV) (Huang et al., 2005; Channappanavar and Perlman, 2017), middle east respiratory syndrome CoV (MERS-CoV) (Channappanavar and Perlman, 2017), highly pathogenic avian influenza viruses (including H5N1 and H7N9) (Kalil and Thomas, 2019), and novel coronavirus (SARS-CoV2) (Yao et al., 2020).

Inflammation under physiological conditions is a protective mechanism that acts to eliminate exogenous agents invading to living bodies, remove necrotic tissues and cells, and promote damage repair (Netea et al., 2017). Being said that the inflammation initiates a protective immune response when it is confined to locally affected tissues. However, when the negative regulatory mechanism is suppressed, a persistent and extensive inflammatory reaction occurs, which can reach pathological levels causing fatally systemic damage (Torres et al., 2017). Such an inflammatory response, including overproduction of immune cells and pro-inflammatory cytokines, is defined as the cytokine storm that usually occurs in viral infection and causes acute lung injury (ALI) and ARDS. Resulting symptoms include congestion, atelectasis, and pulmonary edema, which affects oxygen exchange in the lung and eventually lead to death (Wheeler and Bernard, 2007). There is no effective regime for cytokine storm and resultant lung injury. Therefore, drugs to suppress the cytokine storm are urgently needed to treat deadly virus infection that causes lung damage and ARDS.

Curcumin[(1E,6E)-1,7bis(4-hydroxy-3-methoxyphenyl)-1,6-heptadiene-3,5-dione] is a natural medicine mainly extracted from plants of the Curcuma longa that has a long history to be used in humans in treating diseases without overt side effects. Numerous *in vitro* and *in vivo* studies indicate that curcumin has antioxidant, anti-inflammatory, anti-cancer, and anti-diabetic activity (Xu et al., 2018). Several clinical investigations have reported beneficial effects in treating cardiovascular diseases, metabolic syndrome, or diabetes, and infectious diseases, especially viral infection (Yang et al., 2014; Basu et al., 2013; Amalraj et al., 2017; Alizadeh et al., 2018; Asadi et al., 2019). All of these clinical findings point to that curcumin alleviates these diseases mainly via modulation of immune responses. Indeed, some preclinical studies have suggested that curcumin could inhibit the cytokine storm induced by the viral infection (Dai et al., 2018; Richart et al., 2018; Praditya et al., 2019; Vitali et al., 2020). Therefore, in this review, we outline the relationship between virus infections and cytokine storm and discuss the potential use of curcumin in treating viral infection-triggered ARDS. We hope to provide useful information and references for clinicians in combating devastating severe pneumonia caused by SARS-CoV2, a current global pandemic.

VIRAL INFECTION AND CYTOKINE STORM

Cytokine storm arises from different factors that could derive from autoimmune, inflammatory, iatrogenic, and infectious origins (Behrens and Koretzky, 2017). It is characterized by the production of excessive amounts of inflammatory cytokines as a result of unchecked feedforward activation and amplification of immune cells. Its clinical manifestations include systemic inflammation, multi-organ failure, hyperferritinemia, which is referred to as "cytokine storm syndrome" and could be lethal if untreated.

Under physiological conditions, the steady-state cytokine levels are maintained by negative and positive feedback regulation of their expression (Behrens and Koretzky, 2017). A large amount of virus in the body will induce over-reacted innate and adaptive immune response, triggering extravagant cytokines release and lymphocytes activation. Common to cytokine storm syndromes engendered by all insults is a loss of negative regulation of the production of inflammatory cytokines, which in turn drives a positive feedback regulation, leading to exponentially growing inflammation and multi-organ failure.

At an early stage, virus infection induces host cells to generate cytokines and chemokines, inflammatory mediators, and apoptosis of the host cells, which then attracts immune cells to the damaged areas (Liu et al., 2016). Macrophages, dendritic cells, and mast cells engulf antigen fragments, virus, and virus-bearing damaged cells, which triggers the production of the inflammatory mediators. Myeloid cells, including monocytes, neutrophils, and dendritic cells, contain multiple pattern recognition receptors (PRRs) on their surfaces to help them recognize and bind to viruses via Pathogen-associated molecular patterns (PAMPs) such as viral RNA/DNA, or damage-associated molecular patterns (DAMPs) from necrotic tissue and cells in aseptic inflammation. Subsequently, the immune cells are activated and produce pro-inflammatory cytokines, including tumor necrosis factor-α (TNF-α), interleukin (e.g., IL-1β, IL-6), and interferon-gamma (IFN-γ) (Taniguchi and Karin, 2018). The release of cytokine causes increased vascular permeability; consequently, the leukocytes increasingly migrate to damaged tissues through margination, rolling, adhesion, transmigration, and chemotaxis. Activated leukocytes simultaneously release prostaglandins and inflammatory factors, and activate the complement system, producing C3a and C5a components that kill pathogens (Medzhitov, 2008; Straub et al., 2015; Netea et al., 2017).

An additional effect of cytokines is to activate NADPH oxidase in leukocytes, leading to the generation of reactive oxygen species (ROS) such as superoxide, hydroxyl radicals, and singlet oxygen (Liu et al., 2016). On the one hand, ROS helps to remove proteins, lipids, and nuclear acids of the damaged cells and activate immune cells to eliminate foreign microorganisms through extracellular mechanisms (Zhang et al., 2016). On the other hand, ROS acts as a second messenger to regulate intracellular signaling events. For example, it activates the nuclear factor-κB (NF-κB) to promote further production of pro-inflammatory cytokines such as TNF-α, IL-6, IL-8, and other inflammatory factors (Baldwin, 1996; Cohen et al., 2009; Zhang et al., 2016; Hellebrekers et al., 2018; Khan and Khan, 2018). Therefore, pro-inflammatory cytokines and ROS exert forward feedback regulation of their production.

The inflammatory response can be turned off by the anti-inflammatory cytokine IL-10 (Opal and DePalo, 2000). The positive and negative regulatory inputs maintain normal innate immunity. However, if the balance is disturbed in some cases, for instance, inhibition of the immuo-suppressor cytokine IL-10, a cytokine storm takes place. Infections from such viruses as Ebola, avian influenza, dengue, and coronavirus, can lead to cytokine storms, producing a massive amount of pro-inflammatory cytokines. The concerted action of these inflammatory mediators causes the destruction of tissues and

cells, manifested by clinical syndromes such as extensive pulmonary edema, alveolar hemorrhage, ARDS, and multiple organ failures (Matthay and Zimmerman, 2005; Lau et al., 2013; Sordillo and Helson, 2015; Channappanavar and Perlman, 2017; Amini et al., 2018) (**Figure 1**).

There is clear evidence from coronavirus infected patients with both high cytokine levels and pathological changes in the lung (Wang et al., 2007; Channappanavar et al., 2016; Chen et al., 2020; Wu et al., 2020). For example, in plasma of COVID-19 patients, high concentrations of IL-2, IL-6, and IL-7 have been observed (Chen et al., 2020; Green, 2020; McGonagle et al., 2020; Wu et al., 2020). In particular, IL-6 was significantly elevated in critically ill patients with ARDS compared to patients without ARDS and was statistically significantly correlated with death (Wu et al., 2020). Both patients with mild or severe symptoms had pneumonia, and 29% of patients developed ARDS (Wang et al., 2020).

CURCUMIN INHIBITS INFLAMMATORY REACTION

Inhibition of the Production of Pro-Inflammatory Cytokine

Numerous *in vivo* and *in vitro* studies have been shown that curcumin and its analogs markedly inhibit the production and release of pro-inflammatory cytokines, such as IL-1, IL-6, IL-8, TNF-α (Avasarala et al., 2013; Zhang et al., 2015; Dai et al., 2018; Zhang et al., 2019). In line with this, Zhang et al. (2019) have observed that direct pulmonary delivery of solubilized curcumin dramatically diminishes pro-inflammatory cytokines IL-1β, IL-6, TNF-α in the BAL cells, the lung and serum of mice with severe pneumonia induced by Klebsiella. In addition, curcumin also decreases expression of many other inflammatory mediators, including MCP1(CCL2), MIPI1 (CCL3), GROα (CXCL1), GROβ (CXCL2), IP10 (CXCL10), SDF1 (CXCL12), MMP-2, IFN-γ, and MMP-9, which regulate the activity of immune cells and inflammatory responses and promote fibrosis in the lung after infection (Sordillo and Helson, 2015; Dai et al., 2018).

The mechanism underlying curcumin modulation of inflammation has been extensively investigated and engages diverse signaling pathways, among which NF-κB plays an essential role (Cohen et al., 2009; Salminen et al., 2011; Han et al., 2018). It was reported that curcumin effectively regulates NF-κB signaling through multiple mechanisms (**Figure 2**): First, curcumin inhibits activation of IKKβ (Cohen et al., 2009). In a study of patients with head and neck cancer receiving curcumin, reduced activity of IKKβ was observed in saliva samples, associated with a decrease in the expression of IL-8, TNF-α, and IFN-γ (Kim et al., 2011). Second, curcumin enhances the expression or stability of IκBα (Jobin et al., 1999; Han et al., 2018; Chen et al., 2019). Curcumin inhibits the IκBα degradation, phosphorylation of IκB serine 32 to block the cytokine-mediated

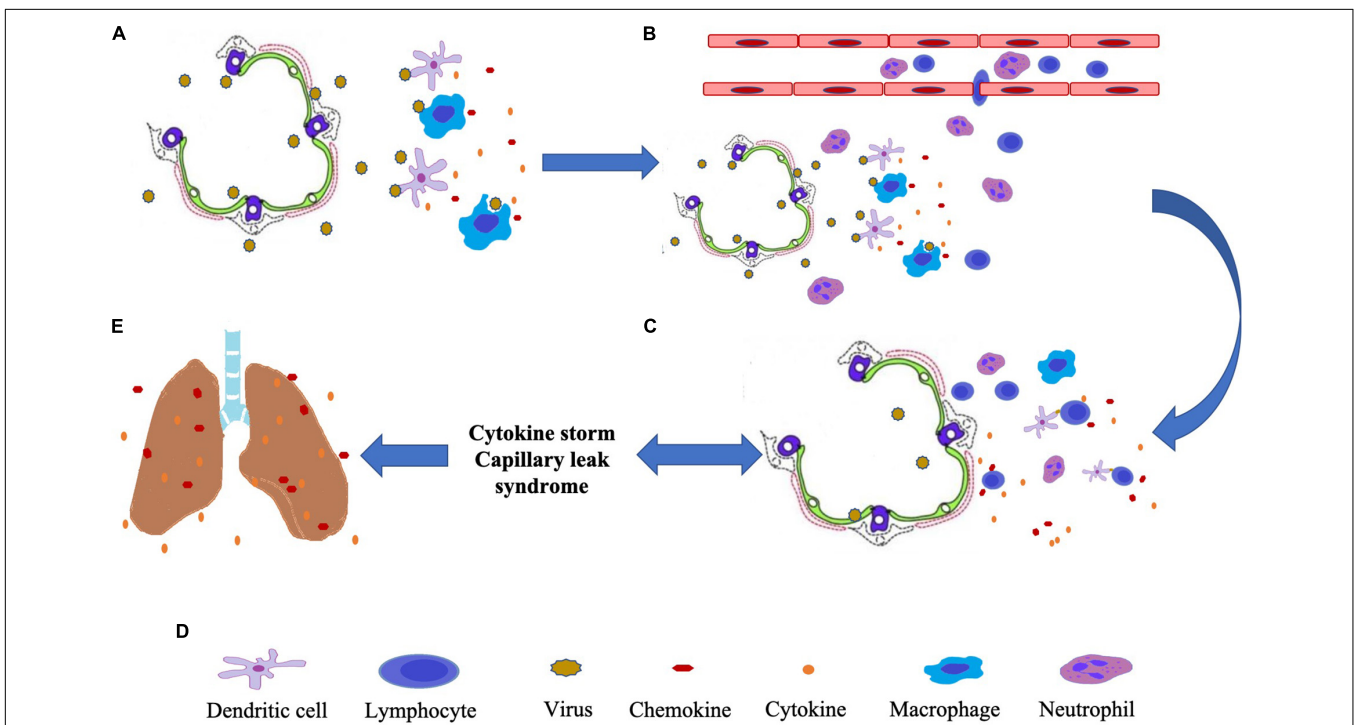

FIGURE 1 | The diagram of lung injury caused by virus-induced cytokine storms. **(A)** The viruses attack alveolar epithelial cells and are recognized by dendritic cells and macrophages, which then release cytokines. **(B)** Cytokines and chemokines help white blood cells in the blood reach the alveoli. **(C)** Antigen-presenting cells (dendritic cells) activate lymphocytes. Activated lymphocytes produce and release large amounts of cytokines while attacking infected alveolar epithelial cells. **(D)** Induce cytokine storm, and capillary leak syndrome. **(E)** Causes atelectasis, pulmonary edema, pulmonary congestion, and ARDS.

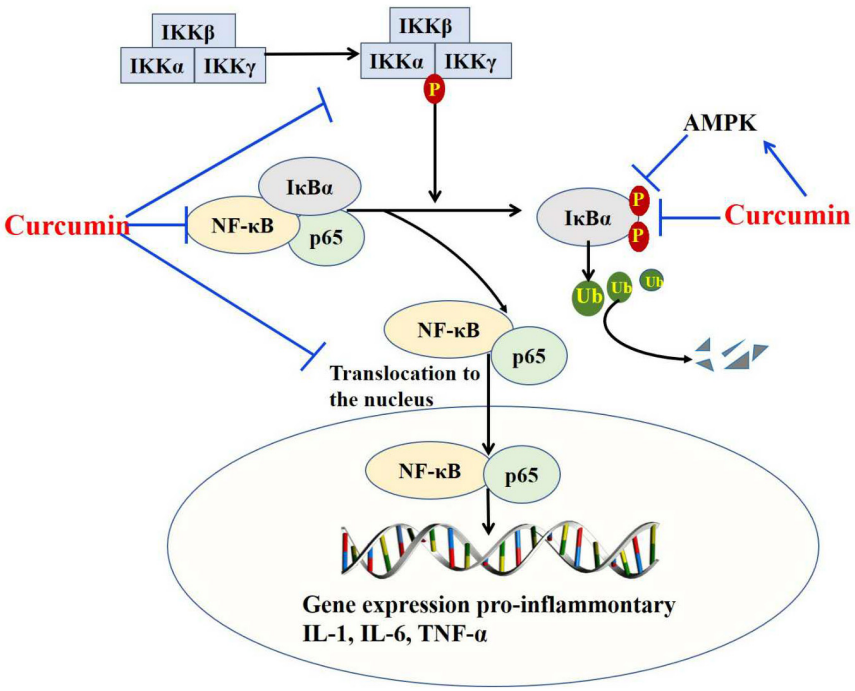

FIGURE 2 | Curcumin inhibits the production of pro-inflammatory cytokine by targeting the NF-κB pathway. Curcumin targets NF-κB signaling through inhibiting activation of IKKβ, enhancing expression or stability of IκBα, activating AMPK, and targeting P65.

NF-κB activation and thus pro-inflammatory gene expression (Jobin et al., 1999). Third, curcumin activates AMPK (Han et al., 2018). It has been documented that curcumin blocks NF-κB signaling upon infection with Influenza A virus (IAV) as a consequence of AMPK activation (Han et al., 2018). Fourth, curcumin acts on p65 to disturb the NF-κB pathway (Xu and Liu, 2017). Infection with IAV led to a decrease of p65 in the cytosol of macrophages and a corresponding increase in the nucleus, where it forms a functional complex with NF-κB, ultimately upregulating transcription of pro-inflammatory cytokines. In contrast, the use of curcumin blocks the nuclear translocation of NF-κB and p65, downregulating transcription of the cytokine genes (Xu and Liu, 2017).

Other inflammatory mediators have been reported to be regulated by curcumin. One of them is cyclooxygenase 2 (COX-2), a key enzyme for the synthesis of prostaglandin (Khan and Khan, 2018). In an animal model of chronic obstructive pulmonary disease, it has been shown that curcumin treatment effectively inhibits the degradation of IκBα and disturbs the production of COX-2 (Yuan et al., 2018). In addition to disrupting the NF-κB pathway, curcumin inhibits the virus-induced expression of TLR2/4/7, MyD88, TRIF, and TRAF6 genes, and blocks IAV-induced phosphorylation of Akt, p38, JNK as well (Sordillo and Helson, 2015; Dai et al., 2018).

Regulation of Anti-inflammatory Cytokines

In contrast to its negative effect on pro-inflammatory molecules, curcumin has been shown to regulate anti-inflammatory cytokines positively, in particular IL-10 (Larmonier et al., 2008; Chen et al., 2018; Mollazadeh et al., 2019; Chai et al., 2020). The latter is an essential negative regulator for inflammatory responses and is secreted by the dendritic cells that bind to DAMP released from damaged cells during aseptic or antigenic inflammatory reactions. IL-10 acts on inflammatory monocytes to reduce the release of TNF-α, IL-6, and ROS, thereby alleviating tissue damage caused by the continuous inflammatory response (Bamboat et al., 2010). Moreover, IL-10 drives the differentiation of Tregs (Mollazadeh et al., 2019). An early study has shown that IL-10 reduces the expression of intercellular adhesion molecule-1 (ICAM-1) on pulmonary vascular and TNF-α levels, which cause reduction of the expression of myeloperoxidase and the number of neutrophils in BAL fluids, consequently alleviating the lung damage (Mulligan et al., 1993).

Many studies have revealed that curcumin and curcuminoids potently increase the expression, production, and activity of IL-10 (Larmonier et al., 2008; Chen et al., 2018; Mollazadeh et al., 2019; Chai et al., 2020). Chai et al. (2020) have depicted the effect of curcumin on ALI/ARDS using cecal ligation and puncture (CLP)-induced ALI mouse model. In this study, curcumin noticeably attenuates lung injury by inducing the differentiation of regulatory T cells (Tregs) and upregulating IL-10 production. Similar effects have been observed in the neuropathic model, colitis model, and other inflammatory diseases. Therefore, in the context of inflammation, curcumin can act as a double-edged sword, downregulating pro-inflammatory cytokines, and upregulating anti-inflammatory IL-10 (Chai et al., 2020).

SCAVENGES ROS

It has been described that curcumin acts to directly scavenge ROS as a polyphenolic antioxidant (Wang et al., 2008). Curcumin has two active groups, one hydroxy hydrogen on the benzene ring that has an anti-oxidation effect and the other a β-diketone moiety. *In vitro* experiments have shown that curcumin effectively scavenges on ROS removal and anti-oxidation, curcumin has been shown effective at scavenging the superoxide anion radical produced by illuminating riboflavin and the OH^- produced by the Fenton reaction. Curcumin also inhibits the peroxidation of lecithin and DNA oxidative damage caused by ROS (Wang et al., 2008).

The ability of curcumin to scavenge ROS can be indirect via enzymatic regulation. For example, curcumin can upregulate superoxide dismutase 2 (SOD2), a key enzyme to convert O^{2-} to H_2O_2, which is then reduced to H_2O by glutathione (GSH) redox system (Forrester et al., 2018). In a study examining liver damage in rats, the GSH redox system was shown to be inhibited by the folic acid antagonist Methotrexate, resulting in hepatic oxidative damage. Curcumin is able to reverse this effect and enhance the effectiveness of SOD so as to maintain the oxidant/antioxidant balance and mitigate liver damage (Hemeida and Mohafez, 2008). Recently, curcumin was reported to oppose the effect of ROS on pro-inflammatory cytokine expression (e.g., IL-1b, IL-18) by downregulation of the thioredoxin interacting protein/NLR pyrin domain containing 3 (TXNIP/NLRP3) (Ren et al., 2019).

ANTIVIRAL ACTIVITY OF CURCUMIN

Many studies have documented that curcumin disrupts the viral infection process via multiple mechanisms, including directly targeting viral proteins, inhibiting particle production and gene expression, and blocking the virus entry, replication, and budding (Wen et al., 2007; Basu et al., 2013; Ou et al., 2013; Du et al., 2017; Kannan and Kolandaivel, 2017; Yang et al., 2017; Dai et al., 2018; Praditya et al., 2019). A recently *in vitro* study has demonstrated that curcumin inhibits respiratory syndrome virus (RSV) by blocking attachment to host cells (Yang et al., 2017). In this study, curcumin was also found to prevent the replication of RSV in human nasal epithelial cells. Additional evidence suggests that curcumin inhibits Porcine reproductive and RSV (PRRSV) attachment, possibly by disrupting the fluidity of viral envelopes (Du et al., 2017). Curcumin also obstructs virus infection by inhibiting PRRSV-mediated cell fusion, virus internalization, and uncoating (Du et al., 2017).

For a century, different subtypes of IAV, H1N1, H2N2, H3N2, and H5N1 have been the leading cause of pandemic outbreaks in the world. It has been reported that curcumin and its derivatives have a high binding affinity to hemagglutinin (HA), a major capsid glycoprotein of influenza virus that mediates virus attachment (Kannan and Kolandaivel, 2017). Ou et al. (2013) have demonstrated that curcumin interacts with HA and disturbs the integrity of membrane structure to block virus binding to host cells and prevent IAV entry. In another study with cells infected by IAV, it was found that curcumin directly inactivates various strains of IAV, disturbs their adsorption, and inhibits their replication (Dai et al., 2018). Further, the study showed that curcumin inhibits IAV absorption and replication by activating the NF-E2-related factor 2 (Nrf2)-hemeoxygenase-1 (HO-1)-axis, a classical anti-inflammatory and antioxidative signaling, which possesses antiviral activity (Dai et al., 2018).

Furthermore, curcumin acts against SARS-CoV (Wen et al., 2007). Accordingly, a study on the anti-SARS-CoV activity of 221 phytocompounds revealed that 20 μM of curcumin exhibits significant inhibitory effects in a Vero E6 cell-based cytopathogenic effect (CPE) assay. The authors presented evidence for a mild effect of curcumin against SARS-CoV replication and the inhibitory effect of curcumin on SARS-CoV 3CL protease activity, which is essential for the replication of SARS-CoV. This study provides promising evidence for curcumin as a potential anti-SARS-CoV agent (Wen et al., 2007).

CURCUMIN ALLEVIATES EXUDATION AND EDEMA CAUSED BY INFLAMMATION

Inflammation plays a pivotal role in the pathogenesis of lung complications of viral infection, as manifested by lung edema, hemorrhage, neutrophil infiltration, and alveolar thickening. Studies indicate that curcumin and its analogs are capable of attenuating lung injury (Suresh et al., 2012; Avasarala et al., 2013; Zhang et al., 2015; Xiao et al., 2019). Polymorphonuclear neutrophils (PMNs) infiltration is associated with pulmonary edema and could release oxidants and proteases, which consequently damage the alveolar-capillary membrane, leading to leakage of plasma proteins out of blood vessels, thereby causing pulmonary edema (Matthay and Zimmerman, 2005). It has been shown that curcumin can inhibit the infiltration of PMNs, including $(GR1^+)$, $CD4^+$, $CD19^+$ B cells, NK cells, and $CD8^+$ T cells, and promote the apoptosis of PMN by increasing the level of P-p38 (Avasarala et al., 2013). More recently, Xiao et al. (2019) have reported that curcumin analog C66 protects lipopolysaccharide (LPS)-induced ALI through suppression of the JNK pathway and subsequent inhibition of inflammatory cytokine expression. Similar protective effects of curcumin have been reported in the rodent model of ventilator-induced lung injury (Wang et al., 2018) and Staphylococcus *S.aureus*-induced ALI (Xu et al., 2015) as evidenced by attenuation of inflammatory cell infiltration, lung edema due to its anti-inflammatory and antioxidant effects. In a chronic obstructive pulmonary disease model, curcumin treatment effectively reduces the degree of airway inflammation and disrupts airway remodeling by inhibiting the proliferation of bronchial epithelial cells (Yuan et al., 2018).

Mechanistically, curcumin protects the lung by inhibiting inflammation and production of ROS through regulation of multiple signaling pathways engaging peroxisome proliferator-activated receptor γ (PPARγ) (Cheng et al., 2018), JNK (Xiao et al., 2019), NF-κB (Suresh et al., 2012; Wang et al., 2018),

and Nrf2 (Dai et al., 2018; Han et al., 2018). Notably, the role of curcumin in regulating Nrf2/HO-1 has been reported in IAV infection (Dai et al., 2018; Han et al., 2018). The Nrf2 enhances the expression of HO-1, an immunoregulatory and anti-inflammation molecule, and other enzymes for maintaining redox homeostasis. The increased expression of HO-1 can alleviate the pathological remolding of the lung during viral infection and increase the survival rate in mice following IAV infection. Curcumin has been shown to stimulate transcription of Nrf2 and thus enhance HO-1 expression *in vivo*, protecting alveoli from merging, inflating and enlarging, and decreasing inflammatory exudation of proteins to alveoli spaces after infection (Dai et al., 2018; Han et al., 2018).

CURCUMIN SUPPRESSES FIBROSIS

The ALI after the viral infection is often followed by pulmonary fibrosis, which can lead to the death. It has been reported that curcumin can inhibit pulmonary fibrosis. Thus, in paraquat-treated mice, collagen deposition in the lung causes diffused fibrosis, while treatment with curcumin reduces collagen deposition and decelerates the development of pulmonary fibrosis (Chen et al., 2017). In the radiation-induced lung damage model, cytokine accumulation and collagen deposition occur in the interstitial space, concurrent with fibrosis of the lung tissue (Amini et al., 2018). However, curcumin reduces the expression of cytokines such as IL-4 and TGF-β, inhibits the infiltration of macrophages and lymphocytes, and ameliorates fibrosis (Amini et al., 2018). In another study on ALI using a mouse model infected with reovirus, curcumin treatment effectively inhibits the production of collagen and procollagen I mRNA (Avasarala et al., 2013). α-SMA, a marker of epithelial to mesenchymal transition, and Tenascin-C (TN-C), both of which are indicators of pulmonary fibrosis, are highly expressed in the adult lung parenchyma after ALI. The high expression of E-cadherin, accompanied by cell proliferation and repair, is associated with pulmonary remodeling after lung injury. Treatment with curcumin reduces the expression of TN-C, α-SMA, and E-cadherin attenuates myofibroblast differentiation and mitigates pulmonary fibrosis. Furthermore, curcumin decreases the expression of the TGF-β receptor II (TGF-ß RII), suggesting that it prevents TGF-β-mediated pulmonary fibrosis. In bleomycin/SiO2/amiodarone-induced pulmonary fibrosis experiments, it was also demonstrated that curcumin directly reduces the expression of TGF-β protein and its mRNA (Avasarala et al., 2013). All these studies support that curcumin alleviates pulmonary fibrosis.

THE POTENTIAL ROLE OF CURCUMIN IN THE PREVENTION AND TREATMENT OF CORONAVIRUS INFECTION

In the last two decades, coronavirus infection has gained much attention for its high mortality. The consensus from recent research is that the cytokine storm plays a crucial role in the development and progression of fatal pneumonia. Among those who experienced SARS-CoV infection in 2003, many manifested ALI and developed ARDS, and the death rate was greater than 10% (Peiris et al., 2004). Similar syndromes are seen in the MERS-CoV, H5N1, H7N9, and SARS-CoV2 infection. The high mortality rate from fatal pneumonia is due to the over-activation of immune cells in the lung (Channappanavar and Perlman, 2017).

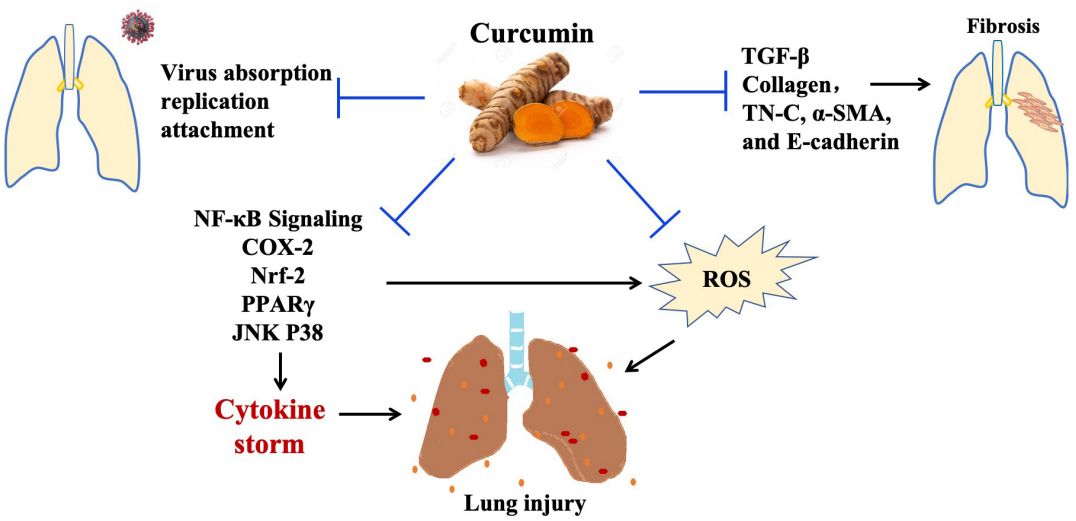

FIGURE 3 | The effects of curcumin in virus associated with severe pneumonia. Curcumin inhibits virus-induced lung injury through its antivirus, anti-inflammation, antioxidant activity. In addition, curcumin could suppress fibrosis by targeting TGF-β signaling. Abbreviations: Nrf2, nuclear factor erythroid-derived 2; NF-κB, nuclear factor-κB; PPARγ, peroxisome proliferator-activated receptor γ; TNF-α, tumor necrosis factor-alpha; COX2, cyclooxygenase-2; IκB, inhibitor of kappa B; IL, interleukin; JNK, c-Jun N-terminal Kinase; TN-C, tenascin-C; α-SMA, alpha-smooth muscle actin.

Targeting cytokine storm is considered as an essential strategy for CoV infections. In clinical settings, glucocorticoids have been used to treat fatal viral pneumonia and shown therapeutic benefits. In the treatment of patients with SARS in 2003, glucocorticoids were widely used to suppress the cytokine storm in severe cases (Buchman, 2001). However, it has been found that large doses of glucocorticoids create many side effects such as osteoporosis and secondary infection with other pathogenic microbes, and small doses have little effect on improving lung injury (Buchman, 2001). These clinical findings indicate that it is increasingly important to seek alternative agents with effectiveness and low toxicity.

Many studies on virus-induced pneumonia have highlighted the potential usage of curcumin in the improvement of lung index and survival rate (Avasarala et al., 2013; Xu and Liu, 2017; Dai et al., 2018; Han et al., 2018; Lai et al., 2020). Curcumin mitigates the severity of viral pneumonia through inhibiting the production of inflammatory cytokines and NF-κB signaling in macrophages (Xu and Liu, 2017; Han et al., 2018). Curcumin has also been shown to activate Nrf2 in association with reduced oxidative stress and inhibit TLR2/4, p38/JNK MAPK, and NF-κB in response to IAV infection; and as a result, pneumonia is improved (Dai et al., 2018).

Up to now, it has been claimed that curcumin benefits human health and prevents diseases (DiSilvestro et al., 2012; Zhu et al., 2019). A recent study suggested that a low dose of curcumin (80 mg/day) produced a variety of health-promoting actions, such as direct and indirect antioxidant actions (DiSilvestro et al., 2012). Additionally, accumulating evidence from animal studies has shown that curcumin prevents the development of severe pneumonia. Thus, pre-treatment of curcumin (5 mg/kg/day) inhibits paraquat-induced lung inflammation and structural remodeling of the lung at an early phase of ALI (Tyagi et al., 2016). Bansal and Chhibber (2010) have demonstrated that pre-treatment of mice with curcumin (150 mg/kg) for 15 days before Klebsiella *pneumonia* infection prevents the tissue from injury and reduces ALI-associated pneumonia by the anti-inflammatory action of curcumin. The similar protective role of curcumin has been found in preclinical studies of viral-induced pneumonia. Treatment with curcumin (50 mg/kg/day) beginning at 5 days prior to reovirus 1/L infection protects CBA/J mice from the development of ALI/ARDS and suppresses subsequent fibrosis (Avasarala et al., 2013). Lai et al. (2020) have reported that pre-infection or post-infection administration of curcumin significantly improves the lung index and prolongs the survival rate. Interestingly, the fatality rate is also reduced by pre-administration with curcumin (Lai et al., 2020). All these studies suggest that curcumin administration could have both prophylactic and therapeutic effects on virus-induced pneumonia and mortality.

Clinical investigations have suggested that curcumin might be effective in improving inflammation and the treatment of virus infections. A clinical trial conducted by Alizadeh et al. (2018) have demonstrated that curcumin nanomicelle supplement ameliorates oxidative stress, and reduces inflammatory biomarker, including TNF-α, compared to a placebo. Furthermore, a phase II randomized controlled study has reported that the topical application of curcumin and curcumin polyherbal cream has a higher HPV clearance rate than the placebo (Basu et al., 2013).

Currently, no data in humans on the link between curcumin and coronavirus infection have been available, but in light of and its preventative and therapeutic role in viral infection and cytokine storms common to all viral infections, curcumin could conceivably be considered as an attractive agent for the management of coronavirus infections.

CONCLUSION

Cytokine storm syndrome triggered by viral infections is the culprit of death. It is exacerbated by unchecked regulation of the production of pro-inflammatory cytokines and ROS, leading to pneumonia, ALI, multiple organs failures, and eventually death. No effective therapy is available for the cytokine storm syndrome and associated lung and other organ failures. Curcumin is a natural plant extract with high safety and low toxicity such that people take it as a diet supplement, and growing evidence from preclinical studies demonstrates that it effectively inhibits viral infection, alleviates the severity of lung injury through offsetting the cytokine storm, inhibits subsequent fibrosis, and increases survival rates (**Figure 3**). Additionally, its anti-SARS-CoV replication and 3CL protease have been reported in an *in vitro* study (Wen et al., 2007). In sum, the preclinical studies we have reviewed here motivate a call for attention to the clinical investigation of curcumin as a therapeutic agent for the cytokine storm syndrome following coronavirus infections, especially pneumonia caused by the coronavirus.

AUTHOR CONTRIBUTIONS

ZL contributed to the preparation of the manuscript and editing. YY contributed to the literature research, revision, and final approval of the manuscript.

FUNDING

This study was supported by the National Natural Science Foundation of China (Nos. 81560299 and 81660163), and Innovation and Entrepreneurship grant from Jiangxi Province Bureau of Foreign Experts.

ACKNOWLEDGMENTS

We are grateful to Professor Zhijun Luo for his comments, constructive suggestions, and generous help in the preparation of this manuscript.

REFERENCES

Alizadeh, F., Javadi, M., Karami, A. A., Gholaminejad, F., Kavianpour, M., and Haghighian, H. K. (2018). Curcumin nanomicelle improves semen parameters, oxidative stress, inflammatory biomarkers, and reproductive hormones in infertile men: a randomized clinical trial. *Phytother. Res.* 32, 514–521. doi: 10.1002/ptr.5998

Amalraj, A., Varma, K., Jacob, J., Divya, C., Kunnumakkara, A. B., Stohs, S. J., et al. (2017). A novel highly bioavailable curcumin formulation improves symptoms and diagnostic indicators in rheumatoid arthritis patients: a randomized, double-blind, placebo-controlled, two-dose, three-arm, and parallel-group study. *J. Med. Food* 20, 1022–1030. doi: 10.1089/jmf.2017.3930

Amini, P., Saffar, H., Nourani, M. R., Motevaseli, E., Najafi, M., Ali Taheri, R., et al. (2018). Curcumin mitigates radiation-induced lung pneumonitis and fibrosis in rats. *Int. J. Mol. Cell. Med.* 7, 212–219. doi: 10.22088/ijmcm.Bums.7.4.212

Asadi, S., Gholami, M. S., Siassi, F., Qorbani, M., Khamoshian, K., and Sotoudeh, G. (2019). Nano curcumin supplementation reduced the severity of diabetic sensorimotor polyneuropathy in patients with type 2 diabetes mellitus: a randomized double-blind placebo- controlled clinical trial. *Complement. Ther. Med.* 43, 253–260. doi: 10.1016/j.ctim.2019.02.014

Avasarala, S., Zhang, F., Liu, G., Wang, R., London, S. D., and London, L. (2013). Curcumin modulates the inflammatory response and inhibits subsequent fibrosis in a mouse model of viral-induced acute respiratory distress syndrome. *PLoS One* 8:e57285. doi: 10.1371/journal.pone.0057285

Baldwin, A. S. Jr. (1996). The NF-κB and IκB proteins: new discoveries and insights. *Annu. Rev. Immunol.* 14, 649–683.

Bamboat, Z. M., Ocuin, L. M., Balachandran, V. P., Obaid, H., Plitas, G., and DeMatteo, R. P. (2010). Conventional DCs reduce liver ischemia/reperfusion injury in mice via IL-10 secretion. *J. Clin. Investig.* 120, 559–569. doi: 10.1172/jci40008

Bansal, S., and Chhibber, S. (2010). Curcumin alone and in combination with augmentin protects against pulmonary inflammation and acute lung injury generated during *Klebsiella pneumoniae* B5055-induced lung infection in BALB/c mice. *J. Med. Microbiol.* 59(Pt 4), 429–437. doi: 10.1099/jmm.0.016873-0

Basu, P., Dutta, S., Begum, R., Mittal, S., Dutta, P. D., Bharti, A. C., et al. (2013). Clearance of cervical human papillomavirus infection by topical application of curcumin and curcumin containing polyherbal cream: a phase II randomized controlled study. *Asian Pac. J. Cancer Prev.* 14, 5753–5759. doi: 10.7314/apjcp.2013.14.10.5753

Behrens, E. M., and Koretzky, G. A. (2017). Cytokine storm syndrome: looking toward the precision medicine era. *Arthritis Rheumatol.* 69, 1135–1143. doi: 10.1002/art.40071

Buchman, A. L. (2001). Side effects of corticosteroid therapy. *J. Clin. Gastroenterol.* 33, 289–294. doi: 10.1097/00004836-200110000-00006

Chai, Y. S., Chen, Y. Q., Lin, S. H., Xie, K., Wang, C. J., Yang, Y. Z., et al. (2020). Curcumin regulates the differentiation of naïve CD4+T cells and activates IL-10 immune modulation against acute lung injury in mice. *Biomed. Pharmacother.* 125:109946. doi: 10.1016/j.biopha.2020.109946

Channappanavar, R., Fehr, A. R., Vijay, R., Mack, M., Zhao, J., Meyerholz, D. K., et al. (2016). Dysregulated type I interferon and inflammatory monocyte-macrophage responses cause lethal pneumonia in SARS-CoV-infected mice. *Cell Host Microbe* 19, 181–193. doi: 10.1016/j.chom.2016.01.007

Channappanavar, R., and Perlman, S. (2017). "Pathogenic human coronavirus infections: causes and consequences of cytokine storm and immunopathology. *Semin. Immunopathol.* 39, 529–539. doi: 10.1007/s00281-017-0629-x

Chen, B., Li, H., Ou, G., Ren, L., Yang, X., and Zeng, M. (2019). Curcumin attenuates MSU crystal-induced inflammation by inhibiting the degradation of IκBα and blocking mitochondrial damage. *Arthritis Res. Ther.* 21:193. doi: 10.1186/s13075-019-1974-z

Chen, H., Yang, R., Tang, Y., Xu, J., Feng, Y., Liu, S., et al. (2017). Effects of curcumin on pulmonary fibrosis and functions of paraquat-challenged rats. *Zhonghua Wei Zhong Bing Ji Jiu Yi Xue* 29, 973–976.

Chen, L., Lu, Y., Zhao, L., Hu, L., Qiu, Q., Zhang, Z., et al. (2018). Curcumin attenuates sepsis-induced acute organ dysfunction by preventing inflammation and enhancing the suppressive function of Tregs. *Int. Immunopharmacol.* 61, 1–7. doi: 10.1016/j.intimp.2018.04.041

Chen, X., Zhao, B., Qu, Y., Chen, Y., Xiong, J., Feng, Y., et al. (2020). Detectable serum SARS-CoV-2 viral load (RNAaemia) is closely correlated with drastically elevated interleukin 6 (IL-6) level in critically ill COVID-19 patients. *Clin. Infect. Dis.* doi: 10.1093/cid/ciaa449 [Epub ahead of print].

Cheng, K., Yang, A., Hu, X., Zhu, D., and Liu, K. (2018). Curcumin attenuates pulmonary inflammation in lipopolysaccharide induced acute lung injury in neonatal rat model by activating peroxisome proliferator-activated receptor γ (PPARγ) pathway. *Med. Sci. Monit.* 24, 1178–1184. doi: 10.12659/msm.908714

Cohen, A. N., Veena, M. S., Srivatsan, E. S., and Wang, M. B. (2009). Suppression of interleukin 6 and 8 production in head and neck cancer cells with curcumin via inhibition of Iκβ kinase. *Arch. Otolaryngol. Head Neck Surg.* 135, 190–197.

Dai, J., Gu, L., Su, Y., Wang, Q., Zhao, Y., Chen, X., et al. (2018). Inhibition of curcumin on influenza A virus infection and influenzal pneumonia via oxidative stress, TLR2/4, p38/JNK MAPK and NF-κB pathways. *Int. Immunopharmacol.* 54, 177–187. doi: 10.1016/j.intimp.2017.11.009

DiSilvestro, R. A., Joseph, E., Zhao, S., and Bomser, J. (2012). Diverse effects of a low dose supplement of lipidated curcumin in healthy middle aged people. *Nutr. J.* 11:79. doi: 10.1186/1475-2891-11-79

Du, T., Shi, Y., Xiao, S., Li, N., Zhao, Q., Zhang, A., et al. (2017). Curcumin is a promising inhibitor of genotype 2 porcine reproductive and respiratory syndrome virus infection. *BMC Vet. Res.* 13:298. doi: 10.1186/s12917-017-1218-x

Forrester, S. J., Kikuchi, D. S., Hernandes, M. S., Xu, Q., and Griendling, K. K. (2018). Reactive oxygen species in metabolic and inflammatory signaling. *Circ. Res.* 122, 877–902. doi: 10.1161/circresaha.117.311401

Green, M. S. (2020). Did the hesitancy in declaring COVID-19 a pandemic reflect a need to redefine the term? *Lancet* 395, 1034–1035. doi: 10.1016/s0140-6736(20)30630-9

Han, S., Xu, J., Guo, X., and Huang, M. (2018). Curcumin ameliorates severe influenza pneumonia via attenuating lung injury and regulating macrophage cytokines production. *Clin. Exp. Pharmacol. Physiol.* 45, 84–93. doi: 10.1111/1440-1681.12848

Hellebrekers, P., Vrisekoop, N., and Koenderman, L. (2018). Neutrophil phenotypes in health and disease. *Eur. J. Clin. Invest.* 48(Suppl. 2):e12943. doi: 10.1111/eci.12943

Hemeida, R., and Mohafez, O. M. (2008). Curcumin attenuates methotraxate-induced hepatic oxidative damage in rats. *J. Egypt. Natl. Canc. Inst.* 20, 141–148.

Huang, K. J., Su, I. J., Theron, M., Wu, Y. C., Lai, S. K., Liu, C. C., et al. (2005). An interferon-γ-related cytokine storm in SARS patients. *J. Med. Virol.* 75, 185–194. doi: 10.1002/jmv.20255

Jobin, C., Bradham, C. A., Russo, M. P., Juma, B., Narula, A. S., Brenner, D. A., et al. (1999). Curcumin blocks cytokine-mediated NF-κB activation and pro-inflammatory gene expression by inhibiting inhibitory factor I-κB kinase activity. *J. Immunol.* 163, 3474–3483.

Kalil, A. C., and Thomas, P. G. (2019). Influenza virus-related critical illness: pathophysiology and epidemiology. *Crit. Care* 23:258.

Kannan, S., and Kolandaivel, P. (2017). Antiviral potential of natural compounds against influenza virus hemagglutinin. *Comput. Biol. Chem.* 71, 207–218. doi: 10.1016/j.compbiolchem.2017.11.001

Khan, M. A., and Khan, M. J. (2018). Nano-gold displayed anti-inflammatory property via NF-kB pathways by suppressing COX-2 activity. *Artif. Cells Nanomed. Biotechnol.* 46, 1149–1158. doi: 10.1080/21691401.2018.1446968

Kim, S. G., Veena, M. S., Basak, S. K., Han, E., Tajima, T., Gjertson, D. W., et al. (2011). Curcumin treatment suppresses IKKβ kinase activity of salivary cells of patients with head and neck cancer: a pilot study. *Clin. Cancer Res.* 17, 5953–5961. doi: 10.1158/1078-0432.ccr-11-1272

Lai, Y., Yan, Y., Liao, S., Li, Y., Ye, Y., Liu, N., et al. (2020). 3D-quantitative structure-activity relationship and antiviral effects of curcumin derivatives as potent inhibitors of influenza H1N1 neuraminidase. *Arch Pharm Res.* doi: 10.1007/s12272-020-01230-5 [Epub ahead of print].

Larmonier, C. B., Uno, J. K., Lee, K. M., Karrasch, T., Laubitz, D., Thurston, R., et al. (2008). Limited effects of dietary curcumin on Th-1 driven colitis in IL-10 deficient mice suggest an IL-10-dependent mechanism of protection. *Am. J. Physiol. Gastrointest. Liver Physiol.* 295, G1079–G1091. doi: 10.1152/ajpgi.90365.2008

Lau, S. K., Lau, C. C., Chan, K.-H., Li, C. P., Chen, H., Jin, D.-Y., et al. (2013). Delayed induction of pro-inflammatory cytokines and suppression of innate antiviral response by the novel Middle East respiratory syndrome coronavirus: implications for pathogenesis and treatment. *J. Gen. Virol.* 94(Pt 12), 2679–2690. doi: 10.1099/vir.0.055533-0

Liu, Q., Zhou, Y.-H., and Yang, Z.-Q. (2016). The cytokine storm of severe influenza and development of immunomodulatory therapy. *Cell. Mol. Immunol.* 13, 3–10. doi: 10.1038/cmi.2015.74

Matthay, M. A., and Zimmerman, G. A. (2005). Acute lung injury and the acute respiratory distress syndrome: four decades of inquiry into pathogenesis and rational management. *Am. J. Respir. Cell Mol. Biol.* 33, 319–327. doi: 10.1165/rcmb.F305

McGonagle, D., Sharif, K., O'Regan, A., and Bridgewood, C. (2020). The role of cytokines including interleukin-6 in COVID-19 induced pneumonia and macrophage activation syndrome-like disease. *Autoimmun. Rev.* 19:102537. doi: 10.1016/j.autrev.2020.102537

Medzhitov, R. (2008). Origin and physiological roles of inflammation. *Nature* 454, 428–435. doi: 10.1038/nature07201

Mollazadeh, H., Cicero, A. F. G., Blesso, C. N., Pirro, M., Majeed, M., and Sahebkar, A. (2019). Immune modulation by curcumin: the role of interleukin-10. *Crit. Rev. Food Sci. Nutr.* 59, 89–101. doi: 10.1080/10408398.2017.1358139

Mulligan, M., Jones, M., Vaporciyan, A. A., Howard, M., and Ward, P. (1993). Protective effects of IL-4 and IL-10 against immune complex-induced lung injury. *J. Immunol.* 151, 5666–5674.

Netea, M. G., Balkwill, F., Chonchol, M., Cominelli, F., Donath, M. Y., Giamarellos-Bourboulis, E. J., et al. (2017). A guiding map for inflammation. *Nat. Immunol.* 18, 826–831.

Opal, S. M., and DePalo, V. A. (2000). Anti-inflammatory cytokines. *Chest* 117, 1162–1172.

Ou, J. L., Mizushina, Y., Wang, S. Y., Chuang, D. Y., Nadar, M., and Hsu, W. L. (2013). Structure–activity relationship analysis of curcumin analogues on anti-influenza virus activity. *FEBS J.* 280, 5829–5840. doi: 10.1111/febs.12503

Peiris, J. S., Guan, Y., and Yuen, K. Y. (2004). Severe acute respiratory syndrome. *Nat. Med.* 10(Suppl. 12) S88–S97. doi: 10.1038/nm1143

Praditya, D., Kirchhoff, L., Brüning, J., Rachmawati, H., Steinmann, J., and Steinmann, E. (2019). Anti-infective properties of the golden spice curcumin. *Front. Microbiol.* 10:912. doi: 10.3389/fmicb.2019.00912

Ren, Y., Yang, Z., Sun, Z., Zhang, W., Chen, X., and Nie, S. (2019). Curcumin relieves paraquat-induced lung injury through inhibiting the thioredoxin interacting protein/NLR pyrin domain containing 3-mediated inflammatory pathway. *Mol. Med. Rep.* 20, 5032–5040.

Richart, S. M., Li, Y. L., Mizushina, Y., Chang, Y. Y., Chung, T. Y., Chen, G. H., et al. (2018). Synergic effect of curcumin and its structural analogue (Monoacetylcurcumin) on anti-influenza virus infection. *J. Food Drug Anal.* 26, 1015–1023. doi: 10.1016/j.jfda.2017.12.006

Salminen, A., Hyttinen, J. M., and Kaarniranta, K. (2011). AMP-activated protein kinase inhibits NF-κB signaling and inflammation: impact on healthspan and lifespan. *J. Mol. Med.* 89, 667–676. doi: 10.1007/s00109-011-0748-0

Sordillo, P. P., and Helson, L. (2015). Curcumin suppression of cytokine release and cytokine storm. A potential therapy for patients with Ebola and other severe viral infections. *In Vivo* 29, 1–4.

Straub, J. M., New, J., Hamilton, C. D., Lominska, C., Shnayder, Y., and Thomas, S. M. (2015). Radiation-induced fibrosis: mechanisms and implications for therapy. *J. Cancer Res. Clin. Oncol.* 141, 1985–1994. doi: 10.1007/s00432-015-1974-6

Suresh, M. V., Wagner, M. C., Rosania, G. R., Stringer, K. A., Min, K. A., Risler, L., et al. (2012). Pulmonary administration of a water-soluble curcumin complex reduces severity of acute lung injury. *Am. J. Respir. Cell Mol. Biol.* 47, 280–287. doi: 10.1165/rcmb.2011-0175OC

Taniguchi, K., and Karin, M. (2018). NF-κB, inflammation, immunity and cancer: coming of age. *Nat. Rev. Immunol.* 18, 309–324. doi: 10.1038/nri.2017.142

Torres, J., Mehandru, S., and Colombel, J. (2017). F, Peyrin-Biroulet L. Crohn's disease. *Lancet* 389, 1741–1755.

Tyagi, N., Dash, D., and Singh, R. (2016). Curcumin inhibits paraquat induced lung inflammation and fibrosis by extracellular matrix modifications in mouse model. *Inflammopharmacology* 24, 335–345. doi: 10.1007/s10787-016-0286-z

Vitali, D., Bagri, P., Wessels, J. M., Arora, M., Ganugula, R., Parikh, A., et al. (2020). Curcumin can decrease tissue inflammation and the severity of HSV-2 infection in the female reproductive mucosa. *Int. J. Mol. Sci.* 21:337. doi: 10.3390/ijms21010337

Wang, W., Ye, L., Ye, L., Li, B., Gao, B., Zeng, Y., et al. (2007). Up-regulation of IL-6 and TNF-alpha induced by SARS-coronavirus spike protein in murine macrophages via NF-kappaB pathway. *Virus Res.* 128, 1–8. doi: 10.1016/j.virusres.2007.02.007

Wang, X., An, X., Wang, X., Bao, C., Li, J., Yang, D., et al. (2018). Curcumin ameliorated ventilator-induced lung injury in rats. *Biomed. Pharmacother.* 98, 754–761. doi: 10.1016/j.biopha.2017.12.100

Wang, X.-M., Zhang, J.-S., Gao, Y.-T., and Dai, Y. (2008). Scavenging effects of curcumin on active oxygens and its anti-oxidation *in vitro*. *Sci. Technol. Food Ind.* 7, 94–98.

Wang, Y., Wang, Y., Chen, Y., and Qin, Q. (2020). Unique epidemiological and clinical features of the emerging 2019 novel coronavirus pneumonia (COVID-19) implicate special control measures. *J. Med. Virol.* [Epub ahead of print].

Wen, C.-C., Kuo, Y.-H., Jan, J.-T., Liang, P.-H., Wang, S.-Y., Liu, H.-G., et al. (2007). Specific plant terpenoids and lignoids possess potent antiviral activities against severe acute respiratory syndrome coronavirus. *J. Med. Chem.* 50, 4087–4095. doi: 10.1021/jm070295s

Wheeler, A. P., and Bernard, G. R. (2007). Acute lung injury and the acute respiratory distress syndrome: a clinical review. *Lancet* 369, 1553–1564.

Wu, C., Chen, X., Cai, Y., Xia, J., Zhou, X., Xu, S., et al. (2020). Risk factors associated with acute respiratory distress syndrome and death in patients with coronavirus disease 2019 Pneumonia in Wuhan, China. *JAMA Intern. Med.* [Epub ahead of print].

Xiao, Z., Xu, F., Zhu, X., Bai, B., Guo, L., Liang, G., et al. (2019). Inhibition Of JNK phosphorylation by curcumin analog C66 Protects LPS-induced acute lung injury. *Drug Des. Dev. Ther.* 13, 4161–4171. doi: 10.2147/dddt.S215712

Xu, F., Diao, R., Liu, J., Kang, Y., Wang, X., and Shi, L. (2015). Curcumin attenuates staphylococcus aureus-induced acute lung injury. *Clin. Respir. J.* 9, 87–97. doi: 10.1111/crj.12113

Xu, X.-Y., Meng, X., Li, S., Gan, R.-Y., Li, Y., and Li, H.-B. (2018). Bioactivity, health benefits, and related molecular mechanisms of curcumin: current progress, challenges, and perspectives. *Nutrients* 10:1553. doi: 10.3390/nu10101553

Xu, Y., and Liu, L. (2017). Curcumin alleviates macrophage activation and lung inflammation induced by influenza virus infection through inhibiting the NF-κB signaling pathway. *Influenza Other Respir. Viruses* 11, 457–463. doi: 10.1111/irv.12459

Yang, X. X., Li, C. M., Li, Y. F., Wang, J., and Huang, C. Z. (2017). Synergistic antiviral effect of curcumin functionalized graphene oxide against respiratory syncytial virus infection. *Nanoscale* 9, 16086–16092. doi: 10.1039/c7nr06520e

Yang, Y. S., Su, Y. F., Yang, H. W., Lee, Y. H., Chou, J. I., and Ueng, K. C. (2014). Lipid-lowering effects of curcumin in patients with metabolic syndrome: a randomized, double-blind, placebo-controlled trial. *Phytother. Res.* 28, 1770–1777. doi: 10.1002/ptr.5197

Yao, X., Ye, F., Zhang, M., Cui, C., Huang, B., Niu, P., et al. (2020). In vitro antiviral activity and projection of optimized dosing design of hydroxychloroquine for the treatment of severe acute respiratory syndrome coronavirus 2 (SARS-CoV-2). *Clin. Infect. Dis.* [Epub ahead of print].

Yuan, J., Liu, R., Ma, Y., Zhang, Z., and Xie, Z. (2018). Curcumin attenuates airway inflammation and airway remolding by inhibiting NF-κB signaling and COX-2 in cigarette smoke-induced COPD mice. *Inflammation* 41, 1804–1814. doi: 10.1007/s10753-018-0823-6

Zhang, B., Swamy, S., Balijepalli, S., Panicker, S., Mooliyil, J., Sherman, M. A., et al. (2019). Direct pulmonary delivery of solubilized curcumin reduces severity of lethal pneumonia. *FASEB J.* 33, 13294–13309. doi: 10.1096/fj.201901047rr

Zhang, J., Wang, X., Vikash, V., Ye, Q., Wu, D., Liu, Y., et al. (2016). ROS and ROS-mediated cellular signaling. *Oxid. Med. Cell. Longev.* 2016:4350965. doi: 10.1155/2016/4350965

Zhang, Y., Liang, D., Dong, L., Ge, X., Xu, F., Chen, W., et al. (2015). Anti-inflammatory effects of novel curcumin analogs in experimental acute lung injury. *Respir. Res.* 16:43.

Zhu, L. N., Mei, X., Zhang, Z. G., Xie, Y. P., and Lang, F. (2019). Curcumin intervention for cognitive function in different types of people: a systematic review and meta-analysis. *Phytother. Res.* 33, 524–533. doi: 10.1002/ptr.6257

Conflict of Interest: The authors declare that the research was conducted in the absence of any commercial or financial relationships that could be construed as a potential conflict of interest.

frontiers in Cell and Developmental Biology

REVIEW
published: 12 June 2020
doi: 10.3389/fcell.2020.00474

The Role of RNA Splicing Factors in Cancer: Regulation of Viral and Human Gene Expression in Human Papillomavirus-Related Cervical Cancer

*Andrea Cerasuolo, Luigi Buonaguro, Franco M. Buonaguro and Maria Lina Tornesello**

Molecular Biology and Viral Oncology Unit, Istituto Nazionale Tumouri IRCCS–Fondazione G. Pascale, Naples, Italy

The spliceosomal complex components, together with the heterogeneous nuclear ribonucleoproteins (hnRNPs) and serine/arginine-rich (SR) proteins, regulate the process of constitutive and alternative splicing, the latter leading to the production of mRNA isoforms coding multiple proteins from a single pre-mRNA molecule. The expression of splicing factors is frequently deregulated in different cancer types causing the generation of oncogenic proteins involved in cancer hallmarks. Cervical cancer is caused by persistent infection with oncogenic human papillomaviruses (HPVs) and constitutive expression of viral oncogenes. The aberrant activity of hnRNPs and SR proteins in cervical neoplasia has been shown to trigger the production of oncoproteins through the processing of pre-mRNA transcripts either derived from human genes or HPV genomes. Indeed, hnRNP and SR splicing factors have been shown to regulate the production of viral oncoprotein isoforms necessary for the completion of viral life cycle and for cell transformation. Target-therapy strategies against hnRNPs and SR proteins, causing simultaneous reduction of oncogenic factors and inhibition of HPV replication, are under development. In this review, we describe the current knowledge of the functional link between RNA splicing factors and deregulated cellular as well as viral RNA maturation in cervical cancer and the opportunity of new therapeutic strategies.

Keywords: splicing factors, cervical cancer, human papillomavirus (HPV), RNA, heterogeneous nuclear ribonucleoproteins (hnRNPs), serine/arginine-rich proteins (SR)

OPEN ACCESS

Edited by:
Giulia De Falco,
Queen Mary University of London,
United Kingdom

Reviewed by:
Alok Chandra Bharti,
University of Delhi, India
John Charles Rotondo,
University of Ferrara, Italy

****Correspondence:***
Maria Lina Tornesello
m.tornesello@istitutotumouri.na.it

Specialty section:
This article was submitted to Molecular Medicine, a section of the journal Frontiers in Cell and Developmental Biology

Received: *24 March 2020*
Accepted: *20 May 2020*
Published: *12 June 2020*

Citation:
Cerasuolo A, Buonaguro L, Buonaguro FM and Tornesello ML (2020) The Role of RNA Splicing Factors in Cancer: Regulation of Viral and Human Gene Expression in Human Papillomavirus-Related Cervical Cancer. Front. Cell Dev. Biol. 8:474. doi: 10.3389/fcell.2020.00474

INTRODUCTION

The large majority of human genes are transcribed as pre-mRNAs, containing non-coding (introns) and coding sequences (exons), that are processed by spliceosomal complexes to remove introns and produce mature mRNAs (Shi, 2017). The alternative removal of introns from pre-mRNAs and joining of exons into different mature transcripts enables the translation of multiple proteins from the transcription of a single gene (Bush et al., 2017). For this reason, the approximately 20,000 human genes are able to encode at least 100,000 different proteins (Wang et al., 2015).

Cell proteins generated by alternative splicing are selectively expressed in a tissue-specific and time-dependent manner and contribute to the regulation of numerous metabolic pathways

involved in cell cycle control, differentiation and apoptosis (Baralle and Giudice, 2017). Aberrant splicing may cause the production of abnormal mRNA isoforms encoding mutated proteins with gain or loss of functions that are involved in neoplastic cell transformation, cancer development and metastasis (Oltean and Bates, 2014).

The role of spliceosome complexes and splicing regulatory factors in cancer has been widely investigated (Oltean and Bates, 2014). In particular, the snRNPs, the hnRNPs and the SR proteins have been shown to act either as oncoproteins or tumor suppressor proteins in different cancer types, including cervical neoplasia (Sorlie et al., 2001; Dvinge et al., 2016; Kohler et al., 2016; Cheng et al., 2017).

The aim of this review was to summarize the current studies on the role played by splicing factors in different cancer types with a particular focus on their peculiar activity in HPV-related cervical neoplasia. Indeed, in HPV infected cells the splicing factors are able to modulate the maturation either of cellular transcripts or of viral RNAs leading to the viral life cycle completion or production of viral and host cell transcripts encoding oncoproteins that cause transformation of cervical epithelium.

Abbreviations: BARD1, BRCA1 associated RING domain 1; BCLAF1, BCL2 associated transcription factor 1; BIN1, bridging integrator-1; BRCA1, breast cancer 1, early onset; BRM, brahma; BTG3, BTG anti-proliferation factor 3; Casp, caspase; CCAR1, cell cycle and apoptosis regulator 1; CCK, cholecystokinin; CCND1, cyclin D1; CDK, cyclin dependent kinase; CFTR, cystic fibrosis transmembrane conductance regulator; CIN, cervical intraepithelial neoplasia; Clk/Sty kinases, Cdc2-like kinase/Ser-Thr-Tyr kinase; COX-2, cyclooxygenase 2; CPSF30, cleavage polyadenylation specificity factor 30; CRH-R1, corticotropin-releasing hormone receptor type 1; CTGF, connective tissue growth factor; E2F1, E2F transcription factor 1; EFTUD2, elongation factor Tu GTP binding domain containing 2; EGFR, epidermal growth factor receptor; EIF3H, eukaryotic translation initiation factor 3 subunit H; EIF4A3, eukaryotic translation initiation factor 4A3; eIF4E, eukaryotic translation initiation factor 4E; EMT, epithelial-mesenchymal transition; ERK, extracellular signal-regulated kinase; ESE, exonic splicing enhancer; ESS, exonic splicing silencer; FASN, fatty acid synthase; FOXO4, forkhead box O4; GATA3, GATA binding protein 3; GCH1, GTP cyclohydrolase 1; GLUT1, glucose transporter; GSK3β, glycogen synthase kinase 3 beta; HDAC1, histone deacetylase 1; HIF-1α, hypoxia-inducible factor-1; hnRNP, heterogeneous nuclear ribonucleoprotein; HPV, human papillomavirus; Hsp90α/7C, heat shock protein 90α/7C; HSPA2, heat shock protein family A; IL1RAP, interleukin 1 receptor accessory protein; ILF3, interleukin enhancer-binding factor 3; ISE, intronic splicing enhancer; ISS, intronic splicing silencer; ITGA6, integrin subunit alpha 6; KH domain, K homology domain; LCR, long control region; LDHA, lactate dehydrogenase A; lncRNA, long non-coding RNA; MAPK, mitogen-activated protein kinase; MCM2/4, minichromosome maintenance complex component 2/4; miR, micro-RNA; MKNK2, MAPK interacting serine/threonine kinase 2; MMP3, matrix metallopeptidase 3; mTOR, mechanistic target of rapamycin kinase; NASP, nuclear autoantigenic sperm protein; NCL, nucleolin; NEK2, NIMA related kinase 2; NF-κB, nuclear factor kappa-light-chain-enhancer of activated B cells; NLS, nuclear localization signal; NMD, non-sense mediated decay; ORF, open reading frame; pAE/pAL, early/late polyadenylation signal; PARP, poly ADP-ribose polymerase; PCNA, proliferating cell nuclear antigen; PDCD4, programmed cell death 4; PDK1, pyruvate dehydrogenase kinase 1; pRb, retinoblastoma protein; Pre-mRNA, pre-messenger RNA; PTEN, phosphatase and tensin homolog; PTGS2, prostaglandin-endoperoxide synthase 2; RAC1, ras-related C3 botulinum toxin substrate 1; RASA1, RAS protein activator 1; Ron, recepteur d'origine nantais; RRM, RNA recognition motif; Sam68, Src-associated in mitosis 68 kDa; S6K2, S6 kinase 2; SD/SA, splice donor/acceptor site; SH2/SH3, Sarc homology 2/3; snRNP, small nuclear ribonucleoprotein; SR protein, serine/arginine-rich protein; SREBP1c, sterol regulatory element-binding transcription factor 1; SRPK, serine/arginine kinase; SRSF, serine/arginine-rich splicing factor; STAR, signal transduction and activation of RNA; STAT, signal transducer and activator of transcription; STK, serine/threonine kinase; SUMO1, small ubiquitin-like modifiers 1; SWI/SNF, SWItch/sucrose non-fermentable; TCGA, The Cancer Genome Atlas; TERC, telomerase RNA component; TOPO1, topoisomerase 1; TRA2B, transformer-2 protein homolog beta; TRF2, telomeric repeat-binding factor 2; U2AF65, U2 small nuclear RNA auxiliary factor 2; UTR, untranslated region; VEGF, vascular endothelial growth factor; WNK2, WNK lysine deficient protein kinase 2; XIAP, X-linked inhibitor of apoptosis; XIST, X inactive specific transcript; ZO-1, tight junction protein-1.

RNA SPLICING FACTORS

The removal of introns from pre-mRNAs is a process catalyzed by two large ribonucleoprotein complexes, namely major and minor spliceosomes, in cooperation with numerous splicing factors (Grabowski et al., 1985; Papasaikas and Valcarcel, 2016). The major spliceosome, responsible for more than 99% of splicing reactions in human cells, is composed of five uridine-rich small nuclear RNAs (snRNA U1, U2, U4, U5, and U6) and over 100 snRNA associated proteins (snRNPs) that undergo complex conformational changes during the different phases of splicing reactions (Frendewey and Keller, 1985; Wahl et al., 2009; Will and Luhrmann, 2011; Kastner et al., 2019). On the other hand, the minor spliceosome, including the U5 snRNA as well as functional analogs of the major spliceosome snRNAs (U11, U12, U4atac and U6atac), catalyzes the splicing of the less abundant U12-type introns (Tarn and Steitz, 1997; Turunen et al., 2013).

The splicing process consists of several sequential reactions involving recruitment of spliceosome components and interaction with *cis*-acting regulatory intronic sequences, such as the 5′ splice donor (SD) and 3′ splice acceptor (SA) sites, the intervening branch-point and the polypyrimidine tract (Aebi et al., 1986; Wang and Burge, 2008). Briefly, the formation of an early spliceosome complex involves the interaction of the U1 snRNP with the 5′ splice site through the base pairing of the U1 snRNA component, the binding of the U2 accessory factor (U2AF) to the polypyrimidine region and the connection of U2AF to U1 through the bridging splicing factor SF1. Binding of U2 snRNA to the branch sequence and 3′ splice site facilitates the U1 and U2 snRNPs interaction and the formation of the spliceosome complex A. Then, the U4/U5/U6 snRNP trimer interacts with the U1 and U2 snRNPs forming the spliceosome complex B, which releases the U1 and U4 snRNPs and becomes activated (complex C) (Wahl et al., 2009). The active spliceosome causes the final exclusion of the intron through: (1) the cleavage of the intron 5′-end; (2) the formation of a lariat (the 5′-end of the intron binds to the branch point); (3) the cleavage of the intron 3′-end; (4) the release of the lariat/U2/U5/U6 complex; and (5) the joining of exons (Lee and Rio, 2015; Papasaikas and Valcarcel, 2016) (**Figure 1**).

The alternative recognition of differential splice donor and acceptor sites allows the production of several mRNA isoforms according to five different figures: (1) the exon is totally or partially skipped; (2) mutually exclusive exons are included; (3) introns are retained; (4) alternative splice donor; or (5) splice acceptor sites are selectively chosen leading to the production of exons with different lengths (Lee and Rio, 2015; Wang et al., 2015) (**Figure 2**).

The fine tuning of pre-mRNA maturation is regulated by *trans*-acting splicing factors including hnRNPs, that generally

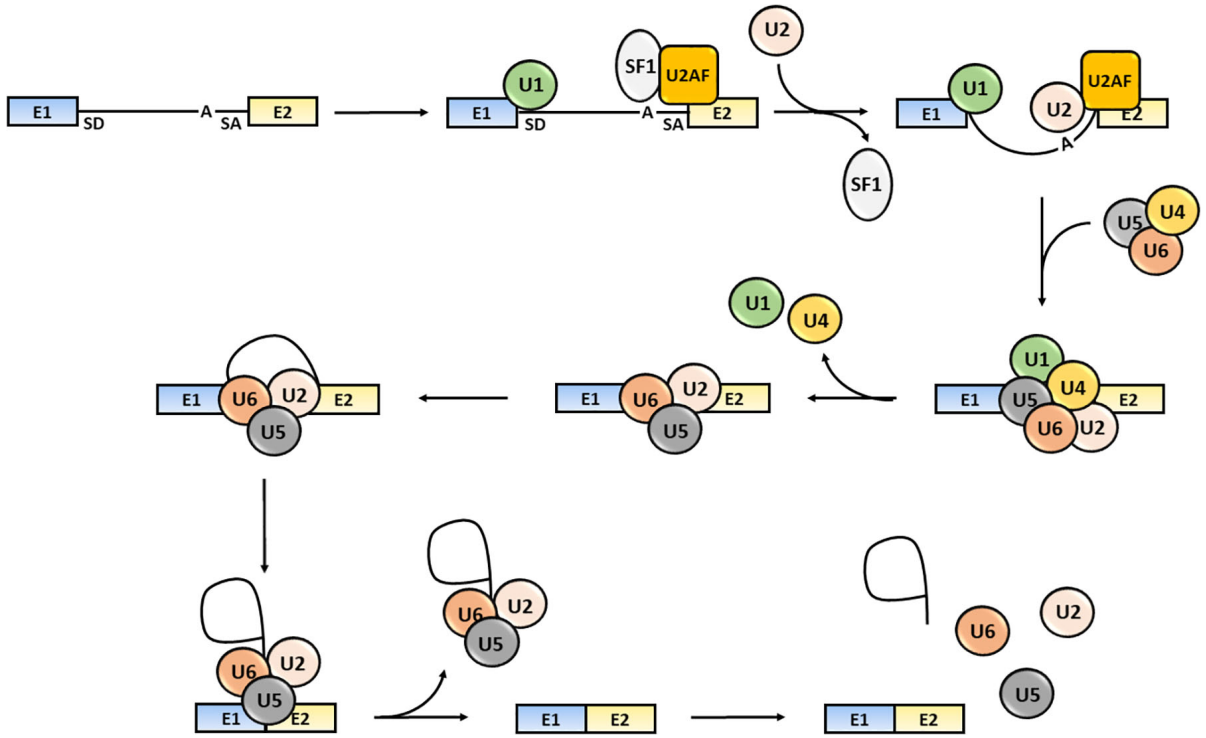

FIGURE 1 | Steps of the splicing process. The snRNP U1, SF1 and U2AF bind to the intron 5′-end SD site, to an intronic branch point site (A) and to the intron 3′-end SA site, respectively. The U2 displaces SF1 and the U4/U5/U6 snRNPs trimer interacts with snRNPs U1 and U2 causing U1 and U4 release. The activated spliceosome catalyzes the cleavage of the intron 5′-end, the formation of a lariat, the intron the cleavage of the intron 3′-end, the release of the lariat/U2/U5/U6 complex release and joining of exons (Shi, 2017). Exons are defined as "E"; the intron is represented as a black solid line.

inhibit the splicing by binding to exonic (ESSs) or intronic splicing silencers (ISSs) sequences, and SR proteins that typically activate the splicing by interacting with exonic (ESEs) and intronic (ISEs) splicing enhancers (Wang and Burge, 2008; Chen and Manley, 2009) (**Figure 3**).

The hnRNPs are a protein family comprising 20 major RNA-binding proteins that contain a RRM, a quasi-RRM domain and a K Homology (KH) domain binding to pre-mRNA sequences as well as a glycine-rich domain interacting with other hnRNPs (Busch and Hertel, 2012). The canonical function of hnRNPs is the inhibition of splicing reactions through their binding to cognate sites and repression of either the assembly of the spliceosome complex on the 5′-SD and 3′-SA sites or the recruitment of SR proteins on ESEs and ISEs following multimerization along exons or by looping out entire exons (Nasim et al., 2002; Geuens et al., 2016; Dvinge, 2018; Ule and Blencowe, 2019) (**Figure 3**). On the other hand, some hnRNPs have been shown to promote splicing through their interaction with ISE sequences containing G triplets. Indeed, hnRNP A1 and hnRNP F have been recognized to bind a AGGGA sequence in the 5′ GA-rich enhancer within the intron 10 of the insulin receptor gene (INSR) transcript as well as similar motifs located at the 3′ end of the same intron and to regulate the skipping or the inclusion of exon 11 causing the differential expression of the insulin receptor A or B isoforms, respectively (Talukdar et al., 2011).

Most of the hnRNPs, including hnRNP A1/A2, hnRNP B1/B2, hnRNP E, hnRNP J, and hnRNP K, are localized to the nucleus and after homomeric and heteromeric complexes formation they shuttle to the cytoplasm via the transportins binding (Siomi and Dreyfuss, 1995; Mili et al., 2001; Geuens et al., 2016). On the other hand, hnRNP C and hnRNP U possess a nuclear retention sequence that inhibits transfer to the cytoplasm (Nakielny and Dreyfuss, 1996; Mili et al., 2001). Post-translational modifications of hnRNPs, such as serine and threonine phosphorylation, arginines methylation, SUMOylation and ubiquitination, affect their sub-cellular localization and modulate positively or negatively their activity (Lee et al., 2012; Friend et al., 2013; Moujalled et al., 2015; Wang et al., 2017). For instance, the ERK kinase was shown to phosphorylate hnRNP K serines 284 and 353 in response to stress stimuli and to cause cytoplasmic accumulation and inhibition of hnRNP K-mediated translation in HeLa cells (Habelhah et al., 2001). In addition, the hnRNPs are able to modulate also the mRNA stability, capping, transport and poly-adenylation as well as to regulate the telomeres maintenance and chromatin organization (Han et al., 2010; Geuens et al., 2016).

The SR proteins family includes twelve serine-arginine rich splicing factors (SRSF1 to 12) characterized by canonical RRM, that interact with the ESE and ISE elements, and C-terminal serine-arginine repeats, which facilitate the recruitment of the spliceosome components to the splice sites (i.e., the binding of

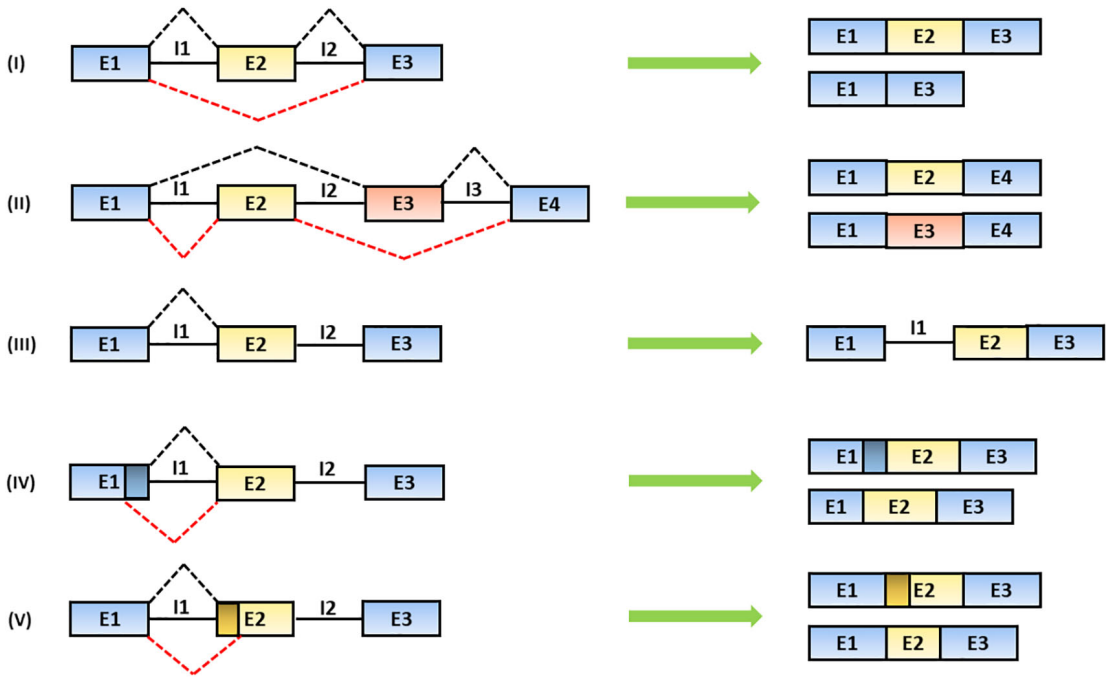

FIGURE 2 | Mechanisms of alternative splicing. The spliceosome generates distinct mRNA isoforms by alternative usage of splice donor (SD) and acceptor (SA) sites, located at the 5′ and 3′ end of introns, respectively. The splicing products include: (I) exon skipping (the partial or total removal of exons), (II) inclusion of mutually exclusive exons, (III) intron retention and the use of alternative (IV) SD or (V) SA sites (Baralle and Giudice, 2017). In the figure, black solid lines represent introns; black and red dashed lines represent alternative splicing mechanisms. Exons are indicated as "E" and introns are indicated as "I."

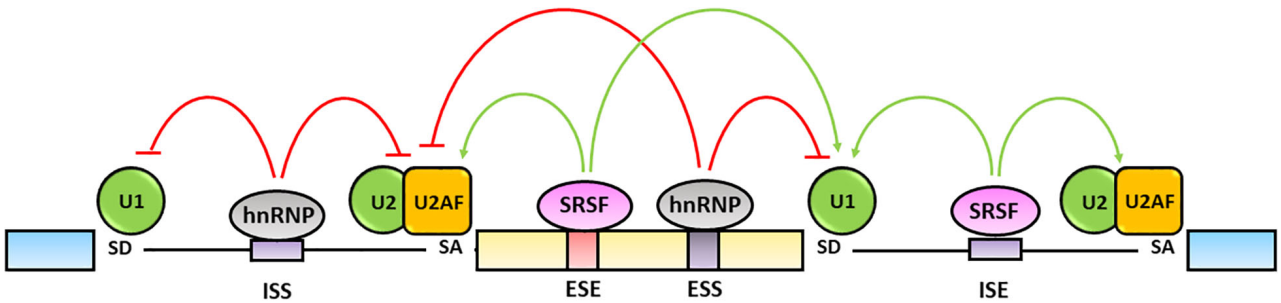

FIGURE 3 | Regulation of alternative splicing. Alternative splicing is finely regulated by trans-acting hnRNPs and SRSFs protein families. The hnRNPs generally bind exonic (ESSs) and intronic splicing silencers (ISSs), antagonize SRs activity and inhibit spliceosome assembly on the splicing sites (red lines). The SRSFs bind to exonic (ESEs) and intronic (ISEs) splicing enhancers and increase the splicing efficiency by favoring the spliceosome recruitment and assembly on the splicing sites (green lines) (Chen and Manley, 2009; Wang et al., 2015).

U1 to the 5′-SD site) and promote splicing processes (Manley and Krainer, 2010; Shen and Mattox, 2012; Bradley et al., 2015; Jeong, 2017) (**Figure 3**). In a few cases the SR proteins have been shown to bind silencer elements and to repress splicing (Kanopka et al., 1996; Shin et al., 2004; Shen and Mattox, 2012). For example, SRSF1 (SF2/ASF), SRSF4 (SRp75), SRSF5 (SRp40), and SRSF6 (SRp55) are able to bind an ISS located in the intron 9 of the CFTR transcript and to skip the exon 9 causing the production of a nonfunctional protein associated with cystic fibrosis development (Pagani et al., 2000).

The localization of SR proteins is regulated by dynamic serine-arginine repeats phosphorylation/dephosphorylation cycles that also modify their protein–protein interaction and functional activities (Zhou and Fu, 2013; Long et al., 2019). For example, the SRSF1, SRSF3 (SRp20), and SRSF7 (9G8) phosphorylated proteins are bound and shuttled by transportin SR2 from the cytoplasm to the nucleus (Lai et al., 2000, 2001). The serine-arginine rich proteins are specifically phosphorylated by the serine/arginine-protein kinases (SRPKs) and the Cdc2-like kinase/Ser-Thr-Tyr (Clk/Sty) kinases (Colwill et al., 1996; Giannakouros et al., 2011). The SRPKs are constitutively active in normal cells and localize either in the cytoplasm or into the nucleus (Giannakouros et al., 2011). The nuclear kinase CLK1 has been shown to phosphorylate the RS2 domain of SRSF1 and

to cause the re-localization from speckles to the nucleoplasm (Aubol et al., 2018). In particular conditions, the SR proteins are phosphorylated by other kinases such as topoisomerase 1 (TOPO1), which becomes active in response to extra-cellular stimuli, and by Akt kinase and MAP kinases (MAPKs) that are constitutively active in cancer cells (Rossi et al., 1996; Naro and Sette, 2013). The SRSFs, similarly to hnRNPs, have also a variety of non-canonical activities related to the stability, export and translation of mRNAs as well as to the chromatin remodeling, nucleolar stress response, genome stability and cell cycle regulation (Howard and Sanford, 2015).

DEREGULATION OF THE SPLICING MACHINERY IN CANCER

Several studies demonstrated that deregulation of constitutive and alternative splicing plays a crucial role in carcinogenesis and could be considered a novel cancer hallmark (Oltean and Bates, 2014; El and Younis, 2018; Wang and Lee, 2018; Zhang Y. et al., 2019; Che and Fu, 2020). Indeed, recent transcriptome sequencing analyses demonstrated that splicing factors expression is commonly deregulated in a multitude of cancer types and is associated with alterations of the tissue-specific transcripts as well as modification of protein–protein interactions (Buljan et al., 2012; Singh and Eyras, 2017).

Characterization of known transcripts from RNA-seq data of 4,542 tumor samples from 11 cancer types recorded in TCGA revealed the presence of 8,122 switches in the RNA isoforms encoded by 6,442 genes, the most common being RAC1 gaining an extra Ras domain and TP53 losing coding capacity (Climente-Gonzalez et al., 2017). Such changes were found mainly associated with alterations in apoptosis, ubiquitin-mediated proteolysis, ERBB-signaling, RNA transcription and splicing pathways (Climente-Gonzalez et al., 2017). In addition, the comprehensive analysis of whole exome sequencing and RNA-seq data of 8,705 tumor samples and 640 normal control tissues from 32 cancer types, including cervical cancer, showed approximately 251,000 new exon–exon junctions in tumors (around 930 per sample), of which 18,000 were recurrent events detected in at least 100 samples (Kahles et al., 2018). Such novel exon–exon junctions were predicted to produce "neoantigens" and to affect the immune response (Kahles et al., 2018). David et al. (2020) extended the analysis of exon–exon junctions to 10,549 tumor samples across 33 TCGA cancer types and observed that more than 50% of new junctions were not shared among cancer samples. Importantly, in cervical cancer they identified a total of 14,086,434 exon–exon junctions of which 2,263,326 were specific to cervical cancer (David et al., 2020).

Several mechanisms are responsible for aberrant splicing processes in human cancers. First, the uncontrolled overexpression of splicing factors may cause anomalous splicing events in tumors (Sveen et al., 2016). The up-regulation of hnRNPs and SRSFs has shown to be commonly caused by gene rearrangements and copy number variations in a variety of cancer types (Shilo et al., 2015). For example, the HNRNPA2B1 gene was found amplified in glioblastoma and its copy number was demonstrated to be inversely correlated with patients survival (Golan-Gerstl et al., 2011). Moreover, the amplification of the chromosome 17q23 and chromosome 6p21 regions has been shown to cause the overexpression of SRSF1 in breast cancer and SRSF3 in lung and cervical carcinoma, respectively (Parssinen et al., 2007; Jia et al., 2010).

The expression of hnRNP A1, hnRNP A2 and hnRNP I (also known as polypyrimidine tract binding protein, PTB) was demonstrated to be trans-activated by Myc oncoprotein. Specifically, the Myc mediated up-regulation of hnRNP A1, hnRNP A2 and hnRNP I induces the production of the pyruvate kinase embryonic isoform PKM2 and the activation of the aerobic glycolysis in different cancer cells (Christofk et al., 2008; David et al., 2010; Chen H. et al., 2018). Myc was also demonstrated to bind E-boxes in the SRSF1 promoter and to transactivate the SRSF1 overexpression that cause production of MKNK2 +13B and TEAD1 +5 isoforms and enhanced proliferation of lung cancer cells (Das et al., 2012).

Altered processing of splicing regulator transcripts represents a further mechanism of abnormal pre-mRNA maturation (Czubaty and Piekielko-Witkowska, 2017). For instance, knockdown experiments of S6K2 kinase, that phosphorylates the serine^{6} residue in hnRNP A1 protein, caused enhanced production of the PKM2 isoform and increased glycolysis in colorectal cancer cells (Sun Y. et al., 2017). The overexpression of SRPK1 causes the hyper-phosphorylation of SRSF1, leading to increased production of Rac1b, an oncogenic variant of the GTPase Rac1 signaling protein that promotes survival and proliferation of colorectal cancer cells (Goncalves et al., 2014; Patel et al., 2019). The overexpression of Clk2 kinase was also shown to sustain cell growth in breast cancer, while its silencing was demonstrated to reduce the SRSF1 phosphorylation and to induce the production of the ENAH isoform, which is typical of the mesenchymal phenotype and associated with tumor invasion and metastasis (Yoshida et al., 2015). *In vitro* studies demonstrated that the up-regulation of the NEK2 kinase promotes the production of the anti-apoptotic BCL-X_L variant through the anomalous phosphorylation of SRSF1 (Naro et al., 2014). In addition, the PI3K/Akt signaling pathway, constitutively activated by mutated EGFR, leads to SRSF1 hyper-phosphorylation and consequent reduction of the anti-apoptotic isoform Casp-9b in lung cancer (Shultz et al., 2010).

Other post-translational modifications, such as acetylation and ubiquitination, are important modulators of splicing factors activity. For example, the hyper-acetylation of hnRNP A1 induced by high glucose levels in hepatocellular carcinoma cells promotes the production of the PKM2 variant and consequent enhancement of glucose metabolism as well as transcription of genes responsible for cell proliferation and growth, such as GLUT1, LDHA, PDK1, CCND1, and MYC (Yang et al., 2019). In addition, the hyper-acetylation of SRSF5 by Tip60 acetyl-transferase causes the production of the CCAR1 isoform S, which favors tumor growth by promoting glucose consumption and acetyl-CoA production (Chen et al., 2018a). On the other hand, the hypo-acetylation and consequent degradation of SRSF5 by the Smurf1 ubiquitin ligase causes CCAR1S reduction under low intracellular glucose levels (Chen et al., 2018a).

The hyper-*O*-GlcNAcylation of hnRNP-K in cholangiocarcinoma cells induces its translocation to the nucleus, where it drives the expression of genes involved in the extracellular matrix composition, cell movement, angiogenesis and epithelial mesenchymal transition, such as CCK, MMP3, PTGS2, and CTGF as well as CCND1 and XIAP (Gao R. et al., 2013; Phoomak et al., 2019). The overexpression of the SUMO1 was shown to cause the sumoylation of hnRNP K and increased *c-Myc* transcription associated with cell proliferation in Burkitt lymphoma (Suk et al., 2015).

Recurrent somatic mutations in splicing factors encoding genes have also been shown to affect the splicing processes in cancer (Kandoth et al., 2013; Watson et al., 2013; Sveen et al., 2016). Specifically, oncogenic driver mutations have been identified in 119 genes encoding for splicing factors in a variety of tumors (Seiler et al., 2018). For instance, point mutations and deletions in the HNRNPK gene, causing hnRNP K down-regulation, have been suggested to have a role in the development of acute myeloid leukemia (Sweetser et al., 2005; Gallardo et al., 2015). Moreover, hotspot mutations in the SRSF2 gene, such as P95H, change the binding properties of the SRSF2 protein and cause genome-wide splicing network alteration and aberrant maturation of different hnRNPs, including HNRNPA2B1, HNRNPM, HNRNPH1, and HNRNPH3, especially in myelodysplastic syndromes (Komeno et al., 2015; Arbab et al., 2018; Aujla et al., 2018; Liang et al., 2018; Masaki et al., 2019).

Moreover, nucleotide changes within the exonic or intronic *cis*-acting splicing factors binding motifs may result in the disruption or creation of binding sites and aberrant splicing reactions (Wang and Cooper, 2007; Sterne-Weiler and Sanford, 2014). A recent whole-exome and transcriptome comprehensive study including 31 cancer types identified 14,438 splicing-associated variants, most of which were shown to disrupt donor and acceptor sites and to cause exon skipping, intron retention and alternative 5′ or 3′ splicing site usage particularly in TP53 and GATA3 genes (Shiraishi et al., 2018).

Additionally, non-coding RNAs, such as miRNAs, are able to regulate splicing and transcription both in normal and tumor tissues for their ability to target the 3′-UTR of hnRNPs and SRSFs mRNAs (Anczukow and Krainer, 2016). For instance, the miR-15a-5p and miR-25-3p have been described as negative regulators of hnRNP A1 expression, required for the maturation of miR-18a-3p, that in turn inhibits the K-RAS oncogene in ovarian cancer (Rodriguez-Aguayo et al., 2017). Besides, miR-183-5p and miR-200c-3p in renal cancer as well as miR-193a-3p in gastric cancer have been demonstrated to target the SRSF2 (SC35) 3′-UTR mRNA, affecting the maturation of several pre-mRNAs involved in the apoptosis (Sokol et al., 2018; Lee et al., 2019).

On the other hand, the hnRNP and SRSF proteins are able to control directly or indirectly the expression of several miRNAs and other non-coding RNAs involved in cancer development (Ratnadiwakara et al., 2018). Indeed, the hnRNP A1 has been shown to interact with pri-miR-18a conserved terminal loop and to induce a relaxation in the stem loop that facilitates the cleavage by Drosha and production of mature miR-18a in prostate, esophageal, pancreatic, hepatocellular, and colorectal cancer (Guil and Caceres, 2007; Komatsu et al., 2014; Kooshapur et al., 2018). Moreover, the hnRNP D reduces the Dicer1 levels by targeting the 3′-UTR of DICER1 mRNA, causing down-regulation of tumor suppressor miR-122 and increased viability of PLC/PRF/5 hepatoma as well as Huh7 liver derived cell lines (Wu et al., 2018). Among SRSF proteins, the SRSF3 was demonstrated to enhance the processing of miR-16-1, miR-30a and miR-223 through the binding of a CNNC motif located 17-18 nucleotides downstream the Drosha cleavage signal (Auyeung et al., 2013).

Several hnRNPs, especially hnRNP K, are also able to modulate the expression of genes involved in the carcinogenic processes through their interaction with lncRNAs (Sun X. et al., 2017). In particular, Li et al. (2018) observed that linc00460 was overexpressed in non-small cell lung tumors and was able to interact with hnRNP K promoting migration and invasion of H460 and A549 human lung cancer cell lines. Furthermore, the analysis of RNA binding proteins-lncRNAs interaction network in the POSTAR2 database and co-immunoprecipitation experiments showed that SRSF1 was able to interact with and to stabilize the lncRNA NEAT1 causing increased cell proliferation in U87MG glioma cell line (Zhou et al., 2019).

Recently, hnRNPs have also been demonstrated to modulate the production of circular RNAs (Kramer et al., 2015). Specifically, the profiling of circular RNAs transcriptome in LNCaP prostate cancer cells expressing HNRNPL compared to HNRNPL-knockdown cells revealed the differential production of circ-PRKAR1B, circ-ZMIZ1, circ-FOXJ3, and circ-CCNY that have been suggested to be involved in prostate cancer development (Fei et al., 2017).

Oncogenic Functions of hnRNPs and SRSFs

Several hnRNP and SRSF proteins have been demonstrated to be overexpressed in tumors and to possess multiple oncogenic functions (El and Younis, 2018) (**Table 1**). In particular, hnRNP A1 is upregulated in lung cancer and its silencing in lung cancer cell line A549 causes cell cycle arrest in G0/G1 phase (Liu et al., 2016). The hnRNP A1 expression enhances the production of a cyclin dependent kinase 2 (CDK2) isoform, characterized by the exon 5 retention, that promotes cell growth, while its inhibition causes the cell cycle arrest at the G2/M phase in oral squamous cancer cell lines (Yu et al., 2015). The overexpression of hnRNP A1 in gastric cancer and hnRNP A2/B1 in lung cancer has been shown to enhance the metastatic potential of tumor cells by inducing a shift from the expression of epithelial markers (i.e., E-cadherin) to mesenchymal markers (i.e., vimentin and snail) phenotype (Boukakis et al., 2010; Tauler et al., 2010; Chen et al., 2018b). The hnRNP A1 also mediates the production of the CD44v6 isoform, associated with larger tumor size, microvascular invasion and tumor recurrence in hepatocellular carcinoma patients (Zhou et al., 2013).

The hnRNP D, that is overexpression in Eca-109 esophageal cancer cell line, has been recognized to bind the 3′-UTR AU-rich motifs of GTP cyclohydrolase (GCH1) transcripts causing GCH1 overexpression and enhanced cell proliferation and colony

TABLE 1 | Splicing factors and regulated oncogenic processes: physiological functions and oncogenic activities in different cancer types and cell lines.

Splicing factors (aliases)	Regulated processes	Oncogenic activities	Pathologic mechanism	Experimental model	Cancer types and cell lines	References
hnRNPs						
hnRNP A1	Splicing, mRNA export and stability, telomeres maintenance, translation	Induction of cell growth by regulation of CDK2 exon 5 alternative splicing	OE	KD	CAL 27 cell line	Yu et al. (2015)
hnRNP A2/B1	Splicing, mRNA localization and stability	Induction of EMT markers expression	OE	OE, KD	A549 cell line	Tauler et al. (2010)
hnRNP C1/C2	Splicing, mRNA transport and stabilization, translation	Maturation of miR-21, down-regulation of PDCD4, reduction of apoptosis, increase of proliferation and invasiveness	OE	KD	T98G cell line	Park et al. (2012)
hnRNP D	Telomeres maintenance, development, apoptosis, DNA recombination, mRNA decay	Up-regulation of GCH1, promoting cell proliferation and colony formation	OE	KD	Eca-109 cell line	Gao et al. (2016)
hnRNP E1	Splicing, mRNA stability, transcription, translation	Production of integrin β1A isoform promoting lymph node and hepatic metastases	OE	OE, KD	Pancreatic cancer	Jiang et al. (2017)
hnRNP E2	Splicing, mRNA stability, transcription, translation	Up-regulation of CDK2 stimulating cell proliferation	OE	KD	HGC-27 and MKN-45 cell lines	Chen C. et al. (2018)
hnRNP K	Splicing, transcription, translation, mRNA stability	Enhancement of cell migration and metastatization by up-regulation of MMP3, MMP10, PTGS2, ITGA6, CTGF, and RASA1	OE	OE	U2OS cell line	Gao R. et al. (2013)
hnRNP L	Splicing, mRNA export and stability, riboswitch	Activation of MAPK signaling and inhibition of caspase-3, -6, and -9	OE	OE, KD	UM-UC-3, EJ, T24 and RT4 cell lines	Lv et al. (2017)
hnRNP M	Splicing	Production of CD44 standard isoform, associated with poor outcome and metastases	OE	OE	Breast cancer	Sun H. et al. (2017)
SRSFs						
SRSF1 (SF2/ASF)	Splicing, mRNA export, mRNA NMD, nucleolar stress response, miRNA processing, mTOR activation, translation	Production of cyclin D1b isoform promoting cell proliferation	OE	KD	Prostate cancer	Olshavsky et al. (2010)
SRSF2 (SC35)	Splicing, mRNA export, transcription	Production of GCH1-L and STK39-L isoforms increasing cell growth and colony forming efficiency	OE	OE, KD	Huh7 cell lines	Luo et al. (2017)
SRSF3 (SRp20)	Splicing, translation, mRNA export and decay	Inhibition of apoptosis by down-regulating PDCD4	OE	KD	SW480 and U2OS cell lines	Kim et al. (2014)
SRSF5 (SRp40)	Splicing, translation	Induction of MCM2 and MCM4 expression, enhancing cell proliferation and colony formation efficiency	OE	KD	CAL 27 and SCC-9 cell line	Yang et al. (2018)
SRSF6 (SRp55)	Splicing	Regulation of CRH-R1 production and cell proliferation	OE	KD	Breast cancer	Lal et al. (2013)
SRSF7 (9G8)	Splicing, mRNA transport, translation	Production of exon 6 deleted Fas variant promoting cell survival	OE	KD	HCT116 and A549 cell lines	Fu and Wang (2018)
SRSF9 (SRp30c)	Splicing, RNA editing	Enhanced expression of β-catenin	OE	OE, KD	HCT116 and SW620 cell lines	Fu et al. (2013)
SRSF10 (SRp38)	Splicing	Production of BCLAF1-L variant promoting cell proliferation and growth	OE	KD	RKO and HCT116 cell lines	Zhou et al. (2014)
Others						
Tra2β	Splicing	Production of NASP-T isoform enhancing the HSPA2 ATPase, which increases proliferation and reduced apoptosis	OE	KD	PC-3 cell line	Alekseev et al. (2011)
Sam68	Splicing, translation, transcription, mRNA export	Production of constitutively active androgen receptor V7 variant	OE	OE, KD	LNCaP cell line	Stockley et al. (2015)

OE, overexpression; KD, knock-down.

formation (Gao et al., 2016). Moreover, the hnRNP D protein can specifically bind to single-stranded d(TTAGGG)n human telomeric repeats through its C-terminal binding domain (BD2), thus impeding the formation of a DNA-quadruplex while favoring telomeres elongation and maintenance (Enokizono et al., 2005). The ectopic expression of p42 and/or p45 hnRNP D isoforms in hnRNP D-deleted mouse embryonic fibroblasts demonstrated that such isoforms are able to bind TERT promoter and to strongly transactivate TERT expression, thus reducing cell senescence (Pont et al., 2012).

The hnRNP E1 plays a major role in the production of integrin β1A isoform, whose expression has been found to correlate with lymph node and hepatic metastasis of pancreatic cancer, while the upregulation of hnRNP E2 was shown to promote the expression of CDK2 causing increased proliferation of gastric cancer cells (Jiang et al., 2017; Chen C. et al., 2018).

The hnRNP K expression has been demonstrated to enhance the transcription of genes involved in the extracellular matrix composition, especially MMP3 and MMP10, as well as of genes responsible for cell motility, such as PTGS2 and ITGA6, and angiogenesis, like CTGF and RASA1 (Gao R. et al., 2013).

The hnRNP L was shown to activate MAPK signaling while inhibiting caspase-3, -6 and -9 in bladder cancer cells as well as to suppress p53 expression and bcl-2/caspase-9/3 signaling via TP53 mRNA and bcl-2 binding, respectively, in prostate cancer cells (Lv et al., 2017; Zhou et al., 2017).

Overexpressed hnRNP M has been demonstrated to mediate the reduction of CD44v6 and increase of the CD44 standard isoform, that is associated with shorter overall survival and axillary lymph node metastases in breast cancer patients (Sun H. et al., 2017).

Among the SRSFs family, the SRSF1 gene was the first to be identified as a proto-oncogene with overexpression in colon, thyroid, small intestine, kidney and lung tumors (Karni et al., 2007). In particular, Karni et al. (2007) showed that SRSF1 regulates the alternative splicing of the tumor suppressor BIN1 and kinases MNK2 and S6K1 causing the production of a BIN1 isoform lacking tumor-suppressor activity, a MNK2 isoform promoting MAP kinase-independent eIF4E phosphorylation, and an oncogenic S6K1 isoform in transformed NIH 3T3 and Rat1 cell lines. The overexpression of SRSF1 was also shown to increase cell proliferation through the production of the exon 5 lacking-variant cyclin D1b in prostate cancer and to induce epithelial mesenchymal transition by stimulating the production of the ΔRon variant in breast cancer (Ghigna et al., 2005; Olshavsky et al., 2010).

Thereafter, several other SR proteins have been demonstrated to possess oncogenic activities in several tumor types (**Table 1**). For example, the knockdown of SRSF2 in Huh7 liver cancer cell line revealed 966 splicing alterations in cancer-related gene transcripts, favoring the production of oncogenic mRNA variants, such as the GCH1-L and STK39-L isoforms, that are involved in cell-cycle control and DNA repair (Luo et al., 2017).

The overexpression of SRSF3 into "normal" lung cell line WI-38 was able to modify the alternative splicing of the interleukin enhancer-binding factor 3 (ILF3) pre-mRNA and to increase the production of isoform-1 and isoform-2, both required for cell proliferation (Jia et al., 2019). Moreover, SRSF3 is able to deregulate the apoptotic pathway by binding to 5′-UTR of PDCD4 mRNA and by inhibiting the expression of the PDCD4, a critical suppressor of apoptosis (Kim et al., 2014).

The SRSF 5-7 proteins are particularly abundant in small cell lung cancer and associated with pleural metastasis (Kim et al., 2016). The SRSF5 enhances the expression of the MCM family members MCM2 and MCM4, that are involved in the initiation and elongation processes of DNA replication, as well as cell growth and colony formation when transfected in CAL 27 and SCC-9 oral squamous cell carcinoma cell lines (Yang et al., 2018). The SRSF6 is involved in the abnormal alternative splicing of the corticotropin-releasing hormone receptor type 1 (CRH-R1) causing indirect perturbation of oncogenic kinases, such as p38 MAPK, Akt and GSK3β, and accumulation of β-catenin in breast cancer (Lal et al., 2013). Knockdown experiments of SRSF7 in HCT116 colon and A549 lung cancer cell lines revealed the production of an exon 6-lacking isoform of the Fas receptor mRNA, that promotes cell survival (Fu and Wang, 2018).

The SRSF9 protein is frequently overexpressed in glioblastoma, colon adenocarcinoma, squamous cell lung carcinoma and malignant melanoma (Fu et al., 2013). The enhanced co-expression of SRSF9 and SRSF1 has been shown to promote tumourigenesis by Wnt signaling activation in a mTOR-dependent manner and to enhance translation of β-catenin mRNA (Fu et al., 2013).

The SRSF10 (SRp38) is an atypical SR protein acting as a potent general splicing repressor in its dephosphorylated form and as a sequence-specific splicing activator in its phosphorylated status (Feng et al., 2008). It was shown to mediate the expression of the BCLAF1 exon5a isoform (BCLAF1-L) that promotes cell proliferation and growth in colon cancer cell lines RKO and HCT116 (Zhou et al., 2014).

Other Oncogenic Splicing Factors

Splicing factors other than hnRNPs and SR family members, such as Tra2β, Brm and Sam68, have been also demonstrated to play a role in cancer development. The Tra2β is an SR-like protein characterized by a double N- and C-terminal RS domains that is able to promote alternative exons inclusion in a dose-dependent manner (Tacke et al., 1998; Stoilov et al., 2004; Venables et al., 2005; Grellscheid et al., 2011; Elliott et al., 2012). The TRA2B gene is amplified in several tumor types, including lung, head and neck, ovary, stomach and uterus cancers (Gabriel et al., 2009; Gao J. et al., 2013). Increased levels of Tra2β promote the production of the NASP-T isoform, enhances the ATPase activity of heat shock protein HSPA2 and causes increased proliferation as well as reduced apoptosis in PC-3 prostate cancer cell line (Alekseev et al., 2011; Best et al., 2013).

The Brm is a member of SWI/SNF (mating-type switch/sucrose non-fermentable) proteins family, involved in chromatin structure remodeling and DNA-damage response (Sudarsanam and Winston, 2000; Roberts and Orkin, 2004; Smith-Roe et al., 2015). The Brm factor interacts with U1, U3, and U5 snRNPs of the major spliceosome complex and favors the inclusion of alternative exons in gene transcripts involved in carcinogenesis (Smith-Roe et al., 2015; Pulice and Kadoch, 2016).

In particular, the overexpression of BRM gene enhances the inclusion of exon 9 in the E-caderin mRNA in the MCF-7 human breast cancer cell line, while the Brm knockdown promotes the production of a cyclin D1b variant lacking exon 27 in Caco2 cell lines (Batsche et al., 2006).

The Sam68 is the prototypic member of the STAR family proteins that regulates alternative splicing and RNA processing in response to signaling pathways (Taylor et al., 1995). This factor contains a 200 amino acids long domain (GRP33/SAM68/GLD-1, GSG) that bind to RNA sequences as well as C-terminal six-proline-rich and tyrosine-rich sequences that interact with SRC homology 2 (SH2) and 3 (SH3) domains of BRK, FYN and Itk/Tec/BTK kinases (Andreotti et al., 1997; Derry et al., 2000; Paronetto et al., 2003; Najib et al., 2005). Sam68 was found overexpressed and associated with poor prognosis in several cancer types, including non-small cell lung carcinoma and breast, hepatocellular, renal, prostate and gastric cancers (Busa et al., 2007; Zhang et al., 2009, 2014, 2015; Song et al., 2010; Xiao et al., 2018). In addition, it was shown to modulate the splicing of transcripts encoded by genes involved in oncogenic pathways (Bielli et al., 2011). In particular, Paronetto et al. (2010) demonstrated that ERK-phosphorylated Sam68 was able to inhibit the U1 snRNP recruitment to the intron-exon 4 junction of CCND1 mRNA in the presence of the rs9344 (870A>G) polymorphism, thus favoring the production of the cyclin D1b. Moreover, Sam68 was also demonstrated to bind an ESE located near the cryptic exon 3b 3′ splice site of the androgen receptor mRNA, promoting the inclusion of exon 3b in the transcript and its translation into the androgen receptor V7 variant in the LNCaP prostate cancer cell line (Stockley et al., 2015).

ALTERNATIVE SPLICING IN HPV-RELATED CERVICAL NEOPLASIA

The cell splicing factors contribute to cervical neoplasia by two distinct but converging mechanisms: (1) by mediating the differential maturation of HPV RNA isoforms, required for virus replication and for viral oncoprotein expression; and (2) by promoting the production of cell mRNA variants and proteins with oncogenic functions that may have roles in cervical neoplasia development and in the progression to later stages of cervical carcinogenesis (Mole et al., 2009a; Johansson and Schwartz, 2013; Oltean and Bates, 2014) (**Table 2**).

HPV Infection and Viral Gene Expression

Persistent infection with high-risk HPVs, most commonly HPV16 and HPV18, is the main risk factor for development of almost all cases of cervical cancer (Doorbar, 2006; Schiffman et al., 2016), and of significant fraction of penile and anal cancers (Moscicki and Palefsky, 2011), vulvar cancer (Preti et al., 2020), as well as tumors of the upper respiratory tract, including head and neck cancers (Bzhalava et al., 2020). Most HPV infections of the cervix are successfully cleared by the host immune system in 2–3 years, but in several cases the infection may persist over the time leading to CIN graded 1 to 3 that eventually evolve during a long lasting period in invasive cervical carcinoma (McCredie et al., 2008; Doorbar et al., 2012; Oyervides-Munoz et al., 2018).

HPV genomes are double stranded circular DNAs of approximately 8000 bp which can be divided into three main regions: (1) the early region, containing the E1, E2, E3, E4, E5, E6 and E7 ORFs, encoding for regulatory proteins; (2) the late region, including L1 and L2 ORFs, encoding for viral capsid proteins and 3) the LCR, comprising the origin of replication and multiple transcription factor binding sites (Zheng and Baker, 2006; Doorbar et al., 2015). An early polyadenylation site (pA_E) is located between the early and the late ORFs, while a late polyadenylation site (pA_L) is positioned between the late genes and the LCR sequence (Zheng and Baker, 2006; Graham, 2010) (**Figure 4**).

The HPV 16 genome contains three promoters: 1) the early promoter P97 located in the LCR region driving the transcription of early polycistronic RNAs; 2) the late promoter P670 within the E7 ORF driving the expression of late polycistronic transcripts and 3) the recent discovered E8 promoter within the ORF E8, regulating the production of the E8^E2 transcript which has been demonstrated to control the viral copy number in undifferentiated keratinocytes (Schmitt and Pawlita, 2011; Chen et al., 2014; Straub et al., 2015) (**Figure 4**).

The HPV gene expression during the viral life cycle is dependent on cellular differentiation stages (Doorbar, 2005). Briefly, the E1 and E2 proteins as well as the E6 and E7 proteins are expressed at low levels in the basal cell stratum of the cervical epithelium and become overexpressed once the keratinocytes move from the basal to the mid layers (Doorbar, 2006; Xue et al., 2010; Doorbar et al., 2012). The L1 and L2 genes, encoding viral capsid proteins, are only produced in the terminally differentiated layers of the cervical epithelium (Doorbar et al., 1997, 2012). In high grade CIN and cervical cancer the viral genome usually integrates into host genome, causing disruption of the E2 ORF, E6 and E7 up-regulation as well as loss of late proteins expression (Collins et al., 2009; Oyervides-Munoz et al., 2018).

Splicing of HPV16 Transcripts

The balanced production of HPV16 early and late proteins is necessary for completion of the viral life cycle. The viral polycistronic transcripts are processed by cell splicing factors in order to remove introns through the differential usage of alternative splice sites and the production of viral proteins isoforms (Graham and Faizo, 2017). In particular, splicing sites SD226, SD880, SA409, SA526, SA742, SA2582, SA2709, and SA3358 in viral pre-mRNAs generated from the P97 promoter are recognized by the major spliceosome complex of the epithelial cells (Johansson and Schwartz, 2013). The SA3358 is the most used 3′ splice site, since these spliced mRNAs can either be polyadenylated at pA_E to generate mRNAs encoding E6, E7, E4, or E5, or polyadenylated at pA_L to produce mRNAs encoding L2 structural protein (Schmitt et al., 2010; Wu et al., 2017) (**Figures 4B,C**).

At late stages of productive viral infection, the binding of splicing factors to SD880, SD3632 and SA5639 sites in the

TABLE 2 | Splicing factors that have been recognized to affect splicing of HPV16 and host cell transcripts in cervical cancer.

Splicing factors (aliases)	Cancer hallmarks	References	HPV16 mRNAs	References
hnRNPs				
hnRNP A1	Regulation of apoptosis by procaspase-3 and PARP cleavage	Patry et al. (2003)	Production of E6*I/E7 isoform, inhibition of SA5639 and of L1 mRNAs production	Cheunim et al. (2008); Rosenberger et al. (2010)
hnRNP A2/B1	Up-regulation of p21 and p27, enhanced cleavage of caspase-3, down-regulation of p-Akt	Shi et al. (2018)	Production of E6*I/E7 isoform, inhibition of SA5639 and of L1 mRNAs production	Rosenberger et al. (2010); Li et al. (2013b)
hnRNP C	–	–	Activation of SD3632 and of L1 mRNAs production	Dhanjal et al. (2015)
hnRNP D	–	–	Inhibition of SD3632 and of late mRNAs production	Li et al. (2013b)
hnRNP E1/E2	–	–	Inhibition of L2 mRNAs production	Chaudhury et al. (2010)
hnRNP F	Production of ENOX2 exon 4 minus splice variant, promoting cell growth	Tang et al. (2011)	–	–
hnRNP G	–	–	Activation of SA3358 and late mRNAs production	Yu et al. (2018)
hnRNP H	–	–	Activation of pA_E and inhibition of late mRNAs production	Oberg et al. (2005); Zheng et al. (2013)
hnRNP I (PTB)	Regulation of cell proliferation, anchorage-independent growth and invasiveness	Wang et al. (2008)	Inhibition of pA_L, activation of SD3632 and of late mRNAs production	Somberg et al. (2008)
hnRNP K	Regulation of cell cycle	Lu and Gao (2016)	Inhibition of L2 mRNAs production	Collier et al. (1998)
hnRNP L	–	–	Activation of SA3358 and pA_E, inhibition of late mRNAs production	Kajitani et al. (2017)
hnRNP P2	Promotion of EMT and cell proliferation	Zhu et al. (2018)	–	–
SRSFs				
SRSF1 (ASF/SF2)	Up-regulation of caspase 9a/9b ratio	Shultz et al. (2011)	Activation of SA3358 and of E6/E7 mRNA production, production of E4, E5, L1, and L2 mRNAs, inhibition of SA3632 and of late mRNAs production, inhibition of SA2709 and of E2 mRNA production	Rush et al. (2005); Somberg and Schwartz (2010); Li et al. (2013a); McFarlane et al. (2015)
SRSF2 (SC35)	Reduction of apoptosis, increased anchorage-independent growth, cell cycle progression	McFarlane et al. (2015)	Production of E6/E7 mRNAs	McFarlane et al. (2015)
SRSF3 (SRp30)	Enhancement of cell proliferation	Jia et al. (2010)	Production of E6/E7 mRNA and of E4/L1 mRNA, inhibition of SA3358 and of late mRNAs production	Rush et al. (2005); McFarlane et al. (2015); Klymenko et al. (2016)
SRSF9 (SRp30c)	Increased colony formation and proliferation, reduced apoptosis	Zhang et al. (2019a)	Inhibition of SA3358, activation of SA5639 and of late mRNAs production	Somberg et al. (2011)
SRSF10 (SRp38)	Increased cell proliferation and tumor growth, production of mIL1RAP, activation of IL-1β signal transduction and NF-κB, immune evasion	Liu et al. (2018)	–	–
SRSF11 (SRp54)	Telomeres elongation	Lee et al. (2015)	–	–
Others				
Tra2β	Increased lymph node metastatization, tumor grade, size and invasion depth	Gabriel et al. (2009)	–	–
Brm	Production of pro-metastatic CD44v5 in cooperation with Sam68	Batsche et al. (2006)	Production of E6/E7 mRNA	Rosenberger et al. (2010)
Sam68	Increased lymph node metastases and EMT, production of CD44v5 and of anti-apoptotic DEx3 variant	Li et al. (2012)	Production of E6/E7 mRNA	Rosenberger et al. (2010)

transcripts generated from the P670 regulates late splicing events to produce E1^E4^L1 mRNAs, encoding both E4 and L1 proteins as well as the E1^E4 mRNAs (Johansson and Schwartz, 2013).

Alternative splicing plays a major role in the regulation of the HPV16 E6 and E7 oncogene expression. In fact, the E6 and E7 ORFs are transcribed as E6/E7 bicistronic mRNAs that can

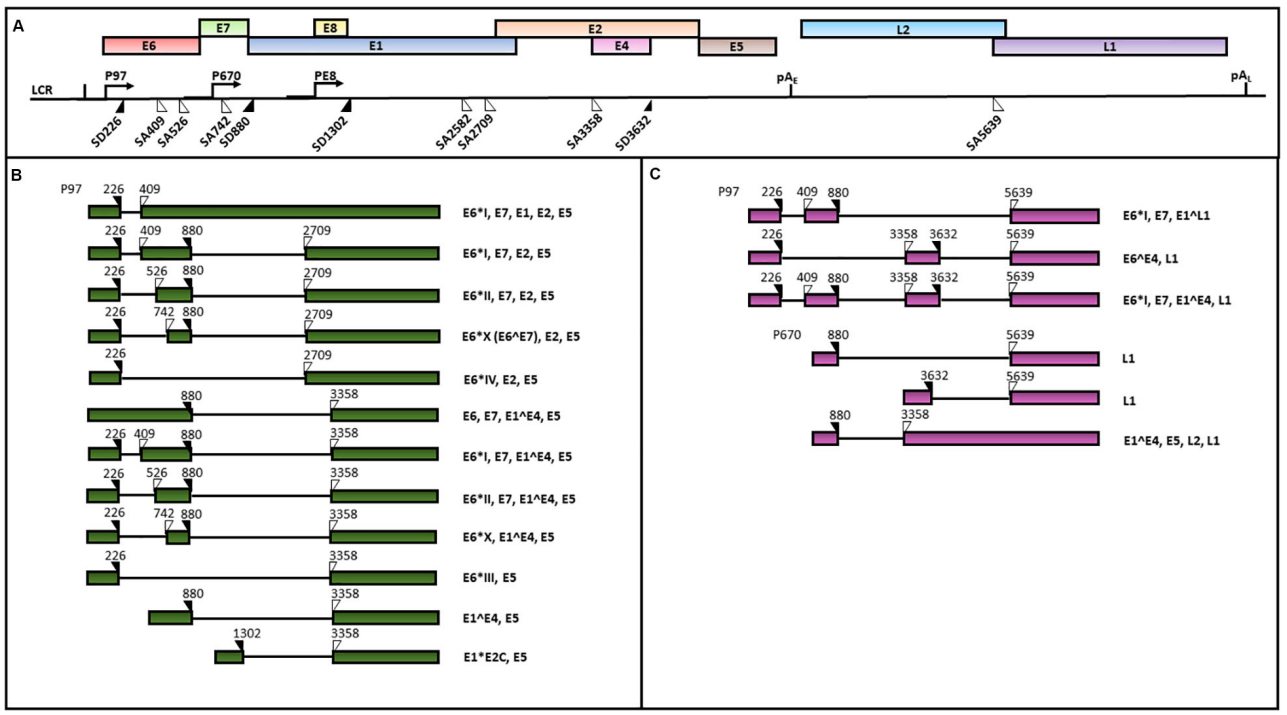

FIGURE 4 | A schematic representation of the HPV16 genome and transcripts. The scheme is based on the HPV episteme (van et al., 2017). **(A)** The P97 derived early mRNAs are polyadenylated at the early polyadenylation site (pAE). The P670 and PE8 derived late mRNAs are polyadenylated at the late polyadenylation site (pAL). Both the early **(B)** and late **(C)** transcripts are polycistronic and subjected to alternative splicing (Zheng and Baker, 2006; Graham, 2010; Graham and Faizo, 2017). The donor (DS) and the acceptor (AS) splice sites in the HPV16 genome are indicated as black and white triangles, respectively. The coding potential of each transcript is also indicated.

be spliced into diverse isoforms, such as E6*I, E6*II, E6*III, E6*IV, E6*V, E6*VI, E6^E7 (E6*X), E6^E7*I, and E6^E7*II (Ajiro and Zheng, 2015; Brant et al., 2018; Olmedo-Nieva et al., 2018). Among these, the E6*I and E6*II, resulting from the SD226^SA409 and SD226^SA526 splicing, respectively, are the two major E6 isoforms expressed in cervical cancer (Zheng and Baker, 2006; Ajiro et al., 2012; Cerasuolo et al., 2017) (**Figure 4B**). McFarlane et al. (2015) analyzed the E6/E7 mRNA splicing pattern in cell subclones with transformed or differentiated phenotype obtained from the W12 cell line, originally derived from a HPV16-positive low grade cervical lesion (Doorbar et al., 1990). The analysis revealed the concomitant presence of E6, E6*I and E6*II in both transformed and differentiated W12 cell clones. However, the E6*X isoform was only detected in W12 transformed cells, suggesting that the E6/E7 RNA splicing pattern may depend on specific cell transformation stages (McFarlane et al., 2015).

The alternative splicing of viral transcripts is also important to maximize the coding potential of the HPV16 genome. In fact, while the unspliced E6/E7 mRNA encodes for the full length E6 protein, the E6*I and E6*II mRNAs may favor the E7 expression by a termination-reinitiation process or leaky scanning mechanisms and the production of shorter E6 peptides (Zheng et al., 2004; Tang et al., 2006; Filippova et al., 2014). The E6 and E7 oncoproteins play a major role in cervical carcinogenesis for their ability to abrogate the functions of p53 and pRb oncosuppressors, respectively (Moody and Laimins, 2010; Tornesello et al., 2018; Yeo-Teh et al., 2018). Moreover, recent studies showed that the HPV16 E6*I isoform have oncogenic activities, such as the disruption of mitochondrial functions and promotion of ROS production (Williams et al., 2014; Evans et al., 2016). Such activities are abrogated by the full-length E6 protein suggesting that the HPV-related cell transformation is regulated by the concerted expression of diverse E6 isoforms (Paget-Bailly et al., 2019). Further studies are needed to understand the precise role of viral mRNA splicing processes, especially E6/E7 mRNA, in high grade cervical neoplasia and cervical carcinoma.

The Role of Splicing Factors in HPV RNAs Splicing

The splicing of HPV RNAs is modulated by cellular hnRNPs and SRSFs factors, that recognize specific enhancer and silencers motifs in the viral transcripts (Graham and Faizo, 2017; Wu et al., 2017) (**Table 3**).

The hnRNP A1 was shown to favor the production of the E6*I isoform in the absence of EGFR, although its binding site on the E6/E7 transcript has not yet been identified (Rosenberger et al., 2010). On the other hand, the hnRNP A1 was shown to bind an ESS in the L1 coding region and to inhibit the production of L1 protein (Zhao et al., 2004, 2007; Cheunim et al., 2008; Zhao

TABLE 3 | Binding motifs recognized by hnRNPs and SRSFs on HPV16 transcripts.

Splicing factors*	Binding motifs (5′–3′)	HPV binding regions	References
hnRNPs			
hnRNP A1	CAGGGU	L1	Zhao et al. (2004); Zhao and Schwartz (2008)
hnRNP A2/B1	AUAGUA	E4	Li et al. (2013b)
hnRNP C	Poly-U	Early 3′-UTR	Dhanjal et al. (2015)
hnRNP D	AUAGUA	E4	Li et al. (2013b)
hnRNP E1/E2	Poly-C	L2	Collier et al. (1998)
hnRNP G	CCGAAGAA	E4	Yu et al. (2018)
hnRNP H	GGG-repeats	L2	Oberg et al. (2005)
hnRNP I (PTB)	Poly-U	Early 3′-UTR	Zhao et al. (2005)
hnRNP K	Poly-C	L2	Collier et al. (1998)
hnRNP L	CA-repeats	E4, L1	Kajitani et al. (2017)
SRSFs			
SRSF1	ACCGAAGAA	E4	Somberg and Schwartz (2010)
SRSF3	ACACC, CCACACCAC	E4	Jia et al. (2009)
SRSF9	CCGAAGAA	E4	Somberg et al. (2011)

**Splicing factors whose exact binding site has not been determined yet were not reported in the table.*

and Schwartz, 2008) (**Figure 5**). Recently, Ajiro et al. (2016b) demonstrated that hnRNP A1 regulates the splicing of HPV18 transcripts by binding to the ESS located at nucleotides 612-639 thus inhibiting the removal of the intron comprised between SD233 and SA416 in the E6/E7 mRNA.

Similarly, the hnRNP A2/B1 has been shown to mediate the production of the E6*I isoform and to inhibit the splicing at SA5639 by preventing the binding of the U2AF65 splicing factor (Rosenberger et al., 2010; Kajitani et al., 2017). Moreover, the hnRNP A2/B1 and hnRNP D factors were demonstrated to bind two AUAGUA motifs located upstream the SD3632 and to inhibit L1 mRNA maturation and protein production in HeLa and C33A2 cervical cancer cell lines transfected with HPV16 complete genome (Li et al., 2013b) (**Figure 5**).

On the other hand, the hnRNP C1 has been demonstrated to increase the L1 and L2 mRNA levels through its binding to the HPV16 early untranslated region and to the AUAGUA silencer upstream the SD3632 in HPV16 -transfected HeLa and C33A cells (Dhanjal et al., 2015) (**Figure 5**). Recently, Nilsson et al. (2018) showed that the alkylating cancer drug melphalan induces the inhibition of HPV16 transcripts early poly-adenylation, by inducing hnRNP C interaction with the pA_E site, and the expression of HPV16 late gene by inhibiting CPSF30-mediated suppression of the pA_L.

Furthermore, the hnRNP E1/E2 were shown to interact with hnRNP K and to block the L2 mRNA translation by binding to a *cis*-acting inhibitory sequence located at the 3′-end of the L2 transcript (Collier et al., 1998; Chaudhury et al., 2010).

The hnRNP G has recently been shown to bind a 8-nucleotide sequence (CCGAAGAA) located downstream the SA3358 in HPV16, thus promoting the production of late mRNAs and skipping of the exon comprised between SA3358 and SD3632 in the L1 mRNA (Yu et al., 2018) (**Figure 5**).

The hnRNP H was shown to promote the polyadenylation at pA_E site and to prevent late genes transcription in HeLa cells transfected with sub-genomic HPV16 plasmids through its interaction with the cut stimulating factor (CStF-64) and with G-rich motifs located in the L2 ORF (Oberg et al., 2005) (**Figure 5**). The late protein L1 was shown to interact with hnRNP H and to activate late genes transcription in differentiated keratinocytes (Zheng et al., 2013).

The hnRNP I binds a U-rich region in the 3′-UTR of HPV16 genome and induces L1/L2 mRNAs production by interfering with a polyadenylation signal at the pA_E and with splicing inhibitory elements located upstream and downstream the SD3632 (Zhao et al., 2005; Somberg et al., 2008) (**Figure 5**).

Kajitani et al. (2017) showed that the hnRNP L phosphorylation by Akt causes its association with HPV16 late splice sites (SA3358, SD3632) and pA_E, the inhibition of U2AF65 binding and decreased L1 mRNA production. Accordingly, the siRNA mediated knockdown of hnRNP L restored the expression of HPV16 L1 and L2 proteins confirming the this splicing factor performs a fine tuning of HPV16 late transcripts (Kajitani et al., 2017) (**Figure 5**).

The SRSF1 factor has been shown to bind the 8-nucleotide purine-rich enhancer downstream the SA3358 site in the E4 ORF and to activate the splicing of early transcripts (except E1 and E2) as well as late mRNAs in different phases of the viral life cycle (Rush et al., 2005; Milligan et al., 2007; Somberg and Schwartz, 2010; Li et al., 2013a) (**Figure 5**). In addition, the SRSF1 is able to bind the exon between SA3358 and SD3632 sites causing partial inhibition of the splicing at SA3632 and production of L1 mRNAs (Somberg and Schwartz, 2010). The SRSF1 has also been shown to reduce the splicing at SA2709 causing inhibition of E2 mRNA production while favoring production of E6 and E7 transcripts in the early phases of HPV16 life cycle (Somberg and Schwartz, 2010).

The SRSF2 and SRSF3 factors promote the early viral transcripts maturation, while their knockdown induces a strong reduction of E6 mRNA isoforms and E6 and E7 oncoproteins expression in CaSki cell lines (McFarlane et al., 2015; Klymenko et al., 2016). Interestingly, the transcriptional activity of the P97 promoter was not affected by SRSF2 levels suggesting it may favor the accumulation of E6/E7 RNAs by regulating the nonsense mediated decay (McFarlane et al., 2015). In addition, SRSF3 depletion causes reduction of E4/L1 mRNA and L1 protein production in W12E cells (McFarlane et al., 2015; Klymenko et al., 2016). Moreover, the SRSF3 is able to bind an A/C-rich enhancer downstream the SA3358 and to promote early genes expression and polyadenylation while inhibiting the late genes expression in CaSki and HeLa cells (Rush et al., 2005; Jia et al., 2009) (**Figure 5**).

The SRSF9 was also shown to inhibit the HPV16 SA3358 enhancer and to promote the production of L1 mRNAs through

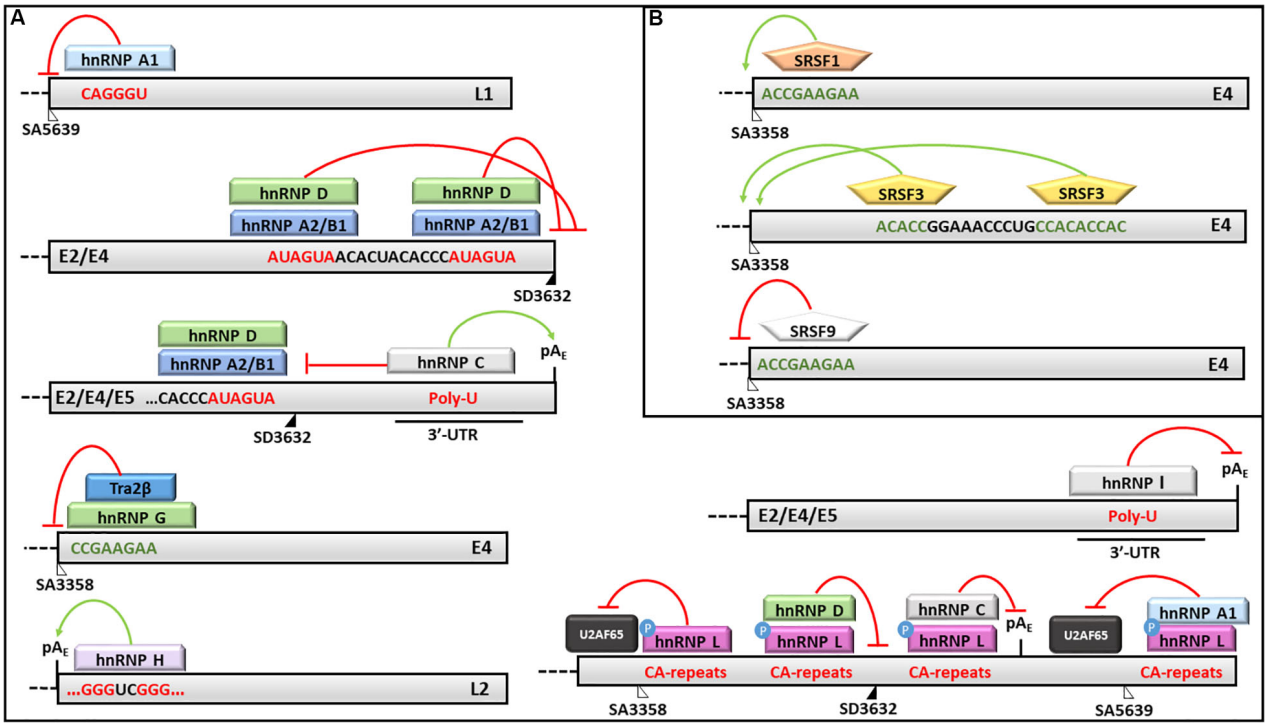

FIGURE 5 | Splicing regulation of HPV16 mRNAs. Activities of **(A)** hnRNPs and **(B)** SRSFs and their binding motifs on HPV16 transcripts are shown. In particular: red lines indicate silencing activities; green arrows indicate enhancing activities; red sequences are silencing elements; while green sequences are enhancer elements. The donor (SD) and acceptor (AS) splice sites are indicated as black and white triangles, respectively.

the skipping of the exon between SA3358 and SD3632 sites as well as through the activation of the splicing at SA5639 (Somberg et al., 2011) (**Figure 5**).

Finally, the cooperation of Sam68 and Brm has been shown to promote the production of full-length E6/E7 transcripts following the activation of Sam68 by Erk1/2 kinase in the presence of EGF in E6-transfected immortalized foreskin keratinocytes (Rosenberger et al., 2010).

HPV Proteins and Cell Splicing Factors

The HPV E2 protein has been shown to possess SRSF-like activities and to regulate viral transcription and replication thus playing a key role in the HPV life cycle (Hegde, 2002; Graham, 2016). An interactome analysis showed that E2 protein binds to several RNA processing proteins and spliceosome components, such as EFTUD2, EIF4A3, SRPK1 and SRPK2, suggesting that it may be involved in the mRNA maturation processes (Jang et al., 2015). Bodaghi et al. (2009) showed that E2 binds to SA408 in the E6/E7 pre-mRNA and interacts with SRSF5, SRSF4, SRSF6 and SRSF9 through its C-terminal domain causing intron 1 exclusion from E6 and E7 mRNAs. Moreover, in mid layers HPV infected keratinocytes the levels of E2 correlate with the expression of SR proteins and both of them increase in cervical neoplasia during CIN progression from grade 1 to grade 3 (Coupe et al., 2012).

On the other hand, chromatin immunoprecipitation assays showed that E2 binds a region comprised between nucleotides 565-363 upstream the SRSF1 AUG starting site through its N-terminal domain and transactivates the SRSF1 expression in the U2OS human osteosarcoma cell line (Mole et al., 2009b). The E2 protein has also been shown to highly transactivate the SRSF3 promoter in the E2-gene transfected U2OS cells (Klymenko et al., 2016). Mole et al. (2020) recently observed that E2-transfected keratinocytes showed an increased expression of SRPK1 and hyper-phosphorylation of SRSF1, that translocate from the nucleus to the cytoplasm in a keratinocyte differentiation-specific manner.

Furthermore, the HPV16 E6 oncoprotein was demonstrated to interact with SRSF4, SRSF6, SRSF9 and with the E6/E7 pre-mRNA promoting intron 1 retention through a NLS3 sequence localized within its C-terminal domain (Bodaghi et al., 2009).

In HPV infected cells the release of E2F1 transcription factor, caused by the E7 binding to pRb, and its recruitment to binding sites in the SRSF10 promoter region determined increased expression of SRSF10 (Liu et al., 2018). Accordingly, the silencing of E6/E7 mRNA was shown to cause downregulation of SRSF10 in cervical cancer as well as in cervical cancer cell line SiHa (Liu et al., 2018).

Splicing Factors Deregulation in Cervical Cancer

The hnRNPs and SRSFs are generally upregulated in the basal and middle layers of the cervical epithelium and are

downregulated in the terminal differentiated layers, while several of them have been found hyper-expressed in cervical carcinoma and suggested to play important roles in cervical carcinogenesis (Fay et al., 2009; Johansson and Schwartz, 2013).

In particular, the hnRNP A1 is significantly overexpressed either in high grade CIN or in cervical carcinoma compared to normal cervical epithelium representing a candidate diagnostic biomarker of cervical cancer (Kim et al., 2017; Qing et al., 2017). Interestingly, a transcriptome analysis of HPV16 E6 and E7 immortalized epithelial cells showed up-regulation of hnRNP A1 in cells cultured under hypoxic condition, suggesting that its expression could be induced by stress (Denko et al., 2000). The hnRNP A1 facilitates the production of mature miR-18a thus promoting proliferation and invasion of SiHa cells (Dong P. et al., 2019). The miR-18a suppresses the expression of PTEN, WNK2, SOX6, BTG3, and RBSP3 genes by binding to their 3′-UTR transcripts, and causes PD-L1 expression and Wnt/β-catenin pathway activation in cervical carcinoma (Dong P. et al., 2019). Moreover, the siRNA-mediated hnRNP A1/A2 knockdown caused shortening of telomeres, procaspase-3 and PARP cleavage as well as increased apoptosis in HeLa cells, suggesting that it plays a significant role in cervical cancer cell viability (Patry et al., 2003).

The role of hnRNP A2/B1 in cervical cancer has been recently investigated (Li et al., 2014). Interestingly, Li et al. (2014) observed that lobaplatin induced cell cycle arrest and apoptosis via downregulation of hnRNP A2/B1 in Caski cells. Moreover, the hnRNP A2/B1 knockdown was shown to suppress cell proliferation, migration and invasion, while increasing the apoptosis and the sensitivity to irinotecan or lobaplatin through the up-regulation of p21, p27 and cleaved caspase-3 as well as p-AKT down-regulation in HeLa and CaSki cell lines (Shi et al., 2018).

The hnRNP E1 and E2 expression decreases during the progress from low grade to high grade cervical neoplasia with an inverse correlation with HPV16 E6 protein levels (Pillai et al., 2003). Indeed, both factors may act as oncosuppressors, being under-expressed in CIN 2-3 and cervical carcinoma compared to CIN 1 (Gao et al., 2020).

Tang et al. (2011) demonstrated that hnRNP F binds to a GGGA ESS motif, located within ENOX2 exon 4, causing enhanced production of ENOX2 exon 4 minus splicing variant, that is overexpressed in cervical cancer and involved in increased cell growth.

The levels of hnRNP H and I are higher in cervical cancer and high grade CIN compared to low grade CIN and normal tissues (Oberg et al., 2005; Fay et al., 2009). The hnRNP I knockdown reduces the proliferation and anchorage-independent growth while increasing invasiveness of HeLa cells (Wang et al., 2008). The hnRNP I was also shown to regulate gene expression by forming a dimer with PTB-associated splicing factor (PSF) in SiHa and CaSki cells (Zhang et al., 2020). Moreover, Zhang et al. (2020) demonstrated that lncRNA ARAP1-AS1 interacts with PSF causing the release of hnRNP I, which in turns enhances the c-Myc IRES-dependent translation by binding to c-Myc mRNA 5′-UTR enhancing SiHa and Caski cell proliferation.

The hnRNP P2 (FUS/TLS) is highly expressed in cervical cancer as well as in SiHa and HeLa cells, dependently from the activation of XIST lncRNA/miR-200a axis, and induces the epithelial mesenchymal transition phenotype and proliferation while inhibiting apoptosis in cervical cancer cells (Zhu et al., 2018).

The SRSF1, SRSF2 and SRSF3 proteins are overexpressed in CIN 1 upper differentiated layers, in the CIN3 entire epithelium as well as in W12 cells (Mole et al., 2009a). The SRSF1 down-regulation causes the caspase 9a/9b decreased ratio and increased sensitivity of cancer cells to DNA damaging agents (Shultz et al., 2011). Similarly, the SRSF2 depletion causes increased p53 expression and apoptosis in W12 transformed subclones as well as decreased anchorage-independent growth and cell cycle arrest at G2/M checkpoint both in W12 and C33A cells (McFarlane et al., 2015). Wu et al. (2010) first demonstrated that SRSF1 was able to bind to CGGACAC motifs in the pri-miR-7-1, pri-miR-221 and pri-miR-222 stem loops thus enhancing Drosha cleavage and accumulation of miR-7, miR-221 and miR-222, promoting cervical cancer development (Pan et al., 2019). Moreover, Dong M. et al. (2019) demonstrated that the lncRNA MIR205HG, which is overexpressed in cervical cancer, targets SRSF1 and up-regulates KRT17 causing cell proliferation and apoptosis inhibition in CaSKi, Hela, MS751 and SiHa cells. The silencing of SRSF3 in HeLa cells was shown to promote the production of ILF3 isoforms 1 and 2 as well as cell cycle progression to the S and G2/M phases and proliferation enhancement (Jia et al., 2019). In addition, a miRNA array analysis showed that SRSF3 knockdown in HeLa cells caused the down-regulation of miR-16, miR-18a, miR-21, miR-92b, miR-128, miR-182, miR-629, miR-629, miR-1180, and miR-1308, and the up-regulation of miR-7, miR-26a, miR-30a, miR-99a, miR100, miR-125b, miR-181a, miR-206, miR-378, and miR-923, all involved in carcinogenic processes (Ajiro et al., 2016a; Tornesello et al., 2020).

The SRSF9 is overexpressed in cervical carcinoma, due to the down regulation of miRNA-802 that in normal epithelium binds the 3′-UTR region of SRSF9 transcript inhibiting translation, and causes increase in cell proliferation (Zhang et al., 2019b).

Similarly, the SRSF10 is increasingly overexpressed in CIN and cervical cancer cells. Its expression is higher in HPV16 and HPV18-positive compared to HPV-negative cervical cancers, but becomes strongly downregulated following the E6/E7 silencing in CaSki cells (Liu et al., 2018). Moreover, the injection of SRSF10-knockdown SiHa cells in nude mice reduced tumor growth suggesting that this factor promotes cell proliferation (Liu et al., 2018). The overexpression of SRSF10 has shown to favor the transcription of the CD47 immune evasion signal and the production of the mIL1RAP isoform, which induces the NF-κB activation and the IL-1β signal transduction associated with production of pro-inflammatory cytokines (Liu et al., 2018).

Finally, the SRSF11 (SRp54) has been observed to interact with TERC and TRF2 factors and to promote the telomerase association with telomeric repeats and telomeres elongation in HeLa cells (Lee et al., 2015).

Other Splicing Factors in Cervical Cancer

Other proteins involved in splicing processes, including Tra2β, Brm and Sam68, have been found deregulated in cervical cancer and derived cell lines and proposed to have significant roles in cervical carcinogenesis. Specifically, the over expression of Tra2β protein, which localizes to the cervical carcinoma cell nuclei, was demonstrated to correlate with lymph node metastasis, higher tumor grade, size and depth of invasion (Gabriel et al., 2009; Best et al., 2013). The Brm factor is able to interact with ERK phosphorylated Sam68 causing the production of the CD44v5 variant by its direct binding to the exon 5 splice-regulatory elements and exon 5 retention in CD44 mRNA in HeLa cell line (Doorbar, 2005).

The Sam68 is highly expressed in cervical carcinoma and its cytoplasmic localization is shown to be associated with pelvic lymph node metastasis and poor prognosis in patients with early-stage cervical cancer (Li et al., 2012). Li et al. (2012) also demonstrated that down-regulation of Sam68 in cervical cancer cells reduced the cell motility and invasion as well as reversed the epithelial mesenchymal transition phenotype through the inhibition of the Akt/GSK-3β/Snail pathway. In HeLa cells the Sam68 was shown to bind a UAAAAAGCAU sequence within the exon 3 of survivin mRNA thus promoting the production of the anti-apoptotic DEx3 variant. Such variant has been found over-expressed in cervical adenocarcinoma HeLa cell line as well as in cervical carcinoma tissues (Futakuchi et al., 2007; Gaytan-Cervantes et al., 2017). Moreover, Sam68 was observed to interact with SRm160, a SR-rich splicing co-activator, to stimulate the inclusion of the v5 exon into the CD44 mRNA in a Ras-signaling dependent manner causing increased invasiveness of HeLa cells (Cheng and Sharp, 2006).

Splicing-Targeted Therapeutic Strategies

The relevant role of aberrant splicing in carcinogenesis highlights the need for novel splicing-targeted therapies. Currently, different strategies have been adopted to target deregulated splicing factors and abnormal splicing variants, including the usage of small bacteria-derived molecules against the core spliceosome, splicing regulators inhibitors and anti-sense oligonucleotides against oncogenic mRNA isoforms (Lee and Abdel-Wahab, 2016; Bates et al., 2017; Lin, 2017; Di et al., 2019; Bonnal et al., 2020) (**Table 4**).

Several bacterial derived small molecules or their synthetic analogs have been used to inhibit the spliceosome assembly or the post-translational modifications of the core spliceosome components (Effenberger et al., 2017). Particularly, spliceostatins and pladienolides derived from *Pseudomonas* and *Streptomyces,* respectively, have shown to bind the SF3b component of U2 snRNP causing the inhibition of the spliceosome assembly and cell cycle arrest at G1 and G2/M phases (Nakajima et al., 1996; Sakai et al., 2002, 2004). The binding of spliceostatin A to SF3b1 has been demonstrated to stimulate the production of unspliced p27 mRNA encoding the C-terminal truncated p27* variant which causes cell cycle arrest at G1 phase by inhibiting CDK2 in HeLa cells (Kaida et al., 2007; Satoh and Kaida, 2016). Treatment with pladienolide B caused reduction of SF3b1 expression in a dose-dependent manner, cell cycle arrest at the G2/M phase and induction of apoptosis by increasing the expression of Tap73, cytochrome C and pro-apoptotic Bax, while decreasing the levels of ΔNp73 and anti-apoptotic Bcl-2 in HeLa cells (Zhang et al., 2019a).

Targeting of kinases regulating the splicing factors activity, such as SRPK1 and CLK2, represents a further promising

TABLE 4 | Splicing-targeted strategies.

Splicing-targeted strategies	Molecules	Targets	Activity	References
Bacteria-derived compounds	Spliceostatins	SF3b	Inhibition of spliceosome assembly, splicing disruption and cell cycle arrest	Kaida et al. (2007); Zhang et al. (2019a)
	Pladienolides			
Splicing regulators inhibitors	SPHINX, SRPIN340	SRPK1	Reduced phosphorylation, altered localization and activity of SRSFs	Lu et al. (2014); Araki et al. (2015); Mavrou et al. (2015); Chang et al. (2017); Otsuka et al. (2018)
	Cpd-1, Cpd-2, Cpd-3	Clk1, Clk2		
	Resveratrol, caffeine, theophylline	hnRNPs and SRSFs mRNAs	Inhibition of hnRNPs and SRSFs expression, rescuing of aberrant splicing events and reduction of cell proliferation	
Splice-switching antisense oligonucleotides (SSOs)	2′-*O*-methylated SSO	Splicing factors binding sites (i.e., splicing acceptor and donor sited, splicing enhancers and silencers)	Inhibition of splicing factors interaction with binding sites by steric hindrance and reduction of oncogenic mRNA isoforms production	Bauman et al. (2010); Mogilevsky et al. (2018)
	2′-*O*-methoxyethylated SSO			

therapeutic model (Urbanski et al., 2018). Either SRPK1 siRNA knockdown or treatment by SPHINX and SRPIN340 inhibitors reduced the SRSF1, SRSF2 and SRSF5 phosphorylation causing increased production of the anti-apoptotic VEGF165b isoform in PC-3 prostate cancer cell line (Mavrou et al., 2015). Araki et al. (2015) showed that Cpd-1, Cpd-2, and Cpd-3 compounds inhibit the Clk1 and Clk2 kinases activity causing reduction of SRSF4 and SRSF6 phosphorylation and modifying genome-wide splicing patterns. In particular, the transcriptome analyses performed after treatment with Cpd-2 showed changes in the splicing patterns of gene transcripts involved in growth and survival, such as EGFR, CD44, EIF3H, AURKA, HDAC1, and PARP, leading to reduced proliferation and increased apoptosis in colorectal cancer COLO205 and COLO320DM, lung cancer NCI-H23 as well as breast cancer MDA-MB-468 cell lines (Araki et al., 2015).

Splice-switching antisense oligonucleotides (SSOs) are synthetic 15–30 nucleotide long sequences that bind matched splice sites and inhibit the splicing factors interaction by steric hindrance (Havens and Hastings, 2016). Chemical modifications, such as 2′-*O*-methylation and 2′-*O*-methoxyethylation are necessary to prevent degradation of pre-mRNA-SSO complexes by RNase H (Rigo et al., 2014). The 2′-*O*-methoxyethylated Bcl-x SSO oligonucleotide is able to target the 5′-splice site in exon 2 of Bcl-x mRNA causing switch from anti-apoptotic Bcl-xL to pro-apoptotic Bcl-xS in a dose dependent manner and apoptosis via PARP cleavage in B16F10 mouse melanoma cells (Bauman et al., 2010). Furthermore, 2′-*O*-methylated SSO, targeting the 3′-splice site in exon 14b of MKNK2 mRNA, enhances the tumor-suppressor Mnkn2a isoform levels, leading to increased phosphorylation and activation of p38α–MAPK and overexpression of cFOS, COX2 and IL-6 target genes (Mogilevsky et al., 2018). The treatment with 2′-*O*-methylated SSO causes reduction of anchorage independent growth and survival in glioblastoma U87MG, hepatocellular carcinoma HuH7 and breast cancer MDA–MB–231 cell lines (Mogilevsky et al., 2018).

The resveratrol has been shown to regulate the miR-424 and miR-503 expression that inhibit hnRNP A1 production and cell proliferation in human breast cancer cell line MCF7 (Otsuka et al., 2018). In addition, bortezomib has found to reduce the expression of hnRNP K, hnRNP H, Hsp90α, Grp78, and Hsp7C in Burkytt lymphoma cell lines such as CA46 and Daudi, as determined by a proteomic analysis (Suk et al., 2015).

A natural compound, caffeine, was demonstrated to reduce the SRSF3 levels by causing increased expression of the p53β variant, reduced expression of SRSF3 targets, such as HIF-1α, SREBP1c, COX-2, FASN, and EGFR, and enhanced cell senescence (Lu et al., 2014). Similarly, theophylline down-regulates SRSF3 expression and switches the production from p53α to p53β isoform in HeLa and MCF-7 cell lines causing apoptosis, senescence, and decreased colony formation (Chang et al., 2017). Another natural drug namely indacaterol was shown to rescue SRSF6 associated aberrant splicing events, such as ZO-1 exon 23 skipping, and to reduce the viability of RKO, HCT116, and HCT8 colorectal cancer cells as well as to inhibit cancer growth in a colorectal cancer mouse model (Wan et al., 2019).

Aberrant protein isoforms have also been proposed as potential therapeutic targets (Le et al., 2015). A comprehensive genomic analysis of 38'028 tumors allowed the discovery of recurrent somatic mutations in the splice donor and acceptor sites in MET transcripts causing skipping of exon 14 in lung adenocarcinoma (Frampton et al., 2015). The expression of exon 14-lacking MET in NIH3T3 cells conferred higher sensitivity to MET-specific inhibitors, such as capmatinib, compared to cells expressing wild type MET (Frampton et al., 2015).

CONCLUSION

In recent years, there is a growing experimental evidence of the key role played by deregulated splicing in cancer development and progression. Several genome-wide studies have revealed tumor specific splicing profiles at mRNA and protein level, identifying a multitude of aberrant splice variants with oncogenic functions. Different protein isoforms have been demonstrated to have a prognostic value and to modify the sensitivity of cancer cells to chemotherapeutic agents. On the other hand, therapies targeting deregulated splicing factors or pathogenic splicing isoforms are under development. Several data have been published on the role of splicing factors in cervical cancer development and further studies are needed to clarify the relevance of such factors in the production of viral or cell genome encoded oncogenic isoforms as well as in the promotion of pre-neoplastic lesions progression to invasive cancer. Much more needs to be done for the development and the clinical application of splicing-targeted therapeutic agents that would inhibit cervical cancer as well as other HPV-related tumors by affecting both cell oncogenic pathways as well as HPV life cycle.

AUTHOR CONTRIBUTIONS

AC performed bibliography analysis and wrote the manuscript. LB and FB supervised the whole project. MT designed the study and drafted the manuscript. All authors read and approved the final manuscript.

FUNDING

This work and the publication costs were supported by the research grants Ricerca Corrente (N. 2611892) and Ministero della Salute (RF-2018-12366163).

ACKNOWLEDGMENTS

We are grateful to Clorinda Annunziata, Francesca Pezzuto, and Noemy Starita for helpful discussion.

REFERENCES

Aebi, M., Hornig, H., Padgett, R. A., Reiser, J., and Weissmann, C. (1986). Sequence requirements for splicing of higher eukaryotic nuclear pre-mRNA. *Cell* 47, 555–565. doi: 10.1016/0092-8674(86)90620-3

Ajiro, M., Jia, R., Yang, Y., Zhu, J., and Zheng, Z. M. (2016a). A genome landscape of SRSF3-regulated splicing events and gene expression in human osteosarcoma U2OS cells. *Nucleic Acids Res.* 44, 1854–1870. doi: 10.1093/nar/gkv1500

Ajiro, M., Jia, R., Zhang, L., Liu, X., and Zheng, Z. M. (2012). Intron definition and a branch site adenosine at nt 385 control RNA splicing of HPV16 E6*I and E7 expression. *PLoS One* 7:e46412. doi: 10.1371/journal.pone.0046412

Ajiro, M., Tang, S., Doorbar, J., and Zheng, Z. M. (2016b). Serine/Arginine-rich splicing factor 3 and heterogeneous nuclear ribonucleoprotein A1 regulate alternative RNA splicing and gene expression of human papillomavirus 18 through two functionally distinguishable cis elements. *J. Virol.* 90, 9138–9152. doi: 10.1128/jvi.00965-16

Ajiro, M., and Zheng, Z. M. (2015). E6ˆE7, a novel splice isoform protein of human papillomavirus 16, stabilizes viral E6 and E7 oncoproteins via HSP90 and GRP78. *mBio* 6:e02068-14.

Alekseev, O. M., Richardson, R. T., Tsuruta, J. K., and O'Rand, M. G. (2011). Depletion of the histone chaperone tNASP inhibits proliferation and induces apoptosis in prostate cancer PC-3 cells. *Reprod. Biol. Endocrinol.* 9:50. doi: 10.1186/1477-7827-9-50

Anczukow, O., and Krainer, A. R. (2016). Splicing-factor alterations in cancers. *RNA* 22, 1285–1301. doi: 10.1261/rna.057919.116

Andreotti, A. H., Bunnell, S. C., Feng, S., Berg, L. J., and Schreiber, S. L. (1997). Regulatory intramolecular association in a tyrosine kinase of the Tec family. *Nature* 385, 93–97. doi: 10.1038/385093a0

Araki, S., Dairiki, R., Nakayama, Y., Murai, A., Miyashita, R., Iwatani, M., et al. (2015). Inhibitors of CLK protein kinases suppress cell growth and induce apoptosis by modulating pre-mRNA splicing. *PLoS One* 10:e0116929. doi: 10.1371/journal.pone.0116929

Arbab, J. P., Ayatollahi, H., Sadeghi, R., Sheikhi, M., and Asghari, A. (2018). Prognostic significance of SRSF2 mutations in myelodysplastic syndromes and chronic myelomonocytic leukemia: a meta-analysis. *Hematology* 23, 778–784. doi: 10.1080/10245332.2018.1471794

Aubol, B. E., Keshwani, M. M., Fattet, L., and Adams, J. A. (2018). Mobilization of a splicing factor through a nuclear kinase-kinase complex. *Biochem. J.* 475, 677–690. doi: 10.1042/bcj20170672

Aujla, A., Linder, K., Iragavarapu, C., Karass, M., and Liu, D. (2018). SRSF2 mutations in myelodysplasia/myeloproliferative neoplasms. *Biomark. Res.* 6:29.

Auyeung, V. C., Ulitsky, I., McGeary, S. E., and Bartel, D. P. (2013). Beyond secondary structure: primary-sequence determinants license pri-miRNA hairpins for processing. *Cell* 152, 844–858. doi: 10.1016/j.cell.2013.01.031

Baralle, F. E., and Giudice, J. (2017). Alternative splicing as a regulator of development and tissue identity. *Nat. Rev. Mol. Cell Biol.* 18, 437–451. doi: 10.1038/nrm.2017.27

Bates, D. O., Morris, J. C., Oltean, S., and Donaldson, L. F. (2017). Pharmacology of modulators of alternative splicing. *Pharmacol. Rev.* 69, 63–79. doi: 10.1124/pr.115.011239

Batsche, E., Yaniv, M., and Muchardt, C. (2006). The human SWI/SNF subunit Brm is a regulator of alternative splicing. *Nat. Struct. Mol. Biol.* 13, 22–29. doi: 10.1038/nsmb1030

Bauman, J. A., Li, S. D., Yang, A., Huang, L., and Kole, R. (2010). Anti-tumor activity of splice-switching oligonucleotides. *Nucleic Acids Res.* 38, 8348–8356. doi: 10.1093/nar/gkq731

Best, A., Dagliesh, C., Ehrmann, I., Kheirollahi-Kouhestani, M., Tyson-Capper, A., and Elliott, D. J. (2013). Expression of Tra2 beta in cancer cells as a potential contributory factor to neoplasia and metastasis. *Int. J. Cell Biol.* 2013:843781.

Bielli, P., Busa, R., Paronetto, M. P., and Sette, C. (2011). The RNA-binding protein Sam68 is a multifunctional player in human cancer. *Endocr. Relat. Cancer* 18, R91–R102.

Bodaghi, S., Jia, R., and Zheng, Z. M. (2009). Human papillomavirus type 16 E2 and E6 are RNA-binding proteins and inhibit in vitro splicing of pre-mRNAs with suboptimal splice sites. *Virology* 386, 32–43. doi: 10.1016/j.virol.2008.12.037

Bonnal, S. C., Lopez-Oreja, I., and Valcarcel, J. (2020). Roles and mechanisms of alternative splicing in cancer – implications for care. *Nat. Rev. Clin. Oncol.* doi: 10.1038/s41571-020-0350-x [Epub ahead of print].

Boukakis, G., Patrinou-Georgoula, M., Lekarakou, M., Valavanis, C., and Guialis, A. (2010). Deregulated expression of hnRNP A/B proteins in human non-small cell lung cancer: parallel assessment of protein and mRNA levels in paired tumour/non-tumour tissues. *BMC Cancer* 10:434. doi: 10.1186/1471-2407-10-434

Bradley, T., Cook, M. E., and Blanchette, M. (2015). SR proteins control a complex network of RNA-processing events. *RNA* 21, 75–92. doi: 10.1261/rna.043893.113

Brant, A. C., Menezes, A. N., Felix, S. P., de Almeida, L. M., Sammeth, M., and Moreira, M. A. M. (2018). Characterization of HPV integration, viral gene expression and E6E7 alternative transcripts by RNA-Seq: a descriptive study in invasive cervical cancer. *Genomics* 111, 1853–1861. doi: 10.1016/j.ygeno.2018.12.008

Buljan, M., Chalancon, G., Eustermann, S., Wagner, G. P., Fuxreiter, M., Bateman, A., et al. (2012). Tissue-specific splicing of disordered segments that embed binding motifs rewires protein interaction networks. *Mol. Cell* 46, 871–883. doi: 10.1016/j.molcel.2012.05.039

Busa, R., Paronetto, M. P., Farini, D., Pierantozzi, E., Botti, F., Angelini, D. F., et al. (2007). The RNA-binding protein Sam68 contributes to proliferation and survival of human prostate cancer cells. *Oncogene* 26, 4372–4382. doi: 10.1038/sj.onc.1210224

Busch, A., and Hertel, K. J. (2012). Evolution of SR protein and hnRNP splicing regulatory factors. *Wiley Interdiscip. Rev. RNA* 3, 1–12. doi: 10.1002/wrna.100

Bush, S. J., Chen, L., Tovar-Corona, J. M., and Urrutia, A. O. (2017). Alternative splicing and the evolution of phenotypic novelty. *Philos. Trans. R. Soc. Lond. B Biol. Sci.* 2017:372.

Bzhalava, Z., Arroyo Muhr, L. S., and Dillner, J. (2020). Transcription of human papillomavirus oncogenes in head and neck squamous cell carcinomas. *Vaccine* 38, 4066–4070. doi: 10.1016/j.vaccine.2020.04.049

Cerasuolo, A., Annunziata, C., Tortora, M., Starita, N., Stellato, G., Greggi, S., et al. (2017). Comparative analysis of HPV16 gene expression profiles in cervical and in oropharyngeal squamous cell carcinoma. *Oncotarget* 8, 34070–34081. doi: 10.18632/oncotarget.15977

Chang, Y. L., Hsu, Y. J., Chen, Y., Wang, Y. W., and Huang, S. M. (2017). Theophylline exhibits anti-cancer activity via suppressing SRSF3 in cervical and breast cancer cell lines. *Oncotarget* 8, 101461–101474. doi: 10.18632/oncotarget.21464

Chaudhury, A., Chander, P., and Howe, P. H. (2010). Heterogeneous nuclear ribonucleoproteins (hnRNPs) in cellular processes: focus on hnRNP E1's multifunctional regulatory roles. *RNA* 16, 1449–1462. doi: 10.1261/rna.2254110

Che, Y., and Fu, L. (2020). Aberrant expression and regulatory network of splicing factor-SRSF3 in tumors. *J. Cancer* 11, 3502–3511. doi: 10.7150/jca.42645

Chen, C., Lei, J., Zheng, Q., Tan, S., Ding, K., and Yu, C. (2018). Poly(rC) binding protein 2 (PCBP2) promotes the viability of human gastric cancer cells by regulating CDK2. *FEBS Open Bio.* 8, 764–773. doi: 10.1002/2211-5463.12408

Chen, H., Liu, H., and Qing, G. (2018). Targeting oncogenic Myc as a strategy for cancer treatment. *Signal. Transduct. Target Ther.* 3:5.

Chen, J., Xue, Y., Poidinger, M., Lim, T., Chew, S. H., Pang, C. L., et al. (2014). Mapping of HPV transcripts in four human cervical lesions using RNAseq suggests quantitative rearrangements during carcinogenic progression. *Virology* 46, 14–24. doi: 10.1016/j.virol.2014.05.026

Chen, M., and Manley, J. L. (2009). Mechanisms of alternative splicing regulation: insights from molecular and genomics approaches. *Nat. Rev. Mol. Cell Biol.* 10, 741–754. doi: 10.1038/nrm2777

Chen, Y., Huang, Q., Liu, W., Zhu, Q., Cui, C. P., Xu, L., et al. (2018a). Mutually exclusive acetylation and ubiquitylation of the splicing factor SRSF5 control tumor growth. *Nat. Commun.* 9:2464.

Chen, Y., Liu, J., Wang, W., Xiang, L., Wang, J., Liu, S., et al. (2018b). High expression of hnRNPA1 promotes cell invasion by inducing EMT in gastric cancer. *Oncol. Rep.* 39, 1693–1701.

Cheng, C., and Sharp, P. A. (2006). Regulation of CD44 alternative splicing by SRm160 and its potential role in tumor cell invasion. *Mol. Cell Biol.* 26, 362–370. doi: 10.1128/mcb.26.1.362-370.2006

Cheng, Z., Sun, Y., Niu, X., Shang, Y., Ruan, J., Chen, Z., et al. (2017). Gene expression profiling reveals U1 snRNA regulates cancer gene expression. *Oncotarget* 8, 112867–112874. doi: 10.18632/oncotarget.22842

Cheunim, T., Zhang, J., Milligan, S. G., McPhillips, M. G., and Graham, S. V. (2008). The alternative splicing factor hnRNP A1 is up-regulated during virus-infected epithelial cell differentiation and binds the human papillomavirus type 16 late regulatory element. *Virus Res.* 131, 189–198. doi: 10.1016/j.virusres.2007.09.006

Christofk, H. R., Vander Heiden, M. G., Harris, M. H., Ramanathan, A., Gerszten, R. E., Wei, R., et al. (2008). The M2 splice isoform of pyruvate kinase is important for cancer metabolism and tumour growth. *Nature* 452, 230–233. doi: 10.1038/nature06734

Climente-Gonzalez, H., Porta-Pardo, E., Godzik, A., and Eyras, E. (2017). The functional impact of alternative splicing in cancer. *Cell Rep.* 20, 2215–2226. doi: 10.1016/j.celrep.2017.08.012

Collier, B., Goobar-Larsson, L., Sokolowski, M., and Schwartz, S. (1998). Translational inhibition in vitro of human papillomavirus type 16 L2 mRNA mediated through interaction with heterogenous ribonucleoprotein K and poly(rC)-binding proteins 1 and 2. *J. Biol. Chem.* 273, 22648–22656. doi: 10.1074/jbc.273.35.22648

Collins, S. I., Constandinou-Williams, C., Wen, K., Young, L. S., Roberts, S., Murray, P. G., et al. (2009). Disruption of the E2 gene is a common and early event in the natural history of cervical human papillomavirus infection: a longitudinal cohort study. *Cancer Res.* 69, 3828–3832. doi: 10.1158/0008-5472.can-08-3099

Colwill, K., Pawson, T., Andrews, B., Prasad, J., Manley, J. L., Bell, J. C., et al. (1996). The Clk/Sty protein kinase phosphorylates SR splicing factors and regulates their intranuclear distribution. *EMBO J.* 15, 265–275. doi: 10.1002/j.1460-2075.1996.tb00357.x

Coupe, V. M., Gonzalez-Barreiro, L., Gutierrez-Berzal, J., Melian-Boveda, A. L., Lopez-Rodriguez, O., Alba-Dominguez, J., et al. (2012). Transcriptional analysis of human papillomavirus type 16 in histological sections of cervical dysplasia by in situ hybridisation. *J. Clin. Pathol.* 65, 164–170. doi: 10.1136/jclinpath-2011-200330

Czubaty, A., and Piekielko-Witkowska, A. (2017). Protein kinases that phosphorylate splicing factors: roles in cancer development, progression and possible therapeutic options. *Int. J. Biochem. Cell Biol.* 91(Pt B), 102–115. doi: 10.1016/j.biocel.2017.05.024

Das, S., Anczukow, O., Akerman, M., and Krainer, A. R. (2012). Oncogenic splicing factor SRSF1 is a critical transcriptional target of MYC. *Cell Rep.* 1, 110–117. doi: 10.1016/j.celrep.2011.12.001

David, C. J., Chen, M., Assanah, M., Canoll, P., and Manley, J. L. (2010). HnRNP proteins controlled by c-Myc deregulate pyruvate kinase mRNA splicing in cancer. *Nature* 463, 364–368. doi: 10.1038/nature08697

David, J., Maden, S., Weeder, B., Thompson, R., and Nellore, A. (2020). Putatively cancer-specific exonΓÇôexon junctions are shared across patients and present in developmental and other non-cancer cells. *NAR Cancer* 1:2.

Denko, N., Schindler, C., Koong, A., Laderoute, K., Green, C., and Giaccia, A. (2000). Epigenetic regulation of gene expression in cervical cancer cells by the tumor microenvironment. *Clin. Cancer Res.* 6, 480–487.

Derry, J. J., Richard, S., Valderrama, C. H., Ye, X., Vasioukhin, V., Cochrane, A. W., et al. (2000). Sik (BRK) phosphorylates Sam68 in the nucleus and negatively regulates its RNA binding ability. *Mol. Cell Biol.* 20, 6114–6126. doi: 10.1128/mcb.20.16.6114-6126.2000

Dhanjal, S., Kajitani, N., Glahder, J., Mossberg, A. K., Johansson, C., and Schwartz, S. (2015). Heterogeneous nuclear ribonucleoprotein C proteins interact with the human papillomavirus type 16 (HPV16) Early 3′-untranslated region and alleviate suppression of HPV16 late L1 mRNA splicing. *J. Biol. Chem.* 290, 13354–13371. doi: 10.1074/jbc.m115.638098

Di, C., Syafrizayanti, Zhang Q, Chen, Y., Wang, Y., Zhang, X., et al. (2019). Function, clinical application, and strategies of Pre-mRNA splicing in cancer. *Cell Death Differ.* 26, 1181–1194. doi: 10.1038/s41418-018-0231-3

Dong, M., Dong, Z., Zhu, X., Zhang, Y., and Song, L. (2019). Long non-coding RNA MIR205HG regulates KRT17 and tumor processes in cervical cancer via interaction with SRSF1. *Exp. Mol. Pathol.* 111:104322. doi: 10.1016/j.yexmp.2019.104322

Dong, P., Xiong, Y., Yu, J., Chen, L., Tao, T., Yi, S., et al. (2019). Correction: control of PD-L1 expression by miR-140/142/340/383 and oncogenic activation of the OCT4-miR-18a pathway in cervical cancer. *Oncogene* 38:3972. doi: 10.1038/s41388-019-0677-x

Doorbar, J. (2005). The papillomavirus life cycle. *J. Clin. Virol.* 32(Suppl. 1), S7–S15.

Doorbar, J. (2006). Molecular biology of human papillomavirus infection and cervical cancer. *Clin. Sci.* 110, 525–541. doi: 10.1042/cs20050369

Doorbar, J., Egawa, N., Griffin, H., Kranjec, C., and Murakami, I. (2015). Human papillomavirus molecular biology and disease association. *Rev. Med. Virol.* 25(Suppl. 1), 2–23. doi: 10.1002/rmv.1822

Doorbar, J., Foo, C., Coleman, N., Medcalf, L., Hartley, O., Prospero, T., et al. (1997). Characterization of events during the late stages of HPV16 infection in vivo using high-affinity synthetic Fabs to E4. *Virology* 238, 40–52. doi: 10.1006/viro.1997.8768

Doorbar, J., Parton, A., Hartley, K., Banks, L., Crook, T., Stanley, M., et al. (1990). Detection of novel splicing patterns in a HPV16-containing keratinocyte cell line. *Virology* 178, 254–262. doi: 10.1016/0042-6822(90)90401-c

Doorbar, J., Quint, W., Banks, L., Bravo, I. G., Stoler, M., Broker, T. R., et al. (2012). The biology and life-cycle of human papillomaviruses. *Vaccine* 30(Suppl. 5), F55–F70.

Dvinge, H. (2018). Regulation of alternative mRNA splicing: old players and new perspectives. *FEBS Lett.* 592, 2987–3006. doi: 10.1002/1873-3468.13119

Dvinge, H., Kim, E., Abdel-Wahab, O., and Bradley, R. K. (2016). RNA splicing factors. *Nat. Rev. Cancer* 16, 413–430.

Effenberger, K. A., Urabe, V. K., and Jurica, M. S. (2017). Modulating splicing with small molecular inhibitors of the spliceosome. *Wiley Interdiscip. Rev. RNA* 8:10.1002/wrna.1381.

El, M. E., and Younis, I. (2018). The cancer spliceome: reprograming of alternative splicing in cancer. *Front. Mol. Biosci.* 5:80. doi: 10.3389/fmolb.2018.00080

Elliott, D. J., Best, A., Dalgliesh, C., Ehrmann, I., and Grellscheid, S. (2012). How does Tra2beta protein regulate tissue-specific RNA splicing? *Biochem. Soc. Trans.* 40, 784–788. doi: 10.1042/bst20120036

Enokizono, Y., Konishi, Y., Nagata, K., Ouhashi, K., Uesugi, S., Ishikawa, F., et al. (2005). Structure of hnRNP D complexed with single-stranded telomere DNA and unfolding of the quadruplex by heterogeneous nuclear ribonucleoprotein D. *J. Biol. Chem.* 280, 18862–18870. doi: 10.1074/jbc.m411822200

Evans, W., Filippova, M., Filippov, V., Bashkirova, S., Zhang, G., Reeves, M. E., et al. (2016). Overexpression of HPV16 E6* alters beta-integrin and mitochondrial dysfunction pathways in cervical cancer cells. *Cancer Genomics Proteomics* 13, 259–273.

Fay, J., Kelehan, P., Lambkin, H., and Schwartz, S. (2009). Increased expression of cellular RNA-binding proteins in HPV-induced neoplasia and cervical cancer. *J. Med. Virol.* 81, 897–907. doi: 10.1002/jmv.21406

Fei, T., Chen, Y., Xiao, T., Li, W., Cato, L., Zhang, P., et al. (2017). Genome-wide CRISPR screen identifies HNRNPL as a prostate cancer dependency regulating RNA splicing. *Proc. Natl. Acad. Sci. U.S.A.* 114, E5207–E5215.

Feng, Y., Chen, M., and Manley, J. L. (2008). Phosphorylation switches the general splicing repressor SRp38 to a sequence-specific activator. *Nat. Struct. Mol. Biol.* 15, 1040–1048. doi: 10.1038/nsmb.1485

Filippova, M., Evans, W., Aragon, R., Filippov, V., Williams, V. M., Hong, L., et al. (2014). The small splice variant of HPV16 E6, E6, reduces tumor formation in cervical carcinoma xenografts. *Virology* 45, 153–164. doi: 10.1016/j.virol.2013.12.011

Frampton, G. M., Ali, S. M., Rosenzweig, M., Chmielecki, J., Lu, X., Bauer, T. M., et al. (2015). Activation of MET via diverse exon 14 splicing alterations occurs in multiple tumor types and confers clinical sensitivity to MET inhibitors. *Cancer Discov.* 5, 850–859. doi: 10.1158/2159-8290.cd-15-0285

Frendewey, D., and Keller, W. (1985). Stepwise assembly of a pre-mRNA splicing complex requires U-snRNPs and specific intron sequences. *Cell* 42, 355–367. doi: 10.1016/s0092-8674(85)80131-8

Friend, L. R., Landsberg, M. J., Nouwens, A. S., Wei, Y., Rothnagel, J. A., and Smith, R. (2013). Arginine methylation of hnRNP A2 does not directly govern its subcellular localization. *PLoS One* 8:e75669. doi: 10.1371/journal.pone.0075669

Fu, Y., Huang, B., Shi, Z., Han, J., Wang, Y., Huangfu, J., et al. (2013). SRSF1 and SRSF9 RNA binding proteins promote Wnt signalling-mediated tumorigenesis by enhancing beta-catenin biosynthesis. *EMBO Mol. Med.* 5, 737–750. doi: 10.1002/emmm.201202218

Fu, Y., and Wang, Y. (2018). SRSF7 knockdown promotes apoptosis of colon and lung cancer cells. *Oncol. Lett.* 15, 5545–5552.

Futakuchi, H., Ueda, M., Kanda, K., Fujino, K., Yamaguchi, H., and Noda, S. (2007). Transcriptional expression of survivin and its splice variants in cervical carcinomas. *Int. J. Gynecol. Cancer* 17, 1092–1098. doi: 10.1111/j.1525-1438.2007.00833.x

Gabriel, B., Zur, H. A., Bouda, J., Boudova, L., Koprivova, M., Hirschfeld, M., et al. (2009). Significance of nuclear hTra2-beta1 expression in cervical cancer. *Acta Obstet. Gynecol. Scand.* 88, 216–221. doi: 10.1080/00016340802503021

Gallardo, M., Lee, H. J., Zhang, X., Bueso-Ramos, C., Pageon, L. R., McArthur, M., et al. (2015). hnRNP K is a haploinsufficient tumor suppressor that regulates proliferation and differentiation programs in hematologic malignancies. *Cancer Cell* 28, 486–499. doi: 10.1016/j.ccell.2015.09.001

Gao, J., Aksoy, B. A., Dogrusoz, U., Dresdner, G., Gross, B., Sumer, S. O., et al. (2013). Integrative analysis of complex cancer genomics and clinical profiles using the cBioPortal. *Sci. Signal.* 6:pl1. doi: 10.1126/scisignal.2004088

Gao, R., Yu, Y., Inoue, A., Widodo, N., Kaul, S. C., and Wadhwa, R. (2013). Heterogeneous nuclear ribonucleoprotein K (hnRNP-K) promotes tumor metastasis by induction of genes involved in extracellular matrix, cell movement, and angiogenesis. *J. Biol. Chem.* 288, 15046–15056. doi: 10.1074/jbc.m113.466136

Gao, W., Ding, L., Song, Z. C., Feng, M. J., Liu, C. L., Li, X. X., et al. (2020). [The role of human papillomavirus 16 early genes E2 and E6 and heterogeneous nuclear ribonucleoprotein E2 in cervical carcinogenesis and their interaction effect]. *Zhonghua Yu Fang Yi Xue Za Zhi* 54, 92–98.

Gao, Y., Wang, W., Cao, J., Wang, F., Geng, Y., Cao, J., et al. (2016). Upregulation of AUF1 is involved in the proliferation of esophageal squamous cell carcinoma through GCH1. *Int. J. Oncol.* 49, 2001–2010. doi: 10.3892/ijo.2016.3713

Gaytan-Cervantes, J., Gonzalez-Torres, C., Maldonado, V., Zampedri, C., Ceballos-Cancino, G., and Melendez-Zajgla, J. (2017). Protein Sam68 regulates the alternative splicing of survivin DEx3. *J. Biol. Chem.* 292, 13745–13757. doi: 10.1074/jbc.m117.800318

Geuens, T., Bouhy, D., and Timmerman, V. (2016). The hnRNP family: insights into their role in health and disease. *Hum. Genet.* 135, 851–867. doi: 10.1007/s00439-016-1683-5

Ghigna, C., Giordano, S., Shen, H., Benvenuto, F., Castiglioni, F., Comoglio, P. M., et al. (2005). Cell motility is controlled by SF2/ASF through alternative splicing of the Ron protooncogene. *Mol. Cell* 20, 881–890. doi: 10.1016/j.molcel.2005.10.026

Giannakouros, T., Nikolakaki, E., Mylonis, I., and Georgatsou, E. (2011). Serine-arginine protein kinases: a small protein kinase family with a large cellular presence. *FEBS J.* 278, 570–586. doi: 10.1111/j.1742-4658.2010.07987.x

Golan-Gerstl, R., Cohen, M., Shilo, A., Suh, S. S., Bakacs, A., Coppola, L., et al. (2011). Splicing factor hnRNP A2/B1 regulates tumor suppressor gene splicing and is an oncogenic driver in glioblastoma. *Cancer Res.* 71, 4464–4472. doi: 10.1158/0008-5472.can-10-4410

Goncalves, V., Henriques, A. F., Pereira, J. F., Neves, C. A., Moyer, M. P., Moita, L. F., et al. (2014). Phosphorylation of SRSF1 by SRPK1 regulates alternative splicing of tumor-related Rac1b in colorectal cells. *RNA* 20, 474–482. doi: 10.1261/rna.041376.113

Grabowski, P. J., Seiler, S. R., and Sharp, P. A. (1985). A multicomponent. *Cell* 42, 345–353.

Graham, S. V. (2010). Human papillomavirus: gene expression, regulation and prospects for novel diagnostic methods and antiviral therapies. *Future Microbiol.* 5, 1493–1506. doi: 10.2217/fmb.10.107

Graham, S. V. (2016). Human papillomavirus E2 protein: linking replication, transcription, and RNA processing. *J. Virol.* 90, 8384–8388. doi: 10.1128/jvi.00502-16

Graham, S. V., and Faizo, A. A. A. (2017). Control of human papillomavirus gene expression by alternative splicing. *Virus Res.* 231, 83–95. doi: 10.1016/j.virusres.2016.11.016

Grellscheid, S., Dalgliesh, C., Storbeck, M., Best, A., Liu, Y., Jakubik, M., et al. (2011). Identification of evolutionarily conserved exons as regulated targets for the splicing activator tra2beta in development. *PLoS Genet.* 7:e1002390. doi: 10.1371/journal.pgen.1002390

Guil, S., and Caceres, J. F. (2007). The multifunctional RNA-binding protein hnRNP A1 is required for processing of miR-18a. *Nat. Struct. Mol. Biol.* 14, 591–596. doi: 10.1038/nsmb1250

Habelhah, H., Shah, K., Huang, L., Ostareck-Lederer, A., Burlingame, A. L., Shokat, K. M., et al. (2001). ERK phosphorylation drives cytoplasmic accumulation of hnRNP-K and inhibition of mRNA translation. *Nat .Cell Biol.* 3, 325–330. doi: 10.1038/35060131

Han, S. P., Tang, Y. H., and Smith, R. (2010). Functional diversity of the hnRNPs: past, present and perspectives. *Biochem. J.* 430, 379–392. doi: 10.1042/bj20100396

Havens, M. A., and Hastings, M. L. (2016). Splice-switching antisense oligonucleotides as therapeutic drugs. *Nucleic Acids Res.* 44, 6549–6563. doi: 10.1093/nar/gkw533

Hegde, R. S. (2002). The papillomavirus E2 proteins: structure, function, and biology. *Annu. Rev. Biophys. Biomol. Struct.* 31, 343–360. doi: 10.1146/annurev.biophys.31.100901.142129

Howard, J. M., and Sanford, J. R. (2015). The RNAissance family: SR proteins as multifaceted regulators of gene expression. *Wiley Interdiscip. Rev. RNA* 6, 93–110. doi: 10.1002/wrna.1260

Jang, M. K., Anderson, D. E., van, D. K., and McBride, A. A. (2015). A proteomic approach to discover and compare interacting partners of papillomavirus E2 proteins from diverse phylogenetic groups. *Proteomics* 15, 2038–2050. doi: 10.1002/pmic.201400613

Jeong, S. (2017). SR proteins: binders, regulators, and connectors of RNA. *Mol. Cells* 40, 1–9. doi: 10.14348/molcells.2017.2319

Jia, R., Ajiro, M., Yu, L., McCoy, P. Jr., and Zheng, Z. M. (2019). Oncogenic splicing factor SRSF3 regulates ILF3 alternative splicing to promote cancer cell proliferation and transformation. *RNA* 25, 630–644. doi: 10.1261/rna.068619.118

Jia, R., Li, C., McCoy, J. P., Deng, C. X., and Zheng, Z. M. (2010). SRp20 is a proto-oncogene critical for cell proliferation and tumor induction and maintenance. *Int. J. Biol. Sci.* 6, 806–826. doi: 10.7150/ijbs.6.806

Jia, R., Liu, X., Tao, M., Kruhlak, M., Guo, M., Meyers, C., et al. (2009). Control of the papillomavirus early-to-late switch by differentially expressed SRp20. *J. Virol.* 83, 167–180. doi: 10.1128/jvi.01719-08

Jiang, P., Li, Z., Tian, F., Li, X., and Yang, J. (2017). Fyn/heterogeneous nuclear ribonucleoprotein E1 signaling regulates pancreatic cancer metastasis by affecting the alternative splicing of integrin beta1. *Int. J. Oncol.* 51, 169–183. doi: 10.3892/ijo.2017.4018

Johansson, C., and Schwartz, S. (2013). Regulation of human papillomavirus gene expression by splicing and polyadenylation. *Nat. Rev. Microbiol.* 11, 239–251. doi: 10.1038/nrmicro2984

Kahles, A., Lehmann, K. V., Toussaint, N. C., Huser, M., Stark, S. G., Sachsenberg, T., et al. (2018). Comprehensive analysis of alternative splicing across tumors from 8,705 patients. *Cancer Cell* 34, 211–224.

Kaida, D., Motoyoshi, H., Tashiro, E., Nojima, T., Hagiwara, M., Ishigami, K., et al. (2007). Spliceostatin A targets SF3b and inhibits both splicing and nuclear retention of pre-mRNA. *Nat. Chem. Biol.* 3, 576–583. doi: 10.1038/nchembio.2007.18

Kajitani, N., Glahder, J., Wu, C., Yu, H., Nilsson, K., and Schwartz, S. (2017). hnRNP L controls HPV16 RNA polyadenylation and splicing in an Akt kinase-dependent manner. *Nucleic Acids Res.* 45, 9654–9678. doi: 10.1093/nar/gkx606

Kandoth, C., McLellan, M. D., Vandin, F., Ye, K., Niu, B., Lu, C., et al. (2013). Mutational landscape and significance across 12 major cancer types. *Nature* 502, 333–339. doi: 10.1038/nature12634

Kanopka, A., Muhlemann, O., and Akusjarvi, G. (1996). Inhibition by SR proteins of splicing of a regulated adenovirus pre-mRNA. *Nature* 381, 535–538. doi: 10.1038/381535a0

Karni, R., de, S. E., Lowe, S. W., Sinha, R., Mu, D., and Krainer, A. R. (2007). The gene encoding the splicing factor SF2/ASF is a proto-oncogene. *Nat. Struct. Mol. Biol.* 14, 185–193. doi: 10.1038/nsmb1209

Kastner, B., Will, C. L., Stark, H., and Luhrmann, R. (2019). Structural insights into nuclear pre-mRNA splicing in higher eukaryotes. *Cold Spring Harb. Perspect. Biol.* 11:a032417. doi: 10.1101/cshperspect.a032417

Kim, H. R., Lee, G. O., Choi, K. H., Kim, D. K., Ryu, J. S., Hwang, K. E., et al. (2016). SRSF5: a novel marker for small-cell lung cancer and pleural metastatic cancer. *Lung Cancer* 99, 57–65. doi: 10.1016/j.lungcan.2016.05.018

Kim, J., Park, R. Y., Chen, J. K., Kim, J., Jeong, S., and Ohn, T. (2014). Splicing factor SRSF3 represses the translation of programmed cell death 4 mRNA by associating with the 5′-UTR region. *Cell Death Differ.* 21, 481–490. doi: 10.1038/cdd.2013.171

Kim, Y. J., Kim, B. R., Ryu, J. S., Lee, G. O., Kim, H. R., Choi, K. H., et al. (2017). HNRNPA1, a splicing regulator, is an effective target protein for cervical cancer detection: comparison with conventional tumor markers. *Int. J. Gynecol. Cancer* 27, 326–331. doi: 10.1097/igc.0000000000000868

Klymenko, T., Hernandez-Lopez, H., MacDonald, A. I., Bodily, J. M., and Graham, S. V. (2016). Human papillomavirus E2 regulates SRSF3 (SRp20) to promote capsid protein expression in infected differentiated keratinocytes. *J. Virol.* 90, 5047–5058. doi: 10.1128/jvi.03073-15

Kohler, J., Schuler, M., Gauler, T. C., Nopel-Dunnebacke, S., Ahrens, M., Hoffmann, A. C., et al. (2016). Circulating U2 small nuclear RNA fragments as a diagnostic and prognostic biomarker in lung cancer patients. *J. Cancer Res. Clin. Oncol.* 142, 795–805. doi: 10.1007/s00432-015-2095-y

Komatsu, S., Ichikawa, D., Takeshita, H., Morimura, R., Hirajima, S., Tsujiura, M., et al. (2014). Circulating miR-18a: a sensitive cancer screening biomarker in human cancer. *In Vivo* 28, 293–297.

Komeno, Y., Huang, Y. J., Qiu, J., Lin, L., Xu, Y., Zhou, Y., et al. (2015). SRSF2 is essential for hematopoiesis, and its myelodysplastic syndrome-related mutations dysregulate alternative pre-mRNA splicing. *Mol. Cell Biol.* 35, 3071–3082. doi: 10.1128/mcb.00202-15

Kooshapur, H., Choudhury, N. R., Simon, B., Muhlbauer, M., Jussupow, A., Fernandez, N., et al. (2018). Structural basis for terminal loop recognition and stimulation of pri-miRNA-18a processing by hnRNP A1. *Nat. Commun.* 9:2479.

Kramer, M. C., Liang, D., Tatomer, D. C., Gold, B., March, Z. M., Cherry, S., et al. (2015). Combinatorial control of *Drosophila* circular RNA expression by intronic repeats, hnRNPs, and SR proteins. *Genes Dev.* 29, 2168–2182. doi: 10.1101/gad.270421.115

Lai, M. C., Lin, R. I., Huang, S. Y., Tsai, C. W., and Tarn, W. Y. (2000). A human importin-beta family protein, transportin-SR2, interacts with the phosphorylated RS domain of SR proteins. *J. Biol. Chem.* 275, 7950–7957. doi: 10.1074/jbc.275.11.7950

Lai, M. C., Lin, R. I., and Tarn, W. Y. (2001). Transportin-SR2 mediates nuclear import of phosphorylated SR proteins. *Proc. Natl. Acad. Sci. U.S.A.* 98, 10154–10159. doi: 10.1073/pnas.181354098

Lal, S., Allan, A., Markovic, D., Walker, R., Macartney, J., Europe-Finner, N., et al. (2013). Estrogen alters the splicing of type 1 corticotropin-releasing hormone receptor in breast cancer cells. *Sci. Signal.* 6:ra53. doi: 10.1126/scisignal.2003926

Le, K. Q., Prabhakar, B. S., Hong, W. J., and Li, L. C. (2015). Alternative splicing as a biomarker and potential target for drug discovery. *Acta Pharmacol. Sin.* 36, 1212–1218. doi: 10.1038/aps.2015.43

Lee, J. H., Jeong, S. A., Khadka, P., Hong, J., and Chung, I. K. (2015). Involvement of SRSF11 in cell cycle-specific recruitment of telomerase to telomeres at nuclear speckles. *Nucleic Acids Res.* 43, 8435–8451. doi: 10.1093/nar/gkv844

Lee, S. C., and Abdel-Wahab, O. (2016). Therapeutic targeting of splicing in cancer. *Nat. Med.* 22, 976–986. doi: 10.1038/nm.4165

Lee, S. D., Yu, D., Lee, D. Y., Shin, H. S., Jo, J. H., and Lee, Y. C. (2019). Upregulated microRNA-193a-3p is responsible for cisplatin resistance in CD44(+) gastric cancer cells. *Cancer Sci.* 110, 662–673. doi: 10.1111/cas.13894

Lee, S. W., Lee, M. H., Park, J. H., Kang, S. H., Yoo, H. M., Ka, S. H., et al. (2012). SUMOylation of hnRNP-K is required for p53-mediated cell-cycle arrest in response to DNA damage. *EMBO J.* 31, 4441–4452. doi: 10.1038/emboj.2012.293

Lee, Y., and Rio, D. C. (2015). Mechanisms and regulation of alternative Pre-mRNA splicing. *Annu. Rev. Biochem.* 84, 291–323.

Li, K., Sun, D., Gou, Q., Ke, X., Gong, Y., Zuo, Y., et al. (2018). Long non-coding RNA linc00460 promotes epithelial-mesenchymal transition and cell migration in lung cancer cells. *Cancer Lett.* 420, 80–90. doi: 10.1016/j.canlet.2018.01.060

Li, X., Johansson, C., Cardoso, P. C., Mossberg, A., Dhanjal, S., Bergvall, M., et al. (2013a). Eight nucleotide substitutions inhibit splicing to HPV-16 3′-splice site SA3358 and reduce the efficiency by which HPV-16 increases the life span of primary human keratinocytes. *PLoS One* 8:e72776. doi: 10.1371/journal.pone.0072776

Li, X., Johansson, C., Glahder, J., Mossberg, A. K., and Schwartz, S. (2013b). Suppression of HPV-16 late L1 5′-splice site SD3632 by binding of hnRNP D proteins and hnRNP A2/B1 to upstream AUAGUA RNA motifs. *Nucleic Acids Res.* 41, 10488–10508. doi: 10.1093/nar/gkt803

Li, X., Ran, L., Fang, W., and Wang, D. (2014). Lobaplatin arrests cell cycle progression, induces apoptosis and alters the proteome in human cervical cancer cell Line CaSki. *Biomed. Pharmacother.* 68, 291–297. doi: 10.1016/j.biopha.2013.10.004

Li, Z., Yu, C. P., Zhong, Y., Liu, T. J., Huang, Q. D., Zhao, X. H., et al. (2012). Sam68 expression and cytoplasmic localization is correlated with lymph node metastasis as well as prognosis in patients with early-stage cervical cancer. *Ann. Oncol.* 23, 638–646. doi: 10.1093/annonc/mdr290

Liang, Y., Tebaldi, T., Rejeski, K., Joshi, P., Stefani, G., Taylor, A., et al. (2018). SRSF2 mutations drive oncogenesis by activating a global program of aberrant alternative splicing in hematopoietic cells. *Leukemia* 32, 2659–2671. doi: 10.1038/s41375-018-0152-7

Lin, J. C. (2017). Therapeutic applications of targeted alternative splicing to cancer treatment. *Int. J. Mol. Sci.* 19:75. doi: 10.3390/ijms19010075

Liu, F., Dai, M., Xu, Q., Zhu, X., Zhou, Y., Jiang, S., et al. (2018). SRSF10-mediated IL1RAP alternative splicing regulates cervical cancer oncogenesis via mIL1RAP-NF-kappaB-CD47 axis. *Oncogene* 37, 2394–2409. doi: 10.1038/s41388-017-0119-6

Liu, X., Zhou, Y., Lou, Y., and Zhong, H. (2016). Knockdown of HNRNPA1 inhibits lung adenocarcinoma cell proliferation through cell cycle arrest at G0/G1 phase. *Gene* 576(2 Pt 2), 791–797. doi: 10.1016/j.gene.2015.11.009

Long, Y., Sou, W. H., Yung, K. W. Y., Liu, H., Wan, S. W. C., Li, Q., et al. (2019). Distinct mechanisms govern the phosphorylation of different SR protein splicing factors. *J. Biol. Chem.* 294, 1312–1327. doi: 10.1074/jbc.ra118.003392

Lu, G. Y., Huang, S. M., Liu, S. T., Liu, P. Y., Chou, W. Y., and Lin, W. S. (2014). Caffeine induces tumor cytotoxicity via the regulation of alternative splicing in subsets of cancer-associated genes. *Int. J. Biochem. Cell Biol.* 47, 83–92. doi: 10.1016/j.biocel.2013.12.004

Lu, J., and Gao, F. H. (2016). Role and molecular mechanism of heterogeneous nuclear ribonucleoprotein K in tumor development and progression. *Biomed. Rep.* 4, 657–663. doi: 10.3892/br.2016.642

Luo, C., Cheng, Y., Liu, Y., Chen, L., Liu, L., Wei, N., et al. (2017). SRSF2 Regulates alternative splicing to drive hepatocellular carcinoma development. *Cancer Res.* 77, 1168–1178. doi: 10.1158/0008-5472.can-16-1919

Lv, D., Wu, H., Xing, R., Shu, F., Lei, B., Lei, C., et al. (2017). HnRNP-L mediates bladder cancer progression by inhibiting apoptotic signaling and enhancing MAPK signaling pathways. *Oncotarget* 8, 13586–13599. doi: 10.18632/oncotarget.14600

Manley, J. L., and Krainer, A. R. (2010). A rational nomenclature for serine/arginine-rich protein splicing factors (SR proteins). *Genes Dev.* 24, 1073–1074. doi: 10.1101/gad.1934910

Masaki, S., Ikeda, S., Hata, A., Shiozawa, Y., Kon, A., Ogawa, S., et al. (2019). Myelodysplastic syndrome-associated SRSF2 mutations cause splicing changes by altering binding motif sequences. *Front. Genet.* 10:338. doi: 10.3389/fgene.2019.00338

Mavrou, A., Brakspear, K., Hamdollah-Zadeh, M., Damodaran, G., Babaei-Jadidi, R., Oxley, J., et al. (2015). Serine-arginine protein kinase 1 (SRPK1) inhibition as a potential novel targeted therapeutic strategy in prostate cancer. *Oncogene* 34, 4311–4319. doi: 10.1038/onc.2014.360

McCredie, M. R., Sharples, K. J., Paul, C., Baranyai, J., Medley, G., Jones, R. W., et al. (2008). Natural history of cervical neoplasia and risk of invasive cancer in women with cervical intraepithelial neoplasia 3: a retrospective cohort study. *Lancet Oncol.* 9, 425–434. doi: 10.1016/s1470-2045(08)70103-7

McFarlane, M., MacDonald, A. I., Stevenson, A., and Graham, S. V. (2015). Human papillomavirus 16 oncoprotein expression is controlled by the cellular splicing factor SRSF2 (SC35). *J. Virol.* 89, 5276–5287. doi: 10.1128/jvi.03434-14

Mili, S., Shu, H. J., Zhao, Y., and Pinol-Roma, S. (2001). Distinct RNP complexes of shuttling hnRNP proteins with pre-mRNA and mRNA: candidate intermediates in formation and export of mRNA. *Mol. Cell Biol.* 21, 7307–7319. doi: 10.1128/mcb.21.21.7307-7319.2001

Milligan, S. G., Veerapraditsin, T., Ahamet, B., Mole, S., and Graham, S. V. (2007). Analysis of novel human papillomavirus type 16 late mRNAs in differentiated W12 cervical epithelial cells. *Virology* 360, 172–181. doi: 10.1016/j.virol.2006.10.012

Mogilevsky, M., Shimshon, O., Kumar, S., Mogilevsky, A., Keshet, E., Yavin, E., et al. (2018). Modulation of MKNK2 alternative splicing by splice-switching oligonucleotides as a novel approach for glioblastoma treatment. *Nucleic Acids Res.* 46, 11396–11404. doi: 10.1093/nar/gky921

Mole, S., Faizo, A. A. A., Hernandez-Lopez, H., Griffiths, M., Stevenson, A., Roberts, S., et al. (2020). Human papillomavirus type 16 infection activates the

host serine arginine protein kinase 1 (SRPK1) – splicing factor axis. *J. Gen. Virol.* doi: 10.1099/jgv.0.001402 [Epub ahead of print].

Mole, S., McFarlane, M., Chuen-Im, T., Milligan, S. G., Millan, D., and Graham, S. V. (2009a). RNA splicing factors regulated by HPV16 during cervical tumour progression. *J. Pathol.* 219, 383–391. doi: 10.1002/path.2608

Mole, S., Milligan, S. G., and Graham, S. V. (2009b). Human papillomavirus type 16 E2 protein transcriptionally activates the promoter of a key cellular splicing factor, SF2/ASF. *J. Virol.* 83, 357–367. doi: 10.1128/jvi.01414-08

Moody, C. A., and Laimins, L. A. (2010). Human papillomavirus oncoproteins: pathways to transformation. *Nat. Rev. Cancer* 10, 550–560. doi: 10.1038/nrc2886

Moscicki, A. B., and Palefsky, J. M. (2011). Human papillomavirus in men: an update. *J. Low. Genit. Tract. Dis.* 15, 231–234. doi: 10.1097/lgt.0b013e318203ae61

Moujalled, D., James, J. L., Yang, S., Zhang, K., Duncan, C., Moujalled, D. M., et al. (2015). Phosphorylation of hnRNP K by cyclin-dependent kinase 2 controls cytosolic accumulation of TDP-43. *Hum. Mol. Genet.* 24, 1655–1669. doi: 10.1093/hmg/ddu578

Najib, S., Martin-Romero, C., Gonzalez-Yanes, C., and Sanchez-Margalet, V. (2005). Role of Sam68 as an adaptor protein in signal transduction. *Cell. Mol. Life Sci.* 62, 36–43. doi: 10.1007/s00018-004-4309-3

Nakajima, H., Sato, B., Fujita, T., Takase, S., Terano, H., and Okuhara, M. (1996). New antitumor substances, FR901463, FR901464 and FR901465. I. Taxonomy, fermentation, isolation, physico-chemical properties and biological activities. *J. Antibiot.* 49, 1196–1203. doi: 10.7164/antibiotics.49.1196

Nakielny, S., and Dreyfuss, G. (1996). The hnRNP C proteins contain a nuclear retention sequence that can override nuclear export signals. *J. Cell Biol.* 134, 1365–1373. doi: 10.1083/jcb.134.6.1365

Naro, C., Barbagallo, F., Chieffi, P., Bourgeois, C. F., Paronetto, M. P., and Sette, C. (2014). The centrosomal kinase NEK2 is a novel splicing factor kinase involved in cell survival. *Nucleic Acids Res.* 42, 3218–3227. doi: 10.1093/nar/gkt1307

Naro, C., and Sette, C. (2013). Phosphorylation-mediated regulation of alternative splicing in cancer. *Int. J. Cell Biol.* 2013:151839.

Nasim, F. U., Hutchison, S., Cordeau, M., and Chabot, B. (2002). High-affinity hnRNP A1 binding sites and duplex-forming inverted repeats have similar effects on 5′ splice site selection in support of a common looping out and repression mechanism. *RNA* 8, 1078–1089. doi: 10.1017/s1355838202024056

Nilsson, K., Wu, C., Kajitani, N., Yu, H., Tsimtsirakis, E., Gong, L., et al. (2018). The DNA damage response activates HPV16 late gene expression at the level of RNA processing. *Nucleic Acids Res.* 46, 5029–5049. doi: 10.1093/nar/gky227

Oberg, D., Fay, J., Lambkin, H., and Schwartz, S. (2005). A downstream polyadenylation element in human papillomavirus type 16 L2 encodes multiple GGG motifs and interacts with hnRNP H. *J. Virol.* 79, 9254–9269. doi: 10.1128/jvi.79.14.9254-9269.2005

Olmedo-Nieva, L., Munoz-Bello, J. O., Contreras-Paredes, A., and Lizano, M. (2018). The role of E6 spliced isoforms (E6*) in human papillomavirus-induced carcinogenesis. *Viruses* 10:45. doi: 10.3390/v10010045

Olshavsky, N. A., Comstock, C. E., Schiewer, M. J., Augello, M. A., Hyslop, T., Sette, C., et al. (2010). Identification of ASF/SF2 as a critical, allele-specific effector of the cyclin D1b oncogene. *Cancer Res.* 70, 3975–3984. doi: 10.1158/0008-5472.can-09-3468

Oltean, S., and Bates, D. O. (2014). Hallmarks of alternative splicing in cancer. *Oncogene* 33, 5311–5318. doi: 10.1038/onc.2013.533

Otsuka, K., Yamamoto, Y., and Ochiya, T. (2018). Regulatory role of resveratrol, a microRNA-controlling compound, in HNRNPA1 expression, which is associated with poor prognosis in breast cancer. *Oncotarget* 9, 24718–24730. doi: 10.18632/oncotarget.25339

Oyervides-Munoz, M. A., Perez-Maya, A. A., Rodriguez-Gutierrez, H. F., Gomez-Macias, G. S., Fajardo-Ramirez, O. R., Trevino, V., et al. (2018). Understanding the HPV integration and its progression to cervical cancer. *Infect. Genet. Evol.* 61, 134–144. doi: 10.1016/j.meegid.2018.03.003

Pagani, F., Buratti, E., Stuani, C., Romano, M., Zuccato, E., Niksic, M., et al. (2000). Splicing factors induce cystic fibrosis transmembrane regulator exon 9 skipping through a nonevolutionary conserved intronic element. *J. Biol. Chem.* 275, 21041–21047. doi: 10.1074/jbc.m910165199

Paget-Bailly, P., Meznad, K., Bruyere, D., Perrard, J., Herfs, M., Jung, A. C., et al. (2019). Comparative RNA sequencing reveals that HPV16 E6 abrogates the effect of E6*I on ROS metabolism. *Sci. Rep.* 9:5938.

Pan, Z. X., Zhang, X. Y., Chen, S. R., and Li, C. Z. (2019). Upregulated exosomal miR-221/222 promotes cervical cancer via repressing methyl-CpG-binding domain protein 2. *Eur. Rev. Med. Pharmacol. Sci.* 23, 3645–3653.

Papasaikas, P., and Valcarcel, J. (2016). The spliceosome: the ultimate RNA chaperone and sculptor. *Trends Biochem. Sci.* 41, 33–45. doi: 10.1016/j.tibs.2015.11.003

Park, Y. M., Hwang, S. J., Masuda, K., Choi, K. M., Jeong, M. R., Nam, D. H., et al. (2012). Heterogeneous nuclear ribonucleoprotein C1/C2 controls the metastatic potential of glioblastoma by regulating PDCD4. *Mol. Cell Biol.* 32, 4237–4244. doi: 10.1128/mcb.00443-12

Paronetto, M. P., Cappellari, M., Busa, R., Pedrotti, S., Vitali, R., Comstock, C., et al. (2010). Alternative splicing of the cyclin D1 proto-oncogene is regulated by the RNA-binding protein Sam68. *Cancer Res.* 70, 229–239. doi: 10.1158/0008-5472.can-09-2788

Paronetto, M. P., Venables, J. P., Elliott, D. J., Geremia, R., Rossi, P., and Sette, C. (2003). Tr-kit promotes the formation of a multimolecular complex composed by Fyn. PLCgamma1 and Sam68. *Oncogene* 22, 8707–8715. doi: 10.1038/sj.onc.1207016

Parssinen, J., Kuukasjarvi, T., Karhu, R., and Kallioniemi, A. (2007). High-level amplification at 17q23 leads to coordinated overexpression of multiple adjacent genes in breast cancer. *Br. J. Cancer* 96, 1258–1264. doi: 10.1038/sj.bjc.6603692

Patel, M., Sachidanandan, M., and Adnan, M. (2019). Serine arginine protein kinase 1 (SRPK1): a moonlighting protein with theranostic ability in cancer prevention. *Mol. Biol. Rep.* 46, 1487–1497. doi: 10.1007/s11033-018-4545-5

Patry, C., Bouchard, L., Labrecque, P., Gendron, D., Lemieux, B., Toutant, J., et al. (2003). Small interfering RNA-mediated reduction in heterogeneous nuclear ribonucleoparticule A1/A2 proteins induces apoptosis in human cancer cells but not in normal mortal cell lines. *Cancer Res.* 63, 7679–7688.

Phoomak, C., Park, D., Silsirivanit, A., Sawanyawisuth, K., Vaeteewoottacharn, K., Detarya, M., et al. (2019). O-GlcNAc-induced nuclear translocation of hnRNP-K is associated with progression and metastasis of cholangiocarcinoma. *Mol. Oncol.* 13, 338–357. doi: 10.1002/1878-0261.12406

Pillai, M. R., Chacko, P., Kesari, L. A., Jayaprakash, P. G., Jayaram, H. N., and Antony, A. C. (2003). Expression of folate receptors and heterogeneous nuclear ribonucleoprotein E1 in women with human papillomavirus mediated transformation of cervical tissue to cancer. *J. Clin. Pathol.* 56, 569–574. doi: 10.1136/jcp.56.8.569

Pont, A. R., Sadri, N., Hsiao, S. J., Smith, S., and Schneider, R. J. (2012). mRNA decay factor AUF1 maintains normal aging, telomere maintenance, and suppression of senescence by activation of telomerase transcription. *Mol. Cell* 47, 5–15. doi: 10.1016/j.molcel.2012.04.019

Preti, M., Rotondo, J. C., Holzinger, D., Micheletti, L., Gallio, N., McKay-Chopin, S., et al. (2020). Role of human papillomavirus infection in the etiology of vulvar cancer in Italian women. *Infect. Agent Cancer* 15:20.

Pulice, J. L., and Kadoch, C. (2016). Composition and function of mammalian SWI/SNF chromatin remodeling complexes in human disease. *Cold Spring Harb. Symp. Quant. Biol.* 81, 53–60. doi: 10.1101/sqb.2016.81.031021

Qing, S., Tulake, W., Ru, M., Li, X., Yuemaier, R., Lidifu, D., et al. (2017). Proteomic identification of potential biomarkers for cervical squamous cell carcinoma and human papillomavirus infection. *Tumour Biol.* 39, 1010428317697547.

Ratnadiwakara, M., Mohenska, M., and Anko, M. L. (2018). Splicing factors as regulators of miRNA biogenesis - links to human disease. *Semin. Cell Dev. Biol.* 79, 113–122. doi: 10.1016/j.semcdb.2017.10.008

Rigo, F., Seth, P. P., and Bennett, C. F. (2014). Antisense oligonucleotide-based therapies for diseases caused by pre-mRNA processing defects. *Adv. Exp. Med. Biol.* 825, 303–352. doi: 10.1007/978-1-4939-1221-6_9

Roberts, C. W., and Orkin, S. H. (2004). The SWI/SNF complex–chromatin and cancer. *Nat. Rev. Cancer* 4, 133–142.

Rodriguez-Aguayo, C., Monroig, P. D. C., Redis, R. S., Bayraktar, E., Almeida, M. I., Ivan, C., et al. (2017). Regulation of hnRNPA1 by microRNAs controls the miR-18a-K-RAS axis in chemotherapy-resistant ovarian cancer. *Cell Discov.* 3:17029.

Rosenberger, S., De-Castro, A. J., Langbein, L., Steenbergen, R. D., and Rosl, F. (2010). Alternative splicing of human papillomavirus type-16 E6/E6* early mRNA is coupled to EGF signaling via Erk1/2 activation. *Proc. Natl. Acad. Sci. U.S.A.* 107, 7006–7011. doi: 10.1073/pnas.1002620107

Rossi, F., Labourier, E., Forne, T., Divita, G., Derancourt, J., Riou, J. F., et al. (1996). Specific phosphorylation of SR proteins by

mammalian DNA topoisomerase I. *Nature* 381, 80–82. doi: 10.1038/381080a0

Rush, M., Zhao, X., and Schwartz, S. (2005). A splicing enhancer in the E4 coding region of human papillomavirus type 16 is required for early mRNA splicing and polyadenylation as well as inhibition of premature late gene expression. *J. Virol.* 79, 12002–12015. doi: 10.1128/jvi.79.18.12002-12015.2005

Sakai, T., Asai, N., Okuda, A., Kawamura, N., and Mizui, Y. (2004). Pladienolides, new substances from culture of Streptomyces platensis Mer-11107. II. Physico-chemical properties and structure elucidation. *J. Antibiot.* 57, 180–187. doi: 10.7164/antibiotics.57.180

Sakai, Y., Yoshida, T., Ochiai, K., Uosaki, Y., Saitoh, Y., Tanaka, F., et al. (2002). GEX1 compounds, novel antitumor antibiotics related to herboxidiene, produced by *Streptomyces* sp. I. Taxonomy, production, isolation, physicochemical properties and biological activities. *J. Antibiot.* 55, 855–862. doi: 10.7164/antibiotics.55.855

Satoh, T., and Kaida, D. (2016). Upregulation of p27 cyclin-dependent kinase inhibitor and a C-terminus truncated form of p27 contributes to G1 phase arrest. *Sci. Rep.* 6:27829.

Schiffman, M., Doorbar, J., Wentzensen, N., de, S. S., Fakhry, C., Monk, B. J., et al. (2016). Carcinogenic human papillomavirus infection. *Nat. Rev. Dis. Primers* 2:16086.

Schmitt, M., Dalstein, V., Waterboer, T., Clavel, C., Gissmann, L., and Pawlita, M. (2010). Diagnosing cervical cancer and high-grade precursors by HPV16 transcription patterns. *Cancer Res.* 70, 249–256. doi: 10.1158/0008-5472.can-09-2514

Schmitt, M., and Pawlita, M. (2011). The HPV transcriptome in HPV16 positive cell lines. *Mol. Cell Probes* 25, 108–113. doi: 10.1016/j.mcp.2011.03.003

Seiler, M., Peng, S., Agrawal, A. A., Palacino, J., Teng, T., Zhu, P., et al. (2018). Somatic mutational landscape of splicing factor genes and their functional consequences across 33 cancer types. *Cell Rep.* 23, 282–296.

Shen, M., and Mattox, W. (2012). Activation and repression functions of an SR splicing regulator depend on exonic versus intronic-binding position. *Nucleic Acids Res.* 40, 428–437. doi: 10.1093/nar/gkr713

Shi, X., Ran, L., Liu, Y., Zhong, S. H., Zhou, P. P., Liao, M. X., et al. (2018). Knockdown of hnRNP A2/B1 inhibits cell proliferation, invasion and cell cycle triggering apoptosis in cervical cancer via PI3K/AKT signaling pathway. *Oncol. Rep.* 39, 939–950.

Shi, Y. (2017). Mechanistic insights into precursor messenger RNA splicing by the spliceosome. *Nat. Rev. Mol. Cell Biol.* 18, 655–670. doi: 10.1038/nrm.2017.86

Shilo, A., Siegfried, Z., and Karni, R. (2015). The role of splicing factors in deregulation of alternative splicing during oncogenesis and tumor progression. *Mol. Cell Oncol.* 2:e970955. doi: 10.4161/23723548.2014.970955

Shin, C., Feng, Y., and Manley, J. L. (2004). Dephosphorylated SRp38 acts as a splicing repressor in response to heat shock. *Nature* 427, 553–558. doi: 10.1038/nature02288

Shiraishi, Y., Kataoka, K., Chiba, K., Okada, A., Kogure, Y., Tanaka, H., et al. (2018). A comprehensive characterization of cis-acting splicing-associated variants in human cancer. *Genome Res.* 28, 1111–1125. doi: 10.1101/gr.231951.117

Shultz, J. C., Goehe, R. W., Murudkar, C. S., Wijesinghe, D. S., Mayton, E. K., Massiello, A., et al. (2011). SRSF1 regulates the alternative splicing of caspase 9 via a novel intronic splicing enhancer affecting the chemotherapeutic sensitivity of non-small cell lung cancer cells. *Mol. Cancer Res.* 9, 889–900. doi: 10.1158/1541-7786.mcr-11-0061

Shultz, J. C., Goehe, R. W., Wijesinghe, D. S., Murudkar, C., Hawkins, A. J., Shay, J. W., et al. (2010). Alternative splicing of caspase 9 is modulated by the phosphoinositide 3-kinase/Akt pathway via phosphorylation of SRp30a. *Cancer Res.* 70, 9185–9196. doi: 10.1158/0008-5472.can-10-1545

Singh, B., and Eyras, E. (2017). The role of alternative splicing in cancer. *Transcription* 8, 91–98. doi: 10.1080/21541264.2016.1268245

Siomi, H., and Dreyfuss, G. (1995). A nuclear localization domain in the hnRNP A1 protein. *J. Cell Biol.* 129, 551–560. doi: 10.1083/jcb.129.3.551

Smith-Roe, S. L., Nakamura, J., Holley, D., Chastain, P. D., Rosson, G. B., Simpson, D. A., et al. (2015). SWI/SNF complexes are required for full activation of the DNA-damage response. *Oncotarget* 6, 732–745. doi: 10.18632/oncotarget.2715

Sokol, E., Kedzierska, H., Czubaty, A., Rybicka, B., Rodzik, K., Tanski, Z., et al. (2018). microRNA-mediated regulation of splicing factors SRSF1, SRSF2 and hnRNP A1 in context of their alternatively spliced 3′UTRs. *Exp. Cell Res.* 363, 208–217. doi: 10.1016/j.yexcr.2018.01.009

Somberg, M., Li, X., Johansson, C., Orru, B., Chang, R., Rush, M., et al. (2011). Serine/arginine-rich protein 30c activates human papillomavirus type 16 L1 mRNA expression via a bimodal mechanism. *J. Gen. Virol.* 92(Pt 10), 2411–2421. doi: 10.1099/vir.0.033183-0

Somberg, M., and Schwartz, S. (2010). Multiple ASF/SF2 sites in the human papillomavirus type 16 (HPV-16) E4-coding region promote splicing to the most commonly used 3′-splice site on the HPV-16 genome. *J. Virol.* 84, 8219–8230. doi: 10.1128/jvi.00462-10

Somberg, M., Zhao, X., Frohlich, M., Evander, M., and Schwartz, S. (2008). Polypyrimidine tract binding protein induces human papillomavirus type 16 late gene expression by interfering with splicing inhibitory elements at the major late 5′ splice site, SD3632. *J. Virol.* 82, 3665–3678. doi: 10.1128/jvi.02140-07

Song, L., Wang, L., Li, Y., Xiong, H., Wu, J., Li, J., et al. (2010). Sam68 up-regulation correlates with, and its down-regulation inhibits, proliferation and tumourigenicity of breast cancer cells. *J. Pathol.* 222, 227–237. doi: 10.1002/path.2751

Sorlie, T., Perou, C. M., Tibshirani, R., Aas, T., Geisler, S., Johnsen, H., et al. (2001). Gene expression patterns of breast carcinomas distinguish tumor subclasses with clinical implications. *Proc. Natl. Acad. Sci. U.S.A.* 98, 10869–10874. doi: 10.1073/pnas.191367098

Sterne-Weiler, T., and Sanford, J. R. (2014). Exon identity crisis: disease-causing mutations that disrupt the splicing code. *Genome Biol.* 15:201. doi: 10.1186/gb4150

Stockley, J., Markert, E., Zhou, Y., Robson, C. N., Elliott, D. J., Lindberg, J., et al. (2015). The RNA-binding protein Sam68 regulates expression and transcription function of the androgen receptor splice variant AR-V7. *Sci. Rep.* 5:13426.

Stoilov, P., Daoud, R., Nayler, O., and Stamm, S. (2004). Human tra2-beta1 autoregulates its protein concentration by influencing alternative splicing of its pre-mRNA. *Hum. Mol. Genet.* 13, 509–524. doi: 10.1093/hmg/ddh051

Straub, E., Fertey, J., Dreer, M., Iftner, T., and Stubenrauch, F. (2015). Characterization of the human papillomavirus 16 E8 promoter. *J. Virol.* 89, 7304–7313. doi: 10.1128/jvi.00616-15

Sudarsanam, P., and Winston, F. (2000). The Swi/Snf family nucleosome-remodeling complexes and transcriptional control. *Trends Genet.* 16, 345–351.

Suk, F. M., Lin, S. Y., Lin, R. J., Hsine, Y. H., Liao, Y. J., Fang, S. U., et al. (2015). Bortezomib inhibits Burkitt's lymphoma cell proliferation by downregulating sumoylated hnRNP K and c-Myc expression. *Oncotarget* 6, 25988–26001. doi: 10.18632/oncotarget.4620

Sun, H., Liu, T., Zhu, D., Dong, X., Liu, F., Liang, X., et al. (2017). HnRNPM and CD44s expression affects tumor aggressiveness and predicts poor prognosis in breast cancer with axillary lymph node metastases. *Genes Chromosomes Cancer* 56, 598–607. doi: 10.1002/gcc.22463

Sun, X., Haider Ali, M. S. S., and Moran, M. (2017). The role of interactions of long non-coding RNAs and heterogeneous nuclear ribonucleoproteins in regulating cellular functions. *Biochem. J.* 474, 2925–2935. doi: 10.1042/bcj20170280

Sun, Y., Luo, M., Chang, G., Ren, W., Wu, K., Li, X., et al. (2017). Phosphorylation of Ser6 in hnRNPA1 by S6K2 regulates glucose metabolism and cell growth in colorectal cancer. *Oncol. Lett.* 14, 7323–7331.

Sveen, A., Kilpinen, S., Ruusulehto, A., Lothe, R. A., and Skotheim, R. I. (2016). Aberrant RNA splicing in cancer; expression changes and driver mutations of splicing factor genes. *Oncogene* 35, 2413–2427. doi: 10.1038/onc.2015.318

Sweetser, D. A., Peniket, A. J., Haaland, C., Blomberg, A. A., Zhang, Y., Zaidi, S. T., et al. (2005). Delineation of the minimal commonly deleted segment and identification of candidate tumor-suppressor genes in del(9q) acute myeloid leukemia. *Genes Chromosomes Cancer* 44, 279–291. doi: 10.1002/gcc.20236

Tacke, R., Tohyama, M., Ogawa, S., and Manley, J. L. (1998). Human Tra2 proteins are sequence-specific activators of pre-mRNA splicing. *Cell* 93, 139–148. doi: 10.1016/s0092-8674(00)81153-8

Talukdar, I., Sen, S., Urbano, R., Thompson, J., Yates, J. R. III, and Webster, N. J. (2011). hnRNP A1 and hnRNP F modulate the alternative splicing of exon 11 of the insulin receptor gene. *PLoS One* 6:e27869. doi: 10.1371/journal.pone.0027869

Tang, S., Tao, M., McCoy, J. P. Jr., and Zheng, Z. M. (2006). The E7 oncoprotein is translated from spliced E6*I transcripts in high-risk human papillomavirus type 16- or type 18-positive cervical cancer cell lines via translation reinitiation. *J. Virol.* 80, 4249–4263. doi: 10.1128/jvi.80.9.4249-4263.2006

Tang, X., Kane, V. D., Morre, D. M., and Morre, D. J. (2011). hnRNP F directs formation of an exon 4 minus variant of tumor-associated NADH oxidase (ENOX2). *Mol. Cell Biochem.* 357, 55–63. doi: 10.1007/s11010-011-0875-5

Tarn, W. Y., and Steitz, J. A. (1997). Pre-mRNA splicing: the discovery of a new spliceosome doubles the challenge. *Trends Biochem. Sci.* 22, 132–137. doi: 10.1016/s0968-0004(97)01018-9

Tauler, J., Zudaire, E., Liu, H., Shih, J., and Mulshine, J. L. (2010). hnRNP A2/B1 modulates epithelial-mesenchymal transition in lung cancer cell lines. *Cancer Res.* 70, 7137–7147. doi: 10.1158/0008-5472.can-10-0860

Taylor, S. J., Anafi, M., Pawson, T., and Shalloway, D. (1995). Functional interaction between c-Src and its mitotic target, Sam 68. *J. Biol. Chem.* 270, 10120–10124. doi: 10.1074/jbc.270.17.10120

Tornesello, M. L., Annunziata, C., Tornesello, A. L., Buonaguro, L., and Buonaguro, F. M. (2018). Human oncoviruses and p53 tumor suppressor pathway deregulation at the origin of human cancers. *Cancers* 10:213. doi: 10.3390/cancers10070213

Tornesello, M. L., Faraonio, R., Buonaguro, L., Annunziata, C., Starita, N., Cerasuolo, A., et al. (2020). The role of microRNAs, long non-coding RNAs, and circular RNAs in cervical cancer. *Front. Oncol.* 10:150. doi: 10.3389/fonc.2020.00150

Turunen, J. J., Niemela, E. H., Verma, B., and Frilander, M. J. (2013). The significant other: splicing by the minor spliceosome. *Wiley Interdiscip. Rev. RNA* 4, 61–76. doi: 10.1002/wrna.1141

Ule, J., and Blencowe, B. J. (2019). Alternative splicing regulatory networks: functions, mechanisms, and evolution. *Mol. Cell* 76, 329–345. doi: 10.1016/j.molcel.2019.09.017

Urbanski, L. M., Leclair, N., and Anczukow, O. (2018). Alternative-splicing defects in cancer: splicing regulators and their downstream targets, guiding the way to novel cancer therapeutics. *Wiley Interdiscip. Rev. RNA* 9:e1476. doi: 10.1002/wrna.1476

van, D. K., Li, Z., Xirasagar, S., Maes, P., Kaminsky, D., Liou, D., et al. (2017). The Papillomavirus Episteme: a major update to the papillomavirus sequence database. *Nucleic Acids Res.* 45, D499–D506.

Venables, J. P., Bourgeois, C. F., Dalgliesh, C., Kister, L., Stevenin, J., and Elliott, D. J. (2005). Up-regulation of the ubiquitous alternative splicing factor Tra2beta causes inclusion of a germ cell-specific exon. *Hum. Mol. Genet.* 14, 2289–2303. doi: 10.1093/hmg/ddi233

Wahl, M. C., Will, C. L., and Luhrmann, R. (2009). The spliceosome: design principles of a dynamic RNP machine. *Cell* 136, 701–718. doi: 10.1016/j.cell.2009.02.009

Wan, L., Yu, W., Shen, E., Sun, W., Liu, Y., Kong, J., et al. (2019). SRSF6-regulated alternative splicing that promotes tumour progression offers a therapy target for colorectal cancer. *Gut* 68, 118–129. doi: 10.1136/gutjnl-2017-314983

Wang, B. D., and Lee, N. H. (2018). Aberrant RNA splicing in cancer and drug resistance. *Cancers* 10:458. doi: 10.3390/cancers10110458

Wang, C., Norton, J. T., Ghosh, S., Kim, J., Fushimi, K., Wu, J. Y., et al. (2008). Polypyrimidine tract-binding protein (PTB) differentially affects malignancy in a cell line-dependent manner. *J. Biol. Chem.* 283, 20277–20287. doi: 10.1074/jbc.m803682200

Wang, F., Fu, X., Chen, P., Wu, P., Fan, X., Li, N., et al. (2017). SPSB1-mediated HnRNP A1 ubiquitylation regulates alternative splicing and cell migration in EGF signaling. *Cell Res.* 27, 540–558. doi: 10.1038/cr.2017.7

Wang, G. S., and Cooper, T. A. (2007). Splicing in disease: disruption of the splicing code and the decoding machinery. *Nat. Rev. Genet.* 8, 749–761. doi: 10.1038/nrg2164

Wang, Y., Liu, J., Huang, B. O., Xu, Y. M., Li, J., Huang, L. F., et al. (2015). Mechanism of alternative splicing and its regulation. *Biomed. Rep.* 3, 152–158.

Wang, Z., and Burge, C. B. (2008). Splicing regulation: from a parts list of regulatory elements to an integrated splicing code. *RNA* 14, 802–813. doi: 10.1261/rna.876308

Watson, I. R., Takahashi, K., Futreal, P. A., and Chin, L. (2013). Emerging patterns of somatic mutations in cancer. *Nat. Rev. Genet.* 14, 703–718. doi: 10.1038/nrg3539

Will, C. L., and Luhrmann, R. (2011). Spliceosome structure and function. *Cold Spring Harb. Perspect. Biol.* 3:a003707.

Williams, V. M., Filippova, M., Filippov, V., Payne, K. J., and Duerksen-Hughes, P. (2014). Human papillomavirus type 16 E6* induces oxidative stress and DNA damage. *J. Virol.* 88, 6751–6761. doi: 10.1128/jvi.03355-13

Wu, C., Kajitani, N., and Schwartz, S. (2017). Splicing and polyadenylation of human papillomavirus type 16 mRNAs. *Int. J. Mol. Sci.* 18:366. doi: 10.3390/ijms18020366

Wu, H., Sun, S., Tu, K., Gao, Y., Xie, B., Krainer, A. R., et al. (2010). A splicing-independent function of SF2/ASF in microRNA processing. *Mol. Cell* 38, 67–77. doi: 10.1016/j.molcel.2010.02.021

Wu, X., Yang, Y., Huang, Y., Chen, Y., Wang, T., Wu, S., et al. (2018). RNA-binding protein AUF1 suppresses miR-122 biogenesis by down-regulating Dicer1 in hepatocellular carcinoma. *Oncotarget* 9, 14815–14827. doi: 10.18632/oncotarget.24079

Xiao, J., Wang, Q., Yang, Q., Wang, H., Qiang, F., He, S., et al. (2018). Clinical significance and effect of Sam68 expression in gastric cancer. *Oncol. Lett.* 15, 4745–4752.

Xue, Y., Bellanger, S., Zhang, W., Lim, D., Low, J., Lunny, D., et al. (2010). HPV16 E2 is an immediate early marker of viral infection, preceding E7 expression in precursor structures of cervical carcinoma. *Cancer Res.* 70, 5316–5325. doi: 10.1158/0008-5472.can-09-3789

Yang, H., Zhu, R., Zhao, X., Liu, L., Zhou, Z., Zhao, L., et al. (2019). Sirtuin-mediated deacetylation of hnRNP A1 suppresses glycolysis and growth in hepatocellular carcinoma. *Oncogene* 38, 4915–4931. doi: 10.1038/s41388-019-0764-z

Yang, S., Jia, R., and Bian, Z. (2018). SRSF5 functions as a novel oncogenic splicing factor and is upregulated by oncogene SRSF3 in oral squamous cell carcinoma. *Biochim. Biophys. Acta Mol. Cell Res.* 1865, 1161–1172. doi: 10.1016/j.bbamcr.2018.05.017

Yeo-Teh, N. S. L., Ito, Y., and Jha, S. (2018). High-risk human papillomaviral oncogenes E6 and E7 target key cellular pathways to achieve oncogenesis. *Int. J. Mol. Sci.* 19:1706. doi: 10.3390/ijms19061706

Yoshida, T., Kim, J. H., Carver, K., Su, Y., Weremowicz, S., Mulvey, L., et al. (2015). CLK2 is an oncogenic kinase and splicing regulator in breast cancer. *Cancer Res.* 75, 1516–1526. doi: 10.1158/0008-5472.can-14-2443

Yu, C., Guo, J., Liu, Y., Jia, J., Jia, R., and Fan, M. (2015). Oral squamous cancer cell exploits hnRNP A1 to regulate cell cycle and proliferation. *J. Cell Physiol.* 230, 2252–2261. doi: 10.1002/jcp.24956

Yu, H., Gong, L., Wu, C., Nilsson, K., Li-Wang, X., and Schwartz, S. (2018). hnRNP G prevents inclusion on the HPV16 L1 mRNAs of the central exon between splice sites SA3358 and SD3632. *J. Gen. Virol.* 99, 328–343. doi: 10.1099/jgv.0.001019

Zhang, Q., Di, C., Yan, J., Wang, F., Qu, T., Wang, Y., et al. (2019a). Inhibition of SF3b1 by pladienolide B evokes cycle arrest, apoptosis induction and p73 splicing in human cervical carcinoma cells. *Artif Cells Nanomed. Biotechnol.* 47, 1273–1280. doi: 10.1080/21691401.2019.1596922

Zhang, Q., Lv, R., Guo, W., and Li, X. (2019b). microRNA-802 inhibits cell proliferation and induces apoptosis in human cervical cancer by targeting serine/arginine-rich splicing factor 9. *J. Cell Biochem.* 120, 10370–10379. doi: 10.1002/jcb.28321

Zhang, T., Wan, C., Shi, W., Xu, J., Fan, H., Zhang, S., et al. (2015). The RNA-binding protein Sam68 regulates tumor cell viability and hepatic carcinogenesis by inhibiting the transcriptional activity of FOXOs. *J. Mol. Histol.* 46, 485–497. doi: 10.1007/s10735-015-9639-y

Zhang, Y., Wu, D., and Wang, D. (2020). Long non-coding RNA ARAP1-AS1 promotes tumorigenesis and metastasis through facilitating proto-oncogene c-Myc translation via dissociating PSF/PTB dimer in cervical cancer. *Cancer Med.* 9, 1855–1866. doi: 10.1002/cam4.2860

Zhang, Y., Yan, L., Zeng, J., Zhou, H., Liu, H., Yu, G., et al. (2019). Pan-cancer analysis of clinical relevance of alternative splicing events in 31 human cancers. *Oncogene* 38, 6678–6695. doi: 10.1038/s41388-019-0910-7

Zhang, Z., Li, J., Zheng, H., Yu, C., Chen, J., Liu, Z., et al. (2009). Expression and cytoplasmic localization of SAM68 is a significant and independent prognostic marker for renal cell carcinoma. *Cancer Epidemiol. Biomarkers Prev.* 18, 2685–2693. doi: 10.1158/1055-9965.epi-09-0097

Zhang, Z., Xu, Y., Sun, N., Zhang, M., Xie, J., and Jiang, Z. (2014). High Sam68 expression predicts poor prognosis in non-small cell lung cancer. *Clin. Transl. Oncol.* 16, 886–891. doi: 10.1007/s12094-014-1160-3

Zhao, X., Fay, J., Lambkin, H., and Schwartz, S. (2007). Identification of a 17-nucleotide splicing enhancer in HPV-16 L1 that counteracts the effect of multiple hnRNP A1-binding splicing silencers. *Virology* 369, 351–363. doi: 10.1016/j.virol.2007.08.002

Zhao, X., Oberg, D., Rush, M., Fay, J., Lambkin, H., and Schwartz, S. (2005). A 57-nucleotide upstream early polyadenylation element in human papillomavirus type 16 interacts with hFip1, CstF-64, hnRNP C1/C2, and polypyrimidine tract binding protein. *J. Virol.* 79, 4270–4288. doi: 10.1128/jvi.79.7.4270-4288.2005

Zhao, X., Rush, M., and Schwartz, S. (2004). Identification of an hnRNP A1-dependent splicing silencer in the human papillomavirus type 16 L1 coding region that prevents premature expression of the late L1 gene. *J. Virol.* 78, 10888–10905. doi: 10.1128/jvi.78.20.10888-10905.2004

Zhao, X., and Schwartz, S. (2008). Inhibition of HPV-16 L1 expression from L1 cDNAs correlates with the presence of hnRNP A1 binding sites in the L1 coding region. *Virus Genes* 36, 45–53. doi: 10.1007/s11262-007-0174-0

Zheng, Z. M., and Baker, C. C. (2006). Papillomavirus genome structure, expression, and post-transcriptional regulation. *Front. Biosci.* 11:2286–2302. doi: 10.2741/1971

Zheng, Z. M., Tao, M., Yamanegi, K., Bodaghi, S., and Xiao, W. (2004). Splicing of a cap-proximal human Papillomavirus 16 E6E7 intron promotes E7 expression, but can be restrained by distance of the intron from its RNA 5′ cap. *J. Mol. Biol.* 337, 1091–1108. doi: 10.1016/j.jmb.2004.02.023

Zheng, Z. Z., Sun, Y. Y., Zhao, M., Huang, H., Zhang, J., Xia, N. S., et al. (2013). Specific interaction between hnRNP H and HPV16 L1 proteins: implications for late gene auto-regulation enabling rapid viral capsid protein production. *Biochem. Biophys. Res. Commun.* 430, 1047–1053. doi: 10.1016/j.bbrc.2012.12.042

Zhou, X., Li, Q., He, J., Zhong, L., Shu, F., Xing, R., et al. (2017). HnRNP-L promotes prostate cancer progression by enhancing cell cycling and inhibiting apoptosis. *Oncotarget* 8, 19342–19353. doi: 10.18632/oncotarget.14258

Zhou, X., Li, X., Cheng, Y., Wu, W., Xie, Z., Xi, Q., et al. (2014). BCLAF1 and its splicing regulator SRSF10 regulate the tumorigenic potential of colon cancer cells. *Nat. Commun.* 5:4581.

Zhou, X., Li, X., Yu, L., Wang, R., Hua, D., Shi, C., et al. (2019). The RNA-binding protein SRSF1 is a key cell cycle regulator via stabilizing NEAT1 in glioma. *Int. J. Biochem. Cell Biol.* 113, 75–86. doi: 10.1016/j.biocel.2019.06.003

Zhou, Z., and Fu, X. D. (2013). Regulation of splicing by SR proteins and SR protein-specific kinases. *Chromosoma* 122, 191–207. doi: 10.1007/s00412-013-0407-z

Zhou, Z. J., Dai, Z., Zhou, S. L., Fu, X. T., Zhao, Y. M., Shi, Y. H., et al. (2013). Overexpression of HnRNP A1 promotes tumor invasion through regulating CD44v6 and indicates poor prognosis for hepatocellular carcinoma. *Int. J. Cancer* 132, 1080–1089. doi: 10.1002/ijc.27742

Zhu, H., Zheng, T., Yu, J., Zhou, L., and Wang, L. (2018). LncRNA XIST accelerates cervical cancer progression via upregulating Fus through competitively binding with miR-200a. *Biomed. Pharmacother.* 105, 789–797. doi: 10.1016/j.biopha.2018.05.053

Conflict of Interest: The authors declare that the research was conducted in the absence of any commercial or financial relationships that could be construed as a potential conflict of interest.

frontiers in Cell and Developmental Biology

ORIGINAL RESEARCH
published: 02 October 2020
doi: 10.3389/fcell.2020.563693

LncRNA MALAT1 Affects *Mycoplasma pneumoniae* Pneumonia via NF-κB Regulation

Haiyan Gu†, Yifan Zhu†, Yao Zhou, Tianyu Huang, Siqing Zhang, Deyu Zhao and Feng Liu**

Department of Respiratory Medicine, Children's Hospital of Nanjing Medical University, Nanjing, China

Our aim was to determine whether the long non-coding RNA (lncRNA) metastasis-associated lung adenocarcinoma transcript 1 (MALAT1) is involved in *Mycoplasma pneumoniae* pneumonia (MPP), and its possible mechanism of action. MALAT1 expression in the bronchoalveolar lavage fluid of 50 hospitalized children with MPP was compared to its expression in 30 children with intrabronchial foreign bodies. MALAT1 expression was higher in children with MPP, accompanied by increased inflammatory mediators interleukin 8 (IL-8) and tumor necrosis factor alpha (TNF-α), compared to the controls. In human airway epithelial cells infected with wild-type *Mycoplasma pneumoniae* (strain M129), MALAT1, IL-8, and TNF-α expression significantly increased, and increased expression of IL-8 and TNF-α could be suppressed by MALAT1 knockdown. Luciferase reporter gene assay and western blot showed that knockdown of MALAT1 reduced nuclear factor-κB (NF-κB) activation. *In vivo*, RNAi packaged with adenovirus (Adv) was nasally transfected into BALB/c mice to silence MALAT1, and an MP-infected mouse pneumonia model was prepared. The results demonstrated that the degree of pulmonary inflammatory injury, vascular permeability, secretion of inflammatory factors, and expression of phosphorylated p65 (pp65) in MP-infected mice were partly reversed after MALAT1 knockdown compared to those in the controls. In conclusion, MALAT1 is involved in the regulation of airway and pulmonary inflammation caused by MP infection via NF-κB regulation.

Keywords: metastasis associated lung adenocarcinoma transcript 1, *Mycoplasma pneumoniae* pneumonia, nuclear factor-κB, inflammation, lncRNA

OPEN ACCESS

Edited by:
Pier Paolo Piccaluga, University of Bologna, Italy

Reviewed by:
Fabienne Gally, National Jewish Health, United States
Chian-Jiun Liou, Chang Gung University of Science and Technology, Taiwan

****Correspondence:***
Deyu Zhao
zhaodeyu98@126.com
Feng Liu
axsliu@163.com

† These authors have contributed equally to this work

Specialty section:
This article was submitted to Molecular Medicine, a section of the journal Frontiers in Cell and Developmental Biology

Received: *19 May 2020*
Accepted: *08 September 2020*
Published: *02 October 2020*

Citation:
Gu H, Zhu Y, Zhou Y, Huang T, Zhang S, Zhao D and Liu F (2020) LncRNA MALAT1 Affects Mycoplasma pneumoniae Pneumonia via NF-κB Regulation. Front. Cell Dev. Biol. 8:563693. doi: 10.3389/fcell.2020.563693

INTRODUCTION

Mycoplasma pneumoniae (MP) is one of the main causes of community-acquired pneumonia in children (Jain et al., 2015). Pneumonia caused by MP often leads to serious complications that affect the quality of life in children (Zhang et al., 2016). In patients with *Mycoplasma pneumoniae* pneumonia (MPP), excessive inflammatory response is a leading cause of pulmonary inflammation and is predictive of poor prognosis. However, the mechanism that leads to the uncontrolled inflammatory response in MPP is still unclear, and further investigation is necessary.

Metastasis-associated lung adenocarcinoma transcript 1 (MALAT1), one of the first lncRNAs associated with human disease to be identified, is of interest because it is widely evolutionarily conserved. MALAT1 was originally identified as a prognostic marker for poor clinical prognosis

in patients with early non-small cell lung cancer (NSCLC) (Ji et al., 2003). After that discovery, the function of MALAT1 was studied in various cancers for its role in cancer development and progression (Sun and Ma, 2019). Recent findings suggest that MALAT1 also plays an important regulatory role in inflammatory diseases. For example, MALAT1 was reported to be involved in the regulation of lipopolysaccharide (LPS)-induced acute kidney injury (Ding et al., 2018) and lung injury (Liang et al., 2019). MALAT1 is also an inflammatory regulator in human systemic lupus erythematosus (Yang H. et al., 2017). Downregulation of MALAT1 alleviates saturated fatty acid-induced myocardial inflammatory injury (Jia et al., 2019), while silencing of MALAT1 ameliorated inflammatory injury after lung transplant ischemia-reperfusion (Wei et al., 2019). Therefore, we aimed to determine whether MALAT1 also plays a regulatory role in the inflammatory response in MPP.

Previous reports have shown that MALAT1 regulates the nuclear factor-κB (NF-κB) signaling pathway to modulate the inflammatory response (Lei et al., 2019). MALAT1 affects NF-κB via direct binding or indirect modulation, thus altering the transcription and activation of its downstream inflammatory factors and resulting in varied inflammatory responses (Dai et al., 2018; Ding et al., 2018). Cytokine production in airway epithelial cells can lead to inflammation associated with respiratory diseases. Interleukin-8 (IL-8), a potent chemoattractant and activator of neutrophils, is associated with the initiation and maintenance of inflammation (Pease and Sabroe, 2002). In humans, the airway epithelium is the main source of IL-8, and the pathogenesis of pneumonia is positively correlated with IL-8 expression (Martin et al., 1997). Tumor necrosis factor alpha (TNF-α) is an important bioactive inflammatory mediator that plays a pivotal role in inflammation and immune regulation. High levels of TNF-α can damage capillary endothelial cells, promote microthrombosis, and lead to ischemic necrosis; thus, TNF-α is related to the severity of pneumonia (Salvatore et al., 2007). Therefore, we conducted experiments *in vitro* and *in vivo* to investigate the role of MALAT1 in MPP.

MATERIALS AND METHODS

Study Population

Fifty children who were diagnosed with MPP and underwent bronchoscopy while hospitalized at Children's Hospital of Nanjing Medical University were included in the study. Thirty children with intrabronchial foreign bodies (FB) were included as the control group. MP infection was diagnosed by polymerase chain reaction (PCR) testing of MP in nasopharyngeal secretions and/or serological testing of MP immunoglobulin M (IgM) by enzyme-linked immunosorbent assay (ELISA). Patients with chronic disease, heart disease, immune deficiency disease, or immunosuppressive drugs were excluded. All enrolled children tested negative for respiratory syncytial virus, influenza virus, parainfluenza virus, pneumovirus, adenovirus, chlamydia trachomatis, and bacterial culture. The study protocol was approved by the Ethics Committee of the Children's Hospital of Nanjing Medical University (approval number: 201801126-1), and the informed written consent of at least one parent/guardian of each patient was obtained.

Bronchoalveolar Lavage (BAL)

Guidelines for bronchoscopy and alveolar lavage were reviewed previously (Yang M. et al., 2017; Gao et al., 2018). Children with MPP underwent bronchoscopy and bronchoalveolar lavage fluid (BALF) collection within 1 week after admission. Children with FB were immediately treated with bronchoscopy to remove the foreign bodies, and BALF specimens were collected during reexamination. Irrigation was performed with sterile normal saline (0.3–0.5 mL/kg). Within 1 h after BALF collection, the supernatant was separated, divided, and stored at −20°C. RNA was isolated with TRIzol reagent (Invitrogen, Carlsbad, United States) and stored at −80°C.

Mycoplasma Culture, Preparation, and Infection

Mycoplasma pneumoniae (strain M129) was provided by Professor Chen Z. M. (Children's Hospital, Zhejiang province), as described in our previous study (Shi et al., 2019). The strain was cultured in a *Mycoplasma* broth, which consists of *Mycoplasma* broth base (Oxoid, Basingstoke, United Kingdom), 0.5% glucose, 0.002% phenol red, and *Mycoplasma* selective supplement G (Oxoid). MP was quantified by counting the number of colony-forming units (CFU) in *Mycoplasma* agar plates.

Cell Culture and MP Infection

Two human epithelial cell lines, A549 and BEAS-2B (Shanghai Cellular Research Institute, Shanghai, China), were cultured in Dulbecco's modified Eagle medium (DMEM, Gibco, Grand Island, NY, United States), with 10% fetal bovine serum (FBS, Gibco, Grand Island, NY, United States), in a humidified 5% CO_2 incubator at 37°C. MP was harvested by centrifugation (10,000 *g* for 20 min), washed, and resuspended in PBS to yield 1×10^8 CFU/mL.A549 and BEAS-2B cells were co-incubated with MP (MOI = 100) for 24 h.

siRNA and Cell Transfection

SiRNA against MALAT1 and scrambled siRNA were designed and synthesized by RiboBio biotech (RiboBio, Guangzhou, China). Vector transfection was performed using the ribo FECT^{TM} CP transfection kit (RiboBio, Guangzhou, China) in accordance with the manufacturer's protocol. Sequences of custom siRNA are listed in **Table 1**.

Laboratory Animals

Forty male specific-pathogen-free (SPF) BALB/c mice aged 6–8 weeks (body weight: 20–25 g) were purchased from the Laboratory Animals Center of Nanjing Medical University. The mice were housed in conditions with temperatures between 21 and 25°C and relative humidity between 55 and 65%, with free access to food and water. This study was approved by and

TABLE 1 | Sequences for siRNAs.

siNC	5′-UUCUCCGAACGUGUCACGU-3′
siMALAT1-1	5′-CACAGGGAAAGCGAGTGGTTGGTAA-3′
siMALAT1-2	5′-GAG GTGTAAAGGGATTTAT-3′

performed in accordance with the Institutional Animal Care and Use Committee, Nanjing Medical University (IACUC-1904054).

Adenovirus (Adv)-RNAi Transfection and Subsequent Establishment of Mouse Model of MP Infection

Fluorescent (GFP)-labeled adenovirus packaged with short-hairpin RNA (shRNA) against MALAT1 (Adv-MALAT1-RNAi) and scrambled shRNA (Adv-shNC) were synthesized by GeneChem (Shanghai, China). Mice were randomly divided into four groups (n = 10 per group): shNC + PBS; sh-MALAT1 + PBS; shNC + MP; and shMALAT1 + MP. To administer the virus, 4% chloral hydrate (0.1 mL/10 g body weight) was given by intraperitoneal to lightly anesthetize the mice, and 30 μL of virus containing 5×10^8 PFU of Adv-shMALAT1-RNAi was inhaled into the lungs through the nose of each mouse. Two doses of this virus were administered to each mouse in 24 h intervals. Mice in the shNC group were treated with control recombinant adenovirus containing scrambled shRNA. After 3 days, mice in the MP group were intranasally administered 10^8 CFU of M129 in a 50 μL solution, and mice in the PBS group were administered 50 μL of PBS. During administration, their heads were kept tilted at an angle of 30°–45° to ensure fluid flow through the lower respiratory tract. After 4 days, the mice were euthanized, and test samples were collected. Sequences for shRNA are listed in **Table 2**.

Biochemical Analysis of Oxidative Stress in Lung Homogenate Samples

After the mice were euthanized, left lung tissue samples were collected, and 10% homogenate was prepared by addition of PBS and centrifugation at 12,000 × g at 4°C for 15 min. The supernatant was stored at −80°C for analysis. The concentrations of superoxide dismutase (SOD) and malondialdehyde (MDA) were determined by visible spectrophotometry (Jiancheng Bioengineering Institute, Nanjing, China).

Collection of Blood and BALF Samples

After euthanasia, 1 mL of blood from each mouse was collected from the eye socket in 1.5 mL Eppendorf tubes. The trachea of each mouse was carefully separated, and 1 mL of normal saline was used to wash and collect the BALF samples three times. Both the blood and BALF samples were centrifuged at 3,000 × g at 4°C for 5 min, and the supernatant was stored at −80°C for analysis.

TABLE 2 | Sequences for shRNAs.

shNC	5′-TTCTCCGAACGTGTCACGT-3′
shMALAT1	5′-GCAGTTTAGAAGAGTCTTTAG-3′

Hematoxylin-Eosin (HE) Staining

After mice were euthanized using a chloral hydrate injection, specimens of the lower lobe of the right lung were fixed in 4% formaldehyde solution, followed by dehydration, paraffin embedding, sectioning, and HE staining for histopathological analysis.

Quantitative Real-Time PCR (qRT-PCR)

Total RNA was extracted from cells or mouse lung tissue using TRIzol reagent according to manufacturer's instructions (Invitrogen, New York, United States). RNA was reverse-transcribed to complementary DNA (cDNA) using PCR Master Mix (Vazyme Biotech, Jiangsu, China). Real-time quantitative PCR was performed using an AceR qPCR SYBR Green Master Mix (Vazyme Biotech, Jiangsu, China). The expression of MALAT1 was normalized to GAPDH and calculated using the $2^{-\Delta\Delta Ct}$ method. The primers used for qRT-PCR are listed in **Table 3**.

Enzyme-Linked Immunosorbent Assay (ELISA)

Concentrations of IL-8 and TNF-α in the cell culture supernatant or BALF of children with MPP or FB were detected using the Human IL-8 ELISA Kit (Novus Biologicals, Littleton, United States) and Human TNF-α ELISA Kit (BD Pharmingen, San Diego, United States), respectively. Concentrations of IL-8 and TNF-α in mouse lung homogenate and BALF were detected using the Mouse IL-8 ELISA Kit (Fcmacs Biotech, Nanjing, China) and Mouse TNF-α ELISA Kit (RayBiotech, Atlanta, United States), respectively, according to the manufacturer's instructions.

Western Blot

Nuclear protein was extracted from cells and mouse lung tissue using a Nuclear Cytoplasm Extraction Kit (KeyGen Biotech,

TABLE 3 | Primers for qRT-PCR.

Human MALAT1-F	5′-CTCCCCACAAGCAACTTCTC-3′
Human MALAT1-R	5′-TTCAACCCACCAAAGACCTC-3′
Human GAPDH-F	5′-GCTCTCTGCTCCTCCTGTTC-3′
Human GAPDH-R	5′-ACGACCAAATCCGTTGACTC-3′
Mouse MALAT1-F	5′-GCGAGCAGGCATTGTGGAGAG-3′
Mouse MALAT1-R	5′-GCCGACCTCAAGAATGTTACCG-3′
Mouse IL-8-F	5′-GGGTGGGGAGTTCGTGTAGA-3′
Mouse IL-8-R	5′-CTACTACACAGGGATCAGGGC-3′
Mouse TNF-α-F	5′-GTGCCAGCCGATGGGTTGTAC-3′
Mouse TNF-α-R	5′-TGACGGCAGAGAGGAGGTTGAC-3′
Mouse GAPDH-F	5′-GGTTGTCTCCTGCGACTTCA-3′
Mouse GAPDH-R	5′-TGGTCCAGGGTTTCTTACTCC-3′

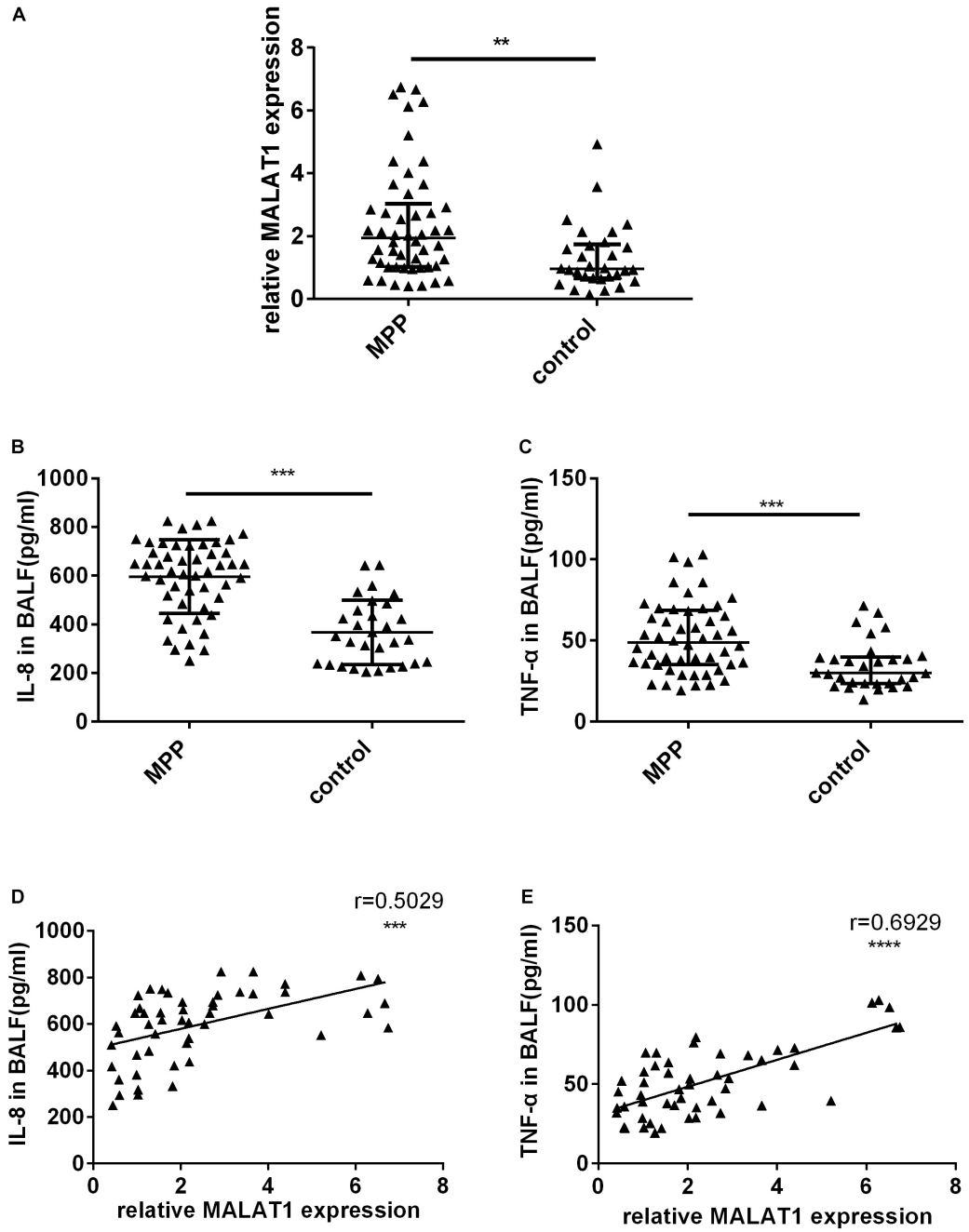

FIGURE 1 | The expression of MALAT1 and inflammatory cytokines in BALF. **(A)** MALAT1 was increased in BALF of 50 children with MPP compared with 30 children with FB. The expression of MALAT1 was measured by qRT-PCR and normalized to GAPDH. Results are shown as median with interquartile range (**$P < 0.01$ by Mann-Whitney test). **(B,C)** Levels of cytokines (IL-8 and TNF-α) in BALF of children with MPP were much higher than that in BALF of children with FB. Data are shown as mean ± standard deviation **(B)** or median with interquartile range **(C)** (***$P < 0.001$). **(D,E)** The expression of MALAT1 in BALF of children with MPP was positively correlated with the levels of IL-8 and TNF-α (***$P < 0.001$, ****$P < 0.0001$).

Nanjing, China). Aliquots of 30 μg of protein lysate were separated using SDS polyacrylamide gel electrophoresis and transferred to PVDF membranes (Millipore, Bedford, MA). After blocking with 5% skim milk at room temperature for 1 h the membrane was incubated overnight with primary antibody at 4°C, and then incubated with secondary antibody at room temperature for 1 h. Finally, ECL reagent (Beyotime, Nanjing, China) was used for chemiluminescent detection. Primary antibodies used for immunoblot analysis included phosphorylated p65 (Cell Signaling Technology, Danvers, United States) and histone H3 (Proteintech, Rosemont, United States).

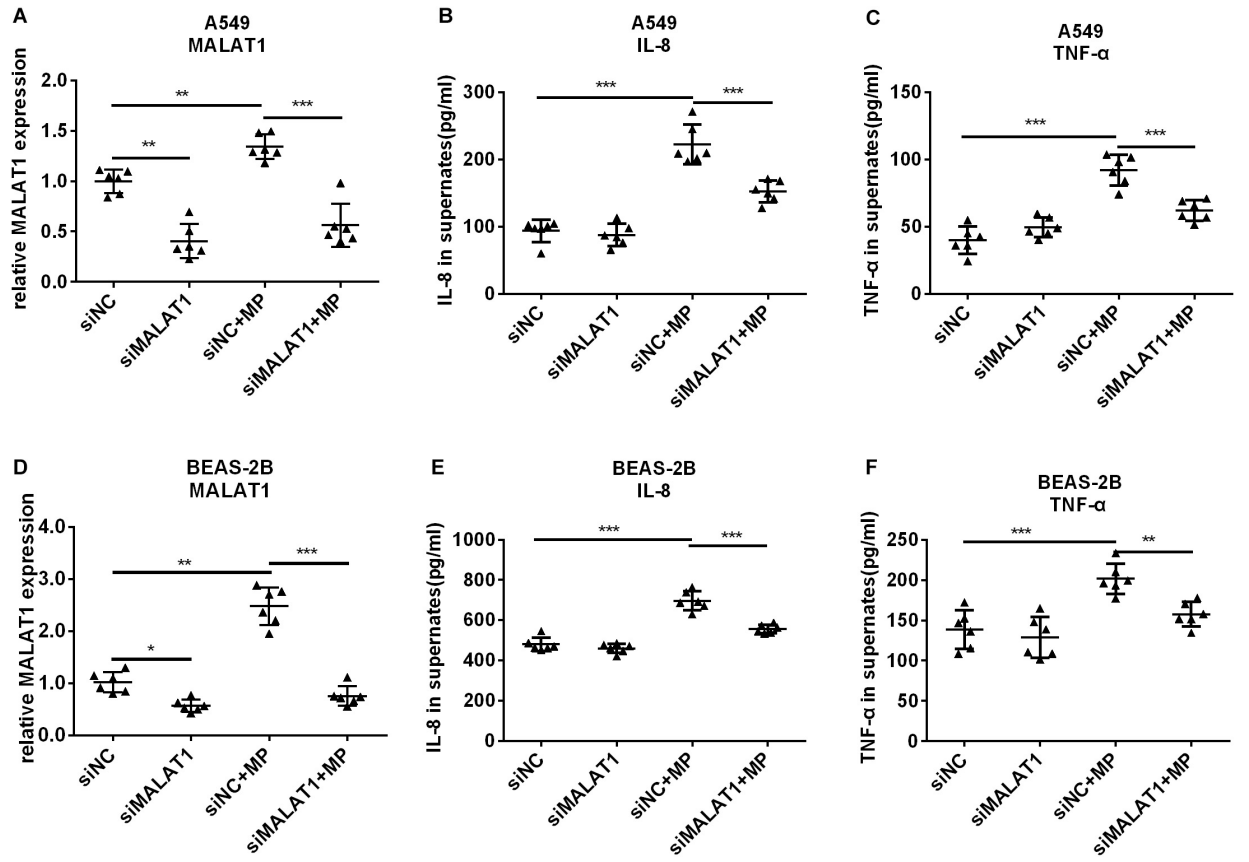

FIGURE 2 | Knockdown of MALAT1 inhibited the secretion of inflammatory cytokines by airway epithelial cells induced by Mycoplasma pneumoniae infection. SiRNA transfection was used to knockdown MALAT1. The expression of MALAT1 was detected by qRT-PCR and normalized to GAPDH. 24 h after MP infection, the expression of MALAT1 in A549 and BEAS-2B cells increased **(A,D)** along with increased levels of IL-8 and TNF-α in cell supernatant **(B,C,E,F)**. The above changes were reversed after MALAT1 was knocked down. Data are shown as mean ± standard deviation (SD) from three experiments ($n = 6$, $^{***}P < 0.001$, $^{**}P < 0.01$, $^{*}P < 0.05$).

Luciferase Reporter Assays

NF-κB transcriptional activity reporter plasmid pNFκB-luc (Beyotime Institute of Biotechnology) and *Renilla* luciferase expression vector pRL-TK (Promega, Madison, United States) were co-transfected into normal or MALAT1-depleted A549 and BEAS-2B cells using Lipofectamine 2000 (Invitrogen, Carlsbad, United States). After 24 h, cells were treated with MP and harvested 24 h later. Luciferase activity was measured using the dual-luciferase reporter assay system (Promega, Madison, United States) in accordance with the manufacturer's protocol. Relative firefly luciferase activity was normalized to *Renilla* luciferase activity.

Statistical Analysis

Each experiment was performed in triplicate. All statistical analyses were conducted by SPSS software, version 19.0 (IBM, Armonk, United States). One-way ANOVA, Student's *t*-test, or Mann-Whitney test were used for statistical comparisons as indicated. $P < 0.05$ was defined as statistically significant.

RESULTS

Analysis of MALAT1 Expression in BALF From Children

First, qRT-PCR was used to detect MALAT1 expression in BALF from children. Expression of MALAT1 in BALF from children with MPP was significantly increased compared to the control group (**Figure 1A**, $P < 0.01$). In addition, ELISA results suggested that the level of inflammatory factors IL-8 and TNF-α in BALF of the MP group was significantly higher than that of the control group (**Figures 1B,C**, $P < 0.001$). Further, correlation analysis showed that expression of MALAT1 was positively correlated with expression of IL-8 and TNF-α (**Figures 1D,E**, $P < 0.001$).

Knockdown of MALAT1 Inhibited the Increased Secretion of Inflammatory Cytokines by Airway Epithelial Cells After MP Infection

To investigate the role of MALAT1 in MP infection-induced inflammation, siRNA was used to knockdown MALAT1 in A549

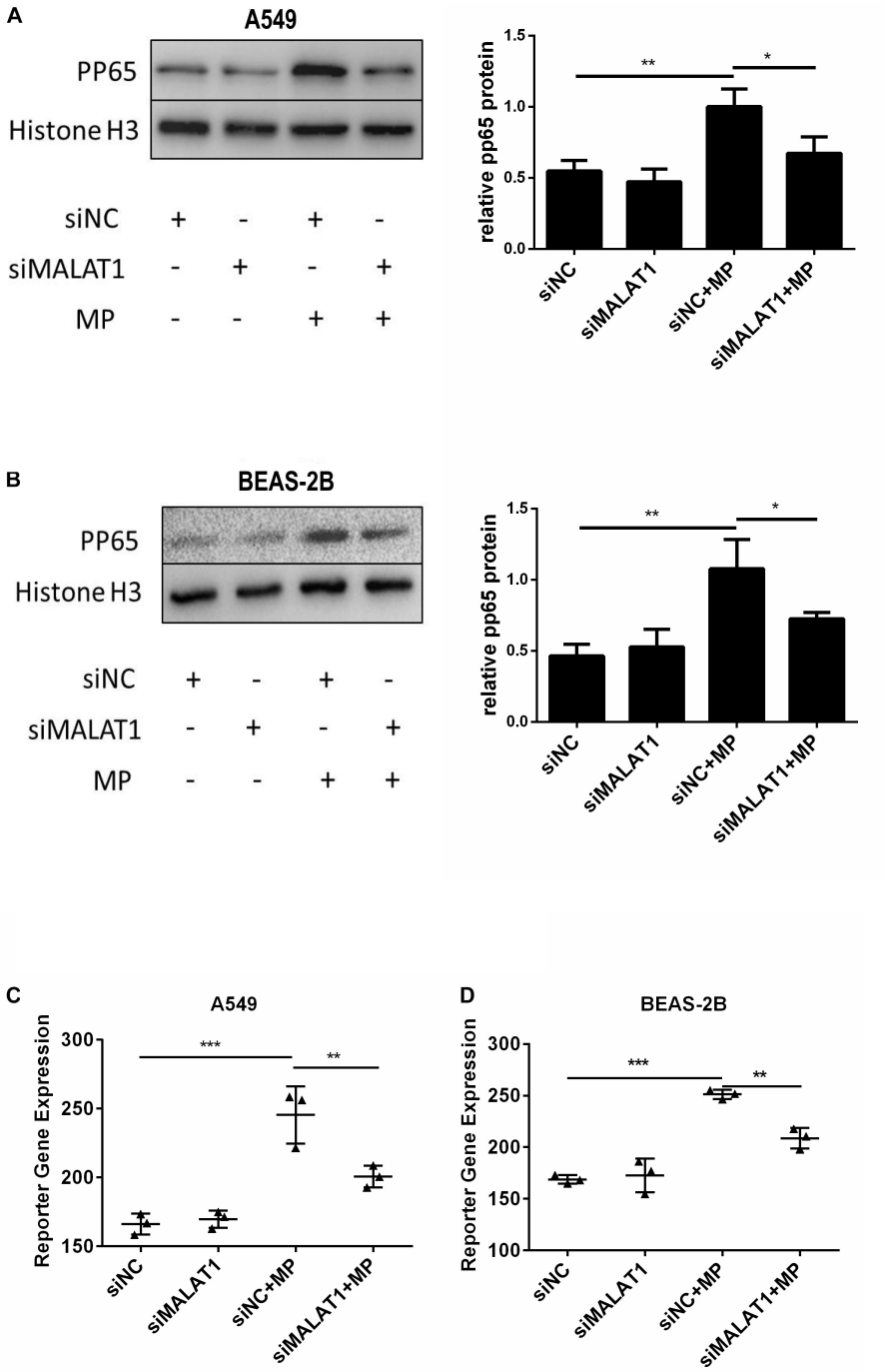

FIGURE 3 | Knockdown of MALAT1 inhibited NF-κB activation of airway epithelial cells induced by MP infection. The expression of phosphorylated p65 protein in A549 **(A)** and BEAS-2B **(B)** cells was detected by western blot. Compared with the normal group, the expression of phosphorylated p65 decreased after MP infection in the knockdown group. The activity of NF-κB was measured by the dual- luciferase reporter gene assay. Compared with the control group, the NF-κB activity of the MALAT1 silent group decreased after MP infection **(C,D)**. Data are shown as mean ± standard deviation (SD) from three experiments ($n = 3$, $^{***}P < 0.001$, $^{**}P < 0.01$, $^{*}P < 0.05$).

and BEAS-2B cells. Then cells were treated with *Mycoplasma pneumoniae* strain M129 for 24 h, and MALAT1 expression was detected using qRT-PCR. As shown in **Figures 2A,D**, the expression of MALAT1 increased in MP-treated cells, while knockdown of MALAT1 decreased the expression, even after MP infection (all $P < 0.05$). In addition, the levels of inflammatory factors in the cell supernatant were detected using ELISA. The results demonstrated that

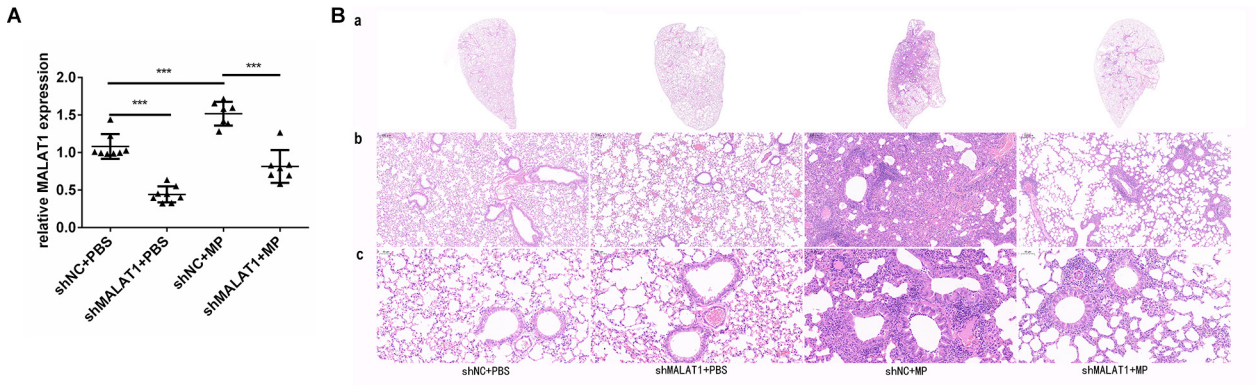

FIGURE 4 | MALAT1 knockdown reduced histopathological damage in BALB/c mice caused by MP infection. Lung tissue samples were collected from each group of mice, then the expression of MALAT1 was detected by qRT-PCR. **(A)** The expression of MALAT1 in the lung tissues of mice was up-regulated in shNC + MP group, while it was decreased in shMALAT1 + PBS group, compared to the shNC + PBS group. In addition, the expression of MALAT1 was inhibited in shMALAT1 + MP group compared with the shNC + MP group. Data are shown as mean ± standard deviation (SD) from three experiments ($n = 8$, $^{***}P < 0.001$). **(B)** Histopathological changes were evaluated by HE staining of lung-tissue samples. The shNC + MP group showed significant histological changes, including cell infiltration, alveolar wall thickening, significantly increased secretion, and even structural collapse, while the above changes were reversed in shMALAT1 + MP group. (a) Representative scans (original magnification × 5) of HE stained FFPE sections of left lungs; (b) digital zoom of the lung mid region; (c) representative images (original magnification × 200) for histopathology changes ($n = 6$).

levels of IL-8 and TNF-α secreted by A549 and BEAS-2B cells were increased after MP infection compared to the control group, while the inflammatory cytokines levels decreased in MALAT1-depleted epithelial cells compared to those of the non-knockdown group after MP infection (**Figures 2B,C,E,F**, all $P < 0.05$).

Knockdown of MALAT1 Inhibited NF-κB Activation Induced by MP Infection in Airway Epithelial Cells

When NF-κB is activated, the subunit of NF-κB, p65, is phosphorylated and translocated to the nucleus. Therefore, we detected pp65 in the nucleus of A549 and BEAS-2B cells by western blot, and the results showed that MALAT1 knockdown reduced pp65 expression in the nucleus of MP infected cells (**Figures 3A,B**, $P < 0.05$). This is in accordance with the results of the dual luciferase reporter assay (**Figures 3C,D**, $P < 0.01$). These results suggest that MALAT1 knockdown inhibited NF-κB activation induced by MP infection in airway epithelial cells.

MALAT1 Knockdown Reduced Histopathological Damage Caused by MP Infection in BALB/c Mice

Lung tissue samples were collected from each group of mice, and MALAT1 expression was detected using qRT-PCR. The expression of MALAT1 was upregulated in the shNC + MP group and downregulated in the shMALAT1 + PBS group, compared to the shNC + PBS group. In addition, the expression of MALAT1 was decreased in the shMALAT1 + MP group compared to the shNC + MP group (**Figure 4A**, $P < 0.001$). As shown in **Figure 4B**, histopathological changes were evaluated by HE staining of the lung tissue samples. The shNC + MP group showed significant histological changes, including cell infiltration, alveolar wall thickening, significantly increased secretion, and even structural collapse. These changes were reversed upon MALAT1 knockdown in the infected group.

MALAT1 Knockdown Reduced Lung Injury Caused by MP Infection in BALB/c Mice

After MP infection, the shNC + MP group exhibited increases in protein concentration in lung homogenate and ratio of protein concentration in lung homogenate and serum. In terms of these two indexes, the shNC + MP group exhibited a greater increase than the shMALAT1 + MP group (**Figures 5A,B**, $P < 0.05$). The level of SOD activity indirectly reflects the body's ability to remove oxygen free radicals, and the level of MDA indirectly reflects the severity of free radical attack on cells. The results showed that compared with the shNC + MP group, the SOD activity of mice in the shMALAT1 + MP group significantly increased, while the MDA concentration decreased (**Figures 5C,D**, $P < 0.05$).

MALAT1 Knockdown Reduced the Expression of Inflammatory Cytokines in Mice With MP Infection

The mRNA expression of IL-8 and TNF-α in mouse lung tissue was detected using qRT-PCR, and the protein expression of IL-8 and TNF-α in mouse lung homogenate and BALF was detected using ELISA. The results showed that both the mRNA and protein expression of IL-8 and TNF-α in the shNC + MP group significantly increased compared to the shNC + PBS group,

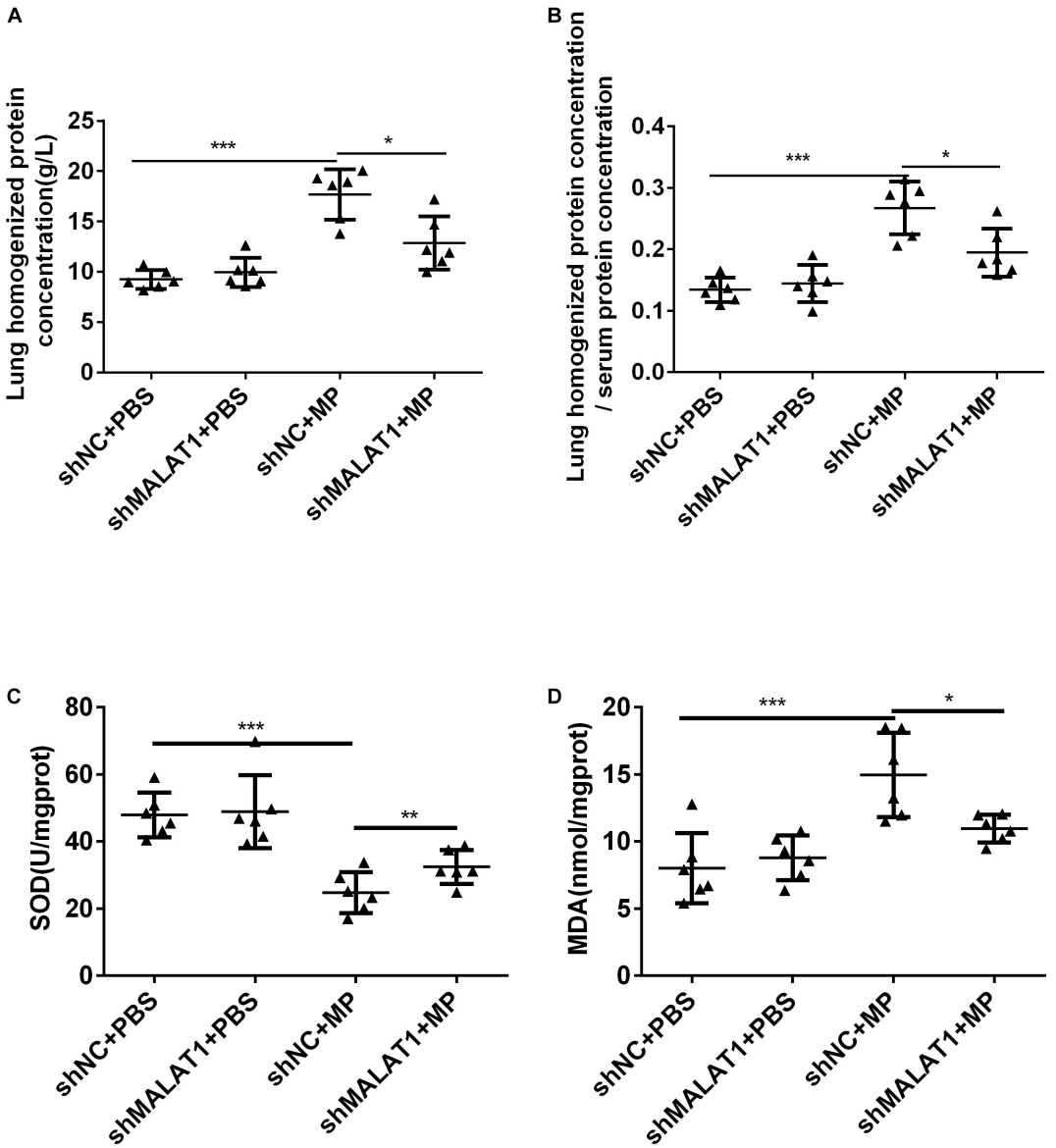

FIGURE 5 | MALAT1 knockdown reduced lung injury in BALB/c mice caused by MP infection. **(A,B)** The shNC + MP group mice exhibited increases in protein concentration in lung homogenate and ratio of protein concentration in lung homogenate and serum compared to the shNC+PBS group. The two indexes were decreased upon MALAT1 knocked down in MP infected group. **(C,D)** Compared with shNC + MP group, SOD level in lung homogenate of mice in the shMALAT1 + MP group was significantly increased, while MDA level was decreased. Data are shown as mean ± standard deviation (SD) from three experiments ($n = 6$, $^{***}P < 0.001$,$^{*}P < 0.05$).

and knockdown of MALAT1 reversed the increase (**Figure 6**, all $P < 0.05$).

NF-κB Is Involved in MALAT1-Mediated Regulation of the Inflammatory Response Induced by MP Infection

Using western blot, we detected phosphorylated p65 expression in the lung tissue of each group. As shown in **Figure 7**, expression of phosphorylated p65 in the shNC + MP group was significantly increased compared to the shNC + PBS group; however, the above change was reversed after MALAT1 knockdown. These results suggested that the NF-κB signaling pathway is involved in MALAT1-mediated regulation of the inflammatory response induced by MP infection.

DISCUSSION

MP infection may cause severe local inflammation, leading to cytotoxicity and tissue damage. For this reason, patients with MPP are prone to atelectasis and necrotizing lesions and often

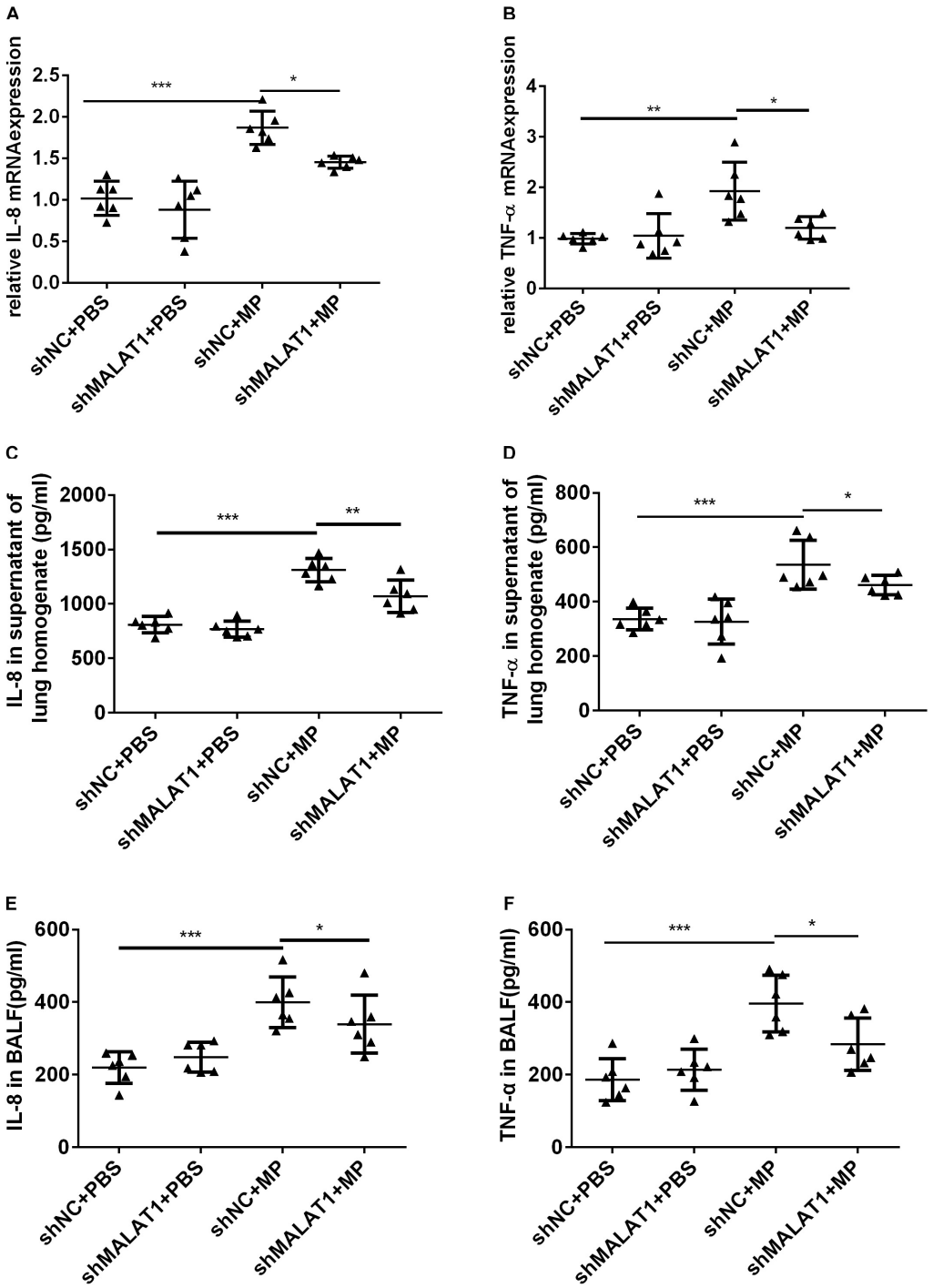

FIGURE 6 | MALAT1 knockdown reduced the expression of inflammatory cytokines in mice with MP infection. The mRNA expressions of IL-8 and TNF-α in lung tissues were detected by qRT-PCR **(A,B)**, and the protein level of IL-8 and TNF-α in mice lung homogenate **(C,D)** and BALF **(E,F)** were detected by ELISA. Data are shown as mean ± standard deviation (SD) from three experiments ($n = 6$, $^{***}P < 0.001$, $^{**}P < 0.01$, $^{*}P < 0.05$).

require fiberoptic bronchoscopy. According to previous studies, the local inflammatory response is initiated by the release of pro-inflammatory cytokines from epithelial cells (Yang et al., 2002). Among the induced cytokines, IL-8 and TNF-α play pivotal roles in the inflammatory response of MPP. Our data showed that the levels of IL-8 and TNF-α were significantly elevated in BALF from children with MPP, supernatants of MP-infected epithelial cells, and lung tissues and BALF of mice infected with MP compared

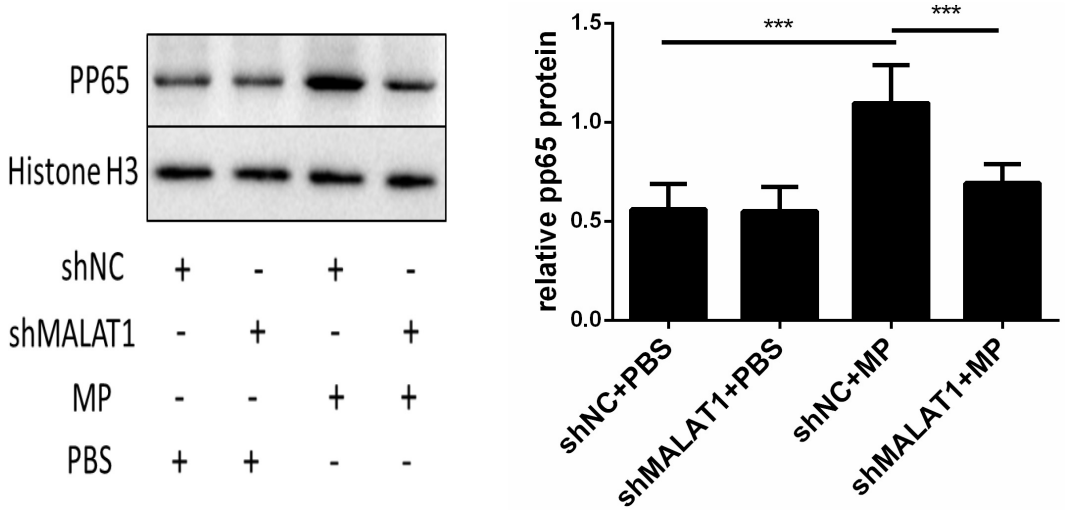

FIGURE 7 | NF-κB is involved in the role of MALAT1 in regulating the inflammatory response induced by MP infection. The expression of phosphorylated p65 in lung tissues of each group was detected by western blot. Densitometry results of the western-blot are shown in the bar graph. The expression of phosphorylated p65 in the shNC + MP group was significantly increased, comparing with the shNC + PBS group, however, the above change was reversed after MALAT1 knocking down. Data are shown as mean ± standard deviation (SD) from three experiments ($n = 6$, $^{***}P < 0.001$).

to the non-infected groups. These results confirmed the role of IL-8 and TNF-α in airway inflammation caused by MPP.

MALAT1 has been reported to be involved in multiple diseases. Recently, researchers have focused on its role in inflammatory diseases. Based on the findings in this study that MALAT1 was highly expressed and expression was positively correlated with inflammatory factors IL-8 and TNF−α in BALF from children with MPP, we performed *in vitro* and *in vivo* experiments to determine the role of this lncRNA in MP-induced inflammation. Our *in vitro* results showed that MALAT1 knockdown inhibited the secretion of inflammatory factors from epithelial cells after MP stimulation. *In vivo*, after MP infection, the expression of IL-8 and TNF-α in lung homogenate and alveolar lavage fluid increased. SOD activity in lung homogenate decreased, while MDA concentration increased, indicating the existence of anti-oxidation imbalance. The ratio of lung homogenate protein concentration to serum total protein concentration was significantly increased, indicating the presence of pulmonary permeability damage, which is consistent with the previous study (Shi et al., 2019). However, MALAT1 knockdown in BALB/c mice alleviated lung inflammation and lung injury induced by MP infection. These results demonstrated for the first time the regulatory role of MALAT1 in MP-induced inflammation.

Previous studies have shown that the regulatory role of MALAT1 in inflammation is complex. For instance, a recent study reported that MALAT1 knockdown markedly reduced lung injury induced by sepsis (Lin et al., 2019). Furthermore, knockdown of MALAT1 was reported to suppress inflammatory response in LPS-induced acute lung injury and kidney injury (Dai et al., 2018; Ding et al., 2018; Cui et al., 2019; Liang et al., 2019). Knockdown of *Malat1* in mice alleviated inflammatory injury after cerebral ischemia, and overexpression of *Malat1* aggravated ischemic brain inflammation (Cao et al., 2019). In addition, MALAT1 has been reported to promote inflammation in septic heart damage (Chen et al., 2018), systemic lupus erythematosus (Yang H. et al., 2017), and hyperglycemia-induced inflammatory process (Puthanveetil et al., 2015). The above findings together with the results from the current study suggest that MALAT1 plays a pro-inflammatory role in many diseases. However, other studies demonstrated that lncRNA MALAT1 performs a protective function against inflammation in several diseases (Zhao et al., 2016; Cremer et al., 2019; Sun et al., 2019; Zhu and Men, 2019). These inconsistencies may be due to the complex mechanisms of MALAT1 regulation in different diseases.

With respect to the mechanism of MALAT1, our study indicated that the pro-inflammatory function of MALAT1 at least in part depends on NF-κB. NF-κB is involved in the inflammatory response of MPP. The lipoprotein components of MP recognize toll-like receptors and activate NF-κB (Shimizu et al., 2007, 2008). In our present study, we detected NF-κB activation in MP-infected epithelial cells and mouse lung tissue and confirmed that MP infection activates NF-κB. According to previous studies, MALAT1 can regulate inflammation by modulating the activation of NF-κB. MALAT1 can bind directly to the subunit of NF-κB (Zhao et al., 2016; Zhu and Men, 2019) or act as competing endogenous RNA (ceRNA) and compete with miRNA functions toward NF-κB (Ding et al., 2018; Cao et al., 2019; Jia et al., 2019; Li et al., 2019; Liang et al., 2019). Our data suggested that MALAT1 knockdown inhibits phosphorylation of p65 caused by MP infection in airway epithelial cells and lung tissue of mice. Therefore, the regulatory role of MALAT1 in inflammation of MPP is associated with NF-κB activation. Although the precise mechanism remains unclear, acting as a certain ceRNA might be the way by which MALAT1

facilitate p65 phosphorylation in MP infection. Further study is needed to reveal the exact regulatory mechanism.

CONCLUSION

In conclusion, our present study demonstrates that lncRNA MALAT1 plays a key regulatory role in MP-induced inflammation. The regulatory function of MALAT1 likely proceeds through NF-κB signaling. By performing *in vivo* experiments, we found that downregulation of MALAT1 reduces pulmonary inflammation caused by MP infection. Our results suggest that MALAT1 may be a new therapeutic target for MPP.

DATA AVAILABILITY STATEMENT

All datasets generated for this study are included in the article.

ETHICS STATEMENT

The studies involving human participants were reviewed and approved by the Ethics Committee of the Children's Hospital of Nanjing Medical University. Written informed consent to participate in this study was provided by the participants' legal guardian/next of kin. The animal study was reviewed and approved by the Institutional Animal Care and Use Committee, Nanjing Medical University.

AUTHOR CONTRIBUTIONS

HG performed the experiments and statistical analysis, contributed to the interpretation of data, made the figures and tables, and drafted the manuscript. YiZ participated in study design, collected and interpreted the clinical information, and determined the clinical status for each children involved in the study. YaZ, TH, and SZ participated in animal experiments and data interpretation. DZ and FL designed the study, analyzed the data, and revised the manuscript. All authors contributed to the article and approved the submitted version.

FUNDING

This work was supported, in part, by grants from the Jiangsu Province Special Funds for Key Program (Social Development) (BE2019607), the Key Projects of Nanjing Health and Planning Commission (ZKX18041), the Jiangsu Province Young Medical Talents (QNRC2016087), the Nanjing Medical Science and Technique Development Foundation (JQX15008), the Nanjing Science and Technology Commission (Social Development) (201723003), the Southeast University-Nanjing Medical University Cooperative Research Project (2242018K3DN20), and the Project of Nanjing Medical University (2017njmuzd054, NMUB2018104).

ACKNOWLEDGMENTS

We would like to thank Editage (www.editage.cn) for English language editing.

REFERENCES

Cao, D., Liu, M., Duan, R., Tao, Y., Zhou, J., Fang, W., et al. (2019). The lncRNA Malat1 functions as a ceRNA to contribute to berberine-mediated inhibition of HMGB1 by sponging miR-181c-5p in poststroke inflammation. *Acta Pharmacol. Sin.* 41, 22–33. doi: 10.1038/s41401-019-0284-y

Chen, H., Wang, X., Yan, X., Cheng, X., He, X., and Zheng, W. (2018). LncRNA MALAT1 regulates sepsis-induced cardiac inflammation and dysfunction via interaction with miR-125b and p38 MAPK/NFκB. *Int. Immunopharmacol.* 55, 69–76. doi: 10.1016/j.intimp.2017.11.038

Cremer, S., Michalik, K. M., Fischer, A., Pfisterer, L., Jaé, N., Winter, C., et al. (2019). Hematopoietic deficiency of the long noncoding RNA MALAT1 promotes atherosclerosis and plaque inflammation. *Circulation* 139, 1320–1334. doi: 10.1161/circulationaha.117.029015

Cui, H., Banerjee, S., Guo, S., Xie, N., Ge, J., Jiang, D., et al. (2019). Long noncoding RNA Malat1 regulates differential activation of macrophages and response to lung injury. *JCI Insight.* 4:e124522.

Dai, L., Zhang, G., Cheng, Z., Wang, X., Jia, L., Jing, X., et al. (2018). Knockdown of LncRNA MALAT1 contributes to the suppression of inflammatory responses by up-regulating miR-146a in LPS-induced acute lung injury. *Connect. Tissue Res.* 59, 581–592. doi: 10.1080/03008207.2018.1439480

Ding, Y., Guo, F., Zhu, T., Li, J., Gu, D., Jiang, W., et al. (2018). Mechanism of long non-coding RNA MALAT1 in lipopolysaccharide-induced acute kidney injury is mediated by the miR-146a/NF-kappaB signaling pathway. *Int. J. Mol. Med.* 41, 446–454.

Gao, M., Wang, K., Yang, M., Meng, F., Lu, R., Zhuang, H., et al. (2018). Transcriptome analysis of *Bronchoalveolar lavage* fluid from children with *Mycoplasma pneumoniae* pneumonia reveals natural killer and T cell-proliferation responses. *Front. Immunol.* 9:1403. doi: 10.3389/fimmu.2018.01403

Jain, S., Williams, D. J., Arnold, S. R., Ampofo, K., Bramley, A. M., Reed, C., et al. (2015). Community-acquired pneumonia requiring hospitalization among U.S. children. *N. Engl. J. Med.* 372, 835–845.

Ji, P., Diederichs, S., Wang, W., Boing, S., Metzger, R., Schneider, P. M., et al. (2003). MALAT-1, a novel noncoding RNA, and thymosin beta4 predict metastasis and survival in early-stage non-small cell lung cancer. *Oncogene* 22, 8031–8041. doi: 10.1038/sj.onc.1206928

Jia, P., Wu, N., Jia, D., and Sun, Y. (2019). Downregulation of MALAT1 alleviates saturated fatty acid-induced myocardial inflammatory injury via the miR-26a/HMGB1/TLR4/NF-κB axis. *Diabetes Metab. Syndrom. Obes.* 12, 655–665. doi: 10.2147/dmso.s203151

Lei, L., Chen, J., Huang, J., Lu, J., Pei, S., Ding, S., et al. (2019). Functions and regulatory mechanisms of metastasis-associated lung adenocarcinoma transcript 1. *J. Cell. Physiol.* 234, 134–151. doi: 10.1002/jcp.26759

Li, J., Wang, M., Song, L., Wang, X., Lai, W., and Jiang, S. (2019). LncRNA MALAT 1 regulates inflammatory cytokine production in lipopolysaccharide-stimulated human gingival fibroblasts through sponging miR-20a and activatingTLR 4 pathway. *J. Periodont. Res.* 55, 182–190. doi: 10.1111/jre.12700

Liang, W., Zeng, X., Jiang, S., Tan, H., Yan, M., and Yang, H. (2019). Long non-coding RNA MALAT1 sponges miR-149 to promote inflammatory responses of LPS-induced acute lung injury by targeting MyD88. *Cell Biol. Int.* 44, 1–10. doi: 10.1002/cbin.11235

Lin, L., Niu, G., and Zhang, X. (2019). Influence of lncRNA MALAT1 on septic lung injury in mice through p38 MAPK/p65 NF-κB pathway. *Eur. Rev. Med. Pharmacol.* 23, 1296–1304.

Martin, L. D., Rochelle, L. G., Fischer, B. M., Krunkosky, T. M., and Adler, K. B. (1997). Airway epithelium as an effector of inflammation: molecular regulation of secondary mediators. *Eur. Respir. J.* 10, 2139–2146. doi: 10.1183/09031936.97.10092139

Pease, J. E., and Sabroe, I. (2002). The role of interleukin-8 and its receptors in inflammatory lung disease. *Am. J. Respirat. Med.* 1, 19–25. doi: 10.1007/bf03257159

Puthanveetil, P., Chen, S., Feng, B., Gautam, A., and Chakrabarti, S. (2015). Long non-coding RNA MALAT1 regulates hyperglycaemia induced inflammatory process in the endothelial cells. *J. Cell Mol. Med.* 19, 1418–1425. doi: 10.1111/jcmm.12576

Salvatore, C. M., Fonseca-Aten, M., Katz-Gaynor, K., Gomez, A. M., Mejias, A., Somers, C., et al. (2007). Respiratory tract infection with *Mycoplasma pneumoniae* in interleukin-12 knockout mice results in improved bacterial clearance and reduced pulmonary inflammation. *Infect. Immun.* 75, 236–242. doi: 10.1128/iai.01249-06

Shi, S., Zhang, X., Zhou, Y., Tang, H., Zhao, D., and Liu, F. (2019). Immunosuppression reduces lung injury caused by *Mycoplasma pneumoniae* infection. *Sci. Rep.* 9:7147.

Shimizu, T., Kida, Y., and Kuwano, K. (2007). Triacylated lipoproteins derived from *Mycoplasma pneumoniae* activate nuclear factor-kappaB through toll-like receptors 1 and 2. *Immunology* 121, 473–483. doi: 10.1111/j.1365-2567.2007.02594.x

Shimizu, T., Kida, Y., and Kuwano, K. (2008). *Mycoplasma pneumoniae*-derived lipopeptides induce acute inflammatory responses in the lungs of mice. *Infect. Immun.* 76, 270–277. doi: 10.1128/iai.00955-07

Sun, J., Sun, J., and Zhou, X. (2019). Protective functions of myricetin in LPS-induced cardiomyocytes H9c2 cells injury by regulation of MALAT1. *Eur. J. Med. Res.* 24:20.

Sun, Y., and Ma, L. (2019). New insights into long non-coding RNA MALAT1 in cancer and metastasis. *Cancers* 11:216. doi: 10.3390/cancers11020216

Wei, L., Li, J., Han, Z., Chen, Z., and Zhang, Q. (2019). Silencing of lncRNA MALAT1 prevents inflammatory injury after lung transplant ischemia-reperfusion by downregulation of IL-8 via p300. *Mol. Ther. Nucleic Acids* 18, 285–297. doi: 10.1016/j.omtn.2019.05.009

Yang, H., Liang, N., Wang, M., Fei, Y., Sun, J., Li, Z., et al. (2017). Long noncoding RNA MALAT-1 is a novel inflammatory regulator in human systemic lupus erythematosus. *Oncotarget* 8, 77400–77406. doi: 10.18632/oncotarget.20490

Yang, J., Hooper, W. C., Phillips, D. J., and Talkington, D. F. (2002). Regulation of proinflammatory cytokines in human lung epithelial cells infected with *Mycoplasma pneumoniae*. *Infect. Immun.* 70, 3649–3655. doi: 10.1128/iai.70.7.3649-3655.2002

Yang, M., Meng, F., Wang, K., Gao, M., Lu, R., Li, M., et al. (2017). Interleukin 17A as a good predictor of the severity of *Mycoplasma pneumoniae* pneumonia in children. *Sci. Rep.* 7:12934.

Zhang, Y., Zhou, Y., Li, S., Yang, D., Wu, X., and Chen, Z. (2016). The clinical characteristics and predictors of refractory *Mycoplasma pneumoniae* pneumonia in children. *PLoS One* 11:e156465. doi: 10.1371/journal.pone.0156465

Zhao, G., Su, Z., Song, D., Mao, Y., and Mao, X. (2016). The long noncoding RNA MALAT1 regulates the lipopolysaccharide-induced inflammatory response through its interaction with NF-kappaB. *FEBS Lett.* 590, 2884–2895. doi: 10.1002/1873-3468.12315

Zhu, W., and Men, X. (2019). Negative feedback of NF-κB signaling by long noncoding RNA MALAT1 controls lipopolysaccharide-induced inflammation injury in human lung fibroblasts WI-38. *J. Cell Biochem.* 121, 1945–1952. doi: 10.1002/jcb.29429

Conflict of Interest: The authors declare that the research was conducted in the absence of any commercial or financial relationships that could be construed as a potential conflict of interest.

frontiers in Cell and Developmental Biology

BRIEF RESEARCH REPORT
published: 19 October 2020
doi: 10.3389/fcell.2020.569729

The Recombinant Protein Based on *Trypanosoma cruzi* P21 Interacts With CXCR4 Receptor and Abrogates the Invasive Phenotype of Human Breast Cancer Cells

Bruna Cristina Borges[1,2], Isadora Akemi Uehara[2], Marlus Alves dos Santos[1], Flávia Alves Martins[1], Fernanda Carvalho de Souza[2], Álvaro Ferreira Junior[3], Felipe Andrés Cordero da Luz[2], Mylla Spirandelli da Costa[1], Ana Flávia Oliveira Notário[4], Daiana Silva Lopes[5], Samuel Cota Teixeira[1], Thaise Lara Teixeira[6], Patrícia de Castilhos[1], Claudio Vieira da Silva[1] and Marcelo José Barbosa Silva[2]*

[1] Laboratório de Tripanosomatídeos, Departamento de Imunologia, Instituto de Ciências Biomédicas, Universidade Federal de Uberlândia, Uberlândia, Brazil, [2] Laboratório de Biomarcadores Tumorais e Osteoimunologia, Departamento de Imunologia, Instituto de Ciências Biomédicas, Universidade Federal de Uberlândia, Uberlândia, Brazil, [3] Departamento de MedicinaVeterinária, Escola de Veterinária e Zootecnia, Universidade Federal de Goiás, Goiânia, Brazil, [4] Laboratório de Nanobiotecnologia, Instituto de Genético e Bioquímica, Universidade Federal de Uberlândia, Uberlândia, Brazil, [5] Instituto Multidisciplinar em Saúde, Universidade Federal da Bahia, Vitória da Conquista, Brazil, [6] Laboratório de Biologia Molecular de Trypanosoma Cruzi, Departamento de Parasitologia, Universidade Federal de São Paulo, São Paulo, Brazil

OPEN ACCESS

Edited by:
Pier Paolo Piccaluga, University of Bologna, Italy

Reviewed by:
Daniela Carlisi, University of Palermo, Italy
Zhihao Jia, Purdue University, United States

***Correspondence:**
Bruna Cristina Borges
brunacb90@gmail.com

Specialty section:
This article was submitted to Molecular Medicine, a section of the journal Frontiers in Cell and Developmental Biology

Received: *04 June 2020*
Accepted: *22 September 2020*
Published: *19 October 2020*

Citation:
Borges BC, Uehara IA, dos Santos MA, Martins FA, de Souza FC, Junior ÁF, da Luz FAC, da Costa MS, Notário AFO, Lopes DS, Teixeira SC, Teixeira TL, de Castilhos P, da Silva CV and Silva MJB (2020) The Recombinant Protein Based on Trypanosoma cruzi P21 Interacts With CXCR4 Receptor and Abrogates the Invasive Phenotype of Human Breast Cancer Cells. Front. Cell Dev. Biol. 8:569729. doi: 10.3389/fcell.2020.569729

Trypanosoma cruzi P21 is a protein secreted by the parasite that plays biological roles directly involved in the progression of Chagas disease. The recombinant protein (rP21) demonstrates biological properties, such as binding to CXCR4 receptors in macrophages, chemotactic activity of immune cells, and inhibiting angiogenesis. This study aimed to verify the effects of rP21 interaction with CXCR4 from non-tumoral cells (MCF-10A) and triple-negative breast cancer cells (MDA-MB-231). Our data showed that the MDA-MB-231 cells expressed higher levels of CXCR4 than did the non-tumor cell lines. Besides, cytotoxicity assays using different concentrations of rP21 showed that the recombinant protein was non-toxic and was able to bind to the cell membranes of both cell lineages. In addition, rP21 reduced the migration and invasion of MDA-MB-231 cells by the downregulation of *MMP-9* gene expression. In addition, treatment with rP21 blocked the cell cycle, arresting it in the G1 phase, mainly in MDA-MB-231 cells. Finally, rP21 prevents the chemotaxis and proliferation induced by CXCL12. Our data showed that rP21 binds to the CXCR4 receptors in both cells, downregulates CXCR4 gene expression, and decreases the receptors in the cytoplasm of MDA-MB-231 cells, suggesting CXCR4 internalization. This internalization may explain the desensitization of the receptors in these cells. Thus, rP21 prevents migration, invasion, and progression in MDA-MB-231 cells.

Keywords: *Trypanosoma cruzi*, recombinant protein P21, CXCR4, triple-negative breast cancer cells, invasion cell

INTRODUCTION

Triple-negative breast cancer (TNBC) is characterized by a tumor subtype void of hormone receptors, such as the estrogen receptors (ER), progesterone receptors (PR), and human epidermal growth factor receptor 2 (HER2) (Zhou et al., 2018); thus, this tumor is associated with poor prognosis (Den Brok et al., 2017). Poor prognosis involves a distinct metastatic pattern involving regional lymph nodes, bone marrow, the lungs, and liver (Müller et al., 2001) and ineffective treatments owing to the lack of therapeutic targets (Venkitaraman, 2010; Voduc et al., 2010).

Most deaths caused by breast cancer are not due to the primary tumor itself but are a result of metastasis to other organs in the body (Weigelt et al., 2005). Chemokines and receptors regulate tumor cell migration and metastasis. The CXCR4 receptor is a seven-transmembrane domain G-protein-coupled receptor (GPCR) superfamily member (Cojoc et al., 2013). CXCL12 is a chemokine that binds to this receptor. The CXCR4/CXCL12 axis can promote tumor metastasis by mediating cell invasion and proliferation and also enhancing tumor-associated neoangiogenesis (Cojoc et al., 2013). It is involved in orientating cancer cell migration to metastasis sites, increased survival of cancer cells in suboptimal conditions, and the establishment of a tumor-promoting cytokine/chemokine network (Balkwill, 2004). This receptor is expressed constitutively in a wide variety of normal tissues, including lymphatic tissues, thymus, brain, spleen, stomach, and small intestine, but it is also expressed in several types of tumor cells (Balkwill, 2004). Tumor cells increase the CXCR4 levels and CXCL12 production, transmitting autocrine and paracrine signals, leading to enhanced tumor growth and metastasis (Liekens et al., 2010).

Microorganisms and viruses can contribute to cancer initiation and progression (Whisner and Aktipis, 2019), such as *Helicobacter pylori* in stomach cancer (Martel et al., 2008), *Herpes papillomavirus* in cervical cancer (Schiffman et al., 2007), and hepatitis C or B in liver cancer (Chan et al., 2016; Axley et al., 2018). Several studies involving parasites demonstrate that bioactive molecules and parasites promote antitumor effects, such as *Strongyloides stercoralis*, *Toxoplasma gondii*, *Plasmodium*, and *Trypanosoma cruzi* (Plumelle et al., 1997; Kim et al., 2007; Chen et al., 2011; Lukasiewicz and Fol, 2018). It has been demonstrated that parasite anticancer activity is mediated by antitumor immunity induction and immunomodulation (Ubillos et al., 2016; Mohamadi et al., 2019; Riaz, 2019), gene regulation (Lu et al., 2019), and anticancer effects by parasite molecule production (Atayde et al., 2008; Valck et al., 2010; Darani and Yousefi, 2012; Ramírez et al., 2012).

Different strains of *T. cruzi* were used for carcinoma treatment and showed that high parasitemia is related to a decreased tumor development in animal models (Krementsov, 2009), and parasite extracts had the same effect (Krementsov, 2009). Thus, the immune response elicited by *T. cruzi* could be effective toward tumor cells due to the molecular mimicry of antigens (Zhigunova et al., 2013; Ubillos et al., 2016). Besides that, it is known that *T. cruzi* has a component with pro-apoptotic activity in tumor cells (Mucci et al., 2006) and antitumor membrane proteins, such as GP82 and calreticulin protein (Atayde et al., 2008; Valck et al., 2010; Ramírez et al., 2012).

P21 is a *T. cruzi* protein involved in parasite–host cell invasion and parasite perpetuation during infection (Silva et al., 2009). Some results have shown that the recombinant form of this protein (rP21) acts as a phagocytosis inducer by binding to the CXCR4 chemokine receptor and activating actin polymerization in macrophages (Rodrigues et al., 2012). This recombinant protein can also increase sFlt-1 production by macrophages. This soluble molecule inhibits endothelial cell proliferation, ensuring an anti-angiogenic action (Teixeira et al., 2015; Teixeira et al., 2017); besides that, rP21 can promote the chemotaxis of immune cells (Teixeira et al., 2015). In this way, it is interesting to consider novel studies exploring rP21 in the tumoral microenvironment. This study aimed to evaluate the effects of the rP21 protein on breast cancer cells *in vitro*.

MATERIALS AND METHODS

Cell Culture

Non-tumorigenic human breast cells (MCF-10A) and human triple-negative breast tumoral cells (MDA-MB-231) were purchased from Banco de Células do Rio de Janeiro. MCF-10A cells were cultivated in Dulbecco's modified Eagle's/Ham's Nutrient Mixture F12 (DMEM/F12; Life Technologies, Carlsbad, CA, United States) supplemented with epidermal factor growth (20 ng/ml), insulin from bovine pancreas (10 μg/ml), hydrocortisone (0.5 μg/ml), and 5% fetal bovine serum (FBS). MDA-MB-231 cells were cultivated in DMEM medium (Sigma-Aldrich, MO, United States) supplemented with 10% FBS and 2 mM sodium bicarbonate. Both cells were maintained with 100 U/ml penicillin and 100 μg/ml streptomycin and incubated at 37°C in a humidified atmosphere containing 5% CO_2.

Production and Purification of rP21

The rP21 (GenBank: EU004210.1) protein was purified as previously described (Silva et al., 2009; Santos et al., 2014). After purification, the protein was incubated with a polymyxin B column. The quality of purification was demonstrated by sodium dodecyl sulfate–polyacrylamide gel electrophoresis (SDS-PAGE) and Western blotting (**Supplementary Figure 1**).

Flow Cytometry

To determine CXCR4 levels, the cells were fixed with 4% paraformaldehyde for at least 1 h and permeabilized with saponin PGN, and stained cells were labeled with PE anti-human CD184 antibodies (BioLegend, CA, United States) for 1 h at 4°C. Data from 12,000 cells were collected by a CytoFLEX (Beckman Coulter). Results were obtained using Kaluza software (Beckman Coulter). The mean fluorescence intensities (MFI) were calculated using the median of samples on a logarithmic scale.

The binding of rP21 to cells was determined. The cells (1×10^5) were treated with rP21 (100 μg/ml) for 1 h. Next, they were washed two times in phosphate-buffered saline (PBS). The protein was stained using primary IgY anti-rP21 antibodies

diluted in 1:10 in 2.5% bovine serum albumin (BSA) for 1 h. The cells were washed twice and secondary anti-IgY fluorescein isothiocyanate (FITC) antibodies were diluted 1:1,000 in 2.5% BSA for 1 h. After this, the samples were collected in the BD FACSVerse (Becton Dickinson, United States). The results were obtained using FlowJo software (FlowJo, LLC).

To verify whether rP21 binding to cells interferes with the CXCR4 receptors, cells (1×10^5) were treated for 1 and 72 h (100 μg/ml rP21). For labeling of the CXCR4 receptor in the membrane, after treatment, the cells were washed and labeled with PE anti-human CD184 antibodies diluted in 2.5% BSA solution (3 μl of antibody in 100 μl of solution). To label the CXCR4 in the cytoplasm, the cells were fixed with 4% paraformaldehyde for 1 h after the PE anti-human CD184 antibodies were diluted in saponin PGN (saline buffer with gelatin) for 1 h at 4°C. Data from 12,000 cells were collected by a CytoFLEX (Beckman Coulter). The results were obtained using Kaluza software (Beckman Coulter).

Confocal Microscopy

To detect CXCR4, 1×10^5 cells were seeded in 24-well coverslips. Next, the cells were fixed with 4% formaldehyde for 1 h and washed three times with PBS. Then, they were permeabilized and blocked with saponin PGN and labeled with PE anti-human CD184 antibodies (BioLegend, CA, United States) for 1 h at 4°C. The images qualitatively show the CXCR4 levels.

To analyze the co-localization between rP21 and CXCR4, 1×10^5 cells were seeded in 24-well coverslips and treated at 1, 6, and 24 h with 100 μg/ml rP21. The cells were stained with primary antibody IgY anti-rP21 overnight. Next, the secondary antibody anti-IgY FITC, PE anti-human CD184 antibodies, and DAPI were added. Images were obtained in a Zeiss LSM 510 META microscope at × 63 magnification.

Quantitative Reverse Transcription PCR

MDA-MB-231 and MCF-10A (1×10^4 cells/well) were seeded in 24-well microplates that had previously been coated with a thin Matrigel. The cells were incubated with rP21 (100 μg/ml), CXCL12 (20 ng/ml), or culture medium (control group) for 72 h. Total RNA was extracted using a Maxwell® RSC simplyRNA Cells Kit (Promega, Madison, WI, United States) and GoScript RT Mix (Promega) was used for reverse transcription according to the manufacturer's instructions. Quantitative RT-PCR was performed using a GoTaq® Master Mix qPCR (Promega) and StepOnePlus™ (Applied Biosystems, Carlsbad, CA, United States) was used to analyze the received data. The data were normalized using HPRT-1 as a housekeeping gene and CXCR4 and MMP9 genes were analyzed. The primers used were: CXCR4, 5′-GGGATCAGTATATACACTTCAGATA-3′ (forward) and 5′-GCTGTGACCTGCTGTTATT-3′ (reverse); MMP-9, 5′-AAGGACCGGTTCATTTGG-3′ (forward) and 5′-CCTCGTATACCGCATCAATC-3′ (reverse); and HPRT-1, 5′-GGCGTCGTGATTAGTGATG-3′ (forward) and 5′-AACACCCTTTCCAAATCCTC-3′ (reverse). The analysis was done by the comparative threshold cycle (C_T) method to calculate fold changes in expression in treated groups compared to the control group. The fold changes in gene expression for the treated groups were then calculated as $2^{-\Delta\Delta CT}$.

Viability Assay

The effect of rP21 on TNBC and normal cells was determined using the 3-[4,5-dimethylthiazol-2-yl]-2,5-diphenyl tetrazolium bromide (MTT) assay. The cells (1×10^4) were seeded in 96-well plates. After adhesion, the cells were treated with different concentrations of rP21 (6.25, 12.5, 25, 50, and 100 μg/ml) for 72 h. Afterward, the cells were incubated with 10 μl MTT (5 mg/ml) per well for 4 h. The dye crystals were dissolved in dimethylformamide (50%) containing 10% SDS overnight. Absorbance was measured at 570 nm on the multiwell scanning spectrophotometer GloMax Explorer (Promega, United States). Cell viability was expressed in percentage, which was calculated as follows: (%) = [(absorbance of the control group – absorbance of the test group)/absorbance of the control group] × 100%. Concentrations that present less than 50% of viable cells would be considered toxic.

Migration/Invasion Assay

A wound healing assay was made by migration analysis. The cells were cultured as confluent monolayers for 24 h and wounded by removing a strip of cells across the well with a standard 10-μl pipette tip. Wounded monolayers were washed twice to remove non-adherent cells. Then, they were treated for 72 h with only the culture medium, 20 ng/ml CXCL12, and 100 μg/ml rP21 and pretreated with 100 μg/ml rP21 for 1 h and then treated with 20 ng/ml CXCL12. Wound healing was quantified using ImageJ software as the mean percentage of the remaining cell-free area compared to the area of the initial wound.

Invasion assay was made using transwells with 8-μm pores (Costar, Corning, United States) with Matrigel (Corning® Matrigel® Growth Factor Reduced). The upper chamber contained cells in the culture medium (1×10^5/ml) and the lower chamber contained the culture medium (negative control), 20 ng/ml CXCL12 (chemoattractant), and 100 μg/ml rP21. In one group, the cells were pretreated with 100 μg/ml rP21 for 1 h and then added in the upper chamber. The lower chamber contained 20 ng/ml CXCL12 (chemoattractant). The cells were incubated for 72 h at 37°C in 5% CO_2. Non-migrated cells were scraped from the upper surface of the membrane with a cotton swab and the migrated cells remaining on the bottom surface were counted after staining with crystal violet. Cell counting was done using a Leica DM 500 microscope at × 10 magnification. The images were used to count the number of cells using ImageJ software.

Cell Cycle Assay

For cell cycle analysis, 7×10^4 cells were seeded in 24-well plates. After 24 h, the cells were treated with culture medium, 20 ng/ml CXCL12, and 100 μg/ml rP21 and pretreated with 100 μg/ml rP21 for 1 h and then 20 ng/ml CXCL12 for 72 h. Then, they were collected, washed once with PBS, and fixed with 70% ethanol at 20°C for 24 h. Fixed cells were washed three times and incubated for 45 min with propidium iodide (PI) solution (10 μg/ml) containing RNase A (0.1 μg/ml). The cells were analyzed for determining DNA contents by flow cytometry. Cell

debris was excluded based on forward vs. side scatter. Data from 12,000 events were collected in the final gated histograms. The cell histogram was divided into three regions according to the cell cycle phase: G1, S, and G2/M. Cells before the row represent unstained events. The inhibition percentage of the cell cycle was calculated as follows: (% inhibition) = (% G1 treated with rP21 –% G1 treated with CXCL12).

Statistical Analysis

All data are presented as the mean ± standard error of the mean of experiments performed at least three times in triplicate. All data were first checked for normal distribution. Significant differences were determined by one-way ANOVA, Tukey's multiple comparisons test, and Student's *t*-test (two-sided) for parametric data or the Mann–Whitney test for non-parametric data according to the experimental design. $P < 0.05$ was considered significant. All the statistical analyses were performed using GraphPad Prism software version 8.0.

RESULTS

CXCR4 Has a Distinct Amount in Non-tumoral and MDA-MB-231 Cells and rP21 Was Not Cytotoxic and Binds in Both Cells

First, we evaluated total CXCR4 levels in the plasma membrane and cytoplasm by confocal microscopy and CXCR4 on the cell surface by flow cytometry. Our data demonstrated higher labeling of the CXCR4 receptors in MDA-MB-231 cells than in MCF-10A cells, and MDA-MB-231 showed higher MFI values than did MCF-10A (**Figures 1A,B**).

Then, MCF-10A and MDA-MB-231 cells were treated with 100, 50, 25, 12.5, or 6.25 μg/ml rP21 for 72 h followed by the MTT assay to determine the effect of rP21 on cell viability. MCF-10A (**Figure 1C**) and MDA-MB-231 (**Figure 1D**) viability did not change with treatment.

As long as the cell lines expressed CXCR4, we addressed the ability of the rP21 protein to bind to the plasma membranes of these cell lineages. The data showed that rP21 adhered to MCF-10A (**Figure 1E**) and MDA-MB-231 membranes (**Figure 1F**) after treatment for 1 h.

rP21 Modulates the Migration and Invasion of MDA-MB-231 by MMP-9 Downregulation

Our next goal was to analyze the potential of rP21 to induce the migration and invasion of these cell lines. For this, the wound healing and Transwell assays were performed (**Figure 2A**). In the wound healing assay, treatment with rP21 for 72 h reduced the invasion of MCF-10A cells when compared to treatment with CXCL12 (**Figure 2B**). However, the reduction in invasion was much more expressed in MDA-MB-231 in the presence of rP21 (**Figure 2C**). In addition, when we pretreated the cells with rP21 and then added CXCL12, the inhibition of migration caused by rP21 was not altered in both cells (**Figures 2B,C**).

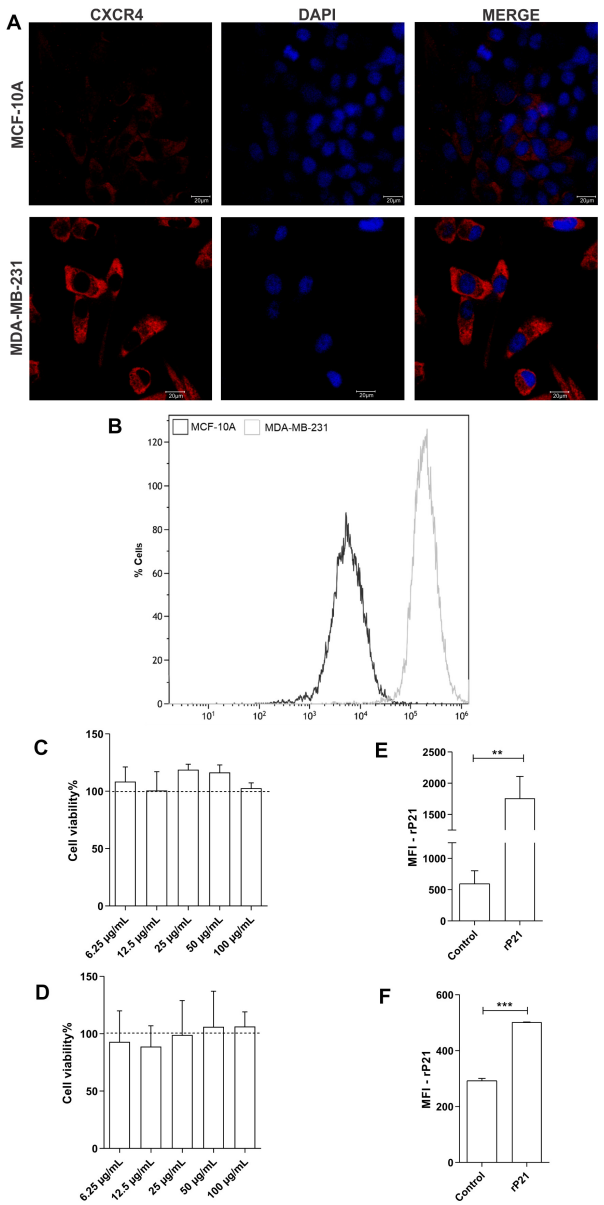

FIGURE 1 | Differential expression of CXCR4 in membrane cells and total receptors in MDA-MB-231 and MCF-10A. Recombinant protein (rP21) is not cytotoxic and binds in cells. Evaluation of CXCR4 levels by confocal microscopy **(A)** and flow cytometry **(B)**. MCF-10A **(C)** and MDA-MB-231 **(D)** were treated with rP21 at different concentrations (100, 50, 25, 12.5 and 6.25 μg/mL) and did not exhibit alterations in cell viability. These data are from one experiment representative of three independent experiments. The cells were incubated for 1 hour with rP21 (100 μg/mL). rP21 labeling by flow cytometry showed protein binding in the MCF-10 A **(E)** and MDA-MB-231 **(F)** cells. These results are representative of at least three independent experiments. Data show the mean ± SEM. Significant differences were determined using student *t*-tests and one-way ANOVA. Differences were considered significant when $p < 0.05$. $^{**}p = 0.0025$, $^{***}p = 0.0005$, and $^{****}p < 0.0001$.

In the Transwell assay, treatment with rP21 as well as pre-incubation with rP21, and the subsequent addition of

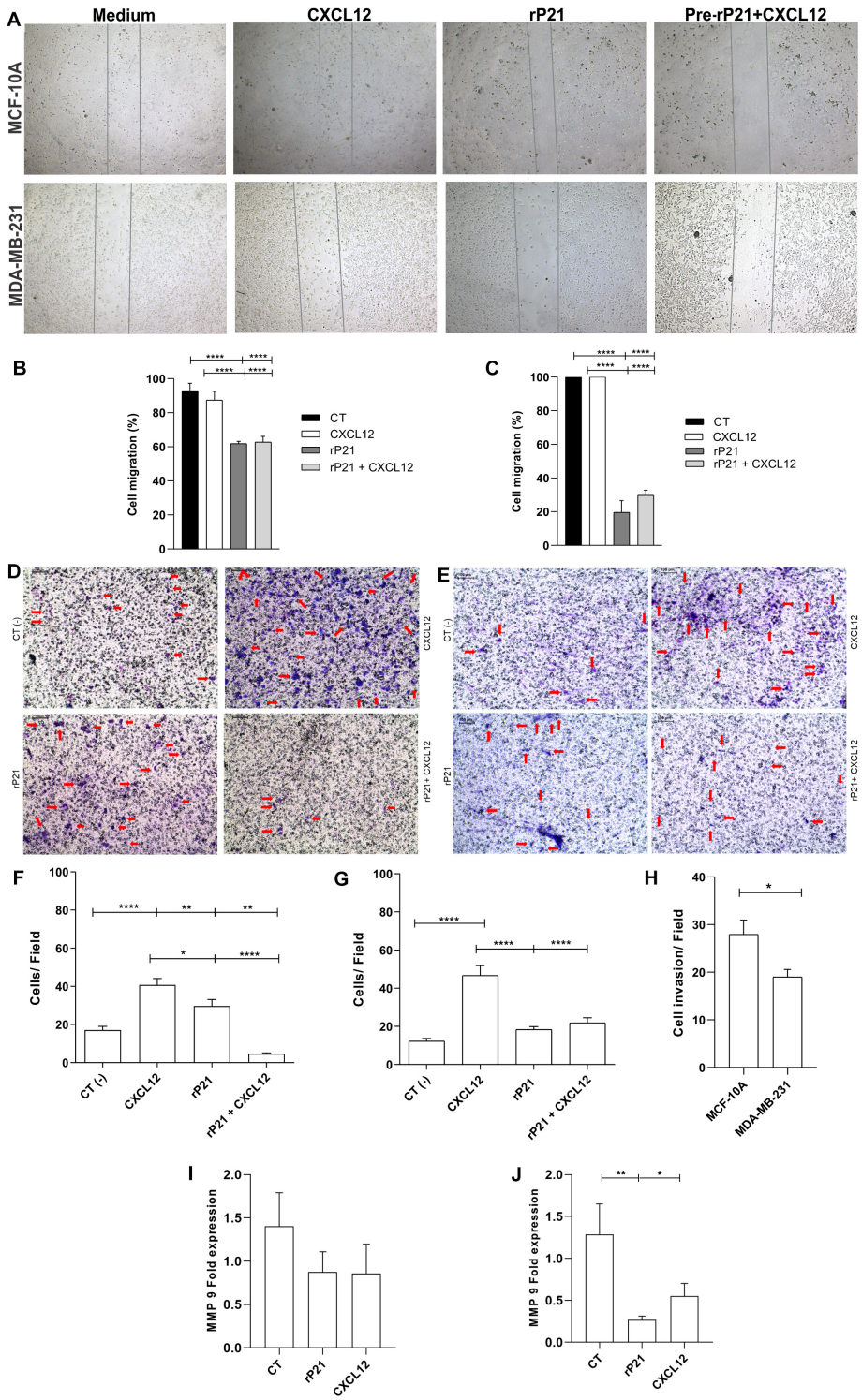

FIGURE 2 | The rP21 protein decreased the migration and invasion of triple-negative breast cancer (TNBC) cells by downregulating MMP-9 gene expression. **(A)** Representative images show the differences in cell migration at 72 h in the wound healing assay. Percentages of MCF-10A **(B)** and MDA-MB-231 **(C)** cell closure of the wound healing assay area after treatments. Transwell cell invasion of MCF-10A **(D,F)** and MDA-MB-231 **(E,G)**. The percentage of cells invaded was determined using CXCL12 as 100%. Negative control: serum-free medium; positive control: medium 17 containing CXCL12 **(H)**. Bars, 100 μm represents × 10 objective. Red arrows indicate invaded cells. Gene expressions of MMP-9 in MCF-10A **(I)** and MDA-MB-231 **(J)**. These results are representative of at least three independent experiments. Data show the mean ± SEM. Significant differences were determined using one-way ANOVA and Tukey's multiple comparisons test. Differences were considered significant when $p < 0.05$. *$p < 0.05$, **$p < 0.01$, and ****$p < 0.0001$.

CXCL12, reduced cell invasion in MCF-10A (**Figures 2D,F**), but was further reduced in MDA-MB-231 (**Figures 2E,G**). Similar to the migration test, in this one, rP21 also prevented the chemotactic action of CXCL12. These data were more evident when comparing treatment with rP21 and the negative control. The invasion of MCF-10A cells was high (**Figure 2F**), while the invasion of MDA-MB-231 was less than that of the negative control (**Figure 2G**). Thus, in both cells, the invasion is smaller than that the CXCL12 group, but the invasion percentage of MDA-MB-231 is smaller than that in MCF-10A (**Figure 2H**).

We proved that rP21 can decrease the migration and invasion, mainly in MDA-MB-231. To assess this effect, matrix metalloproteinase 9 (MMP-9) expression was analyzed. In MCF-10A cells, MMP-9 gene expression remained similar between the control and treatment groups (**Figure 2I**), but in MDA-MB-231, rP21 treatment significantly decreased MMP-9 expression and CXCL12 slightly decreased MMP-9 expression (**Figure 2J**).

rP21 Arrested Cell Cycle of MDA-MB-231 Cell Progression

We further characterized the effects of rP21 on cell cycle. The percentages of MCF-10A and MDA-MB-231 cells in each cycle phase in different treatments are shown in **Figures 3A,B**, respectively. rP21 treatment in MCF-10A decreased cells in the G1 phase (69.50%), while rP21 pretreatment followed by CXCL12 kept MCF-10A cells equal to the control (75.55%; **Figures 3A,C**). Thus, rP21 treatment or pretreatment does not interfere in the cell cycle when compared to the control. When compared with CXCL12, the rP21 protein increases the cells in the G1 phase, even with the rP21 pretreatment. However, rP21 also induces a slight increase in the G1 phase in MCF-10A when compared with CXCL12 (**Figures 3A,C**).

In the MDA-MB-231 treatment with rP21 or pretreatment with rP21 + CXCL12, the cells in the G1 phase increased by 51.52 and 53%, respectively, when compared to both the control and CXCL12 (**Figures 3B,D**). In the rP21 treatment, MDA-MB-231 cells also had an increase in the G1 phase when compared to CXCL12, which was significantly higher than in the MCF-10A cells (**Figure 3E**). In the rP21 pretreatment followed by CXCL12, MDA-MB-231 cells had an increase in the G1 phase when compared to CXCL12, which was also more significant than that in MCF-10A (**Figure 3F**). Thus, rP21 interferes in the cell cycle, increasing the G1 phase in MDA-MB-231, besides interfering with the CXCL12 action in these cells.

rP21-Induced CXCR4 Internalization in MDA-MB-231

To further gain insights into the MDA-MB-231-specific impact of rP21 in impairing cellular invasion and cell cycle, we analyzed CXCR4 after treatment with rP21. First, the CXCR4 gene expression was analyzed. In MCF-10A cells, rP21 and CXCL12 treatments did not alter CXCR4 expression. In MDA-MB-231, CXCL12 treatment downregulated the CXCR4 gene, but rP21 treatment downregulated the CXCR4 gene expression even less than CXCL12 (**Figures 4A,B**).

rP21 treatment for 1 h decreased the CXCR4 levels on the cell surface of MCF-10A (**Figure 4C**), in MDA-MB-231 this decreased is higher than in MCF-10A (**Figure 4D**), suggesting that rP21 binds in the same site as the anti-CXCR4 antibody or receptor internalization. The CXCR4 levels in the cytoplasm are also decreased. In MCF-10A, at both times, the decrease remains the same, being small relative to the control (**Figure 4E**). In MDA-MB-231, the decrease in CXCR4 increases over time (**Figure 4F**). A decreased CXCR4 labeling in the cytoplasm can indicate that rP21 may bind to the same region used by the antibody, or rP21 ligation in CXCR4 causes the internalization and desensitization of the receptors.

To explain these phenomena, rP21 binding kinetics were performed. The recombinant protein was adhered to the MCF-10A plasmatic membrane and not co-localized with CXCR4 at all times (**Figure 4G**). In contrast, in MDA-MB-231, rP21 co-localized with the CXCR4 receptor in 24 h, leaving the cell membrane surface and appearing in the cytoplasm, suggesting the internalization of P21 by its binding to the receptor (**Figure 4H**). In this way, rP21 binds to the CXCR4 receptor, and after 24 and 72 h of treatment, CXCR4 is internalized and its expression in the cytoplasm is lower in MDA-MB-231 than in MCF-10A cells. Besides that, rP21 downregulates CXCR4 gene expression in tumoral cells, but not in MCF-10A cells. Thus, the internalization of rP21 binding in the CXCR4 receptor interferes in tumor cell activity.

DISCUSSION

Trypanosoma cruzi-derived products have antitumor activities, such as a recombinant protein from GP82 (J18) that induces apoptosis in melanoma cells *in vitro* and reduces tumor *in vivo* (Atayde et al., 2008). Another product, calreticulin, is a calcium-binding protein from *T. cruzi* that can inhibit the activation of the complement cascade system favoring infection, besides the anti-angiogenic activity and antitumor properties *in vivo* (Valck et al., 2010; Ramírez et al., 2012).

P21 is an important protein during Chagas disease development (Rodrigues et al., 2012; Santos et al., 2014; Teixeira et al., 2015). The recombinant protein, rP21, has biological activities such as anti-angiogenic features (Teixeira et al., 2017) and promotes the chemotaxis of inflammatory cells (Teixeira et al., 2015) and actin cytoskeletal polymerization (Rodrigues et al., 2012). The rP21 protein did not interfere in cellular viability in any cell type, such as macrophages (Rodrigues et al., 2012), endothelial cell lines (Teixeira et al., 2017), myoblasts (Martins et al., 2020), and breast cells, such as the non-tumoral and tumoral cells shown here. Our results showed that rP21 binds to the CXCR4 receptors in MCF-10A and MDA-MB-231 cells and interferes in the migration/invasion and proliferation phenotypes of these cells. Corroborating these data, rP21 also binds to the CXCR4 of endothelial cells and inhibits vessel formation by inhibiting cell proliferation and increasing the cell numbers in the S phase (Teixeira et al., 2017).

CXCR4 is expressed in various cell types, including tumor cells. This receptor in prostate tumor cells, glioma, oral squamous

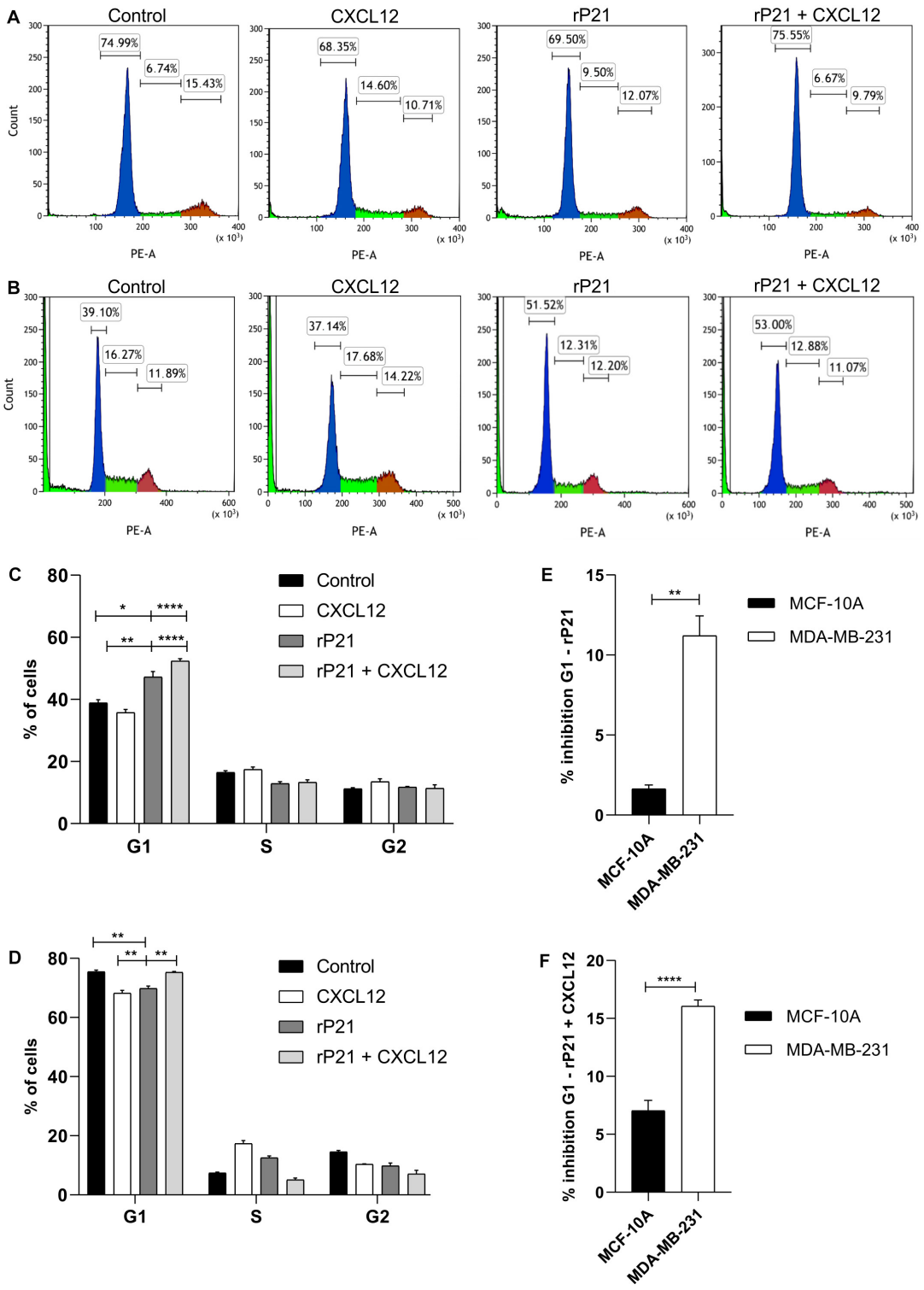

FIGURE 3 | The rP21 protein caused G1 to be arrested in the MDA-MB-231 cell cycle. The DNA content of MCF-10A and MDA-MB-231 cells treated with different treatments at 72 h was analyzed by propidium iodide (PI) staining. Treatments: culture medium (control), CXCL12, rP21, rP21 for 1 h, and followed by CXCL12. Percentages of MCF-10A **(A,C)** and MDA-MB-231 **(B,D)** cells in each cell phase at different treatments. Inhibition percentages of the cell cycle in the rP21 treatment **(E)** and rP21 pretreatment followed by CXCL12 **(F)**. These results are representative of at least three independent experiments. Values are the mean ± SEM. Significant differences were determined using one-way ANOVA and Tukey's multiple comparisons test. Differences were considered significant when $p < 0.05$. $^{*}p < 0.05$, $^{**}p < 0.01$, and $^{****}p < 0.0001$.

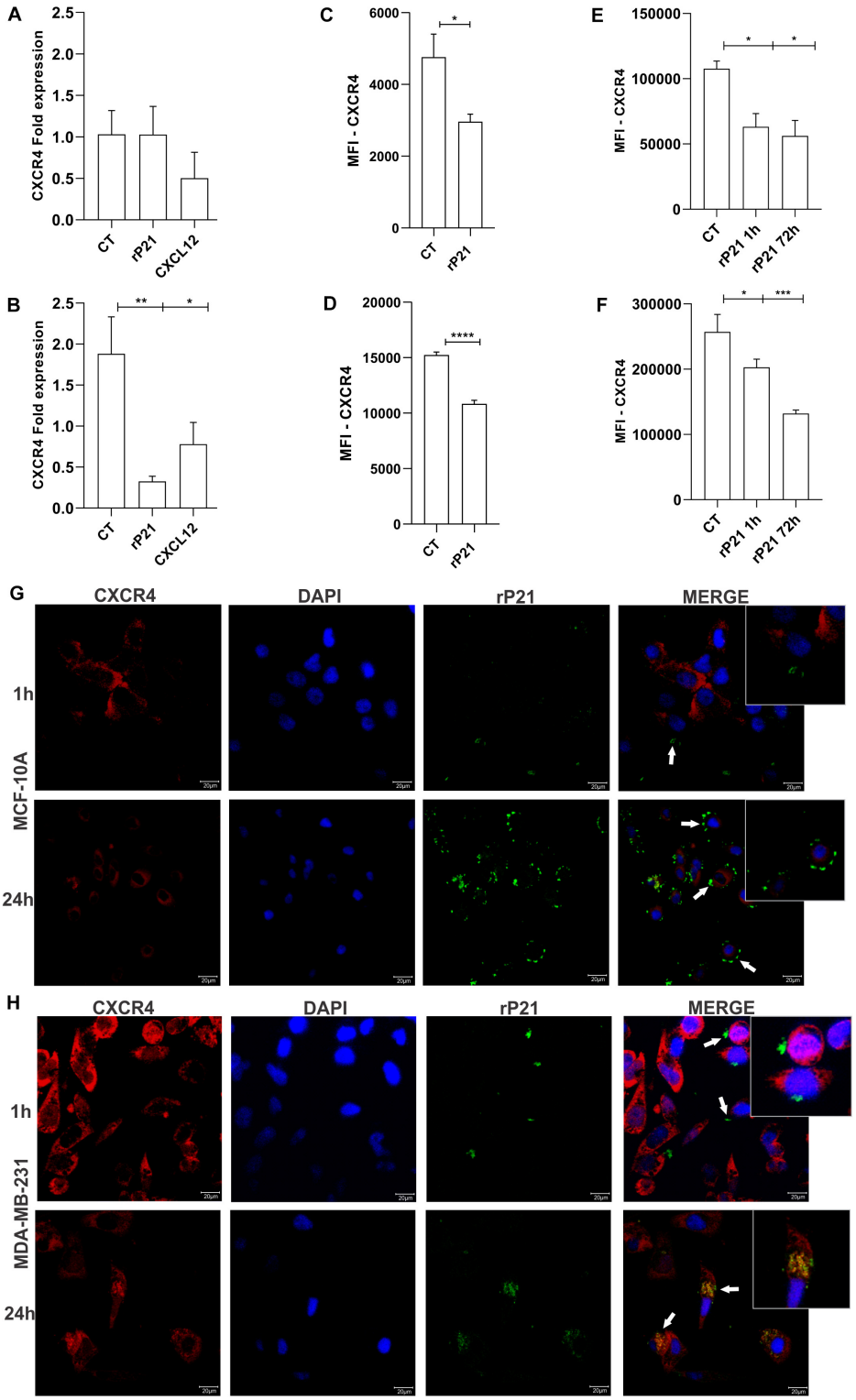

FIGURE 4 | The rP21 protein downregulated CXCR4 gene expression, decreased the CXCR4 levels, and is internalized in MDA-MB-231. Gene expression of CXCR4 in MCF-10A **(A)** and MDA-MB-231 **(B)** after 72 h of treatment. Evaluation of CXCR4 in a membrane cell after rP21 treatment for 1 h in MCF-10A **(C)** and MDA-MB-231 **(D)** cells. Evaluation of CXCR4 in the cytoplasm after rP21 treatment for 1 and 72 h in MCF-10A **(E)** and MDA-MB-231 **(F)** cells. MCF-10A **(G)** and MDA-MB-231 **(H)** cells were treated with rP21 (100 μg/ml) for 1 and 24 h, fixed, permeabilized, rP21 (green) and CXCR4 (red) stained, and analyzed by confocal microscopy. Blue, cell nuclei. White arrows indicate the location of rP21. Bars, 20 μm represents × 63 objective. These results are representative of at least three independent experiments. Data show the mean ± SEM. Significant differences were determined using t-test. Differences were considered significant when $p < 0.05$. *$p < 0.05$, **$p < 0.01$, ***$p < 0.001$, and ****$p < 0.0001$.

carcinoma, pancreatic, and breast tumor cells is overexpressed when compared to non-tumor cells (Balkwill, 2004). Thus, CXCR4 can be studied as a potential therapeutic target for various types of tumors (Zhou et al., 2018). When the cells were treated with rP21, CXCR4 was downregulated. This downregulation of CXCR4 expression could also inhibit the distant metastasis of cancer (Sun et al., 2009). In MDA-MB-231, besides rP21, CXCL12 induces the downregulation of CXCR4. The constant presence of CXCL12 in the culture medium can induce the downregulation of CXCR4 and decrease the migration of these cells (Chatterjje and Gawaz, 2013).

In addition, to regulate CXCR4 gene expression, rP21 decreased the CXCR4 levels in the plasma membrane and cytoplasm of MDA-MB-231 cells, suggesting receptor internalization and desensitization. Our previous studies have shown that rP21 can bind to CXCR4 in HeLa cells, macrophages, and endothelial cells (Silva et al., 2009; Rodrigues et al., 2012; Teixeira et al., 2017). Pretreatment with rP21 in HeLa cells inhibited invasion by extracellular amastigote, suggesting that pre-incubation with rP21 could desensitize these cells (Silva et al., 2009). Thus, recombinant proteins can cause receptor desensitization to favor an infection, but they can cause receptor desensitization and generate beneficial effects in the tumor microenvironment. Chemokine internalization receptors occur after binders bind to a receptor. Depending on the receptor percentage being activated, this process may dramatically reduce the CXCR4 membrane expression levels and therefore change functionality (Neel et al., 2005). Internalization can cause receptor desensitization and unresponsiveness. CXCR4 desensitization in tumor cells is a potential therapy in TNBC and other overexpressed CXCR4 tumor cells. The CXCR4 antagonist AMD3100 is used in leukemia and solid tumor treatments to sensitize the cells to chemotherapy (Liu et al., 2016).

CXCR4 is implicated in promoting migratory phenotypes and proliferation in various types of tumors, and CXCL12 induces chemotactic response and cell proliferation (Tanaka et al., 2005). CXCR4-positive cells are driven by the CXCL12 concentration gradient; thus, tumoral cells leave the primary site toward organs that express more CXCL12, causing metastasis (Teicher and Fricker, 2010). rP21 treatment can modulate these phenomena and decrease invasion and proliferation, mainly in MDA-MB-231 cells. Besides, CXCL12-induced chemotaxis was reduced when cells were pretreated with rP21, showing that the recombinant protein blocks the CXCL12 effects. On the other hand, other drugs with cyclophosphamide, indicated for the treatment of cancerous diseases such as breast cancer and cervical cancer, induce the cell surface expression of CXCR4 and enhance the migration of MDA-MB-231 cells (Hung et al., 2017). Thus, CXCR4-positive cell invasion is dependent on CXCL12–CXCR4 binding. rP21 may bind to CXCR4 in a way that partially blocks CXCL12 downstream effects. The rP21 protein causes neutrophil and macrophage chemotaxis *in vivo* and *in vitro* (Teixeira et al., 2015) and has the same effect in MCF-10A cells, but our data showed that rP21 may act differently on tumor cells. This action in tumor cells can be explained by the rP21 downregulation of MMP-9 gene expression, while in MCF-10, the MMP-9 expression was not altered. MMP-9, as an indicator of migration, has been reported to be a downstream target of CXCL12/CXCR4 (Zuo et al., 2017). Thus, curcumin and luteolin impair the migratory activity in tumor cells by the repression of the CXCL12/CXCR4 biological axis, as a consequence of the downregulation of MMP-9 by luteolin (Qin et al., 2018; Bu and Zhao, 2020). Our results imply that rP21 repressed CXCL12-induced migration and invasion and decreased MMP-9 expression. However, in endothelial cells, rP21 upregulated the expression of MMP-9 after 72 h (Teixeira et al., 2017), but the role of MMP-9 during angiogenesis remains uncertain (Bendeck, 2004).

CXCR4 overexpression promotes migration, adhesion, and invasion in tumor cells, besides promoting epithelium–mesenchyme transition and acting in tumor development (Liu et al., 2016). Some compounds are capable of transforming normal cells, such as MCF-10A, altering important cell cycle proteins as well as inducing cell migration and invasion (Pierozan et al., 2018). Thus, rP21 does not interfere in the MCF-10A cell cycle, while this recombinant protein can arrest the TNBC cell cycle in the G1 phase. Cell cycle block is important in tumor cells because it may influence cell proliferation and migration (Kümper et al., 2016).

In this study, we demonstrate that the rP21 protein based on native *T. cruzi* reduces invasion, migration, and proliferation in MDA-MB-231 cells. The rP21 protein binds to the CXCR4 receptor in MCF-10A and MDA-MB-231, but this recombinant protein decreased the CXCR4 levels and was internalized only in tumoral cells. This internalization suggests that rP21 could desensitize CXCR4, triggering signaling events that decrease migration and invasion and, in addition, cause cell cycle arrest in tumoral breast cancer cells. The ability of rP21 to modulate cell cycle and invasiveness of breast malignant cell lines shed light on the potential use of this protein in triple-negative breast cancer therapeutic approaches to avoid tumor progression and metastasis.

DATA AVAILABILITY STATEMENT

The datasets generated for this study can be found in online repositories. The names of the repository/repositories and accession number(s) can be found below: http://dx.doi.org/10.14393/ufu.te.2019.1265.

AUTHOR CONTRIBUTIONS

BB was responsible for project development, designed the experimental approaches, performed the experimental manipulations, interpreted the data, and drafted the manuscript. IU, MAS, FM, FS, FL, AN, DL, ST, TT, and PC performed the experiments and participated in the data interpretation. IU designed the graphical abstract. AJ produced the rP21 anti-IgY and participated in the data interpretation. MC participated in the data interpretation and edited the manuscript. CS and MS coordinated and designed the biological experiments, analyzed

and interpreted the data, and edited the manuscript. All authors read and approved the final manuscript.

FUNDING

This study was supported by the grants from Fundação de Amparo à Pesquisa do Estado de Minas Gerais (FAPEMIG), Conselho Nacional de Desenvolvimento Científico e Tecnológico (CNPq), and Coordenação de Aperfeiçoamento de Pessoal de Nível Superior (CAPES).

SUPPLEMENTARY MATERIAL

The Supplementary Material for this article can be found online at: https://www.frontiersin.org/articles/10.3389/fcell.2020.569729/full#supplementary-material

REFERENCES

Atayde, V. D., Jasiulionis, M. G., Cortez, M., and Yoshida, N. (2008). A recombinant protein based on Trypanosoma cruzi surface molecule gp82 induces apoptotic cell death in melanoma cells. *Melan. Res.* 18, 172–183. doi: 10.1097/CMR.0b013e3282feeaab

Axley, P., Ahmed, Z., Ravi, S., and Singal, A. K. (2018). Review Article Hepatitis C Virus and Hepatocellular Carcinoma: A Narrative Review. *J. clin. Transl. Hepatol.* 6, 79–84. doi: 10.14218/JCTH.2017.00067

Balkwill, F. (2004). The significance of cancer cell expression of the chemokine receptor CXCR4. *Sem. Cancer Biol.* 14, 171–179. doi: 10.1016/j.semcancer.2003.10.003

Bendeck, M. P. (2004). Macrophage Matrix Metalloproteinase-9 Regulates Angiogenesis in Ischemic Muscle. *Circul. Res.* 94, 138–139. doi: 10.1161/01.RES.0000117525.23089.1A

Bu, Y., and Zhao, D. (2020). Luteolin retards CXCL12-induced Jurkat cells migration by disrupting transcription of CXCR4. *Exp. Mol. Pathol.* 113:104370. doi: 10.1016/j.yexmp.2020.104370

Chan, S. L., Wong, V. W. S., Qin, S., Chan, H. L. Y., Chan, S. L., and Wong, V. W. S. (2016). Infection and Cancer: The Case of Hepatitis B. *J. Clin. Oncol.* 34, 83–90. doi: 10.1200/JCO.2015.61.5724

Chatterjje, M., and Gawaz, M. (2013). Platelet-derived CXCL12 (SDF-1a): basic mechanisms and clinical implications. *J. Throm. Haemos.* 11, 1954–1967. doi: 10.1111/jth.12404

Chen, L., He, Z., Qin, L., Li, Q., Shi, X., Zhao, S., et al. (2011). Antitumor effect of malaria parasite infection in a murine lewis lung cancer model through induction of innate and adaptive immunity. *PLoS One* 6. doi: 10.1371/journal.pone.0024407

Cojoc, M., Peitzsch, C., Trautmann, F., Polishchuk, L., Telegeev, G. D., and Dubrovska, A. (2013). Emerging targets in cancer management: role of the CXCL12 / CXCR4 axis. *Onco. Target. Ther.* 30, 1347–1361. doi: 10.2147/OTT.S36109

Darani, H. Y., and Yousefi, M. (2012). Parasites and cancers: parasite antigens as possible targets for cancer immunotherapy. *Fut. Oncol.* 8, 1529–1535. doi: 10.2217/fon.12.155

Den Brok, W. D., Speers, C. H., Gondara, L., Baxter, E., Tyldesley, S. K., and Lohrisch, C. A. (2017). Survival with metastatic breast cancer based on initial presentation, de novo versus relapsed. *Breast Cancer Res. Treat*. 161, 549–556. doi: 10.1007/s10549-016-4080-9

Hung, C., Hsu, Y., Chen, T., Chang, C., and Lee, M. (2017). Cyclophosphamide promotes breast cancer cell migration through CXCR4 and matrix metalloproteinases. *Cell Bio. Int.* 41, 345–352. doi: 10.1002/cbin.10726

Kim, J. O., Jung, S. S., Kim, S. Y., Tae, Y. K., Shin, D. W., Lee, J. H., et al. (2007). Inhibition of Lewis lung carcinoma growth by *Toxoplasma gondii* through induction of Th1 immune responses and inhibition of angiogenesis. *J. Korean Med. Sci.* 22, 38–46. doi: 10.3346/jkms.2007.22.s.s38

Krementsov, N. (2009). Trypanosoma cruzi, cancer and the Cold War. *Hist. Ciên. Saúde Mang.* 16, 75–94. doi: 10.1590/s0104-59702009000500005

Kümper, S., Mardakheh, F. K., McCarthy, A., Yeo, M., Stamp, G. W., Paul, A., et al. (2016). Rho-associated kinase (ROCK) function is essential for cell cycle progression, senescence and tumorigenesis. *Elife* 5, 1–24. doi: 10.7554/eLife.12203.001

Liekens, S., Schols, D., and Hatse, S. (2010). CXCL12-CXCR4 Axis in Angiogenesis, Metastasis and Stem Cell Mobilization. *Curr. Pharm. Des.* 16, 3903–3920. doi: 10.2174/138161210794455003

Liu, T., Li, X., You, S., Bhuyan, S. S., and Dong, L. (2016). Effectiveness of AMD3100 in treatment of leukemia and solid tumors: from original discovery to use in current clinical practice. *Exp. Hematol. Oncol.* 5:1. doi: 10.1186/s40164-016-005055

Lu, G., Zhou, J., Zhao, Y., Li, Q., Gao, Y., Wang, L., et al. (2019). Transcriptome Sequencing Investigated the Tumor-Related Factors Changes After T . *gondii Infection*. *Front. microbiol.* 10:181. doi: 10.3389/fmicb.2019.00181

Lukasiewicz, K., and Fol, M. (2018). Microorganisms in the Treatment of Cancer: advantages and Limitations. *J. Immunol. Res.* doi: 10.1155/2018/2397808

Martel, C., De, Ferlay, J., Franceschi, S., Vignat, J., Bray, F., et al. (2008). Global burden of cancers attributable to infections in 2008?. *Lancet Oncol.* 13, 607–615. doi: 10.1016/S1470-2045(12)701370137

Martins, F. A., Alves, M., Santos, J. D. G., Alves, A., Borges, B. C., Spirandelli, M., et al. (2020). The Recombinant Form of Trypanosoma cruzi P21 Controls Infection by Modulating Host Immune Response. *Front. Immunol.* 11, 1–17. doi: 10.3389/fimmu.2020.01010

Mohamadi, F., Shakibapour, M., and Sharafi, S. M. (2019). Anti- Toxoplasma gondii antibodies attach to mouse cancer cell lines but not normal mouse lymphocytes. *Biomed. Rep.* 10, 183–188. doi: 10.3892/br.2019.1186

Mucci, J., Risso, M. G., Leguizamón, M. S., Frasch, A. C. C., and Campetella, O. (2006). The trans sialidase from Trypanosoma cruzi triggers apoptosis by target cell sialylation. *Cell Microbiol.* 8, 1086–1095. doi: 10.1111/j.1462-5822.2006.00689.x

Müller, A., Homey, B., Soto, H., Ge, N., Catron, D., Buchanan, M. E., et al. (2001). Involvement of chemokine receptors in breast cancer metastasis. *Nature* 410, 50–56. doi: 10.1038/35065016

Neel, N. F., Schutyser, E., Sai, J., Fan, G., and Richmond, A. (2005). Chemokine receptor internalization and intracellular trafficking. *Cytokine Growth Factor Rev.* 16, 637–658. doi: 10.1016/j.cytogfr.2005.05.008

Pierozan, P., Jerneren, F., and Karlsson, O. (2018). Perfluorooctanoic acid (PFOA) exposure promotes proliferation, migration and invasion potential in human breast epithelial cells. *Arch. Toxicol.* 92, 1729–1739. doi: 10.1007/s00204-018-21812184

Plumelle, Y., Gonin, C., and Edouard, A (1997). Effect of *Strongyloides stercoralis* infection and eosinophilia on age at onset and prognosis of adult T-cell leukemia. *Am. J. Clin. Pathol.* 107, 81–87. doi: 10.1093/ajcp/107.1.81

Qin, L., Qin, J., Zhen, X., Yang, Q., and Huang, L. (2018). Biomedicine & Pharmacotherapy Curcumin protects against hepatic stellate cells activation and migration by inhibiting the CXCL12 / CXCR4 biological axis in liver fibrosis: A study in vitro and in vivo. *Biomed. Pharmacother.* 101, 599–607. doi: 10.1016/j.biopha.2018.02.091

Ramírez, G., Valck, C., Aguilar, L., Kemmerling, U., López-mu, R., Cabrera, G., et al. (2012). Roles of Trypanosoma cruzi calreticulin in parasite-host interactions and in tumor growth. *Mol. Immunol.* 52, 133–140. doi: 10.1016/j.molimm.2012.05.006

Riaz, A. (2019). Immunotherapeutic Potential of Plasmodium Against Cancer by Inducing Immunomodulation. *IJAR* 70, 8–18. doi: 10.7176/ALST

Rodrigues, A. A., Clemente, T. M., dos Santos, M. A., Machado, F. C., Gomes, R. G. B., Moreira, H. H. T., et al. (2012). A Recombinant Protein Based on Trypanosoma cruzi P21 Enhances Phagocytosis. *PLoS One* 7, 1–9. doi: 10.1371/journal.pone.0051384

Santos, M. A., Dos, Teixeira, F. B., Moreira, H. H. T., Rodrigues, A. A., Machado, F. C., et al. (2014). A successful strategy for the recovering of active P21, an insoluble recombinant protein of trypanosoma cruzi. *Sci. Rep.* 4, 1–6. doi: 10.1038/srep04259

Schiffman, M., Castle, P. E., Jeronimo, J., Rodriguez, A. C., and Wacholder, S. (2007). Human papillomavirus and cervical cancer. *Lancet* 370, 890–907. doi: 10.1016/S0140-6736(07)61416-0

Silva, C. V., Kawashita, S. Y., Probst, C. M., Dallagiovanna, B., Cruz, M. C., da Silva, E. A., et al. (2009). Characterization of a 21 kDa protein from Trypanosoma cruzi associated with mammalian cell invasion. *Microb. Infect.* 11, 563–570. doi: 10.1016/j.micinf.2009.03.007

Sun, Y. X., Schneider, A., Jung, Y., Wang, J., Dai, J., Wang, J., et al. (2009). Skeletal Localization and Neutralization of the SDF-1(CXCL12)/CXCR4 Axis Blocks Prostate Cancer Metastasis and Growth in Osseous Sites In Vivo. *J. Bone Min. Res.* 20, 318–329. doi: 10.1359/JBMR.041109

Tanaka, T., Bai, Z., Srinoulprasert, Y., Yang, B. G., Hayasaka, H., and Miyasaka, M. (2005). Chemokines in tumor progression and metastasis. *Cancer Sci.* 96, 317–322. doi: 10.1111/j.1349-7006.2005.00059.x

Teicher, B. A., and Fricker, S. P. (2010). CXCL12 (SDF-1)/ CXCR4 Pathway in Cancer. *Clin. Cancer Res.* 16, 2927–2932. doi: 10.1158/1078-0432.CCR-092329

Teixeira, S. C., Lopes, D. S., Natalie, S., Gimenes, C., Teixeira, T. L., Santos, M., et al. (2017). Mechanistic Insights into the Anti- angiogenic Activity of Trypanosoma cruzi Protein 21 and its Potential Impact on the Onset of Chagasic Cardiomyopathy. *Sci. Rep.* 7:44978. doi: 10.1038/srep44978

Teixeira, T. L., Machado, F. C., Alves, da Silva, A., Teixeira, S. C., Borges, B. C., et al. (2015). Trypanosoma cruzi P21: a potential novel target for chagasic cardiomyopathy therapy. *Sci. Rep.* 5:16877. doi: 10.1038/srep16877

Ubillos, L., Freire, T., Berriel, E., Chiribao, M. L., Chiale, C., Festari, M. F., et al. (2016). Trypanosoma cruzi extracts elicit protective immune response against chemically induced colon and mammary cancers. *Int. J. Cancer* 138, 1719–1731. doi: 10.1002/ijc.29910

Valck, C., Ramı, G., Rodrı, M., Ribeiro, C., Lo, N. C., Maldonado, I., et al. (2010). Antiangiogenic and Antitumor Effects of Trypanosoma cruzi Calreticulin. *PLoS Negl. Trop. Dis.* 4, 1–9. doi: 10.1371/journal.pntd.0000730

Venkitaraman, R. (2010). Triple-negative/basal-like breast cancer: Clinical, pathologic and molecular features. *Exp. Rev. Anti. Ther.* 10, 199–207. doi: 10.1586/ERA.09.189

Voduc, K. D., Cheang, M. C. U., Tyldesley, S., Gelmon, K., Nielsen, T. O., and Kennecke, H. (2010). Breast cancer subtypes and the risk of local and regional relapse. *J. Clin. Oncol.* 28, 1684–1691. doi: 10.1200/JCO.2009.24.9284

Weigelt, B., Peterse, J. L., and Van't Veer, L. J. (2005). Breast cancer metastasis: Markers and models. *Nat. Rev. Cancer* 5, 591–602. doi: 10.1038/nrc1670

Whisner, C. M., and Aktipis, C. A. (2019). The Role of the Microbiome in Cancer Initiation and Progression: How Microbes and Cancer Cells Utilize Excess Energy and Promote One Another's Growth. *Curr. Nutr. Rep.* 8, 42–51. doi: 10.1007/s13668-019-0257252

Zhigunova, A. V., Kravtsov, E. G., Yashina, N. V., Dalin, M. V., and Karpenko, L. P. (2013). Effects of Specific Antibodies and Immunocompetent Cells on Tumor Growth in Passive Transfer Experiment. *Bull. Exp. Biol. Med.* 154, 762–764. doi: 10.1007/s10517-013-2050-3

Zhou, K. X., Xie, L. H., Peng, X., Guo, Q. M., Wu, Q. Y., Wang, W. H., et al. (2018). CXCR4 antagonist AMD3100 enhances the response of MDA-MB-231 triple-negative breast cancer cells to ionizing radiation. *Cancer Lett.* 418, 196–203. doi: 10.1016/j.canlet.2018.01.009

Zuo, J., Wen, M., Li, S. A. I., Lv, X. I. U., Wang, L. E. I., Ai, X., et al. (2017). Overexpression of CXCR4 promotes invasion and migration of non-small cell lung cancer via EGFR and MMP – 9. *Oncol. Lett.* 14, 7513–7521. doi: 10.3892/ol.2017.7168

Conflict of Interest: The authors declare that the research was conducted in the absence of any commercial or financial relationships that could be construed as a potential conflict of interest.

frontiers in Cell and Developmental Biology

ORIGINAL RESEARCH
published: 26 October 2020
doi: 10.3389/fcell.2020.570484

Fine Particulate Matter Exposure Alters Pulmonary Microbiota Composition and Aggravates Pneumococcus-Induced Lung Pathogenesis

Yu-Wen Chen[1†], Shiao-Wen Li[2†], Chia-Der Lin[3†], Mei-Zi Huang[1], Hwai-Jeng Lin[4,5], Chia-Yin Chin[2], Yi-Ru Lai[1], Cheng-Hsun Chiu[1,6], Chia-Yu Yang[1,2,7] and Chih-Ho Lai[1,3,6,8]**

[1] Department of Microbiology and Immunology, Graduate Institute of Biomedical Sciences, College of Medicine, Chang Gung University, Taoyuan, Taiwan, [2] Molecular Medicine Research Center, Chang Gung University, Taoyuan, Taiwan, [3] Department of Otolaryngology-Head and Neck Surgery, School of Medicine, China Medical University and Hospital, Taichung, Taiwan, [4] Division of Gastroenterology and Hepatology, Department of Internal Medicine, Shuang-Ho Hospital, New Taipei, Taiwan, [5] Division of Gastroenterology and Hepatology, Department of Internal Medicine, School of Medicine, College of Medicine, Taipei Medical University, Taipei, Taiwan, [6] Molecular Infectious Disease Research Center, Department of Pediatrics, Chang Gung Memorial Hospital, Linkou, Taiwan, [7] Department of Otolaryngology-Head and Neck Surgery, Chang Gung Memorial Hospital, Taoyuan, Taiwan, [8] Department of Nursing, Asia University, Taichung, Taiwan

OPEN ACCESS

Edited by:
Davide Gibellini, University of Bologna, Italy

Reviewed by:
Laurent Pierre Nicod, University of Lausanne, Switzerland
Leah Cuthbertson, Imperial College London, United Kingdom

***Correspondence:**
Chia-Yu Yang
chiayu-yang@mail.cgu.edu.tw
Chih-Ho Lai
chlai@mail.cgu.edu.tw

[†] These authors have contributed equally to this work

Specialty section:
This article was submitted to Molecular Medicine, a section of the journal Frontiers in Cell and Developmental Biology

Received: *08 June 2020*
Accepted: *14 September 2020*
Published: *26 October 2020*

Citation:
Chen Y-W, Li S-W, Lin C-D, Huang M-Z, Lin H-J, Chin C-Y, Lai Y-R, Chiu C-H, Yang C-Y and Lai C-H (2020) Fine Particulate Matter Exposure Alters Pulmonary Microbiota Composition and Aggravates Pneumococcus-Induced Lung Pathogenesis. Front. Cell Dev. Biol. 8:570484. doi: 10.3389/fcell.2020.570484

Exposure to fine particulate matter (PM) with aerodynamic diameter $\leq$2.5 μm ($PM_{2.5}$) is closely correlated with respiratory diseases. Microbiota plays a key role in maintaining body homeostasis including regulation of host immune status and metabolism. As reported recently, $PM_{2.5}$ exposure causes microbiota dysbiosis and thus promotes disease progression. However, whether $PM_{2.5}$ alters pulmonary microbiota distribution and aggravates bacteria-induced pathogenesis remains unknown. In this study, we used mouse experimental models of $PM_{2.5}$ exposure combined with *Streptococcus pneumonia* infection. We characterized the airway microbiota of bronchoalveolar lavage fluid (BALF) by sequencing the 16S rRNA V3–V4 amplicon on the Illumina MiSeq platform, followed by a combination of bioinformatics and statistical analyses. Shannon-diversity index, observed ASVs, and Fisher's diversity index indicated that microbiota richness was significantly decreased in the mice treated with either $PM_{2.5}$ or pneumococcus when compared with the control group. The genera *Streptococcus*, *Prevotella*, *Leptotrichia*, and *Granulicatella* were remarkably increased in mice exposed to $PM_{2.5}$ combined with pneumococcal infection as compared to mice with pneumococcal infection alone. Histopathological examination exhibited that a more pronounced inflammation was present in lungs of mice treated with $PM_{2.5}$ and pneumococcus than that in mouse groups exposed to either $PM_{2.5}$ or pneumococcal infection alone. Our results demonstrate that $PM_{2.5}$ alters the microbiota composition, thereby enhancing susceptibility to pneumococcal infection and exacerbating lung pathogenesis.

Keywords: $PM_{2.5}$, pulmonary inflammation, microbiota, pneumococcus, pathogenesis

INTRODUCTION

Air pollution is the cause and aggravating factor of many respiratory diseases, including respiratory infections, allergies, asthma, and chronic obstructive pulmonary disease (COPD) (Feng et al., 2016). Particles and gases are the major air pollution components that invade into the human lungs during respiration (Falcon-Rodriguez et al., 2016). These particles with an aerodynamic diameter $\leq$2.5 μm ($PM_{2.5}$) can penetrate and deposit in the bronchi and can affect human health, leading to severe consequences such as respiratory and cardiovascular diseases (Madrigano et al., 2013; Habre et al., 2014; Guo et al., 2018; Zhao et al., 2020). More importantly, $PM_{2.5}$ exposure has been linked to increased cardiopulmonary diseases and other related mortalities (Gehring et al., 2015; Pope et al., 2019), indicating that they pose a potent public health risk.

Pneumococcal pneumonia, caused by *Streptococcus pneumoniae*, which is a Gram-positive bacterium with the shape of diplococci. Pneumococcal infection often occurred in children with high morbidity and mortality, and the incidence of community-acquired pneumonia increases with age (Neupane et al., 2010). Notably, air pollution is closely related to the occurrence of community-acquired pneumonia (Shears et al., 2020). However, the mechanism how particulate matter influences the host defenses against pneumococcal infection remains to be elucidated.

The bacterial community plays an important role in host physiology, such as defenses against pathogens, regulation of immune response, and modulation of metabolism (Shapiro et al., 2014; Liu et al., 2015). Alterations in the bacterial dynamic ecosystem can directly influence immune homeostasis and aggravate inflammatory diseases (Rakoff-Nahoum et al., 2004; Pascal et al., 2018). Recent studies have shown that $PM_{2.5}$ exposure causes bacterial community dysbiosis and exacerbate disease development (Mariani et al., 2018; Qin et al., 2019; Wang et al., 2019). However, whether $PM_{2.5}$ influences respiratory microbiota distribution and facilitates bacterial infection remains unknown.

High-throughput 16S rRNA sequencing has been widely utilized to analyze the microbiota community in recent years. $PM_{2.5}$ exposure is reported to alter bacterial composition in the nasal pathway (Mariani et al., 2018), airway (Qin et al., 2019; Wang et al., 2019), and gut (Mutlu et al., 2018; Wang et al., 2018). However, the mechanisms by which $PM_{2.5}$ influences the microbiota community in lungs and enhances pathogenic bacterial infection in respiratory tract are unclear. For this purpose, a murine experimental model was established by exposing the mice to $PM_{2.5}$ for 3 weeks followed by pneumococcal infection. The BALF microbiota composition and altered metabolism in response to $PM_{2.5}$ exposure were analyzed. Our results indicated that $PM_{2.5}$ influences the microbiota composition that associated with pneumococcus-induced pulmonary pathogenesis.

MATERIALS AND METHODS

Cell and Bacterial Culture

Macrophage cell line RAW264.7 (ATCC TIB-71) cells were cultured in Dulbecco's Modified Eagle Medium (DMEM) supplemented with 10% complement-inactivated fetal bovine serum (FBS). Pneumococcus (*Streptococcus pneumoniae* strain TIGR4, ATCC BAA-334) was cultured on blood agar plates (Becton Dickinson, Sparks, MD, United States) as described previously (Lee et al., 2018). The bacteria were refreshed in Todd Hewitt Broth (Becton Dickinson) for 3 h and prepared for conducting the experiments in murine.

Macrophage Killing Assay

RAW264.7 (5×10^5) cells were suspended with $PM_{2.5}$ (5 or 20 μg/ml) and incubated at 37°C for 2 h. The cells were infected with pneumococcus at multiplicity of infection (MOI) of 100 for 30 min as described previously (Thevaranjan et al., 2018). The uninfected bacteria were removed, and the supernatant was collected from the following each 15 min and cultured on blood agar plates. Visible colony-forming units (CFU) were calculated, and macrophage killing activity was determined.

Animal Study

Male BALB/c mice (aged 6 weeks) were purchased from the National Laboratory Animal Center (Taipei, Taiwan). The animal studies were performed in accordance with the Animal Care and Use Guidelines for Chang Gung University under a protocol approved by the Institutional Animal Care Use Committee (IACUC Approval No.: CGU16-019). Three mice are housed in each cage and kept under normal conditions (21 ± 2°C and in a 12/12-h dark-light cycle) with sterile drinking water, feed, litter, and cages. Particulate matter with diameter smaller than 2.5 μm ($PM_{2.5}$) (RM8785) was purchased from the National Institute of Standards and Technology (Gaithersburg, MD, United States), as described previously (Klouda et al., 2005). Mice were divided into four groups for the treatments with PBS (control), $PM_{2.5}$, pneumococcus, and $PM_{2.5}$ + pneumococcus (six mice each group), respectively. $PM_{2.5}$ was administered by intratracheal (i.t.) instillation twice per week (six times for 3 weeks and for a total of 200 μg) (**Figure 1**). Mice were placed in the chambers for 4 days resting and then infected with pneumococcus by intranasal (i.n.) injection (1×10^8 CFU/10 μl). After infection for 48 h, the mice were euthanized and the BALF (n = 4) and lungs (n = 2) were prepared as described previously (Lin et al., 2014). During the experimental procedure, one mouse in the control treatment and one mouse in the pneumococcal infection group died and were excluded in the following studies. A total of 14 BALF samples were used for sequencing, including the groups control (n = 3), $PM_{2.5}$ (n = 4), pneumococcus (n = 3), and $PM_{2.5}$ + pneumococcus (n = 4).

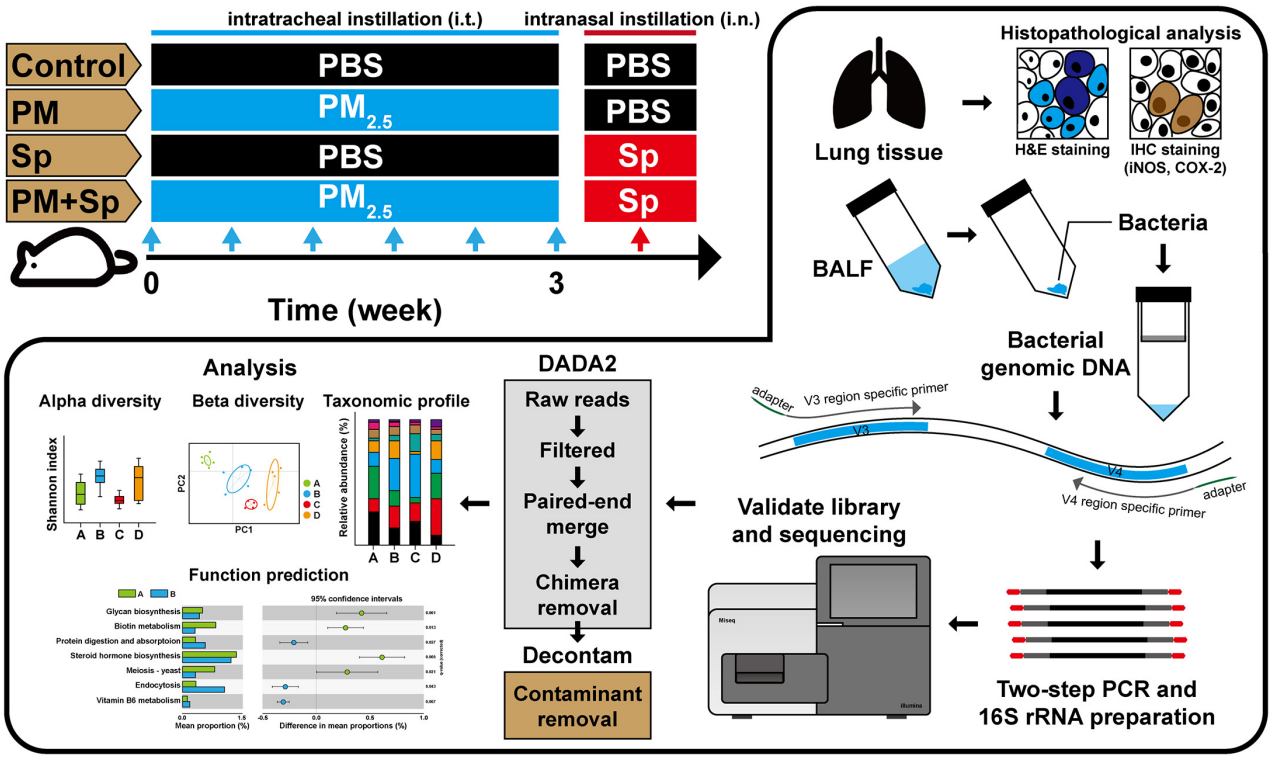

FIGURE 1 | Experimental design of the animal study. Mice were intratracheally administered $PM_{2.5}$ (for a total of 200 μg) and then pneumococcus-infected (1×10^8) via intranasal instillation. After pneumococcal infection for 48 h, the mice were euthanized. Their BALF were then prepared for microbiota analysis, and lung tissues were subjected to histopathological examination.

Histopathological Analysis

Lung tissues isolated from mice were washed with PBS and prepared for hematoxylin–eosin (H&E) and immunohistochemistry (IHC) staining as described previously (Chen et al., 2018). The lung sections were stained with the COX-2 and iNOS, respectively. The stained tissues were observed and examined using a microscope (AXIO IMAGER M2, Carl Zeiss, Germany) by a histopathologist with the scoring evaluation (Lin et al., 2014): 0, normal lung tissue; 1, slight erythrocyte infiltration (interstitium/parenchyma) and slight cell infiltration around the bronchi; 2, obvious erythrocyte infiltration, injured interstitial lung, and slight cell infiltration around the bronchi; 3, substantial erythrocyte infiltration which diffused the interstitium/parenchyma and caused the lung inflammation; and 4, severe inflammation with substantial erythrocyte/immune cell infiltration and obvious thickening bronchial wall.

Genomic DNA Extraction

The total bacterial genomic DNAs of BALF were extracted using the QIAamp DNA Microbiome Kit (Qiagen, Germantown, MD, United States) as per manufacturer's instructions as described previously (Yang et al., 2018). Briefly, the AHL buffer was used to lyse host cells and the nucleic acids were digested, followed by removing the host DNA. ATL buffer was added to the bacterial cells in a pathogen lysis tube L and vortexed using a TissueLyser LT. The bacterial genomic DNA was then eluted using nuclease-free water and stored at −80°C until the preparation of sequencing libraries.

16S rRNA Sequencing

The bacterial 16S rRNA V3–V4 regions were amplified by PCR using primers as described previously (Yang et al., 2018). There was no product generated on reagent-only controls after the PCR amplification. Illumina adaptor overhang nucleotide sequences were added to these gene-specific sequences. The sequences of primers are forward: 5'-TCGTCGGCAGCGTCAGATGTGTATAAGAGACAGCCTACG GGNGGCWGCAG-3'; and reverse: 5'-GTCTCGTGGGCTCGG AGATGTGTATAAGAGACAGGACTACHVGGGTATCTAA TCC-3' (Yang et al., 2018). Each PCR reaction mixture included bacterial genomic DNA (20 ng), aliquots of both forward and reverse primers (1 μM), and 1 × KAPA HiFi Hotstart Ready Mix. The first PCR program was performed with the following cycling: initial denaturation at 95°C for 3 min, followed by 30 cycles of denaturation at 95°C for 30 s, annealing at 55°C for 30 s, and extension at 72°C for 30 s; and a final 72°C extension for 10 min. The first PCR products of the 16S V3–V4 amplicons (~550 bp) were purified using AMPure XP beads (Beckman Coulter, Indianapolis, IN, United States) and subjected to index PCR. Each index PCR reaction mixture included the purified

first PCR products, Nextera XT index primer 1 and primer 2, and 1 × KAPA HiFi Hotstart Ready Mix. The index PCR program was performed with the following cycling: initial denaturation at 95°C for 3 min; 8 cycles of denaturation at 95°C for 30 s, annealing at 55°C for 30 s, extension at 72°C for 30 s, and a final extension at 72°C for 5 min. The index PCR products were purified by AMPure XP beads. The final amplicon libraries were validated using an HT DNA High Sensitivity LabChip kit (Caliper, PerkinElmer, MA, United States). The multiplexed amplified libraries were then sequenced using the Illumina MiSeq system (Illumina, San Diego, CA, United States). The raw sequence files supporting the findings of this article are available in the NCBI Sequence Read Archive under the BioProject ID PRJNA661979 (biosamples SAMN16072462 to SAMN16072475)[1].

Bioinformatic Analysis

The 16S rRNA V3–V4 sequencing reads were demultiplexed using MiSeq Reporter v2.6. The amplicon sequences were analyzed in accordance with MiSeq SOP (Kozich et al., 2013). 16S rRNA gene sequences were processed using the DADA2 pipeline to classify microbial constituents (Callahan et al., 2016). Following the DADA2 tutorial, paired-end sequences were separated through quality-filtering, dereplication, denoising, merging, and chimera removal. The quality-filtering step was performed with the filterAndTrim function in DADA2, and we used standard filtering parameters: maxN = 0, truncQ = 2, rm.phix = TRUE, and maxEE = 2. The truncate forward and reverse sequences were defined at positions 290 and 220, respectively, and the first 13 bases of each sequence were trimmed. A total of 1,521,645 sequences were used to construct amplicon sequence variants (ASVs), and ASVs comprising fewer than two reads were filtered from the dataset. The "Decontam" frequency method was used for contaminant removal by correlation with DNA concentration (Davis et al., 2018). As a result, 2,363 ASVs with quality-filtered sequences were obtained. A Naïve Bayes classifier was trained using the most recent available version of Silva (version 132) sequences for taxonomy assignment for each ASV through the assigned Taxonomy function (Wang et al., 2007). Comparison of species richness (observed ASVs, Shannon index, and Fisher's index) between different groups was determined with phyloseq (McMurdie and Holmes, 2013). Beta diversity was performed using weighted Unifrac phylogenetic distance matrices (Lozupone and Knight, 2005). Two-dimensional PCoA plots to visualize bacterial community populations between two groups were generated with phyloseq. A PERMANOVA (α = 0.05) with 999 random permutations was performed to determine differences between groups using the function "Adonis" of the Vegan package. The microbial functionality profiles were predicted using PICRUSt2 (Douglas et al., 2020) to generate the Kyoto Encyclopedia of Genes and Genomes (KEGG) pathway based on 16S rRNA gene sequencing data. The predicted genes and their functions were aligned to the KEGG database, and the differences among groups were compared using STAMP (version 2.1.3). Two-side Welch's *t*-test and Benjamini–Hochberg FDR correction were employed for comparisons of two groups.

Statistical Analysis

Student's *t*-test was employed to analyze the statistical significance of the experimental results between two groups. The statistical analysis was performed by using the SPSS program (version 18.0 for windows, SPSS Inc., Chicago, IL, United States). A *p*-value less than 0.05 was considered statistically significant. Differential abundance analysis was using the Kruskal–Wallis to detect main effect differences followed by the Wilcoxon rank-sum test for pairwise comparisons, with a *P* value cutoff of 0.05 and a linear discriminant analysis (LDA) score of 3.0 for identifying discriminative features by LEfSe with default parameters (Segata et al., 2011). We used the cladogram functionality of LEfSe to illustrate differences in BALF microbiota composition between with and without $PM_{2.5}$ treatments. In the cladogram, differences between groups are illustrated at phyla, class, order, family, and genus levels.

RESULTS

$PM_{2.5}$ Exposure Influences Microbiota Profiles

Firstly, we investigated whether $PM_{2.5}$ exposure affected the microbiota community in the respiratory tract. Mice were divided into four groups consisting of animals treated with either PBS (control), $PM_{2.5}$, pneumococcus (Sp), or $PM_{2.5}$ + pneumococcus (PM + Sp). After completing the treatment, mice were euthanized and BALF were collected for analyzing bacterial profiles. The bacterial genomic DNA were purified and analyzed using PCR amplification targeting 16S rRNA V3–V4 amplicons. The average number of raw reads per sample was 169,417 in 14 BALF samples (**Supplementary Table 1**). We obtained a total of 1,517,437 high-quality filtered reads, or 107,926.4 ± 21,089.7 reads per participant. The reads were constructed into 2,363 ASVs, and the sequence variants were used in the taxonomic analysis. The ASVs were classified into known taxa (22 phyla, 38 classes, 68 orders, 110 families, 285 genera, and 201 species) and unclassified groups. Taxonomic and phylogenetic information on the ASVs was shown in **Supplementary Table 2**. As an initial step, we compared the bacterial diversity and composition of BALF in mice subjected to different treatments. The BALF microbiota communities in $PM_{2.5}$-exposure mice showed a significantly lower value of the Shannon-diversity index than the control group (**Figure 2A**). In addition, the two other richness factors, observed ASVs and Fisher index, were also decreased in mice exposed to $PM_{2.5}$ when compared with the control group (**Figures 2B,C**). Similarly, the microbiota communities in the pneumococcus infection group were less diverse than those in the control group. Next, the beta-diversity was assessed using principal coordinate analysis (PCoA) to determine the microbiota diversity in different groups. According to the weighted Unifrac distance calculation performed on microbiota profiles followed by the

[1].http://www.ncbi.nlm.nih.gov/bioproject/661979

Adonis test (p = 0.001 and R^2 = 0.48), the PCoA plot showed that the BALF bacterial compositions with spatial separations were varied among different groups (**Supplementary Figure 1**). These results suggest that the BALF microbiota communities were divergent among the control, $PM_{2.5}$, and/or pneumococcal treatment groups.

Alterations in Most Abundant Bacterial Taxa in $PM_{2.5}$-Treated Mice

The most abundant bacteria at the phylum and genus levels within groups were investigated. The dataset indicated a total of 6 phyla (frequency higher than 0.001 in four groups), and 5 of them accounted for 97% bacteria. In the control mice, the top five relatively abundant bacteria were *Firmicutes* (41.5 ± 2.6%), *Proteobacteria* (23.0 ± 1.9%), *Actinobacteria* (22.8 ± 3.7%), *Bacteroidetes* (5.5 ± 2.8%), and *Fusobacteria* (4.7 ± 1.0%) (**Figure 3A**). There was no significant difference in *Firmicutes* and *Proteobacteria* levels between the $PM_{2.5}$-exposed and pneumococcus-infected groups (**Figures 3B,C**). In pneumococcus-infected mice, *Actinobacteria* (28.5%, p = 0.0135) was increased but *Bacteroidetes* (2.3%, p = 0.0001) and *Fusobacteria* (3.0%, p < 0.0001) were decreased as compared with the control group (**Figures 3D-F**). In mice exposed to

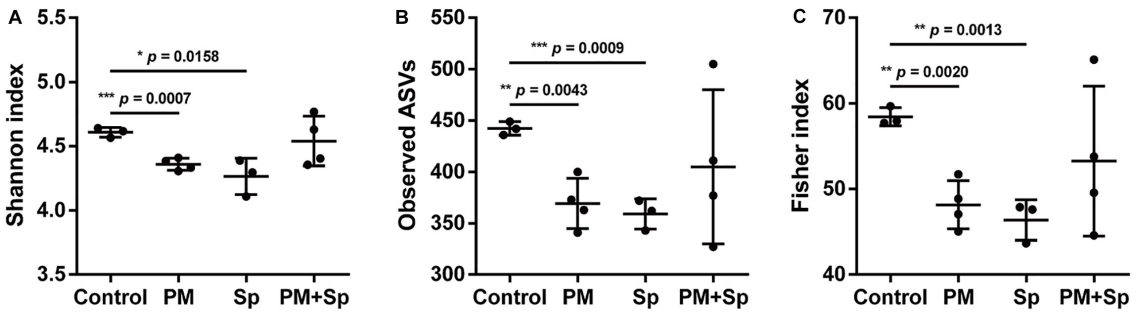

FIGURE 2 | $PM_{2.5}$ alters BALF microbiota communities. **(A)** Shannon-diversity index, **(B)** observed ASVs, and **(C)** Fisher's diversity index were conducted to assess microbiome diversity in BALF. Student's *t*-test was used to analyze the statistical significance of the experimental results between two groups. *P < 0.05; **P < 0.01; ***P < 0.001. PM, $PM_{2.5}$ exposure; Sp, pneumococcal infection.

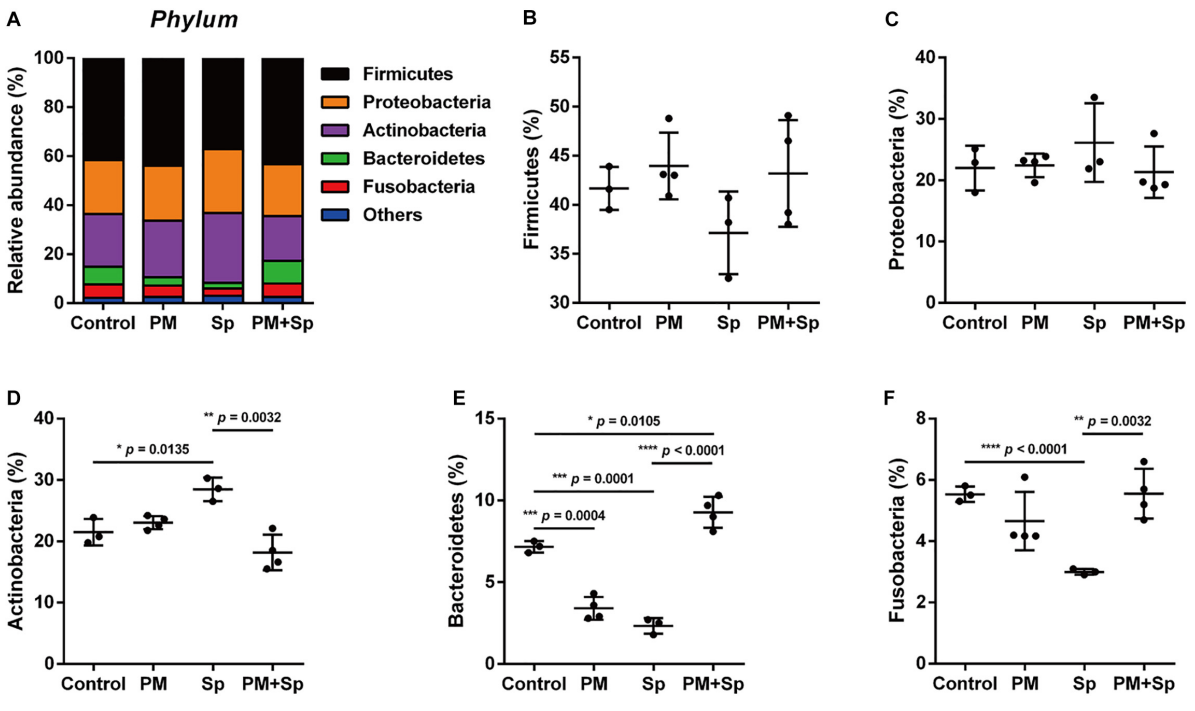

FIGURE 3 | Relative abundance of bacterial phyla in mice exposed to $PM_{2.5}$ and pneumococcus. The bacteria taxonomic profiles at the phylum level in BALF microbiota from $PM_{2.5}$-treated (PM) and/or pneumococcus-infected (Sp) mice. **(A)** The top 5 most abundant phyla in the four groups were shown. Relative abundances of **(B)** *Firmicutes*, **(C)** *Proteobacteria*, **(D)** *Actinobacteria*, **(E)** *Bacteroidetes*, and **(F)** *Fusobacteria* in the BALF microbiota community were analyzed. Student's *t*-test was used to analyze the statistical significance of the experimental results between two groups. *P < 0.05; **P < 0.01; ***P < 0.001.

$PM_{2.5}$, *Bacteroidetes* (3.4%, $p = 0.0004$) and *Fusobacteria* (4.7%, $p < 0.0001$) were decreased. Noticeably, *Actinobacteria* (18.2%, $p = 0.0032$) was decreased, but both *Bacteroidetes* (9.3%, $p < 0.0001$) and *Fusobacteria* (5.5%, $p = 0.0032$) were significantly higher in mice exposed to $PM_{2.5}$ + pneumococcus than in the pneumococcus-infected group.

The profiles of major microbiota at the genus level were further analyzed. Our data showed a total of 16 genera (all frequency higher than 0.01), of which the top 15 genera were identified (**Figure 4A** and **Supplementary Figure 2**). The 5 predominant genera were *Rothia* (12.0 ± 1.7%), *Halomonas* (7.1 ± 1.4%), *Streptococcus* (6.4 ± 3.2%), *Ezakiella* (6.0 ± 0.7%), and *Pelagibacterium* (5.8 ± 1.3%) in the control group. In the 15 genera of most relative abundance, 7 were significantly modulated among different treatment groups (**Figures 4B–H** and **Supplementary Figure 2**). In mice exposed to $PM_{2.5}$, 5 genera were altered, with an increase in 3 genera (*Lachnoanaerobaculum*, *Peptoniphilus*, and *Actinomyces*)

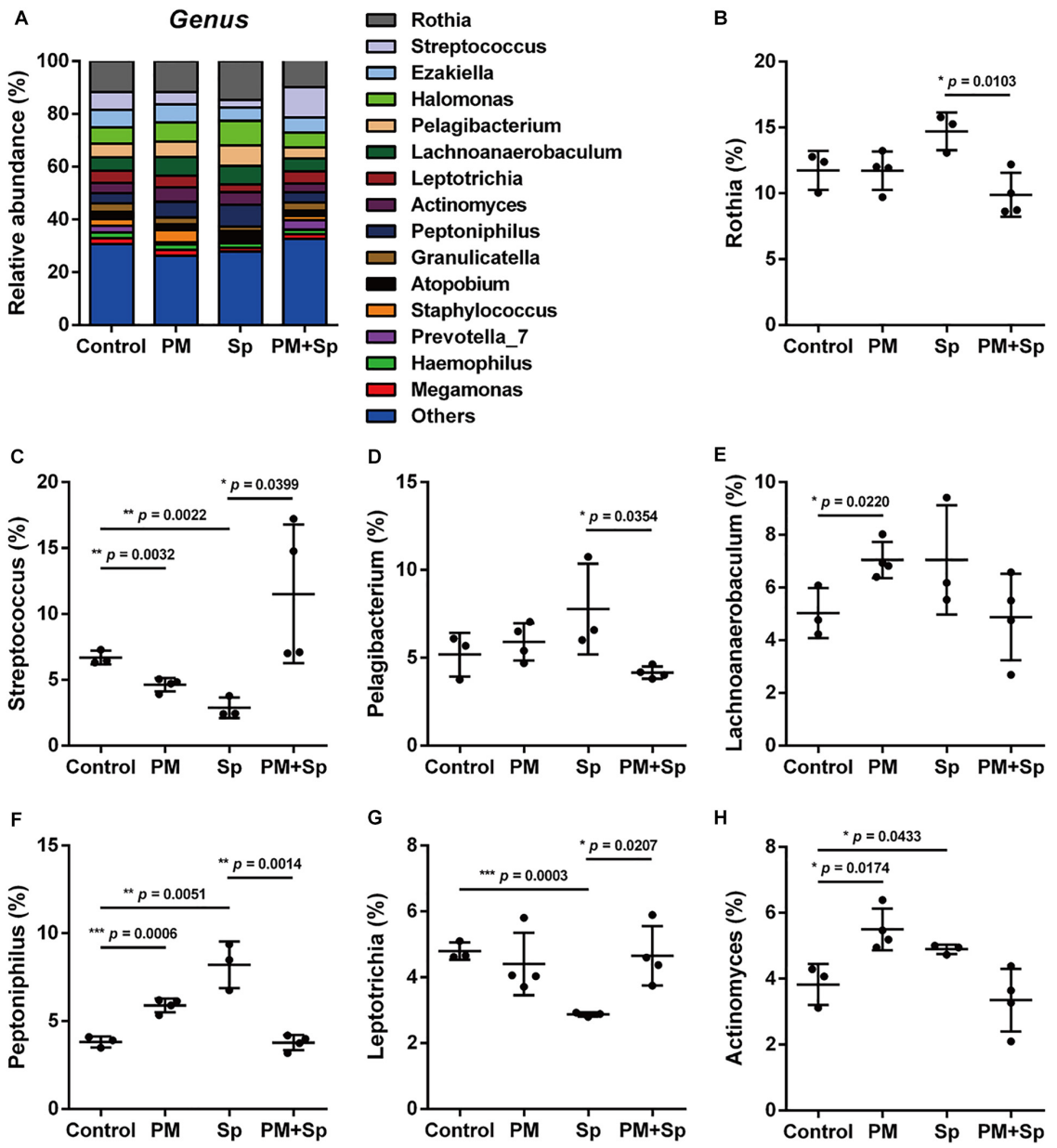

FIGURE 4 | Relative abundance of bacterial genera in mice treated with $PM_{2.5}$ and pneumococcus. The bacteria taxonomic profiles at the genus level in BALF microbiome from $PM_{2.5}$-treated (PM) and/or pneumococcus-infected (Sp) mice. **(A)** The top 15 most abundant genera among four groups were shown. Relative abundances of **(B)** *Rothia*, **(C)** *Streptococcus*, **(D)** *Pelagibacterium*, **(E)** *Lachnoanaerobaculum*, **(F)** *Peptoniphilus*, **(G)** *Leptotrichia*, and **(H)** *Actinomyces* in BALF microbiota community were analyzed. Student's *t*-test was used to analyze the statistical significance of the experimental results between two groups. $^{*}P < 0.05$; $^{**}P < 0.01$; $^{***}P < 0.001$.

($p < 0.05$), and a decrease in 2 genera (*Streptococcus* and *Prevotella*) ($p < 0.05$). Compared to the pneumococcus-infected group, mice exposed to $PM_{2.5}$ + pneumococcus showed changes in 8 genera, with an increase in 4 genera (*Streptococcus*, *Leptotrichia*, *Granulicatella*, and *Prevotella*) ($p < 0.05$) and a decrease in the 4 genera (*Rothia*, *Pelagibacterium*, *Peptoniphilus*, and *Atopobium*) ($p < 0.05$). These results indicate that microbial abundance was altered in mice treated with either $PM_{2.5}$ and/or pneumococcus.

$PM_{2.5}$ Alters Microbiota Composition

LEfSe analysis was performed to analyze the relatively enriched bacteria at genus and species levels among different groups. Many bacteria at the genus level were enriched in different groups; therefore, we selected a linear discriminant analysis (LDA) score higher than 3 or lower than -3 to represent the most significantly enriched genus in respective groups. As shown in **Figure 5A**, the relative abundances of *Actinomyces*, *Lachnoanaerobaculum*, *Peptoniphilus*, and *Murdochiella* were significantly increased in $PM_{2.5}$-exposed mice than in the control group. Notably, the relative abundance of *Streptococcus*, *Prevotella*, *Leptotrichia*, *Granulicatella*, *Porphyromonas*, and *Bacteroides* were mostly increased in mice co-treated with $PM_{2.5}$ and pneumococcus group than in the pneumococcus-infection alone group (**Figure 5B**). The specific enriched bacteria at the species level were then compared in $PM_{2.5}$-exposed to pneumococcus-uninfected or infected mice (**Supplementary Figure 3**). The significantly increased bacteria in the $PM_{2.5}$ + pneumococcus group were *Prevotella melaninogenica*, *Prevotella histicola*, *Veillonella dispar*, *Fusobacterium periodonticum*, and *Bacteroides coprocola* than in the pneumococcus-infection alone group. Moreover, the taxonomy and phylogenetic analysis were performed as cladogram. With $PM_{2.5}$ exposure, the microbiota richness was remarkably decreased than in the control group (**Figure 6A**). Furthermore, the enriched bacteria had notably different clusters in the $PM_{2.5}$ + pneumococcus group as compared to the pneumococcus-infection-alone group (**Figure 6B**). These results indicate that $PM_{2.5}$ exposure alters the microbiota composition and may increase the susceptibility of *Streptococcus* infection in mice.

Functional Prediction of BALF Microbiota

To understand the influence of the microbiota community on disease progression, the functions of bacterial communities were analyzed using Phylogenetic Investigation of Communities by Reconstruction of Unobserved States 2 (PICRUSt2). Glycan biosynthesis, glycan degradation, lipopolysaccharide biosynthesis, biotin, vitamin B6, linoleic acid, and nitrogen metabolisms were associated with $PM_{2.5}$ exposure (**Figure 7** and **Supplementary Figure 4**). Furthermore, the predominate pathways related to metabolisms such as glycan biosynthesis, glycan degradation, fatty acid biosynthesis, and several metabolisms were associated with $PM_{2.5}$ exposure followed by pneumococcal infection. These results indicate that

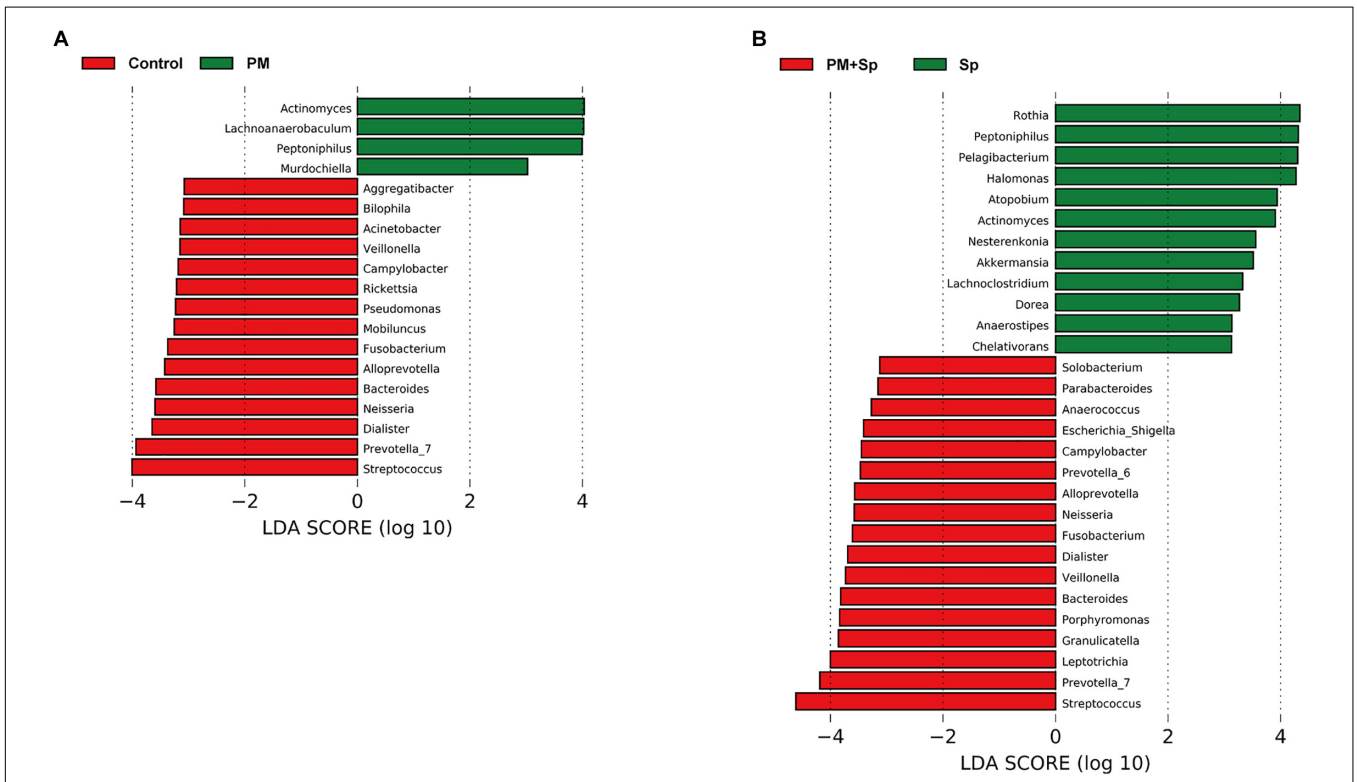

FIGURE 5 | The differentially enriched microbiota genus in mice exposed to $PM_{2.5}$ and pneumococcus. LEfSe analysis showed abundance of bacterial genus (LDA > 3) was altered as compared between **(A)** control and $PM_{2.5}$ (PM); **(B)** pneumococcus (Sp) and $PM_{2.5}$ + pneumococcus (PM + Sp), respectively.

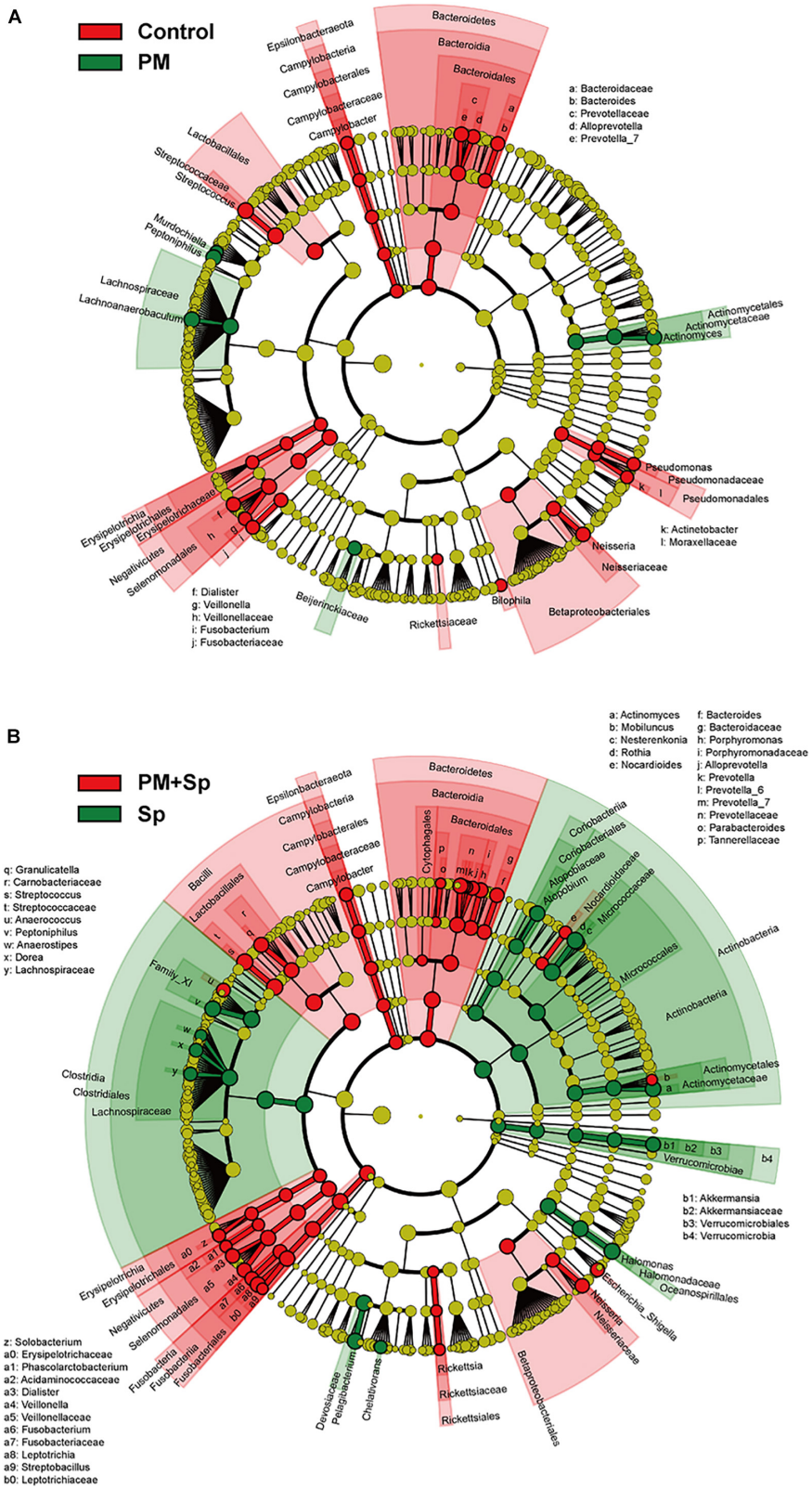

FIGURE 6 | Circular taxonomic and phylogenetic trees of microbiota diversity. Comparison of the taxonomy for the $PM_{2.5}$-exposed in uninfected and pneumococcus-infected mice. The taxonomy was analyzed and performed as cladogram. Compared the effect of $PM_{2.5}$ altered microbiota composition in panels **(A)** control and **(B)** pneumococcus-infected (Sp) mice. The relative color represented the more abundance bacterial taxonomy in each group.

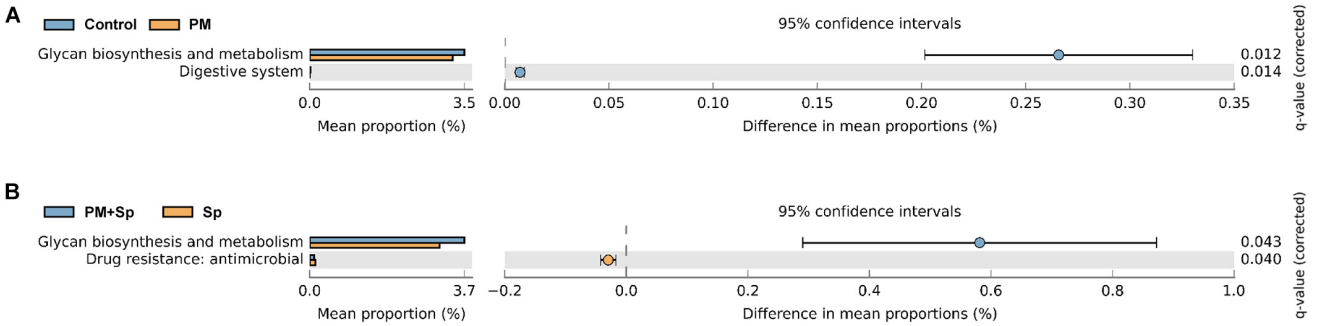

FIGURE 7 | Putative ecological functions of bacterial communities altered by $PM_{2.5}$ and pneumococcus. The functions of bacterial communities were analyzed based on PICRUSt2 by KEGG annotation at level 2. Comparison of the functional profiles between **(A)** $PM_{2.5}$-exposed (PM) and unexposed (control) mice; **(B)** pneumococcal infection (Sp) and $PM_{2.5}$ plus pneumococcus (PM + Sp) infection.

differentially abundant features in mice treated with $PM_{2.5}$ and pneumococcus were correlated with host metabolisms, which may lead to disease development.

$PM_{2.5}$ Exposure Combined With Pneumococcal Infection Exacerbated Pulmonary Pathogenesis

To further analyze whether $PM_{2.5}$ enhanced pneumococcus-induced pathogenesis in the lungs, mouse pulmonary tissues were prepared for histopathological analysis. As shown in **Figure 8A**, the lung tissue sections from the control group showed a clearly defined epithelium with healthy alveoli. $PM_{2.5}$ exposure or pneumococcal infection caused pronounced inflammatory cell infiltration around the bronchi. Noticeably, by treating with $PM_{2.5}$ plus pneumococcus, enhanced inflammation and exuded erythrocytes in the pulmonary parenchyma were observed. Furthermore, significant bronchial wall thickening was observed in mice exposed to $PM_{2.5}$ combined with pneumococcal infection than that in either $PM_{2.5}$ or pneumococcal infection alone (**Figure 8B**). In addition, IHC analysis showed that the expression levels of iNOS and COX-2 were increased in $PM_{2.5}$ + pneumococcus mice compared with the control group (**Supplementary Figure 5**). The total bacterial survivals were increased in cells pretreated with $PM_{2.5}$ when compared to the untreated cells (**Supplementary Figure 6**). Collectively, our results demonstrate that $PM_{2.5}$ exposure alters the airway microbiota community and aggravates pneumococcus-induced lung pathogenesis.

DISCUSSION

$PM_{2.5}$ exposure is reported to change microbiota composition in respiratory and intestinal tracts (Mariani et al., 2018; Mutlu et al., 2018; Wang et al., 2018, 2019; Qin et al., 2019). However, the association between $PM_{2.5}$ and airway microbiota and its influence on pathogenic infection has not been investigated. In this study, we hypothesized that $PM_{2.5}$ interferes with the airway ecosystem to influence the bacterial community and disrupts pulmonary function, leading to increased susceptibility to pneumococcal infection. By using 16S rRNA sequencing analysis with Shannon-diversity index, observed ASVs, and Fisher's diversity profiles, we observed that the abundance of BALF microbiota communities was decreased in both $PM_{2.5}$-exposure and $PM_{2.5}$ + pneumococcal infection groups than in control mice. It is known that resident microbiota contributes to host defense against pathogen infection (Liu et al., 2015). Once respiratory dysbiosis occurs, the fundamental roles performed by indigenous microbiota end up being modified, thereby leading to disease development (Marsland et al., 2013; Pascal et al., 2018). Intriguingly, the beta-diversity and cladogram indicated that the dominant community was similar in the control and PM + Sp groups. However, this restoration cannot be considered to suggest that the functions of microbiota were normal. Indeed, the histological analysis indicated severe pulmonary inflammation in mice with the combined treatment (PM + Sp). In addition, our recent study reported that macrophage functions were impaired by $PM_{2.5}$ exposure, which enhanced pneumococcal infectivity (Chen et al., 2020). These lines of evidence indicate that $PM_{2.5}$ alters the microbial ecosystem to benefit pneumococcus infection.

The predominant genera enriched in the $PM_{2.5}$ + pneumococcus group were *Streptococcus*, *Prevotella*, *Leptotrichia*, *Granulicatella*, *Porphyromonas*, and *Bacteroides*, which are involved in glycan biosynthesis and metabolism in compliance with the results from PICRUSt2 analysis (Thompson and Pikis, 2012; Zhou et al., 2016; Emerson and Weimer, 2017; Robinson et al., 2017). The bacterial cell wall is coated with diverse glycoproteins that help respond to the environment. They participate in biological processes like virulence and are linked to pathogenesis in the progression of many diseases (Tra and Dube, 2014; Williams et al., 2020). Intriguingly, the glycosylation process in *Streptococcus* is associated with the ability of adherence to the host and taking part in immune evasion (Schmidt et al., 2003). These findings indicated that glycan biosynthesis and metabolism are closely related to bacterial infectivity and pathogenesis. However, the mechanism underlying how the glycosylation process senses environmental factors requires further exploration.

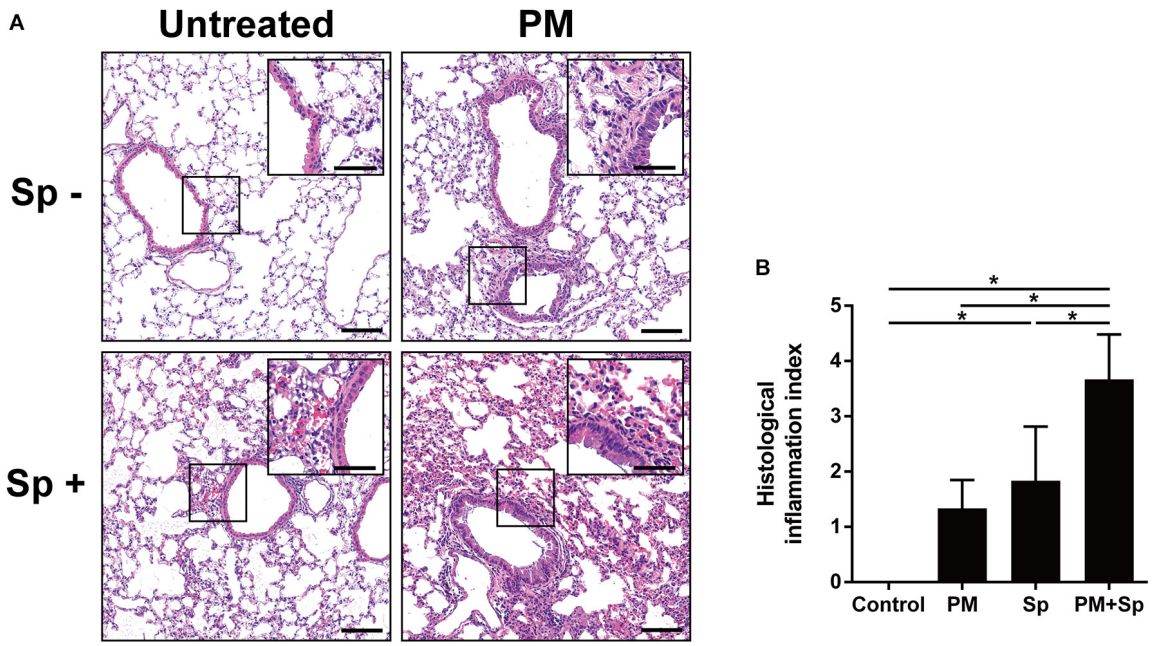

FIGURE 8 | $PM_{2.5}$ exposure aggravated pneumococcus-induced lung inflammation. **(A)** Lung tissues were subjected to H&E staining. The magnified images were shown in the inset from each cropped area. **(B)** The stained tissues were examined and scored. PM, $PM_{2.5}$ treatment; Sp, pneumococcal infection. Scale bar in each panel, 100 μm, and in each inset, 50 μm.

The genera observed in our study were similar to those observed in humans who smoked and were exposed to air pollution (Hosgood et al., 2014; Shen et al., 2016; Li et al., 2019; Qin et al., 2019). Chronic $PM_{2.5}$ exposure altered microbiota richness and induced abnormalities in glucose homeostasis (Li et al., 2020), which correlated with diabetes development (Liu et al., 2018, 2019). Although these studies revealed the link between $PM_{2.5}$ and glucose-metabolic effects, the underlying mechanism of microbiota in the regulation of host glucose homeostasis needs further investigations.

Short-chain fatty acids and lipid metabolites produced from commensal microbiota are shown to impair the inflammatory responses and promote disease development, including asthma, colitis, and intestine atherosclerosis (Maslowski et al., 2009). Moreover, the recognition of commensal bacteria-derived products by toll-like receptors is an important line in intestine homeostasis (Rakoff-Nahoum et al., 2004). These findings indicate the importance of the metabolites in influencing the commensal microbiota to cause diseases. In addition to regulating metabolism, our study also calls attention to the role of the modulation in resident bacterial genera in infectious disease and pathogenesis. For instance, *Streptococcus*, a Gram-positive coccus, is the most common cause of human respiratory diseases and several diseases are associated with *S. pneumoniae* infection, including bacteremia, meningitis, and pneumonia, a lower respiratory tract disease (Wardlaw et al., 2006). Notably, *Streptococcus* was abundant in patients infected with *Mycobacterium tuberculosis* and influenza virus (De Lastours et al., 2016; Ding et al., 2019; Eshetie and van Soolingen, 2019). For genera *Bacteroides* and *Prevotella*, which are commonly observed in Gram-negative lung microbiota, a recent study demonstrated their role in promoting fibrotic pathogenesis through their outer membrane vesicle-mediated IL-17R signaling (Yang et al., 2019). In addition, *Leptotrichia* has been found in BALF as a potentially causative bacterium for severe pneumonia (Kawanami et al., 2009). These lines of evidence indicate that $PM_{2.5}$ alters the microbiota community and particularly enhances the clinically important bacteria, which may collectively participate in exacerbating lung pathogenesis.

Macrophages play a crucial role in the clearance of pathogens. We recently demonstrated that $PM_{2.5}$ adversely influences macrophage activity to enhance pneumococcal infectivity and exacerbate pulmonary pathogenesis (Chen et al., 2020). Our results showed that $PM_{2.5}$ impairs macrophage functions, such as phagocytosis and cytokine production, resulting in reduction in its bacterial clearance activity. In addition, $PM_{2.5}$ manipulates macrophage polarization by suppressing M1 macrophage markers and then subverts macrophage defense against bacterial infection, thereby aggravating inflammation. It is worth noting that $PM_{2.5}$ exposure altered the microbiota community and led to disease progression (Mariani et al., 2018; Qin et al., 2019). Although the commensal microbiota can protect from asthma and allergic responses (Kirjavainen et al., 2019), an aberrant microbiota community is correlated with airway diseases (Hoggard et al., 2017, 2018). Along with the results of previous reports, the outcomes of our present study reveal that $PM_{2.5}$ affects both immune defense and microbiota dysbiosis, thereby exacerbating pathogen infection in the respiratory tract.

Although this study provides evidence that $PM_{2.5}$ exposure-altered airway microbiota is associated with an increased

susceptibility of pneumococcal infection, some limitations exist. First, the sample size of each treatment group is small in the LEfSe analysis for characterizing the changed microbiota composition among different experimental groups. The features of LEfSe analysis included the tests of biological consistency and effect-size estimation, particularly given the small number of test samples (Segata et al., 2011; Goodrich et al., 2014). The inclusion of more mice in the future studies was required to reduce any bias in the sequencing analysis. Second, the detailed mechanism underlying the $PM_{2.5}$-altered microbiota community to induce pathogenesis was not explored in the current study. Third, the pathogenic patterns and $PM_{2.5}$ natural exposure ways are different between mice and human, and hence, a direct clinical study merits further investigation. Therefore, further studies of the samples isolated from patients with pneumococcal infection living in $PM_{2.5}$-exposed areas are required to support the clinical manifestations. Since the composition of indigenous microbiota is quite complicated and plays crucial roles in the regulation of human immunity, physiology, and metabolism, systemic human studies with extensive investigation of airway microbiota and the ecosystems in long-term exposure to $PM_{2.5}$ are warranted.

CONCLUSION

In summary, our results showed that $PM_{2.5}$ exposure is associated with a decrease of lung microbiota diversity. Further, the microbiota community is dynamically altered in response to $PM_{2.5}$ exposure followed by pneumococcal infection. The results from this study provide a better understanding of the adverse effects of $PM_{2.5}$ on the pulmonary microbiota community, which may enhance pathogen infection and aggravate lung pathogenesis.

DATA AVAILABILITY STATEMENT

The datasets presented in this study can be found in online repositories. The names of the repository/repositories and accession number(s) can be found in the article/**Supplementary Material.**

ETHICS STATEMENT

The animal study was reviewed and approved by Institutional Animal Care Use Committee, Chang Gung University (IACUC Approval No.: CGU16-019).

AUTHOR CONTRIBUTIONS

C-DL, C-HC, C-YY, and C-HL: conception or design of this work. Y-WC, S-WL, M-ZH, H-JL, and C-YC: experimental study. Y-WC, S-WL, and Y-RL: data analysis and interpretation. Y-WC, S-WL, C-DL, C-HC, C-YY, and C-HL: writing the manuscript. All authors contributed to the article and approved the submitted version.

FUNDING

This work was funded by the Ministry of Science and Technology (109-2320-B-182-025-MY3 and 109-2320-B-182-029-MY3), Chang Gung Memorial Hospital (CMRPD1F0431-3, CMRPD1I0061-3, CMRPD1J0021-3, CMRPD1K0361, and BMRPE90), and Tomorrow Medical Foundation.

ACKNOWLEDGMENTS

The authors would like to thank the editor and reviewers for the editorial assistance and their valuable comments. The authors sincerely appreciate the assistance for analyzing 16S rRNA sequences and bioinformatic analysis (Next Generation Sequencing Core, Bioinformatics Core, and Molecular Medicine Research Center, Chang Gung University, Taoyuan, Taiwan, CLRPD1J0012, EMRPD1K0281).

SUPPLEMENTARY MATERIAL

The Supplementary Material for this article can be found online at: https://www.frontiersin.org/articles/10.3389/fcell.2020.570484/full#supplementary-material

Supplementary Figure 1 | Comparison of BALF microbiota diversity. PCoA was conducted to analyze the BALF microbiota compositions in mice treated with control (red), $PM_{2.5}$ (PM, green), pneumococcus (Sp, purple), $PM_{2.5}$ + pneumococcus (PM + Sp, blue).

Supplementary Figure 2 | Relative abundance of bacterial genera in mice exposed to $PM_{2.5}$ and pneumococcus. The bacteria taxonomic profiles at genus level in BALF microbiota from $PM_{2.5}$-treated and/or pneumococcus-infected mice. Relative abundance of **(A)** *Halomonas*, **(B)** *Ezakiella*, **(C)** *Granulicatella*, **(D)** *Staphylococcus*, **(E)** *Atopobium*, **(F)** *Haemophilus*, **(G)** *Prevotella*, and **(H)** *Megamonas* in BALF microbiota were analyzed. Statistical significance was analyzed using the Student's *t*-test. $^{*}P < 0.05$; $^{**}P < 0.01$; $^{***}P < 0.001$; $^{***}P < 0.0001$. PM, $PM_{2.5}$ exposure; Sp, pneumococcal infection.

Supplementary Figure 3 | The differentially enriched bacterial species compared with $PM_{2.5}$ exposure and pneumococcus-infected mice. LEfSe analysis indicated the abundance bacterial species compared with **(A)** control and $PM_{2.5}$ exposure (PM); **(B)** pneumococcus (Sp) and $PM_{2.5}$ + pneumococcus (PM + Sp).

Supplementary Figure 4 | Putative functions of microbiota communities altered by $PM_{2.5}$ and pneumococcus. The functions of microbiota were predicted based PICRUSt2 by KEGG annotation at level 3. **(A)** Comparison of the functional profiles between **(A)** control and $PM_{2.5}$ exposure (PM); **(B)** pneumococcus (Sp) and $PM_{2.5}$ + pneumococcus (PM + Sp).

Supplementary Figure 5 | $PM_{2.5}$ exposure aggravated pneumococcus-induced pulmonary inflammation. Mice were euthanized and lung tissues were subjected to immunohistochemical (IHC) staining with specific antibody against iNOS and COX-2 (original magnification: 200×). The magnified images are shown in the panel of each cropped area. Scale bar in each panel, 100 μm, and in each inset, 50 μm.

Supplementary Figure 6 | $PM_{2.5}$ suppresses macrophage clearance to increase bacterial survival. RAW264.7 cells were exposed to low (5 μg/ml) or high (20 μg/ml) doses of $PM_{2.5}$ for 2 h, and then incubated with and pneumococcus (MOI = 100) for the indication times. Total pneumococcal survival was determined and expressed as viable CFU. Results are represented mean ± standard deviation from triplicate independent experiments. Statistical significance was analyzed using the Student's *t*-test ($^{*}P < 0.05$ compared to $PM_{2.5}$-untreated group).

REFERENCES

Callahan, B. J., McMurdie, P. J., Rosen, M. J., Han, A. W., Johnson, A. J., and Holmes, S. P. (2016). DADA2: high-resolution sample inference from Illumina amplicon data. *Nat. Methods* 13, 581–583. doi: 10.1038/nmeth.3869

Chen, Y. A., Tzeng, D. T. W., Huang, Y. P., Lin, C. J., Lo, U. G., Wu, C. L., et al. (2018). Antrocin sensitizes prostate cancer cells to radiotherapy through inhibiting PI3K/AKT and MAPK Signaling Pathways. *Cancers* 11:34. doi: 10.3390/cancers11010034

Chen, Y. W., Huang, M. Z., Chen, C. L., Kuo, C. Y., Yang, C. Y., Chiang-Ni, C., et al. (2020). PM2.5 impairs macrophage functions to exacerbate pneumococcus-induced pulmonary pathogenesis. *Part Fibre Toxicol.* 17:37. doi: 10.1186/s12989-020-00362-2

Davis, N. M., Proctor, D. M., Holmes, S. P., Relman, D. A., and Callahan, B. J. (2018). Simple statistical identification and removal of contaminant sequences in marker-gene and metagenomics data. *Microbiome* 6:226. doi: 10.1186/s40168-018-0605-2

De Lastours, V., Malosh, R., Ramadugu, K., Srinivasan, U., Dawid, S., Ohmit, S., et al. (2016). Co-colonization by *Streptococcus pneumoniae* and *Staphylococcus aureus* in the throat during acute respiratory illnesses. *Epidemiol. Infect.* 144, 3507–3519. doi: 10.1017/S0950268816001473

Ding, T., Song, T., Zhou, B., Geber, A., Ma, Y., Zhang, L., et al. (2019). Microbial composition of the human nasopharynx varies according to influenza virus type and vaccination status. *mBio* 10:e01296-19. doi: 10.1128/mBio.01296-19

Douglas, G. M., Maffei, V. J., Zaneveld, J. R., Yurgel, S. N., Brown, J. R., Taylor, C. M., et al. (2020). PICRUSt2 for prediction of metagenome functions. *Nat. Biotechnol.* 38, 685–688. doi: 10.1038/s41587-020-0548-6

Emerson, E. L., and Weimer, P. J. (2017). Fermentation of model hemicelluloses by *Prevotella* strains and *Butyrivibrio fibrisolvens* in pure culture and in ruminal enrichment cultures. *Appl. Microbiol. Biotechnol.* 101, 4269–4278. doi: 10.1007/s00253-017-8150-7

Eshetie, S., and van Soolingen, D. (2019). The respiratory microbiota: new insights into pulmonary tuberculosis. *BMC Infect. Dis.* 19:92. doi: 10.1186/s12879-019-3712-1

Falcon-Rodriguez, C. I., Osornio-Vargas, A. R., Sada-Ovalle, I., and Segura-Medina, P. (2016). Aeroparticles, composition, and lung diseases. *Front. Immunol.* 7:3. doi: 10.3389/fimmu.2016.00003

Feng, S., Gao, D., Liao, F., Zhou, F., and Wang, X. (2016). The health effects of ambient PM2.5 and potential mechanisms. *Ecotoxicol. Environ. Saf.* 128, 67–74. doi: 10.1016/j.ecoenv.2016.01.030

Gehring, U., Beelen, R., Eeftens, M., Hoek, G., de Hoogh, K., de Jongste, J. C., et al. (2015). Particulate matter composition and respiratory health: the PIAMA Birth Cohort study. *Epidemiology* 26, 300–309. doi: 10.1097/EDE.0000000000000264

Goodrich, J. K., Di Rienzi, S. C., Poole, A. C., Koren, O., Walters, W. A., Caporaso, J. G., et al. (2014). Conducting a microbiome study. *Cell* 158, 250–262. doi: 10.1016/j.cell.2014.06.037

Guo, C., Zhang, Z., Lau, A. K. H., Lin, C. Q., Chuang, Y. C., Chan, J., et al. (2018). Effect of long-term exposure to fine particulate matter on lung function decline and risk of chronic obstructive pulmonary disease in Taiwan: a longitudinal, cohort study. *Lancet Planet Health* 2, e114–e125. doi: 10.1016/S2542-5196(18)30028-7

Habre, R., Moshier, E., Castro, W., Nath, A., Grunin, A., Rohr, A., et al. (2014). The effects of PM2.5 and its components from indoor and outdoor sources on cough and wheeze symptoms in asthmatic children. *J. Exp. Sci. Environ. Epidemiol.* 24, 380–387. doi: 10.1038/jes.2014.21

Hoggard, M., Biswas, K., Zoing, M., Wagner Mackenzie, B., Taylor, M. W., and Douglas, R. G. (2017). Evidence of microbiota dysbiosis in chronic rhinosinusitis. *Int. Forum Allergy Rhinol.* 7, 230–239. doi: 10.1002/alr.21871

Hoggard, M., Nocera, A., Biswas, K., Taylor, M. W., Douglas, R. G., and Bleier, B. S. (2018). The sinonasal microbiota, neural signaling, and depression in chronic rhinosinusitis. *Int. Forum Allergy Rhinol.* 8, 394–405. doi: 10.1002/alr.22074

Hosgood, H. D. III, Sapkota, A. R., Rothman, N., Rohan, T., Hu, W., Xu, J., et al. (2014). The potential role of lung microbiota in lung cancer attributed to household coal burning exposures. *Environ. Mol. Mutagen.* 55, 643–651. doi: 10.1002/em.21878

Kawanami, T., Fukuda, K., Yatera, K., Kido, T., Yoshii, C., Taniguchi, H., et al. (2009). Severe pneumonia with *Leptotrichia* sp. detected predominantly in bronchoalveolar lavage fluid by use of 16S rRNA gene sequencing analysis. *J. Clin. Microbiol.* 47, 496–498. doi: 10.1128/JCM.01429-08

Kirjavainen, P. V., Karvonen, A. M., Adams, R. I., Taubel, M., Roponen, M., Tuoresmaki, P., et al. (2019). Farm-like indoor microbiota in non-farm homes protects children from asthma development. *Nat. Med.* 25, 1089–1095. doi: 10.1038/s41591-019-0469-4

Klouda, G. A., Filliben, J. J., Parish, H. J., Chow, J. C., Watson, J. G., and Cary, R. A. (2005). Reference material 8785: air particulate matter on filter media. *Aerosol. Sci. Technol.* 39, 173–183. doi: 10.1080/027868290916453

Kozich, J. J., Westcott, S. L., Baxter, N. T., Highlander, S. K., and Schloss, P. D. (2013). Development of a dual-index sequencing strategy and curation pipeline for analyzing amplicon sequence data on the MiSeq Illumina sequencing platform. *Appl. Environ. Microbiol.* 79, 5112–5120. doi: 10.1128/AEM.01043-13

Lee, H. Y., Wu, T. L., Su, L. H., Li, H. C., Janapatla, R. P., Chen, C. L., et al. (2018). Invasive pneumococcal disease caused by ceftriaxone-resistant *Streptococcus pneumoniae* in Taiwan. *J. Microbiol. Immunol. Infect.* 51, 500–509. doi: 10.1016/j.jmii.2016.12.004

Li, J., Hu, Y., Liu, L., Wang, Q., Zeng, J., and Chen, C. (2020). PM2.5 exposure perturbs lung microbiome and its metabolic profile in mice. *Sci. Total Environ.* 721:137432. doi: 10.1016/j.scitotenv.2020.137432

Li, K. J., Chen, Z. L., Huang, Y., Zhang, R., Luan, X. Q., Lei, T. T., et al. (2019). Dysbiosis of lower respiratory tract microbiome are associated with inflammation and microbial function variety. *Respir. Res.* 20:272. doi: 10.1186/s12931-019-1246-0

Lin, C. D., Kou, Y. Y., Liao, C. Y., Li, C. H., Huang, S. P., Cheng, Y. W., et al. (2014). Zinc oxide nanoparticles impair bacterial clearance by macrophages. *Nanomedicine* 9, 1327–1339. doi: 10.2217/nnm.14.48

Liu, C. M., Price, L. B., Hungate, B. A., Abraham, A. G., Larsen, L. A., Christensen, K., et al. (2015). *Staphylococcus aureus* and the ecology of the nasal microbiome. *Sci. Adv.* 1:e1400216. doi: 10.1126/sciadv.1400216

Liu, C. W., Lee, T. L., Chen, Y. C., Liang, C. J., Wang, S. H., Lue, J. H., et al. (2018). PM2.5-induced oxidative stress increases intercellular adhesion molecule-1 expression in lung epithelial cells through the IL-6/AKT/STAT3/NF-kappaB-dependent pathway. *Part Fibre Toxicol.* 15:4. doi: 10.1186/s12989-018-0240-x

Liu, T., Chen, X., Xu, Y., Wu, W., Tang, W., Chen, Z., et al. (2019). Gut microbiota partially mediates the effects of fine particulate matter on type 2 diabetes: evidence from a population-based epidemiological study. *Environ. Int.* 130:104882. doi: 10.1016/j.envint.2019.05.076

Lozupone, C., and Knight, R. (2005). UniFrac: a new phylogenetic method for comparing microbial communities. *Appl. Environ. Microbiol.* 71, 8228–8235. doi: 10.1128/AEM.71.12.8228-8235.2005

Madrigano, J., Kloog, I., Goldberg, R., Coull, B. A., Mittleman, M. A., and Schwartz, J. (2013). Long-term exposure to PM2.5 and incidence of acute myocardial infarction. *Environ. Health Perspect.* 121, 192–196. doi: 10.1289/ehp.1205284

Mariani, J., Favero, C., Spinazze, A., Cavallo, D. M., Carugno, M., Motta, V., et al. (2018). Short-term particulate matter exposure influences nasal microbiota in a population of healthy subjects. *Environ. Res.* 162, 119–126. doi: 10.1016/j.envres.2017.12.016

Marsland, B. J., Yadava, K., and Nicod, L. P. (2013). The airway microbiome and disease. *Chest* 144, 632–637. doi: 10.1378/chest.12-2854

Maslowski, K. M., Vieira, A. T., Ng, A., Kranich, J., Sierro, F., Yu, D., et al. (2009). Regulation of inflammatory responses by gut microbiota and chemoattractant receptor GPR43. *Nature* 461, 1282–1286. doi: 10.1038/nature08530

McMurdie, P. J., and Holmes, S. (2013). phyloseq: an R package for reproducible interactive analysis and graphics of microbiome census data. *PLoS One* 8:e61217. doi: 10.1371/journal.pone.0061217

Mutlu, E. A., Comba, I. Y., Cho, T., Engen, P. A., Yazici, C., Soberanes, S., et al. (2018). Inhalational exposure to particulate matter air pollution alters the composition of the gut microbiome. *Environ. Pollut.* 240, 817–830. doi: 10.1016/j.envpol.2018.04.130

Neupane, B., Jerrett, M., Burnett, R. T., Marrie, T., Arain, A., and Loeb, M. (2010). Long-term exposure to ambient air pollution and risk of hospitalization with community-acquired pneumonia in older adults. *Am. J. Respir. Crit. Care Med.* 181, 47–53. doi: 10.1164/rccm.200901-0160OC

Pascal, M., Perez-Gordo, M., Caballero, T., Escribese, M. M., Lopez Longo, M. N., Luengo, O., et al. (2018). Microbiome and allergic diseases. *Front. Immunol.* 9:1584. doi: 10.3389/fimmu.2018.01584

Pope, C. A. III., Lefler, J. S., Ezzati, M., Higbee, J. D., Marshall, J. D., Kim, S.-Y., et al. (2019). Mortality risk and fine particulate air pollution in a large, representative cohort of U.S. *Adults. Environ. Health Perspect.* 127, 1–9.

Qin, T., Zhang, F., Zhou, H., Ren, H., Du, Y., Liang, S., et al. (2019). High-Level PM2.5/PM10 exposure is associated with alterations in the human pharyngeal microbiota composition. *Front. Microbiol.* 10:54. doi: 10.3389/fmicb.2019.00054

Rakoff-Nahoum, S., Paglino, J., Eslami-Varzaneh, F., Edberg, S., and Medzhitov, R. (2004). Recognition of commensal microflora by toll-like receptors is required for intestinal homeostasis. *Cell* 118, 229–241. doi: 10.1016/j.cell.2004.07.002

Robinson, L. S., Lewis, W. G., and Lewis, A. L. (2017). The sialate O-acetylesterase EstA from gut *Bacteroidetes* species enables sialidase-mediated cross-species foraging of 9-O-acetylated sialoglycans. *J. Biol. Chem.* 292, 11861–11872. doi: 10.1074/jbc.M116.769232

Schmidt, M. A., Riley, L. W., and Benz, I. (2003). Sweet new world: glycoproteins in bacterial pathogens. *Trends Microbiol.* 11, 554–561. doi: 10.1016/j.tim.2003.10.004

Segata, N., Izard, J., Waldron, L., Gevers, D., Miropolsky, L., Garrett, W. S., et al. (2011). Metagenomic biomarker discovery and explanation. *Genome Biol.* 12:R60. doi: 10.1186/gb-2011-12-6-r60

Shapiro, H., Thaiss, C. A., Levy, M., and Elinav, E. (2014). The cross talk between microbiota and the immune system: metabolites take center stage. *Curr. Opin. Immunol.* 30, 54–62. doi: 10.1016/j.coi.2014.07.003

Shears, R. K., Jacques, L. C., Naylor, G., Miyashita, L., Khandaker, S., Lebre, F., et al. (2020). Exposure to diesel exhaust particles increases susceptibility to invasive pneumococcal disease. *J. Allergy Clin. Immunol.* 145, 1272.e6–1284.e6. doi: 10.1016/j.jaci.2019.11.039

Shen, P., Morissette, M. C., Vanderstocken, G., Gao, Y., Hassan, M., Roos, A., et al. (2016). Cigarette smoke attenuates the nasal host response to *Streptococcus pneumoniae* and predisposes to invasive pneumococcal disease in mice. *Infect. Immun.* 84, 1536–1547. doi: 10.1128/IAI.01504-15

Thevaranjan, N., Puchta, A., Schulz, C., Naidoo, A., Szamosi, J. C., Verschoor, C. P., et al. (2018). Age-associated microbial dysbiosis promotes intestinal permeability, systemic inflammation, and macrophage dysfunction. *Cell Host Microbe* 21, 455.e4–466.e4. doi: 10.1016/j.chom.2018.03.006

Thompson, J., and Pikis, A. (2012). Metabolism of sugars by genetically diverse species of oral *Leptotrichia*. *Mol. Oral. Microbiol.* 27, 34–44. doi: 10.1111/j.2041-1014.2011.00627.x

Tra, V. N., and Dube, D. H. (2014). Glycans in pathogenic bacteria - potential for targeted covalent therapeutics and imaging agents. *Chem. Commun.* 50, 4659–4673. doi: 10.1039/c4cc00660g

Wang, L., Cheng, H., Wang, D., Zhao, B., Zhang, J., Cheng, L., et al. (2019). Airway microbiome is associated with respiratory functions and responses to ambient particulate matter exposure. *Ecotoxicol. Environ. Saf.* 167, 269–277. doi: 10.1016/j.ecoenv.2018.09.079

Wang, Q., Garrity, G. M., Tiedje, J. M., and Cole, J. R. (2007). Naive Bayesian classifier for rapid assignment of rRNA sequences into the new bacterial taxonomy. *Appl. Environ. Microbiol.* 73, 5261–5267. doi: 10.1128/AEM.00062-07

Wang, W., Zhou, J., Chen, M., Huang, X., Xie, X., Li, W., et al. (2018). Exposure to concentrated ambient PM2.5 alters the composition of gut microbiota in a murine model. *Part Fibre Toxicol.* 15:17. doi: 10.1186/s12989-018-0252-6

Wardlaw, T., Salama, P., Johansson, E. W., and Mason, E. (2006). Pneumonia: the leading killer of children. *Lancet* 368, 1048–1050. doi: 10.1016/S0140-6736(06)69334-3

Williams, D. A., Pradhan, K., Paul, A., Olin, I. R., Tuck, O. T., Moulton, K. D., et al. (2020). Metabolic inhibitors of bacterial glycan biosynthesis. *Chem. Sci.* 11, 1761–1774. doi: 10.1039/c9sc05955e

Yang, C. Y., Yeh, Y. M., Yu, H. Y., Chin, C. Y., Hsu, C. W., Liu, H., et al. (2018). Oral microbiota community dynamics associated with oral squamous cell carcinoma staging. *Front. Microbiol.* 9:862. doi: 10.3389/fmicb.2018.00862

Yang, D., Chen, X., Wang, J., Lou, Q., Lou, Y., Li, L., et al. (2019). Dysregulated lung commensal bacteria drive interleukin-17B production to promote pulmonary fibrosis through their outer membrane vesicles. *Immunity* 50, 692.e7–706.e7. doi: 10.1016/j.immuni.2019.02.001

Zhao, C., Wang, Y., Su, Z., Pu, W., Niu, M., Song, S., et al. (2020). Respiratory exposure to PM2.5 soluble extract disrupts mucosal barrier function and promotes the development of experimental asthma. *Sci. Total Environ.* 730:139145. doi: 10.1016/j.scitotenv.2020.139145

Zhou, Y., Yang, J., Zhang, L., Zhou, X., Cisar, J. O., and Palmer, R. J. Jr. (2016). Differential utilization of basic proline-rich glycoproteins during growth of oral bacteria in saliva. *Appl. Environ. Microbiol.* 82, 5249–5258. doi: 10.1128/AEM.01111-16

Conflict of Interest: The authors declare that the research was conducted in the absence of any commercial or financial relationships that could be construed as a potential conflict of interest.

frontiers in Cell and Developmental Biology

ORIGINAL RESEARCH
published: 27 October 2020
doi: 10.3389/fcell.2020.534268

Advances in CMV Management: A Single Center Real-Life Experience

Michele Malagola[1], Caterina Pollara[2], Nicola Polverelli[1], Tatiana Zollner[1], Daria Bettoni[3], Lisa Gandolfi[1], Doriana Gramegna[1], Enrico Morello[1], Alessandro Turra[1], Silvia Corbellini[2], Liana Signorini[4], Giovanni Moioli[4], Simona Bernardi[1,5], Camilla Zanaglio[1,5], Mirko Farina[1], Tullio Elia Testa[3], Arnaldo Caruso[2] and Domenico Russo[1]*

[1] Chair of Hematology, Bone Marrow Transplant Unit, ASST-Spedali Civili Brescia, Department of Clinical and Experimental Sciences, University of Brescia, Brescia, Italy, [2] ASST-Spedali Civili, Section of Microbiology, Department of Experimental and Applied Medicine, University of Brescia, Brescia, Italy, [3] UO Farmacia Aziendale, ASST Spedali Civili of Brescia, Brescia, Italy, [4] Department of Infectious and Tropical Diseases, University of Brescia, ASST Spedali Civili di Brescia, Brescia, Italy, [5] CREA Laboratory (Hematological-Research AIL Centre), ASST-Spedali Civili Brescia, Brescia, Italy

CMV infection is a major challenge in allogeneic stem cell transplantation (allo-SCT). The changing landscape in CMV management includes the introduction of letermovir in prophylaxis of high-risk patients and the source of CMV DNA monitoring (plasma—PL vs. whole blood—WB), for pre-emptive therapy (PET) initiation. We report here how our real-life experience in CMV management evolved, following letermovir registration. We focus on: (i) the effects of systematic use of letermovir for CMV prophylaxis in high-risk patients, (ii) the results of a longitudinal comparison of CMV DNAemia monitoring in PL and WB. From December 2018 to April 2020, 60 allo-SCTs have been performed in our center (LET *ERA*), of whom 45 received letermovir in prophylaxis from day 0 to day + 100, because of recipient positivity of anti CMV IgG. These patients were compared with a cohort of 41 allo-SCTs performed between November 2017 and November 2018 (NO LET *ERA*). Firstly, the incidence of CMV clinically significant infections, CMV disease, bacterial infections, proven/probable fungal infections, hospital re-admissions after allo-SCT by day + 100 in the two ERA were 8 vs. 44% ($p = 0.0006$), 2 vs. 12% ($p = 0.02$), 37 vs. 56% ($p = 0.05$), 8 vs. 19% ($p = 0.09$), and 23 vs. 39% ($p = 0.09$), respectively. By day + 180 these differences were 17 vs. 68% ($p < 0.00001$), 2 vs. 12% ($p = 0.02$), 45 vs. 78% ($p = 0.09$), 8 vs. 22% ($p = 0.05$), and 40 vs. 66% ($p = 0.01$), respectively. Secondly, from February to May 2019, we comparatively measured CMV DNA from WB and PL and we confirmed that there is a linear correlation between CMV DNA level in WB and PL (Spearman's test $r = 0.86$). Moreover, CMV DNAemia at the time of PET in the 12 patients with a clinically significant CMV infection was higher in WB vs. PL (5.202 vs. 4.981 copies/ml, $p = 0.1$). Our real-life experience confirms that: (i) letermovir is highly effective, leading to a significant drop in CMV clinically significant infections and CMV-related complications by day + 100 and + 180 after allo-SCT; (ii) WB may be an effective alternative to PL as a source for CMV DNA monitoring, as a linear correlation of DNAemia was confirmed between WB and PL, even if the CMV DNAemia at PET initiation was comparable in the two sources.

Keywords: CMV, allogeneic stem cell transplantation, prophylaxis, pre-emptive therapy, CMV DNA monitoring

OPEN ACCESS

Edited by:
Davide Gibellini, University of Bologna, Italy

Reviewed by:
Pilar Perez-Romero, Carlos III Health Institute (ISCIII), Spain
Rafael De La Camara, Princess University Hospital, Spain

****Correspondence:***
Michele Malagola
michele.malagola@unibs.it

Specialty section:
This article was submitted to Molecular Medicine, a section of the journal Frontiers in Cell and Developmental Biology

Received: *11 February 2020*
Accepted: *28 August 2020*
Published: *27 October 2020*

Citation:
Malagola M, Pollara C, Polverelli N, Zollner T, Bettoni D, Gandolfi L, Gramegna D, Morello E, Turra A, Corbellini S, Signorini L, Moioli G, Bernardi S, Zanaglio C, Farina M, Testa TE, Caruso A and Russo D (2020) Advances in CMV Management: A Single Center Real-Life Experience. Front. Cell Dev. Biol. 8:534268. doi: 10.3389/fcell.2020.534268

INTRODUCTION

Cytomegalovirus (CMV) infection is a challenge in allogeneic stem cell transplantation (allo-SCT) (Boeckh and Nichols, 2004; Boeckh and Ljungman, 2009). In the first 100 days after transplant, it is detected in more than 60% of CMV seropositive recipients, in whom it produces a number of direct and indirect relevant effects, leading to an increase in non-relapse mortality (NRM). CMV disease, drug-related peripheral blood cytopenia, bacterial or fungal infections, and graft vs. host disease (GVHD) are the main CMV-related complications (Ariza-Heredia et al., 2014).

Before the availability of letermovir, the management of CMV infection was based on the monitoring of CMV DNAemia by RT-qPCR and on the prompt use of pre-emptive therapy (PET), either with foscarnet, ganciclovir, or valganciclovir. CMV DNA cut-off values for PET are still a matter of debate: Italian guidelines suggest more than 1,000 copies/ml in plasma (PL) or 10,000 copies/ml in whole blood (WB), in two consecutive assessments (Girmenia et al., 2019), while the ECIL-7 guidelines suggest that it should be adapted according to the monitoring technique used at the transplant center (Ljungman et al., 2019). PET is generally continued for at least 2 weeks, and stopped after at least one (Ljungman et al., 2019) or preferably two consecutive negative tests (Girmenia et al., 2019). Although anti-CMV hyper-immunoglobulins (Megalotect) can be safely used (Malagola et al., 2019), no conclusive data are available to recommend a routine use, and both the ECIL-7 guidelines and the Italian guidelines do not recommend the routine use of anti-CMV hyper-immunoglobulins (Girmenia et al., 2019; Ljungman et al., 2019).

Recently, significant improvements have been made in the management of CMV infection. They include: (i) the introduction of letermovir for prophylaxis in CMV seropositive patients; (ii) the advances in laboratory monitoring of CMV infection.

Letermovir has been licensed in Italy (December 2018) for prophylaxis in high-risk patients from day 0 to day + 100, following the conclusive data reported in the registration trial (Marty et al., 2017), showing a reduction of CMV clinically significant infection. In this study, the incidence of CMV reactivation was significantly lower in patients receiving letermovir vs. placebo (37 vs. 60%, respectively, $p < 0.001$), with an excellent safety profile (Marty et al., 2017).

Although ganciclovir and foscarnet were widely investigated in the 80s and 90s for CMV prophylaxis and have been proven to be effective in reducing CMV infection and disease, they showed significant toxicity (myelotoxicity for ganciclovir and nephrotoxicity for foscarnet), that hampered their extensive use in clinical practice (Chen et al., 2018). Thus, letermovir is, at present, the most effective and safe drug for CMV prophylaxis and the only licensed one for this indication.

During the last few years, the laboratory monitoring of CMV and the diagnosis of CMV infection moved from CMV antigenemia (Cariani et al., 2007) to molecular quantitative RT-qPCR (Girmenia et al., 2019; Ljungman et al., 2019), but a unique standardized method for detection of DNAemia has not been defined yet. Even though it is true that both WB and PL are valid sources for CMV DNA monitoring after allo-SCT, recently, WB has been suggested to be more reliable than PL as a source for RT-qPCR. In fact, in WB both intra-cellular and extra-cellular CMV DNA is detected, and during PET the clearance of CMV DNA appears to be faster in WB than in PL, where free particles of non-infective DNA are measured for many days after the complete clearance of the virus. This latter point is crucial, because it reduces the duration of PET and its side effects (Lazzarotto et al., 2018).

The aim of our study is to depict if and how letermovir and the availability of different sources for CMV DNAemia monitoring have impacted on daily CMV management. Thus, we report here a real-life single center experience in CMV management, conducted in our transplant center since letermovir registration in Italy (LET *ERA*) from December 2018 to April 2020, during which 60 allo-SCTs have been performed. We compared these data with a cohort of 41 patients allotransplanted before letermovir registration (from November 2017 to November 2018, NO LET *ERA*). We highlight two major issues: (i) the effects of the systematic use of letermovir for CMV prophylaxis in CMV positive recipients; (ii) the comparative monitoring of CMV DNAemia from WB and PL, to evaluate the reliability of the two methods in the era of prophylaxis with letermovir.

PATIENTS AND METHODS

CMV Management Before Letermovir Introduction (Before December 2018)

For the purpose of this study, we report the policy and the results of CMV management before and after December 2018, that is when letermovir was licensed in Italy and routinely used by us for CMV prophylaxis in CMV seropositive patients undergoing allo-SCT.

Data were obtained by local databases and clinical charts, and special queries were addressed on missing data. The allo-SCT procedures, in terms of conditioning regimens, GVHD prophylaxis, and antimicrobial prophylaxis, were based on local guidelines and protocols, were undertaken upon written informed consent for transplant procedures and they remained unchanged following letermovir registration.

In order to define the risk of developing CMV infection and/or disease, standard practice included a serological test for CMV IgG of both the patient and the donor: patient's CMV IgG positivity defined the high-risk category. Additional risk-factors were considered: the presence of a seronegative donor for a seropositive recipient, the presence of a mismatch donor, and the presence of GHVD, as reported in the literature (Styczynski, 2018). Up to December 2018, no prophylaxis against CMV was adopted, and all the patients received a standard-dose of acyclovir for other herpes virus prophylaxis. PET consisted of foscarnet, ganciclovir, or valganciclovir. Foscarnet was chosen in cases of peripheral blood cytopenia, ganciclovir in cases of renal impairment, and valganciclovir in cases of management of CMV once the patient has been discharged. PET was started in cases of a clinically significant CMV infection, defined as CMV reactivation

with at least two positive controls (>1,000 copies/ml from PL) (Boeckh and Ljungman, 2009). From 2016, anti-CMV hyper-immunoglobulins (Megalotect) have been used in three settings: with anti-CMV specific drugs (during PET), in monotherapy for secondary prophylaxis (prevention of CMV breakthrough infection in very high-risk patients), and in order to control a CMV reactivation not requiring PET. Megalotect was used at the conventional dose of 100 UI/Kg every 2 weeks.

CMV Management After Letermovir Introduction (After December 2018)

Following letermovir registration and availability in our hospital (January 2019), all high-risk patients were selected to receive standard prophylaxis with letermovir from day 0 to day + 100, at the conventional dose of 240 or 480 mg/day orally, based on the immunosuppressive drug co-administered for GVHD prophylaxis. No changes were made in PET approach, as well as in the supportive care with Megalotect. In particular, we maintained the clinical practice to start PET following two consecutive CMV positive samples with more than 1000 copies/ml in PL. Nevertheless, soon after the introduction of letermovir (from February 2019 to May 2019), we conducted a comparative assessment of CMV-DNA from PL and WB, in order to verify WB reliability, with the intent to move from PL to WB, as a source for CMV DNA monitoring (from June 2019). During this time-frame, any decision for PET initiation was made considering the CMV-DNA on PL. After May 2019, a cut-off of 10,000 copies/ml in two consecutive samples was adopted for PET initiation. Moreover, for DNAemia between 1000 and 10,000 copies/ml the presence of additional risk factors for CMV-related complications was carefully considered for a prompt PET start, even with copies < 10,000/ml in two consecutive samples (e.g., aGVHD under steroids and haploidentical donor).

CMV DNAemia Monitoring

Up to February 2019, the clinical practice in our transplant center was to monitor CMV-DNA from PL at least once a week until day + 100, and to start PET in cases of clinical significant CMV infection as above reported. From February to May 2019, in collaboration with the microbiology unit of our hospital, we carried out a CMV DNAemia monitoring protocol for allotransplanted patients for comparative determination of quantitative CMV DNA from WB and PL. In particular, this comparative evaluation was performed both in patients who were transplanted between February and March 2019 (n = 21) and in patients who have been previously transplanted and were monitored during the follow up and transplanted before letermovir availability (n = 47). Extraction, detection, and quantification of CMV-DNA in paired WB and PL samples were performed using a commercial automated platform (ELITe InGenius®, Elitechgroup, Italy) (CMV ELITe MGB® Kit, 2017, SCH mRTK015PLD_11, of 10/03/17, Elitechgroup). The ELITe InGenius® instrument is the first fully automated sample-to-result solution, integrating sample preparation, amplification, and result analysis, validated with a quantitative transplant pathogen monitoring menu, based on the real-time PCR MGB technology. Results interpretation and analysis are automatically done by the ELITe InGenius® system. In comparison to conventional PCR platforms and conventional methods in microbiology, the ELITe InGenius® system simplified and reduced the duration of the pre-analytical and analytical phases in the laboratory (2 h 30' to process one sample) and proved to be a reliable and sensitive tool for a sample-in answer-out detection of CMV directly from clinical samples.

Briefly, primary samples were loaded directly and processed in the ELITe InGenius® system, according to the manufacturer's instructions. The instrument collected only 200 μL for each sample (WB and PL) and the purified nucleic acid was eluted into a total volume of 100 μL and amplification was performed using 20 μL. For each protocol, the limit of detection (LoD) and the lower limit of quantification (LLoQ) were as reported by the manufacturer. In particular, the LoD was 156 and 293 copies/ml from WB and PL, respectively, and the LLoQ was 254 and 593 copies/ml from WB and PL, respectively. Quantitative results were reported as log10 copies/mL of the sample. Positive samples (WB and PL) below the LLoQ were considered negative; while all samples with a value < 156 copies/mL for WB and < 293 copies/ml for PL were considered really negative (0 copies/mL) samples. For the ELITe InGenius® real-time CMV assay, the manufacturer has determined the conversion factor and provides a conversion factor whatever the matrix used (WB or plasma). The conversion factor for WB is 2.9 IU/copies, while for PL is 1.9 IU/copies.

Statistical Analysis

CMV DNA levels between whole blood and plasma samples were compared by a Mann-Whitney U-test. The correlation between CMV DNA in the two groups was analyzed using the Spearman's correlation coefficient (Dioverti et al., 2017). The differences between the groups were analyzed using the Chi-square test or the Fisher's exact test, as appropriate. A P-value of < 0.05 was considered as statistically significant.

RESULTS

Results of Letermovir Prophylaxis

For the purpose of this study, we consider 110 allogeneic transplants performed from November 2017 to April 2020 in our transplant center, divided into two cohorts: 41 transplants performed before the registration of letermovir in Italy (NO LET *ERA*—November 2017–November 2018) and 60 transplants performed after letermovir registration in Italy (LET *ERA*—December 2018–April 2020).

Table 1 reports the clinical and transplant characteristics of the two cohorts. Focusing on the 60 transplants of the LET *ERA*, more than 50% were performed for acute leukemia, 53% were made in complete remission, and 57% following a myeloablative conditioning regimen. In 70% of them peripheral blood stem cells were used, and 27% were performed with a haploidentical transplantation. No statistical significant differences were observed in the two cohorts, with the exception of the expected difference in letermovir use: letermovir

TABLE 1 | Clinical and transplant characteristics of the 101 patients transplanted from November 2017 to April 2020.

Characteristics	NO LETERMOVIR *ERA*		LETERMOVIR *ERA*		
	Nov 2017–Nov 2018 *N* = 41		Dec 2018–Apr 2020 *N* = 60		P
	N	%	N	%	
Patient age, median (range)	56 (19–71)	–	52 (21–71)	–	
Patient sex, female/male	19/22	46/54	27/33	45/55	0.89
Disease					
AL	27	66	32	53	0.20
MFI	4	10	9	15	0.43
MM	4	1014	8	13	0.58
NHL	6	0	5	8	0.31
HL	0	0	2	3	n.e.
SAA	0		2	3	n.e.
Other			2	3	n.e.
Disease status at transplant					
CR	21	51	32	53	0.83
CMV serostatus (R +)	32	78	51	85	0.37
Donor type					
Sibling	11	27	11	18	0.07
MUD	24	58	32	53	0.69
Haplo	15	15	16	27	0.38
UCB	0	0	1	2	1
Stem cell source					
PBSC	34	83	42	70	0.16
BM	7	17	17	28	0.24
UCB	0	0	1	2	1
Conditioning intensity					
RIC	21	51	26	43	0.54
MAC	20	49	34	57	
aGVHD grade II-IV	12	29	14	23	0.64
cGVHD	3	7	2	3	0.39
Letermovir					
YES	0	0	45	45	< 0.0001
NO	41	100	15	15	
Letermovir duration					
Discontinued at day + 100	–	–	25	56	–
Ongoing	–	–	13	29	–
Discontinued before day + 100	–	–	7	15	–
Dose					
240 mg/day	–	–	36	80	–
480 mg/day	–	–	9	20	–

AL, acute leukemia; MFI, primary myelofibrosis; HL, Hodgkin lymphoma; NHL, Non-Hodgkin lymphoma; MM, multiple myeloma; CR, complete remission; MUD, matched unrelated donor; Haplo, haploidentical; UCB, umbilical cord blood; PBSC, peripheral blood stem cell; BM, bone marrow; MAC, myeloablative conditioning; RIC, reduced intensity conditioning; aGVHD, acute graft vs. host disease; cGVHD, chronic graft vs. host disease; n.e., not evaluable.

prophylaxis was used in 45/60 transplants of the LET *ERA* (75%) and in none of the transplant of the previous period ($p < 0.0001$). All the patients who received letermovir were IgG positive. Additional CMV risk factors were: matched unrelated donor (23 cases) and haploidentical donor (14 cases). Most of the patients (80%) who received letermovir prophylaxis took 240 mg/daily together with cyclosporine. Nine patients (20%) received letermovir 480 mg together with sirolimus (6 cases) or tacrolimus (3 cases). At the last follow up (April 20, 2020), 25/45 patients (56%) discontinued letermovir because they completed the planned 100 days of treatment, while 13/45 patients (29%) were still receiving letermovir and 7/45 (15%) discontinued letermovir for CMV clinically significant infection or death before day + 100.

Overall, the treatment was very well tolerated. In particular, no drug-related grade ł 2 WHO adverse events were reported (diarrhea, vomiting, skin rash, fever, cough, or peripheral edema) (Marty et al., 2017).

As above reported, considering the 60 transplants of the LET *ERA* letermovir prophylaxis was used in 45 cases (75%, **Table 2a**). In total, 14/45 (31%) developed a CMV reactivation (before day + 100, during letermovir prophylaxis in 8 cases and after day + 100 in 6 cases). In 7 cases (7/45, 15%) the infection was clinically significant and required PET (2 cases—4%—during letermovir prophylaxis, before day + 100 and 5 cases—11%—after day + 100).

A total of 15/60 (25%) patients of the LET ERA did not receive letermovir prophylaxis (CMV seronegativity in 9 cases, letermovir temporary unavailability at our institution in 3 cases, second transplant in 2 cases, who previously received letermovir for the first transplant and received an anti-CMV drug during the follow up and CMV DNA positivity at day −2 in 1 case; **Table 2b**). In total, 5/15 of these patients (45%) developed a CMV-related complication: two patients developed a clinically significant CMV infection at day +13 and +24, one at day −2 and two patients developed a CMV disease (1 lung localization before day + 100 and 1 gut localization after day + 100, both without CMV DNAemia).

Considering all the 12 cases of CMV clinically significant infection or disease observed in the LET *ERA* (7 in the letermovir group—**Table 2a**—and 5 in the non-letermovir group—**Table 2b**), the treatment consisted of foscarnet (5 cases), valganciclovir (6 cases), and ganciclovir (1 case). All the patients who received PET for a clinically significant CMV infection achieved a complete clearance of CMV DNA after a median of 14 days (range 7–26). In 5/12 cases (42%) a breakthrough CMV infection was observed, that was successfully treated with second line anti-CMV drugs. No resistance to ganciclovir or foscarnet was observed.

In order to assess the impact of letermovir prophylaxis in the clinical management of allotransplanted patients, we compared the most relevant transplant outcomes in the NO LET *ERA* (Nov 2017–Nov 2018; 41 transplants) vs. the LET *ERA* (Dec 2018–Apr 2020; 60 transplants) (**Table 3**). Focusing on the first 100 days after allo-SCT, the incidence of clinically significant CMV infections, CMV disease, bacterial infections, proven/probable fungal infections, and hospital readmission was 44 vs. 5% ($p = 0.0006$), 12 vs. 2% ($p = 0.02$), 56 vs. 37% ($p = 0.05$), 19 vs. 8% ($p = 0.09\%$), and 39 vs. 23% ($p = 0.09$), respectively. Moreover, the incidence of grade ł 2 aGVHD was 29 vs. 23%, in

TABLE 2a | CMV course in the 45 high-risk (CMV IgG+) patients who received prophylaxis with letermovir from day 0 to day + 100.

Pt N°	SCT date	CMV IgG D/R	Day of 1st CMV reactivation	CMV DNAemia	Source	PET	LET duration	Pt last f up
1	Mar 2020	−/+	+10	<1,000 copies/ml	WB	–	27	+27
2	Jul 2019	+/+	+11	<1,000 copies/ml	WB	–	100	+234
3	Oct 2019	+/+	+11	<1,000 copies/ml	WB	–	82	+192
4	Jan 2019	+/+	+12	2,779 copies/ml	PL	FOS	12	Dead
5*	Mar 2019	−/+	+13	10,099 copies/ml	PL	FOS	13	Dead
6	May 2019	+/+	+20	<1,000 copies/ml	WB	–	100	Dead
7	May 2019	−/+	+20	<1,000 copies/ml	WB	–	100	+343
8	Jan 2019	−/+	+78	<1,000 copies/ml	PL	–	100	+493
9	Feb 2019	+/+	+120	2,280 copies/ml	PL	VAL	100	+433
10	Feb 2019	+/+	+130	<1,000 copies/ml	WB	–	100	+443
11	Mar 2019	−/+	+133	10,744 copies/ml	WB	VAL	100	+383
12	Oct 2019	+/+	+146	10,900 copies/ml	WB	VAL	100	+186
13	May 2019	+/+	+147	4,675 copies/ml	WB	VAL	100	+332
14	Jul 2019	+/+	+150	5,451 copies/ml	WB	VAL	100	+178
15	Jan 2019	+/+	–	–	–	–	100	Dead
16	Jun 2019	+/+	–	–	–	–	18	Dead
17	Jun 2019	+/+	–	–	–	–	68	Dead
18	Jun 2019	+/+	–	–	–	–	100	+307
19	Jul 2019	+/+	–	–	–	–	100	+292
20	Jul 2019	−/+	–	–	–	–	100	+283
21	Jul 2019	−/+	–	–	–	–	100	+270
22	Sep 2019	+/+	–	–	–	–	100	+214
23	Oct 2019	+/+	–	–	–	–	100	+193
24	Oct 2019	−/+	–	–	–	–	100	+116
25**	Nov 2019	−/+	–	–	–	–	40	Dead
26	Nov 2019	−/+	–	–	–	–	100	+156
27	Nov 2019	+/+	–	–	–	–	100	+155
28	Nov 2019	+/+	–	–	–	–	24	Dead
29	Nov 2019	+/+	–	–	–	–	100	+143
30	Dec 2019	−/+	–	–	–	–	100	+129
31	Dec 2019	−/+	–	–	–	–	100	+122
33	Jan 2020	−/+	–	–	–	–	100	+102
33	Jan 2020	+/+	–	–	–	–	100	+101
34	Jan 2020	+/+	–	–	–	–	95	+95
35	Jan 2020	+/+	–	–	–	–	80	+80
36	Feb 2020	+/+	–	–	–	–	20	Dead
37	Feb 2020	−/+	–	–	–	–	66	+66
38	Feb 2020	+/+	–	–	–	–	60	+60
39	Feb 2020	+/+	–	–	–	–	56	+56
40	Mar 2020	+/+	–	–	–	–	41	+41
41	Mar 2020	+/+	–	–	–	–	25	+25
42	Apr 2020	+/+	–	–	–	–	11	+11
43	Apr 2020	+/+	–	–	–	–	10	+10
44	Apr 2020	−/+	–	–	–	–	6	+6
45	Apr 2020	+/+	–	–	–	–	3	+3

**First transplant for primary myelofibrosis.*
***First transplant for primary myelofibrosis. Letermovir discontinuation at day + 40 because of foscarnet therapy for HHV6 reactivation.*

the two periods (p = 0.5). The observed differences were more evident prolonging the observation up to 180 days after allo-SCT: 68 vs. 17% for CMV clinically significant infection ($p < 0.00001$), 12 vs. 2% for CMV disease (p = 0.02), 78 vs. 45% for bacterial infections (p = 0.009), 22 vs. 8% for proven/probable fungal infections (p = 0.05), and 66 vs. 40% for hospital re-admission (p = 0.01). The costs of PET showed a reduction from Euro 38,000 to Euro 10,000, that only partially balanced the costs of letermovir from day 0 to day + 100 (Euro 13,700/pt for 240 mg/daily and Euro 29,000/pt for 480 mg/daily).

Comparative Monitoring of CMV DNAemia From PL and WB

From February to May 2019 (4 months), a total of 566 consecutive samples were collected, for comparative assessment of CMV

TABLE 2b | CMV course in the 15 patients who did not receive prophylaxis with letermovir from day 0 to day + 100.

Pt ID	SCT date	CMV IgG D/R	Day of 1st CMV reactivation	CMV DNAemia	Source	Anti CMV therapy	Pts last f up
46*	Feb 2019	−/+	−2	2,605 copies/ml	PL	FOS	+421
47	Apr 2019	−/−	+13	1,347 copies/ml	PL	VAL	+376
48	Mar 2019	+/−	+20	–	–	FOS[#]	Dead
49[@]	Dec 2018	−/+	+24	2,273 copies/ml	PL	FOS	+485
50[@]	Dec 2018	−/+	+240	–	–	GAN[§]	+478
51	Dec 2018	−/+	–	–	–	–	Dead
56	Apr 2019	–/–	–	–	–	–	+335
5**	Apr 2019	–/+	–	–		–	Dead
57	Jun 2019	–/–	–	–		–	+294
58	Aug 2019	−/−	–	–		–	+260
25***	Dec 2019	−/+	–	–		–	Dead

**Letermovir was not used because of CMV positive DNA before SCT (day −2).*
[#]FOS for CMV disease (lung) on day + 16, with negative CMV DNA on PL.
[@]Letermovir was not used because, although registered, it became available in our hospital from January 2019.
[§] GAN for CMV disease (gut) on day + with negative CMV DNA on PL.
***Letermovir was not used because this is a second transplant. Letermovir was used in the first transplant and discontinued at day + 13 for CMV clinically significant infection (see **Table 2a**).*
****Letermovir was discontinued at day + 40 after the first transplant because of foscarnet therapy for HHV6 reactivation (see **Table 2a**).*

TABLE 3 | Impact of letermovir on the management of patients undergoing allo-SCT.

	Nov 2017–Nov 2018 NO LET *"ERA"*	Dec 2018–APR 2020 LET *"ERA"*	*P*
No. of allo-SCT	41	60	–
Letermovir prophylaxys day 0 → + 100	0	45	–
Clinically significant CMV infection (≤ 100 days)	18 (44%)	5* (8%)	0.0006
Clinically significant CMV infection (≤ 180 days)	28 (68%)	10 (17%)	<0.00001
CMV disease (≤100 days)	5 (12%)	1** (2%)	0.02
CMV disease (≤180 days)	5 (12%)	1 (2%)	0.02
Bacterial infections (≤100 days)	23 (56%)	22 (37%)	0.05
Bacterial infections (≤180 days)	32 (78%)	27 (45%)	0.009
Fungal infections (probable/proven) (≤100 days)	8 (19%)	5 (8%)	0.09
Fungal infections (probable/proven) (≤180 days)	9 (22%)	5 (8%)	0.05
aGVHD grade ≥ 2	12 (29%)	14 (23%)	0.5
Hospital re-admission (≤100 days)	16 (39%)	14 (23%)	0.09
Hospital re-admission (≤180 days)	27 (66%)	24 (40%)	0.01
Cumulative cost for PET[#]	Euro 38,000	Euro 10,000	–
Letermovir costs			
−240 mg day 0 → + 100	–	Euro 13,700/pt	–
−480 mg day 0 → + 100	–	Euro 29,000/pt	–

Two patients in the letermovir group (CE and CP in **Table 2a) and **3** patients in the no-letermovir group (CN, BG, and FB in **Table 2b**).*
***Two patients in the no-letermovir group (BA and FG in **Table 2b**).*
[#]This indicates the cumulative cost with the different anti-CMV specific drug actually administered (FOS, GAN, VAL), calculated for 15 days and for a standard of 70 Kg of body weight.

DNA from PL and WB. The samples came from 68 patients (21 females and 47 males, mean age 50 ± 21 years), of whom 21 allotransplanted in the same period of time (250 samples) and 47 allotransplanted before February 2019 and who were monitored during follow up (316 samples). The median number of samples per patient was 8 (range: 1–29).

The first objective of this analysis was to confirm the data reported in the literature of a linear correlation between the results of the RT-qPCR on PL and WB (Lazzarotto et al., 2018). Considering all the 566 samples, including 294 samples with undetectable CMV DNAemia, the median number of copies/ml was 293 (range 293–169,769) and 156 (range 156–202,261) on PL and WB, respectively. The Spearman's test clearly showed a linear correlation between the two sources ($r = 0.87$). Considering the 272 samples coming from the 18 patients who had a CMV reactivation, the median value of CMV DNA was 593 copies/ml on PL and 402 copies/mL on WB, respectively (**Figure 1A**). The mean was 4,664 copies/ml on PL and 4,679 copies/mL on WB, respectively (**Figure 1A**). **Figure 1B** confirms the linear correlation between the values ($r = 0.86$).

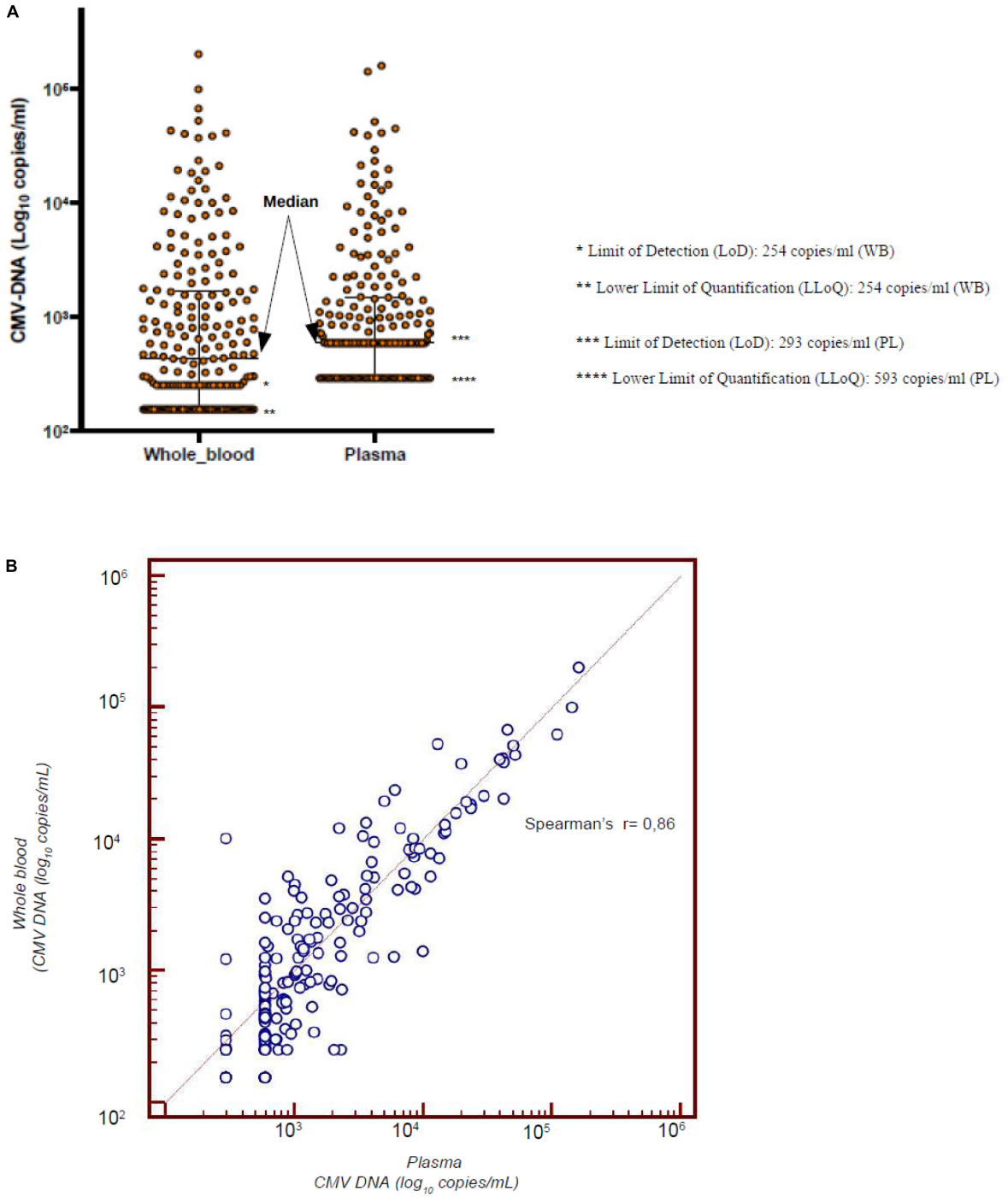

FIGURE 1 | (A) Median value of CMV-DNAemia of the 18 patients with CMV reactivation who were monitored simultaneously from PL and WB. **(B)** Linear correlation between the CMV DNAemia assessed on PL and WB in the 18 patients who experienced a CMV reactivation.

We then grouped the CMV DNA level as detected from PL and WB of the 208 samples from the 12/18 patients who experienced a CMV reactivation that required PET. **Figures 2A,B** report this analysis. Time-point zero of each figure includes the peak value of CMV DNA which correspond to the first day of anti-CMV treatment; negative time-points include the weekly assessment before PET initiation and positive timepoints include the weekly assessment during PET. At time-point zero, the DNAemia on WB (**Figure 2B**, median 5,202 copies/mL) was higher than that detected on PL (**Figure 2A**, median 4,981 copies/mL). The difference was not significant (p = 0.1). The kinetics of CMV DNAemia during PET was similar

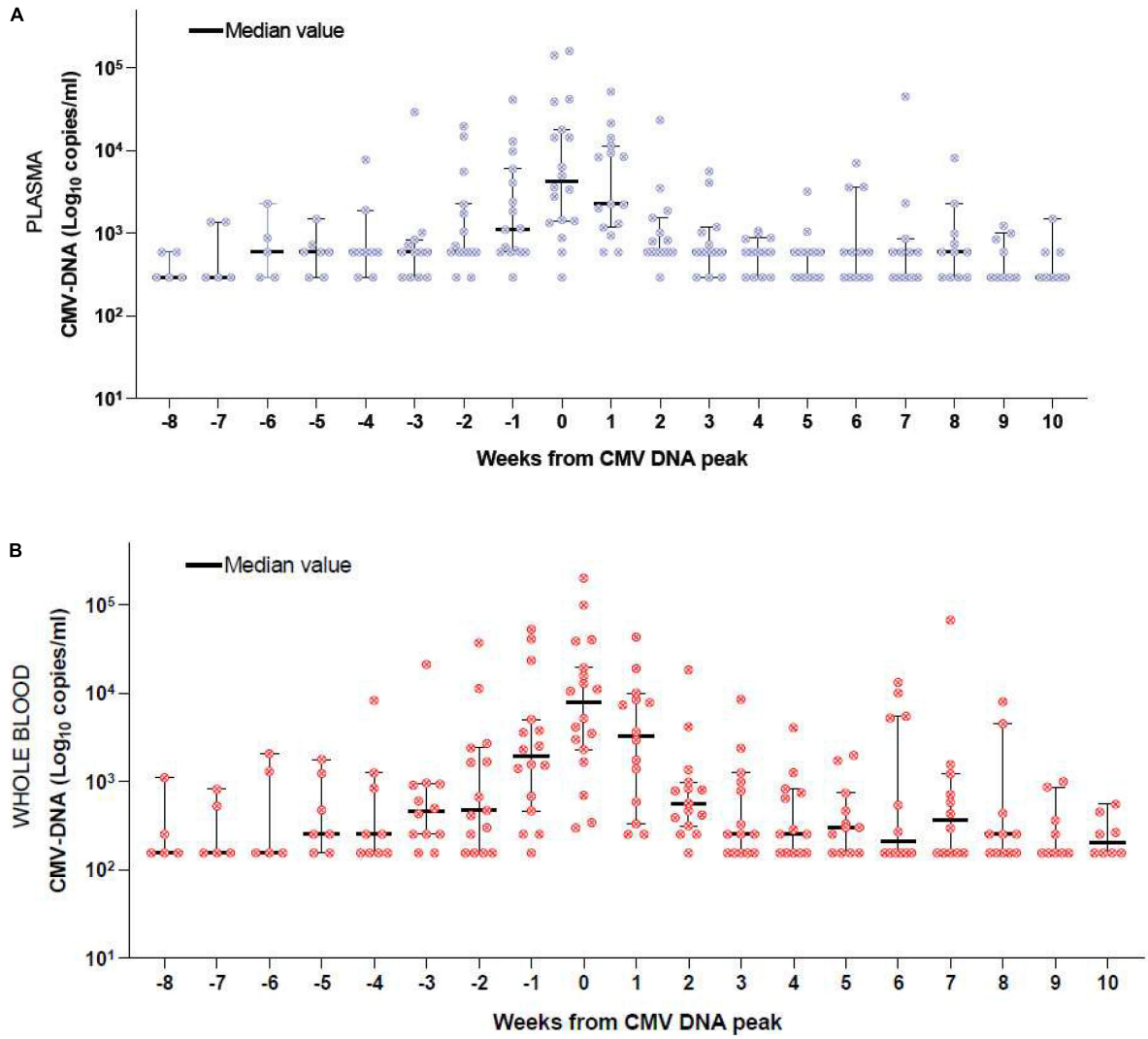

FIGURE 2 | (A) CMV DNAemia monitored on PL of the 12 patients who received PET. Week 0 includes the maximum DNAemia. Negative weeks include the DNAemia before the peak and positive weeks include the DNAemia during PET. **(B)** CMV DNAemia monitored on WB of the 12 patients who received PET. Week 0 includes the maximum DNAemia. Negative weeks include the DNAemia before the peak and positive weeks include the DNAemia during PET.

when considering PL (**Figure 2A**) or WB (**Figure 2B**). The comparative CMV DNAemia expressed in copies/ml and IU/ml according to the manufacturer conversion factor is reported in **Supplementary Table 1**.

DISCUSSION

CMV management is a major challenge for patients admitted for allo-SCT and a raise in CMV reactivation is expected in the next few years following the extensive use of haploidentical transplantation and the progressive increase of patients' age at transplant (Boeckh and Ljungman, 2009). In both these settings, acute and chronic GVHD incidence is expected to be higher in comparison to conventional transplants in younger patients. Thus the prolonged immunosuppression and the long-lasting immune-reconstitution are expecting to expose these patients to more frequent CMV infections.

The attention of the transplant community on CMV is particularly high, and recently the Gruppo Italiano Trapianto di Midollo Osseo (GITMO) published a guideline addressing the major points of CMV management (Girmenia et al., 2019). Nevertheless, the real-life policy of CMV management is still heterogeneous in this transition period, considering that letermovir has been recently registered for CMV prophylaxis (Marty et al., 2017) and that CMV DNA monitoring from WB instead of PL for definition of the CMV clinically significant infection has been proposed to be preferable, even though not definitively demonstrated and largely applied (Lazzarotto et al., 2018).

These clinical and laboratory aspects have been recently highlighted by Marty et al. (2017) in their registration studies

and by Lazzarotto et al. (2018) in their experimental work. The results of both papers are considered as reference, but few data on real-life experience are currently available, taking into account that the number of patients who received primary prophylaxis with letermovir in the real-life published studies is very limited (Lin et al., 2019; Anderson et al., 2020; Johnsrud et al., 2020; Sharma et al., 2020).

In the present paper, we report a real-life experience on CMV management in our transplant center following letermovir registration in Italy (December 2018) and we compare a cohort of 60 transplants performed after letermovir registration (LET *ERA*, December 2018–April 2020) with a historical cohort of transplants performed before letermovir registration (NO LET *ERA*, November 2017–November 2018), with the aim to evaluate the efficacy of letermovir prophylaxis and its impact on CMV reactivation and incidence of clinically significant CMV infections. The results of our experience confirms that letermovir is highly effective and safe in reducing the incidence of CMV reactivation, when used from day 0 to day + 100. Impressively, the incidence of clinically significant CMV infection by day + 100 in the LET *ERA* was 8%, significantly lower than the 44% observed in the NO LET *ERA* (**Table 3**, $p = 0.0006$), even if, as reported in **Table 2a**, 8/45 patients (18%) and 11/45 patients (24%) have not completed the first 60 and 90 days of prophylaxis, respectively. The effectiveness of letermovir in reducing CMV infections and CMV-related events is even more evident if we prolong the observation up to day + 180 after allo-SCT. Our data are in line with the observations of Johnsrud and colleagues, as we found that by day + 180 the incidence of CMV clinically significant CMV infection, CMV disease, bacterial infection, probable/proven fungal infections, and the incidence of hospital re-admission reduced from 68, 12, 78, 22, and 66% to 17, 2, 45, 8, and 40%, respectively ($p < 0.00001$, $p = 0.02$, $p = 0.009$, $p = 0.05$, and $p = 0.01$, respectively; **Table 3**).

Facing the costs of PET before and after letermovir introduction, we observed a reduction in PET cost/year from Euro 38,000 to Euro 10,000, that was partially balanced by letermovir costs (Euro 13,700/pt at the dose of 240 mg/daily and Euro 29,000/pt at the dose of 480 mg/daily for 100 days). However, the cost-effectiveness should be calculated not only on the basis of the cost of drugs, but also considering the cost of hospital readmission, antibiotics, antifungal drugs, supportive therapy, and their impact on quality of life (Restelli et al., 2019).

Concerning the safety profile we confirm that the drug is highly safe, with neither hematological nor non-hematological adverse events. The drug was used at the dose reported in the investigator's brochure: 240 mg/daily in 36 patients treated with cyclosporine and 480 mg/daily in 9 patients treated with other immunosuppressive drugs. No cumulative drug-related adverse events were recorded, the drug was used from day 0 in all the patients, and no detrimental effects on engraftment and/or negative effects on the frequency and severity of GVHD were observed.

According to the registration indication, letermovir was discontinued by day + 100, but the patients continued to be monitored and 5/45 (11%) additional patients had late-onset new CMV reactivation at the last follow up (**Table 2a**). This event is of interest, and a higher number of late CMV-related events (infections and disease) are expected to be registered in the next few years, following the extensive use of haploidentical transplantation and the increasing age of patients. Thus, we think that letermovir may be useful also after day + 100 too and, in order to clearly demonstrate this, we need to wait the results of the randomized phase III multicentric trial exploring letermovir vs. placebo from day + 100 to day + 200, in which we are currently recruiting patients in our center (Clinicaltrials.gov: NCT03930615).

The need to harmonize CMV management is crucial, in order to make data comparable between different centers. This harmonization also includes the specimen for CMV monitoring (PL or WB) and the cut-off for PET initiation. The pivotal paper by Lazzarotto and colleagues suggested that, at infection onset, CMV DNA in WB is usually higher than in PL (approximately 1 log) and that the kinetic of CMV DNA clearance during PET is more effectively depicted when WB is used, with a significant reduction in the number of days on PET (Lazzarotto et al., 2018). In our cohort of 12 patients who developed CMV reactivation and received PET between February and May 2019, we observed that the peak of CMV DNA on WB displayed an insignificantly higher number copies of DNA/ml vs. PL (5.502 vs. 4.891 copies/ml) (**Figures 2A,B**). Moreover, the kinetic of CMV DNA clearance during PET was comparable in the two sources (**Figures 2A,B**). We can speculate that this finding could be related to the small number of patients or could depend on technical reasons. Our system (ELITe InGenius®) is completely automatic and thus can optimally reduce the bias eventually associated with manual manipulation of blood samples. The next step will be the expression of CMV DNA in IU instead of copies/ml, by applying a conversion factor, with the aim to abolish any inter-laboratory variation (Sidoti et al., 2019). This process is ongoing in our center and in the GITMO scientific society, in the context of a multicentric study. From June 2019 we definitively moved from PL to WB and adopted 10,000 copies/ml in two consecutive samples as the threshold for PET initiation. When the DNAemia is > 1,000 copies/ml, but < 10,000 copies/ml, we usually perform a twice weekly longitudinal monitoring of CMV DNA, in accordance with the recently published guidelines, considering additional risk factors (e.g., GHVD, mismatch transplant, early infection, and alternative donor transplantation) (Girmenia et al., 2019). This is the case of patients 13 and 14 reported in **Table 2a**, who were treated with PET given a CMV DNAemia of 4,675 and 5,451 copies/ml, respectively, because of aGVHD under steroids in both cases.

CONCLUSION

In conclusion, our real-life experience, moving from NO LET *ERA* to LET *ERA*, confirms the high efficacy and the safety of letermovir for CMV prophylaxis from day 0 to day + 100. The use of letermovir led to a significant reduction of CMV-indirect effects, such as bacterial infections, fungal infections, and hospital readmission by day + 180. We confirmed the data of the linear

correlation between CMV DNA assessed in PL and WB, but we were not able to confirm two other observations reported in the literature (Lazzarotto et al., 2018): the 1-log higher DNAemia in WB vs. PL at the time of PET initiation and the more rapid reduction in CMV DNA during PET when WB is used. Thus, we suggest that each laboratory should perform internal analysis before moving definitively from PL to WB and we consider it good clinical practice to assess two or three consecutive RT-qPCR showing at least 0.5 Log of DNAemia increase as a sign of a clinically significant CMV reactivation which requires PET.

DATA AVAILABILITY STATEMENT

The datasets generated for this study are available on request to the corresponding author.

AUTHOR CONTRIBUTIONS

MM, CP, NP, AC, and DR designed the study. MM, TZ, LG, DG, EM, NP, AT, LS, GM, SB, CZ, and MF collected and analyzed the data. CP, SC, and AC performed the laboratory analysis form CMV DNA monitoring. DB and TT performed the costs analysis. MM, CP, and DR wrote the manuscript. All authors gave their final approval before submission.

SUPPLEMENTARY MATERIAL

The Supplementary Material for this article can be found online at: https://www.frontiersin.org/articles/10.3389/fcell.2020.534268/full#supplementary-material

REFERENCES

Anderson, A., Raja, M., Vaquez, N., Morris, M., Komanduri, K., and Camargo, J. (2020). Clinical "real-world" experience with letermovir for prevention of cytomegalovirus infection in allogeneic hematopoietic cell transplantation recipients. *Clin. Transplant.* 3:e13866.

Ariza-Heredia, E. J., Nesher, L., and Chemaly, R. F. (2014). Cytomegalovirus disease after stem cell transplantation: a mini-review. *Cancer Lett.* 342, 1–8.

Boeckh, M., and Ljungman, P. (2009). How we treat cytomegalovirus in hematopoietic cell transplant recipients. *Blood* 113, 5711–5719.

Boeckh, M., and Nichols, W. G. (2004). The impact of cytomegalovirus serostatus of donor and recipient before hematopoietic stem cell transplantation in the era of antiviral prophylaxis and preemptive therapy. *Blood* 103, 2003–2008.

Cariani, E., Pollara, C., Valloncini, B., Perandin, F., Bonfanti, C., and Manca, N. (2007). Relationship between pp65 antigenemia levels and real-time quantitative DNA PCR for human cytomegalovirus (HCMV) management in immunocompromised patients. *BMC Infect. Dis.* 7:138. doi: 10.1186/1471-2334-7-138

Chen, K., Cheng, M. P., Hammond, S. P., Einsele, H., and Marty, F. M. (2018). Antiviral prophylaxis for cytomegalovirus infection in allogeneic hematopoietic cell transplantation. *Blood Adv.* 2, 2159–2175.

CMV ELITe MGB® Kit (2017). *SCH mRTK015PLD_11 of 10/03/17*. Puteaux: Elitechgroup.

Dioverti, M. V., Lahr, B. D., Germer, J. J., Yao, J. D., Gartner, M. L., and Razonable, R. R. (2017). Comparison of standardized cytomegalovirus (CMV) viral load thresholdsin whole blood and plasma of solid organ and hematopoietic stem cell transplant recipients with CMV infection and disease. *Open Forum Infect. Dis.* 4:ofx143. doi: 10.1093/ofid/ofx143

Girmenia, C., Lazzarotto, T., Bonifazi, F., Patriarca, F., Irrera, G., Ciceri, F., et al. (2019). Assessment and prevention of cytomegalovirus infection in allogeneic hematopoietic stem cell transplant and in solid organ transplant: a multidisciplinary consensus conference by the Italian GITMO, SITO, and AMCLI societies. *Clin. Transplant.* 33:e13666. doi: 10.1111/ctr.13666

Johnsrud, J. J., Nguyen, I. T., Domingo, W., Narasimhan, B., Efron, B., and Brown, J. W. (2020). Letermovir prophylaxis reduces the burden of Cytomegalovirus (CMV) in patients at high risk for CMV disease following hematopoietic cell transplant. *Bone Marrow Transplant.* 9, S1083–S8791.

Lazzarotto, T., Chiereghin, A., Piralla, A., Piccirilli, G., Girello, A., Campanini, G., et al. (2018). Cytomegalovirus and epstein-barr virus DNA kinetics in whole blood and plasma of allogeneic hematopoietic stem cell transplantation recipients. *Biol. Blood Marrow Transplant.* 24, 1699–1706.

Lin, A., Maloy, M., Su, Y., Bhatt, V., DeRespiris, L., Griffin, M., et al. (2019). Letermovir for primary and secondary cytomegalovirus prevention in allogeneic hematopoietic cell transplant recipients: real-world experience. *Transpl. Infect. Dis.* 21:e13187. doi: 10.1111/tid.13187

Ljungman, P., de la Camara, R., Robin, C., Crocchiolo, R., Einsele, H., Hill, J. A., et al. (2019). 2017 European Conference on infections in leukaemia group. Guidelines for the management of cytomegalovirus infection in patients with haematological malignancies and after stem cell transplantation from the 2017 European Conference on Infections in Leukaemia (ECIL 7). *Lancet Infect. Dis.* 9, e260–e272. doi: 10.1016/S1473-3099(19)30107-0

Malagola, M., Greco, R., Santarone, S., Natale, A., Iori, A. P., and Qoatrocchi, L. (2019). CMV management with specific immunoglobulins: a multicentric retrospective analysis on 92 allotransplanted patients. *Mediterr. J. Hematol. Infect. Dis.* 1:e2019048. doi: 10.4084/MJHID.2019.048

Marty, F. M., Ljungman, P., Chemalay, R. F., Maertens, J., Dadwal, S. S., Duarte, R. F., et al. (2017). Letermovir prophylaxis for cytomegalovirus in hematopoietic-cell transplantation. *N. Engl. J. Med.* 377, 2433–2444.

Restelli, U., Croce, D., Pacelli, V., Ciceri, F., and Girmenia, C. (2019). Cost-effectiveness analysis of the use of letermovir for the prophylaxis of cytomegalovirus in adult cytomegalovirus seropositive recipients undergoing allogeneic hematopoietic stem cell transplantation in Italy. *Infect. Drug Resist.* 12, 1127–1138.

Sharma, P., Gakar, N., Mac Donald, J., Abidi, M. Z., Benamu, E., Bajrovic, V., et al. (2020). Letermovir prophylaxis through day 100 post transplant is safe and effective compared with alternative CMV prophylaxis strategies following adult cord blood and haploidentical cord blood transplantation. *Bone Marrow Transplat.* 55, 780–786.

Sidoti, F., Piralla, A., Costa, C., Scarasciulli, M. L., Calvario, A., Conaldi, P. G., et al. (2019). Collaborative national multicenter for the identification of conversion factors from copies/mL to international units/mL for the normalization of HCMV DNA load. *Diagn. Microbiol. Infect. Dis.* 95, 152–158.

Styczynski, J. (2018). Who is the patient at risk of CMV recurrence: a review of the current scientific evidence with a focus on hematopoietic cell transplantation. *Infect. Dis. Ther.* 7, 1–16.

Conflict of Interest: MM was included in Biotest Advisory Board. DR was included in Merck Sharp and Dohme Advisory Board.

The remaining authors declare that the research was conducted in the absence of any commercial or financial relationships that could be construed as a potential conflict of interest.

frontiers in Cell and Developmental Biology

REVIEW
published: 03 November 2020
doi: 10.3389/fcell.2020.566702

Genome-Scale Metabolic Modeling for Unraveling Molecular Mechanisms of High Threat Pathogens

Mustafa Sertbas[1,2] *and Kutlu O. Ulgen*[1]*

[1] *Department of Chemical Engineering, Bogazici University, Istanbul, Turkey,* [2] *Department of Chemical Engineering, Istanbul Technical University, Istanbul, Turkey*

Pathogens give rise to a wide range of diseases threatening global health and hence drawing public health agencies' attention to establish preventative and curative solutions. Genome-scale metabolic modeling is ever increasingly used tool for biomedical applications including the elucidation of antibiotic resistance, virulence, single pathogen mechanisms and pathogen-host interaction systems. With this approach, the sophisticated cellular system of metabolic reactions inside the pathogens as well as between pathogen and host cells are represented in conjunction with their corresponding genes and enzymes. Along with essential metabolic reactions, alternate pathways and fluxes are predicted by performing computational flux analyses for the growth of pathogens in a very short time. The genes or enzymes responsible for the essential metabolic reactions in pathogen growth are regarded as potential drug targets, as *a priori* guide to researchers in the pharmaceutical field. Pathogens alter the key metabolic processes in infected host, ultimately the objective of these integrative constraint-based context-specific metabolic models is to provide novel insights toward understanding the metabolic basis of the acute and chronic processes of infection, revealing cellular mechanisms of pathogenesis, identifying strain-specific biomarkers and developing new therapeutic approaches including the combination drugs. The reaction rates predicted during different time points of pathogen development enable us to predict active pathways and those that only occur during certain stages of infection, and thus point out the putative drug targets. Among others, fatty acid and lipid syntheses reactions are recent targets of new antimicrobial drugs. Genome-scale metabolic models provide an improved understanding of how intracellular pathogens utilize the existing microenvironment of the host. Here, we reviewed the current knowledge of genome-scale metabolic modeling in pathogen cells as well as pathogen host interaction systems and the promising applications in the extension of curative strategies against pathogens for global preventative healthcare.

Keywords: genome-scale metabolic models, pathogen, systems biology, pathogen-host interactions, gene essentiality, flux balance analysis (FBA), flux variability analysis, infection

OPEN ACCESS

Edited by:
Giulia De Falco,
Queen Mary University of London, United Kingdom

Reviewed by:
Sayed-Amir Marashi,
University of Tehran, Iran
Meiyappan Lakshmanan,
*Bioprocessing Technology Institute (A*STAR), Singapore*

***Correspondence:**
Kutlu O. Ulgen
ulgenk@boun.edu.tr

Specialty section:
This article was submitted to Molecular Medicine, a section of the journal Frontiers in Cell and Developmental Biology

Received: *28 May 2020*
Accepted: *30 September 2020*
Published: *03 November 2020*

Citation:
Sertbas M and Ulgen KO (2020) Genome-Scale Metabolic Modeling for Unraveling Molecular Mechanisms of High Threat Pathogens. Front. Cell Dev. Biol. 8:566702. doi: 10.3389/fcell.2020.566702

INTRODUCTION

Pathogens give rise to a wide range of diseases threatening global health and drawing public health agencies' attention to establish preventative and curative solutions (Sweileh, 2017; World Health Organization, 2017). As antibiotics lose their effectiveness in the course of time due to the emergence of bacterial resistance, researches on antibiotics necessitate continuous improvements. However, the interest of pharmaceutical companies in antibiotic development dwindled over the last decades owing to scientific, regulatory, and economic difficulties (Brown and Wright, 2016; Luepke et al., 2016). Based on 10 different criteria including community and health-care burden, mortality, pipeline, prevalence of resistance, preventability in community and health-care setting, transmissibility, treatability and trend of resistance, 20 bacterial species among 25 antibiotic-resistant bacteria were classified into three priority groups as critical, high and medium priority. Multidrug-resistant *Mycobacterium tuberculosis* takes the global priority.

Over the quarter century after the first genome sequenced for pathogenic *Haemophilus influenzae* Rd in 1995, the advances in experimental and computational technologies have accelerated context-specific understanding of complex biological networks and the emergence of a new field of science, called systems biology (Fleischmann et al., 1995; Aggarwal and Lee, 2003). Metabolic reactions in conjunction with their corresponding metabolites and genes constitute a sophisticated cellular system inside the pathogens. This interconnection among genes, metabolites and reactions are converted into mathematical representation by using genome-scale metabolic modeling which is an ever increasingly used computational approach in the field of systems biology to elucidate pathogenic mechanisms along with their host interactions. Numerous pathogen-specific genome-scale metabolic models (GEMs) were reconstructed in the last two decades (**Table 1**). The key aspects such as predicting cellular and disease phenotypes, production of virulence factors, and evolution of antibiotic resistance related to human pathogens have been effectively studied by GEMs. In addition to identifying the cellular phenotype of a single pathogen, this modeling approach can be extended to interactions between pathogen and host cells (Jamshidi and Raghunathan, 2015).

Essential genes are mandatory for the cellular growth, and their computational prediction plays a fundamental role in genome-scale modeling of pathogens. These genes are regarded as potential drug targets for killing pathogenic microorganisms. Instead of tedious and time-consuming experimental work, *a priori* computational analysis of gene essentiality and drug targeting by using constraint-based metabolic models can save considerable time and effort. The deletion of a single gene in the laboratory and observation of phenotypic change may take a few days or weeks; however, computational analysis of gene deletion is performed within seconds. An important point that need to be considered in the gene essentiality analysis for drug targeting studies, is essential genes be specific to pathogenic microorganisms.

Since their emergence two decades ago, GEMs have extended our knowledge toward system-level understanding of pathogenesis of microbial infections. They have provided irreplaceable contributions to elucidate antibiotic resistance, virulence, single pathogenic as well as pathogen-host interaction mechanisms. Pathogens change the key metabolic processes both in themselves and the host cell depending on the nutrient sources present in the infected host niche. Therefore, revealing cellular mechanisms of pathogenesis, identifying strain-specific biomarkers and developing new therapeutic approaches have great importance. Here, we reviewed the current knowledge of genome-scale metabolic modeling in pathogen cells with the specific examples mainly from WHO prioritization list as well as pathogen host interaction systems and its promising applications in the extension of curative strategies against pathogens for global preventative healthcare. GEMs integrated with genomic, proteomic and metabolomic data may be the first step toward the quantitative analysis of the pathogen metabolism, and thus can provide a remarkable benefit for the researchers as *a priori* guide in the drug target studies.

GENOME-SCALE METABOLIC MODELING AND ANALYSIS

First genome sequences were published for bacterial pathogens *Haemophilus influenzae* and *Mycoplasma genetalium* in 1995. Since then, continual improvements in genome sequencing technologies and their applications to genome analysis of pathogens have resulted in the comprehensive gene and cellular network information specific to microorganism of interest (Reed et al., 2006; Land et al., 2015). The cutting-edge technologies facilitated the understanding of complex cellular mechanisms behind the genomic variations in pathogens (Bryant et al., 2012). Starting with the genome annotation, the genome-scale metabolic modeling aims to reconstruct the mathematical representation of interconnected biochemical relationship among genes, reactions, and metabolites (**Figure 1**).

A crucial component of the pathogen-specific GEM reconstruction is the accurate inclusion of microbial metabolism to investigate cellular mechanism. In addition to common metabolic pathways, different pathogens have particular pathways, which are hallmark to expand models toward better understanding of pathogenic mechanisms. For example, mycolic acid is the unique component of the mycobacterial cell envelope and essential for the growth of devastating pathogen *M. tuberculosis* causing tuberculosis (Marrakchi et al., 2014). The metabolic reactions in mycolic acid biosynthetic pathway should thus be included in the GEM of *M. tuberculosis*. Moreover, virulence factors are the critical molecules in the infection mechanism and their synthesis pathways need to be incorporated into reconstructed GEM for valuable insight into virulence factor metabolism (Bartell et al., 2017).

In accordance with pathogen-specific data, validated experimentally or available in the literature, the localization of metabolic reactions into the different cellular compartments, the addition of transport reactions between the compartments inside the cell and the determination of biomass reaction with correct composition of its constituents (i.e., stoichiometric

TABLE 1 | Reconstructed GEM examples of priority pathogens reported by World Health Organization (2017).

Pathogen	Priority	Model name	Number of metabolites	Number of genes	Number of reactions	References
Mycobacterium tuberculosis	Global	iNJ661	826	661	1,025	Jamshidi and Palsson, 2007
		GSMN-TB	645	726	856	Beste et al., 2007
		GSMN-TB 1.1	766	759	876	Lofthouse et al., 2013
		sMtb	929	915	1,192	Rienksma et al., 2014
		iOSDD890	961	890	1,152	Vashisht et al., 2014
		iSM810	723	810	938	Ma et al., 2015
		iEK1011	998	1011	1,128	Kavvas et al., 2018
Acinetobacter baumannii	Critical	AbyMBEL891	778	650	891	Kim et al., 2010
		iLP844	1,509	844	1,628	Presta et al., 2017
		iCN718	890	718	1,016	Norsigian et al., 2018
Pseudomonas aeruginosa	Critical	iMO1056	760	1,056	883	Oberhardt et al., 2008
		iMO1086	1,021	1,086	1,031	Oberhardt et al., 2011
		iPae1146	1,284	1146	1,493	Bartell et al., 2017
		iPau1129	1,286	1,129	1,495	Bartell et al., 2017
		iPAO1	3,022	1,458	4,265	Zhu et al., 2018
Escherichia coli	Critical	15 pathogenic strain	1,378–1,484	4,584–5,784	1,473–1,564	Vieira et al., 2011
Klebsiella pneumoniae	Critical	iYL1228	1,685	1,228	1,970	Liao et al., 2011
Helicobacter pylori	High	iCS291	403	291	388	Schilling et al., 2002
		iIT341	485	341	554	Thiele et al., 2005
Salmonella typhimurium	High	iRR1083	774	1,083	1,087	Raghunathan et al., 2009
		iMA945	1,036	945	1,964	AbuOun et al., 2009
		STM_v1.0	1,119	1,270	2,201	Thiele et al., 2011
		MetaSal	1,088	824	1„097	Hartman et al., 2014
Staphylococcus aureus	High	iSB619	571	619	641	Becker and Palsson, 2005
		iMH551	604	551	712	Heinemann et al., 2005
		iSA863	1,379	863	1,545	Mazharul Islam et al., 2020
Campylobacter jejuni	High	-	467	388	536	Metris et al., 2011
Streptococcus pneumoniae	Medium	iDS372	355	372	462	Dias et al., 2019
Haemophilus influenzae	Medium	iJE296	343	296	488	Edwards and Palsson, 1999
		iCS400	451	400	561	Schilling and Palsson, 2000

coefficients) play crucial roles in GEMs. When hundreds or thousands of metabolic reactions occurring inside the pathogenic cells and their literature-based distribution among different compartments are taken into consideration, the reconstruction process is extensively time-consuming and needs to be standardized. This reconstruction process was described by various studies (Francke et al., 2005; Rocha et al., 2008; Feist et al., 2009). A comprehensive protocol (**Figure 1**) with four main stages (draft reconstruction, manual curation, conversion to mathematical model and network analysis) in genome-scale metabolic modeling was published by Thiele and Palsson (2010). In a very recent publication, this protocol was extended toward developing multi-strain GEMs from a reference model (Norsigian et al., 2020).

Different tools and softwares have been developed to facilitate and accelerate metabolic reconstruction process (Hamilton and Reed, 2014; Mendoza et al., 2019). The biochemical databases such as KEGG, BRENDA, and MetaCyc have become remarkable sources in this reconstruction process to obtain collective information on genes, enzymes, reactions, metabolites and pathways (Kanehisa, 2000; Schomburg, 2002; Caspi et al., 2012). High-throughput phenotype microarrays technology (Biolog) provide clues toward the viability of the pathogenic microorganisms on hundreds of nutrient sources simultaneously (Bochner et al., 2001). Biolog phenotype microarrays take full advantage of respiration of the cells, detected by tetrazolium dye, as a reporter system. Therefore, in addition to the model refinement, Biolog data have been used in the validation of a wide range of GEMs (Oberhardt et al., 2008, 2011; Baumler et al., 2011; Liao et al., 2011; Metris et al., 2011; Bartell et al., 2017; Norsigian et al., 2018; Zhu et al., 2018).

Genome-scale metabolic models have many key advantages in the investigation of pathogenic processes. They allow to perform thousands of different infection scenario simulations in a very short time in an effective manner. Cellular phenotypes such as growth and virulence factor production are predicted by changing nutrient sources present in the host environment. Different infected locations within the human body show

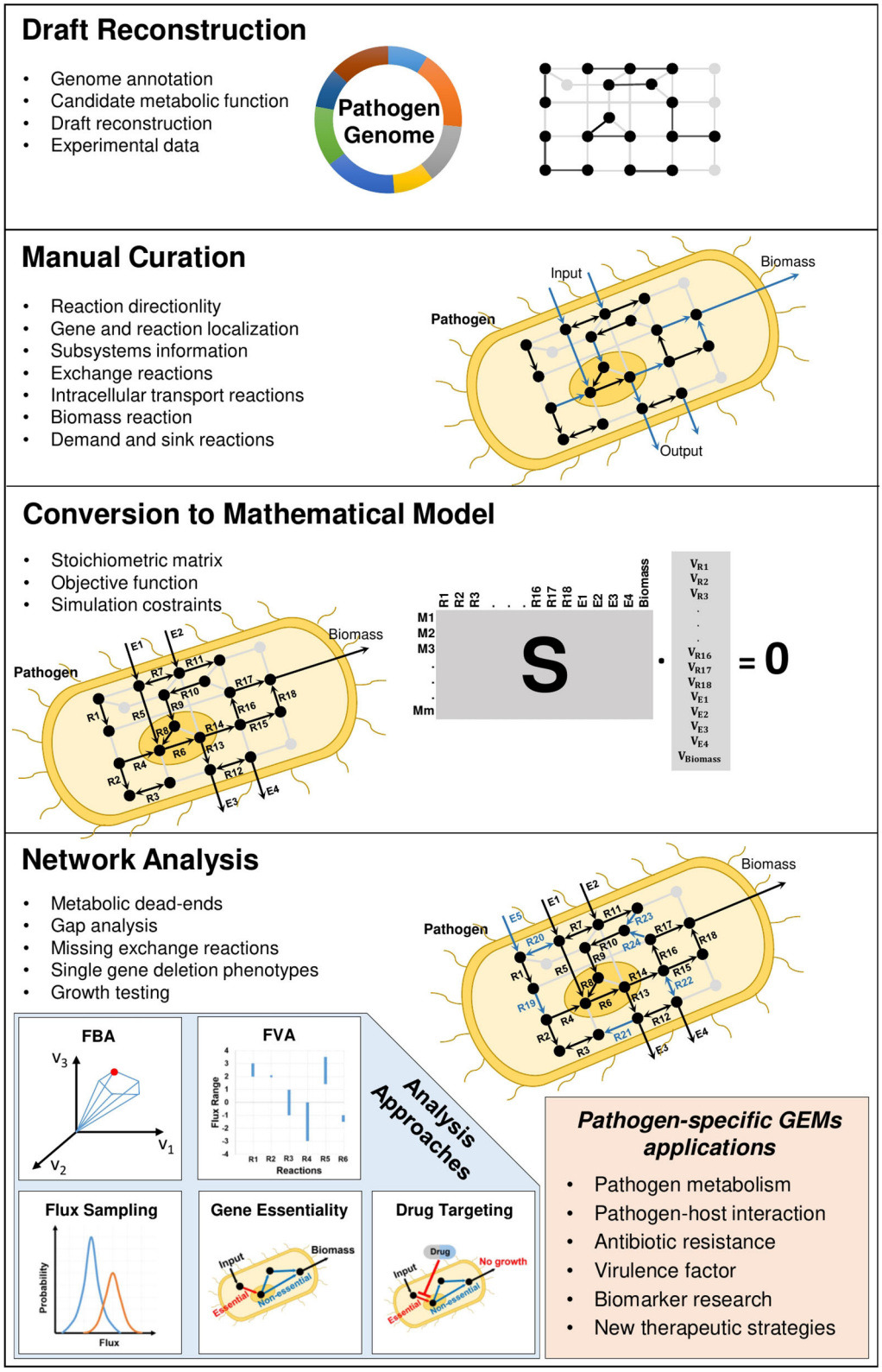

FIGURE 1 | Reconstruction process of pathogen-specific GEMs.

different nutrient distributions and thus different infection features and growth phenotypes that can be rapidly deduced from GEMs. They are highly cost-effective in gene deletion analysis. Thus, essential genes are examined by carrying out *in silico* simulations with gene deletion one by one in the genome-scale network. These predicted essential genes and their products are considered as putative drug targets to fight against pathogen of interest. Multi-omics data can be easily mapped to GEMs to investigate condition-specific pathogenicity. The integrated analysis of pathogen and host GEMs enables us to identify essential metabolic connections between host and pathogen and thus to unlock the mechanisms behind their interactions.

Flux Balance Analysis

Flux balance analysis (FBA) is a frequently used constraint-based modeling approach to represent the possible behavior of microbial metabolism and plays an irreplaceable role in genome-scale metabolic modeling (Kauffman et al., 2003; Orth et al., 2010). FBA uses metabolic reaction stoichiometry together with the physiochemical and environmental constraints at steady state condition. Subsequent to conversion of genome-scale metabolic reconstruction to mathematical matrix format at steady state, FBA finds a flux distribution which maximizes the objective function. Stoichiometric coefficients of the metabolic reactions compose stoichiometric matrix (S), where the rows and columns are represented by metabolites and reactions, respectively. Metabolic fluxes constitute flux vector (v) of the metabolic reactions in the GEM. At steady state, a system of linear equations obtained from the metabolic network, is given by:

$$\mathrm{S.v} = 0$$

Constraints, arising from reaction directionalities and experimental measurements, are imposed by arranging upper and lower limits. The exchange fluxes between the pathogen cell and environment are involved in accordance with the metabolites in the growth medium. Maximization of biomass is defined as objective function in order to simulate pathogen growth. The linear optimization problem used in FBA is summarized below:

$$\begin{aligned} &max\, f^T v \\ &s.t\ S.v = 0 \\ &v_{lower} \leq v \leq v_{upper} \end{aligned}$$

where f is objective function vector, the vector of coefficients assigning the cellular objective to each reaction.

Flux Variability Analysis

Constraint-based modeling leaves open the possibility of alternate optimal solutions which mean that the same objective value can be achieved by a diverse set of flux distributions and the solution is not unique. Flux variability analysis (FVA) determines the possible range of flux quantities which is allowable with the given objective value (Mahadevan and Schilling, 2003). First, the value of the objective function that is maximization of growth in pathogenic microorganisms is computed by FBA. By adding and fixing calculated objective value in the model, a series of FBA/FVA is performed for each reaction in the GEM with the maximization and minimization objective function for allowable range of fluxes for each reaction. The reactions with the same minimum and maximum non-zero fluxes computed by FVA are essential in accomplishing certain objective. There are no alternative pathways for those in which these reactions exist and therefore these reactions and pathways are essentially involved in the GEM to succeed objective of interest. Mathematical formulation of FVA is given by:

$$\begin{aligned} &max\ v_i \text{ and } min\ v_i \\ &\text{s.t S.v} = 0 \\ &f^T v = Z_{obj} \\ &v_{lower} \leq v_i \leq v_{upper} \text{ for } i = 1, \ldots n \end{aligned}$$

where Z_{obj} is previously computed objective function value by using FBA.

Growth and metabolic state predictions are calculated by FBA and FVA. Flux variability analysis determines all possible alternate routes for growth of a microorganism and thus identifies a minimal set of reactions required for pathogen intracellular survival. FBA and FVA are used in testing and validation of the GEMs by comparing with the experimental data. The consistency between *in silico* growth simulations and experimental studies demonstrate the predictive power of the model.

Flux Sampling

Flux sampling calculates all feasible solutions throughout the entire solution space in a statistical meaningful way (Price et al., 2004; Schellenberger and Palsson, 2009; Bordel et al., 2010; Herrmann et al., 2019). Sufficient and uniform data points are required for the accurate and unbiased analysis of the solution space. Both flux sampling and FVA computes feasible flux range; i.e., set of possible flux distributions. However, flux sampling gives additional information on probability of flux solutions. Different from FBA, flux sampling does not require an objective function. Therefore, it is an effective and alternative approach in analyzing the GEMs when certain objective of cell is not clear. Several algorithms were developed for flux sampling. Artificial centering hit-and-run (ACHR) algorithm calculates the random flux distributions by using the center estimate and random flux vector direction (Kaufman and Smith, 1998). Coordinate hit-and-run with rounding (CHRR) applies a rounding preprocessing to the anisotropic flux sets (Haraldsdóttir et al., 2017). *optGpSampler* provides an opportunity of use of large samples via parallel sampling to reduce computation process (Megchelenbrink et al., 2014).

Gene Essentiality

Essential genes are necessary for completeness of metabolic network and proper functioning of the cell. They have crucial roles in the development of phenotypic features of microorganism. Their knockouts give rise to failure in the cellular metabolism and no growth condition eventually. Therefore, essential gene studies in pathogenic microorganisms gain further importance to fight against pathogens. Experimental analyses of

essential genes are performed by different methods including random mutagenesis, targeted mutagenesis and knockdown approaches (Rancati et al., 2018; Gonyar et al., 2019). These studies constitute a significant platform for computational gene essentiality predictions by using pathogen-specific GEMs (Joyce and Palsson, 2007). Computationally predicted genes are compared with the experimentally obtained essential gene datasets for the predictive capacity of the GEMs. FBA is widely used in gene essentiality predictions. Genes are deleted from the model on an individual basis by setting the flux value of corresponding reactions to zero. The objective function, used in the optimization, is the maximization of biomass production. If the flux analysis results in no growth, the corresponding gene is predicted to be essential.

The formulation of the biomass reaction (equation) in the GEM holds a great importance (Thiele and Palsson, 2010). It should include accurate chemical compositions of the pathogen obtained from experimental studies. In addition to growth associated maintenance, required energy for macromolecular synthesis, the content of amino acid, nucleotide, lipid, soluble pool (polyamines, vitamins, and cofactors) and ions are required in the generation of biomass equation. The composition of the biomass reaction is critical for the analysis of essential genes. If a biomass precursor is not included in the biomass reaction, its synthesis reactions may not be necessary for the cellular growth and these reactions are regarded as non-essential with the associated genes in the computational analysis.

Drug Targeting

Target identification is the primary and indispensable step in drug discovery and development to combat infection. Impairments in the metabolic functionalities of the investigated microorganisms give rise to cell death due to drug inhibition (Fischbach and Walsh, 2009). Conventional methods require an extensive and expensive experimental research to detect therapeutic targets. On the other hand, computational studies reveal a rapid and cost-effective alternative route by predicting novel targets, which are critical for cell growth. Over the last decade, genome-scale metabolic modeling has fulfilled an inevitable rise in the prediction of pathogenic drug targets. Within this scope, essential genes and their corresponding products, obtained from *in silico* analysis of pathogen-specific GEMs, are regarded as putative drug targets to inhibit cell survival.

The ideal drug target is the target with little or no harm to the host organism. Fungal sphingolipid pathways are different in many ways from their mammalian analogs in terms of enzymes and products. The glucosylceramide (GlcCer) lowering antifungal agents have an important potential to control and prevent infections. Acyhydrazones have been identified as the inhibitor of glucosylceramide synthase enzyme. When the glycosylceramide synthesis gene is deleted in *Cryptococcus neoformans*, the strain does not produce glycosylceramide and is avirulent in host organism. In this context, glucosylceramide (GlcCer) lowering agents or inhibitors of glycosylceramide synthesis can be considered as new opportunities to prevent fungal infections (Rittershaus et al., 2006; Raj et al., 2017).

Other Methods

Constraint-based methods mentioned above are the most frequent techniques used in the analysis of pathogen-specific GEMs. Investigation of the *in silico* killing strategies of pathogenic bacteria is the main goal of the pathogen-specific GEMs; however, the maximum amount of production of valuable metabolites takes great importance in industrial microorganisms' GEMs with the minimum cost. Depending on the application of the GEMs, various approaches are also available in the literature. Among them, dynamic FBA (dFBA) was suggested for the study of the metabolic network dynamics since the classical FBA is used for steady state systems (Mahadevan et al., 2002). Minimization of metabolic adjustments (MOMA) and regulatory on-off minimization (ROOM) are used in the analysis of response to gene deletion or insertion (Segrè et al., 2002; Shlomi et al., 2005). Metabolic reactions controlled by the genes of interest are deleted from the GEM and the new reaction fluxes are optimized with the minimum metabolic change.

GENOME-SCALE METABOLIC MODELS OF PATHOGENIC MICROORGANISMS AND ANTIBIOTIC RESISTANCE

Antibiotic resistance is a growing problem threatening global health. Development of promising novel treatments require a complete understanding of resistance mechanisms. For this purpose, adaptive laboratory evolution experiments are frequently used where the pathogens are treated with certain antibiotics and tested whether to develop resistance (Conrad et al., 2011; Dragosits and Mattanovich, 2013; Zampieri et al., 2017; Dunphy et al., 2019). Multi-omics technologies, including transcriptomics, proteomics and metabolomics, have become crucial components of these experiments since they provide simultaneous measurements of thousands of gene expressions, proteins and metabolites, respectively. Muti-omics data are collected from the wild-type and antibiotic-resistant pathogens at various time points. Then, they are integrated with the pathogen-specific GEMs for system-level understanding of pathogenic shifts due to antibiotic resistance (**Figure 2**). The integration process, that maps high throughput omics data onto high-connected metabolic network, facilitates the prediction of feasible flux distributions throughout pathogenic metabolism. Consequently, the novel therapeutic strategies are proposed to combat antibiotic resistance as well as infection.

Several applications of GEMs in antibiotic resistance have been published by the researchers around the world (Dunphy and Papin, 2018). Recently, the flux distributions and metabolic changes of streptomycin resistant and chloramphenicol resistant *Chromobacterium violaceum* were studied by using its specific GEM (iDB858) and metabolomics data (Banerjee and Raghunathan, 2019). FVA was carried out to predict the metabolic reprogramming due antibiotic pressures. Chloramphenicol resistance enhanced acetate production, whereas streptomycin resistance resulted in increased secretion of both acetate and formate. NAD/NADH ratio of streptomycin resistant population growing on glucose was calculated to

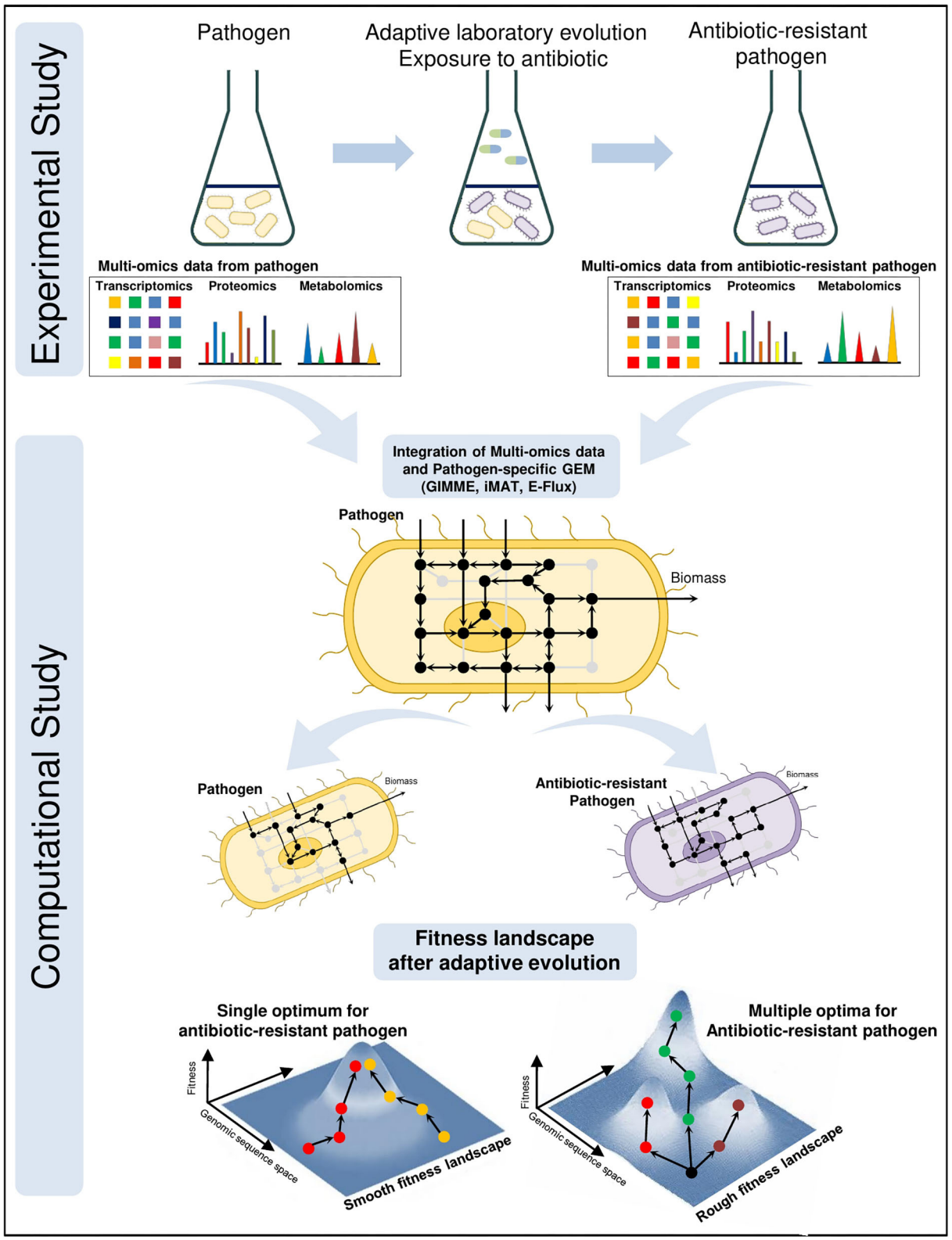

FIGURE 2 | Integrated investigation of the antibiotic resistance by adaptive laboratory evolution (ALE) experiments and pathogen-specific GEMs. Multi-omics data are collected during the ALE experiments from wild-type and antibiotic-resistant pathogens at different time points. To elucidate the evolutionary response at system-level due to antibiotic pressure, high throughput omics data are computationally mapped onto the genome-scale metabolic network. Analysis of metabolic shift in the

(Continued)

FIGURE 2 | cellular metabolism and mechanism of antibiotic-resistant pathogenic GEMs facilitate the discovery of novel potential drug targets and treatment strategies against antibiotic-resistant pathogen. Fitness landscapes demonstrate the optimality in adaptive evolution of antibiotic resistance. Smooth fitness landscapes consist of a single optimum and regardless of the starting point evolutionary tendency converge to this optimum. There exist multiple optima on the rough fitness landscapes and evolutionary tendency diverge even from the same starting point.

be higher than that of chloramphenicol resistant population (2.47–0.28). Further works on this issue will be discussed under the related pathogenic bacteria below.

Mycobacterium tuberculosis

M. tuberculosis is one of the most studied pathogens in genome-scale metabolic modeling due to its global priority. The first GEMs published for this pathogen are iNJ661 and GSMN-TB (Beste et al., 2007; Jamshidi and Palsson, 2007). Genome annotation of *M. tuberculosis* H37Rv was used as the starting point in iNJ661 model reconstruction (Cole et al., 1998). However, GSMN-TB model was initiated with previously developed *Streptomyces coelicolor* genome-scale metabolic model (Borodina et al., 2005). *M. tuberculosis* specific reactions obtained from literature and biochemical databases were added to both models throughout the reconstruction processes. Instead of starting with annotated genome, previously developed genome-scale metabolic models can also be used as a draft in the reconstruction process. Therefore, these initial models became a starting point for the most of the subsequent *M. tuberculosis* genome-scale metabolic models. More than 10 genome-scale models were developed for this pathogen with divergent representations around the world by extending previous ones (Lofthouse et al., 2013; Rienksma et al., 2014, 2018; Vashisht et al., 2014; Ma et al., 2015). They were standardized and updated with a new model iEK1011, including 1228 reactions, 1,011 genes and 998 metabolites (Kavvas et al., 2018). Recently, eight *M. tuberculosis* GEMs were systematically evaluated for accurate model selection (López-Agudelo et al., 2020). By taking genetic information, network topology, blocked reactions, mass and charge balance reactions and gene essentiality predictions into consideration, iEK1011 and sMtb2018 were described as the best performing *M. tuberculosis* GEMs. These two GEMs were further improved and named iEK1011_2.0 and sMtb2.0, respectively. These updated versions allow comprehensive *in silico* investigation of the effects of various environmental and genetic conditions on *M. tuberculosis* metabolism.

Jamshidi and Palsson (2007) analyzed essentiality of glycerol and non-essentiality of glucose in *M. tuberculosis* model iNJ661 by using FVA at maximum biomass production. Glycerol transporter and glycerol kinase in glycerol metabolism were computed as non-zero flux values with no flexibility. This shows that glycerol-3-phosphate production via glycerol kinase is required for membrane and fatty acid metabolism. Beste et al. (2007) investigated *in silico* slow growth mechanism of *M. tuberculosis* by using GSMN-TB. The reactions in the glyoxylate shunt were predicted to be significantly changed due to the slow growth of organism. A high increase was computed in the isocitrate lyase reaction flux. This observation proposed a hypothesis of a key role of isocitrate lyase to sustain growth at the slow growth condition. The activity of isoctrate lyase was measured at slow and fast growth rates experimentally. Consistent with the simulations, the activity of this enzyme was twofold higher in the slow growing cells.

The mechanism of antibiotic resistance evolution in *M. tuberculosis* was investigated by means of *in silico* iEK1011 (Kavvas et al., 2018). Antibiotic-specific pressures were imposed by using an associated metabolic objective function. For example, decaprenylphosphoryl-β-D-arabinose (DPA) production was elevated by *ubiA* mutations, which cause ethambutol resistance. Consequently, the maximization of DPA production was used as the objective function to simulate antibiotic resistance evolution due to ethambutol (Safi et al., 2013). In order to incorporate this evolution into *in silico* iEK1011 model, the minimization of mycothiol production was selected for ethionamide and the maximization of tetrahydrofolate and L-alanine production were chosen as objective functions for para-aminosalicylic acid and d-cycloserine, respectively (Vilchèze et al., 2008; Zheng et al., 2013; Desjardins et al., 2016). The computational analyses of *in vivo* and *in vitro* conditions were performed by FVA, and an important effect of L-alanine due to correlation between the ethambutol and d-cycloserine fluxes was unraveled. These two antibiotics may be less effective *in vivo* owing to the presence of L-alanine.

Acinetobacter baumannii

An important high threat pathogens in hospitals is *A. baumannii,* causing various infections covering pneumonia, blood-stream, urinary-tract and wound infections (Dijkshoorn et al., 2007). First GEM for multi-drug resistant *A. baumannii* AYE is AbyMBEL891, reconstructed from genome annotation data integrated with literature and biological databases (Vallenet et al., 2008; Kim et al., 2010). Similarly, genome-scale metabolic model iLP844 was developed for *A. baumannii* ATCC 19606, which was initiated with a draft model from genome annotation by using Kbase and then manually curated (Davenport et al., 2014; Presta et al., 2017; Arkin et al., 2018). The publications of new studies lead to the inclusion of new knowledge into the model and also to the validation of the model with more experimental work enhancing its prediction quality. In accordance with this purpose, AbyMBEL891 model was updated with the new data produced in experiments and standardized into a new model, iCN718, to provide more accurate representation of the microorganism (Norsigian et al., 2018). iCN718 was used in the simulation of growth behavior and the development of strain-specific GEMs of 74 other *A. baumannii* strains.

The role of reaction reversibility on gene essentiality was simulated using *in silico* AbyMBEL891 model of *A.*

baumannii (Kim et al., 2010). Ornithine carbamoyltransferase and argininosuccinate synthase reactions are experimentally demonstrated to be essential in arginine biosynthesis and cell growth in the *A. baumannii* (Dorsey et al., 2002). These reactions were also computationally estimated to be essential on condition that a series of alternative path reactions toward arginine production were set irreversible. If the reactions in alternative route were set as reversible, two essential reactions became non-essential and AbyMBEL891 lost the capability to synthesize arginine. Thus, *in silico* AbyMBEL891 model gives consistent simulation results with *A. baumannii* phenotype and provides a valuable use in reaction reversibility.

Similar to essential genes, the metabolites whose absence leads to no growth are considered essential metabolites (Kim et al., 2010). They are predicted by using flux balance analysis and removing each metabolite out of the cell to explore their effect on cell growth. Computational investigation of an essential metabolite in the GEM is performed by the deletion (zero flux values) of all outgoing reactions and allowing non-zero flux values of the incoming reactions associated with the interested metabolite (Kim et al., 2007). Kim et al. (2010) presented essential metabolite filtering method (EMFilter) to discover effective drug targets for *in silico* AbyMBEL891. EMFilter includes four steps that are removal of currency metabolites, selection of essential metabolites existing in more than three reactions, removal of metabolites present in human metabolic network and removal of metabolites related with genes which have human homologs. In order to avoid drug interference with any of the human enzymes and identify multi-drug target, EMFilter narrowed 211 essential metabolites down to 9 metabolites for drug targeting by using these four steps. The enzymes catalyzing the outgoing reactions associated with essential metabolites were predicted to be final candidate drug target. D-glutamate and 4-aminobenzoate were predicted as essential metabolites *in silico* and they have critical roles in the biosynthesis of bacterial cell wall and folate, respectively (Lundqvist et al., 2007; Valderas et al., 2008). Six essential metabolites were also predicted to be essential for four pathogens among *A. baumannii, E. coli, H. pylori, M. tuberculosis, P. aeruginosa,* and *S. aureus*. Therefore, the enzymes catalyzing the reactions in which these six essential metabolites are involved could be regarded as broad-spectrum drug targets due to the fact that a broad-spectrum antibiotic acts against a wide range of pathogenic bacteria.

The colistin-resistant *A. baumannii* metabolism was studied by GEM to determine new putative drug targets (Presta et al., 2017). The *in silico* model iLP844 was integrated with transcriptomic response to colistin, sampled at 15 and 60 min after its exposure (Henry et al., 2014). The integration was performed by using MADE (Metabolic Adjustment by Differential Expression) method which maps gene expression data onto genome-scale metabolic network (Jensen and Papin, 2011). Essential genes were computed at 15 and 60 min with and without colistin exposure to analyze the shifts in gene essentiality. In addition to 66 essential genes shared between with and without colistin exposure, 21 and 17 condition-specific essential genes were predicted for 15 and 60 min data, respectively. Following colistin exposure, some essential genes became non-essential and vice versa. These results demonstrated changes in gene essentiality patterns due to colistin and consequently significant drug targets for *A. baumannii* ATCC 19606 strain. Potential drug candidates should be pathogen-specific and should not have orthologs in human to avoid side-effects. Subsequent to BLAST search, they defined four condition-specific and 46 general essential genes without human orthologous (Altschul et al., 1990). To study colistin resistance mechanism, loss of lipopolysaccharide (LPS) production approach was implemented with the transcriptomic data sampled at 60 minutes (Moffatt et al., 2010). LPS component was removed from biomass reaction in iLP844 to simulate LPS deficit *A. baumannii*. They observed 54 shared essential genes in the presence and absence of colistin resistance at 60 min. Eighteen genes switched from non-essential to essential. By applying BLAST search, they demonstrated that five essential genes do not have orthologs in human and these can be considered as specific targets in combination therapy with colistin in LPS deficient strain of *A. baumannii*.

Pseudomonas aeruginosa

Pathogenic genome-scale metabolic modeling can potentially be used for comparative analysis and drug assessment. Genome-scale metabolic model iMO1056 was developed for *P. aeruginosa* PAO1 from annotated genome, published studies and databases (Stover et al., 2000; Oberhardt et al., 2008). Three years later, iMO1056 was updated with iMO1086 and reconciled with non-pathogenic *P. putida* model (iJP962) by the same research group for comparative analysis of these two strains for understanding the pathogenicity (Oberhardt et al., 2011). To reflect different mechanisms in these two microorganisms, a number of unique reactions and pathways were identified including naphthalene and anthracene degradation, phenylalanine metabolism and benzoate degradation in *P. putida* and pyrimidine, purine and beta-alanine metabolism in *P. aeruginosa*. The *in silico* iMO1056 was used in the study of multiple targets in *P. aeruginosa* and 41 putative targets were suggested (Perumal et al., 2011). Recently, Bartell et al. (2017) presented two GEMs for *P. aeruginosa* strain PAO1 and *P. aeruginosa* strain PA14 (iPae1146 and iPau1129, respectively) to provide insight into the relationship between virulence factor production and growth. These two *in silico* models included 112 and 108 virulence-associated genes, respectively. The genes only critical for virulence factor production, growth and both were analyzed and thus non-obvious links between virulence factor production and growth were observed. iMO1056 and Opt208964, an automatically generated GEM by Model SEED, were used as initial drafts in the development of iPAO1, which is then extensively curated using the literature and databases toward the study of polymyxin treatment in *P. aeruginosa* metabolism at the systems level (Henry et al., 2010; Zhu et al., 2018). Together with other biochemical databases, *Pseudomonas aeruginosa* specific database PseudoCAP provides valuable metabolic information for GEM reconstruction of this organism (Winsor et al., 2005).

Oberhardt et al. (2011) performed comparative pathway flexibility analysis of pathogenic *P. aeruginosa* and non-pathogenic *P. putida* by using *in silico* iMO1086 and iJP962, respectively. Three sulfur-associated pathways, which are sulfur

metabolism, taurine and hypotaurine metabolism, and cysteine and methionine metabolism, showed more flexibility in *P. aeruginosa* than in *P. putida*. This finding demonstrated significant probability of sulfur-associated pathways behind the distinct phenotypes. Enhanced flexibility of *P. aeruginosa* was also simulated in terms of nitrogen metabolism and the demand reactions of virulence factor. *P. aeruginosa* is able to carry out denitrification in microaerobic condition which can be seen in lung infections of cystic fibrosis patients (Eschbach et al., 2004), whereas *P. putida* cannot carry out denitrification. Increased flexibility simulation of *P. aeruginosa*, in comparison with *P. putida*, is in agreement with the known role of denitrification in virulence.

The essential genes in *Pseudomonas aeruginosa* were investigated for both virulence factor synthesis and growth by using *in silico* mPA14 and comparing 46 shared essential genes for biomass production and synthesis of at least one virulence factor (Bartell et al., 2017). Seven genes (*aacA, aacB, aacC, aacD, fabB, fabD,* and *fabG*) in fatty acid and phospholipid metabolism were predicted to be essential for growth and production of at least eight virulence factors. Growth-essential genes in aromatic amino acid synthesis (*aroB, aroC, aroE,* and *aroK*) were predicted to be essential for the synthesis of six virulence factors which are chorismate, pyocyanin, 1-carboxyphenazine, salicylate, dihydroaeruginoic acid and pyochelin. Moreover, the interconnectivity for each knockout was computationally researched by plotting virulence factor vs. growth inhibition compared to wild-type simulations. Uncertain connections between growth and virulence factor production were determined from the distribution of data points on plots. Several growth-essential genes partially hindered virulence factor synthesis. The virulence factor-related essential genes were significantly altered and not correlated with pathway complexity.

Investigation of metabolic response of pathogenic *P. aeruginosa* to polymyxin B treatment unlocked its effect on bacterial metabolism with the help of genome-scale metabolic model iPAO1 (Zhu et al., 2018). RNA-seq data obtained in the presence and absence of polymyxin B were combined with the *in silico* model by using E-Flux method constraining fluxes as a function of the gene expression level (Colijn et al., 2009). Several pathways involved in central, amino acid and fatty acid metabolisms were found to be significantly perturbed because of polymyxin B treatment which enhanced oxygen uptake and decreased the growth rate. In TCA cycle, NADH production and the fluxes from citrate to fumarate were increased. The reduction in biomass production due to polymyxin treatment resulted in the downregulation of fluxes in LPS, GPL and peptidoglycan biosynthesis. Spermidine biosynthesis enhanced with the increased expression level of *sdeD* and *speE* encoding S-adenosyl-L-methionine decarboxylase and spermidine synthase, respectively.

Escherichia coli

Due to its genetic simplicity as well as its history in a variety of infections, *Escherichia coli* is one of the most extensively studied microorganisms in genome-scale metabolic modeling. Based on the genome sequence, the first GEM (iJO660) for *E. coli* was reconstructed for K-12 MG1655 commensal and common laboratory strain (Blattner et al., 1997; Edwards and Palsson, 2000). Over the last two decades, several updates were published to expand the understanding of bacterial mechanism via *in silico* network of *E. coli* (Reed et al., 2003; Feist et al., 2007; Orth et al., 2011; Monk et al., 2017). Besides the commensal strains, there also exist pathogenic strains of *E. coli* which brings about different intestinal and extraintestinal infections (Kaper et al., 2004). So as to reveal further insight into evolution mechanism *in silico*, Baumler et al. (2011) developed six strain-specific genome-scale model of *E. coli* (two enterohemorrhagic (EHEC), two uropathogenic (UPEC) and two commensal strains) by means of pangenome and core GEM. In addition to several pathogen specific reaction deletions, eight new reactions unique to EHEC strains were added, which are fructose synthetase, gentisate 1,2,-dioxygenase, perosamine synthetase, salicylate hydroxylase, sucrose transport, urease, tellurite reduction and UDP-N-acetylglucosamine 4-epimerase reactions. UPEC strains included only one addition of propionate CoA-transferase reaction in common. Furthermore, one unique reaction was added to each UPEC strain; hydroxy-pyruvate reaction for UTI89 strain and galactose isomerase reaction for CFT073 strain. The comperative simulations of strain-specific *E. coli* models resulted in variations of biomass yields on glucose due to the strain-specific metabolic reactions.

By increasing the number of the strains investigated, the diversities of the commensal and pathogenic *E. coli* strains were broadened (Vieira et al., 2011; Monk et al., 2013). Vieira et al. (2011) developed a genome-scale metabolic network for the analysis of core and panmetabolism in 29 *E. coli* strains including 21 pathogenic strains and eight commensal strains, which cover six *Shigella* strains. The reconstructed strain-specific GEMs resulted in 1,545 and 885 reactions in panmetabolism and core metabolism, respectively. The removal of *Shigella* strains did not significantly change the reactions in panmetabolism (1,545–1,543); however, increased number of reactions in the core metabolism to 1,065 from 885. This increase in the number of the reactions in the core metabolism among *E. coli* strains indicates a conserved metabolism in *E. coli*. The reactions absent from *Shigella* core metabolism were distributed in various pathways including D-allose degradation, phenylethylamine and phenylacetate degradation, and biosynthesis pathways related amino acids, nucleotides and fatty acids. Another strain-specific GEM was built for 55 strains of *E. coli* and *Shigella* to shine light on adaptations to diverse environments (Monk et al., 2013). This study increased the reactions in core and panmetabolism to 1,773 and 2,501, respectively. Similarly, strain-specific GEMs of 64 strains of *S. aureus* were reconstructed for elucidating the metabolic capabilities associated with the pathogenity (Bosi et al., 2016).

Klebsiella pneumoniae

In the reconstruction and analysis of iYL1228 for *K. pneumoniae* MGH 78578, FBA was performed for the growth phenotype predictions on different nutrition media including carbon, nitrogen, phosphorus and sulfur to compare with the Biolog data (Liao et al., 2011). The discrepancies between computational

results and Biolog data were taken as advantages toward the curation of the model by pioneering and adding experimentally supported metabolic reactions. Subsequent to refinement, iYL1228 was able to predict 84% of phenotypes among 171 growth conditions. In the same study, in addition to *in silico* viability predictions, experimental growth rates of nine carbon sources under aerobic conditions were investigated and two of them (citrate and myo-inositol) were predicted significantly higher than those of experimental results. After adaptive evolution of *K. pneumoniae* to myo-inositol by serial passage, the experimental growth rate increased and the rate of growth error decreased from 80% to 24%. Hence, GEMs can also give remarkable clues toward uncovering adaptive evolution mechanism. In another study, the *in silico* iYL1228 was used as a platform to reconstruct GEMs for 22 *K. pneumoniae* strains (Norsigian et al., 2019). These models were manipulated for the investigation of growth capabilities on carbon, nitrogen, sulfur and phosphorus sources. Carbon, nitrogen and sulfur simulations varied across the strains; however, phosphorus results were largely remained the same.

The screening of putative drug targets in *K. pneumoniae* was studied by iYL1228 with the improved biomass reaction (Cesur et al., 2020). So as to mimic the host microenvironment, the growth simulations were performed by using FBA in three different conditions including human body fluid, sputum-macrophage, and generic host media. Gene-centric (essential genes) and metabolite-centric (essential metabolites) approaches were employed to identify whether they are indispensable for bacterial metabolism or not. Since potential drug targets are required to exist in only pathogen metabolism, homology analysis of essential genes was performed and presence of essential metabolites among human metabolites were examined to eliminate possible side effects in the host metabolism. Further *in silico* prioritization approaches such as subcellular localization, druggability, antibiotic resistance, virulence and broad-spectrum analysis were performed to come up with more effective targets. 2-dehydro-3-deoxyphosphooctonate aldolase (KdsA) was identified as the highest-ranked putative drug target satisfying virulence, druggability and broad-spectrum criteria and ZINC95543764 was suggested as a potential *Klebsiella* inhibitor in gene-centric approach. The enzymes related to essential metabolites were suggested as putative drug targets in metabolite-centric approach. These are enoyl-(acyl carrier protein) reductase (FabI) in fatty acid metabolism, riboflavin synthase subunit α (RibC) and riboflavin synthase subunit β (RibH) in riboflavin metabolism, and penicillin-binding protein 1A-C (PBP 1A, PBP 1B, and PBP 1C) in the peptidoglycan biosynthesis. PBP 1A-C were found to be synthetic lethal and the remaining three were essential.

Salmonella typhimurium

Salmonellae are gram-negative bacterial pathogens with a wide host range, causing millions of human infections and hundreds of thousands of deaths per year worldwide. The serovars of *Salmonella* differ in their antimicrobial host specificity, resistance profiles, and virulence phenotypes. For example, *S. typhimurium* is the leading cause of human gastroenteritis and have more than 2000 serovars. An *in silico* strain-specific metabolic reconstruction was performed for 410 *Salmonella* strains and the metabolic capabilities on minimal media with more than 500 different growth-supporting nutrition sources including carbon, nitrogen, phosphorous, and sulfur were compared across the *Salmonella* genus in aerobic and anaerobic conditions (Seif et al., 2018). One thousand nine hundred thirteen metabolic reactions associated with 1,013 genes and 1,407 metabolites are shared across all 410 strains. The common strains mostly differ in their capability to utilize D-tagatose, myo-inositol, 2,3-diaminopropionate, allantoin, D-galactonate, and 2-aminoethylphosphonate. All 6 Typhi strains were predicted to lack the capability to utilize L-idonate (an available nutrient source in the gut) due to the absence of *idnD* and *idnO* and show lack of fitness (inability of the organism to thrive in a competitive environment). A total of 21 catabolic pathways like the utilization of D-tagatose, L-xylulose, D-xylose, deoxy-D-ribose, L-idonate, D-glyceraldehyde, and allantoin, that form part of the host's diet and/or exist in the intestinal environment, contributed to *Salmonella* fitness during intestinal infection. The compositional differences in the intestinal vs. extraintestinal milieu of the host may reflect differences in pathogenicity of different *Salmonella* types.

The *in silico* model of *S. typhimurium* (iRR1083) provided a suitable platform to analyze the role of reactions important in infection and pathogenesis, such as those required for drug efflux, proton pumps, inhibitory effects of antibiotics, mechanisms for reactive nitrogen species (RNS) and reactive oxygen species (ROS) resistance (Raghunathan et al., 2009). Two hundred (out of 1,083) metabolic genes were predicted as essential. Gene essentiality analysis was extended to virulence predictions study in such a way that *Salmonella* mutants defective in essential and non-essential genes were considered as avirulent (no growth) and virulent (can grow) in the host cells, respectively. Of the 24 *in vivo* essential genes from the literature, the *in silico* analysis correctly predicted 22 virulence characterizations. For example, AceA, which was predicted as non-essential and mutants defective in *AceA* are virulent. AceA is required only for chronic and not for acute *Salmonella* infections (Fang et al., 2005). The double deletion of two genes (*ackA* and *pta*) responsible in acetyl phosphate formation lead to virulent strain. The fatty acid degradation genes *fadA*, *fadD/fadE* genes have been implicated for virulence in chronic *Salmonella* infection, however the model predicted the presence of glucose or pyruvate but not acetate or short chain fatty acids during the early stages of infection (Fang et al., 2005) and these fad genes are not being operational during the early stages of infection. Furthermore, simultaneous upregulation of *cyoE* and *cyoA* (succinate dehydrogenase and electron transport chain genes) was reported suggestive of an aerobic condition *in vivo*, during the early stages of infection (Karatzas et al., 2008). Increased levels of F_1F_0 ATP synthase subunits, heme biosynthesis, upregulated histidine biosynthesis (hisC, hisD, hisG) predictions were consistent with the literature (Eriksson et al., 2003; Shi et al., 2006; Karatzas et al., 2008). The *in silico* model accurately predicted that catalase (*katE* and *katG*) mutants and super oxide dismutase mutants (*sodA* and *sodCII*)

are virulent, confirming the pathogens have multiple defenses to oxidative stresses. On the other hand, the model predicted that mutants defective in aromatic amino acid biosynthesis are avirulent.

Staphylococcus aureus

Taking the evolution due to drug resistance into consideration, GEMs for 13 multidrug-resistant *S. aureus* strains were reconstructed by using genome annotation, functional pathway analysis and comparative genomics approaches (Lee et al., 2009). The number of metabolic reactions in these GEMs varied between 1,444 and 1,497, and over 90% of these metabolic reactions, metabolites and enzymes were shared in common by all 13 strain-specific GEMs. Several amino acid biosynthesis pathways were involved in all strains, but L-histidine, L-serine, L-homocysteine and L-asparagine pathways were absent in all 13 strains. Fatty acid biosynthesis genes (*fabG, fabA, fabZ, fabI, fabK, fabH,* and *fabF*) were present in all strains. All these genes, exluding *fabI*, were determined as essential. The analysis of single unconditionally essential enzymes (essential in rich medium and computed without any limitation on fluxes of uptake reactions) resulted in 70 essential enzymes in one or more of 13 strains and 44 in all *S. aureus* strains. Of the 44 shared essential enzymes, minimum six of them were experimentally supported in *S. aureus* including transketolase, hydroxyl-methylbilane synthase, methionine adenosyltransferase, UDP-N-acetyl-glucosamine 1-carboxyvinyltransferase, protein N (pi)-phospho-histidine-sugar phosphortransferase and acetyl-CoA carboxylase (Forsyth et al., 2002). Simultaneous inactivation of two enzymes in the GEMs could lead to lethality or no growth while their single (one-at-a-time) knockout does not result in lethality. Of the 54 synthetic-lethal pairs of enzymes, 10 pairs were predicted in all 13 strains. Among them, prephenate dehydrogenase and arogenate dehydrogenase pair is involved in amino acid biosynthesis, and UDP-N-acetylglucosamine pyrophosphorylase and phosphoglucosamine mutase pair in cell wall metabolism. The synthetic lethal sets, i.e., the combinations of genes, which when simultaneously deleted, abolish growth *in silico*, allow to decipher complex interactions in reconstructed metabolic networks (Thiele et al., 2011).

Strain-specific GEMs enabled phenotype predictions via metabolic flux distributions of 64 *S. aureus* strains in more than 300 growth conditions (Bosi et al., 2016). The majority of the reactions different between the core and panmodels were identified in amino acid biosynthesis, and these diversities may lead to adaptation of different strains to different nutritional conditions. For all 64 *in silico* strain-specific models, vitamins B1 (thiamin) and B3 (niacin) were additionally required to grow in glucose minimal media. The thiamin and niacin auxotrophy are due to absence of the pathways converting tyrosine to thiamin and nicotinate-nucleotide diphosphorylase, respectively. The prediction of growth capabilities on alternative sources (carbon, nitrogen, phosphorous, and sulfur) indicated 238 nutrients including glucose and glycerol as carbon sources and arginine as nitrogen source are used by all 64 *in silico S. aureus* strains. Among other strain-specific nutrients, both uracil and thymidine were predicted as nitrogen source for 42 strains, and dulcose and inosine as carbon source for 42 and 13 strains, respectively. The simulations of growth resulted in the presence of two virulence factors (staphylokinase and IgG binding protein A precursor) and the ability to catabolize maltotriose distinguished human-associated strains from livestock-associated strains. Thus, the simulations based on genome-scale metabolic modeling allow the classification of *S. aureus* strains according to the presence of virulence factors.

Biothreat Agents

The Centers for Disease Control and Prevention (CDC) evaluated the potential threats from various microorganisms and classify them into three categories (Rotz et al., 2002). Category A consists of the pathogens that are considered the highest risk with mass casualties for public health and necessitates broad-based preparedness efforts, Category B have some risk for large-scale dissemination, and Category C pathogens are emerging infectious disease threats. The discovery of antibiotics against these biological agents may not be economically feasible; however, it is clear that preventative and curative healthcare solutions are urgently needed. Toward this end, in addition to drug repurposing strategy, where the existing medications are searched for new successful treatments, utilization of antimicrobial peptides (AMPs) potentially constitute therapeutic options for high threat pathogens (Findlay et al., 2016; Farha and Brown, 2019; Miró-Canturri et al., 2019). The combinatorial therapeutic potential of one 24-amino acid AMP (WLBU2) and three early generation antibiotics (tigecycline, minocycline and novobiocin) were studied for two Category B pathogens (*Burkholderia mallei* and *Burkholderia pseudomallei*) and three category A pathogens which are *Yersinia pestis Bacillus anthracis* and *Francisella tularensis* causing plague, anthrax, and tularemia, respectively (Cote et al., 2020). By using the checkerboard MIC titration assays, it was observed that the combination of novobiocin-AMP enhanced the sensitivity of all five biological agents of interest. The tetracycline-peptide combinations increased the sensitivities of four agents including *Y. pestis, F. tularensis, B. anthracis, and B. pseudomallei*. The results showed that combinations of antibiotic-AMP are useful tools to fight against biological threat agents. Antimicrobial action mechanisms of AMPs can occur both directly and indirectly (Mahlapuu et al., 2016; Deslouches and Di, 2017). The direct cytotoxicity of AMPs electrostatically affects the bacterial outer surface by disrupting a phospholipid membrane. Subsequent to entry of AMPs into the cell, they interfere with critical intracellular processes including RNA and protein synthesis. Indirect AMP actions occur through immunomodulatory activities such as chemotactic stimulation, immune cells differentiation, inflammatory cell response regulation and cell death pathways.

A GEM study (iPC815) on *Yersinia pestis* revealed essential genes that might contribute to propose possible targets for antibiotic development (Charusanti et al., 2011). The largest group of predicted essential genes was found within amino acid transport and metabolism followed by nucleotide and coenzyme metabolism, cell membrane biogenesis and lipid metabolism. Several essential genes in these metabolisms were also identified

as essential in *in silico E. coli* and *S. typhimurium* GEMs (Feist et al., 2007; Thiele et al., 2011). The predicted essential genes reflect a likely overlap among these three pathogens (*Y. pestis, E. coli* and *S. typhimurium*), the family of Enterobacteriaceae. The shared essential enzymes should be further exploited for the development of broad-spectrum antibiotics that can be used against this group of human pathogens.

The *in silico* analysis of *Francisella* strain demonstrated that *Francisella tularensis* undergoes significant changes of its metabolism upon its entry into the host cell (during intracellular growth) (Raghunathan et al., 2010). A switch from oxidative metabolism (TCA cycle) in the initial stages of infection to glycolysis, fatty acid oxidation, and gluconeogenesis during the later stages was found by flux balance and variability analyses. Moreover, the accumulation of 5-aminoimidazole-4-carboxamide ribonucleotide (AICAR) was found as a regulator of fructose bis phosphatase (*fbp*) gene in *Francisella* and the adenylyosuccinate lyase gene that catalyzes its formation, is a condition independent lethal gene, essential for survival and are proposed as a potential drug target. Thus, the predicted accumulation of AICAR in the host (macrophage) revealed a role as a potential master regulator during infection.

A multidisciplinary approach was applied to *F. tularensis* to select a group of enzymes as drug targets and ∼20,000 small-molecule compounds were screened to list potential inhibitors against these targets (Chaudhury et al., 2013). A set of 40 candidate compounds was identified for antimicrobial activity against *F. tularensis*. Moreover, based on FBA predicted inhibition of NAD^+ synthase (NadE), pantetheine-phosphate adenylyltransferase (CoaD), chorismate synthase (AroC) and sedoheptulose 7-phosphate isomerase (LpcA) enzymes, that are important in various metabolic pathways, these enzymes were suggested as potential drug targets. NadE takes part in NAD^+ biosynthesis, CoaD in coenzyme A biosynthesis, AroC in phenylalanine, tyrosine and tryptophan biosynthesis and LpcA in lipopolysaccharide biosynthesis. These four enzymes are putative drug targets and the experimental validation of their enzymatic inhibition is an important step in the development of candidate antimicrobial compounds.

In a multiple metabolic network analysis, 19 strains of three Category A biothreat agents *Y. pestis*, *B. anthracis* and *F. tularensis* were examined toward having a common drug target. Nine essential enzymes were shared between these three high threat pathogens (Ahn et al., 2014). These enzymes are phosphopantothenoyl cysteine decarboxylase (CoaB), phosphopantothenate cysteine ligase (CoaC), pantetheine-phosphate adenylyltransferase (CoaD), dephospho-CoA kinase (CoaE) in coenzyme A biosynthesis pathway, dihydroneopterin aldolase (FolB), dihydrofolate synthase/tetrahydrofolate synthase (FolC, two distinct enzymatic activities), GTP cyclohydrolase I (FolE) in folate biosynthesis pathway, guanylate kinase (Gmk) and thymidylate kinase (Tmk) in nucleic acid pathways and phosphatidyl serine decarboxylase (Psd) in phosphatidyl-ethanolamine synthesis. The comparison of the predicted essential enzymes in common with the experimental studies showed that CoaE is essential for growth in *M. tuberculosis, S. aureus, H. influenza,* and four other bacteria. Gmk and Tmk were found to be essential in *B. subtilis, E. coli, H. influenza, S. aureus,* and *Mycoplasma genitalium*. A further study of whether existing antibiotics targeted to any of these nine enzymes demonstrated that the antimicrobial compounds, trimethoprim and Rab1, already targeted FolC. Trimethoprim directly inhibits dihydrofolate synthase activity and the accumulation of dihydrofolate indirectly inhibits tetrahydrofolate synthase in *E. coli* (Kwon et al., 2008). It is effective against *Y. pestis*, whereas *B. anthracis* is resistant against trimethoprim (Wong et al., 2000; Barrow et al., 2007). Rab1 demonstrated broad-spectrum applicability and inhibited growth of three category A biothreat agents besides methicillin-resistant *S. aureus* and vancomycin-resistant *S. aureus* (Bourne et al., 2010).

PATHOGEN-HOST MODELING

Genome-scale metabolic models provide an improved understanding of how intracellular pathogens utilize the existing microenvironment of the host (**Figure 3**). It is of utmost importance to understand the pathogen metabolism including metabolic virulence factors like quorum sensing QS, lipopolysaccharides LPS, and rhamnolipids (and more such as siderophores-based iron uptake systems, cable pili for adhesion, motility, hemolysin, proteases, phospholipases, secretion systems, toxins, and extracellular capsules) to unravel mechanisms of pathogenesis. Pathogens reside in a phagosome (a vacuole in the cytoplasm of a cell), or more specifically localize in intracellular, extracellular-interstitial, extracellular-intravascular, extracellular-transcellular and "semi-open" spaces in host cells (e.g., the respiratory or alimentary tracts, etc.). Pathogens demonstrate different biochemical phenotypes and interaction mechanisms when inside the host vs. outside the host. Therefore, the pathogen and host GEMs are re-compartmentalized, and the transport across the macrophage cytoplasm are represented in connection with the other GEM.

An integrated host-pathogen GEM (iAB-AMØ-1410-Mt-661) was reconstructed by combining iAB-AMØ-1410 and iNJ661 which represent *in silico* alveolar macrophage and *M. tuberculosis* metabolism, respectively (Bordbar et al., 2010). iAB-AMØ-1410 was developed by using context-specific model extraction algorithms (GIMME and iMAT) and manual curation based on generic human GEM (Recon1) along with the gene expression data (Duarte et al., 2007; Becker and Palsson, 2008; Shlomi et al., 2008). The distribution of flux states for each reaction in the integrated model was compared with those of the corresponding reactions in the two pioneering models. In spite of the some variations in alveolar macrophage part, most of the changes were found in the pathogen part of the network where flux of glycolysis was reduced with acetyl-CoA synthesis produced from fatty acids. Glucose was produced through gluconeogenesis. Fatty acid oxidation pathways were upregulated; whereas, nucleotides, peptidoglycans and phenolic glycolipid productions were downregulated. In the alveolar macrophage part, nitric oxide production was increased; however, ATP synthesis, nucleotide production and amino acid metabolism were reduced. Due to different infection mechanisms in different tissues, three

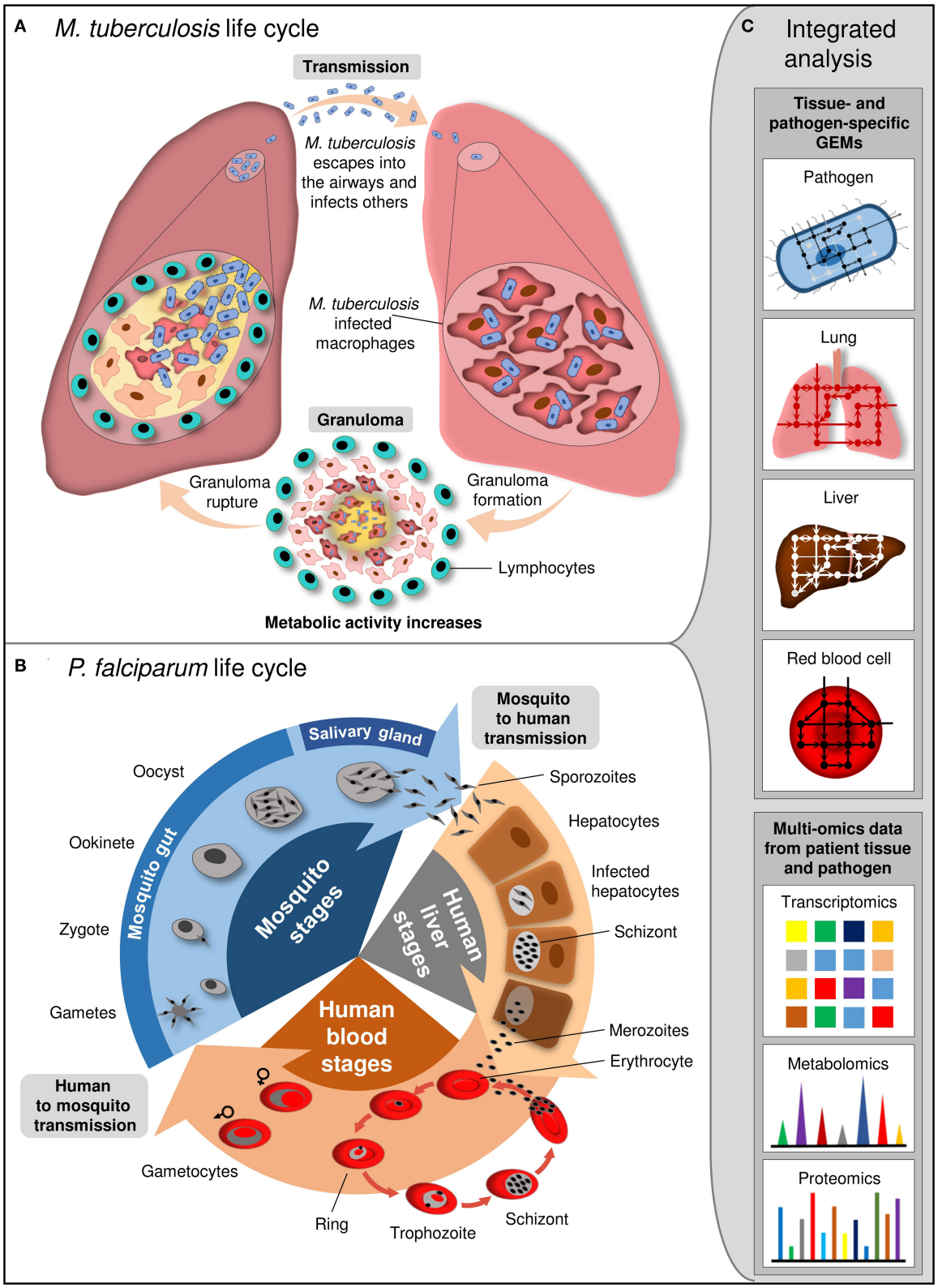

FIGURE 3 | Life cycle of *M. tuberculosis* and *P. falciparum* and integrated analysis at system level. **(A)** *M. tuberculosis* is transmitted by aerosol. Inhaled pathogen reaches the alveoli of the lung and grows inside the alveolar macrophages. Granuloma, where *M. tuberculosis* kills the macrophages and escapes from the cell for division, is formed. Subsequent to maturation, granuloma ruptures and releases *M. tuberculosis* into the airways. **(B)** *P. falciparum* life cycle involves the different

(Continued)

FIGURE 3 | stages in female *Anopheles* mosquito and human. Mosquito transmits sporozoites into the human. They infect hepatocytes and mature into schizonts which release merozoites. Merozoites invade erythrocytes and resulted in release of newly multiplied merozoites by erythrocytes destruction. Some merozoites differentiate into gametocytes which are taken up from host by mosquito. Gametocytes develop into sporozoites within mosquito. **(C)** Integrated analysis of tissue- and pathogen-specific GEMs with the high-throughput multi-omics data provides insight into the cellular and interaction mechanisms between the pathogen and host tissue at different stage of infection.

infection-specific models were developed for latent, pulmonary and meningeal tuberculosis by mapping gene expression data (Thuong et al., 2008). Hyaluronan synthesis was computed to be active only in the pulmonary-specific model, suggesting that the inhibition of hyaluronan synthase as a putative approach to cease the activation from latent to pulmonary condition. Furthermore, vitamin D and folate metabolism were found to be active in pulmonary and meningeal states. Vitamin D is important to fight against infection and folate play a critical role in DNA synthesis and repair.

Salmonella metabolism during infection was studied by using host-cell nutrient environment and gene expression data obtained from *S. typhimurium* growing inside macrophage cell lines (Raghunathan et al., 2009). The genome-scale metabolic model (iRR1083) was reconstructed specific to *S. typhimurium* LT2. FBA and FVA were employed in the prediction of essential genes and active metabolic pathways during infection. 417 and 736 flux-carrying reactions were computed for optimal and suboptimal biomass productions, respectively. Gene expressions and nutrients availability in the host cell environment were used as constraints in the simulations. Blocked reactions were predicted to offer valuable insight into inactive pathways in *Salmonella* metabolism under investigated conditions during infection. Integrated gene expression and optimal growth computations resulted in unexpressed *fad* genes in fatty acid degradation; however, the same genes were predicted to be operational under suboptimal growth conditions. Therefore, the simulations of *in silico* iRR1083 model provided clues toward metabolic shifts from early stages of infection to chronic infection of *Salmonella*. The computational results were compared with the literature-based proteome data, where 315 *S. typhimurium* proteins were identified by isolating this pathogen from macrophage at different time following infection (Shi et al., 2006). Of the 129 proteins, which were shared between experimental proteome data and iRR1080 model, 80 and 34 proteins were found within the reactions computed by FVA during optimal and suboptimal growth, respectively.

Prediction of essential genes for enterobacterial human pathogens (three *E. coli* and one *Salmonella* strains) was performed in three different host niches including human bloodstream, urinary tract and macrophage (Ding et al., 2016). Together with *E.coli* pangenome metabolic model (iEco1712_pan) containing all metabolic reactions and associated genes from 16 *E. coli* genome, the experimentally-based nutrient compositions were used as simulation constraints to mimic these three host environments (Keiter et al., 1955; Putnam, 1971; Raghunathan et al., 2009; Baumler et al., 2011). Among 51 metabolites, only 15 of them were shared for all niches of interest since the different locations inside the human body have diverse nutrients availability, which plays a pivotal role in pathogen survival and infection mechanism. By deleting each gene, essential (no growth) and important (reduction of biomass production >1% of the wild type) genes were predicted through FBA. Only one important reaction (isocitrate dehydrogenase) and 38 essential reactions including allantoinase, ATP synthase, citrate lyase, enolase and pyruvate kinase were predicted in common for all host locations. However, 121 reactions were computed to be important in one or two host environment. Subsequent to defining essential and important genes, these genes were compared with genomes of *E. coli* UT189, *E. coli* 53638, and *Salmonella* LT2 to investigate whether these genes were retained or lost over time. The genome of *E. coli* O157:H7 was utilized as control since it causes infection in a different location of human body (intestine). Therefore, this control strain lost highest number of these genes predicted for each of the three host environments. As expected, most of the lost essential or important genes were computed in intestinal pathogen *E. coli* O157:H7 due to evolutionary outcomes. The simulations of *E. coli* UT189 successfully predicted least amount of essential and important genes lost in human bloodstream and urinary tract where it causes infection. However, the inconsistencies in urinary tract simulations demonstrated a necessity of additional constrains for more accurate predictions in this location.

Similar to host-pathogen modeling at system-level, unraveling of host-parasite interactions via genome-scale metabolic modeling draws researchers' attention. A good example in this sense is the parasite *Plasmodium falciparum* which is responsible for the most severe form of malaria and involves the different stages in mosquito and human (**Figure 3**). Subsequent to reconstructions and integration of GEM for *P. falciparum* and human erythrocyte, antimalarial drug targets were predicted for stage-specific conditions by mapping gene expression data from different life cycles (Huthmacher et al., 2010). Among 57 experimentally supported essential enzymes, 35 enzymes including glutathione reductase, thioredoxin reductase, carbonic anhydrase and acetyl-CoA carboxylase were predicted to be putative drug targets. By applying additional assumptions (transporter constraints of biomass precursors), another 16 enzymes including spermidine synthase and ornithine decarboxylase were also predicted to have antimalarial effects. Drug targets of this parasite in human liver metabolism were simulated by using well-curated GEMs for human hepatocyte (HepatoNet1) and *P. falciparum* (PlasmoNet) (Gille et al., 2010; Huthmacher et al., 2010; Bazzani et al., 2012). Twenty-four out of 48 experimental antimalarial drug targets including serine transferase, sphingomyelin synthase, thioredoxin reductase, and adenylosuccinate synthase were predicted as essential for parasite and non-essential for human. Another study was carried

out to elucidate host response to malarial infection during the intraerythrocytic developmental cycle (IDC) (Wallqvist et al., 2016). Along with time series gene expression data during IDC, the proteomic based reconstruction of red blood cell (iAB-RBC-283) and metabolic network model of *P. falciparum* were coupled to simulate infection metabolism of this parasite inside the human red blood cells (Bordbar et al., 2011; Fang et al., 2014). The glycolytic pathway fluxes of co-cultured uninfected red blood cells were predicted between 13 and 19% of those in normal cells, indicating inactivation of glycolysis pathway due to the presence of infected cells in the same culture. Temporal activation of the glycolytic pathway was observed among the infected and co-cultured red blood cells. During very early and late intraerythrocytic developmental cycle (IDC), infected and co-cultured red blood cells showed similar patterns with high fluxes through phosphoglycerate kinase and low fluxes through diphosphoglycero mutase and diphosphoglycerate phosphatase. However, the low fluxes through phosphoglycerate kinase were predicted in the infected red blood cells during the middle IDC because of ATP secretion from *P. falciparum*.

Considering the different life cycle stages (liver, blood, and mosquito stage of parasites), the metabolism of the parasite *P. falciparum* varies due to fluctuating availability of nutrients in the different host environments. Thus, a stage-specific metabolism of *P. falciparum* was studied by a context specific GEM using gene expression data to get an idea during which stages reactions are essential (Huthmacher et al., 2010). The *in silico* analysis predicted 307 essential reactions for the parasite. All reactions were computed as essential during at least one developmental stage. In blood stages of its life cycle, the parasite *P. falciparum* need to incorporate heme from hemoglobin degradation into hemozoin molecules in order to prevent intoxication and cell lysis. Consistent with this, the predictions demonstrated several essential enzymes involved in heme biosynthesis. In late liver stage, the fatty acid synthesis is only essential in the apicoplast. Essential reaction predictions demonstrated that top ranking reactions were found in the apicoplast. In ring stage, fewer reactions corresponding to folate biosynthesis are predicted to be active compared to subsequent stages. In schizont and early ring stage, an increase in the number of active reactions is predicted for the citric acid cycle and sphingolipid metabolism. In trophozoite and schizont stages, the parasites have a high acyltransferase activity, that can be considered as significant for their fitness (Huthmacher et al., 2010; Bazzani et al., 2012). Among the metabolic reactions, *P. falciparum* involves a pathway to synthesize pyrimidine nucleotides *de novo* of which multiple reactions were predicted to be essential such as those catalyzed by carbonic anhydrase, carbamoylphosphate synthase, dihydroorotase, dihydroorotate oxidase, orotidine-5′-phosphate decarboxylase. Moreover, the enzymatic inhibitions of *Plasmodium falciparum* were investigated by a reconstructed genome-scale network PlasmoNet (Bazzani et al., 2012). Acyl-CoA synthetase inhibition impaired PlasmoNet sphingomyelin production, suggesting a certain amount of sphingolipids is essential for the growth of *Plasmodium falciparum*. Similarly, aspartate carbamoyltransferase inhibition resulted in an impairment of UDP-glucose production in PlasmoNet. The *in silico* inhibition of the enzyme glycerol-3-phosphate acyltransferase impaired the production of phosphatidylethanolamine in PlasmoNet. This enzyme glycerol-3-phosphate acyltransferase is essential for *P. falciparum* growth that necessitates high amount of phospholipids for membrane synthesis.

Several studies have indicated that the time-of-day of host infection influences pathogen progression (Rijo-Ferreira and Takahashi, 2019). For example, the levels of *Salmonella enterica subsp. enterica* serovar Typhimurium (*S. typhimurium*) were higher if the infection occurred during the rest phase compared to the infection initiated in the middle of the active phase (Bellet et al., 2013). Viral infections of herpes, influenza A, and respiratory viruses of the Paramyxoviridae family were worse when host circadian rhythms are disrupted, e.g., by mutation in *Bmal1* gene, the main circadian regulator. The parasite infection similarly depends on the timing of the host circadian cycle, e.g., the load of *Leishmania* parasite is circadian in nature. The circadian clock (mainly BMAL1) can regulate cellular immunity against bacteria, viruses, and parasites (Rijo-Ferreira and Takahashi, 2019). Infections along with the resulting inflammation can disrupt the circadian clock by decreasing the amplitude of circadian rhythms. Some examples are seen with *Trypanosoma cruzi*, *Trypanosoma brucei, Plasmodium chabaudi* (Fernández Alfonso et al., 2003; Rijo-Ferreira et al., 2018).

Host-pathogen (HP) models have unraveled the pathogen adaptation and carbon source utilization *in vivo* and host manipulation by pathogen. These HP models answer questions regarding the causality during the infection process, condition dependent (or context specific) differences. The diagnosis and treatment related challenges can be solved by examining the metabolic fluxes in tissues and develop strategies for treatment options on the basis of few experimental data. In brief, HP models help elucidate the role of host environment on pathogen metabolism during the course of an infection.

SPHINGOLIPIDS RELATED INVASION MECHANISM OF PATHOGENS

During the microbial infection process, the sphingolipid molecules play a critical role in host-pathogen interaction mechanism (Sharma and Prakash, 2017; Kunz and Kozjak-Pavlovic, 2019; Rolando and Buchrieser, 2019). The initial steps of infection is the host-pathogen contact on the cell surface and then penetration of pathogen into the host cell. Many of the pathogens do not have their own sphingolipids; however, they are able to take advantage of host sphingolipid pathway to promote their virulence and invasion. Sphingolipids are bioactive lipids participating in cell membrane and various cellular processes including growth, death, adhesion, inflammation and signaling (Hannun and Obeid, 2008). Ceramide is the central hub metabolite in sphingolipid metabolism due to different formation (*de novo* synthesis from palmitoyl-CoA and serine, sphingomyelin hydrolysis by sphingomyelinases and reacylation of sphingosine catalyzed by ceramide synthase)

and consumption reactions covering conversion to sphingosine, sphingomyelin, glucosylceramide and ceramide 1-phosphate catalyzed by the enzymes of ceramidase, sphingomyelin synthase, glucosylceramide synthase and ceramide kinase, respectively.

Acid sphingomyelinase (ASM) converts sphingomyelin to ceramide and has a great importance in membrane reorganization. Several bacterial pathogens activate the ASM and ceramide-enriched membrane platforms are formed in response to increase in ceramides (Simonis and Schubert-Unkmeir, 2018). These lipid rafts facilitate the uptake of bacterial pathogen into host. Moreover, different pathogens demonstrate specific infection mechanisms based on their own and host cell characteristics. In *P. aeruginosa* infection in cystic fibrosis, the increase in ceramide and ceramide-enriched platforms, where β1-integrins are located on the luminal pole of bronchial cells, lead to the accumulation of β1-integrins (Grassmé et al., 2017). The downregulation of acid ceramidase expression due to β1-integrins causes further accumulation of ceramide and a decrease in surface sphingosine, which kills bacteria. *S. aureus* α-toxin activates ASM and concomitant formation of ceramide in endothelial cells by means of binding to ADAM10 (Becker et al., 2018; Keitsch et al., 2018). In addition to ceramide, sphingosine and sphingosine-1-phosphate (S1P) participate in lung inflammatory injury. S1P is produced by the sphingosine kinase-1 (SPHK1) in cytosol and sphingosine kinase-2 (SPHK2) in nucleus by phosphorylation of sphingosine. *P. aeruginosa* infection resulted in phosphorylation of SPHK2 and increased localization in nucleus leading to enhanced level of S1P and acetylation of histone (Ebenezer et al., 2019). *M. tuberculosis,* which is directly able to use glycosphingolipids of the plasma membrane, can bind to lactosylceramide-enriched lipid rafts of human neutrophils (Nakayama et al., 2016). Sphingomyelin is necessary for *H. pylori* entry, and secreted vacuolating cytotoxin facilitates bacterial colonization (Foegeding et al., 2016).

The successful response of host cell to bacterial invasion takes full advantages of phagolysosome formation or autophagy induction to kill bacteria. On the other hand, pathogens develop various strategies to survive including escaping from phagosome into the cytosol, inhibiting phagocytosis, preventing fusion of phagosomes and lysosomes and blocking autophagy. Sphingolipids participate in these strategies for pathogenic survival in the host. The protein Rv0888 which shows sphingomyelinase activity is synthesized by *M. tuberculosis*. This protein converts host sphingomyelin into ceramide and phosphorylcholine, and these metabolites are used as carbon, nitrogen and phosphorus sources by *M. tuberculosis* (Speer et al., 2015). *P. aeruginosa* infection activates the mitochondrial ASM (Managò et al., 2015). This results in cell death due to formation of mitochondrial ceramide and the release of mitochondrial cytochrome c. Subsequent to invasion, a type-III secretion system is required for *Salmonella* to constitute a specialized bacterial survival and replication niche, which is called *Salmonella*-containing vacuole (SCV) (Owen et al., 2014). Based on the replication stage, *Salmonella* can induce suppression of autophagy so as to increase survival. This can be regulated by sphingolipids since the decreased *Salmonella*-induced autophagy results from inhibition of *de novo* sphingolipid biosynthesis (Huang, 2016).

These examples show that pathogens are willing to use and manipulate sphingolipids in order to invade eukaryotic cell and promote pathogen colonization in the host. The cases are not limited to the above mentioned examples, and can be extended to further pathogens like *Neisseria* strains (*Neisseria meningitidis*, *Neisseria gonorrhoeae*), *H. influenzae*, *Chlamydia trachomatis*, *Legionella pneumophila*, *Candida albicans*, *Cryptococcus neoformans*, *Aspergillus fumigatus*, etc. (Aerts et al., 2019; Kunz and Kozjak-Pavlovic, 2019; Rolando and Buchrieser, 2019). Pharmaceutical reduction of sphingolipids and glycosphingolipids such as glucosylceramide (GlcCer) was proposed as a new strategy to fight against fungal infections. Acylhydrazones have been determined as specific inhibitors since they targets synthesis of fungal and not mammalian GlcCer (Mor et al., 2015; Lazzarini et al., 2018).

CONCLUDING REMARKS

Pathogen-specific genome-scale metabolic models as well as host-pathogen integrative constraint-based methods have become successful tools in the research of infection mechanism that need to be fully understood to develop therapeutical strategies against pathogens. The analysis of essential genes and their associated products provide a valuable insight into how to impair bacterial growth and how these critical biomolecules change in different environmental states which mimic different human niches. Essential biomolecules common in different infected host microenvironment have high potential for targeting in the combat of pathogen in multiple human niches. Similarly, the different stages of infection may show stage-specific essential biomolecules to be targeted by antimicrobial agents. In such cases, molecules shared in all stages are selected as putative drug targets. The identification of conserved metabolic pathways during pathogen invasion may lead to alternative complementary routes that can be targeted by novel interfering compounds. If it is not possible to treat the bacterial infection with a single antibiotic, combined treatment strategies (cocktail of drugs) would be an alternative solution. For the rare bacterial species involved in infections, an economically feasible route for pharmaceutical companies may be the search for broad spectrum antibiotics. Another option would be the development of combinatorial treatment protocols using current drugs that are already in use against infections. Here, it is strictly necessary not to forget the human orthologs, which need to be excluded from being drug targets in order to avoid side effects. The computational genome scale models presented in this review article have not only the ability to reduce the search space for novel drug targets in the pathogen metabolism, but can also give insights on putative side effects on host metabolism. These metabolic network models can be used as an additional screening tool to predict potential toxicity of the predicted target in a healthy cell or tissue model. Many side effects are due to patient-to-patient genetic variability. Using context specific constraint-based models integrated with omics data, the potential causes of the side effects such as drug

off-target binding, downstream transcriptional effects (changes in gene expression that are induced with drug treatment), and the pharmacokinetics of drug clearance can be predicted in patients and serve as *a priori* guide in the drug target studies.

In case of extremely deadly pathogens, this genome scale modeling approach is indispensable since experimental analyses are associated with the need for high-security laboratory conditions, and in some cases prohibited. These models identify novel virulence genes as well as enable the evaluation of pathogen metabolism, predict disease phenotypes and hence get the infection scenario. They offer insight into why the same microbial pathogen may cause disease in some host environments but not others.

Pathogen species, infection stages and host niches have great importance and need to be taken into consideration in clinical and computational studies to extend curative strategies against pathogens for global preventative healthcare. Throughout the infection course, different pathogens develop various stage-specific interaction mechanisms to host cells depending on their invasion and response features. The experimental elucidation of such complex infection process requires long and difficult work alone. An effective application of stage-specific genome-scale metabolic modeling approach guides experimental studies and facilitate the development of novel candidate drugs targeting key essential biomolecules at all stages infection.

AUTHOR CONTRIBUTIONS

MS and KOU contributed to writing the manuscript and preparing the table and figures. Both authors contributed to the article and approved the submitted version.

FUNDING

This work was supported by TUBITAK, The Scientific and Technological Research Council of Turkey [Project Code: 119M923].

REFERENCES

AbuOun, M., Suthers, P. F., Jones, G. I., Carter, B. R., Saunders, M. P., Maranas, C. D., et al. (2009). Genome scale reconstruction of a salmonella metabolic model: Comparison of similarity and differences with a commensal *Escherichia coli* strain. *J. Biol. Chem*. 284, 29480–29488. doi: 10.1074/jbc.M109.005868

Aerts, J. M. F. G., Artola, M., van Eijk, M., Ferraz, M. J., and Boot, R. G. (2019). Glycosphingolipids and infection. Potential new therapeutic avenues. *Front. Cell Dev. Biol.* 7, 1–16. doi: 10.3389/fcell.2019.00324

Aggarwal, K., and Lee, K. H. (2003). Functional genomics and proteomics as a foundation for systems biology. *Briefings Funct. Genomics Proteomics* 2, 175–184. doi: 10.1093/bfgp/2.3.175

Ahn, Y. Y., Lee, D. S., Burd, H., Blank, W., and Kapatral, V. (2014). Metabolic network analysis-based identification of antimicrobial drug targets in category A bioterrorism agents. *PLoS ONE* 9:e85195. doi: 10.1371/journal.pone.0085195

Altschul, S. F., Gish, W., Miller, W., Myers, E. W., and Lipman, D. J. (1990). Basic local alignment search tool. *J. Mol. Biol*. 215, 403–410. doi: 10.1016/S0022-2836(05)80360-2

Arkin, A. P., Cottingham, R. W., Henry, C. S., Harris, N. L., Stevens, R. L., Maslov, S., et al. (2018). KBase: the United States department of energy systems biology knowledgebase. *Nat. Biotechnol*. 36, 566–569. doi: 10.1038/nbt.4163

Banerjee, D., and Raghunathan, A. (2019). Constraints-based analysis identifies NAD + recycling through metabolic reprogramming in antibiotic resistant chromobacterium violaceum. *PLoS ONE* 14:e0210008. doi: 10.1371/journal.pone.0210008

Barrow, E. W., Dreier, J., Reinelt, S., Bourne, P. C., and Barrow, W. W. (2007). *In vitro* efficacy of new antifolates against trimethoprim-resistant *Bacillus anthracis*. *Antimicrob. Agents Chemother*. 51, 4447–4452. doi: 10.1128/AAC.00628-07

Bartell, J. A., Blazier, A. S., Yen, P., Thøgersen, J. C., Jelsbak, L., Goldberg, J. B., et al. (2017). Reconstruction of the metabolic network of *Pseudomonas aeruginosa* to interrogate virulence factor synthesis. *Nat. Commun.* 8:14631. doi: 10.1038/ncomms14631

Baumler, D. J., Peplinski, R. G., Reed, J. L., Glasner, J. D., and Perna, N. T. (2011). The evolution of metabolic networks of *E. coli*. *BMC Syst. Biol*. 5, 1–21. doi: 10.1186/1752-0509-5-182

Bazzani, S., Hoppe, A., and Holzhütter, H. G. (2012). Network-based assessment of the selectivity of metabolic drug targets in *Plasmodium* falciparum with respect to human liver metabolism. *BMC Syst. Biol.* 6:118. doi: 10.1186/1752-0509-6-118

Becker, K. A., Fahsel, B., Kemper, H., Mayeres, J., Li, C., Wilker, B., et al. (2018). Staphylococcus aureus alpha-toxin disrupts endothelial-cell tight junctions via acid sphingomyelinase and ceramide. *Infect. Immun.* 86:e00606-17. doi: 10.1128/IAI.00606-17

Becker, S. A., and Palsson, B. (2005). Genome-scale reconstruction of the metabolic network in *Staphylococcus aureus* N315: an initial draft to the two-dimensional annotation. *BMC Microbiol*. 5:8. doi: 10.1186/1471-2180-5-8

Becker, S. A., and Palsson, B. O. (2008). Context-specific metabolic networks are consistent with experiments. *PLoS Comput. Biol.* 4:e1000082. doi: 10.1371/journal.pcbi.1000082

Bellet, M. M., Deriu, E., Liu, J. Z., Grimaldi, B., Blaschitz, C., Zeller, M., et al. (2013). Circadian clock regulates the host response to Salmonella. *Proc. Natl. Acad. Sci. U.S.A*. 110, 9897–9902. doi: 10.1073/pnas.1120636110

Beste, D. J. V., Hooper, T., Stewart, G., Bonde, B., Avignone-Rossa, C., Bushell, M. E., et al. (2007). GSMN-TB: a web-based genome-scale network model of *Mycobacterium tuberculosis* metabolism. *Genome Biol*. 8:R89. doi: 10.1186/gb-2007-8-5-r89

Blattner, F. R., Plunkett, G., Bloch, C. A., Perna, N. T., Burland, V., Riley, M., et al. (1997). The complete genome sequence of *Escherichia coli* K-12. *Science* 277, 1453–1462. doi: 10.1126/science.277.5331.1453

Bochner, B. R., Gadzinski, P., and Panomitros, E. (2001). Phenotype Microarrays for high-throughput phenotypic testing and assay of gene function. *Genome Res.* 11, 1246–1255. doi: 10.1101/gr.186501

Bordbar, A., Jamshidi, N., and Palsson, B. O. (2011). IAB-RBC-283: A proteomically derived knowledge-base of erythrocyte metabolism that can be used to simulate its physiological and patho-physiological states. *BMC Syst. Biol*. 5:110. doi: 10.1186/1752-0509-5-110

Bordbar, A., Lewis, N. E., Schellenberger, J., Palsson, B., and Jamshidi, N. (2010). Insight into human alveolar macrophage and *M. tuberculosis* interactions via metabolic reconstructions. *Mol. Syst. Biol.* 6:422. doi: 10.1038/msb.2010.68

Bordel, S., Agren, R., and Nielsen, J. (2010). Sampling the solution space in genome-scale metabolic networks reveals transcriptional regulation in key enzymes. *PLoS Comput. Biol*. 6:e1000859. doi: 10.1371/journal.pcbi.1000859

Borodina, I., Krabben, P., and Nielsen, J. (2005). Genome-scale analysis of Streptomyces coelicolor A3(2) metabolism. *Genome Res*. 15, 820–829. doi: 10.1101/gr.3364705

Bosi, E., Monk, J. M., Aziz, R. K., Fondi, M., Nizet, V., and Palsson, B. (2016). Comparative genome-scale modelling of *Staphylococcus aureus* strains identifies strain-specific metabolic capabilities linked to pathogenicity. *Proc. Natl. Acad. Sci. U.S.A*. 113:E3801-9. doi: 10.1073/pnas.1523199113

Bourne, C. R., Barrow, E. W., Bunce, R. A., Bourne, P. C., Berlin, K. D., and Barrow, W. W. (2010). Inhibition of antibiotic-resistant *Staphylococcus aureus* by the

broad-spectrum dihydrofolate reductase inhibitor RAB1. *Antimicrob. Agents Chemother*. 54, 3825–3833. doi: 10.1128/AAC.00361-10

Brown, E. D., and Wright, G. D. (2016). Antibacterial drug discovery in the resistance *era*. *Nature* 529, 336–343. doi: 10.1038/nature17042

Bryant, J., Chewapreecha, C., and Bentley, S. D. (2012). Developing insights into the mechanisms of evolution of bacterial pathogens from whole-genome sequences. *Future Microbiol*. 7, 1283–1296. doi: 10.2217/fmb.12.108

Caspi, R., Altman, T., Dreher, K., Fulcher, C. A., Subhraveti, P., Keseler, I. M., et al. (2012). The MetaCyc database of metabolic pathways and enzymes and the BioCyc collection of pathway/genome databases. *Nucleic Acids Res*. 44, D471–D480. doi: 10.1093/nar/gkr1014

Cesur, M. F., Siraj, B., Uddin, R., Durmuş, S., and Çakir, T. (2020). Network-based metabolism-centered screening of potential drug targets in *klebsiella pneumoniae* at genome scale. *Front. Cell. Infect. Microbiol*. 9:447. doi: 10.3389/fcimb.2019.00447

Charusanti, P., Chauhan, S., McAteer, K., Lerman, J. A., Hyduke, D. R., Motin, V. L., et al. (2011). An experimentally-supported genome-scale metabolic network reconstruction for *Yersinia pestis* CO92. *BMC Syst. Biol.* 5:163. doi: 10.1186/1752-0509-5-163

Chaudhury, S., Abdulhameed, M. D. M., Singh, N., Tawa, G. J., D'haeseleer, P. M., Zemla, A. T., et al. (2013). Rapid countermeasure discovery against francisella tularensis based on a metabolic network reconstruction. *PLoS ONE* 8:e63369. doi: 10.1371/journal.pone.0063369

Cole, S. T., Brosch, R., Parkhill, J., Garnier, T., Churcher, C., Harris, D., et al. (1998). Deciphering the biology of *Mycobacterium tuberculosis* from the complete genome sequence. *Nature*. 393, 537–544. doi: 10.1038/31159

Colijn, C., Brandes, A., Zucker, J., Lun, D. S., Weiner, B., Farhat, M. R., et al. (2009). Interpreting expression data with metabolic flux models: predicting *Mycobacterium tuberculosis* mycolic acid production. *PLoS Comput. Biol.* 5:e1000489. doi: 10.1371/journal.pcbi.1000489

Conrad, T. M., Lewis, N. E., and Palsson, B. O. (2011). Microbial laboratory evolution in the era of genome-scale science. *Mol. Syst. Biol*. 7:509. doi: 10.1038/msb.2011.42

Cote, C. K., Blanco, I. I., Hunter, M., Shoe, J. L., Klimko, C. P., Panchal, R. G., et al. (2020). Combinations of early generation antibiotics and antimicrobial peptides are effective against a broad spectrum of bacterial biothreat agents. *Microb. Pathog*. 142:104050. doi: 10.1016/j.micpath.2020.104050

Davenport, K. W., Daligault, H. E., Minogue, T. D., Bruce, D. C., Chain, P. S. G., Coyne, S. R., et al. (2014). Draft genome assembly of *Acinetobacter baumannii* ATCC 19606. *Genome Announc*. 2:e00832-14. doi: 10.1128/genomeA.00832-14

Desjardins, C. A., Cohen, K. A., Munsamy, V., Abeel, T., Maharaj, K., Walker, B. J., et al. (2016). Genomic and functional analyses of *Mycobacterium tuberculosis* strains implicate ald in D-cycloserine resistance. *Nat. Genet*. 48, 544–551. doi: 10.1038/ng.3548

Deslouches, B., and Di, Y. P. (2017). *Antimicrobial* peptides: a potential therapeutic option for surgical site infections. *Clin. Surg*. 2:1740.

Dias, O., Saraiva, J., Faria, C., Ramirez, M., Pinto, F., and Rocha, I. (2019). IDS372, a phenotypically reconciled model for the metabolism of *streptococcus pneumoniae* strain R6. *Front. Microbiol*. 10:1283. doi: 10.3389/fmicb.2019.01283

Dijkshoorn, L., Nemec, A., and Seifert, H. (2007). An increasing threat in hospitals: multidrug-resistant *Acinetobacter baumannii*. *Nat. Rev. Microbiol*. 5, 939–951. doi: 10.1038/nrmicro1789

Ding, T., Case, K. A., Omolo, M. A., Reiland, H. A., Metz, Z. P., Diao, X., et al. (2016). Predicting essential metabolic genome content of niche-specific enterobacterial human pathogens during simulation of host environments. *PLoS ONE* 11:e0149423. doi: 10.1371/journal.pone.0149423

Dorsey, C. W., Tomaras, A. P., and Actis, L. A. (2002). Genetic and phenotypic analysis of *Acinetobacter baumannii* insertion derivatives generated with a transposome system. *Appl. Environ. Microbiol*. 68, 6353–6360. doi: 10.1128/AEM.68.12.6353-6360.2002

Dragosits, M., and Mattanovich, D. (2013). Adaptive laboratory evolution - principles and applications for biotechnology. *Microb. Cell Fact*. 12:64. doi: 10.1186/1475-2859-12-64

Duarte, N. C., Becker, S. A., Jamshidi, N., Thiele, I., Mo, M. L., Vo, T. D., et al. (2007). Global reconstruction of the human metabolic network based on genomic and bibliomic data. *Proc. Natl. Acad. Sci. U.S.A*. 104, 1777–1782. doi: 10.1073/pnas.0610772104

Dunphy, L. J., and Papin, J. A. (2018). Biomedical applications of genome-scale metabolic network reconstructions of human pathogens. *Curr. Opin. Biotechnol*. 51, 70–79. doi: 10.1016/j.copbio.2017.11.014

Dunphy, L. J., Yen, P., and Papin, J. A. (2019). Integrated experimental and computational analyses reveal differential metabolic functionality in antibiotic-resistant *Pseudomonas aeruginosa*. *Cell Syst*. 8, 3–14.e3. doi: 10.1016/j.cels.2018.12.002

Ebenezer, D. L., Berdyshev, E. V., Bronova, I. A., Liu, Y., Tiruppathi, C., Komarova, Y., et al. (2019). *Pseudomonas aeruginosa* stimulates nuclear sphingosine-1-phosphate generation and epigenetic regulation of lung inflammatory injury. *Thorax* 74, 579–591. doi: 10.1136/thoraxjnl-2018-212378

Edwards, J. S., and Palsson, B. O. (1999). Systems properties of the *Haemophilus* influenzae Rd metabolic genotype. *J. Biol. Chem*. 274, 17410–17416. doi: 10.1074/jbc.274.25.17410

Edwards, J. S., and Palsson, B. O. (2000). The *Escherichia coli* MG1655 in silico metabolic genotype: its definition, characteristics, and capabilities. *Proc. Natl. Acad. Sci. U.S.A*. 97, 5528–5533. doi: 10.1073/pnas.97.10.5528

Eriksson, S., Lucchini, S., Thompson, A., Rhen, M., and Hinton, J. C. D. (2003). Unravelling the biology of macrophage infection by gene expression profiling of intracellular *Salmonella enterica*. *Mol. Microbiol*. 47, 103–118. doi: 10.1046/j.1365-2958.2003.03313.x

Eschbach, M., Schreiber, K., Trunk, K., Buer, J., Jahn, D., and Schobert, M. (2004). Long-term anaerobic survival of the opportunistic pathogen *Pseudomonas aeruginosa* via pyruvate fermentation. *J. Bacteriol*. 186, 4596–4604. doi: 10.1128/JB.186.14.4596-4604.2004

Fang, F. C., Libby, S. J., Castor, M. E., and Fung, A. M. (2005). Isocitrate lyase (AceA) is required for *Salmonella* persistence but not for acute lethal infection in mice. *Infect. Immun*. 73, 2547–2549. doi: 10.1128/IAI.73.4.2547-2549.2005

Fang, X., Reifman, J., and Wallqvist, A. (2014). Modeling metabolism and stage-specific growth of *Plasmodium* falciparum HB3 during the intraerythrocytic developmental cycle. *Mol. Biosyst*. 10, 2526–2537. doi: 10.1039/C4MB00115J

Farha, M. A., and Brown, E. D. (2019). Drug repurposing for antimicrobial discovery. *Nat. Microbiol*. 4, 565–577. doi: 10.1038/s41564-019-0357-1

Feist, A. M., Henry, C. S., Reed, J. L., Krummenacker, M., Joyce, A. R., Karp, P. D., et al. (2007). A genome-scale metabolic reconstruction for *Escherichia coli* K-12 MG1655 that accounts for 1260 ORFs and thermodynamic information. *Mol. Syst. Biol*. 3:121. doi: 10.1038/msb4100155

Feist, A. M., Herrgård, M. J., Thiele, I., Reed, J. L., and Palsson, B. Ø. (2009). Reconstruction of biochemical networks in *microorganisms*. *Nat. Rev. Microbiol*. 7, 129–143. doi: 10.1038/nrmicro1949

Fernández Alfonso, T., Celentano, A. M., Gonzalez Cappa, S. M., and Golombek, D. A. (2003). The circadian system of *Trypanosoma cruzi*-infected mice. *Chronobiol. Int*. 20, 49–64. doi: 10.1081/CBI-120017687

Findlay, F., Proudfoot, L., Stevens, C., and Barlow, P. G. (2016). Cationic host defense peptides; novel antimicrobial therapeutics against category A pathogens and emerging infections. *Pathog. Glob. Health* 110, 137–147. doi: 10.1080/20477724.2016.1195036

Fischbach, M. A., and Walsh, C. T. (2009). Antibiotics for emerging pathogens. *Science* 325, 1089–1093. doi: 10.1126/science.1176667

Fleischmann, R. D., Adams, M. D., White, O., Clayton, R. A., Kirkness, E. F., Kerlavage, A. R., et al. (1995). Whole-genome random sequencing and assembly of *Haemophilus* influenzae Rd. *Science* 269, 496–512. doi: 10.1126/science.7542800

Foegeding, N. J., Caston, R. R., McClain, M. S., Ohi, M. D., and Cover, T. L. (2016). An overview of *Helicobacter pylori* VacA toxin biology. *Toxins (Basel)*. 8:173. doi: 10.3390/toxins8060173

Forsyth, R. A., Haselbeck, R. J., Ohlsen, K. L., Yamamoto, R. T., Xu, H., Trawick, J. D., et al. (2002). A genome-wide strategy for the identification of essential genes in *Staphylococcus aureus*. *Mol. Microbiol*. 43, 1387–1400. doi: 10.1046/j.1365-2958.2002.02832.x

Francke, C., Siezen, R. J., and Teusink, B. (2005). Reconstructing the metabolic network of a bacterium from its *genome*. *Trends Microbiol*. 13, 550–558. doi: 10.1016/j.tim.2005.09.001

Gille, C., Bölling, C., Hoppe, A., Bulik, S., Hoffmann, S., Hübner, K., et al. (2010). HepatoNet1: a comprehensive metabolic reconstruction of the human hepatocyte for the analysis of liver physiology. *Mol. Syst. Biol*. 6:411. doi: 10.1038/msb.2010.62

Gonyar, L. A., Gelbach, P. E., McDuffie, D. G., Koeppel, A. F., Chen, Q., Lee, G., et al. (2019). *In vivo* gene essentiality and metabolism in *Bordetella pertussis*. *mSphere*. 4:e00694-18. doi: 10.1128/mSphere.00694-18

Grassmé, H., Henry, B., Ziobro, R., Becker, K. A., Riethmüller, J., Gardner, A., et al. (2017). β1-integrin accumulates in cystic fibrosis luminal airway epithelial membranes and decreases sphingosine, promoting bacterial infections. *Cell Host Microbe 21*, 707–718.e8. doi: 10.1016/j.chom.2017.05.001

Hamilton, J. J., and Reed, J. L. (2014). Software platforms to facilitate reconstructing genome-scale metabolic networks. *Environ. Microbiol*. 16, 49–59. doi: 10.1111/1462-2920.12312

Hannun, Y. A., and Obeid, L. M. (2008). Principles of bioactive lipid signalling: lessons from sphingolipids. *Nat. Rev. Mol. Cell Biol*. 9, 139–150. doi: 10.1038/nrm2329

Haraldsdóttir, H. S., Cousins, B., Thiele, I., Fleming, R. M. T., and Vempala, S. (2017). CHRR: Coordinate hit-and-run with rounding for uniform sampling of constraint-based models. *Bioinformatics* 33, 1741–1743. doi: 10.1093/bioinformatics/btx052

Hartman, H. B., Fell, D. A., Rossell, S., Jensen, P. R., Woodward, M. J., Thorndahl, L., et al. (2014). Identification of potential drug targets in *Salmonella enterica* sv. *Typhimurium* using metabolic modelling and experimental validation. *Microbiology* 160, 1252–1266. doi: 10.1099/mic.0.076091-0

Heinemann, M., Kümmel, A., Ruinatscha, R., and Panke, S. (2005). *In silico* genome-scale reconstruction and validation of the *Staphylococcus aureus* metabolic network. *Biotechnol. Bioeng*. 92, 850–864. doi: 10.1002/bit.20663

Henry, C. S., Dejongh, M., Best, A. A., Frybarger, P. M., Linsay, B., and Stevens, R. L. (2010). High-throughput generation, optimization and analysis of genome-scale metabolic models. *Nat. Biotechnol*. 28, 977–982. doi: 10.1038/nbt.1672

Henry, R., Crane, B., Powell, D., Lucas, D. D., Li, Z., Aranda, J., et al. (2014). The transcriptomic response of *Acinetobacter baumannii* to colistin and doripenem alone and in combination in an *in vitro* pharmacokinetics/pharmacodynamics model. *J. Antimicrob. Chemother*. 70, 1303–1313. doi: 10.1093/jac/dku536

Herrmann, H. A., Dyson, B. C., Vass, L., Johnson, G. N., and Schwartz, J. M. (2019). Flux sampling is a powerful tool to study metabolism under changing environmental conditions. *NPJ Syst. Biol. Appl*. 5:32. doi: 10.1038/s41540-019-0109-0

Huang, F. C. (2016). *De Novo* sphingolipid synthesis is essential for *Salmonella*-induced autophagy and human beta-defensin 2 expression in intestinal epithelial cells. *Gut Pathog*. 8:5. doi: 10.1186/s13099-016-0088-2

Huthmacher, C., Hoppe, A., Bulik, S., and Holzhütter, H. G. (2010). Antimalarial drug targets in *Plasmodium* falciparum predicted by stage-specific metabolic network analysis. *BMC Syst. Biol*. 4:120. doi: 10.1186/1752-0509-4-120

Jamshidi, N., and Palsson, B. (2007). Investigating the metabolic capabilities of *Mycobacterium tuberculosis* H37Rv using the *in silico* strain iNJ661 and proposing alternative drug targets. *BMC Syst. Biol*. 1:26. doi: 10.1186/1752-0509-1-26

Jamshidi, N., and Raghunathan, A. (2015). Cell scale host-pathogen modeling: another branch in the evolution of constraint-based methods. *Front. Microbiol*. 6:1032. doi: 10.3389/fmicb.2015.01032

Jensen, P. A., and Papin, J. A. (2011). Functional integration of a metabolic network model and expression data without arbitrary thresholding. *Bioinformatics* 27, 541–547. doi: 10.1093/bioinformatics/btq702

Joyce, A. R., and Palsson, B. (2007). Predicting gene essentiality using genome-scale *in Silico* models. *Methods Mol. Biol*. 416, 433–457. doi: 10.1007/978-1-59745-321-9_30

Kanehisa, M. (2000). KEGG: kyoto encyclopedia of genes and genomes. *Nucleic Acids Res*. 28, 27–30. doi: 10.1093/nar/28.1.27

Kaper, J. B., Nataro, J. P., and Mobley, H. L. T. (2004). Pathogenic *Escherichia coli*. *Nat. Rev. Microbiol*. 2, 123–140. doi: 10.1038/nrmicro818

Karatzas, K. A. G., Randall, L. P., Webber, M., Piddock, L. J. V., Humphrey, T. J., Woodward, M. J., et al. (2008). Phenotypic and proteomic characterization of multiply antibiotic-resistant variants of *Salmonella enterica* serovar typhimurium selected following exposure to disinfectants. *Appl. Environ. Microbiol*. 74, 1508–1516. doi: 10.1128/AEM.01931-07

Kauffman, K. J., Prakash, P., and Edwards, J. S. (2003). Advances in flux balance *analysis*. *Curr. Opin. Biotechnol*. 14, 491–496. doi: 10.1016/j.copbio.2003.08.001

Kaufman, D. E., and Smith, R. L. (1998). Direction choice for accelerated convergence in hit-and-run sampling. *Oper. Res*. 46, 84–95. doi: 10.1287/opre.46.1.84

Kavvas, E. S., Seif, Y., Yurkovich, J. T., Norsigian, C., Poudel, S., Greenwald, W. W., et al. (2018). Updated and standardized genome-scale reconstruction of *Mycobacterium tuberculosis* H37Rv, iEK1011, simulates flux states indicative of physiological conditions. *BMC Syst. Biol*. 12:25. doi: 10.1186/s12918-018-0557-y

Keiter, H. G., Berman, H., Jones, H., and Maclachlan, E. (1955). The chemical composition of normal human red blood cells, including variability among centrifuged cells. *Blood*. 10, 370–376. doi: 10.1182/blood.V10.4.370.370

Keitsch, S., Riethmüller, J., Soddemann, M., Sehl, C., Wilker, B., Edwards, M. J., et al. (2018). Pulmonary infection of cystic fibrosis mice with *Staphylococcus aureus* requires expression of α-Toxin. *Biol. Chem*. 399, 1203–1213. doi: 10.1515/hsz-2018-0161

Kim, H. U., Kim, T. Y., and Lee, S. Y. (2010). Genome-scale metabolic network analysis and drug targeting of multi-drug resistant pathogen *Acinetobacter baumannii* AYE. *Mol. Biosyst*. 6, 339–348. doi: 10.1039/B916446D

Kim, P. J., Lee, D. Y., Tae, Y. K., Kwang, H. L., Jeong, H., Sang, Y. L., et al. (2007). Metabolite essentiality elucidates robustness of *Escherichia coli* metabolism. *Proc. Natl. Acad. Sci. U.S.A*. 104, 13638–13642. doi: 10.1073/pnas.0703262104

Kunz, T. C., and Kozjak-Pavlovic, V. (2019). Diverse facets of sphingolipid involvement in bacterial infections. *Front. Cell Dev. Biol*. 7:203. doi: 10.3389/fcell.2019.00203

Kwon, Y. K., Lu, W., Melamud, E., Khanam, N., Bognar, A., and Rabinowitz, J. D. (2008). A domino effect in antifolate drug action in *Escherichia coli*. *Nat. Chem. Biol*. 4, 602–608. doi: 10.1038/nchembio.108

Land, M., Hauser, L., Jun, S. R., Nookaew, I., Leuze, M. R., Ahn, T. H., et al. (2015). Insights from 20 years of bacterial genome sequencing. *Funct. Integr. Genomics* 15, 141–161. doi: 10.1007/s10142-015-0433-4

Lazzarini, C., Haranahalli, K., Rieger, R., Ananthula, H. K., Desai, P. B., Ashbaugh, A., et al. (2018). Acylhydrazones as antifungal agents targeting the synthesis of fungal sphingolipids. *Antimicrob. Agents Chemother*. 62:e00156-18. doi: 10.1128/AAC.00156-18

Lee, D. S., Burd, H., Liu, J., Almaas, E., Wiest, O., Barabási, A. L., et al. (2009). Comparative genome-scale metabolic reconstruction and flux balance analysis of multiple *Staphylococcus aureus* genomes identify novel antimicrobial drug targets. *J. Bacteriol*. 191, 4015–4024. doi: 10.1128/JB.01743-08

Liao, Y. C., Huang, T. W., Chen, F. C., Charusanti, P., Hong, J. S. J., Chang, H. Y., et al. (2011). An experimentally validated genome-scale metabolic reconstruction of *Klebsiella pneumoniae* MGH 78578, iYL1228. *J. Bacteriol*. 193, 1710–1717. doi: 10.1128/JB.01218-10

Lofthouse, E. K., Wheeler, P. R., Beste, D. J. V., Khatri, B. L., Wu, H., Mendum, T. A., et al. (2013). Systems-based approaches to probing metabolic variation within the *Mycobacterium tuberculosis* complex. *PLoS ONE*. 8:e75913. doi: 10.1371/journal.pone.0075913

López-Agudelo, V. A., Mendum, T. A., Laing, E., Wu, H. H., Baena, A., Barrera, L. F., et al. (2020). A systematic evaluation of *Mycobacterium tuberculosis* genome-scale metabolic networks. *PLoS Comput. Biol*. 16:e1007533. doi: 10.1371/journal.pcbi.1007533

Luepke, K. H., Suda, K. J., Boucher, H., Russo, R. L., Bonney, M. W., Hunt, T. D., et al. (2016). Past, present, and future of antibacterial economics : increasing bacterial resistance, limited antibiotic pipeline, and societal *implications*. *Pharmacotherapy* 37, 71–84. doi: 10.1002/phar.1868

Lundqvist, T., Fisher, S. L., Kern, G., Folmer, R. H. A., Xue, Y., Newton, D. T., et al. (2007). Exploitation of structural and regulatory diversity in glutamate racemases. *Nature* 447, 817–822. doi: 10.1038/nature05689

Ma, S., Minch, K. J., Rustad, T. R., Hobbs, S., Zhou, S. L., Sherman, D. R., et al. (2015). Integrated modeling of gene regulatory and metabolic networks in *Mycobacterium tuberculosis*. *PLoS Comput. Biol*. 11:e1004543. doi: 10.1371/journal.pcbi.1004543

Mahadevan, R., Edwards, J. S., and Doyle, F. J. (2002). Dynamic flux balance analysis of diauxic growth in *Escherichia coli*. *Biophys. J*. 83, 1331–1340. doi: 10.1016/S0006-3495(02)73903-9

Mahadevan, R., and Schilling, C. H. (2003). The effects of alternate optimal solutions in constraint-based genome-scale metabolic models. *Metab. Eng.* 5, 264–276. doi: 10.1016/j.ymben.2003.09.002

Mahlapuu, M., Håkansson, J., Ringstad, L., and Björn, C. (2016). Antimicrobial peptides: an emerging category of therapeutic agents. *Front. Cell. Infect. Microbiol.* 6:194. doi: 10.3389/fcimb.2016.00194

Managò, A., Becker, K. A., Carpinteiro, A., Wilker, B., Soddemann, M., Seitz, A. P., et al. (2015). *Pseudomonas aeruginosa* pyocyanin induces neutrophil death via mitochondrial reactive oxygen species and mitochondrial acid sphingomyelinase. *Antioxidants Redox Signal.* 22, 1097–1110. doi: 10.1089/ars.2014.5979

Marrakchi, H., Lanéelle, M. A., and Daffé, M. (2014). Mycolic acids: structures, biosynthesis, and beyond. *Chem. Biol.* 21, 67–85. doi: 10.1016/j.chembiol.2013.11.011

Mazharul Islam, M., Thomas, V. C., Van Beek, M., Ahn, J. S., Alqarzaee, A. A., Zhou, C., et al. (2020). An integrated computational and experimental study to investigate *Staphylococcus aureus* metabolism. *NPJ Syst. Biol. Appl.* 6:3. doi: 10.1038/s41540-019-0122-3

Megchelenbrink, W., Huynen, M., and Marchiori, E. (2014). optGpSampler: an improved tool for uniformly sampling the solution-space of genome-scale metabolic networks. *PLoS ONE* 9:e86587. doi: 10.1371/journal.pone.0086587

Mendoza, S. N., Olivier, B. G., Molenaar, D., and Teusink, B. (2019). A systematic assessment of current genome-scale metabolic reconstruction tools. *Genome Biol.* 20:158. doi: 10.1186/s13059-019-1769-1

Metris, A., Reuter, M., Gaskin, D. J. H., Baranyi, J., and van Vliet, A. H. M. (2011). *In vivo* and in silico determination of essential genes of *Campylobacter jejuni*. *BMC Genomics* 12:535. doi: 10.1186/1471-2164-12-535

Miró-Canturri, A., Ayerbe-Algaba, R., and Smani, Y. (2019). Drug repurposing for the treatment of bacterial and fungal infections. *Front. Microbiol.* 10:41. doi: 10.3389/fmicb.2019.00041

Moffatt, J. H., Harper, M., Harrison, P., Hale, J. D. F., Vinogradov, E., Seemann, T., et al. (2010). Colistin resistance in *Acinetobacter baumannii* is mediated by complete loss of lipopolysaccharide production. *Antimicrob. Agents Chemother.* 54, 4971–4977. doi: 10.1128/AAC.00834-10

Monk, J. M., Charusanti, P., Aziz, R. K., Lerman, J. A., Premyodhin, N., Orth, J. D., et al. (2013). Genome-scale metabolic reconstructions of multiple *Escherichia coli* strains highlight strain-specific adaptations to nutritional environments. *Proc. Natl. Acad. Sci. U.S.A.* 110, 20338–20343. doi: 10.1073/pnas.1307797110

Monk, J. M., Lloyd, C. J., Brunk, E., Mih, N., Sastry, A., King, Z., et al. (2017). iML1515, a knowledgebase that computes *Escherichia coli* traits. *Nat. Biotechnol.* 35, 904–908. doi: 10.1038/nbt.3956

Mor, V., Rella, A., Farnou, A. M., Singh, A., Munshi, M., Bryan, A., et al. (2015). Identification of a new class of antifungals targeting the synthesis of fungal sphingolipids. *MBio* 6:e00647. doi: 10.1128/mBio.00647-15

Nakayama, H., Kurihara, H., Morita, Y. S., Kinoshita, T., Mauri, L., Prinetti, A., et al. (2016). *Lipoarabinomannan* binding to lactosylceramide in lipid rafts is essential for the phagocytosis of mycobacteria by human neutrophils. *Sci. Signal.* 9:ra101. doi: 10.1126/scisignal.aaf1585

Norsigian, C. J., Attia, H., Szubin, R., Yassin, A. S., Palsson, B., Aziz, R. K., et al. (2019). Comparative genome-scale metabolic modeling of metallo-beta-lactamase-producing multidrug-resistant *klebsiella pneumoniae* clinical isolates. *Front. Cell. Infect. Microbiol.* 9:161. doi: 10.3389/fcimb.2019.00161

Norsigian, C. J., Fang, X., Seif, Y., Monk, J. M., and Palsson, B. O. (2020). A workflow for generating multi-strain genome-scale metabolic models of prokaryotes. *Nat. Protoc.* 15, 1–14. doi: 10.1038/s41596-019-0254-3

Norsigian, C. J., Kavvas, E., Seif, Y., Palsson, B. O., and Monk, J. M. (2018). iCN718, an updated and improved genome-scale metabolic network reconstruction of *Acinetobacter baumannii* AYE. *Front. Genet.* 9:121. doi: 10.3389/fgene.2018.00121

Oberhardt, M. A., Puchałka, J., dos Santos, V. A. P. M., and Papin, J. A. (2011). Reconciliation of genome-scale metabolic reconstructions for comparative systems analysis. *PLoS Comput. Biol.* 7:e1001116. doi: 10.1371/journal.pcbi.1001116

Oberhardt, M. A., Puchałka, J., Fryer, K. E., Martins Dos Santos, V. A. P., and Papin, J. A. (2008). Genome-scale metabolic network analysis of the opportunistic pathogen *Pseudomonas aeruginosa* PAO1. *J. Bacteriol.* 190, 2790–2803. doi: 10.1128/JB.01583-07

Orth, J. D., Conrad, T. M., Na, J., Lerman, J. A., Nam, H., Feist, A. M., et al. (2011). A comprehensive genome-scale reconstruction of *Escherichia coli* metabolism-2011. *Mol. Syst. Biol.* 7:535. doi: 10.1038/msb.2011.65

Orth, J. D., Thiele, I., and Palsson, B. O. (2010). What is flux balance analysis? *Nat. Biotechnol.* 28, 245–248. doi: 10.1038/nbt.1614

Owen, K. A., Meyer, C. B., Bouton, A. H., and Casanova, J. E. (2014). activation of focal adhesion kinase by salmonella suppresses autophagy via an Akt/mTOR signaling pathway and promotes bacterial survival in macrophages. *PLoS Pathog.* 10:e1004159. doi: 10.1371/journal.ppat.1004159

Perumal, D., Samal, A., Sakharkar, K. R., and Sakharkar, M. K. (2011). Targeting multiple targets in *Pseudomonas aeruginosa* PAO1 using flux balance analysis of a reconstructed genome-scale metabolic network. *J. Drug Target.* 19, 1–13. doi: 10.3109/10611861003649753

Presta, L., Bosi, E., Mansouri, L., Dijkshoorn, L., Fani, R., and Fondi, M. (2017). Constraint-based modeling identifies new putative targets to fight colistin-resistant A. *baumannii infections. Sci. Rep.* 7:3706. doi: 10.1038/s41598-017-03416-2

Price, N. D., Schellenberger, J., and Palsson, B. O. (2004). Uniform sampling of steady-state flux spaces: means to design experiments and to interpret enzymopathies. *Biophys. J.* 87, 2172–2186. doi: 10.1529/biophysj.104.043000

Putnam, D. F. (1971). *Composition and Concentrative Properties of Human Urine*. Washington, DC: NASA.

Raghunathan, A., Reed, J., Shin, S., Palsson, B., and Daefler, S. (2009). Constraint-based analysis of metabolic capacity of *Salmonella typhimurium* during host-pathogen interaction. *BMC Syst. Biol.* 3:38. doi: 10.1186/1752-0509-3-38

Raghunathan, A., Shin, S., and Daefler, S. (2010). Systems approach to investigating host-pathogen interactions in infections with the biothreat agent *Francisella*. Constraints-based model of *Francisella tularensis*. *BMC Syst. Biol.* 4:118. doi: 10.1186/1752-0509-4-118

Raj, S., Nazemidashtarjandi, S., Kim, J., Joffe, L., Zhang, X., Singh, A., et al. (2017). Changes in glucosylceramide structure affect virulence and membrane biophysical properties of *Cryptococcus neoformans*. *Biochim. Biophys. Acta Biomembr.* 1859, 2224–2233. doi: 10.1016/j.bbamem.2017.08.017

Rancati, G., Moffat, J., Typas, A., and Pavelka, N. (2018). Emerging and evolving concepts in gene essentiality. *Nat. Rev. Genet.* 19, 34–49. doi: 10.1038/nrg.2017.74

Reed, J. L., Famili, I., Thiele, I., and Palsson, B. O. (2006). Towards multidimensional genome annotation. *Nat. Rev. Genet.* 7, 130–141. doi: 10.1038/nrg1769

Reed, J. L., Vo, T. D., Schilling, C. H., and Palsson, B. O. (2003). An expanded genome-scale model of *Escherichia coli* K-12 (iJR904 GSM/GPR). *Genome Biol.* 4:R54. doi: 10.1186/gb-2003-4-9-r54

Rienksma, R. A., Schaap, P. J., dos Santos, V. A. P. M., and Suarez-Diez, M. (2018). Modeling the metabolic state of *Mycobacterium tuberculosis* upon infection. *Front. Cell. Infect. Microbiol.* 8:264. doi: 10.3389/fcimb.2018.00264

Rienksma, R. A., Suarez-Diez, M., Spina, L., Schaap, P. J., and Martins Dos Santos, V. A. P. (2014). Systems-level modeling of mycobacterial metabolism for the identification of new (multi-)drug targets. *Semin. Immunol.* 26, 610–622. doi: 10.1016/j.smim.2014.09.013

Rijo-Ferreira, F., Carvalho, T., Afonso, C., Sanches-Vaz, M., Costa, R. M., Figueiredo, L. M., et al. (2018). Sleeping sickness is a circadian disorder. *Nat. Commun.* 9:62. doi: 10.1038/s41467-017-02484-2

Rijo-Ferreira, F., and Takahashi, J. S. (2019). Genomics of circadian rhythms in health and disease. *Genome Med.* 11:82. doi: 10.1186/s13073-019-0704-0

Rittershaus, P. C., Kechichian, T. B., Allegood, J. C., Merrill, A. H., Hennig, M., Luberto, C., et al. (2006). Glucosylceramide synthase is an essential regulator of pathogenicity of *Cryptococcus neoformans*. *J. Clin. Invest.* 116, 1651–1659. doi: 10.1172/JCI27890

Rocha, I., Förster, J., and Nielsen, J. (2008). "Design and application of genome-scale reconstructed metabolic models," in *Microbial Gene Essentiality: Protocols and Bioinformatics Methods in Molecular Biology*^{TM}, Vol. 416, eds A. L. Osterman and S. Y. Gerdes (Totowa, NJ: Humana Press), 409–431. doi: 10.1007/978-1-59745-321-9_29

Rolando, M., and Buchrieser, C. (2019). A comprehensive review on the manipulation of the sphingolipid pathway by pathogenic bacteria. *Front. Cell Dev. Biol.* 7, 1–8. doi: 10.3389/fcell.2019.00168

Rotz, L. D., Khan, A. S., Lillibridge, S. R., Ostroff, S. M., and Hughes, J. M. (2002). Public health assessment of potential biological terrorism agents. *Emerg. Infect. Dis*. 8, 225–230. doi: 10.3201/eid0802.010164

Safi, H., Lingaraju, S., Amin, A., Kim, S., Jones, M., Holmes, M., et al. (2013). Evolution of high-level ethambutol-resistant tuberculosis through interacting mutations in decaprenylphosphoryl-β-D-arabinose biosynthetic and utilization pathway genes. *Nat. Genet*. 45, 1190–1197. doi: 10.1038/ng.2743

Schellenberger, J., and Palsson, B. (2009). Use of randomized sampling for analysis of metabolic networks. *J. Biol. Chem*. 284, 5457–5461. doi: 10.1074/jbc.R800048200

Schilling, C. H., Covert, M. W., Famili, I., Church, G. M., Edwards, J. S., and Palsson, B. O. (2002). Genome-scale metabolic model of *Helicobacter pylori* 26695. *Society* 184, 4582–4593. doi: 10.1128/JB.184.16.4582-4593.2002

Schilling, C. H., and Palsson, B. (2000). Assessment of the metabolic capabilities of Haemophilus influenzae Rd through a genome-scale pathway analysis. *J. Theor. Biol*. 203, 249–283. doi: 10.1006/jtbi.2000.1088

Schomburg, I. (2002). BRENDA, enzyme data and metabolic information. *Nucleic Acids Res*. 30, 47–49. doi: 10.1093/nar/30.1.47

Segrè, D., Vitkup, D., and Church, G. M. (2002). Analysis of optimality in natural and perturbed metabolic networks. *Proc. Natl. Acad. Sci. U.S.A*. 99, 15112–15117. doi: 10.1073/pnas.232349399

Seif, Y., Kavvas, E., Lachance, J. C., Yurkovich, J. T., Nuccio, S. P., Fang, X., et al. (2018). Genome-scale metabolic reconstructions of multiple *Salmonella* strains reveal serovar-specific metabolic traits. *Nat. Commun*. 9:3771. doi: 10.1038/s41467-018-06112-5

Sharma, L., and Prakash, H. (2017). Sphingolipids are dual specific drug targets for the management of pulmonary infections: perspective. *Front. Immunol*. 8:378. doi: 10.3389/fimmu.2017.00378

Shi, L., Adkins, J. N., Coleman, J. R., Schepmoes, A. A., Dohnkova, A., Mottaz, H. M., et al. (2006). Proteomic analysis of *Salmonella enterica* serovar Typhimurium isolated from RAW 264.7 macrophages: identification of a novel protein that contributes to the replication of serovar Typhimurium inside macrophages. *J. Biol. Chem*. 281, 29131–29140. doi: 10.1074/jbc.M604640200

Shlomi, T., Berkman, O., and Ruppin, E. (2005). Regulatory on/off minimization of metabolic flux changes after genetic perturbations. *Proc. Natl. Acad. Sci. U.S.A*. doi: 10.1073/pnas.0406346102

Shlomi, T., Cabili, M. N., Herrgård, M. J., Palsson, B., and Ruppin, E. (2008). Network-based prediction of human tissue-specific metabolism. *Nat. Biotechnol*. 26, 1003–1010. doi: 10.1038/nbt.1487

Simonis, A., and Schubert-Unkmeir, A. (2018). The role of acid sphingomyelinase and modulation of sphingolipid metabolism in bacterial infection. *Biol. Chem*. 399, 1135–1146. doi: 10.1515/hsz-2018-0200

Speer, A., Sun, J., Danilchanka, O., Meikle, V., Rowland, J. L., Walter, K., et al. (2015). Surface hydrolysis of sphingomyelin by the outer membrane protein Rv0888 supports replication of *Mycobacterium tuberculosis* in macrophages. *Mol. Microbiol*. 97, 881–897. doi: 10.1111/mmi.13073

Stover, C. K., Pham, X. Q., Erwin, A. L., Mizoguchi, S. D., Warrener, P., Hickey, M. J., et al. (2000). Complete genome sequence of *Pseudomonas aeruginosa* PAO1, an opportunistic pathogen. *Nature* 406, 959–964. doi: 10.1038/35023079

Sweileh, W. M. (2017). Global research trends of World Health Organization's top eight emerging pathogens. *Global. Health*. 13:9. doi: 10.1186/s12992-017-0233-9

Thiele, I., Hyduke, D. R., Steeb, B., Fankam, G., Allen, D. K., Bazzani, S., et al. (2011). A community effort towards a knowledge-base and mathematical model of the human pathogen Salmonella Typhimurium LT2. *BMC Syst. Biol*. 5:8. doi: 10.1186/1752-0509-5-8

Thiele, I., and Palsson, B. (2010). A protocol for generating a high-quality genome-scale metabolic reconstruction. *Nat. Protoc*. 5, 93–121. doi: 10.1038/nprot.2009.203

Thiele, I., Vo, T. D., Price, N. D., and Palsson, B. (2005). Expanded metabolic reconstruction of *Helicobacter pylori* (iIT341 GSM/GPR): an *in silico* genome-scale characterization of single- and double-deletion mutants. *J. Bacteriol*. 187, 5818–5830. doi: 10.1128/JB.187.16.5818-5830.2005

Thuong, N. T. T., Dunstan, S. J., Chau, T. T. H., Thorsson, V., Simmons, C. P., Quyen, N. T. H., et al. (2008). Identification of tuberculosis susceptibility genes with human macrophage gene expression profiles. *PLoS Pathog*. 4:e1000229. doi: 10.1371/journal.ppat.1000229

Valderas, M. W., Andi, B., Barrow, W. W., and Cook, P. F. (2008). Examination of intrinsic sulfonamide resistance in *Bacillus anthracis*: a novel assay for dihydropteroate synthase. *Biochim. Biophys. Acta 1780, 848–853. doi: 10.1016/j.bbagen.2008.02.003*

Vallenet, D., Nordmann, P., Barbe, V., Poirel, L., Mangenot, S., Bataille, E., et al. (2008). Comparative analysis of acinetobacters: three genomes for three lifestyles. *PLoS ONE*. 3:e1805. doi: 10.1371/journal.pone.0001805

Vashisht, R., Bhat, A., Kushwaha, S., Bhardwaj, A., Consortium, O., and Brahmachari, S. (2014). Systems level mapping of metabolic complexity in *Mycobacterium tuberculosis* to identify high-value drug targets. *J. Transl. Med*. 12:263. doi: 10.1186/s12967-014-0263-5

Vieira, G., Sabarly, V., Bourguignon, P. Y., Durot, M., Le Fèvre, F., Mornico, D., et al. (2011). Core and panmetabolism in *Escherichia coli*. *J. Bacteriol*. 193, 1461–1472. doi: 10.1128/JB.01192-10

Vilchèze, C., Av-Gay, Y., Attarian, R., Liu, Z., Hazbón, M. H., Colangeli, R., et al. (2008). Mycothiol biosynthesis is essential for ethionamide susceptibility in *Mycobacterium tuberculosis*. *Mol. Microbiol*. 69, 1316–1329. doi: 10.1111/j.1365-2958.2008.06365.x

Wallqvist, A., Fang, X., Tewari, S. G., Ye, P., and Reifman, J. (2016). Metabolic host responses to malarial infection during the intraerythrocytic developmental cycle. *BMC Syst. Biol*. 10:58. doi: 10.1186/s12918-016-0291-2

Winsor, G. L., Lo, R., Ho Sui, S. J., Ung, K. S. E., Huang, S., Cheng, D., et al. (2005). *Pseudomonas aeruginosa* genome database and pseudoCAP: facilitating community-based, continually updated, genome annotation. *Nucleic Acids Res*. 33, 338–343. doi: 10.1093/nar/gki047

Wong, J. D., Barash, J. R., Sandfort, R. F., and Janda, J. M. (2000). Susceptibilities of *Yersinia pestis* strains to 12 antimicrobial agents. *Antimicrob. Agents Chemother*. 44, 1995–1996. doi: 10.1128/AAC.44.7.1995-1996.2000

World Health Organization (2017). *Prioritization of Pathogens to Guide Discovery, Research and Development of New Antibiotics for Drug Resistant Bacterial Infections, Including Tuberculosis*. Geneva.

Zampieri, M., Enke, T., Chubukov, V., Ricci, V., Piddock, L., and Sauer, U. (2017). Metabolic constraints on the evolution of antibiotic resistance. *Mol. Syst. Biol*. 13:917. doi: 10.15252/msb.20167028

Zheng, J., Rubin, E. J., Bifani, P., Mathys, V., Lim, V., Au, M., et al. (2013). Para-aminosalicylic acid is a prodrug targeting dihydrofolate reductase in *Mycobacterium tuberculosis*. *J. Biol. Chem*. 288, 23447–23456. doi: 10.1074/jbc.M113.475798

Zhu, Y., Czauderna, T., Zhao, J., Klapperstueck, M., Maifiah, M. H. M., Han, M. L., et al. (2018). Genome-scale metabolic modeling of responses to polymyxins in *Pseudomonas aeruginosa*. *Gigascience* 7:giy021. doi: 10.1093/gigascience/giy021

Conflict of Interest: The authors declare that the research was conducted in the absence of any commercial or financial relationships that could be construed as a potential conflict of interest.

frontiers in Cell and Developmental Biology

ORIGINAL RESEARCH
published: 05 November 2020
doi: 10.3389/fcell.2020.552020

Chlorogenic Acid Promotes Autophagy and Alleviates *Salmonella* Typhimurium Infection Through the lncRNAGAS5/miR-23a/PTEN Axis and the p38 MAPK Pathway

Shirui Tan[1†], Fang Yan[1†], Qingrong Li[2†], Yaping Liang[1], Junxu Yu[1], Zhenjun Li[3], Feifei He[4], Rongpeng Li[5*] and Ming Li[1*]*

[1] Center of Life Sciences, School of Life Sciences, Yunnan University, Kunming, China, [2] The Second Affiliated Hospital of Kunming Medical University, Kunming, China, [3] Pneumology Department, Suzhou Kowloon Hospital, School of Medicine, Shanghai Jiao Tong University, Suzhou, China, [4] School of Agriculture, Yunnan University, Kunming, China, [5] Key Laboratory of Biotechnology for Medicinal Plants of Jiangsu Province and School of Life Sciences, Jiangsu Normal University, Xuzhou, China

OPEN ACCESS

Edited by:
Davide Gibellini,
University of Bologna, Italy

Reviewed by:
Jing Zhang,
Shanghai Jiao Tong University, China
Alexander Van Parys,
Ghent University, Belgium

***Correspondence:**
Feifei He
hefeifei@ynu.edu.cn
Rongpeng Li
lirongpeng@jsnu.edu.cn
Ming Li
MingL1022@163.com

[†] These authors have contributed equally to this work

Specialty section:
This article was submitted to Molecular Medicine, a section of the journal Frontiers in Cell and Developmental Biology

Received: 15 April 2020
Accepted: 19 October 2020
Published: 05 November 2020

Citation:
Tan S, Yan F, Li Q, Liang Y, Yu J, Li Z, He F, Li R and Li M (2020) Chlorogenic Acid Promotes Autophagy and Alleviates Salmonella Typhimurium Infection Through the lncRNAGAS5/miR-23a/PTEN Axis and the p38 MAPK Pathway. Front. Cell Dev. Biol. 8:552020. doi: 10.3389/fcell.2020.552020

Background: *Salmonella typhimurium (ST)* causes several intestinal diseases. Polyphenols including chlorogenic acid (CGA) inhibit pathogenesis.

Objective: This study aimed to investigate the mechanisms of CGA in *ST* infection.

Methods: The intestinal pathological changes and survival rate of ST-infected mice were measured to verify the protection of CGA on *ST* infection. The antibacterial effects of CGA *in vitro* on the invasion to intestinal epithelial cells and autophagy was evaluated. The relationships among GAS5, miR-23a, and PTEN were verified. Expression of inflammation- and autophagy-related proteins was detected.

Results: CGA treatment alleviated pathological damage, improved the secretion disturbance of intestinal cytokines caused by *ST* infection, and reduced the mortality of mice. Intestinal GAS5 was upregulated after CGA treatment. LncRNA GAS5 competitively bound to miR-23a to upregulate PTEN and inhibit the p38 MAPK pathway. CGA regulated the p38 MAPK pathway through lncRNA GAS5/miR-23a/PTEN axis to promote autophagy in *ST* infection. The functional rescue experiments of miR-23a and PTEN further identified these effects.

Conclusion: CGA promotes autophagy and inhibits *ST* infection through the GAS5/miR-23a/PTEN axis and the p38 MAPK pathway.

Keywords: chlorogenic acid, *Salmonella typhimurium*, lncRNAGAS5, microRNA-23a, PTEN, p38 MAPK, autophagy

Abbreviations: CGA, chlorogenic acid; DMEM, Dulbecco's modified Eagle's medium; TSB, tryptic soy broth; EP, eppendorf; PBS, phosphate buffer saline; SPF, specific pathogen free; TBST, tris-buffered saline with Tween; FISH, fluorescence *in situ* hybridization; DAPI, 4′,6-diamidino-2-phenylindole; RT-qPCR, reverse transcription quantitative polymerase chain reaction; TEM, transmission electron microscope; MDC, monodansylcadaverin; PVDF, polyvinylidene fluoride; BCA, bicinchoninic acid; LDH, lactate dehydrogenase; HE, hematoxylin and eosin; ELISA, enzyme-linked immunosorbent assay; MOI, multiplicity of infection; WT, wild type; MUT, mutant; SDS-PAGE, sodium dodecyl sulfate–polyacrylamide gel electrophoresis; BSA, bovine serum albumin; ANOVA, analysis of variance; NO, nitric oxide; TNF-α, tumor necrosis factor-α; IL, interleukin; miR, microRNA; ceRNA, competing endogenous RNA; lncRNA, long non-coding RNAs.

INTRODUCTION

Salmonella enterica serovar Typhimurium (*S*. Typhimurium, ST) is a Gram-negative facultative intracellular pathogen in humans and animals (Viswanathan et al., 2009; Jiang et al., 2018). The *ST* invades intestinal phagocytic and epithelial cells to achieve its pathogenicity, intracellular replication, and dissemination to other tissues (Birhanu et al., 2018). *ST* is the leading cause of bacterial gastrointestinal infections, enterocolitis, typhoid-like diseases, and severe systemic diseases in human and livestock around the world via oral intake of contamination (Velge et al., 2012). The systemic dissemination of *ST* may cause acute intestinal inflammation, diarrhea and immunodeficiency disorders in people and result in an enormous economic loss in animal husbandry and food industry (Park et al., 2017; Yang et al., 2019). Despite increasing awareness of hygiene and health issues, *ST* infection has increased worldwide and its underlying mechanisms remain unclear (Jain et al., 2018). Therefore, a comprehensive understanding of the mechanisms and new therapeutic agents will provide a novel insight to clarify *ST* infections and develop proper therapies to minimize economic loss.

Antibacterial activities of some agents against a multidrug-resistant strain of *ST* show suppressive actions *in vitro* and in mice (Kim et al., 2018; Mortazavi and Aliakbarlu, 2019). As one of the most abundant polyphenols in human diet, chlorogenic acid (CGA) is mainly from coffee, fruits and vegetables, and is also an important bioactive component in some medicine (Upadhyay and Mohan Rao, 2013). Polyphenols including CGA can inhibit pathogenic bacteria and help regulate intestinal microorganisms (Bao et al., 2019). Studies have shown that CGA has anti-oxidative, anti-inflammatory and antibacterial effects, and improves immune regulation (Tosovic et al., 2017; Zhang et al., 2018; Wang et al., 2019). Importantly, the antibacterial activity of CAG against Salmonella Enteritidis S1 has been reported (Sun et al., 2020). Moreover, *Salmonella* expresses hundreds of small regulatory RNAs, many of which are activated under defined stress and virulence conditions, suggesting a role during host infection (Westermann et al., 2016). Mammalian cells express many long non-coding RNA (lncRNA), which are associated with dysregulation of immunity and host defense (Carpenter and Fitzgerald, 2018). *ST* infection usually causes cell inflammation, and many lncRNAs are differentially expressed in inflammatory diseases. GAS5 is abnormally expressed in autoimmune and inflammatory diseases, especially in patients with bacterial sepsis (Mayama et al., 2016). In some inflammatory diseases, GAS5 affects cell inflammatory responses by regulating TLR4 receptor (Zhao et al., 2020). TLR family including TLR4 is an important cell surface receptor in the process of *ST* infection (Kamble et al., 2017; Muneta et al., 2018; Lin H.H. et al., 2020). However, less attention has been paid to the involvement of lncRNA GAS5 in the molecular mechanism of *ST* infection. In addition, the interaction between CGA and lncRNA has been documented recently, which relieves oxidative stress injury in retinal ganglion cells by upregulation of lncRNA TUG1 expression (Gong et al., 2019). In our preliminary experiments for screening lncRNAs in mice, lncRNA GAS5 expression was remarkably changed after CGA treatment. Hence, we focused on lncRNA GAS5 and tried to figure out the regulatory mechanism of CGA in the treatment of *ST* infections.

In light of the aforementioned information, we hypothesized that CGA upregulates lncRNA GAS5 expression in the model of ST infection. We conducted histochemical and molecular experiments to verify the hypothesis, with the purpose of providing antibacterial agents against *ST* infection.

MATERIALS AND METHODS

Ethics Statement

This study was ratified and supervised by the ethics committee of Yunnan University (Approval number:Yuncae2020334). Significant efforts were made to minimize the animals used and their suffering.

Animal Grouping and Treatments

After normal feeding for 1 week, 6–8-weeks-old specific pathogen free female C57BL/6 mice (purchased from Changchun Yisi Experimental Animal Technology Co., Ltd., Changchun, China) were grouped into: (1) saline group (n = 20, gavaged with 100 μL of normal saline every day for 10 days); (2) Sty group (n = 20, gavaged with 100 μL of normal saline every day for 7 days, and given oral ST (5.19×10^9cfu $mL^{-1}day^{-1}$p.o) on days 8–10 (Dong et al., 2020); (3) treatment groups of different concentrations of CGA (60 mice were assigned into three groups with 20 mice in each group, gavaged with 10, 60, and 120 mg/kg/day of CGA (Sigma, St. Louis, MO, United States), respectively, and given oral *ST* (5.19×10^9cfu $mL^{-1}day^{-1}$p.o (n = 20) on days 8–10 after CGA treatment; (4) ST + CGA + kd-NC group (n = 20, gavaged with 60 mg/kg/day CGA daily, given oral *ST* (5.19×10^9cfu $mL^{-1}day^{-1}$p.o) on days 8–10), and injected with 100 μL of empty vector in the tail vein on days 5 and 10); (5) ST + CGA + kd-GAS5 group (n = 20, the rest operations were the same as those in the kd-NC group, except that the tail vein was injected with 100 μL 7.8×10^7 IFUs GAS5 interfering vector) on the 5th day and the 10th day). Gas5 interference vector kd-GAS5, control kd-NC, and sh-NC and sh-GAS5 used in the following experiments were constructed and synthesized by Shanghai Genechem Co., Ltd. (Shanghai, China).

On the 11th day of CGA gavage, the mesenteric lymph nodes, liver, and spleen of 5 mice in each group were aseptically collected for determining of organ indices and bacterial loads of *Salmonella*. Hematoxylin and eosin (HE) staining was used to detect intestinal pathological changes. Another five mice in each group were used for enzyme-linked immunosorbent assay (ELISA) to detect the intestinal cytokine secretion level. The remaining 10 mice in each group were used for the observation of the living situation. The body weight, general state and mortality rate of mice was monitored and recorded.

HE Staining

The contents of the cecum and colorectum were rinsed with sterile phosphate buffer saline (PBS), and 1 cm of the intestine was cut and fixed in 4% (m/v) paraformaldehyde. After paraffin

embedding, the sections at 4 μm were dewaxed and dehydrated, and stained with HE (Beyotime Biotechnology Co., Ltd., Shanghai, China), followed by observation under a microscopy.

Detection of Bacterial Load of *Salmonella* in Organs

Spleen, liver, cecum, colorectal samples of mice were isolated and weighed. According to organ weight/cadaveric weight, the organ index was calculated. The weighed spleen and liver were ground in pre-cooled PBS, and 100 μL of diluted sample was spread on Luria-Bertani agar plates with 20 mg/mL streptomycin sulfate (Shandong Lukang Pharmaceutical Co., Ltd., Jining, China) at 37°C overnight, for the observation and counting of colonies.

ELISA

The contents of the cecum after PBS washes were ground using liquid nitrogen, and centrifuged at 3,500 r/min, 4°C for 20 min. The supernatant was collected to detect the levels of nitric oxide (NO), interleukin (IL)-12 (IL-12), and IL-10 secreted in the tissue, or the levels of IL-4, IL-6, tumor necrosis factor-α (TNF-α), and IL-1β in the cells after fixing. The detection protocol was in strict accordance with the instructions of the ELISA kits (Shanghai Lengton Bioscience Co., Ltd, Shanghai, China). In short, the ground tissue supernatant was added into the 96-well ELISA plate, and incubated at 37°C for 2 h after adding the coating solution, and then incubated overnight at 4°C. After washing in PBS containing 0.05% (v/v) Tween-20 repeatedly, the sample was blocked using 10% calf serum overnight at 4°C. After washing, the primary antibody was added and incubated at 37°C for 2 h, and the second antibody was incubated at the same temperature for 1.5 h. Then the color reaction was carried out. The termination solution was added to terminate the reaction, and the value was recorded on the microplate.

Cytotoxicity Test

CGA diluted with high-glucose Dulbecco's modified Eagle's medium (DMEM) was added to the mouse intestinal epithelial cells MODE-K (American Type Culture Collection, Manassas, VA, United States) cultured in 96-well microplates, so that the final concentration of CGA was 0, 10, 40, 80, and 160 μg/mL, with 3 replicates for each concentration. The microplates treated with CGA were placed in a 37°C incubator and cultured for 5 h with 5% CO_2. Afterward, the microplates were centrifuged at 1,000 r/min for 10 min. From each well, 100 μL of supernatant was aspirated and placed into new 96-well microplates. Each well was incubated with 100 μL of prepared lactate dehydrogenase (LDH) reagent for 15 min in the dark. Then absorbance at the wavelength of 490 nm was measured with a microplate reader (Shanghai Peiou Analytical Instrument Co., Ltd., Shanghai, China) to calculate the amount of LDH released into the supernatant of each well.

Gentamicin Protection Assay

ST cultured overnight was expanded in a new tryptic soy broth (TSB) tube at 1:20. CGA solution was added to make the concentrations at 0, 10, 20, 30, and 40 μg/mL, and cultured at 37°C for 4 h. Then the bacterial suspension was diluted with high-glucose DMEM, so that the ratio of the bacterial counts to the cells (multiplicity of infection value) was 200:1. The suspension was cultured at 37°C for 24 h. The bacterial suspension and MODE-K cells were mixed, centrifuged at 1,000 r/min for 10 min, and then cultured at 37°C for 50 min, so that the bacteria repeatedly invaded MODE-K cells. Next, 1 mL of gentamicin diluted with high-glucose DMEM (with the final concentration being 100 μg/mL) was added into each well and incubated at 37°C for 1 h. After that, 1 mL of 0.2% (m/v) saponin was added into each well to fully lyse the cells. The lysate was diluted at proper ratios, and spread onto the prepared TSB culture plates, which was then placed into a 37°C incubator for 24 h. The number of colonies was counted, and the invasion rate of *ST* treated with CGA was calculated, with the invasion rate of *ST* in the group without CGA treatment as 100%. Subsequently, CGA at the optimal concentration against ST was cocultured with MODE-K cells and assigned into: ST + CGA + NC group (cells were treated with 40 μg/mL CGA, and transfected with GAS5 empty vector), ST + CGA + sh-GAS5 group (cells were treated with 40 μg/mL CGA, and transfected with 20 nM GAS5 interference vector), ST + CGA + sh-GAS5 + in-miR-23a group (the treatment protocol was the same as ST + CGA + sh-GAS5 group, except that miR-23a inhibitor was transfected). The transfection was performed in line with the instructions of Lipofectamine^{TM} 2000 (Invitrogen, Carlsbad, CA, United States).

Reverse Transcription Quantitative Polymerase Chain Reaction (RT-qPCR)

Total RNA in the tissue and cells was extracted using RNAiso Plus (TAKARA, Otsu, Shiga, Japan) and Trizol LS Reagent (TAKARA), respectively. Subsequently, the reliability of the obtained RNA was verified using denaturing formaldehyde agarose gel electrophoresis. Reverse transcription was performed using the PrimeScript RT kit (TAKARA). Standard real-time qPCR was performed according to the instructions of SYBR Premix Ex Taq (TAKARA), and miR and mRNA levels were quantified according to the $2^{-\Delta\Delta Ct}$ method. U6 or glyceraldehyde-3-phosphate dehydrogenase (GAPDH) was used as the control. All primers were synthesized by Sangon Biotech, Shanghai, China. The primer sequences are shown in **Table 1**.

Western Blot Analysis

The cells and cecum tissues of the above groups and mice were ground and homogenized and added with lysate, and lysed with ultrasound. After that, the samples were centrifuged for 10 min. A small amount of sample was taken to determine the protein concentration using bicinchoninic acid (BCA) protein quantification kit (Thermo Fisher Scientific Inc., Waltham, MA, United States) on the microplate reader. For each sample, 50 μg protein was loaded onto a 10–15% sodium dodecyl sulfate-polyacrylamide gel electrophoresis gel with tris-glycine running buffer, and transferred to polyvinylidene fluoride (PVDF) membranes, which was blocked with 5% (m/v) skimm milk or bovine serum albumin (BSA) for 2 h. The membranes were incubated with primary antibodies (**Table 2**, all from

TABLE 1 | Primer sequences of RT-qPCR.

Gene	Sequence (5′–3′)
GAS5	F: CTTCTGGGCTCAAGTGATCCT
	R: TTGTGCCATGAGACTCCATCAG
miR-23a	F: AATCCCTGGCAATGTGAT
	R: GTGTAACACGTCTATACGCCCA
U6	F: CTCGCTTCGGCAGCACA
	R: GTGTCGTGGAGTCGGCAA
PTEN	F: GAAGTATGACAAAGATGA
	R: AGAGCTTCTTGGAGACTG
IL-1β	F: ATAAGCCCACTCTACACCTCTGA
	R: ATTGGCCCTGAAAGGAGAGAGA
IL-6	F: GCTTCTTAGCGCTAGCCTCAATG
	R: TGG GGCTGATTGGAAACCTTATT
IL-4	F: TGCTGCCTCCAAGAACACAACTG
	R: CATGATCGTCTTTAGCCTTTCCA
TNF-α	F: TCC TGCATCCTGTCTGGAAG
	R: 5'-GTCTTCTGGGCCACTGACTG
GAPDH	F: ACCAGGTATCTGCTGGTTG
	R: TAACCATGATGTCAGCGTGGT

GAS5, growth arrest-specific 5; IL, interleukin; PTEN, gene of phosphate and tension homology deleted on chromsome ten; RT-qPCR, reverse transcription quantitative polymerase chain reaction; GAPDH, glyceraldehyde-3-phosphate dehydrogenase; miR, microRNA; F, forward; R, reverse.

TABLE 2 | Antibodies used in Western blot analysis.

Antibodies	Cat. No. and source	Dilution ratio
P62	ab109012, abcam	1/10,000
LC3I	ab51520, abcam	1/500
LC3II	ab51520, abcam	1/500
P38	ab170099, abcam	1/500
P-P38	ab47363, abcam	1/500
PTEN	ab32199, abcam	1/10,000
GAPDH	ab181602, abcam	1/10,000

LC3, light chain 3; PTEN, gene of phosphate and tension homology deleted on chromsome ten; GAPDH, glyceraldehyde-3-phosphate dehydrogenase. All antibodies were purchased from Abcam (Cambridge, MA, United States).

Abcam Inc., Cambridge, MA, United States) at 4°C overnight. The next day after washing with tris-buffered saline with Tween (TBST), the membranes were incubated with goat anti-mouse secondary antibody (1:2,000, ab7063, Abcam) for 2 h. After visualization using enhanced chemiluminescence, the membranes were imaged using the gel imaging system. The band intensity was quantified with Image-Pro Plus 6.0 software (Olympus Optical Co., Ltd, Tokyo, Japan).

Transmission Electron Microscope (TEM) Observation

The cells were collected, washed twice with PBS, and fixed on ice for 30 min by adding pre-cooled 2.5% glutaraldehyde fixative. Then the cells were transferred to eppendorf tubes and kept overnight. Then the samples were subjected to acetone gradient dehydration, resin embedding, ultra-thin microtome for sectioning, and uranium acetate-lead citrate double staining, and observed under a transmission electron microscope (HF5000 Hitachi, Japan) for changes of intracellular organelles and nuclei.

Monodansylcadaverin (MDC) Fluorescence Staining

Cells were washed twice with pre-cooled PBS, and incubated with 0.05 mmoL/L MDC solution (Shanghai Uteam-Biotech Co., Ltd., Shanghai, China) at 37°C for 30 min. Next, cells were fixed with 4% (m/v) paraformaldehyde for 10 min and washed twice with PBS. After the natural air-drying, the cells were observed and imaged under a fluorescence microscope (Olympus, Japan).

Nuclear/Cytosol Fractionation Experiment

According to the method of a report (Lin H. et al., 2020) and the instructions of the nuclear/cytosol fractionation kit (Invitrogen), the cells were isolated. Briefly, 10^6 cells were mixed with 300 μL cell disruption buffer, incubated on ice for 10 min, and centrifuged for 3 min. The supernatant was cytosol, and the precipitate was the nuclei. The supernatant was aspirated into RNase-free tubes and placed on ice to perform RNA extraction immediately. Subsequently, lncRNA GAS5 in the nucleus and cytoplasm was detected using RT-qPCR.

Fluorescence *in situ* Hybridization (FISH) Assay

The localization of GAS5 was detected in intestinal epithelial cells. The cells were allocated into cell group and control group (the cells were treated only with 4′,6-diamidino-2-phenylindole (DAPI) but no GAS5 probe), and seeded in 24-well microplates with coverslips for 24 h. After diluting the lncRNA-GAS5 FISH probe in the hybridization solution at 1:50, 100 μL the mixture was added to each well and hybridized in a 37°C incubator in the dark overnight. The cells were washed with sodium saline citrate the next day, stained with 10 μL DAPI working solution (10 μg/mL), kept still for 8 min, and washed 3 times with PBS. Finally, the coverslips were sealed, observed and imaged as the kit (Guangzhou RiboBio Co., Ltd., Guangzhou, China) instructed.

RNA Pull-Down Assay

The binding of GAS5 to miR-23a was detected by RNA pull-down assay. Total RNA of tissue (100 μg) was extracted. For each sample, 500 μg streptavidin magnetic beads were mixed with 200 pmol biotin-labeled miR-23a, and incubated with the extracted RNA for 1 h. Elution buffer was added to collect the RNA complex that had been pulled down. Quantitative analysis of lncRNA GAS5 levels was fulfilled using RT-qPCR. The specific operations were based on the instructions of GENEWIZ (China) and biotin-labeled Magnetic RNA-protein pull-down kit (Thermo Fisher Scientific).

Dual Luciferase Reporter Gene Assay

The PTEN and GAS5 sequences containing miR-23a binding site were synthesized, respectively, and PTEN and GAS5 wild-type (WT) plasmids (PTEN/GAS5-WT) were constructed. Based on the WT plasmids, the binding sites were mutated to construct

PTEN and GAS5 mutant (MUT) plasmids (PTEN/GAS5-MUT). These plasmids were mixed with NC and miR-23a and transfected into 293T cells. Cells were collected and lysed 48 h after transfection, and luciferase activity was detected using a luciferase detection kit (BioVision, San Francisco, CA, United States) and a Glomax20/20 luminometer fluorescence detector (Promega, Madison, Wisconsin, United States).

Statistical Analysis

Data were analyzed using SPSS 21.0 (IBM Corp. Armonk, NY, United States). Kolmogorov-SmiRnov test showed a normal distribution of the data, and data are expressed as mean ± standard deviation. Comparisons between two groups were performed using independent sample *t*-tests. Comparisons among multiple groups were performed using one-way or two-way analysis of variance (ANOVA). Pairwise comparisons after ANOVA were performed using Tukey's multiple comparison test. Survival analysis was performed using Kaplan-Meier analysis. The *p*-value was calculated using a two-sided test, and $p < 0.05$ was considered statistically significant.

RESULTS

CGA Alleviated Pathological Damage Caused by *ST* Infection

To evaluate the effect of CGA on *ST* infection, we established a mouse enteritis model induced by *ST* and treated the mice with different concentrations of CGA by gavage. The pathological damage of the colorectum and cecum of mice was evaluated using HE staining. The results showed that the intestinal rectum gland and cecal gland of control mice were intact; while most of the glands of *ST*-infected mice were destroyed, the intestinal mucosa was shed, with massive inflammatory cell infiltration and bleeding spots. With the increasing concentrations of CGA, the structures of rectal and cecal glands of *ST*-infected mice were intact, and inflammatory cell infiltration and bleeding points were gradually reduced (**Figure 1A**). The spleen in *ST*-infected mice was enlarged and the weight was notably increased compared with those of control mice. With increasing concentrations of CGA, the spleen swelling caused by *ST* infection was attenuated, and the decreased contents in cecum and decreased weight were gradually improved (**Figures 1B–D**). In addition, no *Salmonella* was detected in the organs of control mice, while a large amount of *Salmonella* was present in the organs of *ST*-infected mice. Increasing concentrations of CGA significantly reduced the bacterial loads in the spleen, liver and mesenteric lymph nodes of *ST*-infected mice (all $p < 0.01$) (**Figure 1E**). In summary, CGA alleviated the pathological damage of mice caused by *ST* infection.

CGA Regulated the Secretion Balance of Cytokines in the Intestinal Tract of *ST*-Infected Mice and Reduced the Mortality

The levels of NO and IL-12 secretion in the intestinal tissue of *ST*-infected mice were increased, while the level of IL-10 secretion was significantly reduced. These changes were reversed after treatment with different concentrations of CGA (**Figure 2A**) (all $p < 0.01$). It possibly indicated that CGA might maintain the intestinal immune balance and relieve the intestinal inflammatory responses by regulating the secretion of cytokines. The weight of control mice was increased slowly, and the weight of *ST*-infected mice was lost severely, but different concentrations of CGA alleviated the weight loss (**Figure 2B**). In addition, no mice died in the control group, while the survival rate of *ST*-infected mice was only 20% on the 12th day, and the survival rate in *ST*-infected mice treated with CGA was increased (**Figure 2C**). In conclusion, CGA could improve the secretion disturbance of intestinal cytokines caused by *ST* infection, alleviate the weight loss, and reduce the mortality of mice.

CGA Reduced Intestinal Damage Caused by *ST* by Upregulating lncRNA GAS5 Expression

To understand the protective mechanism of CGA against *ST* infection, we referenced a large amount of publications on immunity and anti-inflammation, and found that lncRNAs play a certain role in these physiological processes. Therefore, we selected 10 related lncRNAs in the recent references and detected the expression in the intestinal tissue of *ST*-infected mice using RT-qPCR. It turned out that GAS5 expression in the intestinal tissue of *ST*-infected mice was decreased significantly, but upregulated significantly in *ST*-infected mice treated with a high concentration of CGA (**Figure 3A**). GAS5 is abnormally downregulated in patients with bacterial sepsis (Mayama et al., 2016). In some inflammatory diseases, GAS5 affects cell inflammatory responses by regulating TLR4 receptor (Zhao et al., 2020), which is an important cell surface receptor in *ST* infection (Kamble et al., 2017; Muneta et al., 2018; Lin H.H. et al., 2020). Therefore, we speculated that CGA might upregulate GAS5 expression in the intestinal tissue of *ST*-infected mice, thus exerting a protective effect. To confirm this speculation, we injected the GAS5 interference vector (kd-GAS5) into the *ST*-infected mice via the tail vein, which successfully knocked down GAS5 expression (**Figure 3B**). Then we evaluated the colorectal and cecal pathological damage using HE staining. After GAS5 knockdown, the intestinal glands of mice were destroyed, intestinal mucosa was shed, inflammatory cells infiltrated, and blood spots took place (**Figure 3C**); the spleen and cecum organ index of mice was increased (**Figures 3D,E**); the bacterial loads in the spleen, liver and mesenteric lymph nodes of mice were significantly increased (all $p < 0.01$) (**Figure 3F**). ELISA showed that the levels of NO and IL-12 in the intestinal tissue of *ST*-infected mice were significantly increased, while the IL-10 secretion was reduced after GAS5 knockdown (**Figure 3G**). Furthermore, the mice lost weight significantly (**Figure 3H**) and the survival rate was reduced (**Figure 3I**) after GAS5 knockdown. In summary, GAS5 knockdown could reverse the protective effect of CGA on *ST*-infected intestine.

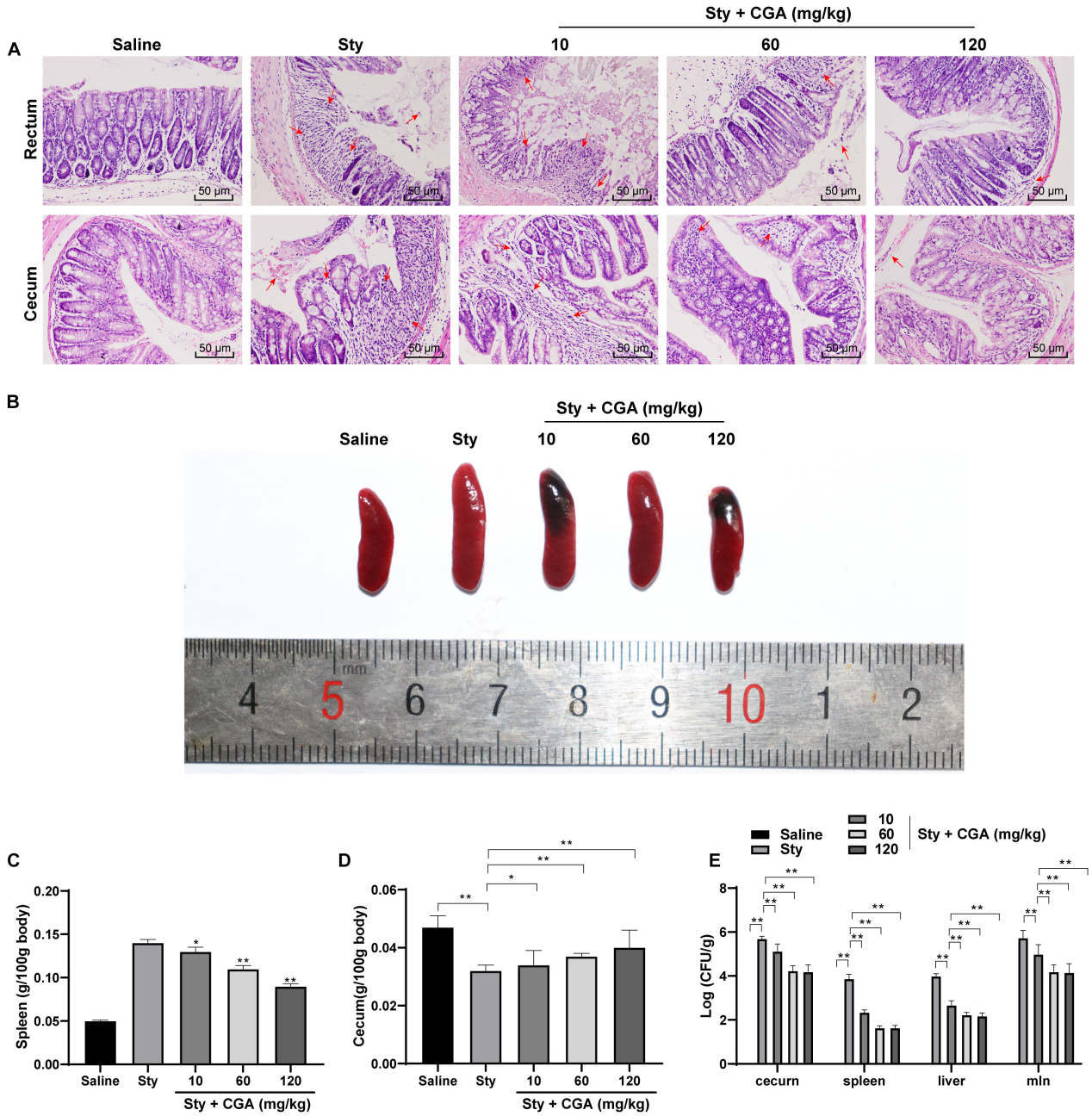

FIGURE 1 | CGA alleviated the pathological damage of *ST*-infected mice. Female C57BL/6 mice were treated with *ST* infection and different concentrations of CGA. **(A)** HE staining detected the pathology of rectum and cecum of mice (×200); the arrow points to the bleeding point; **(B)** spleen morphology of mice in each group; **(C)** spleen organ index of mice in each group; **(D)** cecum organ index of mice in each group; **(E)** *Salmonella* loads in cecum, spleen, liver and mesenteric lymph nodes of mice; $n = 5$. The data in panels C/D were analyzed using one-way ANOVA and Tukey's multiple comparison test, and data in panel E were analyzed using two-way ANOVA and Tukey's multiple comparison test, $^{*}p < 0.05$, $^{**}p < 0.01$.

CGA Inhibited the Invasion of *ST* to Intestinal Epithelial Cells and Improved the Secretion Balance of Inflammatory Cytokines

To investigate whether CGA could inhibit the *in vitro* infection of *ST*, we chose mouse intestinal epithelial cells MODE-K for *in vitro* experiments. First, the cytotoxicity tests found that CGA had no cytotoxicity at the concentrations of 0, 10, and 40 μg/mL, but had weak cytotoxicity at the concentration of 80 μg/mL. The results indicated that when the effective concentration of CGA was from 0 to 40 μg/mL, it did not affect the activity of intestinal epithelial cells (**Figure 4A**). Then gentamicin protection assay found that when the CGA

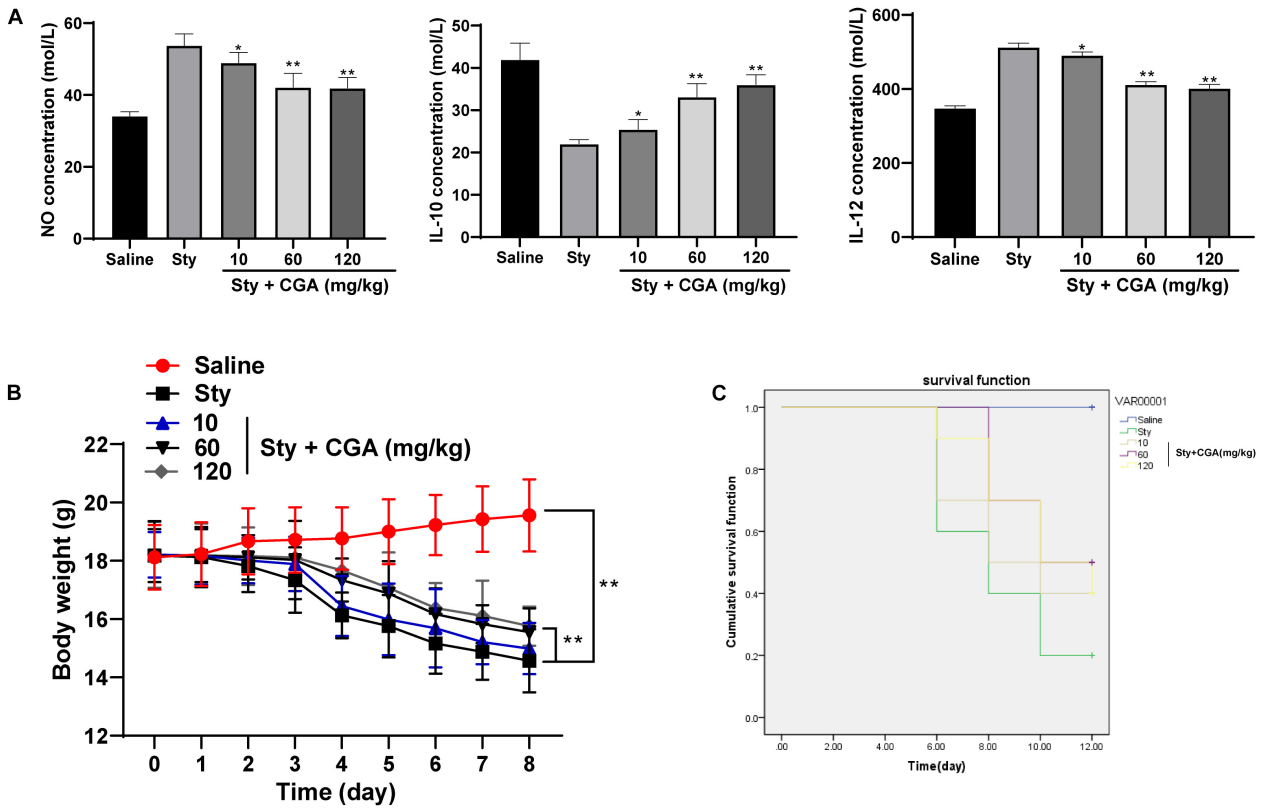

FIGURE 2 | CGA regulates the secretion balance of cytokines in *ST*-infected intestine and alleviates the mortality of mice. *ST*-infected mice were treated with different concentrations of CGA. **(A)** Intestinal cytokine secretion levels of mice in each group measured by ELISA ($n = 5$); **(B)** daily measurement of body weight of mice in each group ($n = 10$); **(C)** survival of mice in each group ($n = 10$). The abscissa is the observation time, and the ordinate is the survival rate. The data in **(A)** were analyzed using one-way ANOVA and Tukey's multiple comparison test, data in panel B were analyzed using two-way ANOVA and Tukey's multiple comparison test, and data in panel C were analyzed using Kaplan-Meier analysis; compared with the sty group, $^{*}p < 0.05$, $^{**}p < 0.01$.

concentration was 40 μg/mL, the invasion rate of *ST* to MODE-K cells was minimal (**Figure 4B**). Moreover, RT-qPCR and ELISA showed that compared with those of the control, the levels of various inflammatory factors (IL-4, IL-6, TNF-α, and IL-1β) in *ST*-infected MODE-K cells were increased significantly, and these levels were gradually reduced after treatments with different doses of CGA (**Figures 4C,D**) ($p < 0.01$).

Low Expression of lncRNA GAS5 Attenuated the Protective Effect of CGA Against *ST* Invasion to Intestinal Epithelial Cells

Similarly, to confirm the effect of CGA on *ST* infection was achieved through lncRNA GAS5 *in vitro*, CGA concentration at 40 μg/mL was selected for experiments and low expression of GAS5 was transfected into MODE-K cells (**Figure 5A**). The gentamicin protection assay found that the bacterial invasion rate to MODE-K cells was increased significantly after GAS5 silencing ($p < 0.05$) (**Figure 5B**). RT-qPCR and ELISA showed that GAS5 silencing caused significant increases in the levels of inflammatory factors in MODE-K cells (all $p < 0.05$) (**Figures 5C,D**).

LncRNA GAS5 Competitively Bound to miR-23a to Upregulate PTEN Expression

From the above results *in vivo* and *in vitro*, we confirmed that CGA exerts a protective effect against *ST* infection by upregulating the expression of GAS5. Recently, the competing endogenous RNA (ceRNA) regulation model describes lncRNA as a sponge for miR to indirectly regulate miR downstream target genes in many disease processes (Han et al., 2020). The ceRNA network of GAS5 has been reported (Liu et al., 2019; Fang et al., 2020). However, we did not know the downstream mechanisms of GAS5. Actually, the activities of lncRNA depend on its subcellular localization. For this purpose, we checked through biological websites and found that GAS5 is partially located in the cytoplasm (**Figure 6A**). Furthermore, nuclear/cytosol fractionation experiments (**Figure 6B**), FISH assay (**Figure 6C**) and dual-luciferase reporter gene assay (**Figure 6F**) confirmed that lncRNA GAS5 was localized in the cytosol in intestinal epithelial cells. GAS5 can play a role in regulating diseases through the ceRNA mechanism. Through literature search, we found that there were many abnormal expression of miR in mesenteric lymph nodes

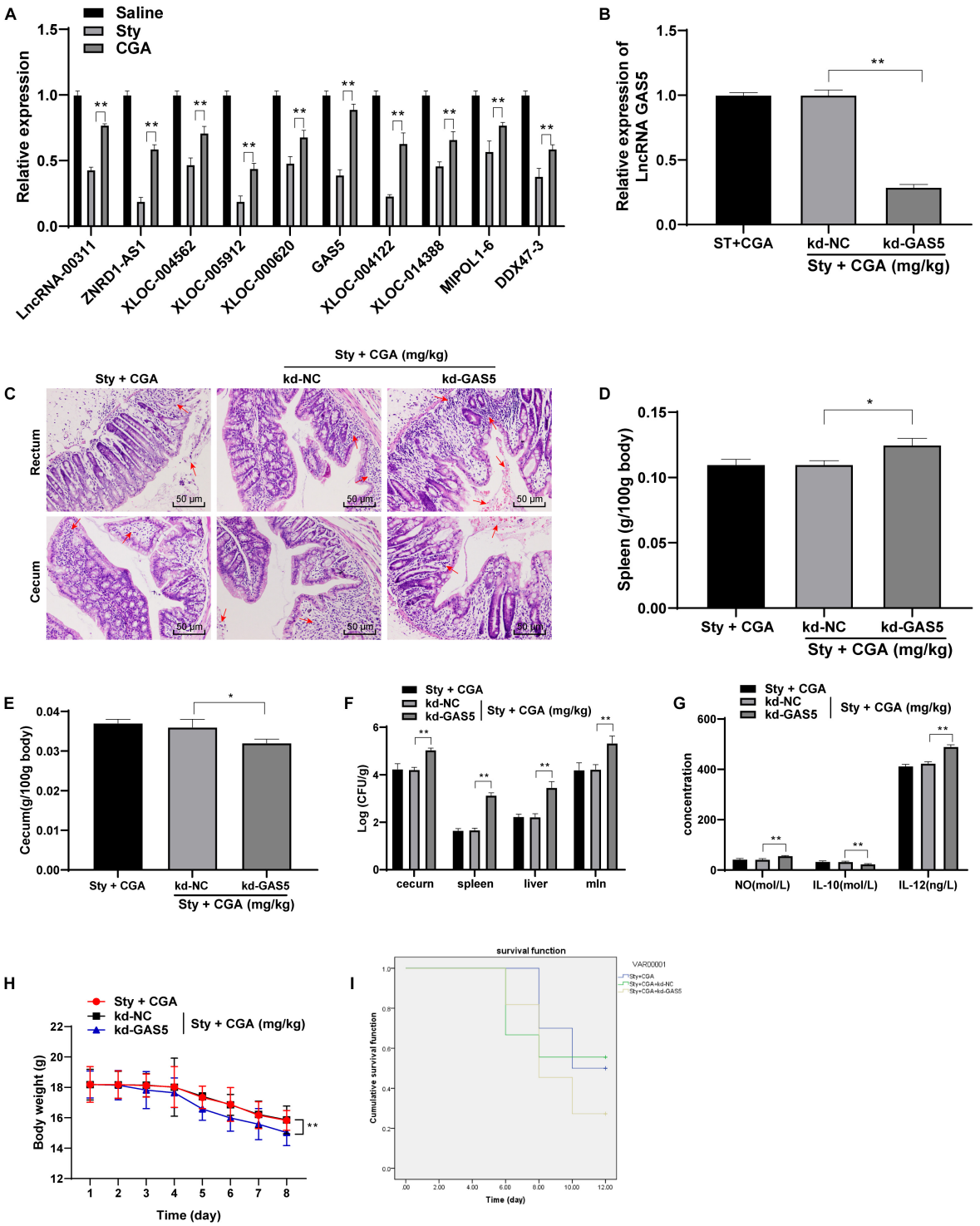

FIGURE 3 | CGA reduced intestinal damage caused by *ST* infection by upregulating lncRNA GAS5 expression. **(A)** RT-qPCR detected differential expression of lncRNAs in intestinal tissue of mice ($n = 5$); **(B)** RT-qPCR detected lncRNA GAS5 expression ($n = 5$); **(C)** HE staining detected pathology of rectum and cecum of mice (×200) ($n = 5$)' the arrow points to the bleeding point; **(D)** spleen organ index of mice in each group ($n = 5$); **(E)** cecum organ index of mice in each group ($n = 5$); **(F)** *Salmonella* loads in the cecum, spleen, liver and mesenteric lymph nodes of mice ($n = 5$); **(G)** intestinal cytokine secretion level of mice in each group ($n = 5$); **(H)** daily measurement of body weight of mice in each group ($n = 10$); **(I)** survival status of each group ($n = 10$). The abscissa is the observation time, and the ordinate is the survival rate. Kd-GAS5 is the interference vector of GAS5, and the empty vector (kd-NC) is used as the control. The data in **(B,D)** were analyzed using one-way ANOVA and Tukey's multiple comparison test, data in **(A,F,G,H)** were analyzed using two-way ANOVA and Tukey's multiple comparison test, and data in **(I)** was analyzed using Kaplan-Meier analysis; $^{*}p < 0.05$, $^{**}p < 0.01$.

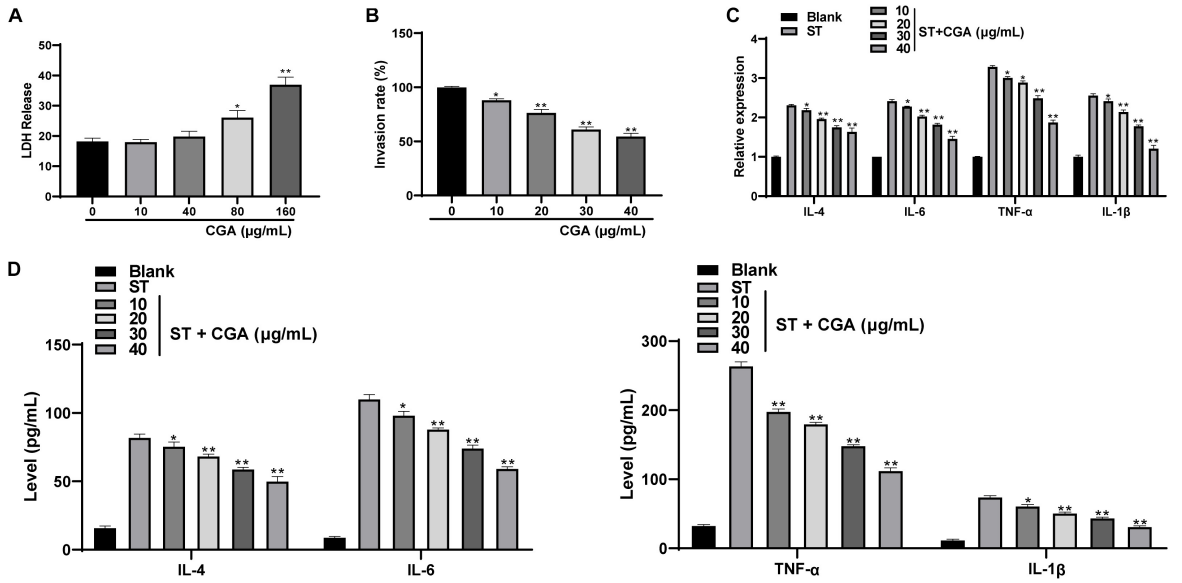

FIGURE 4 | CGA inhibited the proliferation of *ST* in intestinal epithelial cells and regulates the secretion balance of inflammatory factors. *ST*-infected MODE-K cells were treated with different concentrations of CGA. **(A)** cytotoxicity test was performed to detect the cytotoxicity of CGA to MODE-K cells; **(B)** gentamicin protection assay was used to determine the invasion rate of *ST* after different doses of CGA treatments; **(C)** RT-qPCR detected IL-4, IL-6, TNF-α, and IL-1βlevels; **(D)** ELISA detected IL-4, IL-6, TNF-α, and IL-1β levels. All experiments were repeated 3 times. The data in **(A,B)** were analyzed using one-way ANOVA and Tukey's multiple comparison test, and data in **(C,D)** were analyzed using two-way ANOVA and Tukey's multiple comparison test; compared with 0 μg/mL CGA (ST) group. $^{*}p < 0.05$, $^{**}p < 0.01$.

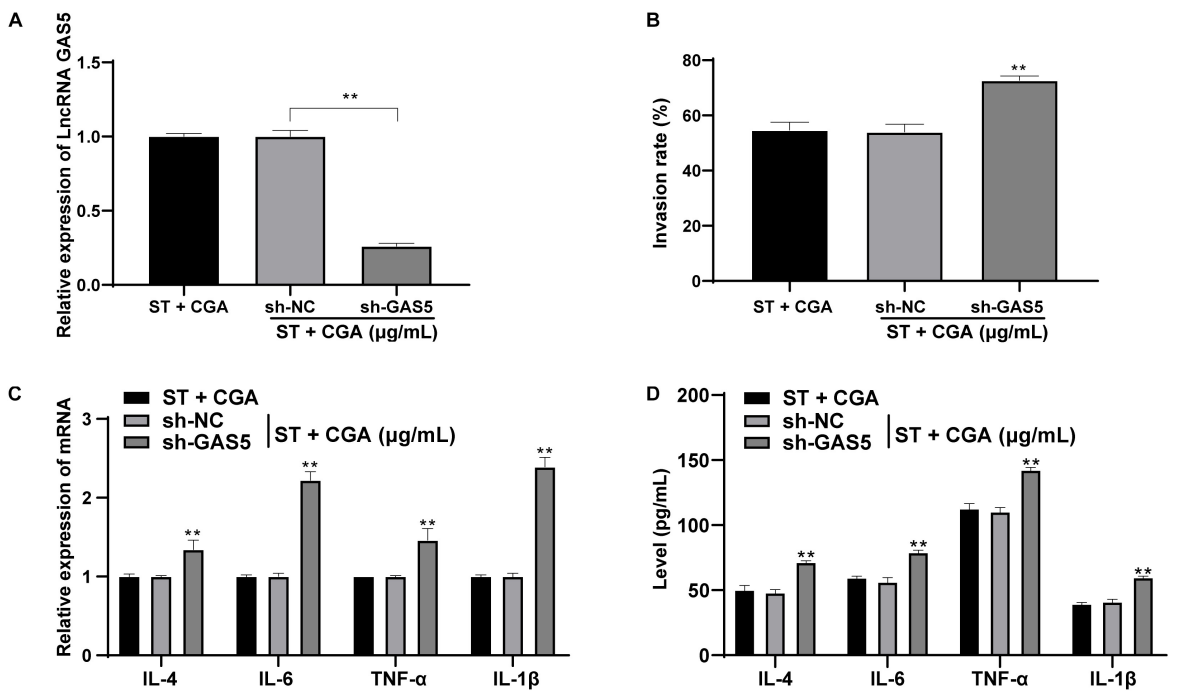

FIGURE 5 | Low expression of lncRNA GAS5 attenuated the protective effect of CGA against *ST* invasion to MODE-K cells. GAS5 expression was knocked down in MODE-K cells, and then the toxic effect of CGA on cells was observed. **(A)** RT-qPCR was used to detect the expression of lncRNA GAS5; **(B)** gentamicin protection assay was used to detect the invasion rate of *ST* to MODE-K cells after different treatments; **(C)** RT-qPCR was used to detect IL-4, IL-6, TNF-α, and IL-1β levels; **(D)** ELISA detected IL-4, IL-6, TNF-α, and IL-1β levels. All experiments were repeated 3 times; The data in **(A,B)** were analyzed using one-way ANOVA and Tukey's multiple comparison test; data in **(C,D)** were analyzed using two-way ANOVA and Tukey's multiple comparison test; compared with ST + CGA group, $^{**}p < 0.01$.

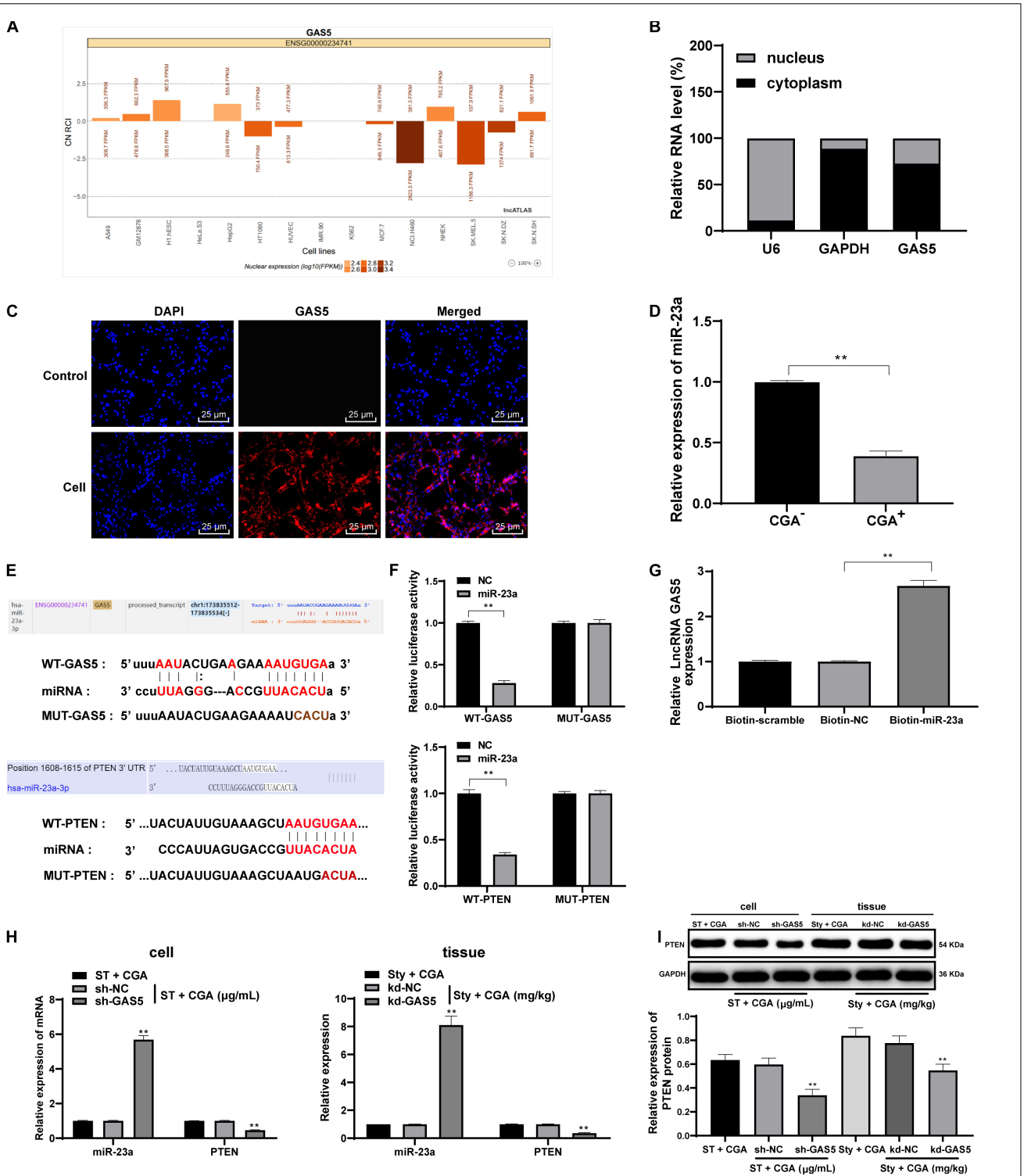

FIGURE 6 | LncRNA GAS5 competitively binds miR-23a to upregulate PTEN expression. The downstream regulatory molecules of GAS5 were analyzed and verified. **(A)** the biological website confirmed that lncRNA GAS5 is located in the cytoplasm; **(B)** nuclear/cytosol fractionation experiments confirmed the subcellular localization of lncRNA; **(C)** FISH assay confirmed that lncRNA GAS5 is localized in the cytoplasm; **(D)** RT-qPCR detection of the expression of mioR-23a in tissue before and after CGA treatment; **(E,F)** dual luciferase gene reporter assay accurately verified the existence of binding regions of lncRNAGAS5 and miR-23a, and miR-23a and PTEN genes; **(G)** RNA pull-down assay found there is a binding region between lncRNA GAS5 and miR-23a; **(H)** RT-qPCR was used to detect the expression of miR-23a and PTEN; **(I)** Western blot was used to detect the protein level of PTEN. All the experiments were repeated 3 times. The data in **(G,I)** were analyzed using one-way ANOVA and Tukey's multiple comparison test; the data in **(B,F,H)** were analyzed using two-way ANOVA and Tukey's multiple comparison test; and the data in **(D)** were analyzed using independent *t*-test; compared with sh-NC or kd-NC groups, $^{**}p < 0.01$.

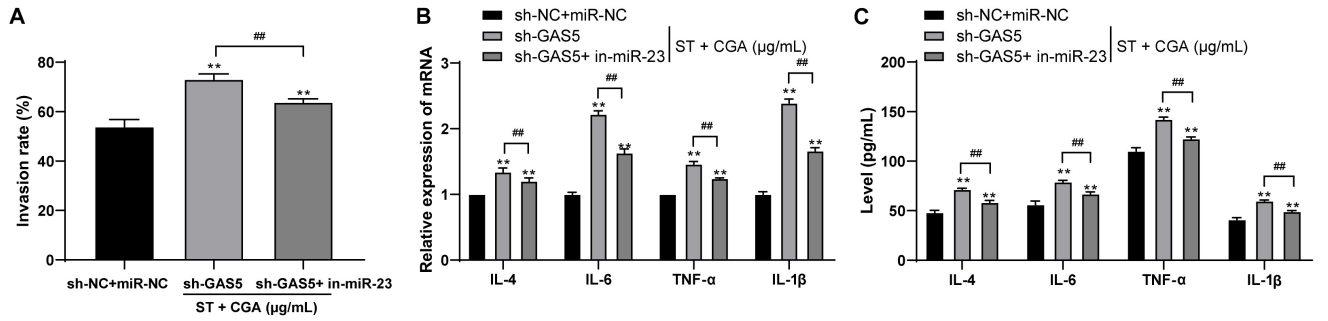

FIGURE 7 | Low expression of miR-23a reversed the promoting effect of low expression of lncRNA GAS5 on the invasion to intestinal epithelial cells by *ST*. *ST*-infected MODE-K cells lowly expressing GAS5 were treated with low miR-23a expression to observe the protective effect of CGA on the cells. **(A)** Gentamicin protection assay was used to detect the invasion rate of *ST* after different CGA treatments; **(B)** RT-qPCR was used to detect the mRNA levels of IL-4, IL-6, TNF-α, and IL-1β; **(C)** ELISA was used to detect the levels of IL-4, IL-6, TNF-α, and IL-1β. All the experiments were repeated 3 times. The data in **(A,B)** were analyzed using *t*-test, and data in **(C)** were analyzed using two-way ANOVA and Tukey's multiple comparison test. Compared with sh-GAS5 group, $^{**}p < 0.01$, $^{\#\#}p < 0.01$.

after *ST* infection (Herrera-Uribe et al., 2018). Therefore, we screened these miRs in the biological websites, and found miR-23a has binding relation to GAS5 (**Figure 6E**). Then we detected the expression of miR-23a in intestinal tissues of *ST*-infected mice before and after CGA treatment by RT-qPCR. The results showed that the expression of miR-23a in intestinal tissues of *ST*-infected mice treated with CGA was significantly downregulated (**Figure 6D**). Therefore, we speculated that GAS5 may protect against ST infection by competitively binding to miR-23a. To confirm this speculation, we found that there was a binding region between GAS5 and miR-23a through RNA pull-down assay and dual-luciferase reporter gene assay (**Figures 6F,G**). It has been reported that PTEN gene deletion can enhance the sensitivity of mice to *ST* infection (Howe et al., 2019). In addition, we predicted through the biological websites that miR-23a has multiple target genes, including PTEN. Then we verified the binding regions of miR-23a and PTEN genes by dual-luciferase reporter gene assay (**Figures 6E,F**). After GAS5 knockdown, miR-23a was upregulated and PTEN levels were significantly downregulated (**Figures 6H,I**) (all $p < 0.01$).

Low Expression of miR-23a Reversed the Promoting Effect of Low Expression of GAS5 on *ST* Invasion to Intestinal Epithelial Cells

To confirm that GAS5 played a protective role against *ST* infection through competitive binding, we performed cell rescue experiments. MODE-K cells poorly expressing GAS5 were transfected with miR-23a inhibitor. Then we measured the bacterial invasion rate to the intestinal epithelial cells using gentamicin protection assay. Compared with those of GAS5 silencing alone, the bacterial invasion rate to MODE-K cells was decreased significantly (**Figure 7A**), and the levels of IL-4, IL-6, TNF-α, and IL-1β in the MODE-K cells were reduced after combined treatment of sh-GAS5 + in-miR-23a (**Figures 7B,C**) (all $p < 0.05$).

CGA Regulated the p38 MAPK Pathway Through the GAS5/miR-23a/PTEN Axis to Promote Autophagy in *ST* Infection

To explore the downstream pathways regulated by PTEN, Western blot analysis was used to detect the expression of p38MAPK pathway-related proteins in intestinal tissue and cells. CGA treatment reduced the activation level of p38 MAPK pathway, and knocking down GAS5 partially reversed the inhibitory effect of CGA on the p38 MAPK pathway (**Figure 8A**). In addition, autophagy plays an important role in *ST* infection, and moderate activation of autophagy is beneficial to inhibit the proliferation of *Salmonella* (Lv et al., 2012). It triggered us to speculate that the effect of CGA on ST infection may relate to autophagy. To confirm this hypothesis, the autophagy of intestinal epithelial cells after CGA treatment was detected by TEM, MDC fluorescence staining and immunoblotting. With increasing CGA concentrations, the autophagic vesicles and intracellular bacteria with bilayer membrane structure were increased, and the intracellular fluorescence distribution intensity and LC3II/LC3I were increased, and P62 gradually was decreased (**Figures 8B–E**). It can be seen that CGA treatment promoted the autophagy of intestinal epithelial cells.

PTEN Knockdown Inhibited Autophagy and Reverses the Protective Effect of CGA Against *ST* Infection

To confirm that CGA regulates the autophagy through the lncRNA GAS5/miR-23a/PTEN axis, we performed an *in vitro* functional rescue experiment. Cells were assigned into CGA group and the CGA + sh-PTEN group. TEM, MDC fluorescence staining and immunoblotting were used to detect the autophagy of MODE-K cells, and the gentamicin protection assay was used to determine the invasion rate of *ST* to MODE-K cells. After the combined treatment with CGA and PTEN knockdown, the autophagy of MODE-K cells infected by *ST* was inhibited, and the invasion rate of *ST* to MODE-K cells was increased significantly (all $p < 0.05$) (**Figures 9A–E**). It is suggested that

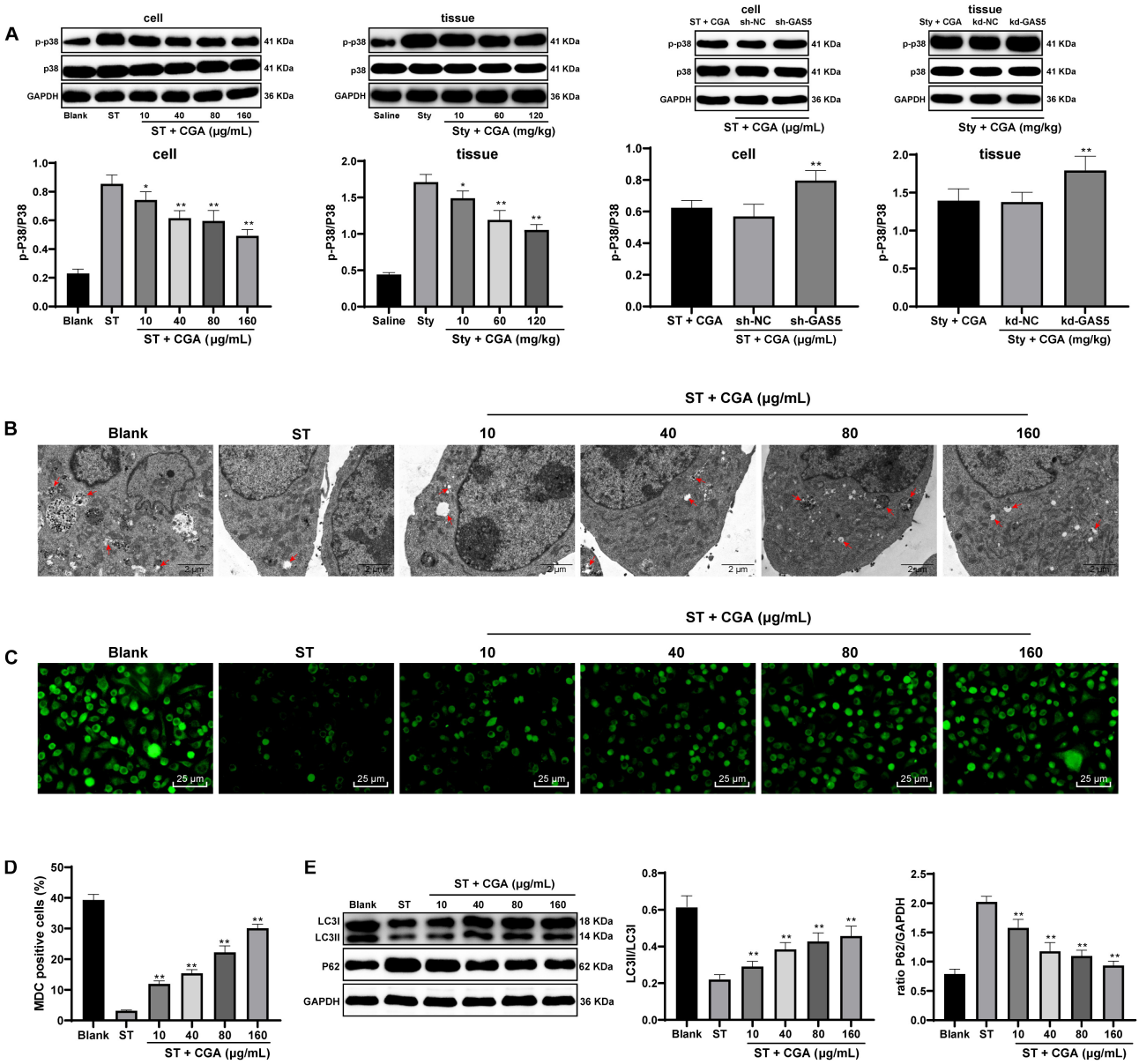

FIGURE 8 | CGA regulated the p38 MAPK signaling pathway through the lncRNAGAS5/miR-23a/PTEN axis to promote autophagy in *ST* infection. Effect of different concentrations of CGA on autophagy of MODE-K cells infected by *ST* was discussed. **(A)** Western blot analysis was used to detect the expression of p38 MAPK signaling pathway-related proteins in tissue and cells; **(B)** autophagosomes and colonies were observed by TEM (×5,000); **(C,D)** MDC fluorescence staining was used to detect cellular autophagy in each group; **(D)** the relative expression in MDC-positive cells; **(E)** Western blot detected the expression of autophagy-related proteins P62 and LC3II/LC3I. All the experiments were repeated 3 times. The data in **(A,D,E)** were analyzed using one-way ANOVA and Tukey's multiple comparison test. Compared with Blank group, ST + CGA group or Sty + CGA group, $^{*}p < 0.05$, $^{**}p < 0.01$.

the promotion of autophagy by CGA is realized through the GAS5/miR-23a/PTEN axis.

DISCUSSION

Beneficial Role of CGA in ST Infection

CGA has antibacterial activities against Gram-negative and Gram-positive bacteria (He et al., 2019). RNAseq profiling of various cell types infected with *Salmonella* has provided a treasure trove of lncRNAs that are regulated upon immune cell stimulation or pathogen invasion, but their molecular functions remain uncharacterized (Garcia-Del Portillo and Pucciarelli, 2017; Yu et al., 2018). But the sole or combined roles of CGA and lncRNA GAS5 in *ST* infection are incompletely understood. In this study, we verified the hypothesis that CGA upregulates lncRNA GAS5 in epithelial cells to promote autophagy in the model of *ST* infection via the miR-23a/PTEN/p38MAPK axis.

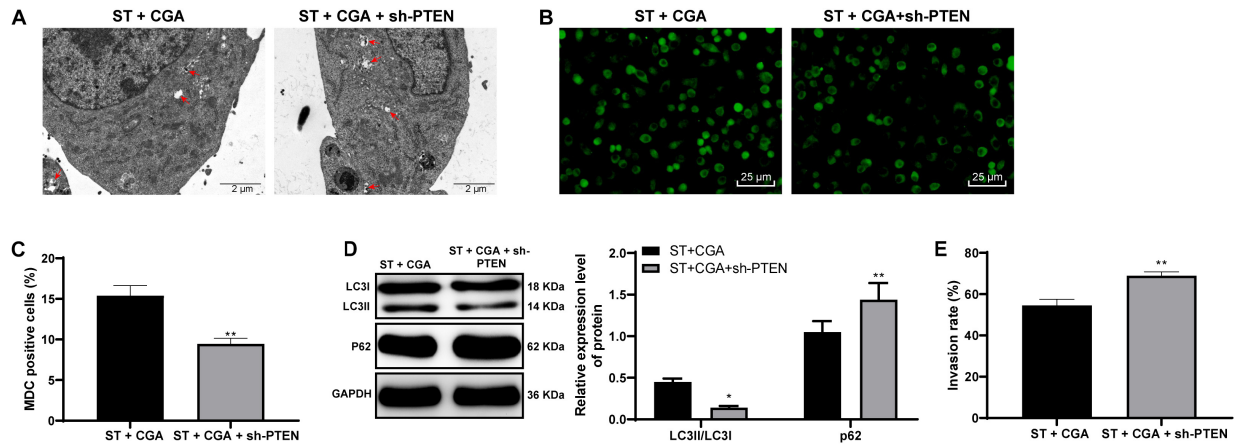

FIGURE 9 | PTEN knockdown inhibited autophagy and reversed the protective effect of CGA on *ST* infection. The autophagy level of MODE-K cells was observed after PTEN expression was knocked down. **(A)** TEM was used to observe the autophagosomes and colonies of cells in each group (×5,000); **(B)** MDC fluorescence staining was used to detect the cellular autophagy in each group; **(C)** the relative expression of MDC-positive cells; **(D)** western blot detection for quantification of the expression of autophagy-related proteins; **(E)** gentamicin protection assay was used to detect the invasion rate of *ST* to MODE-K cells after different CGA treatments. All the experiments were repeated 3 times. The data in **(A,D)** were analyzed using *t*-test for statistical analysis, and data in panel E were analyzed using two-way ANOVA and Tukey's multiple comparison test. Compared with ST + CGA group, $^{*}p < 0.05$, $^{**}p < 0.01$.

CGA has certain therapeutic effects on ulcerative colitis, inhibits intestinal inflammation, weight loss, diarrhea, and improves the immune regulation of intestinal microbes (Zhang et al., 2017). In this experiment, with the increase of CGA concentrations, the structures of rectal and cecal glands of *ST*-infected mice were intact, the inflammatory cell infiltration and bleeding points were decreased gradually, the spleen swelling was attenuated, and bacterial load was decreased significantly. The incorporation of cadmium selenide and CGA into nanoparticles can destroy the cell wall of bacteria and inhibit the proliferation of bacteria, which is probably due to the increase of active oxygen caused by the release of CGA (Wang et al., 2020). Briefly, CGA could improve pathological damage caused by *ST* infection. During the process of inflammation, the secretion of IL-12 is related to the clearance of bacteria by macrophages (Yang et al., 2018). Moreover, after oral administration of CGA, NO, and IL-12 levels were decreased, IL-10 was elevated, and body weight loss and low survival rate of *ST*-infected mice were alleviated. In methicillin-resistant *Staphylococcus aureus*-infected mice, the levels of IL-6, TNF-α and IL-10 are upregulated, and bacterial load in spleen, liver and kidney is surged (Li et al., 2020). CGA inhibits the secretion of IL-2, IFN-g, and IL-12 but facilitates IL-4 and IL-10 with dose dependence (Chauhan et al., 2012). In summary, CGA regulates the balance of cytokines in the intestinal tract and reduces the mortality of *ST*-infected mice. Moreover, to investigate whether CGA could inhibit the *in vitro ST* infection, we chose mouse intestinal epithelial cells MODE-K for *in vitro* experiments. The results revealed that the levels of inflammatory factors (IL-4, IL-6, TNF-α, and IL-1β) in *ST*-infected MODE-K cells were gradually reduced after treatments with different doses of CGA. Consistently, CGA alleviates renal injury by reducing inflammation and inducing epithelial cells proliferation (Arfian et al., 2019). CGA abrogates the upregulation of TNF-α and IL-1β and histological changes induced by NaAsO treatment (Dkhil et al., 2020). Taken together, CGA treatment can alleviate *ST* infection *in vivo* and *in vitro*.

GAS5 Knockdown in the Protective Effect of CGA on the *ST*-Infected Mice and MODE-K Cells

ST infection impacts nuclear RNA decay, which in turn drives the accumulation of unstable nuclear lncRNAs, some of which may have protective effects against this common bacterial pathogen (Koops et al., 2018). After reference retrieval, we focused on GAS5. GAS5 expression was decreased in the intestinal tissue of *ST*-infected mice, but increased after administration of CGA. GAS5 levels are alerted in virus or bacterial infectious diseases. GAS5 is important in immune functions and pathogenesis of inflammatory and infectious diseases (Mayama et al., 2016). GAS5 monitors cell inflammatory responses by regulating TLR4 receptor (Zhao et al., 2020), which is important in *ST* infection (Kamble et al., 2017; Muneta et al., 2018; Lin H.H. et al., 2020). After GAS5 knockdown, the intestinal gland of mice was destroyed, inflammatory cells infiltrated, the spleen and cecum organ index of mice was increased, bacteria were increased, the secretion levels of NO and IL-12 were increased, while IL-10 and the survival rate were decreased. The strain deficient of bacterial sialidase is more easily cleared by reducing the inhibition of GAS5, inducing more IL-12 in macrophages (Yang et al., 2018). *In vivo*, low expression of GAS5 was transfected into MODE-K cells. After GAS5 knockdown, the invasion rate of bacteria into MODE-K cells was increased, and the levels of IL-4, IL-6, TNF-α, and IL-1β increased. GAS5 overexpression inhibited TNF-α, IL-6, and IL-1β, oxidative stress and pyroptosis of high-glucose-induced renal tubular cells (Xie et al., 2019). In conclusion, GAS5 knockdown could reverse the protective effect of CGA on the *ST*-infected mice and MODE-K cells.

The ceRNA Network of GAS5/miR-23a/PTEN

A recent study indicates that mRNAs that co-express with lncRNAs are mainly involved in regulating *ST* infection (Yu et al., 2018). Then our focus shifted to the downstream mechanism of lncRNA GAS5 involving in the protective effect of CGA against *ST* infection. LncRNA GAS5 was located in the cytoplasm of intestinal epithelial cells, suggesting that GAS5 may play a regulatory role in diseases through the ceRNA network. The ceRNA network of GAS5 has been reported (Liu et al., 2019; Fang et al., 2020). After literature search, we found that there were many abnormal expression of miR in mesenteric lymph nodes after ST infection (Herrera-Uribe et al., 2018). Additionally, biological website prediction, RNA pull-down and dual luciferase reporter gene assays confirmed that miR-23a has binding relation to GAS5. The expression of miR-23a in intestinal tissues of *ST*-infected mice treated with CGA was significantly downregulated. Additionally, PTEN gene deletion can enhance the sensitivity of mice to *ST* infection (Howe et al., 2019). miR-23a has multiple target genes, including PTEN. Then we verified the binding regions of miR-23a and PTEN genes by dual-luciferase reporter gene assay. After GAS5 knockdown, miR-23a was upregulated and PTEN levels were significantly downregulated. Intriguingly, lncRNA GAS5 acts as a sponge platform to competitively decrease miR-23a expression, and miR-23a degrading PTEN further influenced the downstream pathway PI3K/Akt/mTOR/Snail in hepatic fibrosis (Dong et al., 2019). To sum up, lncRNA GAS5 competitively bound to miR-23a to upregulate PTEN expression. Furthermore, MODE-K cells poorly expressing GAS5 were transfected with miR-23a inhibitor. After the combined treatment of sh-GAS5 + in-miR-23a, the invasion rate of bacteria into MODE-K cells was decreased, and the levels of inflammatory factors were decreased significantly. Reduction in miR-23a markedly inhibits the levels of TNF-α and IL-6 in lipopolysaccharide-induced macrophages (Peng et al., 2015). Inhibition of miR-23a results in increases in IL-12 levels (Du et al., 2018). Briefly, low expression of miR-23a reversed the promoting effect of GAS5 knockdown on *ST* invasion to intestinal epithelial cells.

p38 MAPK Pathway and Autophagy in CGA Benefit in *ST* Infection

MAPK pathway is a feature of innate immune responses in in *Caenorhabditis elegans* innate immunity (Kim et al., 2002). To explore the downstream pathways regulated by PTEN, Western blot was utilized to detect the expression of p38 MAPK pathway-related proteins. CGA reduced the activation level of p38 MAPK pathway, and knocking down GAS5 partially reversed the inhibitory effect of CGA on p38 MAPK pathway. CGA can block lipopolysaccharide-triggered pro-inflammatory cascades possibly through inhibition of p38 MAPK (Chauhan et al., 2012). CGA attenuates dextran sodium sulfate-induced ulcerative colitis, colonic mucosal damage, inflammation in mice by inactivating the MAPK/ERK/JNK pathway (Gao et al., 2019). When bacteria invade epithelial cells, autophagy is initiated as an autonomous antibacterial defense to prevent intestinal bacterial transmission during *ST* infection (Benjamin et al., 2013). With increasing CGA concentrations, the autophagic vesicles were increased, and LC3II/LC3I was increased, and P62 gradually was decreased. It can be seen that CGA treatment promoted the autophagy of intestinal epithelial cells. To confirm that CGA regulates the autophagy through the lncRNA GAS5/miR-23a/PTEN axis, we performed an *in vitro* functional rescue experiment. Beyond that, after treatment with CGA + sh-PTEN, the autophagy of *ST*-infected MODE-K cells was inhibited, and the invasion rate of *ST* into MODE-K cells increased significantly. In *Caenorhabditis elegans*, CGA improves resistance to thermal via autophagy activation (Carranza et al., 2020). PTEN regulates activation of autophagy in infected macrophages during tularemic infection (Hrstka et al., 2007). Overall, PTEN knockdown inhibited autophagy and reverses the protective effect of CGA against *ST* infection.

Study Limitation

As we mentioned in the results section, 10 lncRNAs related to immune and anti-inflammatory were found and expressed in the intestinal tissues of mice infected with *ST*. Except for lncRNA GAS5, the others may also have some relevance to the process of *ST* infection. In the future, we will make further investigation to identify the possible mechanisms of other 9 lncRNAs in *ST* infection.

CONCLUSION

Overall, our study highlighted the protective effects of CGA on *ST* infection by promoting autophagy in *ST* infection via the GAS5/miR-23a/PTEN axis and p38MAPK pathway.

DATA AVAILABILITY STATEMENT

The original contributions presented in the study are included in the article/supplementary material, further inquiries can be directed to the corresponding authors.

ETHICS STATEMENT

The animal study was reviewed and approved by the Yunnan University.

AUTHOR CONTRIBUTIONS

ST was the guarantor of integrity of the entire study and contributed to the study concepts and definition of intellectual content. FY contributed to the design of this study and manuscript review. QL contributed to the literature research and contributed to the manuscript preparation. YL contributed to the clinical studies. JY took charge of the experimental studies. RL contributed to the data acquisition. ML took charge of the data analysis. ZL contributed to the statistical analysis. FH contributed to the manuscript editing. All authors read and approved the final manuscript.

FUNDING

This study was supported by the National Natural Science Foundation of China (Nos. 31960557, 31560528, 31360454, and 82060669), the Project of Xuzhou Applied and Basic Research (No. KC18009), Yunnan Health Training Project of High Level Talents, Yunnan Fundamental Research Project (Nos. 2019FB136), the Scientifific Research Fund of Yunnan Province of China, Kunming Medical University Joint Research Project [No. 2018FE001(-312)], and the Fund of Yunnan Provincial Health Science and Technology Plan (No. 2018NS0283).

REFERENCES

Arfian, N., Wahyudi, D. A. P., Zulfatina, I. B., Citta, A. N., Anggorowati, N., Multazam, A., et al. (2019). Chlorogenic acid attenuates kidney ischemic/reperfusion injury via reducing inflammation, tubular injury, and myofibroblast formation. *Biomed Res. Int.* 2019:5423703. doi: 10.1155/2019/5423703

Bao, N., Chen, F., and Dai, D. (2019). The regulation of host intestinal microbiota by polyphenols in the development and prevention of chronic kidney disease. *Front. Immunol.* 10:2981. doi: 10.3389/fimmu.2019.02981

Benjamin, J. L., Sumpter, R. Jr., Levine, B., and Hooper, L. V. (2013). Intestinal epithelial autophagy is essential for host defense against invasive bacteria. *Cell Host Microbe* 13, 723–734. doi: 10.1016/j.chom.2013.05.004

Birhanu, B. T., Park, N. H., Lee, S. J., Hossain, M. A., and Park, S. C. (2018). Inhibition of *Salmonella* Typhimurium adhesion, invasion, and intracellular survival via treatment with methyl gallate alone and in combination with marbofloxacin. *Vet. Res.* 49:101. doi: 10.1186/s13567-018-0597-8

Carpenter, S., and Fitzgerald, K. A. (2018). Cytokines and long noncoding RNAs. *Cold Spring Harb. Perspect. Biol.* 10:a028589. doi: 10.1101/cshperspect.a028589

Carranza, A. D. V., Saragusti, A., Chiabrando, G. A., Carrari, F., and Asis, R. (2020). Effects of chlorogenic acid on thermal stress tolerance in C. elegans via HIF-1, HSF-1 and autophagy. *Phytomedicine* 66:153132. doi: 10.1016/j.phymed.2019.153132

Chauhan, P. S., Satti, N. K., Sharma, P., Sharma, V. K., Suri, K. A., and Bani, S. (2012). Differential effects of chlorogenic acid on various immunological parameters relevant to rheumatoid arthritis. *Phytother. Res.* 26, 1156–1165. doi: 10.1002/ptr.3684

Dkhil, M. A., Abdel Moneim, A. E., Bauomy, A. A., Khalil, M., Al-Shaebi, E. M., and Al-Quraishy, S. (2020). Chlorogenic acid prevents hepatotoxicity in arsenic-treated mice: role of oxidative stress and apoptosis. *Mol. Biol. Rep.* 47, 1161–1171. doi: 10.1007/s11033-019-05217-4

Dong, N., Xue, C., Zhang, L., Zhang, T., Wang, C., Bi, C., et al. (2020). Oleanolic acid enhances tight junctions and ameliorates inflammation in *Salmonella* typhimurium-induced diarrhea in mice via the TLR4/NF-kappaB and MAPK pathway. *Food Funct.* 11, 1122–1132. doi: 10.1039/c9fo01718f

Dong, Z., Li, S., Wang, X., Si, L., Ma, R., Bao, L., et al. (2019). lncRNA GAS5 restrains CCl4-induced hepatic fibrosis by targeting miR-23a through the PTEN/PI3K/Akt signaling pathway. *Am. J. Physiol. Gastrointest. Liver Physiol.* 316, G539–G550. doi: 10.1152/ajpgi.00249.2018

Du, Q., Wu, X., Wang, T., Yang, X., Wang, Z., Niu, Y., et al. (2018). Porcine circovirus type 2 suppresses IL-12p40 induction via capsid/gC1qR-mediated MicroRNAs and signalings. *J. Immunol.* 201, 533–547. doi: 10.4049/jimmunol.1800250

Fang, X., Zhong, G., Wang, Y., Lin, Z., Lin, R., and Yao, T. (2020). Low GAS5 expression may predict poor survival and cisplatin resistance in cervical cancer. *Cell Death Dis.* 11:531. doi: 10.1038/s41419-020-2735-2

Gao, W., Wang, C., Yu, L., Sheng, T., Wu, Z., Wang, X., et al. (2019). Chlorogenic acid attenuates dextran sodium sulfate-induced ulcerative colitis in mice through MAPK/ERK/JNK pathway. *Biomed Res. Int.* 2019:6769789. doi: 10.1155/2019/6769789

Garcia-Del Portillo, F., and Pucciarelli, M. G. (2017). RNA-Seq unveils new attributes of the heterogeneous *Salmonella*-host cell communication. *RNA Biol.* 14, 429–435. doi: 10.1080/15476286.2016.1276148

Gong, W., Li, J., Zhu, G., Wang, Y., Zheng, G., and Kan, Q. (2019). Chlorogenic acid relieved oxidative stress injury in retinal ganglion cells through IncRNA-TUG1/Nrf2. *Cell Cycle* 18, 1549–1559. doi: 10.1080/15384101.2019.1612697

Han, T. S., Hur, K., Cho, H. S., and Ban, H. S. (2020). Epigenetic associations between lncRNA/circRNA and miRNA in hepatocellular carcinoma. *Cancers* 12:E2622. doi: 10.3390/cancers12092622

He, X., Deng, Y., Yu, Y., Lyu, H., and Liao, L. (2019). Drug-loaded/grafted peptide-modified porous PEEK to promote bone tissue repair and eliminate bacteria. *Colloids Surf. B Biointerfaces* 181, 767–777. doi: 10.1016/j.colsurfb.2019.06.038

Herrera-Uribe, J., Zaldivar-Lopez, S., Aguilar, C., Luque, C., Bautista, R., Carvajal, A., et al. (2018). Regulatory role of microRNA in mesenteric lymph nodes after *Salmonella* typhimurium infection. *Vet. Res.* 49:9. doi: 10.1186/s13567-018-0506-1

Howe, C., Mitchell, J., Kim, S. J., Im, E., and Rhee, S. H. (2019). Pten gene deletion in intestinal epithelial cells enhances susceptibility to *Salmonella* typhimurium infection in mice. *J. Microbiol.* 57, 1012–1018. doi: 10.1007/s12275-019-9320-3

Hrstka, R., Krocova, Z., Cerny, J., Vojtesek, B., Macela, A., and Stulik, J. (2007). *Francisella tularensis* strain LVS resides in MHC II-positive autophagic vacuoles in macrophages. *Folia Microbiol. (Praha)* 52, 631–636. doi: 10.1007/bf02932193

Jain, P., Sudhanthirakodi, S., Chowdhury, G., Joshi, S., Anandan, S., Ray, U., et al. (2018). Antimicrobial resistance, plasmid, virulence, multilocus sequence typing and pulsed-field gel electrophoresis profiles of *Salmonella enterica* serovar Typhimurium clinical and environmental isolates from India. *PLoS One* 13:e0207954. doi: 10.1371/journal.pone.0207954

Jiang, X., Li, X., Sun, S., and Jiang, L. (2018). The transcriptional regulator VarN contributes to *Salmonella* typhimurium growth in macrophages and virulence in mice. *Res. Microbiol.* 169, 214–221. doi: 10.1016/j.resmic.2018.03.003

Kamble, N. M., Hajam, I. A., and Lee, J. H. (2017). Orally administered live attenuated *Salmonella* typhimurium protects mice against lethal infection with H1N1 influenza virus. *Vet. Microbiol.* 201, 1–6. doi: 10.1016/j.vetmic.2017.01.006

Kim, D. H., Feinbaum, R., Alloing, G., Emerson, F. E., Garsin, D. A., Inoue, H., et al. (2002). A conserved p38 MAP kinase pathway in *Caenorhabditis elegans* innate immunity. *Science* 297, 623–626. doi: 10.1126/science.1073759

Kim, S. P., Lee, S. J., Nam, S. H., and Friedman, M. (2018). Mechanism of antibacterial activities of a rice hull smoke extract (RHSE) against multidrug-resistant *Salmonella* typhimurium in vitro and in mice. *J. Food Sci.* 83, 440–445. doi: 10.1111/1750-3841.14020

Koops, S., Blom, J. D., Bouachmir, O., Slot, M. I., Neggers, B., and Sommer, I. E. (2018). Treating auditory hallucinations with transcranial direct current stimulation in a double-blind, randomized trial. *Schizophr. Res.* 201, 329–336. doi: 10.1016/j.schres.2018.06.010

Li, T., Qian, Y., Miao, Z., Zheng, P., Shi, T., Jiang, X., et al. (2020). Xuebijing injection alleviates Pam3CSK4-induced inflammatory response and protects mice from sepsis caused by methicillin-resistant *Staphylococcus aureus*. *Front. Pharmacol.* 11:104. doi: 10.3389/fphar.2020.00104

Lin, H., Shen, L., Lin, Q., Dong, C., Maswela, B., Illahi, G. S., et al. (2020). SNHG5 enhances paclitaxel sensitivity of ovarian cancer cells through sponging miR-23a. *Biomed. Pharmacother.* 123:109711. doi: 10.1016/j.biopha.2019.109711

Lin, H. H., Chen, H. L., Weng, C. C., Janapatla, R. P., Chen, C. L., and Chiu, C. H. (2020). Activation of apoptosis by *Salmonella* pathogenicity island-1 effectors through both intrinsic and extrinsic pathways in *Salmonella*-infected macrophages. *J. Microbiol. Immunol. Infect.* doi: 10.1016/j.jmii.2020.02.008 [Epub ahead of print].

Liu, L., Wang, H. J., Meng, T., Lei, C., Yang, X. H., Wang, Q. S., et al. (2019). lncRNA GAS5 inhibits cell migration and invasion and promotes autophagy by targeting miR-222-3p via the GAS5/PTEN-signaling pathway in CRC. *Mol. Ther. Nucleic Acids* 17, 644–656. doi: 10.1016/j.omtn.2019.06.009

Lv, J., Wu, S., Wei, L., Li, Y., He, P., and Huang, R. (2012). *Salmonella enterica* serovar typhi plasmid pR ST98-mediated inhibition of autophagy promotes bacterial survival in infected fibroblasts. *Indian J. Med. Microbiol.* 30, 423–430. doi: 10.4103/0255-0857.103763

Mayama, T., Marr, A. K., and Kino, T. (2016). Differential expression of glucocorticoid receptor noncoding RNA repressor Gas5 in autoimmune and

inflammatory diseases. *Horm. Metab. Res.* 48, 550–557. doi: 10.1055/s-0042-106898

Mortazavi, N., and Aliakbarlu, J. (2019). Antibacterial effects of ultrasound, cinnamon essential oil, and their combination against *Listeria monocytogenes* and *Salmonella* typhimurium in milk. *J. Food Sci.* 84, 3700–3706. doi: 10.1111/1750-3841.14914

Muneta, Y., Arai, N., Yakabe, Y., Eguchi, M., Shibahara, T., Sakuma, A., et al. (2018). In vivo effect of a TLR5 SNP (C1205T) on *Salmonella enterica* serovar typhimurium infection in weaned, specific pathogen-free Landrace piglets. *Microbiol. Immunol.* 62, 380–387. doi: 10.1111/1348-0421.12591

Park, K. I., Lee, M. R., Oh, T. W., Kim, K. Y., and Ma, J. Y. (2017). Antibacterial activity and effects of *Colla corii asini* on *Salmonella* typhimurium invasion in vitro and in vivo. *BMC Complement. Altern. Med.* 17:520. doi: 10.1186/s12906-017-2020-9

Peng, P., Li, Z., and Liu, X. (2015). Reduced expression of miR-23a suppresses A20 in TLR-stimulated macrophages. *Inflammation* 38, 1787–1793. doi: 10.1007/s10753-015-0156-7

Sun, Z., Zhang, X., Wu, H., Wang, H., Bian, H., Zhu, Y., et al. (2020). Antibacterial activity and action mode of chlorogenic acid against *Salmonella* Enteritidis, a foodborne pathogen in chilled fresh chicken. *World J. Microbiol. Biotechnol.* 36:24. doi: 10.1007/s11274-020-2799-2

Tosovic, J., Markovic, S., Dimitric Markovic, J. M., Mojovic, M., and Milenkovic, D. (2017). Antioxidative mechanisms in chlorogenic acid. *Food Chem.* 237, 390–398. doi: 10.1016/j.foodchem.2017.05.080

Upadhyay, R., and Mohan Rao, L. J. (2013). An outlook on chlorogenic acids-occurrence, chemistry, technology, and biological activities. *Crit. Rev. Food Sci. Nutr.* 53, 968–984. doi: 10.1080/10408398.2011.576319

Velge, P., Wiedemann, A., Rosselin, M., Abed, N., Boumart, Z., Chausse, A. M., et al. (2012). Multiplicity of *Salmonella* entry mechanisms, a new paradigm for *Salmonella* pathogenesis. *Microbiologyopen* 1, 243–258. doi: 10.1002/mbo3.28

Viswanathan, V. K., Hodges, K., and Hecht, G. (2009). Enteric infection meets intestinal function: how bacterial pathogens cause diarrhoea. *Nat. Rev. Microbiol.* 7, 110–119. doi: 10.1038/nrmicro2053

Wang, H., Chu, W., Ye, C., Gaeta, B., Tao, H., Wang, M., et al. (2019). Chlorogenic acid attenuates virulence factors and pathogenicity of *Pseudomonas aeruginosa* by regulating quorum sensing. *Appl. Microbiol. Biotechnol.* 103, 903–915. doi: 10.1007/s00253-018-9482-7

Wang, Z., Zhai, X., Sun, Y., Yin, C., Yang, E., Wang, W., et al. (2020). Antibacterial activity of chlorogenic acid-loaded SiO2 nanoparticles caused by accumulation of reactive oxygen species. *Nanotechnology* 31:185101. doi: 10.1088/1361-6528/ab70fb

Westermann, A. J., Forstner, K. U., Amman, F., Barquist, L., Chao, Y., Schulte, L. N., et al. (2016). Dual RNA-seq unveils noncoding RNA functions in host-pathogen interactions. *Nature* 529, 496–501. doi: 10.1038/nature16547

Xie, C., Wu, W., Tang, A., Luo, N., and Tan, Y. (2019). lncRNA GAS5/miR-452-5p reduces oxidative stress and pyroptosis of high-glucose-stimulated renal tubular cells. *Diabetes Metab. Syndr. Obes.* 12, 2609–2617. doi: 10.2147/DMSO.S228654

Yang, X., Pan, Y., Xu, X., Tong, T., Yu, S., Zhao, Y., et al. (2018). Sialidase deficiency in *Porphyromonas gingivalis* increases IL-12 secretion in stimulated macrophages through regulation of CR3, lncRNA GAS5 and miR-21. *Front. Cell. Infect. Microbiol.* 8:100. doi: 10.3389/fcimb.2018.00100

Yang, Y., Li, J., Yin, Y., Guo, D., Jin, T., Guan, N., et al. (2019). Antibiofilm activity of coenzyme Q0 against *Salmonella* typhimurium and its effect on adhesion-invasion and survival-replication. *Appl. Microbiol. Biotechnol.* 103, 8545–8557. doi: 10.1007/s00253-019-10095-8

Yu, A., Wang, Y., Yin, J., Zhang, J., Cao, S., Cao, J., et al. (2018). Microarray analysis of long non-coding RNA expression profiles in monocytic myeloid-derived suppressor cells in *Echinococcus granulosus*-infected mice. *Parasit Vectors* 11:327. doi: 10.1186/s13071-018-2905-6

Zhang, L., Fan, Y., Su, H., Wu, L., Huang, Y., Zhao, L., et al. (2018). Chlorogenic acid methyl ester exerts strong anti-inflammatory effects via inhibiting the COX-2/NLRP3/NF-kappaB pathway. *Food Funct.* 9, 6155–6164. doi: 10.1039/c8fo01281d

Zhang, Z., Wu, X., Cao, S., Cromie, M., Shen, Y., Feng, Y., et al. (2017). Chlorogenic acid ameliorates experimental colitis by promoting growth of akkermansia in mice. *Nutrients* 9:677. doi: 10.3390/nu9070677

Zhao, J., Liu, B., and Li, C. (2020). Knockdown of long noncoding RNA GAS5 protects human cardiomyocyte-like AC16 cells against high glucose-induced inflammation by inhibiting miR-21-5p-mediated TLR4/NF-kappaB signaling. *Naunyn Schmiedebergs Arch. Pharmacol.* 393, 1541–1547. doi: 10.1007/s00210-019-01795-z

Conflict of Interest: The authors declare that the research was conducted in the absence of any commercial or financial relationships that could be construed as a potential conflict of interest.

frontiers in Cell and Developmental Biology

REVIEW
published: 10 December 2020
doi: 10.3389/fcell.2020.605972

Severe Acute Respiratory Syndrome Coronavirus 2-Induced Neurological Complications

Shijia Yu[1] *and Mingjun Yu*[2]*

[1] Department of Neurology, Shengjing Hospital of China Medical University, Shenyang, China, [2] Department of Neurosurgery, Shengjing Hospital of China Medical University, Shenyang, China

Our review aims to highlight the neurological complications of severe acute respiratory syndrome coronavirus 2 (SARS-CoV-2) infection and the available treatments according to the existing literature, discussing the underlying mechanisms. Since the end of 2019, SARS-CoV-2 has induced a worldwide pandemic that has threatened numerous lives. Fever, dry cough, and respiratory symptoms are typical manifestations of COVID-19. Recently, several neurological complications of the central and peripheral nervous systems following SARS-CoV-2 infection have gained clinicians' attention. Encephalopathy, stroke, encephalitis/meningitis, Guillain–Barré syndrome, and multiple sclerosis are considered probable neurological signs of COVID-19. The virus may invade the nervous system directly or induce a massive immune inflammatory response via a "cytokine storm." Specific antiviral drugs are still under study. To date, immunomodulatory therapies and supportive treatment are the predominant strategies. In order to improve the management of COVID-19 patients, it is crucial to monitor the onset of new neurological complications and to explore drugs/vaccines targeted against SARS-CoV-2 infection.

Keywords: coronavirus, COVID-19, SARS-CoV-2, neurological complications, inflammation, ACE2

OPEN ACCESS

Edited by:
Giulia De Falco,
Queen Mary University of London, United Kingdom

Reviewed by:
Kuldeep Dhama,
Indian Veterinary Research Institute (IVRI), India
Ruchi Tiwari,
U.P. Pandit Deen Dayal Upadhyaya Veterinary University, India

***Correspondence:**
Mingjun Yu
mjyu@cmu.edu.cn

Specialty section:
This article was submitted to Molecular Medicine, a section of the journal Frontiers in Cell and Developmental Biology

Received: *14 September 2020*
Accepted: *11 November 2020*
Published: *10 December 2020*

Citation:
Yu S and Yu M (2020) Severe Acute Respiratory Syndrome Coronavirus 2-Induced Neurological Complications. Front. Cell Dev. Biol. 8:605972. doi: 10.3389/fcell.2020.605972

INTRODUCTION

A global pandemic named coronavirus disease-2019 (COVID-19) broke out at the end of 2019 caused by the novel human coronaviral pathogen, the severe acute respiratory syndrome-coronavirus type 2 (SARS-CoV-2). In the past few months, it has spread rapidly to almost all continents and infected a large number of individuals. According to the updated COVID-19 dashboard from John Hopkins University (Dong et al., 2020), as of November 9, 2020, over 50 million cases were confirmed in 215 countries, with 1,259,245 reported deaths. Data shows that the United States currently has the highest number of confirmed cases and death rate, followed by India and Brazil. In Europe, most cases have been confirmed in France and Spain, while the death rate in Italy is the highest (Dhama et al., 2020a).

The COVID-19 pandemic is challenging healthcare systems around the whole world. SARS-CoV-2 transmits both zoonotically and human-to-human and can spread via respiratory aerosol and direct contact with contaminated surfaces. COVID-19 patients' age could range from 20s to 80s. In particular, older or immune-comprised individuals with preexisting diseases have high risks of viral infection (Chen et al., 2020; Zhang J. J. et al., 2020). Although the general infection fatality risk merely ranges from 0.3 to 0.6%, patients with high viral loads are more prone to dying. Even though scientists and clinicians have spared no effort on SARS-CoV-2 research, there is no proven

effective therapy yet. People are recommended to work from home and required to engage in social distancing, quarantine, and isolation to reduce the spread. Businesses have been forced to shut down during periods of 2020, causing severe consequences on global finances.

Human coronaviruses are a large group of enveloped, single-stranded, positive-sense RNA viruses, which can induce acute infections in respiratory and digestive systems. According to the full sequence published in January 2020, SARS-CoV-2 belongs to a beta genus of coronaviruses, sharing ∼80% similarity with SARS-CoV (Andersen et al., 2020; Wu et al., 2020). In addition, SARS-CoV-2 possesses over 90% homology with coronaviruses from the bat and the pangolin, which explains its potent cross-species transmitting ability (Koralnik and Tyler, 2020). The virus is composed of four classic proteins: spike (S) glycoprotein, envelope (E) glycoprotein, membrane (M) glycoprotein, and nucleocapsid (N) protein (Lin et al., 2003). Viral detection depends on the conserved N protein, while the S glycoprotein functions as a trimeric fusion to determine the tropism of virus (Almazan et al., 2000). Intriguingly, specific domains encoding polybasic cleavage sites are detected in the S protein of SARS-CoV-2, which may lead its stronger infectiousness (Andersen et al., 2020).

Generally, patients with COVID-19 develop flu-like symptoms such as fever, fatigue, and dry cough (Bhatraju et al., 2020; Guan et al., 2020; Huang et al., 2020). Gastroenteritis, diarrhea, and myocarditis have also been reported in previous studies (Huang et al., 2020). Moreover, around 10% are asymptomatic or present mild pneumonia only (Guan et al., 2020). Some patients with confirmed SARS-CoV-2 infection only complain of weakness, dizziness, or neurological disorders without any respiratory symptoms (Favas et al., 2020). Analyses of the COVID-19-associated neurological manifestations and explorations of the underlying mechanisms are needed for a better understanding of the disease. Here, we present a review of the previously reported cases of various neurological complications associated with SARS-CoV-2 infection and discuss the possible pathogenesis.

PATHOLOGY OF COVID-19

According to former studies, SARS-CoV-2 can invade multiple organs and rapidly replicate to activate inflammatory responses in the human body (Dhama et al., 2020b). Critical illness may progress to acute respiratory distress syndrome (ARDS) or acute respiratory failure. A study of a series of 135 cases reported a high prevalence of lymphopenia (75.4%) and eosinopenia (52.9%) concurrent with SARS-CoV-2 infection (Zhang J. J. et al., 2020). Leukopenia happens more frequently in adult patients, whereas children are prone to leukocytosis and upregulated creatine kinase (Han et al., 2020). D-dimer, procalcitonin, and C-reactive protein are notably increased in patients with high viral loads (Zhang J. J. et al., 2020). Patients may have decreased platelet count and increased blood urea nitrogen (Mao et al., 2020). Severe cases may develop liver damage with elevated transaminases (Dhama et al., 2020b). As reported, CT scans may demonstrate ground-glass opacities, traction bronchiectasis, or even bilateral multilobar consolidation in the lungs (Zhu et al., 2020). Neurological manifestations of SARS-CoV-2 infection can be induced by direct invasion of the nervous system or by inflammatory responses (Alshebri et al., 2020). Affecting either the neurons or the glia cells can lead to neurological pathologies (Ibrahim, 2020).

NEUROLOGICAL COMPLICATIONS OF COVID-19

Neurological manifestations could occur in the central nervous system (CNS), peripheral nervous system (PNS), and relative skeletal muscles (Kutlubaev, 2020; Mao et al., 2020; Puccioni-Sohler et al., 2020). A systematic review about 290 patients revealed that 91% of patients with neurological discomfort present with CNS symptoms, while only PNS symptoms account for 9% (Ibrahim, 2020). Headaches and dizziness are regarded as the most common symptoms in CNS, while smell and taste disorders in PNS (Padda et al., 2020). A retrospective study about 213 patients from Italy with positive SARS-CoV-2 testing results indicates that headache (4.6%), fatigue (32.3%), myalgia (9.3%), anosmia (6.1%), seizure (2.8%), and consciousness disorder (40.3%) are common symptoms accompanied with fever or dyspnea in COVID-19 (Luigetti et al., 2020). Eighteen out of thirty six critically ill cases had consciousness disordered in Japan (Kohara and Kawamoto, 2020).

Neurological Symptoms Induced by Systemic Inflammation

Encephalopathy is considered the most common CNS complication of COVID-19 (caused by hypoxia or systemic diseases) (Kholin et al., 2020). About 50% of the hospitalized COVID-19 cases develop encephalopathy (Nath and Smith, 2020). If the patients' temperature surpasses 39.5°C or if blood oxygen saturation falls below 85%, it can lead to dizziness, ataxia, mental disorder, cognitive dysfunction, or even consciousness impairment. Older or immunosuppressed patients with cardiovascular, hepatic, and renal comorbidities are more susceptible to encephalopathy (Mao et al., 2020). Generally, once the primary diseases are addressed, the neurological impairments can be partially or completely reversible. Based on a survey of 304 COVID-19-confirmed patients including 108 critical patients, there is no evidence of additional risks for acute symptomatic seizure or status epilepticus (Lu et al., 2020). Nevertheless, some individuals manifest sudden seizure due to high fever. For patients with previously diagnosed epilepsy, sleep disorders and apprehension related to the unprecedented worldwide COVID-19 pandemic may pose extra trigger for onset of seizure (Parihar et al., 2020). Four SARS-CoV-2-positive cases in their 60s−70s presented with seizures, and two of them had electroencephalogram (EEG)-indicated epilepsy (Parauda et al., 2020). They were diagnosed with posterior reversible encephalopathy syndrome (PRES), with cerebral angioedema. In addition, a 74-year-old COVID-19 patient manifested altered mental status with epileptiform discharges in

his temporal lobe (Filatov et al., 2020). Postmortem evaluation was conducted in four COVID-19-confirmed patients to reveal the hypoxia-induced cerebral impairments. There were multiple microhemorrhages and enlarged space around the vessels. Leukocytes infiltrated the myelin sheaths and small perivascular lesions appeared in the white matter (Kantonen et al., 2020). Moreover, researchers have recognized abnormal fluid-attenuated inversion recovery (FLAIR) signals in the neuroimaging scans of 44% (12/27) ICU-admitted patients who presented with neurological complications (Kandemirli et al., 2020). Kremer et al. illustrated the neuroradiological patterns in the brain MRIs of 37 COVID-19 patients, revealing multifocal FLAIR/T2 hyperintensities with contrast enhancement, and extensive microhemorrhagic abnormalities in the cerebral white matter (Kremer et al., 2020). Pediatric multisystem inflammatory syndrome (PIMS) induced by SARS-CoV-2 could affect the nervous system as well (Padda et al., 2020). Children may present with headache, weakness, hyporeflexia, and brain parenchyma impaired symptoms (Padda et al., 2020). Abnormal imaging signals are evident in the splenium of the corpus callosum (Abdel-Mannan et al., 2020).

Cerebrovascular disease is considered to be another main neurological complication of SARS-CoV-2 infection, which has a high mortality rate (Chua et al., 2020). The pooled prevalence of COVID-19-related acute cerebrovascular disease is inferred as 2.3% (Favas et al., 2020). A Spanish medical center reported that 1.4% of the total 1,683 hospitalized patients with COVID-19 developed cerebrovascular disease (Hernandez-Fernandez et al., 2020). Among them, 73.9% of cases were diagnosed with ischemic stroke, while 21.7% were diagnosed with hemorrhagic stroke with elevated ferritin levels. The vertebrobasilar artery was the most frequently blocked vessel in the ischemic patients. Their brain biopsies evidenced endothelium injury and thrombotic microangiopathy, rather than necrotizing encephalitis or vasculitis. This suggested that severely infected patients are more likely to develop hemorrhagic or ischemic stroke due to coagulopathy (Tang et al., 2020). Patients with cardiocerebrovascular risk factors have a predisposition for acute stroke during COVID-19 dissemination (Li et al., 2020). Six COVID-19 patients with acute ischemic stroke in large vessels developed aphasia, dysarthria, prosopoplegia, paralysis, sensory loss, and even acute confusion. Two cases had multiple infarctions caused by simultaneous venous and arterial thrombosis. Lupus anticoagulants were positive in five patients, suggesting a coagulation disturbance. The angiograms demonstrated occlusion of the posterior or middle cerebral artery trunk or branches (Beyrouti et al., 2020). Oxley et al. admitted five COVID-19 cases with typical neurological dysfunction signs, such as hemiplegia, sensory deficit, facial weakness, or dysarthria, due to infarction in their large vessel territories. They accepted anticoagulant treatments, and one of them improved greatly within 2 weeks (Oxley et al., 2020). In another series of six cases aged from 57 to 82 years old, four developed ischemic stroke and the other two developed hemorrhagic stroke. All of them presented severe pneumonia and complications in multiple organs with elevated transaminases and LDH levels in blood tests, which indicated poor outcome. However, only one patient had possible vessel-related risk factors for stroke before COVID-19 (Morassi et al., 2020). Four SARS-CoV-2-positive patients from New York showed focal diffusion weighted imaging (DWI) hyperintensities in the splenium of the corpus callosum, including two patients with rare isolated lesions. Their mental status was apparently impaired. Three of them progressed to severe inflammatory hypercoagulable status during admission, requiring mechanical ventilation and dialysis. Subarachnoid hemorrhage (SAH) and hemorrhagic transformation after ischemic stroke occurred in two cases. However, SARS-CoV-2 was negative in their CSF (Sparr and Bieri, 2020). Another five cases infected by SARS-CoV-2 developed intracerebral hemorrhage (ICH) during admission. Four of them had ICHs in the lobe area with no cerebral vascular malformation in computed tomography angiography (CTA) examination (Benger et al., 2020). Hemorrhagic lesions may be caused by the coagulopathy derived from severe systemic infection or by the viral invasion of the vascular endothelium (Al Saiegh et al., 2020). In turn, lesions to the cerebral white matter and the blood vessels may aggravate patients' general condition (Tang et al., 2020). Patients with mechanical ventilation support may develop secondary neurological disorders because of the brain-lung crosstalk. The stress state related to hypoxia and to endothelial cell injury can aggravate inflammation, cause hypercoagulability, and lead to "pulmonary encephalopathy"–like impairments (Battaglini et al., 2020).

Direct Invasion Into the Nervous System

Coronaviruses can directly invade the CNS for their neurotropism, causing encephalitis or meningitis (Alshebri et al., 2020; Serrano-Serrano et al., 2020). Based on the autopsy analyses of 17 COVID-19 patients, 8 individuals were identified SARS-CoV-2 positive in brain tissue with cerebral edema and vascular congestion (Remmelink et al., 2020). A Japanese male developed new-onset seizure and unconsciousness following fever and general weakness. RT-PCR test of SARS-CoV-2 in CSF was positive. Taking these results together with brain MRI results, the patient was likely to suffer from SARS-CoV-2-associated meningitis (Moriguchi et al., 2020). McAbee et al. described a case with encephalitis who was only 11 years old (McAbee et al., 2020). The patient had a sudden status epilepticus and high fever without any preexisting diseases. CSF assay detected positive SARS-CoV-2, together with elevated red and white cells, but normal protein and glucose concentrations. The EEG recorded occasional delta waves in the frontal lobe. A 20-year-old female with COVID-19 presented with mental disorder and urinary incontinence 4 days after flu-like symptoms (Babar et al., 2020). Laboratory assay found predominantly elevated ferritin and D-dimer. No remarkable findings were acquired from MRI and CSF analysis. She received methylprednisolone therapy over 20 days and gained intermittent awareness. Despite absence of direct evidence supporting viral infection in the CSF, the patient was still highly speculated as SARS-CoV-2 encephalitis because the neurological manifestations had significantly improved after SARS-CoV-19 turning negative. Another COVID-19-related encephalitic patient presented with mental disturbances and psychotic features without

early respiratory symptoms. MRI detected multiple lesions in the thalamus, cortex, and corpus callosum with abnormal T2/FLAIR signals (Rebeiz et al., 2020). Moreover, brainstem encephalitis was suspected in a 65-year-old woman with SARS-CoV-2 infection (Khoo et al., 2020). She developed involuntary limb movement with myoclonus, nonsense words, diplopia, and disturbed cognition 2 weeks after presenting dry cough and fever. Neurological examination confirmed hypermyotonia on both sides. However, MRI and CSF analyses reported unrepresented results. An experimental treatment with corticosteroids resulted in neurological improvement, which further verified the original speculated diagnosis of postinfectious brainstem encephalitis. The autopsy of an infant who died from COVID-19 revealed a limited distribution of SARS-CoV-2 in choroid plexus, lateral ventricle, and a few regions in the frontal cortex. It is known that viruses and immune factors enter the developing human brain through a weakened blood–brain barrier and induce neural impairments (da et al., 2020). Although not all cases test positive for SARS-CoV-2 in the CSF, signs of nervous system infection or impairment should arouse clinicians' attention to probable neurological complications of COVID-19 (Puccioni-Sohler et al., 2020).

Moreover, chemosensory disorders, including anosmia and ageusia, affect COVID-19 patients (Koralnik and Tyler, 2020; Padda et al., 2020; Vaira et al., 2020). Over one-third of the patients with COVID-19 present with smell or taste disturbances (Favas et al., 2020). These symptoms can develop before, simultaneously, or after cough and fever (Spinato et al., 2020). About 50% of patients report hyposmia or hypogeusia at the initial stage of COVID-19 (Beltran-Corbellini et al., 2020; Cherry et al., 2020). Statistics suggest that dysosmia and dysgeusia are predictors for COVID-19. When considered together with fever, the sensitivity is 70% and the discrimination accuracy is 75% (Roland et al., 2020). The prevalence of smell and taste dysfunctions decreases in older patients (Agyeman et al., 2020), and female patients are more prone to smell disturbance (Meng et al., 2020). Furthermore, about 12% of the COVID-19 patients develop only anosmia as initial symptom (Puccioni-Sohler et al., 2020). Eight cases developed sudden and complete loss of smell without respiratory symptoms (Gilani et al., 2020). Additionally, patients may present with other sensory dysfunctions, including oropharyngeal and ontological/vestibular disturbances: sore throat, dysphagia, vertigo, tinnitus, and hearing loss are common complications (Krajewska et al., 2020; Ozcelik Korkmaz et al., 2020). For instance, a middle-aged woman with sudden dizziness and dry throat was confirmed to have COVID-19. Although her brain MRI showed no abnormal signs, CT demonstrated ground-glass-like infiltration in the lungs (Kong et al., 2020). Careful assessment of otolaryngologic manifestations, combined with nucleic acid and imaging examinations, may provide great help for the early identification of COVID-19.

Autoimmune-Related Disorders in the Nervous System

SARS-CoV-2 infection can also lead to demyelinating diseases through neurological immune response, both in the CNS and PNS. Guillain–Barré syndrome (GBS) is a common PNS complication caused by an overactivated autoimmune reaction (Wakerley and Yuki, 2013). Progressive flaccid paralysis, dysergia, and areflexia are considered its typical neurological manifestations. The first COVID-19-related GBS patient was reported in January in Wuhan (Zhao et al., 2020). This 61-year-old woman complained of sudden weakness of the lower limbs without history of fever or cough. Lymphocytopenia and thrombocytopenia were determined by laboratory tests. SARS-CoV-2 was positive. CSF results showed an elevation of protein levels but normal cell counts. Electrophysiological examinations detected motor and sensory nerves demyelination with prolonged distal latency and absent F wave, indicating the GBS. Another published series of cases studied five patients with COVID-19-related GBS in Italy (Toscano et al., 2020). These patients presented with facial and/or limb paresis and paresthesia within 5–10 days after the onset of COVID-19 symptoms. CSF tests showed high protein levels without SARS-CoV-2. Antiganglioside antibodies were all negative in the three tested cases. Caudal roots or facial nerve enhancement was observed in MRI, implying an ongoing immune inflammatory response in nerves. Intravenous immunoglobulin (IVIg) was administered to all the patients, but only two improved. Additionally, two Spanish men presented with Miller Fisher syndrome and polycranial neuritis respectively, several days after COVID-19 (Gutierrez-Ortiz et al., 2020). They had diplopia, balance disturbances, and areflexia with albuminocytologic dissociation in the CSF examination. One 50-year-old man presented with right oculomotor palsy and right internuclear ophthalmoparesis. His GD1b-IgG antibodies were positive. Another 39-year-old man developed bilateral palsy of abducens. Both cases were SARS-CoV-2 positive in the oropharyngeal swab sample but negative in CSF. In addition, Dinkin et al. described two COVID-19 cases who developed ophthalmoplegia several days after flu-like symptoms (Dinkin et al., 2020). MRI exhibited enhancement of injured nerves, including the optic nerve and oculomotor nerve. Neither ganglioside antibodies nor SARS-CoV-2 were detected in CSF. Another 51-year-old man presented with limb weakness, sensory disturbances in hands and feet, and areflexia after 2 weeks of fever and cough (Pfefferkorn et al., 2020). Then his condition rapidly deteriorated into ventilator dependence with an almost locked-in syndrome in the PNS. SARS-CoV-2 was positive in a pharyngeal swab test but negative in CSF. Albuminocytologic dissociation was identified in the CSF 13 days later. Electrophysiology revealed demyelination of multiple peripheral nerves, and MRI detected equal enhancement of anterior and posterior nerve roots from different spinal levels. Based on these aforementioned cases, GBS should be regarded as a possible neurological sign of COVID-19, especially in patients with lymphocytopenia. Moreover, GBS with generalized paralysis can further aggravate patients' general conditions.

Multiple sclerosis (MS) is a subacute immune-mediated and demyelinating disease of the CNS. The patients' neurological manifestations often exacerbate and relapse due to infection or stress (Sadeghmousavi and Rezaei, 2020). The mainstay therapy is immunosuppressants. In such cases, patients may suffer from severe lymphopenia with poor prognosis if they are involved in

COVID-19 simultaneously (Dersch et al., 2020; Sadeghmousavi and Rezaei, 2020). Additionally, they may develop emerging MS due to post-inflammatory immune response. The first published case recognized as MS with progressively impaired vision due to optic neuritis was reported in May in Spain (Palao et al., 2020). This 29-year-old woman with COVID-19 complained of retro-ocular pain, transient weakness, and myalgia of her limbs with hyperreflexia on admission. MRI demonstrated enhancement of the right optic nerve and demyelinating lesions surrounding the lateral ventricles, while the spinal cord was normal. Lumbar puncture detected oligoclonal bands of IgG but no aquaporin-4 (AQP4) or MOG antibodies. No SARS-CoV-2 was identified in CSF. High-dose steroids were administered and her vision recovered gradually.

Another reported COVID-19-associated neurological complication induced by autoimmunity is acute disseminated encephalomyelitis (ADEM). Patients may present as encephalopathy and transverse myelitis with weakness and numbness of the limbs and urinary disorders. A 51-year-old German woman with COVID-19 lost consciousness and manifested dull oculocephalic reflex (Parsons et al., 2020). Diffused FLAIR hyperintensive signals were detected in the deep brain tissue and white matter adjacent to cortices. The CSF examination showed xanthochromia, with elevated glucose and protein levels. Pathogen assays were negative, but oligoclonal bands were positive in both serum and CSF. Antibodies for AQP4 were absent. All these findings highly supported ADEM in this case. The patient regained consciousness after weeks of IVIg and steroids treatment. Utukuri et al. reported a 44-year-old man with COVID-19 who developed ADEM (Utukuri et al., 2020). He was initially admitted for urinary retention, inability to walk on his own, and back pain, without any symptoms of respiratory infection. MRI showed slightly increased T2 signals in the spinal cord and hyperintensive FLAIR signals in periventricular or juxtacortical regions, indicating ongoing acute lesions associated with demyelination. The CSF analysis revealed upregulated protein levels with normal IgG and absent oligoclonal bands. No SARS-CoV-2 was found in CSF. Additionally, ADEM occurred in a 64-year-old woman with COVID-19 from Italy (Novi et al., 2020). She complained of alternations in the bilateral visual fields, impaired smell and taste, and numbness of the right lower limb. The Babinski sign was induced on the left side. MRI found dissembled abnormalities in both cerebral hemisphere and a segmental injury at the level of the 8th thoracic vertebra of the spinal cord, with typical T1 enhancement. SAR2-CoV-2 was positive in her CSF. Moreover, CSF and serum analyses found oligoclonal bands, but no AQP4 antibody. She received high-dose steroids together with IVIg for 14 days, partially recovering her vision and reducing T1-enhanced lesions. On the contrary, a 71-year-old man, who was positive for COVID-19 after a coronary artery bypass surgery, rapidly deteriorated to multiple organ dysfunction syndrome (MODS) and did not survive (Reichard et al., 2020). The autopsy revealed disseminated focal hemorrhage and edema in the cerebral white matter. Immunohistochemical analysis indicated ADEM-like lesions around vessels. Acute hemorrhagic necrotizing encephalopathy was diagnosed in a woman about 60 years old with positive SARS-CoV-2 (Poyiadji et al., 2020). She manifested altered mental status after several days of fever and cough. No virus was detected in CSF. Brain MRI revealed patchy and bilateral hemorrhagic signals with enhanced edge in the basal ganglia region and medial temporal lobes. IVIg was applied to get generally recovered consciousness. A 59-year-old woman with aplastic anemia developed epilepsy and consciousness disorder 10 days after flu-like symptoms (Dixon et al., 2020). She was highly suspected of having acute necrotizing encephalopathy as a post-immune consequence. SARS-CoV-2 was positive on the nasopharyngeal swab sample. Radiological examinations revealed a fast-progressing condition from brainstem swelling to disseminated hemorrhage. No microorganism was detected in CSF. She did not improve with steroid treatment and died 8 days after admission. Another woman without preexisting diseases was suspected of acute necrotizing myelitis with neck pain and motor and sensory weakness (Sotoca and Rodriguez-Alvarez, 2020). Spinal MRI showed T2 abnormal hyperintensity in a long segment. There was clinical improvement with plasma exchange and methylprednisolone therapies. In addition, a 32-year-old male with COVID-19 developed acute transverse myelitis with paraplegia and dysuria after a 2-day fever (AlKetbi et al., 2020). MRI showed lesions at the cervical and lumbar levels of the spinal cord. Methylprednisolone was administered to relieve his symptoms.

Other Neurological Complications

Two COVID-19-positive women from New York presented with ophthalmoparesis, headache, and sensory disorder. They both complained of typical diplopia because of abducens nerve palsy. There was neither SARS-CoV-2 RNA nor ganglioside antibodies detected in CSF. The MRI revealed hypothalamic and tegmental mesencephalic hyperintensity in FLAIR and T2 sequences, which is indicative of Wernicke encephalopathy. However, no laboratory evidence supported abnormal thiamine levels (Pascual-Goni et al., 2020).

Additionally, SARS-CoV-2 infection is thought to progress from olfactory bulbs into the diencephalon or the brainstem, causing extrapyramidal symptoms (Mendez-Guerrero et al., 2020; Rabano-Suarez et al., 2020). A 58-year-old man, who previously had good health, was positive for COVID-19 with symptoms of fever, cough, and dyspnea (Mendez-Guerrero et al., 2020). He then developed olfactory disturbances, opsoclonus, bilateral resting myoclonus, consciousness impairment, and asymmetric hypokinetic-rigid syndrome without any metabolic disturbance. Protein level was elevated slightly in CSF. [^{123}I]-ioflupane dopamine transporter single-photon emission CT (DaT-SPECT) images indicated that the presynaptic uptake of dopamine in the bilateral putamina reduced asymmetrically. Three patients were diagnosed with generalized myoclonus (Rabano-Suarez et al., 2020). They all felt decreased taste and developed myoclonus in the face, nasopharynx, and arms, with absence of microorganism in CSF. After methylprednisolone and plasma exchange treatment, their general condition improved gradually.

Musculoskeletal manifestations are another common neurological complication, including fatigue or generalized

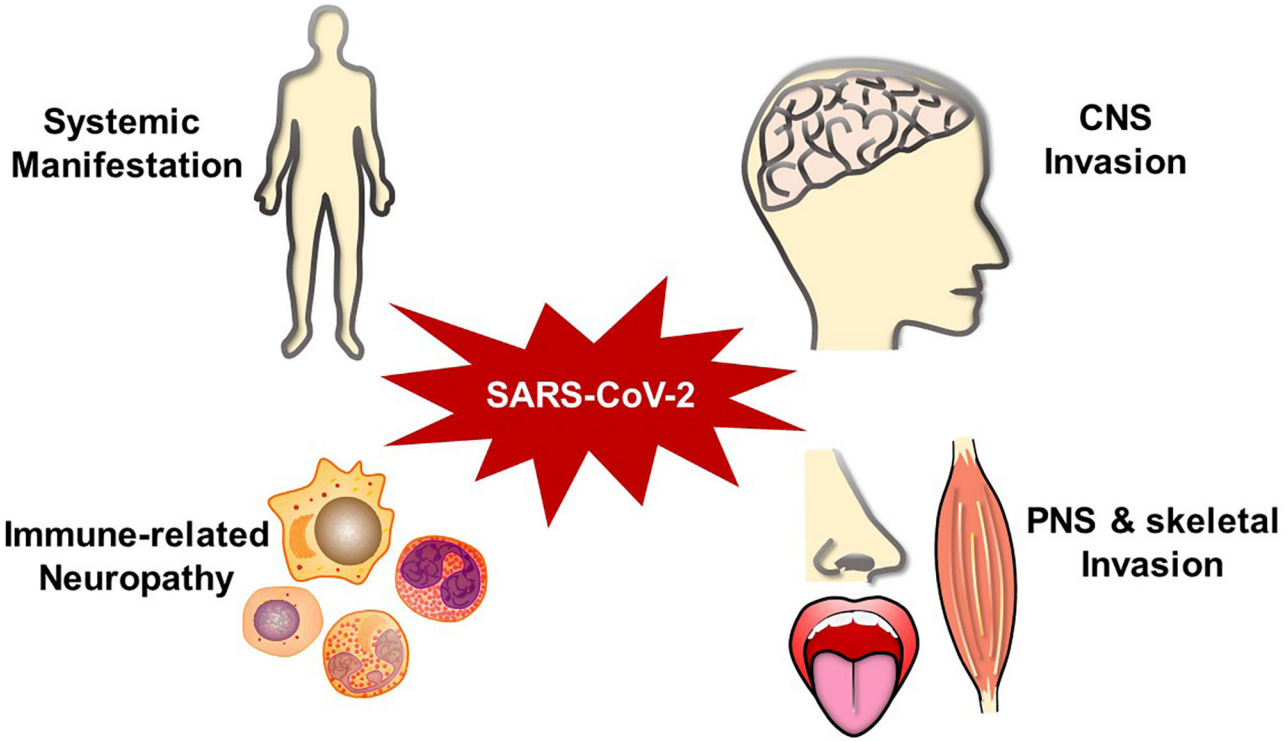

FIGURE 1 | SARS-CoV-2-associated neurological impairments.

weakness, myalgia or myositis, and skeletal muscle injury. Serum creatine kinase (CK) was significantly increased in 124 out of 213 (58.2%) COVID-19 patients (Luigetti et al., 2020). Myalgias may be associated with the severity of infection (Zhang X. et al., 2020). Researchers investigated nine cases that presented with back pain, dyskinesia, and paresthesia in lower limbs. Spinal cord MRI revealed intramuscular edema in seven patients, suggesting paraspinal myositis (Mehan et al., 2020). Besides, SARS infection could cause functional deficits and myalgias in skeletal muscle with elevated CK level (Xu P. et al., 2020). Patients with SARS infection lost about 32% of their grip strength and shortened about 13% of 6 min walking distance (Lau et al., 2005). Virus-induced inflammatory immune response and deconditioning during severe illness may exacerbate the muscular impairments (Disser et al., 2020). However, more clinical cases are needed to explore whether SARS-CoV-2 can affect musculoskeletal sequelae in long term.

As a widely spread pandemic, COVID-19 has influenced thousands of people's lives. In addition to the common respiratory symptoms, patients can develop diverse neurological complications (**Figure 1**). Patients' neurological manifestations may present as the earliest infected signs (Chua et al., 2020). Individuals may suffer months of malaise, generalized fatigue, or decreased exercise tolerance even after recovered (Nath and Smith, 2020). It is important to differentiate SARS-CoV-2-associated neurological complications from other neurological diseases, such as primary epilepsy, mitochondrial encephalomyopathy, paraneoplastic syndromes, chemosensory disturbances in early neurodegenerative diseases, toxin/drug-related neural injury, and other intracranial infections. Although doctors already pay attention to SARS-CoV-2 impacts in multiple organs, a more comprehensive and deeper understanding should be attained for the complex neurological manifestations. It is crucial to inquire patients about their medical histories, perform the neurological physical examination carefully, and combine with imaging and pathogenic examination results.

MECHANISM OF SARS-CoV-2 INFECTION

According to previous literatures, SARS-CoV-2 infection can cause complications via direct invasion and immune disturbance through hematogenous or transsynaptic propagation (**Figure 2**) (Haddadi and Asadian, 2020; Puccioni-Sohler et al., 2020). SARS-CoV-2 is regarded as neurotropic virus. SARS-CoV-2 replicates via synthesizing viral polyproteins and assembling RNA in cells (Shang et al., 2020b). As known, there is an S-protein domain on its surface, with high affinity to angiotensin-converting enzyme 2 (ACE2). ACE2 is widely distributed on the cell membrane in cerebral cortex, vascular endothelium, oral and nasal mucosa (Uhlen et al., 2015; Xu H. et al., 2020). ACE2 receptors are expressed in neurons and glia cells, which may explain the potential neural invasion of SARS-CoV-2 (Baig et al., 2020). Evidence supported that transmembrane protease serine 2 (TMPRSS2) could promote SARS-CoV-2 migration

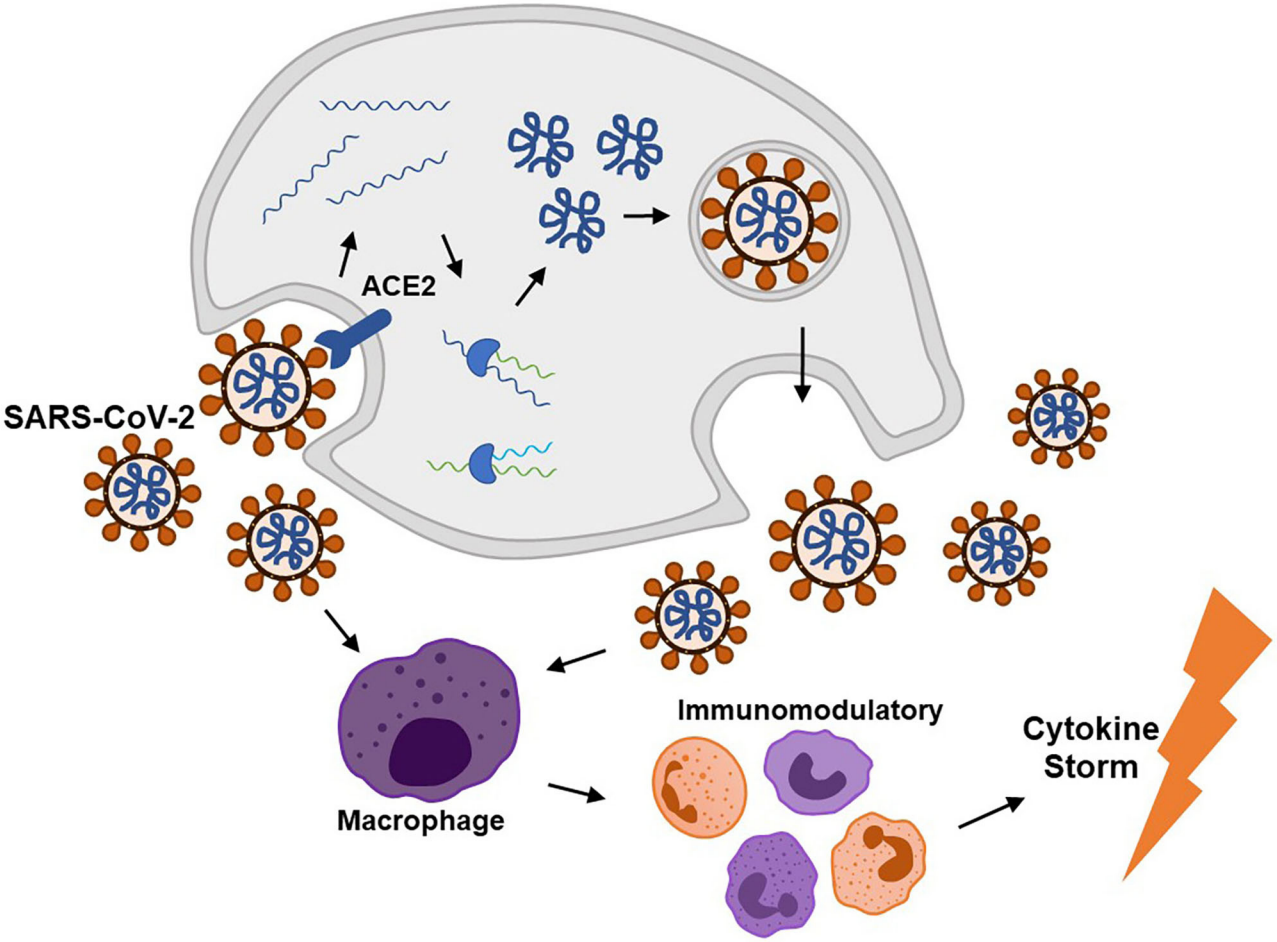

FIGURE 2 | SARS-CoV-2 invades into human cells via the ACE2 receptor and then replicates to cause immunomodulatory disorder through a cytokine storm.

and infection by preactivating S-protein and cleaving ACE2. Endothelial damage and neuronal apoptosis can be induced by SARS-CoV-2 infection (Pranata et al., 2020). ACE2 receptors on vascular endothelial cell membrane may participate in regulating blood pressure, which is closely related to stroke (Tsatsakis et al., 2020; Viana et al., 2020). Also, SARS-CoV-2 may cause vascular endothelial damages, facilitating viral invasion into CNS (Baig et al., 2020). Considering distribution of ACE2 in the muscle system, SARS-CoV-2 could upregulate lactate levels, reduce oxygen/energy supply, and cause myalgia (Kucuk et al., 2020). Besides, virus could spread directly into the brain through the cribriform plate to invade cranial nerves. Bryche et al. studied the SARS-CoV-2-induced deficits of the olfactory system in golden Syrian hamsters. The olfactory epithelium (OE) is severely impaired and massive sustentacular cells were injured, causing numerous cilia loss (Bryche et al., 2020). SARS-CoV-2 may initiate its spread from the nasal mucosa and alveolar epithelium to the circulatory system and attacked cells in other tissues or organs by interacting with ACE2 or TMPRSS2 (Shang et al., 2020a).

On the other hand, SARS-CoV-2 can activate excessive and damaging immune inflammatory response in COVID-19, which is called "cytokine storm." Mononuclear phagocytes are over proliferated with accumulated interleukin (IL)-6, IL-7, tumor necrosis factor (TNF), inflammatory chemokines CCL2, CCL3, and CXCL10 (Pedersen and Ho, 2020). Interferon regulatory factor 7 (IFN-7) may induce astrocytes to secret chemokines (Haddadi and Asadian, 2020). Extensive T cell responses during the cytokine storm could cause lymphopenia in patients. It is hypothesized that the cytokine storm may be induced by the inflamed nucleus tractus solitarius (NTS) in SARS-CoV-2 infection. Both hypothalamic/pituitary/adrenal axis and cholinergic anti-inflammatory pathway do not function in COVID-19 (Ur and Verma, 2020). The abnormal immune response following SARS-CoV-2 infection, in turn, induces autoimmune-related neurological complications. Severe lymphopenia and cytokine storm usually imply a poor prognosis of higher mortality (Tan et al., 2020).

Furthermore, the upregulated inflammatory factors and cytokines in serum can induce systemic hypercoagulable state.

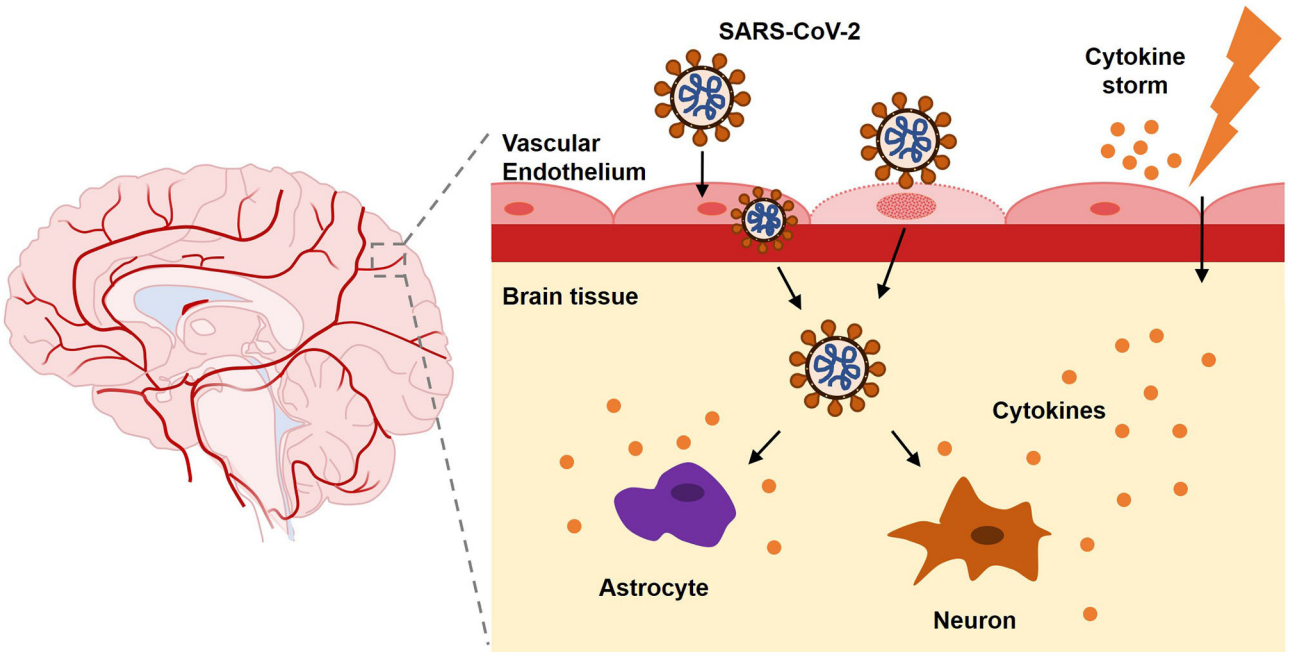

FIGURE 3 | SARS-CoV-2 leads to neurological disorders via different pathways.

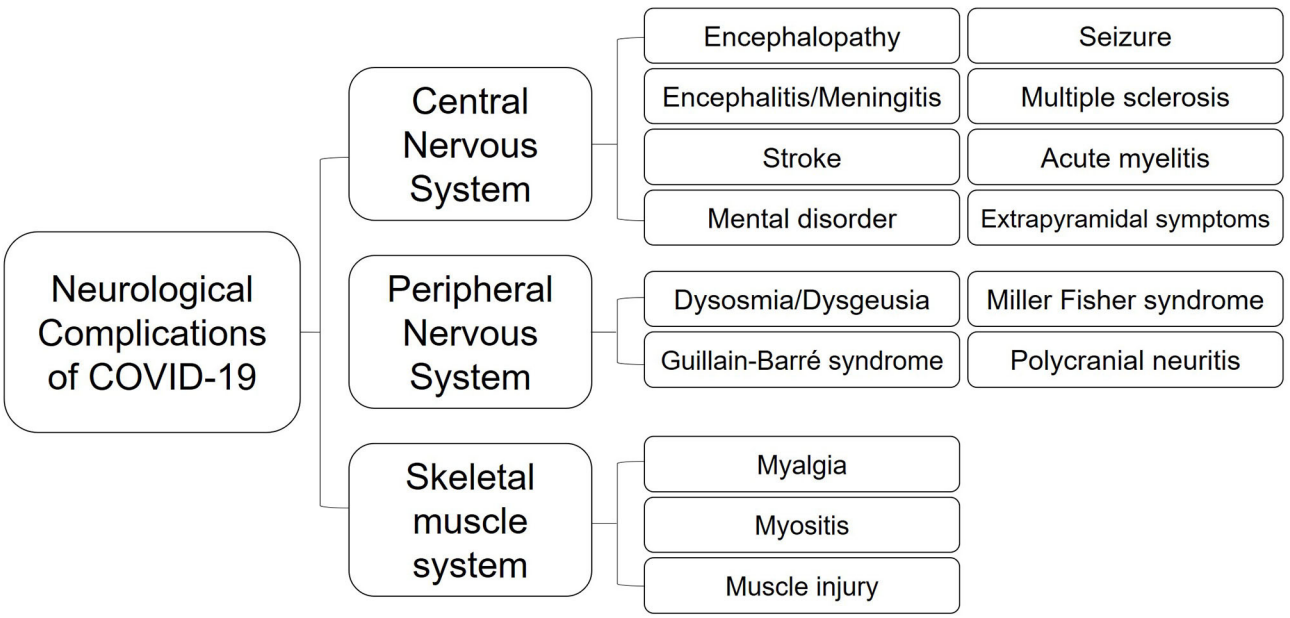

FIGURE 4 | Neurological complications of COVID-19.

Thus, patients with COVID-19 are prone to thrombosis in both arteries and veins (Huang et al., 2020). In addition, increasing lipoprotein(a) (LP(a)) may promote the development of thrombosis in COVID-19. LP(a) could activate phospholipid oxidation to exert proinflammatory roles and split off the preformed atherosclerotic plaques. Besides, the endogenous fibrinolytic system is restrained by the apolipoprotein(a) compartments within Lp(a) molecules (Moriarty et al., 2020). The complicated metabolic mechanism still needs more exploration.

TREATMENT AND CLINICAL MANAGEMENT

To date, no specific drugs or vaccines for COVID-19 have been approved. Symptomatic treatment is performed on the infected organs and systems. For the severely or critically ill, mechanical ventilation and intensive care unit (ICU) admission are performed for life support (Alberti et al., 2020; Dalakas, 2020). Anticoagulant therapy is applied for patients with coagulopathy. Antimalarials are assumed to inhibit the release of pro-inflammatory factors in the CNS by crossing the blood–brain barrier with their high lipophilic properties (Ong et al., 2020). Serotonin, a classic neurotransmitter, could suppress the inflammatory response in CNS and PNS. Luis et al. reported that selective serotonin reuptake inhibitors (SSRI) might act as neuroprotectors and reduce neuropsychiatric disorders (Costa et al., 2020). A recent study found that fluoxetine could contribute to SARS-CoV-2 inhibition (Zimniak et al., 2020). However, inappropriate utilization of SSRIs may overactivate serotoninergic neurons and induce serotonin syndrome with lethal consequences.

Immunotherapies are conducted in the short term to moderate inflammatory responses after SARS-CoV-2 infection (Sharun et al., 2020b). Convalescent serum is used as a rapid therapy to induce passive immunity against COVID-19. Additionally, intravenously administered monoclonal immunoglobulins may block the activation of Fc receptors and reduce the cytokine storm in CNS during inflammation (Iqbal Yatoo et al., 2020). It could be an effective and safe treatment for COVID-19-related encephalopathy (Muccioli et al., 2020).

Corticosteroids and plasma exchange are applied to control the systemic overactivated immune response in severely ill cases with neurological complications (Sharun et al., 2020a). However, there are risks of exacerbated infection induced by immunosuppression. Recently, some monoclonal antibodies (mNA) have been postulated to neutralize SARS-CoV-2 via binding to its spike protein (Sharun et al., 2020b). Studies are required to explore the underlying mechanism in detail and propose a specific treatment with low side effects for COVID-19.

Scientists and researchers are working on various types of vaccines, including live attenuated vaccines; vaccines modified at the protein, DNA, or mRNA levels; and vaccines with or without vectors (Iqbal Yatoo et al., 2020). Great challenges still exist for the development of a stable and relatively long-term vaccine. Both effectiveness and clinical safety should be taken into consideration.

In order to control the source of infection and stop the transmission, strategies of isolation, quarantine, and physical distancing have been implemented. People are encouraged to use masks or face coverings and to follow hand hygiene practices (Rabaan et al., 2020). Other the other hand, the management and treatment of acute or chronic primary neurological diseases cannot be neglected (von Oertzen et al., 2020). Task forces comprised of medical staff have been placed to guarantee emergency care of acute neurovascular events (Al-Jehani et al., 2020). Clinicians can observe their patients with preexisting seizure disorders through regular telemedicine (Parihar et al., 2020). Moreover, because COVID-19 could cause neurological complications in children as well, pediatric neurology should pay more attention to their patients' manifestations for a timely diagnosis and treatment (Bonkowsky et al., 2020).

CONCLUSION AND FUTURE PROSPECTS

Since the outbreak of the COVID-19 pandemic, SARS-CoV-2 poses serious threat to both the CNS and the PNS (Wang et al., 2020). Although it is regarded to mainly affect the respiratory system, more and more neurological complications seem to be appearing which further deteriorate the patients' condition and prognosis. Those in severe or critical states from COVID-19 usually present with consciousness disorders caused by concurrent neurological deficits and require assisted ventilation. Despite intensive care, they may ultimately lose their lives. Aggressive supportive care, such as mechanical ventilation, reduction of intracranial pressure, or anticoagulation therapy, is necessary to improve the patients' systemic condition. On the other hand, mild cases may only present with olfactory or gustatory disorders, which can lead to missed diagnoses (Wang et al., 2020). Neurologists should explore the pathogenesis by CT or MRI scan and laboratory analyses, especially for CSF, since SARS-CoV-2 can affect the nervous system in various manners. The use of high-dose steroid therapy is always a challenge for patients with severe respiratory infections. Experimental treatments should only be undertaken to relieve a worsening critical physical status in patients with negative CSF results. Vaccines are imperative in this fight against the COVID-19 pandemic, but they still need massive research and developments.

Since the virus can lead to multiple neurological disorders by different means (**Figure 3**), more studies are needed to determine the possible influences and moderating factors of SARS-CoV-2 infection. Early manifestations of neurological symptoms should be regarded as possible indicators of COVID-19 (**Figure 4**). Despite possible iatrogenic infections, individuals who feel unwell should seek medical attention immediately. Physicians who examine patients with atypical symptoms should ask for a detailed medical history and conduct the necessary PCR assays for SARS-CoV-2 to obtain an early diagnosis and avoid the wide spread. Further explorations are required on the molecular regulation of COVID-19 for a better understanding of SARS-CoV-2 neurotropism and its possible interferences.

AUTHOR CONTRIBUTIONS

SY designed the conception, searched the literature, draw the schematics, and created the manuscript. MY searched the literature, summarized the opinion, draw the schematics, and revised the manuscript. All authors contributed to the article and approved the submitted version.

FUNDING

This work was supported by the National Natural Science Foundation of China, No. 81902537 (to MY); National Natural Science Foundation of China, No. 82001475 (to SY); Natural Science Foundation of Liaoning Province of China, No. QNZR2020016 (to SY); Natural Science Foundation of Liaoning Province of China, No. 20180550913 (to MY); Shengjing Hospital of China Medical University scientific fund, No. M0124 (to SY); and the 345 Talent Project from Shengjing Hospital of China Medical University (to SY).

ACKNOWLEDGMENTS

The authors thank Dr. Juan Feng for the feedback on a preliminary plan of this review.

REFERENCES

Abdel-Mannan, O., Eyre, M., Lobel, U., Bamford, A., Eltze, C., Hameed, B., et al. (2020). Neurologic and radiographic findings associated with COVID-19 infection in children. *JAMA Neurol.* 77, 1–6. doi: 10.1001/jamaneurol.2020.2687

Agyeman, A. A., Chin, K. L., Landersdorfer, C. B., Liew, D., and Ofori-Asenso, R. (2020). Smell and taste dysfunction in patients with COVID-19: a systematic review and meta-analysis. *Mayo Clin. Proc.* 95, 1621–1631. doi: 10.1016/j.mayocp.2020.05.030

Al Saiegh, F., Ghosh, R., Leibold, A., Avery, M. B., Schmidt, R. F., Theofanis, T., et al. (2020). Status of SARS-CoV-2 in cerebrospinal fluid of patients with COVID-19 and stroke. *J. Neurol. Neurosurg. Psychiatry* 91, 846–848. doi: 10.1136/jnnp-2020-323522

Alberti, P., Beretta, S., Piatti, M., Karantzoulis, A., Piatti, M. L., Santoro, P., et al. (2020). Guillain-Barre syndrome related to COVID-19 infection. *Neurol. Neuroimmunol. Neuroinflamm.* 7:e741. doi: 10.1212/NXI.0000000000000741

Al-Jehani, H., John, S., Hussain, S. I., Al Hashmi, A., Alhamid, M. A., Amr, D., et al. (2020). MENA-SINO consensus statement on implementing care pathways for acute neurovascular emergencies during the COVID-19 pandemic. *Front. Neurol.* 11:928. doi: 10.3389/fneur.2020.00928

AlKetbi, R., AlNuaimi, D., AlMulla, M., AlTalai, N., Samir, M., Kumar, N., et al. (2020). Acute myelitis as a neurological complication of Covid-19: a case report and MRI findings. *Radiol. Case Rep.* 15, 1591–1595. doi: 10.1016/j.radcr.2020.06.001

Almazan, F., Gonzalez, J. M., Penzes, Z., Izeta, A., Calvo, E., Plana-Duran, J., et al. (2000). Engineering the largest RNA virus genome as an infectious bacterial artificial chromosome. *Proc. Natl. Acad. Sci. U.S.A.* 97, 5516–5521. doi: 10.1073/pnas.97.10.5516

Alshebri, M. S., Alshouimi, R. A., Alhumidi, H. A., and Alshaya, A. I. (2020). Neurological complications of SARS-CoV, MERS-CoV, and COVID-19. *SN Compr. Clin. Med.* doi: 10.1007/s42399-020-00589-2. [Epub ahead of print].

Andersen, K. G., Rambaut, A., Lipkin, W. I., Holmes, E. C., and Garry, R. F. (2020). The proximal origin of SARS-CoV-2. *Nat. Med.* 26, 450–452. doi: 10.1038/s41591-020-0820-9

Babar, A., Lewandowski, U., Capin, I., Khariton, M., Venkataraman, A., Okolo, N., et al. (2020). SARS-CoV-2 encephalitis in a 20-year old healthy female. *Pediatr. Infect. Dis. J.* 39, e320–e321. doi: 10.1097/INF.0000000000002855

Baig, A. M., Khaleeq, A., Ali, U., and Syeda, H. (2020). Evidence of the COVID-19 virus targeting the CNS: tissue distribution, host-virus interaction, and proposed neurotropic mechanisms. *ACS Chem. Neurosci.* 11, 995–998. doi: 10.1021/acschemneuro.0c00122

Battaglini, D., Brunetti, I., Anania, P., Fiaschi, P., Zona, G., Ball, L., et al. (2020). Neurological manifestations of severe SARS-CoV-2 infection: potential mechanisms and implications of individualized mechanical ventilation settings. *Front. Neurol.* 11:845. doi: 10.3389/fneur.2020.00845

Beltran-Corbellini, A., Chico-Garcia, J. L., Martinez-Poles, J., Rodriguez-Jorge, F., Natera-Villalba, E., Gomez-Corral, J., et al. (2020). Acute-onset smell and taste disorders in the context of COVID-19: a pilot multicentre polymerase chain reaction based case-control study. *Eur. J. Neurol.* 27:e34. doi: 10.1111/ene.14359

Benger, M., Williams, O., Siddiqui, J., and Sztriha, L. (2020). Intracerebral haemorrhage and COVID-19: clinical characteristics from a case series. *Brain Behav. Immun.* 88, 940–944. doi: 10.1016/j.bbi.2020.06.005

Beyrouti, R., Adams, M. E., Benjamin, L., Cohen, H., Farmer, S. F., Goh, Y. Y., et al. (2020). Characteristics of ischaemic stroke associated with COVID-19. *J. Neurol. Neurosurg. Psychiatry* 91, 889–891. doi: 10.1136/jnnp-2020-323586

Bhatraju, P. K., Ghassemieh, B. J., Nichols, M., Kim, R., Jerome, K. R., Nalla, A. K., et al. (2020). Covid-19 in critically Ill patients in the Seattle Region - case series. *N. Engl. J. Med.* 382, 2012–2022. doi: 10.1056/NEJMoa2004500

Bonkowsky, J. L., deVeber, G., Kosofsky, B. E., and Child Neurology Society Research Committee. (2020). Pediatric neurology research in the twenty-first century: status, challenges, and future directions post-COVID-19. *Pediatr. Neurol.* 113, 2–12. doi: 10.1016/j.pediatrneurol.2020.08.012

Bryche, B., St Albin, A., Murri, S., Lacote, S., Pulido, C., Ar Gouilh, M., et al. (2020). Massive transient damage of the olfactory epithelium associated with infection of sustentacular cells by SARS-CoV-2 in golden Syrian hamsters. *Brain Behav. Immun.* 89, 579–586. doi: 10.1016/j.bbi.2020.06.032

Chen, N., Zhou, M., Dong, X., Qu, J., Gong, F., Han, Y., et al. (2020). Epidemiological and clinical characteristics of 99 cases of 2019 novel coronavirus pneumonia in Wuhan, China: a descriptive study. *Lancet* 395, 507–513. doi: 10.1016/S0140-6736(20)30211-7

Cherry, G., Rocke, J., Chu, M., Liu, J., Lechner, M., Lund, V. J., et al. (2020). Loss of smell and taste: a new marker of COVID-19? Tracking reduced sense of smell during the coronavirus pandemic using search trends. *Expert. Rev. Anti. Infect. Ther.* 18, 1–6. doi: 10.1080/14787210.2020.1792289

Chua, T. H., Xu, Z., and King, N. K. K. (2020). Neurological manifestations in COVID-19: a systematic review and meta-analysis. *Brain Inj.* 14, 1–20. doi: 10.1080/02699052.2020.1831606

Costa, L. H. A., Santos, B. M., and Branco, L. G. S. (2020). Can selective serotonin reuptake inhibitors have a neuroprotective effect during COVID-19? *Eur. J. Pharmacol.* 889:173629. doi: 10.1016/j.ejphar.2020.173629

da, S. G. P. C., Goto-Silva, L., Temerozo, J. R., Gomes, I. C., and Souza, L. R. Q., Vitoria, G., et al. (2020). *Non-Permissive SARS-CoV-2 Infection of Neural Cells in the Developing Human Brain and Neurospheres. bioRxiv [Preprint].* doi: 10.1101/2020.09.11.293951

Dalakas, M. C. (2020). Guillain-Barre syndrome: the first documented COVID-19-triggered autoimmune neurologic disease: more to come with myositis in the offing. *Neurol. Neuroimmunol. Neuroinflamm.* 7:e781. doi: 10.1212/NXI.0000000000000781

Dersch, R., Wehrum, T., Fahndrich, S., Engelhardt, M., Rauer, S., and Berger, B. (2020). COVID-19 pneumonia in a multiple sclerosis patient with severe lymphopenia due to recent cladribine treatment. *Mult. Scler.* 26, 1264–1266. doi: 10.1177/1352458520943783

Dhama, K., Khan, S., Tiwari, R., Sircar, S., Bhat, S., Malik, Y. S., et al. (2020a). Coronavirus disease 2019-COVID-19. *Clin. Microbiol. Rev.* 33:e00028-20. doi: 10.1128/CMR.00028-20

Dhama, K., Patel, S. K., Pathak, M., Yatoo, M. I., Tiwari, R., Malik, Y. S., et al. (2020b). An update on SARS-CoV-2/COVID-19 with particular reference to its clinical pathology, pathogenesis, immunopathology and mitigation strategies. *Travel. Med. Infect. Dis.* 37:101755. doi: 10.1016/j.tmaid.2020.101755

Dinkin, M., Gao, V., Kahan, J., Bobker, S., Simonetto, M., Wechsler, P., et al. (2020). COVID-19 presenting with ophthalmoparesis from cranial nerve palsy. *Neurology* 95, 221–223. doi: 10.1212/WNL.0000000000009700

Disser, N. P., De Micheli, A. J., Schonk, M. M., Konnaris, M. A., Piacentini, A. N., Edon, D. L., et al. (2020). Musculoskeletal consequences of COVID-19. *J. Bone Joint Surg. Am.* 102, 1197–1204. doi: 10.2106/JBJS.20.00847

Dixon, L., Varley, J., Gontsarova, A., Mallon, D., Tona, F., Muir, D., et al. (2020). COVID-19-related acute necrotizing encephalopathy with brain stem involvement in a patient with aplastic anemia. *Neurol. Neuroimmunol. Neuroinflamm.* 7. doi: 10.1212/NXI.0000000000000789

Dong, E., Du, H., and Gardner, L. (2020). An interactive web-based dashboard to track COVID-19 in real time. *Lancet Infect. Dis.* 20, 533–534. doi: 10.1016/S1473-3099(20)30120-1

Favas, T. T., Dev, P., Chaurasia, R. N., Chakravarty, K., Mishra, R., Joshi, D., et al. (2020). Neurological manifestations of COVID-19: a systematic review and meta-analysis of proportions. *Neurol. Sci.* 41, 3437–3470. doi: 10.1007/s10072-020-04801-y

Filatov, A., Sharma, P., Hindi, F., and Espinosa, P. S. (2020). Neurological complications of coronavirus disease (COVID-19): encephalopathy. *Cureus* 12:e7352. doi: 10.7759/cureus.7352

Gilani, S., Roditi, R., and Naraghi, M. (2020). COVID-19 and anosmia in Tehran, Iran. *Med. Hypotheses* 141:109757. doi: 10.1016/j.mehy.2020.109757

Guan, W. J., Ni, Z. Y., Hu, Y., Liang, W. H., Ou, C. Q., He, J. X., et al. (2020). Clinical characteristics of coronavirus disease 2019 in China. *N. Engl. J. Med.* 382, 1708–1720. doi: 10.1056/NEJMoa2002032

Gutierrez-Ortiz, C., Mendez-Guerrero, A., Rodrigo-Rey, S., San Pedro-Murillo, E., Bermejo-Guerrero, L., Gordo-Manas, R., et al. (2020). Miller Fisher syndrome and polyneuritis cranialis in COVID-19. *Neurology* 95, e601–e605. doi: 10.1212/WNL.0000000000009619

Haddadi, K., and Asadian, L. (2020). Coronavirus disease 2019: latest data on neuroinvasive potential. *Iran J. Med. Sci.* 45, 325–332. doi: 10.30476/ijms.2020.85980.1561

Han, Y. N., Feng, Z. W., Sun, L. N., Ren, X. X., Wang, H., Xue, Y. M., et al. (2020). A comparative-descriptive analysis of clinical characteristics in 2019-coronavirus-infected children and adults. *J. Med. Virol*. doi: 10.1002/jmv.25835. [Epub ahead of print].

Hernandez-Fernandez, F., Valencia, H. S., Barbella-Aponte, R. A., Collado-Jimenez, R., Ayo-Martin, O., Barrena, C., et al. (2020). Cerebrovascular disease in patients with COVID-19: neuroimaging, histological and clinical description. *Brain*. 143, 3089–3103. doi: 10.1093/brain/awaa239

Huang, C., Wang, Y., Li, X., Ren, L., Zhao, J., Hu, Y., et al. (2020). Clinical features of patients infected with 2019 novel coronavirus in Wuhan, China. *Lancet* 395, 497–506. doi: 10.1016/S0140-6736(20)30183-5

Ibrahim, W. (2020). Neurological manifestations in coronavirus disease 2019 (COVID-19) patients: a systematic review of literature. *CNS Spectr.* doi: 10.1017/S1092852920001935. [Epub ahead of print].

Iqbal Yatoo, M., Hamid, Z., Parray, O. R., Wani, A. H., Ul Haq, A., Saxena, A., et al. (2020). COVID-19 - recent advancements in identifying novel vaccine candidates and current status of upcoming SARS-CoV-2 vaccines. *Hum. Vaccin Immunother*. doi: 10.1080/21645515.2020.1788310l. [Epub ahead of print].

Kandemirli, S. G., Dogan, L., Sarikaya, Z. T., Kara, S., Akinci, C., Kaya, D., et al. (2020). Brain MRI findings in patients in the intensive care unit with COVID-19 infection. *Radiology*. 297, E232–E235. doi: 10.1148/radiol.2020201697

Kantonen, J., Mahzabin, S., Mayranpaa, M. I., Tynninen, O., Paetau, A., Andersson, N., et al. (2020). Neuropathologic features of four autopsied COVID-19 patients. *Brain Pathol*. doi: 10.1111/bpa.12889. [Epub ahead of print].

Kholin, A. A., Zavadenko, N. N., Nesterovskiy, Y. E., Kholina, E. A., Zavadenko, A. N., and Khondkaryan, G. S. (2020). [Features of neurological manifestations of the COVID-19 in children and adults]. *Zh. Nevrol. Psikhiatr. Im. S.S. Korsakova* 120, 114–120. doi: 10.17116/jnevro2020120091114

Khoo, A., McLoughlin, B., Cheema, S., Weil, R. S., Lambert, C., Manji, H., et al. (2020). Postinfectious brainstem encephalitis associated with SARS-CoV-2. *J. Neurol. Neurosurg. Psychiatry* 91, 1013–1014. doi: 10.1136/jnnp-2020-323816

Kohara, N., and Kawamoto, M. (2020). [COVID-19 and the hospital neurologist: how should we confront the COVID pandemic?]. *Brain Nerve.* 72, 1049–1056. doi: 10.11477/mf.1416201647

Kong, Z., Wang, J., Li, T., Zhang, Z., and Jian, J. (2020). 2019 novel coronavirus pneumonia with onset of dizziness: a case report. *Ann. Transl. Med.* 8:506. doi: 10.21037/atm.2020.03.89

Koralnik, I. J., and Tyler, K. L. (2020). COVID-19: a global threat to the nervous system. *Ann. Neurol.* 88, 1–11. doi: 10.1002/ana.25807

Krajewska, J., Krajewski, W., Zub, K., and Zatonski, T. (2020). COVID-19 in otolaryngologist practice: a review of current knowledge. *Eur. Arch. Otorhinolaryngol.* 277, 1885–1897. doi: 10.1007/s00405-020-05968-y

Kremer, S., Lersy, F., de Seze, J., Ferre, J. C., Maamar, A., Carsin-Nicol, B., et al. (2020). Brain MRI findings in severe COVID-19: a retrospective observational study. *Radiology*. 297, E242–E251. doi: 10.1148/radiol.2020202222

Kucuk, A., Cumhur Cure, M., and Cure, E. (2020). Can COVID-19 cause myalgia with a completely different mechanism? A hypothesis. *Clin. Rheumatol.* 39, 2103–2104. doi: 10.1007/s10067-020-05178-1

Kutlubaev, M. A. (2020). [Clinical and pathogenetic aspects of nervous system impairments in COVID-19]. *Zh. Nevrol. Psikhiatr. Imeni S S Korsakova* 120, 130–136. doi: 10.17116/jnevro2020120091130

Lau, H. M., Lee, E. W., Wong, C. N., Ng, G. Y., Jones, A. Y., and Hui, D. S. (2005). The impact of severe acute respiratory syndrome on the physical profile and quality of life. *Arch. Phys. Med. Rehabil.* 86, 1134–1140. doi: 10.1016/j.apmr.2004.09.025

Li, Y., Li, M., Wang, M., Zhou, Y., Chang, J., Xian, Y., et al. (2020). Acute cerebrovascular disease following COVID-19: a single center, retrospective, observational study. *Stroke Vasc. Neurol.* 5, 279–284. doi: 10.1136/svn-2020-000431

Lin, Y., Shen, X., Yang, R. F., Li, Y. X., Ji, Y. Y., He, Y. Y., et al. (2003). Identification of an epitope of SARS-coronavirus nucleocapsid protein. *Cell Res.* 13, 141–145. doi: 10.1038/sj.cr.7290158

Lu, L., Xiong, W., Liu, D., Liu, J., Yang, D., Li, N., et al. (2020). New onset acute symptomatic seizure and risk factors in coronavirus disease 2019: a retrospective multicenter study. *Epilepsia* 61, e49–e53. doi: 10.1111/epi.16524

Luigetti, M., Iorio, R., Bentivoglio, A. R., Tricoli, L., Riso, V., Marotta, J., et al. (2020). Assessment of neurological manifestations in hospitalized patients with COVID-19. *Eur. J. Neurol*. doi: 10.1111/ene.14444. [Epub ahead of print].

Mao, L., Jin, H., Wang, M., Hu, Y., Chen, S., He, Q., et al. (2020). Neurologic manifestations of hospitalized patients with coronavirus disease 2019 in Wuhan, China. *JAMA Neurol.* 77, 683–690. doi: 10.1001/jamaneurol.2020.1127

McAbee, G. N., Brosgol, Y., Pavlakis, S., Agha, R., and Gaffoor, M. (2020). Encephalitis associated with COVID-19 infection in an 11-year-old child. *Pediatr. Neurol.* 109:94. doi: 10.1016/j.pediatrneurol.2020.04.013

Mehan, W. A., Yoon, B. C., Lang, M., Li, M. D., Rincon, S., and Buch, K. (2020). Paraspinal myositis in patients with COVID-19 infection. *AJNR Am. J. Neuroradiol*. 41, 1949–1952. doi: 10.3174/ajnr.A6711

Mendez-Guerrero, A., Laespada-Garcia, M. I., Gomez-Grande, A., Ruiz-Ortiz, M., Blanco-Palmero, V. A., Azcarate-Diaz, F. J., et al. (2020). Acute hypokinetic-rigid syndrome following SARS-CoV-2 infection. *Neurology*. 95, e2109–e2118. doi: 10.1212/WNL.0000000000010282

Meng, X., Deng, Y., Dai, Z., and Meng, Z. (2020). COVID-19 and anosmia: a review based on up-to-date knowledge. *Am. J. Otolaryngol.* 41:102581. doi: 10.1016/j.amjoto.2020.102581

Morassi, M., Bagatto, D., Cobelli, M., D'Agostini, S., Gigli, G. L., Bna, C., et al. (2020). Stroke in patients with SARS-CoV-2 infection: case series. *J. Neurol.* 267, 2185–2192. doi: 10.1007/s00415-020-09885-2

Moriarty, P. M., Gorby, L. K., Stroes, E. S., Kastelein, J. P., Davidson, M., and Tsimikas, S. (2020). Lipoprotein(a) and its potential association with thrombosis and inflammation in COVID-19: a testable hypothesis. *Curr. Atheroscler. Rep*. 22:48. doi: 10.1007/s11883-020-00867-3

Moriguchi, T., Harii, N., Goto, J., Harada, D., Sugawara, H., Takamino, J., et al. (2020). A first case of meningitis/encephalitis associated with SARS-Coronavirus-2. *Int. J. Infect. Dis.* 94, 55–58. doi: 10.1016/j.ijid.2020.03.062

Muccioli, L., Pensato, U., Bernabe, G., Ferri, L., Tappata, M., Volpi, L., et al. (2020). Intravenous immunoglobulin therapy in COVID-19-related encephalopathy. *J. Neurol*. doi: 10.1007/s00415-020-10248-0. [Epub ahead of print].

Nath, A., and Smith, B. (2020). Neurological complications of COVID-19: from bridesmaid to bride. *Arq. Neuropsiquiatr.* 78, 459–460. doi: 10.1590/0004-282x20200121

Novi, G., Rossi, T., Pedemonte, E., Saitta, L., Rolla, C., Roccatagliata, L., et al. (2020). Acute disseminated encephalomyelitis after SARS-CoV-2 infection. *Neurol. Neuroimmunol. Neuroinflamm.* 7:e797. doi: 10.1212/NXI.0000000000000797

Ong, W. Y., Go, M. L., Wang, D. Y., Cheah, I. K., and Halliwell, B. (2020). Effects of antimalarial drugs on neuroinflammation-potential use for treatment of COVID-19-related neurologic complications. *Mol. Neurobiol*. doi: 10.1007/s12035-020-02093-z. [Epub ahead of print].

Oxley, T. J., Mocco, J., Majidi, S., Kellner, C. P., Shoirah, H., Singh, I. P., et al. (2020). Large-vessel stroke as a presenting feature of covid-19 in the young. *N. Engl. J. Med.* 382:e60. doi: 10.1056/NEJMc2009787

Ozcelik Korkmaz, M., Egilmez, O. K., Ozcelik, M. A., and Guven, M. (2020). Otolaryngological manifestations of hospitalised patients with confirmed COVID-19 infection. *Eur. Arch. Otorhinolaryngol.* doi: 10.1007/s00405-020-06396-8. [Epub ahead of print].

Padda, I., Khehra, N., Jaferi, U., and Parmar, M. S. (2020). The neurological complexities and prognosis of COVID-19. *SN Compr. Clin. Med.* doi: 10.1007/s42399-020-00527-2. [Epub ahead of print].

Palao, M., Fernandez-Diaz, E., Gracia-Gil, J., Romero-Sanchez, C. M., Diaz-Maroto, I., and Segura, T. (2020). Multiple sclerosis following SARS-CoV-2 infection. *Mult. Scler. Relat. Disord.* 45:102377. doi: 10.1016/j.msard.2020.102377

Parauda, S. C., Gao, V., Gewirtz, A. N., Parikh, N. S., Merkler, A. E., Lantos, J., et al. (2020). Posterior reversible encephalopathy syndrome in patients with COVID-19. *J. Neurol. Sci.* 416:117019. doi: 10.1016/j.jns.2020.117019

Parihar, J., Tripathi, M., and Dhamija, R. K. (2020). Seizures and epilepsy in times of corona virus disease 2019 pandemic. *J. Epilepsy. Res.* 10, 3–7. doi: 10.14581/jer.20002

Parsons, T., Banks, S., Bae, C., Gelber, J., Alahmadi, H., and Tichauer, M. (2020). COVID-19-associated acute disseminated encephalomyelitis (ADEM). *J. Neurol.* 267, 2799–2802. doi: 10.1007/s00415-020-09951-9

Pascual-Goni, E., Fortea, J., Martinez-Domeno, A., Rabella, N., Tecame, M., Gomez-Oliva, C., et al. (2020). COVID-19-associated ophthalmoparesis and hypothalamic involvement. *Neurol. Neuroimmunol. Neuroinflamm.* 7:e823. doi: 10.1212/NXI.0000000000000823

Pedersen, S. F., and Ho, Y. C. (2020). SARS-CoV-2: a storm is raging. *J. Clin. Invest.* 130, 2202–2205. doi: 10.1172/JCI137647

Pfefferkorn, T., Dabitz, R., von Wernitz-Keibel, T., Aufenanger, J., Nowak-Machen, M., and Janssen, H. (2020). Acute polyradiculoneuritis with locked-in syndrome in a patient with Covid-19. *J. Neurol.* 267, 1883–1884. doi: 10.1007/s00415-020-09897-y

Poyiadji, N., Shahin, G., Noujaim, D., Stone, M., Patel, S., and Griffith, B. (2020). COVID-19-associated acute hemorrhagic necrotizing encephalopathy: imaging features. *Radiology* 296, E119–E120. doi: 10.1148/radiol.2020201187

Pranata, R., Huang, I., Lim, M. A., Wahjoepramono, E. J., and July, J. (2020). Impact of cerebrovascular and cardiovascular diseases on mortality and severity of COVID-19-systematic review, meta-analysis, and meta-regression. *J. Stroke Cerebrovasc. Dis.* 29:104949. doi: 10.1016/j.jstrokecerebrovasdis.2020.104949

Puccioni-Sohler, M., Poton, A. R., Franklin, M., Silva, S. J. D., Brindeiro, R., and Tanuri, A. (2020). Current evidence of neurological features, diagnosis, and neuropathogenesis associated with COVID-19. *Rev. Soc. Bras. Med. Trop.* 53:e20200477. doi: 10.1590/0037-8682-0477-2020

Rabaan, A. A., Al-Ahmed, S. H., Sah, R., Tiwari, R., Yatoo, M. I., Patel, S. K., et al. (2020). SARS-CoV-2/COVID-19 and advances in developing potential therapeutics and vaccines to counter this emerging pandemic. *Ann. Clin. Microbiol. Antimicrob.* 19:40. doi: 10.1186/s12941-020-00384-w

Rabano-Suarez, P., Bermejo-Guerrero, L., Mendez-Guerrero, A., Parra-Serrano, J., Toledo-Alfocea, D., Sanchez-Tejerina, D., et al. (2020). Generalized myoclonus in COVID-19. *Neurology* 95, e767–e772. doi: 10.1212/WNL.0000000000009829

Rebeiz, T., Lim-Hing, K., Khazanehdari, S., and Rebeiz, K. (2020). Behavioral changes without respiratory symptoms as a presenting sign of COVID-19 encephalitis. *Cureus* 12:e10469. doi: 10.7759/cureus.10469

Reichard, R. R., Kashani, K. B., Boire, N. A., Constantopoulos, E., Guo, Y., and Lucchinetti, C. F. (2020). Neuropathology of COVID-19: a spectrum of vascular and acute disseminated encephalomyelitis (ADEM)-like pathology. *Acta Neuropathol.* 140, 1–6. doi: 10.1007/s00401-020-02166-2

Remmelink, M., De Mendonca, R., D'Haene, N., De Clercq, S., Verocq, C., Lebrun, L., et al. (2020). Unspecific post-mortem findings despite multiorgan viral spread in COVID-19 patients. *Crit. Care* 24:495. doi: 10.1186/s13054-020-03218-5

Roland, L. T., Gurrola, J. G. 2nd, Loftus, P. A., Cheung, S. W., and Chang, J. L. (2020). Smell and taste symptom-based predictive model for COVID-19 diagnosis. *Int. Forum Allergy Rhinol.* 10, 832–838. doi: 10.1002/alr.22602

Sadeghmousavi, S., and Rezaei, N. (2020). COVID-19 and multiple sclerosis: predisposition and precautions in treatment. *SN Compr. Clin. Med.* doi: 10.1007/s42399-020-00504-9. [Epub ahead of print].

Serrano-Serrano, B., Lopez-Hernandez, N., Dahl-Cruz, F., Elvira-Soler, E., and Diaz-Marin, C. (2020). [Multifocal encephalitis as a neurological manifestation of COVID-19 infection]. *Rev. Neurol.* 71, 351–352. doi: 10.33588/rn.7109.2020226

Shang, J., Wan, Y., Luo, C., Ye, G., Geng, Q., Auerbach, A., et al. (2020a). Cell entry mechanisms of SARS-CoV-2. *Proc. Natl. Acad. Sci. U.S.A.* 117, 11727–11734. doi: 10.1073/pnas.2003138117

Shang, J., Ye, G., Shi, K., Wan, Y., Luo, C., Aihara, H., et al. (2020b). Structural basis of receptor recognition by SARS-CoV-2. *Nature* 581, 221–224. doi: 10.1038/s41586-020-2179-y

Sharun, K., Tiwari, R., Dhama, J., and Dhama, K. (2020a). Dexamethasone to combat cytokine storm in COVID-19: clinical trials and preliminary evidence. *Int. J. Surg.* 82, 179–181. doi: 10.1016/j.ijsu.2020.08.038

Sharun, K., Tiwari, R., Iqbal Yatoo, M., Patel, S. K., Natesan, S., Dhama, J., et al. (2020b). Antibody-based immunotherapeutics and use of convalescent plasma to counter COVID-19: advances and prospects. *Expert Opin. Biol. Ther.* 20, 1033–1046. doi: 10.1080/14712598.2020.1796963

Sotoca, J., and Rodriguez-Alvarez, Y. (2020). COVID-19-associated acute necrotizing myelitis. *Neurol. Neuroimmunol. Neuroinflamm.* 7:e803. doi: 10.1212/NXI.0000000000000803

Sparr, S. A., and Bieri, P. L. (2020). Infarction of the splenium of the corpus callosum in the age of COVID-19: a snapshot in time. *Stroke.* 51, e223–e226. doi: 10.1161/STROKEAHA.120.030434

Spinato, G., Fabbris, C., Polesel, J., Cazzador, D., Borsetto, D., Hopkins, C., et al. (2020). Alterations in smell or taste in mildly symptomatic outpatients with SARS-CoV-2 infection. *JAMA.* 323, 2089–2090. doi: 10.1001/jama.2020.6771

Tan, L., Wang, Q., Zhang, D., Ding, J., Huang, Q., Tang, Y. Q., et al. (2020). Lymphopenia predicts disease severity of COVID-19: a descriptive and predictive study. *Signal. Transduct. Target. Ther.* 5:33. doi: 10.1038/s41392-020-0148-4

Tang, N., Li, D., Wang, X., and Sun, Z. (2020). Abnormal coagulation parameters are associated with poor prognosis in patients with novel coronavirus pneumonia. *J. Thromb. Haemost.* 18, 844–847. doi: 10.1111/jth.14768

Toscano, G., Palmerini, F., Ravaglia, S., Ruiz, L., Invernizzi, P., Cuzzoni, M. G., et al. (2020). Guillain-Barre syndrome associated with SARS-CoV-2. *N. Engl. J. Med.* 382, 2574–2576. doi: 10.1056/NEJMc2009191

Tsatsakis, A., Calina, D., Falzone, L., Petrakis, D., Mitrut, R., Siokas, V., et al. (2020). SARS-CoV-2 pathophysiology and its clinical implications: an integrative overview of the pharmacotherapeutic management of COVID-19. *Food Chem. Toxicol.* 146:111769. doi: 10.1016/j.fct.2020.111769

Uhlen, M., Fagerberg, L., Hallstrom, B. M., Lindskog, C., Oksvold, P., Mardinoglu, A., et al. (2015). Proteomics. Tissue-based map of the human proteome. *Science* 347:1260419. doi: 10.1126/science.1260419

Ur, A., and Verma, K. (2020). Cytokine storm in COVID19: a neural hypothesis. *ACS Chem. Neurosci.* 11, 1868–1870. doi: 10.1021/acschemneuro.0c00346

Utukuri, P. S., Bautista, A., Lignelli, A., and Moonis, G. (2020). Possible acute disseminated encephalomyelitis related to severe acute respiratory syndrome coronavirus 2 infection. *AJNR Am. J. Neuroradiol.* 41, E82–E83. doi: 10.3174/ajnr.A6714

Vaira, L. A., Salzano, G., Deiana, G., and De Riu, G. (2020). Anosmia and Ageusia: common findings in COVID-19 patients. *Laryngoscope* 130:1787. doi: 10.1002/lary.28692

Viana, S. D., Nunes, S., and Reis, F. (2020). ACE2 imbalance as a key player for the poor outcomes in COVID-19 patients with age-related comorbidities - role of gut microbiota dysbiosis. *Ageing Res. Rev.* 62:101123. doi: 10.1016/j.arr.2020.101123

von Oertzen, T. J., Macerollo, A., Leone, M. A., Beghi, E., Crean, M., Oztuk, S., et al. (2020). EAN consensus statement for management of patients with neurological diseases during the COVID-19 pandemic. *Eur. J. Neurol.* doi: 10.1111/ene.14521. [Epub ahead of print].

Wakerley, B. R., and Yuki, N. (2013). Infectious and noninfectious triggers in Guillain-Barre syndrome. *Expert Rev. Clin. Immunol.* 9, 627–639. doi: 10.1586/1744666X.2013.811119

Wang, L., Shen, Y., Li, M., Chuang, H., Ye, Y., Zhao, H., et al. (2020). Clinical manifestations and evidence of neurological involvement in 2019 novel coronavirus SARS-CoV-2: a systematic review and meta-analysis. *J. Neurol.* 267, 2777–2789. doi: 10.1007/s00415-020-09974-2

Wu, F., Zhao, S., Yu, B., Chen, Y. M., Wang, W., Song, Z. G., et al. (2020). A new coronavirus associated with human respiratory disease in China. *Nature* 579, 265–269. doi: 10.1038/s41586-020-2008-3

Xu, H., Zhong, L., Deng, J., Peng, J., Dan, H., Zeng, X., et al. (2020). High expression of ACE2 receptor of 2019-nCoV on the epithelial cells of oral mucosa. *Int. J. Oral. Sci.* 12:8. doi: 10.1038/s41368-020-0074-x

Xu, P., Sun, G. D., and Li, Z. Z. (2020). Clinical characteristics of two human-to-human transmitted coronaviruses: corona virus disease 2019 vs. middle east respiratory syndrome coronavirus. *Eur. Rev. Med. Pharmacol. Sci.* 24, 5797–5809. doi: 10.26355/eurrev_202005_21374

Zhang, J. J., Dong, X., Cao, Y. Y., Yuan, Y. D., Yang, Y. B., Yan, Y. Q., et al. (2020). Clinical characteristics of 140 patients infected with SARS-CoV-2 in Wuhan, China. *Allergy* 75, 1730–1741. doi: 10.1111/all.14238

Zhang, X., Cai, H., Hu, J., Lian, J., Gu, J., Zhang, S., et al. (2020). Epidemiological, clinical characteristics of cases of SARS-CoV-2 infection with abnormal imaging findings. *Int. J. Infect. Dis.* 94, 81–87. doi: 10.1016/j.ijid.2020.03.040

Zhao, H., Shen, D., Zhou, H., Liu, J., and Chen, S. (2020). Guillain-Barre syndrome associated with SARS-CoV-2 infection: causality or coincidence? *Lancet Neurol.* 19, 383–384. doi: 10.1016/S1474-4422(20)30109-5

Zhu, J., Zhong, Z., Li, H., Ji, P., Pang, J., Li, B., et al. (2020). CT imaging features of 4121 patients with COVID-19: a meta-analysis. *J. Med. Virol.* 92, 891–902. doi: 10.1002/jmv.25910

Zimniak, M., Kirschner, L., Hilpert, H., Seibel, J., and Bodem, J. (2020). The serotonin reuptake inhibitor fluoxetine inhibits SARS-CoV-2. 2014:150490. doi: 10.1101/2020.06.14.150490

Conflict of Interest: The authors declare that the research was conducted in the absence of any commercial or financial relationships that could be construed as a potential conflict of interest.

frontiers in Cell and Developmental Biology

REVIEW
published: 11 March 2021
doi: 10.3389/fcell.2021.614847

IL-35: A Novel Immunomodulator in Hepatitis B Virus-Related Liver Diseases

Xuefen Li[1†], Xia Liu[2†] and Weilin Wang[3*]*

[1] Key Laboratory of Clinical In Vitro Diagnostic Techniques of Zhejiang Province, Department of Laboratory Medicine, The First Affiliated Hospital, Zhejiang University School of Medicine, Hangzhou, China, [2] Hangzhou Global Scientific and Technological Innovation Center, Zhejiang University, Hangzhou, China, [3] Key Laboratory of Precision Diagnosis and Treatment for Hepatobiliary and Pancreatic Tumor of Zhejiang Province, Division of Hepatobiliary and Pancreatic Surgery, Department of Surgery, Clinical Research Center of Hepatobiliary and Pancreatic Diseases of Zhejiang Province, The Second Affiliated Hospital, Zhejiang University School of Medicine, Hangzhou, China

OPEN ACCESS

Edited by:
Davide Gibellini,
University of Bologna, Italy

Reviewed by:
Sheik Pran Babu Sardar Pasha,
University of California, Davis, United States
Miodrag J. Colic,
Institute for the Application of Nuclear Energy (INEP), Serbia

***Correspondence:**
Xuefen Li
zylxf@zju.edu.cn
Weilin Wang
wam@zju.edu.cn

† These authors have contributed equally to this work

Specialty section:
This article was submitted to Molecular Medicine, a section of the journal Frontiers in Cell and Developmental Biology

Received: 07 October 2020
Accepted: 19 February 2021
Published: 11 March 2021

Citation:
Li X, Liu X and Wang W (2021) IL-35: A Novel Immunomodulator in Hepatitis B Virus-Related Liver Diseases. Front. Cell Dev. Biol. 9:614847. doi: 10.3389/fcell.2021.614847

Chronic hepatitis B virus (HBV) infection is a risk factor for liver cirrhosis (LC) and hepatocellular carcinoma (HCC), however, little is known about the mechanisms involved in the progression of HBV-related diseases. It has been well acknowledged that host immune response was closely related to the clinical outcomes of patients with HBV infection. As the factors closely related to the immunomodulatory process, cytokines are crucial in the cell-cell communication and the host responses to HBV infection. Recently, a newly discovered cytokine, designated as interleukin-35 (IL-35), has been proved to be essential for the progression of chronic HBV infection, the development of cirrhosis, the transformation of cirrhosis to HCC, and the metastasis of HCC. Specifically, it showed various biological activities such as inhibiting the HBV-specific cytotoxic T lymphocyte (CTL) proliferation and cytotoxicity, deactivating the immature effector T-cells (Teffs), as well as delaying the proliferation of dendritic cells. It regulated the immune responses by acting as a "brake" on the activation of Teffs, which subsequently played important roles in the pathogenesis of various inflammatory diseases and malignancies. In this review, we focused on the most recent data on the relationship between IL-35 and chronic HBV infection, LC and HCC.

Keywords: chronic hepatitis B, interleukin-35, cytotoxic T lymphocytes, induced regulatory T-cells, immunopathology

INTRODUCTION

Hepatitis B virus (HBV) infection is still a threat to health worldwide causing chronic infection among 250 million individuals (Lee and Banini, 2019). Patients with HBV infection may develop hepatic failure, liver cirrhosis (LC), and primary hepatocellular carcinoma (HCC), resulting in a death toll of more than 1 million annually (Polaris Observatory Collaborators, 2018; Lee and Banini, 2019). The pathogenesis of HBV infection is rather complicated, which is influenced by several factors including HBV genotype, viral variation and replication. In addition, host factors (e.g., sex, age, and immune status) and other exogenous factors (e.g., hepatitis viral co-infection and alcoholism) were also reported to be involved (Tong et al., 2010; Tang et al., 2018; Terrault et al., 2018; Vlachogiannakos and Papatheodoridis, 2018). Therefore, various manifestations of HBV

infection can be seen clinically at different stages (**Table 1**). HBV is infected through person-to-person transmission at birth or after birth. Although the vaccines against HBV have been developed in the 1980s, about 1/3 of the population worldwide still showed a previous or existing HBV infection in serological tests (World Health Organization, 2013). Globally, viral hepatitis caused 1.34 million deaths in 2015. This result is similar to tuberculosis deaths (1.37 million) and is higher than HIV infections (1.06 million) and malaria (0.44 million). About 96% of these people died from complications of chronic hepatitis and most of them (66%) were diagnosed with chronic hepatitis caused by HBV. It was recognized as the disease with the highest burden by the WHO Western Pacific region (which includes 37 countries) in 2016 (World Health Organization, 2017; Seto et al., 2018).

To date, the pathogenesis of HBV infection is still not well defined. As is known to all, persistent HBV infection has been acknowledged to be closely associated with inadequate immune responses. Both innate and adaptive immunity were reported to be involved in anti-HBV immune response. During early stage of virus infection, innate sensing of viruses can occur through Toll-like receptors (TLRs) and cytosolic sensors that recognize viral DNA and RNA, then transmit a warning message to initiate downstream signals and activate effector components. In the later phase, antigen-presenting cells (APCs), including macrophages and dendritic cells (DCs), initialize the virus-specific adaptive immunity characterized by activation of T helper (Th) lymphocytes and secretion of various cytokines, which then mobilize the $CD8^+$ cytotoxic T lymphocytes (CTLs) to kill the HBV-infected hepatocytes (Bertoletti and Gehring, 2006). Previous work showed that cell-mediated immunity is critical for clearance of HBV infection, in particular, robust and multiple epitope-specific $CD8^+$ T cell responses are necessary for the spontaneous resolution of HBV infection (Thimme et al., 2003). Moreover, HBV-specific $CD4^+$ T cells are also important in determining the outcome of acute HBV infection, as shown in a chimpanzee study that the depletion of $CD4^+$ T cells abrogated the function of $CD8^+$ T cells and resulted in chronic HBV infection (Asabe et al., 2009). In addition to T-cell responses, neutralizing antibodies produced by B cells are believed to play an integral role in of HBV detection and resolution. Unlike the adaptive immune system, the innate lymphoid cells (ILCs) mainly localized at mucosal surfaces acting as sentinel cells, where release of their cytokine suite inhibits establishment and spread of HBV virus infection (Yang et al., 2015). Importantly, there is growing evidence that cytokine-mediated immune responses play an important role in determining clinical outcomes during HBV viral control and virus-induced hepatic injury (Dandri and Locarnini, 2012; Seetharam et al., 2014; Li et al., 2016).

Interleukin (IL)-35 is a newly identified cytokine of the IL-12 family and a potent immunosuppressive cytokine secreted by regulatory T (Treg) cells and the regulatory B (Breg) cells (Xiang and Xie, 2015). IL-35 and iTr35 cells develop a positive feedback loop to interact with each other, as iTr35 cells generation can be induced by IL-35, while more IL-35 is further secreted by iTr35 cells (Collison et al., 2010). Like transforming growth factor-β (TGF-β) and IL-10, IL-35 can also induce the development of induced regulatory T cell (iTreg) population (Collison et al., 2007). Moreover, IL-35 stimulation increased the inhibitory function of $CD4^+CD25^+CD127^{dim/-}$ Tregs by reducing cellular proliferation and enhancing IL-35/IL-10 productions (Mitani et al., 2015; Shi et al., 2015). Thus, the current researches suggested that the elevated proportion of Tregs might be the major source of IL-35 enhancement in the serum of patients with CHB. Besides, IL-35 also induces Breg cells formation *in vivo* and promotes their conversion to a unique Breg subset that produces IL-35 ($IL\text{-}35^+$ Breg) (Wang et al., 2014), and inhibit the proliferation and function of effector T-cells (Teffs) (Collison et al., 2007; Collison et al., 2010). A novel immunosuppresive subset named $CD8^+$ Tregs were reported in both human and mice, exerting immunoregulatory function through secreting cytokines (Flippe et al., 2019). IL-35 has also been described as expressed and playing a suppressive role for tumor-associated $CD8^+$ Tregs (Olson et al., 2012; Zhang et al., 2019). Although very few papers were published on $CD8^+$ Tregs function in HBV infection, based on the anti-inflammation role of $CD8^+$ Tregs in human disease (Vuddamalay and van Meerwijk, 2017), we hypothesize that IL-35 secreted by $CD8^+$ Tregs in CHB patients may similarly contributed to immune tolerance and exhaustion state of CTLs, therefore, targeting IL-35 secreted $CD8^+$ Tregs may provide peculiar thought for treatment of HBV infection. In conclusion, IL-35 can induce the generation of iTr35, Bregs and possibly $CD8^+$ Tregs, which function as an immunosuppressive factor in immune mediated progression of chronic hepatitis B.

The effect of IL-35 on pro-inflammatory cytokines were also reported to be involved in the pathogenesis of HBV. For instance, IL-35 stimulation notably reduced concentrations of interferon-gamma (IFN-γ), IL-1β, IL-6, and IL-8 produced by PBMCs, indicating IL-35 inhibited cytokines-induced antiviral immunity to HBV. Furthermore, the reduction of pro-inflammatory cytokine secretion in HBsAg and IL-35 co-stimulated PBMCs was accompanied by the decreased phosphorylation of STAT1 in comparison of HBsAg stimulation only group (Shao et al., 2017). Previous studies demonstrated that IL-35 showed inhibitory effects on the HBV-specific CTL response, which affected HBV clearance and modulated the pathogenesis of HCC (Li et al., 2015; Xiang and Xie, 2015; Xue et al., 2019). To our best knowledge, although more researches are exploring the role of IL-35 in human disease, few studies have been focused on the roles of IL-35 in HBV infection. In this review, we summarized the possible immunoregulatory roles of IL-35 in the pathogenesis of CHB, LC and the hepatocarcinogenesis related with HBV infection. It contributed to the proposal of potential strategies for reversing exhaustion of T cells and the treatment programs of CHB.

BIOLOGICAL PROPERTIES OF IL-35

IL-35 is a novel cytokine of the IL-12 family (Xiang and Xie, 2015). Each of IL-12 family members (e.g., IL-12, IL-23, IL-27, and IL-39) is a heterodimeric cytokine composed of α chain (i.e., p19, p28, and p35) and β chain including p40 and Epstein-Barr virus-induced gene 3 [EBI3], which contain common subunits

TABLE 1 | Clinical features of patients infected with HBV at different stages (Tong et al., 2010; Tang et al., 2018; Terrault et al., 2018; Vlachogiannakos and Papatheodoridis, 2018).

Clinical parameters	Stages of HBV infection					
	Occult HBV infection	**Inactive carrier**	**Acute self-limit HBV infection**	**Active chronic HBV infection**	**HBV-related LC**	**HBV-related HCC**
Virological markers	HBsAg (–)	HBsAg (+)	HBsAg (+)	HBsAg (+)	HBsAg (+)	HBsAg (+)
	HBeAg (–)	HBeAg (–)	HBeAg (+)	HBeAg (±)	HBeAg (±)	HBeAg (±)
	Anti-HBc (+)	Anti-HBc (±)	Anti-HBc (±)	Anti-HBc (±)	Anti-HBc (±)	Anti-HBc (±)
	Anti-HBe (±)	Anti-HBe (±)	Anti-HBe (±)	Anti-HBe (±)	Anti-HBe (±)	Anti-HBe (±)
	HBV-DNA (+)	HBV-DNA (<2,000 IU/ml)	HBV-DNA (+)	HBV-DNA (+)	HBV-DNA (±)	HBV-DNA (±)
Liver biochemistry	Normalization	Normalization	↑	↑↑	Normalization/↑	Normalization/↑/↑↑
Liver histopathology	No liver damage	Low grade inflammation	Minimal or temple liver damage	Increased liver damage	Increased liver damage	Increased liver damage
Antiviral therapy	No	No	No	Yes	Yes	Yes

HBV, Hepatitis B virus; HBsAg, Hepatitis B surface antigen; HBeAg, Hepatitis B e antigen; Anti-HBc, Antibody to HBcAg; Anti-HBe, Antibody to HBeAg; (–): Negtive; (+): Positive; (±): Positive or Negative; ↑: Increased; ↑↑: Significantly increased.

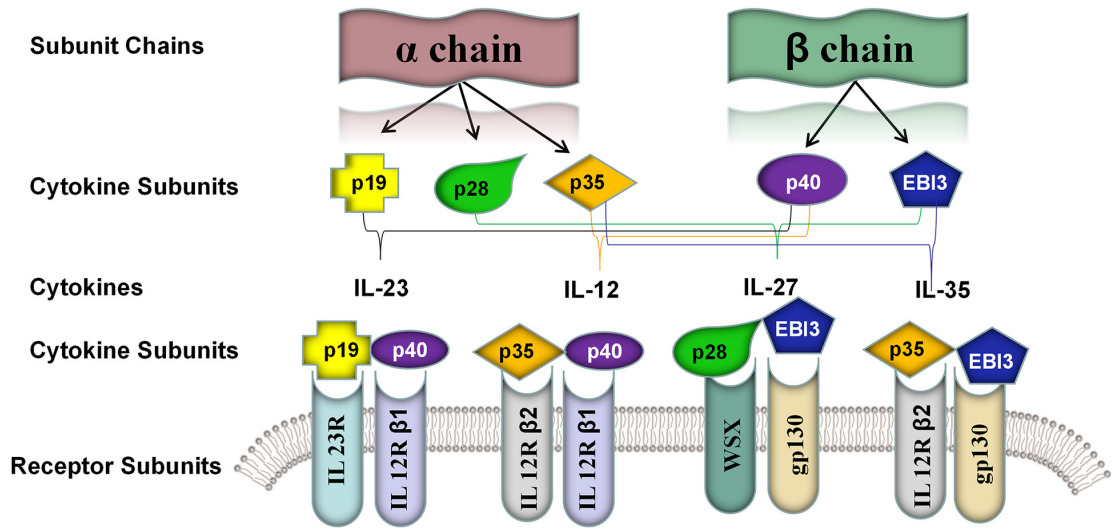

FIGURE 1 | Five known members of the IL-12 family cytokine subunits and their corresponding receptor subunits. The IL-12 family was characterized by different assembling of a α chain consisted of p19, p28, and p35 and β chain consisted of p40 and EBI3. The members of IL-12 shared the subunits and their cognate receptors including IL-23R, IL-12R-β1, IL-12R-β2, IL-27R [WSX] and gp130. IL-23: p19 and p40; IL-12: p35 and p40; IL-27: p28 and EBI3; IL-35: p35 and EBI3; IL-39: p19 and EBI3.

and receptors (**Figure 1**; Bastian et al., 2019). Structurally, it was composed of the IL-27β chain EBI3 subunit and the IL-12α chain p35 subunit. Although IL-12 family members share similar subunit structures, they have significantly different biological properties. Unlike other members of the IL-12 family, IL-35 showed strong immunosuppressive features (Collison et al., 2007; Su et al., 2018).

Human IL-35, expressed in response to inflammatory stimuli, was reported to inhibit proliferation and function of Teffs and convert the conventional $CD4^+$ T cells (Tconv) to highly inhibitory IL-35 induced regulatory T cell (iTr35), which further induced immune tolerance in hosts, and promoted viral infection (Collison et al., 2009; Shen et al., 2014). In a previous study, Collison et al. (2007) demonstrated that IL-35 was implicated in the conversion of naive T cells into iTr35 in human or mouse. Transcriptional analysis revealed that there were highly restricted genes characteristics of iTr35 ($CD4^+Foxp3^-EBI3^+p35^+IL10^-TGF\beta^-$), which were distinct from the other two types of Tregs (iTr), TGF-β-iTr ($CD4^+Foxp3^+TGF\text{-}\beta^+$) and IL-10-iTr ($CD4^+Foxp3^+IL\text{-}10^+$ or $CD4^+Foxp3^{negative}IL\text{-}10^+$), which were regulated by differential transcriptional regulators, respectively (Brockmann et al., 2018). Gene expression analysis indicated that IL-35 was distributed in broad tissues, and was a responsive anti-inflammatory cytokine induced by pro-inflammatory cytokines in a variety of non-T cells such as tumor cells, Bregs, dendritic cells (DCs), endothelial cells, smooth muscle cells, and monocytes (Li et al., 2012; Choi et al., 2015; Dixon et al., 2015).

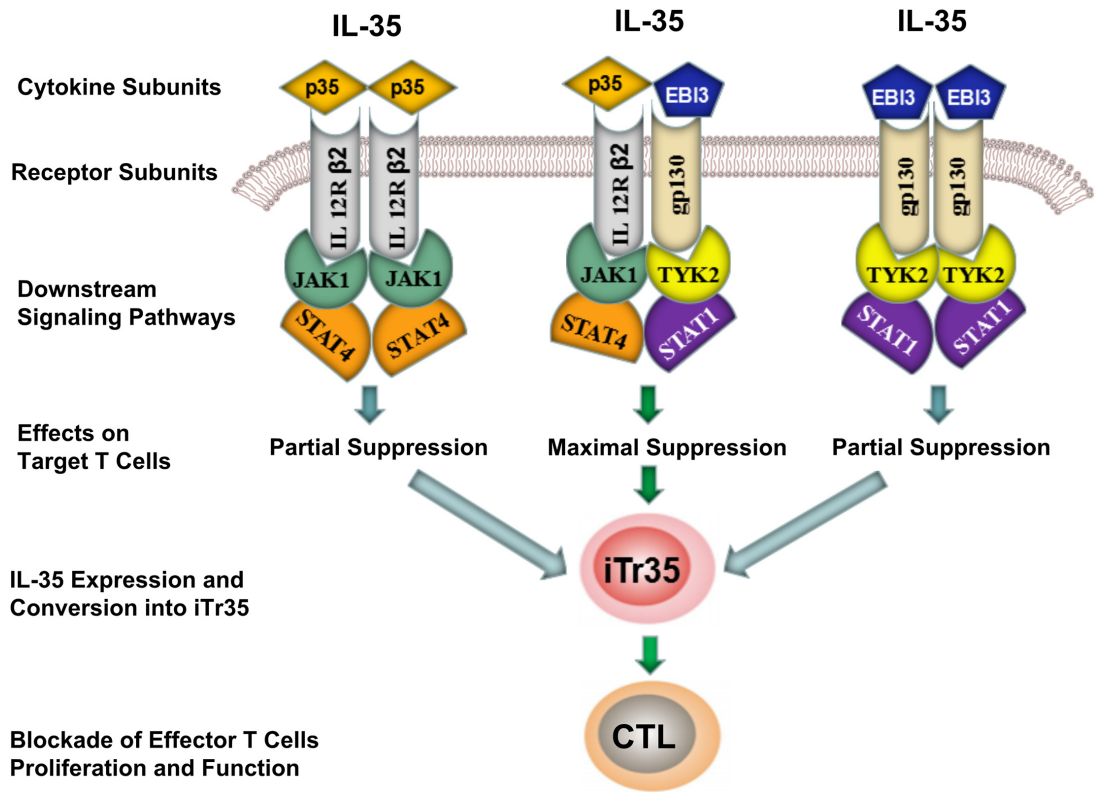

FIGURE 2 | Differences of inhibitory effects between homodimeric and heterodimeric IL-35. IL-35 signal inhibited the differentiation of effector T-cells (Teffs) by activating the intracellular JAK-STAT signaling pathway. Although both homodimeric (EBI3/EBI3 and p35/p35) and heterodimeric (EBI3/p35) IL-35 were capable of producing iTr35, the later showed a maximal suppressive activity by producing iTr35 and blocked the proliferation and function of Teffs. CTL, Cytotoxic T lymphocyte; iTr35, IL-35-producing Treg cells; JAK, Janus kinase; STAT, Signal transducer and activator of transcription.

The transmission of IL-35 signals is mainly relied on a heterodimer formed by gp130 and IL-12Rβ2 receptor chain subunits, or a homodimer of IL-12Rβ2 or gp130 subunits. IL-35 did not fully induce iTr35 transformation despite the fact that homodimeric IL-35 (i.e., EBI3/EBI3 and p35/p35) could block Teffs differentiation by activating one of its signaling pathways. In contrast, heterodimeric IL-35 (EBI3/p35) was capable of inducing iTr35 (**Figure 2**). Such difference was mainly associated with the downstream receptor signaling (Huang et al., 2017). The maximal suppressive activity of IL-35 involves the formation of a unique heterodimers of IL12Rβ2 and gp130, which subsequently binds the downstream transcriptional factors (i.e., STAT1 and STAT4). These combined transcriptional factors could uniquely bind with different sites in the *p35* and *EBI3* gene promoters. Thus, heterodimeric IL-35 contributed to the expression of p35 and EBI3, which formed a positive feedback loop modulating the secretion of IL-35 (Collison et al., 2012). As previously described, IL-35 rather than IL-12 or IFN-γ promoted the conversion of Tconv cells into iTr35. Besides, it could induce STAT1 and STAT4 activation, which demonstrated that IL-35 was highly specific to STAT1 and STAT4 (Thierfelder et al., 1996; Hoey et al., 2003; Collison et al., 2012; Louis, 2016). In future, more studies focusing on the composition and function of these downstream receptors in the IL-35 signaling pathways are required to further illustrate the potential biological properties of IL-35.

Different from IL-12 family cytokines, the inhibitory activity of IL-35 was primarily on the CTL/Th cell proliferation and effector function. Among the subpopulations of Th cells, both Th1 and Th2 have been implicated in the pathogenesis of hepatic inflammation during HBV infection (Bertoletti and Ferrari, 2012). On one hand, IL-35 significantly inhibited immune activation of Th1/CTL cells together with secretion of IL-2 and IFN-γ in inflammation and related diseases of animal disease models (Guo et al., 2017). On the other hand, IL-35 showed attenuating effects on allergen-specific $CD4^+$ memory/effector Th2 cell-mediated airway inflammation (Huang et al., 2011). Th2 cells are in favor of anti-inflammation partly depending on the production of IL-10, as well as the secretion of other cytokines (e.g., IL-4, IL-5, and IL-13), which were induced by IL-35 administration (Guo et al., 2017; Teymouri and Pirro, 2018). IL-10 is recognized as a key cytokine regulating the immune response to HBV infection. Das et al. (2012) reported that the down-regulation of IL-10 restores the function of exhausted HBV-specific $CD8^+$ T cells (Das et al., 2012; Liu et al., 2016). Moreover, IL-10 might substantially affect the antiviral immune response, as it inhibits the production of pro-inflammatory cytokines such as IFN-γ, tumor necrosis factor-alpha (TNF-α),

IL-1β, and IL-6 (Rybicka et al., 2020). As recent studies suggest that rIL-35 fusion proteins can induce Breg cells to secret IL-10 (Wang et al., 2014), hence, is possible that IL-35 induce Th2 and Breg cells to secret IL-10, which was involved in immunologic tolerance in CHB patients.

Furthermore, IL-35 stimulation was shown to inhibit the differentiation of HBV core-specific ($CD4^+CD25^+Foxp3^+$) Tregs into a IL-17-secreting $CD4^+$ T cells (Th17), and both of the Th subsets have been shown to be associated with disease progression or liver damage in CHB patients (Zhang et al., 2011; Cheng et al., 2015; Teng et al., 2019; Yang et al., 2019). Study indicated that the decreased Tregs/Th17 ratio and increased TGF-β1/IL-17 ratio can be used independently to predict the prognosis and disease progression and may be associated with the survival and disease progression of patients (Yu et al., 2014). Besides, *in vitro* IL-35 stimulation reduced Th17 cell subset and Th17 cytokine production in $CD4^+$ T cells from acute hepatitis B (AHB) patients (Teng et al., 2019). Moreover, *in vivo* treatment of IL-35 decreased the HBV-induced liver injury and reduced hepatic NK cells and HBV peptides-induced Th17 cells in HBV plasmid injected mouse model (Teng et al., 2019). Taken together, IL-35 was crucial for regulation of peripheral and hepatic HBV peptides-induced Th17 cells *in vitro* and *in vivo*, which might subsequently modulated hepatocytes damage and liver inflammation during acute HBV infection.

In CHB patients, the major biological roles of IL-35 are mainly associated with the disruption of the balance between the immunocytes, which triggered the increase of immunosuppressive cells in number and functional disorder. Meanwhile, IL-35 could trigger the decline of effector cells and the functional attenuation. It finally induced the pathogenesis and even the progression of inflammation-related diseases.

IL-35 AND CHB

For patient with HBV infection, virus elimination or persistency was closely related to the appropriate immune responses. Cytokines are known as important chemical mediators regulating the differentiation, proliferation and function of immune cells, which could trigger the pathogenesis of liver disease and affect various clinical presentations (Sodsai et al., 2013; Li et al., 2016; Nitschke et al., 2016). Accumulating evidence indicated that serum IL-35 showed significant increase in patients with chronic HBV infection. According to the previous description, serum IL-35 was positively correlated with HBV DNA load and Tregs levels, and there was a negative correlation between IL-35 and circulating effector $CD8^+$ T cells (Li et al., 2015; Moreno-Cubero and Larrubia, 2016; Nitschke et al., 2016). These supported a potential role of IL-35 and iTr35 cells in maintaining the immune tolerance during HBV infection. However, the exact role of IL-35 is still not completely understood, and further experiments and clinical trials are required to illustrate the role of IL-35 in this process.

As a responsive anti-inflammatory cytokine, IL-35 may have multifunctional roles involved in HBV-induced liver diseases (**Figure 3**). Elevation of IL-35 was reported to contribute to immunosuppression in CHB by modulating the balance between Th17 and Tregs (Collison et al., 2010; Yang et al., 2019). Some studies showed that although the plasma IL-35 levels and circulating HBV peptide-induced Th17 frequency showed significant increase in patients with hepatitis B, IL-35 expression was negatively correlated with liver inflammation (Teng et al., 2019; Yang et al., 2019). Besides, *in vivo* IL-35 administration down-regulated HBV peptides-induced Th17 cells in the liver, suggesting IL-35 might be a novel mediator associated with hepatocytes damage and liver inflammation by regulating HBV peptides-induced Th17 cells during acute HBV infection (Teng et al., 2019). Our recent study also indicated that only a small amount of IL-35 could trigger significant inhibition on the proliferation of $CD4^+CD25^-CD45RA^+$ T cells. Similarly, it could significantly inhibit DCs proliferation and promote secretion of IL-10 and IL-6. Upon synergic stimuli by HBV core antigen peptide (Collison et al., 2007, 2010; Olson et al., 2012; Wang et al., 2014; Mitani et al., 2015; Shi et al., 2015; Shao et al., 2017; Vuddamalay and van Meerwijk, 2017; Flippe et al., 2019; Zhang et al., 2019) to the peripheral blood mononuclear cells (PBMCs) of CHB patients *in vitro*, IL-35 significantly inhibited the proliferation of HBV-specific CTL cells and IFN-γ secretion (Li et al., 2015).

The regulation of IL-35 on virus-specific Tregs/Th17 balance may lead to viral persistence in chronic HBV infection. Zhou et al. (2015) showed that the IL-35 level was significant higher in $CD4^+$ T cells in patients with chronic HBV infection compared with that of the healthy individuals. Meanwhile, a high IL-35 level was related to a high HBV cccDNA replication in chronic HBV infection group, which indicated that HBV could induce the production of IL-35 by $CD4^+$ T cells. Moreover, HBV infection also involved in the activation of immune system, while IL-35 showed immunosuppressive effects upon onset of chronic HBV infection. In a previous study, Tao et al. (2018) reported that IL-35 played a novel role in HBV replication. It had shown that IL-35 participated in stimulating the transcription and replication of HBV through interacting with hepatocyte nuclear factor 4α (HNF4α). Recombinant human IL-35 (rhIL-35) promoted HBV DNA replication and secretion of HBV core antigen, hepatitis B surface antigen (HBsAg), and hepatitis B e antigen (HBeAg). This implied that HNF4α may be a target for IL-35. On this basis, mutation of the *HNF4α* binding site on the HBV core promoter or silencing *HNF4α* may abolish the IL-35-induced enhancement on HBV replication.

Among the diseases caused by viral infections, high IL-35 was found to enhance the immunosuppressive activity of Tregs, and was positively correlated with the severity of diseases (e.g., CHB) (Damo and Joshi, 2019). According to previous description, Tregs and Th17 cells were closely interacted in the pathogenesis of viral infection. Specifically, Th17 cells contributed to the immune activation and disease progression, while Tregs may inhibit such process and play crucial roles in the maintenance of immune stability (Wan et al., 2020). In cases of chronic viral infection, there was high expression of Foxp3 and low expression of CD127 in the Tregs, which may directly promote the immune tolerance through direct cellular contact and inhibitory factors (e.g., IL-10 and IL-35) (Klein et al., 2010;

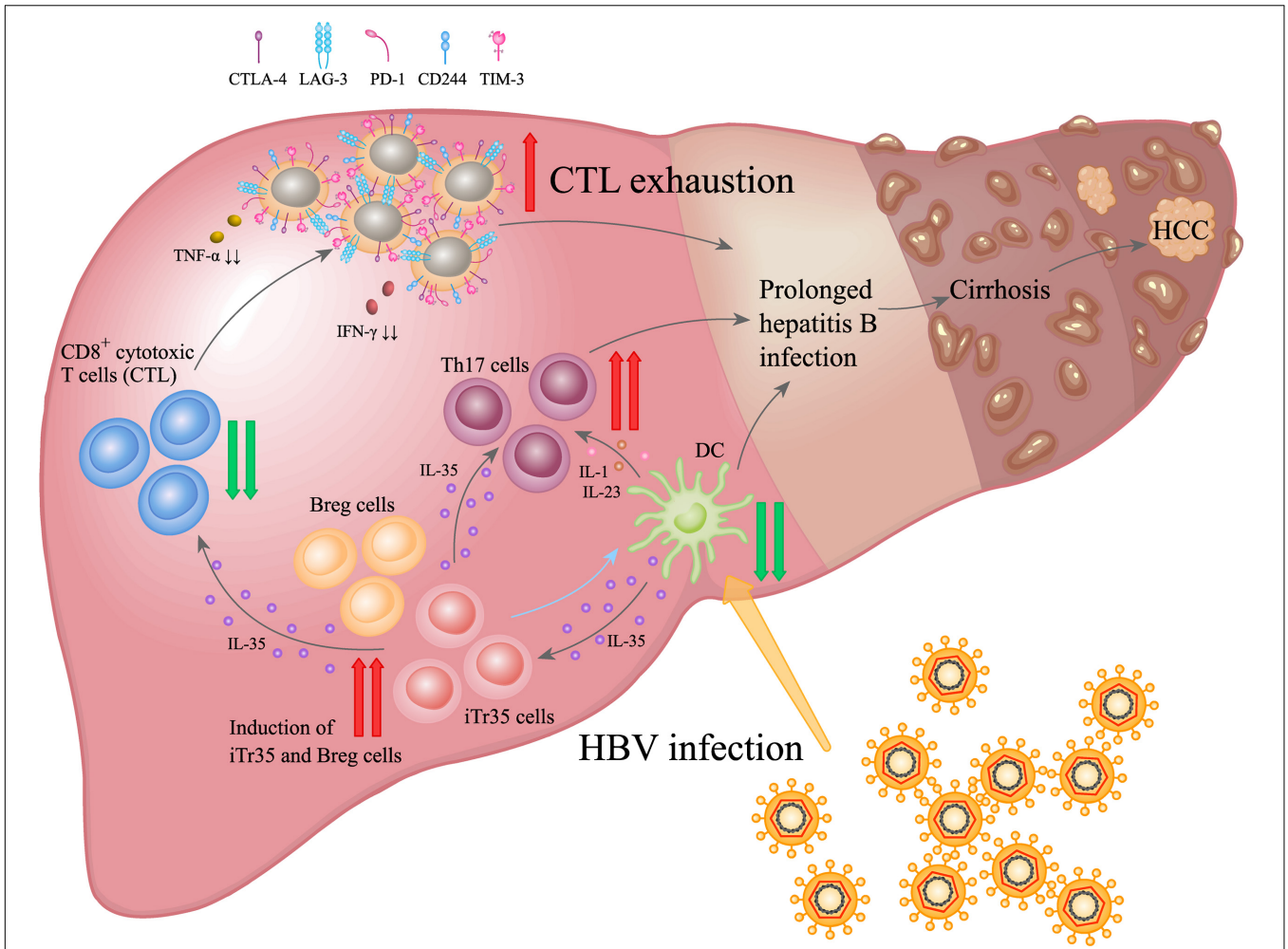

FIGURE 3 | IL-35 promoted the dynamic interaction among disease progression of HBV infection driven by immunocytes. During chronic HBV infection, IL-35 up-regulation appeared as a primary effector in suppressing CTL-mediated immunity response and reducing dendritic cells (DCs) activation. It also induced fibrosis via activating Th17 and Tregs. IL-35-mediated regulatory function was closely related to the inhibition of Teffs proliferation and function, and modulation of T-cell differentiation, as well as induction of iTr35 and Breg (IL-35 and iTr35 develop a positive feedback loop to interact each other: iTr35 can be induced by IL-35, meanwhile, more IL-35 would be further secreted by iTr35 cells), which resulted in persistent HBV infection, liver cirrhosis and hepatocellular carcinoma (HCC).

Karkhah et al., 2018). In Th17 cells, there was high expression of transcriptional factor retinoic acid-related orphan receptor γt (RORγt). Besides, it could secret the IL-17 and IL-22, which induced the hepatic inflammation and fibrosis associated with the HBV infection (Zhang et al., 2011; Zúñiga et al., 2013; Nikoopour et al., 2015; Paquissi, 2017). Tregs and Th17 imbalance was reported to be associated with the liver injury, and was also a risk factor for the hepatic fibrosis and HCC pathogenesis in CHB patients (Li et al., 2017; Liu et al., 2017). Furthermore, effective anti-viral therapy could down-regulate the response of $CD4^+$ T cells or $CD4^+CD25^+CD127^{dim/-}$ Tregs to IL-35 stimulation *in vitro* (Yang et al., 2019). Studies on Tregs in HBV infection indicated that the circulating $CD4^+CD25^+$ Tregs population was expanded in the persistence HBV infection patients (Manigold and Racanelli, 2007). It has been shown that Tregs could inhibit the HBV-specific CTL proliferation and the secretion of cytokines, which plays a role in suppressing antiviral T cell responses and aiding viral persistence (Knolle et al., 2015; Jung and Shin, 2016). Interestingly, in hepatitis B patients received anti-viral therapy, there was a decline of Tregs in the peripheral blood, accompanied with recovery of Teffs response. This contributed to the prediction of the efficiency treatment regimens (Sprengers et al., 2007; Stoop et al., 2007). In a recent study, Tregs derived IL-35 promoted the expression of $CD4^+$ Tconv, $CD8^+$ T cells and B lymphocytes inhibitory receptor, such as programmed cell death protein 1 (PD-1), T cell immunoglobulin and mucin domain 3 (TIM-3), cytotoxic T Lymphocyte-associated antigen-4 (CTLA-4) and lymphocyte activation gene 3 (LAG-3), which played important roles in the tolerance of infection (Sullivan et al., 2020).

The studies discussed above indicated that IL-35 played a double-edged sword role in the pathogenesis of CHB. Specifically, it can induce the generation of Th17 cells, which thereby regulating the inflammation. Moreover, IL-35 played

an important role in modulating the differentiation of Tregs with anti-inflammatory functions. IL-35 could trigger the up-regulation of Tregs and regulate the specific Tregs/Th17 balance, which may contribute to viral persistence in chronic HBV infection. More importantly, $CD4^+CD25^+$ Tregs are able to inhibit activation and proliferation of effective $CD4^+$ or $CD8^+$ T cells, which then suppresses the amplification of HBV-specific CTLs and secretion of cytokines. Therefore, the immunosuppressive effects of IL-35 demonstrate that IL-35 can lead to imbalance of immune response and CTL exhaustion, leading to a poor immune response to HBV. In general, the above results indicated a potential mechanism of IL-35-induced immunoregulation in chronic HBV infection.

IL-35 AND HBV-RELATED LC

Chronic HBV infection may induce deterioration of liver function through triggering liver injury and persistent liver inflammation, which subsequently resulted in paraplasm in the hepatic connective tissues and the consequential HBV-related liver fibrosis (HBV-LF), LC and even HCC (Xu et al., 2012). Various studies have suggested the pathology of HBV-related LC involves various immune components, especially immune cells and cytokines (e.g., IL-35) (Li et al., 2016; Tsai et al., 2018; Luo et al., 2019).

As mentioned above, IL-35 could directly inhibit the proliferation and function of Teffs, as well as the differentiation of Th17 cells. Meanwhile, it could expand the immunoregulatory reactions through the release of IL-35 from iTr35, which enhanced the tolerance to infection (Song and Ma, 2016). According to previous study, IL-35 pathway was closely associated with the progression of CHB to LC (liver cirrhosis), which implied that IL-35 may involve in the HBV-related LC (Shi et al., 2015). Additionally, the serum IL-35 in HBV-related LC patients was significantly higher compared with that of the normal control group, while serum IL-35 was positively correlated with IL-17, IL-22, and IL-33 which all acted as multifunctional roles involved in HBV infection (Wang et al., 2012; Zhao et al., 2014). Sun et al. (2012) indicated that the elevation of Th17 cells in hepatic cirrhosis patients would promote the activation of stellate cells in liver, which finally triggered the disease progression. At the early stage of HBV infection, Th17 could secret pro-inflammatory factors including IL-17, TGF-β and IL-22. It seems that IL-35 in LC may play a role in sustaining the pathologic process, since increase of IL-35 and other inflammatory cytokines (e.g., TGF-β, IL-22, IL-23, IL-31, and IL-33) can augment and extend hepatic inflammation (Cheng et al., 2015; Ming et al., 2015). For example, IL-35 can collaborate with TGF-β to exert immunoregulatory function and then present effective and maximal anti-inflammatory outcome (Slawek et al., 2020). Previous studies found that the mRNA and protein expression of TGF-β1 were significantly up-regulated in both the plasma and liver tissue in patients with fulminant liver failure (Miwa et al., 1997), and overexpression of TGF-β1 delayed liver regeneration and promoted perisinusoidal fibrosis and hepatocyte apoptosis in the rat model of fulminant liver failure (Yoshimoto et al., 2005). Mechanically, IL-35 could prevent the binding of TGF-β and its receptor, which inhibit phosphorylation of Smad3, a downstream effector of TGF-β receptor, thereby preventing the differentiation of Th17 cells and the synthesis of IL-17 in HBV-related LC patients (Ming et al., 2015).

All these indicated that IL-35 involved in the pathogenesis of the HBV related hepatic fibrosis. Therefore, attention should be paid to the side effects of IL-35 inhibition. Indeed, there is a long way for the application of such regimen for treating fibrotic diseases. On this basis, it is necessary to understand the relationship between IL-35 and fibrotic diseases for the development of new therapeutic approaches.

IL-35 AND HBV-RELATED HCC

Similar with the roles of IL-35 in CHB and LC, IL-35 appeared to exhibit immunosuppressive effects in HBV-related HCC. Several studies showed that high IL-35 was associated with poor prognosis in several malignancies, including HCC and gastric cancer (Friedman and Liao, 2015; Fu et al., 2016; Lumley et al., 2018; Teymouri and Pirro, 2018). Up to now, IL-35 played essential roles in restricting anti-cancer immunity and the T cell dysfunction in the tumor microenvironment. Turnis et al. (2016) revealed that Tregs derived IL-35 promoted the expression of several inhibitory receptors such as PD-1, LAG-3, and TIM-3, which then promoted the T cell exhaustion in tumor. In contrast, neutralization with an IL-35-specific antibody or Tregs-restricted deletion of IL-35 production limited tumor growth in multiple murine models of human cancer. Restriction of IL-35 level in tumor tissues contributed to the proliferation of Teffs, as well as their effecting function and the antigenic specificity. Therefore, Tregs and the associated cytokines formed the major barrier for the immunity against tumor.

In HCC tumor tissues, high IL-35 expression was associated with tumor cell invasion and poor prognosis. It was also an independent prognostic factor for HCC recurrence (Long et al., 2016; Damo and Joshi, 2019). To date, little is known about the roles of IL-35 in the pathogenesis of HCC. Secretion of IL-35 by liver tumor cells has been reported to associate with IL-35 up-regulation via a positive feedback, inhibition of proliferation, activation, cytotoxicity of $CD8^+$ T cells that promoted disease progression, and viral gene mutation and induction of tumor immune escape (Qiu et al., 2016; Damo and Joshi, 2019; Xue et al., 2019). IL-35 regulated the tumor microenvironment together with negative regulators (e.g., IL-18BP and IL-10), which played a key role in tumor immune escape, and promoted tumor progression and metastasis. It is an important factor in promoting tumorigenesis and development, and reduction of IL-35 may facilitate the control of disease progression (Xiang and Xie, 2015; Long et al., 2016). Meanwhile, it could limit the infiltration, effector function, and immune memory of antigen-specific T cells and promote the expression of various immunosuppressive receptors (e.g., PD-1, TIM3, CTLA-4, and LAG3), which thereby promoted T cell exhaustion in the tumor, and assisted tumor immune escape, tumor proliferation and

metastasis (Vignali and Kuchroo, 2012; Fu et al., 2016; Sawant and Yano, 2019).

In tumor tissues, IL-35 involved in JAK/STAT pathway phosphorylation by recruiting bone marrow-derived $CD11b^{+}Gr1^{+}$ inhibitory effector cells, which then promoted the tumor angiogenesis and immunosuppression of the tumor microenvironment (Facciabene et al., 2012; Liang et al., 2016; Long et al., 2016; Turnis et al., 2016). Therefore, the immunosuppressive activity and anti-inflammatory properties of IL-35 may be attributed to its potential in inhibiting Teffs amplification, as well as promoting the generation of IL-35 secreted iTr35 and Bregs in the tumor environment. Besides, it promoted host immune tolerance to infection and tumor cells, which played crucial roles in the pathogenesis of various diseases. This indicates that IL-35 may be a new target for the treatment of infectious diseases, malignancies, and inflammatory diseases.

POSSIBLE IMMUNOREGULATORY MECHANISM OF IL-35 IN CHB

As mentioned above, although there are various studies on the role of IL-35 in liver diseases, including CHB, LC, and HCC (**Table 2**), little is known about how IL-35 affects the HBV replication. To illustrate related mechanism, further researches are needed to investigate the immunopathology of IL-35. Currently, the immunoregulatory function of IL-35 can be depicted based on known upstream and downstream pathways (**Figure 4**). Downstream of IL-35, EBI3, and p35 subunits had been shown to form a tetramer by binding to the corresponding receptors (i.e., gp130 and IL-12Rβ2). In turn, intracellular JAK kinase was phosphorylated, which ultimately induced the phosphorylation of the downstream STAT transcriptional factor and certain gene expression upon translocation to a specific promoter site gene expression. The specific signaling pathway may be associated with the function of IL-35 (Olson et al., 2013; Egwuagu et al., 2015; Trehanpati and Vyas, 2017). In previously published study, the inhibition of Teffs proliferation and function mediated by IL-35 *in vitro* was in a dose-dependent manner, while activation of the STAT pathway was reported to participate in this process (Collison et al., 2010). However, our recent study suggested that IL-35 could activate the JAK1/TYK2-STAT1/STAT4 pathway in CTLs *in vitro*, while IFN-γ and TNF-α expression showed increase in CTLs when blocking the JAK-STAT pathway. In addition, the expression of the inhibitory receptors (e.g., PD-1, CTLA-4 and LAG-3) on CTLs was down-regulated in the presence of JAK-STAT pathway blockage (Dong et al., 2020). IL-35 triggered the inhibition of HBV-specific CTLs function by modulating the JAK1/TYK2-STAT1/STAT4 pathway. Meanwhile, JAK-STAT pathway block could recover the function of CTL. In this regard, blockage of IL-10, IL-35, and IL-35 signaling pathways (e.g., JAK1 or STAT1) would lead to restore of Teffs function. This indeed contributed to HBV clearance, which may provide a new experimental basis for immunotherapy for CHB.

More studies are needed to elucidate the possible mechanisms involved in HBV-triggering production of IL-35. Study from Liu et al. (2011) provided first evidence that HBV may act as an inducer for the $CD4^{+}$ T cells to initiate IL-35 secretion based on the data that both the mRNA expression of EBI3/p35 and the protein secretion of IL-35 were detectable in circulating $CD4^{+}$ T cells in patients with chronic hepatitis B. However, there remains a lack of research on IL-35 derived from Breg cells in HBV infection. Future investigations are needed to fully elucidate the molecular mechanism of how HBV trigger IL-35 secretion in persistent HBV infection and its related liver deterioration. With further advances in the understanding of IL-35 and its immunosuppressive mechanisms, it will be possible to design targeted immunotherapies and antivirus approaches to modulate the immune response for controlling persistent chronic HBV infection or deterioration in liver diseases.

HBV related proteins (e.g., HBx, HBs, HBc, HBe, preS1, and preS2) may be upstream protein associated with the IL-35 secretion. The *HBx* gene encoding the HBx protein was recognized as one of the most essential determinants for viral replication, dissemination, and viral-medicated pathogenesis (Slagle and Bouchard, 2018). The HBx protein served as a multifunctional HBV regulator that interacted with multiple

TABLE 2 | Immunoregulatory activities of IL-35 in HBV-related liver diseases.

Disease	Action	Role	Outcomes reported	References
CHB	Significantly increased; Positively correlated with HBV DNA load and Tregs levels	Modulate Tregs/Th17 balance; Induction of effector T-cells exhaustion and immunosuppression; Stimulating HBV transcription and replication	Lead to imbalance of immune response and contribute to viral persistence	Li et al., 2015; Zhou et al., 2015; Teng et al., 2019; Yang et al., 2019
HBV-related LC	Significantly increased; Negatively correlated with the albumin level and the Child-Pugh score	Augment and extend hepatic inflammation; Sustaining the pathologic process	Enhance the tolerance to infection, trigger the disease progression	Cheng et al., 2015; Shi et al., 2015; Sun et al., 2012; Slawek et al., 2020
HBV-related HCC	Notably elevated; Positively correlated with Treg infiltration and HCC aggressiveness; Negatively correlated with TNM stage, histological grade, tumor size, vascular invasion and lymph node metastasis	Reducing perforin expression and IFN-γ production, elevating PD-1 and CTLA-4 expression; Trigger the decline of effector T-cells and the functional attenuation	Limit effective anti-tumor immunity	Fu et al., 2016; Long et al., 2016; Qiu et al., 2016; Damo and Joshi, 2019

CHB, Chronic hepatitis B; LC, Liver cirrhosis; HCC, Hepatocellular carcinoma; TNM, Tumor node metastasis; IFN-γ, Interferon-gamma; PD-1, Programmed cell death protein 1; CTLA-4, Cytotoxic T Lymphocyte-associated antigen-4.

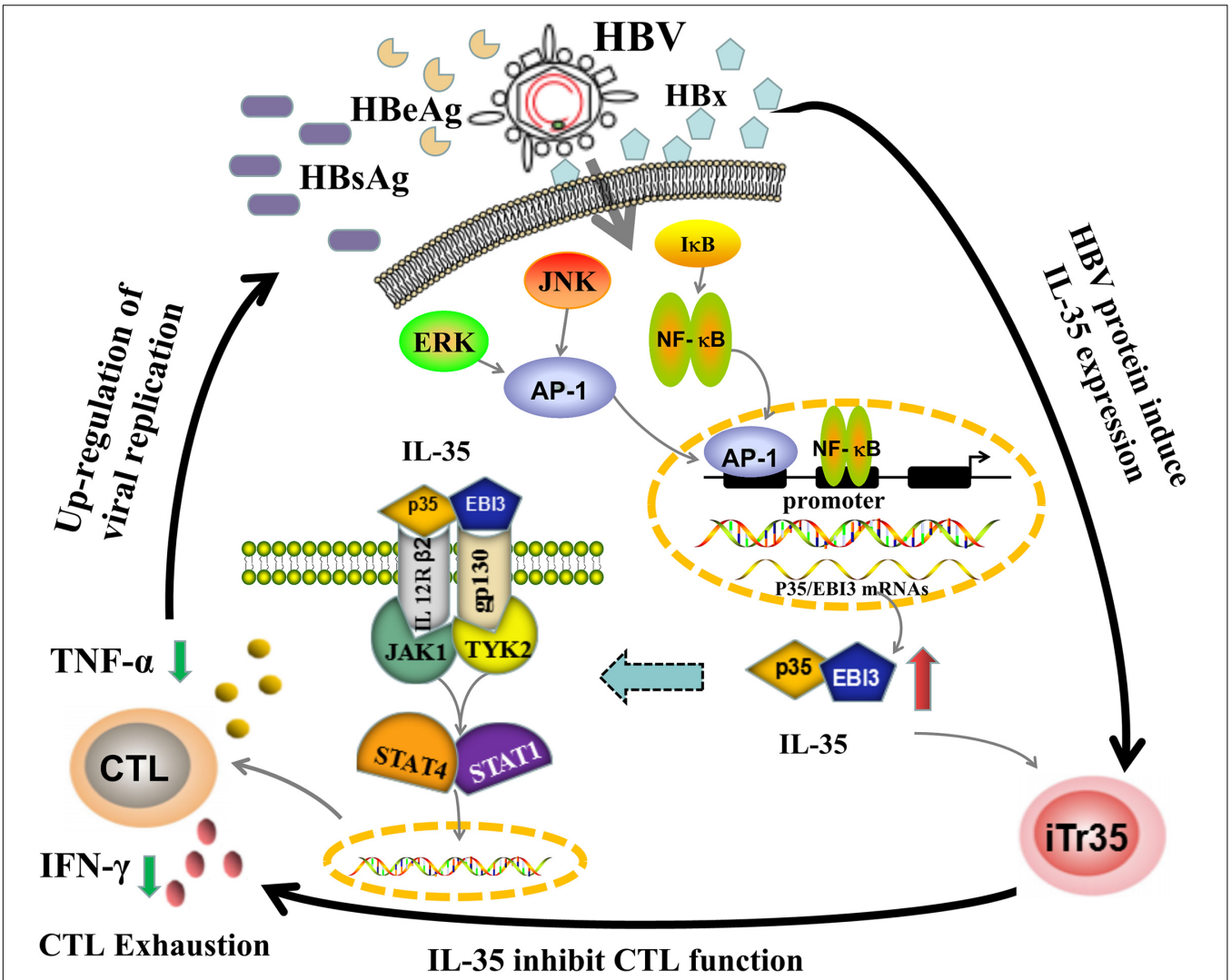

FIGURE 4 | The potential working model of IL-35 immunepathogenesis in chronic HBV infection. The mechanisms of IL-35 mediated immune-suppressive regulation in CHB may be linked to both upstream and downstream pathways. When HBV escaped the host immune system, it would trigger the release of HBV related protein especially HBx, which subsequently activated ERK/AP-1 and IκB/NF-κB signaling pathway to up-regulate IL-35 expression. The increase of IL-35 would bind to IL-12Rβ2/gp130 heterodimers receptors, yielding the formation of a tetramer. After combining to JAK1 and TYK2 kinases, the tetramer was be phosphorylated and eventually activated STAT1/STAT4 pathways by phosphorylation of their transcription factor, which tailed the HBV-specific CTLs into a state of exhaustion. The decrease of number and function of CTLs would further induce the development of chronic HBV infection. The immunological roles of IL-35 were closely related to the etiology of CHB.

protein kinases in the cytosol. Secondly, it could act as a kinase activator or co-stimulatory molecule, which then directly activated target cellular promoters and enhancers to increase viral gene expression and replication. Taken together, HBx protein participated in intracellular signal transduction, colonization and transformation, and inhibited the hepatocellular apoptosis, and invasion and metastasis of HCC (Bagga et al., 2016). In the pathogenesis of CHB, HBx could activate ERK and NF-κB signaling pathways, and then triggered the up-regulation of IL-23 and over-expression of the transcription factor AP-1 of ERK/JNK signaling pathway that contributed to the proliferation of hepatoma cells (Shan et al., 2010; Xia et al., 2012). Also, it was implicated with the metabolism of arachidonic acid and activation of the ERK signaling pathway and its positive feedback loop, which subsequently promoted the pathogenesis of hepatic inflammation (Cho et al., 2015). Recently, it has been proposed that there are binding sites for AP-1 and NF-κB transcription factors in the p35/EBI3 subunit gene promoters. In particular, NF-κB can directly activate the *EBI3* gene promoter in bone marrow-derived DCs (Li et al., 2012; Song and Ma, 2016). Therefore, up-regulation of IL-35 expression in CHB patients may be mediated by the HBx/ERK/NF-κB pathway, which inhibited the function of Teffs and attenuated the antiviral immunity in hosts. Considering the roles of IL-35 on the receptors and/or signaling pathways during HBV infection, it is reasonable to speculate that IL-35 may serve

as a novel immunotherapy target for chronic HBV infection related diseases.

CHALLENGES AND PROSPECTS

HBV infection has caused great health problems and heavy economic burdens. Oral administration of nucleos(t)ide analogs is the main treatment option for anti-HBV therapy with most cases achieving a high virological suppression. For example, in patients treated with entecavir and tenofovir, more than 95% of patients' serum HBV DNA were below the detection limit. In addition, the long-term suppression of the virus by nucleo(t)ide analog therapy also resulted in significant improvement in liver histology and reduced the incidence of liver cirrhosis, as well as hepatocellular carcinoma (Wong et al., 2013; Wu et al., 2014; Seto et al., 2018). Its main disadvantages include the necessity of lifelong treatment, difficulty in the clearance of HBsAg in serum and the possibility of HBV reactivation. Therefore, there is an urgent need to explore new anti-inflammatory points and drug targets in order to establish effective treatment options. For the immunoregulatory therapy in treating HBV infection, it is necessary to develop regimens based on blocking checkpoint inhibitor, specific T cell vaccines and genetically engineered T cells such as chimeric antigen receptor (CAR) and TCR redirected T cells. These contribute to the restoration of aberrant HBV specific responses, which promoted the clearance of serum HBsAg (Ye et al., 2015; Boni et al., 2019a; Bertoletti and Tan, 2020). Previous studies suggested that intervention strategies may be helpful to the recovery of depleted T cells by blocking co-inhibitory pathways (Boni et al., 2019a; Meng et al., 2020). However, most of them are in the preclinical or phase I or II stage. These therapies include HBV-specific immunomodulators, such as immunostimulants [e.g., Inarigivir (SB 9200) and the anti-PD-1 antibody nivolumab] and therapeutic vaccines (e.g., GS-4774 and TG-1050) (Martin et al., 2017; Verdon et al., 2017; Yuen et al., 2018; Boni et al., 2019b). A novel CAR construct is developed to exert a profound influence on the expansion, differentiation, development, and survival of lymphocytes (Boni et al., 2019a; Bertoletti and Tan, 2020). Kruse et al. (2018) also reported that HBsAg-CAR T cells have anti-HBV activity in an authentic preclinical HBV infection animal model. In addition, this new immunoregulatory therapy in treating HBV infection can reduce the HBsAg concentration to varying degrees, and induce HBsAg serum clearance in a few cases. Above experimental evidences suggest that immune-based therapies constitute a promising immune modulatory approach for a therapeutic restoration of protective immunity and serve as a new direction of current research in the field of liver diseases. Therefore, due to the IL-35 play a unique role in the IL-12 family and show immunosuppressive activities on Teffs during HBV infection. Assessing the tissue and cellular origins of IL-35 during chronic HBV infection will help determine its potential as a biomarker for the diagnosis and prognostic evaluation of HBV. Elucidation of the immunopathologic roles of IL-35 in the progression of CHB may contribute to promise candidates for the development of new immunotherapeutic strategies targeting IL-35.

AUTHOR CONTRIBUTIONS

XLi drafted and revised the manuscript. XLiu participated in data collection and modified the figures. WW was critically revised and given the final approval of the version to be published. All authors have read and approved the article.

FUNDING

This work was supported, in part, by the grants from the National Natural Science Foundation of China (Nos. 82072357 and 81672092), and the Major National S&T Projects for Infectious Diseases (2017ZX10202201-002-004).

REFERENCES

Asabe, S., Wieland, S. F., Chattopadhyay, P. K., Roederer, M., Engle, R. E., Purcell, R. H., et al. (2009). The size of the viral inoculum contributes to the outcome of hepatitis B virus infection. *J. Virol.* 83, 9652–9662. doi: 10.1128/JVI.00867-09

Bagga, S., Rawat, S., Ajenjo, M., and Bouchard, M. J. (2016). Hepatitis B virus (HBV) X protein-mediated regulation of hepatocyte metabolic pathways affects viral replication. *Virology* 498, 9–22. doi: 10.1016/j.virol.2016.08.006

Bastian, D., Wu, Y., Betts, B. C., and Yu, X. Z. (2019). The IL-12 cytokine and receptor family in graft-vs.-host disease. *Front. Immunol.* 10:988. doi: 10.3389/fimmu.2019.00988

Bertoletti, A., and Ferrari, C. (2012). Innate and adaptive immune responses in chronic hepatitis B virus infections: towards restoration of immune control of viral infection. *Gut* 61, 1754–1764. doi: 10.1136/gutjnl-2011-301073

Bertoletti, A., and Gehring, A. J. (2006). The immune response during hepatitis B virus infection. *J. Gen. Virol.* 87(Pt 6), 1439–1449. doi: 10.1099/vir.0.81920-0

Bertoletti, A., and Tan, A. T. (2020). HBV as a target for CAR or TCR-T cell therapy. *Curr. Opin. Immunol.* 66, 35–41. doi: 10.1016/j.coi.2020.04.003

Boni, C., Barili, V., Acerbi, G., Rossi, M., Vecchi, A., Laccabue, D., et al. (2019a). HBV immune-therapy: from molecular mechanisms to clinical applications. *Int. J. Mol. Sci.* 20:2754. doi: 10.3390/ijms20112754

Boni, C., Janssen, H. L. A., Rossi, M., Yoon, S. K., Vecchi, A., Barili, V., et al. (2019b). Combined GS-4774 and tenofovir therapy can improve HBV-specific t-cell responses in patients with chronic hepatitis. *Gastroenterology* 157, 227–241 e7. doi: 10.1053/j.gastro.2019.03.044

Brockmann, L., Soukou, S., Steglich, B., Czarnewski, P., Zhao, L., Wende, S., et al. (2018). Molecular and functional heterogeneity of IL-10-producing CD4(+) T cells. *Nat. Commun.* 9:5457. doi: 10.1038/s41467-018-07581-4

Cheng, L. S., Liu, Y., and Jiang, W. (2015). Restoring homeostasis of CD4+ T cells in hepatitis-B-virus-related liver fibrosis. *World J. Gastroenterol.* 21, 10721–10731. doi: 10.3748/wjg.v21.i38.10721

Cho, H. K., Kim, S. Y., Kyaw, Y. Y., Win, A. A., Koo, S. H., Kim, H. H., et al. (2015). HBx induces the proliferation of hepatocellular carcinoma cells via AP1 over-expressed as a result of ER stress. *Biochem. J.* 466, 115–121. doi: 10.1042/bj20140819

Choi, J., Leung, P. S., Bowlus, C., and Gershwin, M. E. (2015). IL-35 and autoimmunity: a comprehensive perspective. *Clin. Rev. Allergy Immunol.* 49, 327–332. doi: 10.1007/s12016-015-8468-9

Collison, L. W., Chaturvedi, V., Henderson, A. L., Giacomin, P. R., Guy, C., Bankoti, J., et al. (2010). IL-35-mediated induction of a potent regulatory T cell population. *Nat. Immunol.* 11, 1093–1101. doi: 10.1038/ni.1952

Collison, L. W., Delgoffe, G. M., Guy, C. S., Vignali, K. M., Chaturvedi, V., Fairweather, D., et al. (2012). The composition and signaling of the IL-35 receptor are unconventional. *Nat. Immunol.* 13, 290–299. doi: 10.1038/ni.2227

Collison, L. W., Pillai, M. R., Chaturvedi, V., and Vignali, D. A. (2009). Regulatory T cell suppression is potentiated by target T cells in a cell contact, IL-35- and IL-10-dependent manner. *J. Immunol.* 182, 6121–6128. doi: 10.4049/jimmunol.0803646

Collison, L. W., Workman, C. J., Kuo, T. T., Boyd, K., Wang, Y., Vignali, K. M., et al. (2007). The inhibitory cytokine IL-35 contributes to regulatory T-cell function. *Nature* 450, 566–569. doi: 10.1038/nature06306

Damo, M., and Joshi, N. S. (2019). T(reg) cell IL-10 and IL-35 exhaust CD8(+) T cells in tumors. *Nat. Immunol.* 20, 674–675. doi: 10.1038/s41590-019-0389-y

Dandri, M., and Locarnini, S. (2012). New insight in the pathobiology of hepatitis B virus infection. *Gut* 61(Suppl. 1), i6–i17. doi: 10.1136/gutjnl-2012-302056

Das, A., Ellis, G., Pallant, C., Lopes, A. R., Khanna, P., Peppa, D., et al. (2012). IL-10-producing regulatory B cells in the pathogenesis of chronic hepatitis B virus infection. *J. Immunol.* 189, 3925–3935. doi: 10.4049/jimmunol.1103139

Dixon, K. O., van der Kooij, S. W., Vignali, D. A., and van Kooten, C. (2015). Human tolerogenic dendritic cells produce IL-35 in the absence of other IL-12 family members. *Eur. J. Immunol.* 45, 1736–1747. doi: 10.1002/eji.201445217

Dong, Y., Li, X., Yu, Y., Lv, F., and Chen, Y. (2020). JAK/STAT signaling is involved in IL-35-induced inhibition of hepatitis B virus antigen-specific cytotoxic T cell exhaustion in chronic hepatitis B. *Life Sci.* 252, 117663. doi: 10.1016/j.lfs.2020.117663

Egwuagu, C. E., Yu, C. R., Sun, L., and Wang, R. (2015). Interleukin 35: critical regulator of immunity and lymphocyte-mediated diseases. *Cytokine Growth Factor Rev.* 26, 587–593. doi: 10.1016/j.cytogfr.2015.07.013

Facciabene, A., Motz, G. T., and Coukos, G. (2012). T-regulatory cells: key players in tumor immune escape and angiogenesis. *Cancer Res.* 72, 2162–2171. doi: 10.1158/0008-5472.can-11-3687

Flippe, L., Bezie, S., Anegon, I., and Guillonneau, C. (2019). Future prospects for CD8(+) regulatory T cells in immune tolerance. *Immunol. Rev.* 292, 209–224. doi: 10.1111/imr.12812

Friedman, A., and Liao, K. L. (2015). The role of the cytokines IL-27 and IL-35 in cancer. *Math. Biosci. Eng.* 12, 1203–1217. doi: 10.3934/mbe.2015.12.1203

Fu, Y.-P., Yi, Y., Cai, X.-Y., Sun, J., Ni, X.-C., He, H.-W., et al. (2016). Overexpression of interleukin-35 associates with hepatocellular carcinoma aggressiveness and recurrence after curative resection. *Br. J. Cancer* 114, 767–776. doi: 10.1038/bjc.2016.47

Guo, H., Zhao, N., Gao, H., and He, X. (2017). Mesenchymal stem cells overexpressing interleukin-35 propagate immunosuppressive effects in mice. *Scand. J. Immunol.* 86, 389–395. doi: 10.1111/sji.12613

Hoey, T., Zhang, S., Schmidt, N., Yu, Q., Ramchandani, S., Xu, X., et al. (2003). Distinct requirements for the naturally occurring splice forms Stat4alpha and Stat4beta in IL-12 responses. *EMBO J.* 22, 4237–4248. doi: 10.1093/emboj/cdg393

Huang, A., Cheng, L., He, M., Nie, J., Wang, J., and Jiang, K. (2017). Interleukin-35 on B cell and T cell induction and regulation. *J. Inflamm. (Lond.)* 14:16. doi: 10.1186/s12950-017-0164-5

Huang, C. H., Loo, E. X. I, Kuo, C., Soh, G. H., Goh, D. L., Lee, B. W., et al. (2011). Airway inflammation and IgE production induced by dust mite allergen-specific memory/effector Th2 cell line can be effectively attenuated by IL-35. *J. Immunol.* 187, 462–471. doi: 10.4049/jimmunol.1100259

Jung, M. K., and Shin, E. C. (2016). Regulatory T cells in hepatitis B and C virus infections. *Immune Netw.* 16, 330–336. doi: 10.4110/in.2016.16.6.330

Karkhah, A., Javanian, M., and Ebrahimpour, S. (2018). The role of regulatory T cells in immunopathogenesis and immunotherapy of viral infections. *Infect. Genet. Evol.* 59, 32–37. doi: 10.1016/j.meegid.2018.01.015

Klein, S., Kretz, C. C., Krammer, P. H., and Kuhn, A. (2010). CD127(low/-) and FoxP3(+) expression levels characterize different regulatory T-cell populations in human peripheral blood. *J. Invest. Dermatol.* 130, 492–499. doi: 10.1038/jid.2009.313

Knolle, P. A., Böttcher, J., and Huang, L. R. (2015). The role of hepatic immune regulation in systemic immunity to viral infection. *Med. Microbiol. Immunol.* 204, 21–27. doi: 10.1007/s00430-014-0371-0

Kruse, R. L., Shum, T., Tashiro, H., Barzi, M., Yi, Z., Whitten-Bauer, C., et al. (2018). HBsAg-redirected T cells exhibit antiviral activity in HBV-infected human liver chimeric mice. *Cytotherapy* 20, 697–705. doi: 10.1016/j.jcyt.2018.02.002

Lee, H. M., and Banini, B. A. (2019). Updates on chronic HBV: current challenges and future goals. *Curr. Treat. Options Gastroenterol.* 17, 271–291. doi: 10.1007/s11938-019-00236-3

Li, K., Liu, H., and Guo, T. (2017). Th17/Treg imbalance is an indicator of liver cirrhosis process and a risk factor for HCC occurrence in HBV patients. *Clin. Res. Hepatol. Gastroenterol.* 41, 399–407. doi: 10.1016/j.clinre.2016.12.004

Li, X., Liu, X., Tian, L., and Chen, Y. (2016). Cytokine-mediated immunopathogenesis of hepatitis B virus infections. *Clin. Rev. Allergy Immunol.* 50, 41–54. doi: 10.1007/s12016-014-8465-4

Li, X., Mai, J., Virtue, A., Yin, Y., Gong, R., Sha, X., et al. (2012). IL-35 is a novel responsive anti-inflammatory cytokine–a new system of categorizing anti-inflammatory cytokines. *PLoS One* 7:e33628. doi: 10.1371/journal.pone.0033628

Li, X., Tian, L., Dong, Y., Zhu, Q., Wang, Y., Han, W., et al. (2015). IL-35 inhibits HBV antigen-specific IFN-γ-producing CTLs in vitro. *Clin. Sci. (Lond.)* 129, 395–404. doi: 10.1042/cs20140511

Liang, Y., Chen, Q., Du, W., Chen, C., Li, F., Yang, J., et al. (2016). Epstein-barr virus-induced gene 3 (EBI3) blocking leads to induce antitumor cytotoxic t lymphocyte response and suppress tumor growth in colorectal cancer by bidirectional reciprocal-regulation STAT3 signaling pathway. *Mediators Inflamm.* 2016:3214105. doi: 10.1155/2016/3214105

Liu, B., Gao, W., Zhang, L., Wang, J., Chen, M., Peng, M., et al. (2017). Th17/Treg imbalance and increased interleukin-21 are associated with liver injury in patients with chronic severe hepatitis B. *Int. Immunopharmacol.* 46, 48–55. doi: 10.1016/j.intimp.2017.02.019

Liu, F., Tong, F., He, Y., and Liu, H. (2011). Detectable expression of IL-35 in CD4+ T cells from peripheral blood of chronic hepatitis B patients. *Clin. Immunol.* 139, 1–5. doi: 10.1016/j.clim.2010.12.012

Liu, Y., Cheng, L. S., Wu, S. D., Wang, S. Q., Li, L., She, W. M., et al. (2016). IL-10-producing regulatory B-cells suppressed effector T-cells but enhanced regulatory T-cells in chronic HBV infection. *Clin. Sci. (Lond.)* 130, 907–919. doi: 10.1042/CS20160069

Long, J., Guo, H., Cui, S., Zhang, H., Liu, X., Li, D., et al. (2016). IL-35 expression in hepatocellular carcinoma cells is associated with tumor progression. *Oncotarget* 7, 45678–45686. doi: 10.18632/oncotarget.10141

Louis, P. R. B. I. V. S. (2016). "Post-transcriptional regulation of cytokine signaling during inflammatory responses," in *Post-Transcriptional Mechanisms in Endocrine Regulation*, eds K. Menon and A. Goldstrohm (Cham: Springer), 55–70. doi: 10.1007/978-3-319-25124-0_3

Lumley, S. F., McNaughton, A. L., Klenerman, P., Lythgoe, K. A., and Matthews, P. C. (2018). Hepatitis B virus adaptation to the CD8+ T cell response: consequences for host and pathogen. *Front. Immunol.* 9:1561. doi: 10.3389/fimmu.2018.01561

Luo, M., Peng, H., Chen, P., and Zhou, Y. (2019). The immunomodulatory role of interleukin-35 in fibrotic diseases. *Expert Rev. Clin. Immunol.* 15, 431–439. doi: 10.1080/1744666x.2019.1564041

Manigold, T., and Racanelli, V. (2007). T-cell regulation by CD4 regulatory T cells during hepatitis B and C virus infections: facts and controversies. *Lancet Infect. Dis.* 7, 804–813. doi: 10.1016/s1473-3099(07)70289-x

Martin, C. F., Sprinzl, F., Leroy, V., Pol, S., Habersetzer, F., Thimme, R., et al. (2017). Phase 1b clinical trial of TG1050 a novel HBV-targeted immunotherapy in NUC suppressed chronic hepatitis B (CHB) patients: safety and early immunological data following single administration. *Hepatology* 66(suppl. 1), 483A–484A.

Meng, Z., Chen, Y., and Lu, M. (2020). Advances in targeting the innate and adaptive immune systems to cure chronic hepatitis B virus infection. *Front. Immunol.* 10:3127. doi: 10.3389/fimmu.2019.03127

Ming, D., Yu, X., Guo, R., Deng, Y., Li, J., Lin, C., et al. (2015). Elevated TGF-β1/IL-31 pathway is associated with the disease severity of hepatitis B virus-related liver cirrhosis. *Viral. Immunol.* 28, 209–216. doi: 10.1089/vim.2014.0142

Mitani, A., Niedbala, W., Fujimura, T., Mogi, M., Miyamae, S., Higuchi, N., et al. (2015). Increased expression of interleukin (IL)-35 and IL-17, but not IL-27, in gingival tissues with chronic periodontitis. *J. Periodontol.* 86, 301–309. doi: 10.1902/jop.2014.140293

Miwa, Y., Harrison, P. M., Farzaneh, F., Langley, P. G., Williams, R., and Hughes, R. D. (1997). Plasma levels and hepatic mRNA expression of transforming growth factor-beta1 in patients with fulminant hepatic failure. *J. Hepatol.* 27, 780–788. doi: 10.1016/s0168-8278(97)80313-3

Moreno-Cubero, E., and Larrubia, J. R. (2016). Specific CD8(+) T cell response immunotherapy for hepatocellular carcinoma and viral hepatitis. *World J. Gastroenterol.* 22, 6469–6483. doi: 10.3748/wjg.v22.i28.6469

Nikoopour, E., Bellemore, S. M., and Singh, B. (2015). IL-22, cell regeneration and autoimmunity. *Cytokine* 74, 35–42. doi: 10.1016/j.cyto.2014.09.007

Nitschke, K., Luxenburger, H., Kiraithe, M. M., Thimme, R., and Neumann-Haefelin, C. (2016). CD8+ T-cell responses in hepatitis B and C: the (HLA-) A, B, and C of hepatitis B and C. *Dig. Dis.* 34, 396–409. doi: 10.1159/000444555

Olson, B. M., Jankowska-Gan, E., Becker, J. T., Vignali, D. A., Burlingham, W. J., and McNeel, D. G. (2012). Human prostate tumor antigen-specific CD8+ regulatory T cells are inhibited by CTLA-4 or IL-35 blockade. *J. Immunol.* 189, 5590–5601. doi: 10.4049/jimmunol.1201744

Olson, B. M., Sullivan, J. A., and Burlingham, W. J. (2013). Interleukin 35: a key mediator of suppression and the propagation of infectious tolerance. *Front. Immunol.* 4:315. doi: 10.3389/fimmu.2013.00315

Paquissi, F. C. (2017). Immunity and fibrogenesis: the role of Th17/IL-17 Axis in HBV and HCV-induced chronic hepatitis and progression to cirrhosis. *Front. Immunol.* 8:1195. doi: 10.3389/fimmu.2017.01195

Polaris Observatory Collaborators (2018). Global prevalence, treatment, and prevention of hepatitis B virus infection in 2016: a modelling study. *Lancet Gastroenterol. Hepatol.* 3, 383–403. doi: 10.1016/s2468-1253(18)30056-6

Qiu, X., Wang, X., Song, Y., and Chen, L. (2016). Plasma level of interleukin-35 as an independent prognostic indicator in hepatocellular carcinoma. *Dig. Dis. Sci.* 61, 3513–3521. doi: 10.1007/s10620-016-4270-7

Rybicka, M., Woziwodzka, A., Sznarkowska, A., Romanowski, T., Stalke, P., Dreczewski, M., et al. (2020). Genetic variation in IL-10 influences the progression of hepatitis B infection. *Int. J. Infect. Dis.* 96, 260–265. doi: 10.1016/j.ijid.2020.04.079

Sawant, D. V., and Yano, H. (2019). Adaptive plasticity of IL-10(+) and IL-35(+) T(reg) cells cooperatively promotes tumor T cell exhaustion. *Nat. Immunol.* 20, 724–735. doi: 10.1038/s41590-019-0346-9

Seetharam, A., Perrillo, R., and Gish, R. (2014). Immunosuppression in patients with chronic hepatitis B. *Curr. Hepatol. Rep.* 13, 235–244. doi: 10.1007/s11901-014-0238-2

Seto, W.-K., Lo, Y.-R., Pawlotsky, J.-M., and Yuen, M.-F. (2018). Chronic hepatitis B virus infection. *Lancet* 392, 2313–2324. doi: 10.1016/s0140-6736(18)31865-8

Shan, C., Xu, F., Zhang, S., You, J., You, X., Qiu, L., et al. (2010). Hepatitis B virus X protein promotes liver cell proliferation via a positive cascade loop involving arachidonic acid metabolism and p-ERK1/2. *Cell Res.* 20, 563–575. doi: 10.1038/cr.2010.49

Shao, X., Ma, J., Jia, S., Yang, L., Wang, W., and Jin, Z. (2017). Interleukin-35 suppresses antiviral immune response in chronic hepatitis B virus infection. *Front. Cell. Infect. Microbiol.* 7:472. doi: 10.3389/fcimb.2017.00472

Shen, P., Roch, T., Lampropoulou, V., O'Connor, R. A., Stervbo, U., Hilgenberg, E., et al. (2014). IL-35-producing B cells are critical regulators of immunity during autoimmune and infectious diseases. *Nature* 507, 366–370. doi: 10.1038/nature12979

Shi, M., Wei, J., Dong, J., Meng, W., Ma, J., Wang, T., et al. (2015). Function of interleukin-17 and -35 in the blood of patients with hepatitis B-related liver cirrhosis. *Mol. Med. Rep.* 11, 121–126. doi: 10.3892/mmr.2014.2681

Slagle, B. L., and Bouchard, M. J. (2018). Role of HBx in hepatitis B virus persistence and its therapeutic implications. *Curr. Opin. Virol.* 30, 32–38. doi: 10.1016/j.coviro.2018.01.007

Slawek, A., Lorek, D., Kedzierska, A. E., and Chelmonska-Soyta, A. (2020). Regulatory B cells with IL-35 and IL-10 expression in a normal and abortion-prone murine pregnancy model. *Am. J. Reprod. Immunol.* 83:e13217. doi: 10.1111/aji.13217

Sodsai, P., Surakiatchanukul, T., Kupatawintu, P., Tangkitvanich, P., and Hirankarn, N. (2013). Association of cytokine and cytokine receptor gene polymorphisms with the risk of chronic hepatitis B. *Asian Pac.J. Allergy Immunol.* 31, 277–285. doi: 10.12932/ap0284.31.4.2013

Song, M., and Ma, X. (2016). The immunobiology of interleukin-35 and its regulation and gene expression. *Adv. Exp. Med. Biol.* 941, 213–225. doi: 10.1007/978-94-024-0921-5_10

Sprengers, D., Stoop, J. N., Binda, R. S., Kusters, J. G., Haagmans, B. L., Carotenuto, P., et al. (2007). Induction of regulatory T-cells and interleukin-10-producing cells in non-responders to pegylated interferon-alpha therapy for chronic hepatitis B. *Antivir. Ther.* 12, 1087–1096.

Stoop, J. N., van der Molen, R. G., Kuipers, E. J., Kusters, J. G., and Janssen, H. L. (2007). Inhibition of viral replication reduces regulatory T cells and enhances the antiviral immune response in chronic hepatitis B. *Virology* 361, 141–148. doi: 10.1016/j.virol.2006.11.018

Su, L. C., Liu, X. Y., Huang, A. F., and Xu, W. D. (2018). Emerging role of IL-35 in inflammatory autoimmune diseases. *Autoimmun. Rev.* 17, 665–673. doi: 10.1016/j.autrev.2018.01.017

Sullivan, J. A., Tomita, Y., Jankowska-Gan, E., Lema, D. A., Arvedson, M. P., Nair, A., et al. (2020). Treg-cell-derived IL-35-coated extracellular vesicles promote infectious tolerance. *Cell Rep.* 30, 1039–1051.e5. doi: 10.1016/j.celrep.2019.12.081

Sun, H. Q., Zhang, J. Y., Zhang, H., Zou, Z. S., Wang, F. S., and Jia, J. H. (2012). Increased Th17 cells contribute to disease progression in patients with HBV-associated liver cirrhosis. *J. Viral. Hepat.* 19, 396–403. doi: 10.1111/j.1365-2893.2011.01561.x

Tang, L. S. Y., Covert, E., Wilson, E., and Kottilil, S. (2018). Chronic hepatitis B infection. *JAMA* 319:1802. doi: 10.1001/jama.2018.3795

Tao, N. N., Gong, R., Chen, X., He, L., Ren, F., Yu, H. B., et al. (2018). Interleukin-35 stimulates hepatitis B virus transcription and replication by targeting transcription factor HNF4α. *J. Gen. Virol.* 99, 645–654. doi: 10.1099/jgv.0.001050

Teng, D. K., Liu, Y., Lv, Y. F., Wang, L., Zhang, W., Wang, J. P., et al. (2019). Elevated interleukin-35 suppresses liver inflammation by regulation of T helper 17 cells in acute hepatitis B virus infection. *Int. Immunopharmacol.* 70, 252–259. doi: 10.1016/j.intimp.2019.02.048

Terrault, N. A., Lok, A. S. F., McMahon, B. J., Chang, K. M., Hwang, J. P., Jonas, M. M., et al. (2018). Update on prevention, diagnosis, and treatment of chronic hepatitis B: AASLD 2018 hepatitis B guidance. *Hepatology* 67, 1560–1599. doi: 10.1002/hep.29800

Teymouri, M., and Pirro, M. (2018). IL-35, a hallmark of immune-regulation in cancer progression, chronic infections and inflammatory diseases. *Int. J. Cancer* 143, 2105–2115. doi: 10.1002/ijc.31382

Thierfelder, W. E., van Deursen, J. M., Yamamoto, K., Tripp, R. A., Sarawar, S. R., Carson, R. T., et al. (1996). Requirement for Stat4 in interleukin-12-mediated responses of natural killer and T cells. *Nature* 382, 171–174. doi: 10.1038/382171a0

Thimme, R., Wieland, S., Steiger, C., Ghrayeb, J., Reimann, K. A., Purcell, R. H., et al. (2003). CD8(+) T cells mediate viral clearance and disease pathogenesis during acute hepatitis B virus infection. *J. Virol.* 77, 68–76. doi: 10.1128/jvi.77.1.68-76.2003

Tong, M. J., Hsu, L., Hsien, C., Kao, J. H., Durazo, F. A., Saab, S., et al. (2010). A comparison of hepatitis B viral markers of patients in different clinical stages of chronic infection. *Hepatol. Int.* 4, 516–522. doi: 10.1007/s12072-010-9179-1

Trehanpati, N., and Vyas, A. K. (2017). Immune regulation by T regulatory cells in hepatitis B virus-related inflammation and cancer. *Scand. J. Immunol.* 85, 175–181. doi: 10.1111/sji.12524

Tsai, K. N., Kuo, C. F., and Ou, J. J. (2018). Mechanisms of hepatitis B virus persistence. *Trends Microbiol.* 26, 33–42. doi: 10.1016/j.tim.2017.07.006

Turnis, M. E., Sawant, D. V., Szymczak-Workman, A. L., Andrews, L. P., Delgoffe, G. M., Yano, H., et al. (2016). Interleukin-35 limits anti-tumor immunity. *Immunity* 44, 316–329. doi: 10.1016/j.immuni.2016.01.013

Verdon, D., Brooks, A. E., Gaggar, A., Woo, J., Schwabe, C., Subramanian, M., et al. (2017). Immunological assessment of HBeAg-negative chronic hepatitis B patient responses following anti-PD-1 treatment. *Hepatology* 66(suppl. 1):23A.

Vignali, D. A., and Kuchroo, V. K. (2012). IL-12 family cytokines: immunological playmakers. *Nat. Immunol.* 13, 722–728. doi: 10.1038/ni.2366

Vlachogiannakos, J., and Papatheodoridis, G. V. (2018). Hepatitis B: who and when to treat? *Liver Int* 38(Suppl. 1), 71–78. doi: 10.1111/liv.13631

Vuddamalay, Y., and van Meerwijk, J. P. (2017). CD28(-) and CD28(low)CD8(+) Regulatory T Cells: of Mice and Men. *Front. Immunol.* 8:31. doi: 10.3389/fimmu.2017.00031

Wan, Z., Zhou, Z., Liu, Y., Lai, Y., Luo, Y., Peng, X., et al. (2020). Regulatory T cells and T helper 17 cells in viral infection. *Scand. J. Immunol.* 91:e12873. doi: 10.1111/sji.12873

Wang, J., Cai, Y., Ji, H., Feng, J., Ayana, D. A., Niu, J., et al. (2012). Serum IL-33 levels are associated with liver damage in patients with chronic hepatitis B. *J. Interferon Cytokine Res.* 32, 248–253. doi: 10.1089/jir.2011.0109

Wang, R. X., Yu, C. R. I, Dambuza, M., Mahdi, R. M., Dolinska, M. B., Sergeev, Y. V., et al. (2014). Interleukin-35 induces regulatory B cells that suppress autoimmune disease. *Nat. Med.* 20, 633–641. doi: 10.1038/nm.3554

Wong, G. L.-H., Chan, H. L.-Y., Mak, C. W.-H., Lee, S. K.-Y., Ip, Z. M.-Y., Lam, A. T.-H., et al. (2013). Entecavir treatment reduces hepatic events and deaths in chronic hepatitis B patients With liver cirrhosis. *Hepatology* 58, 1537–1547. doi: 10.1002/hep.26301

World Health Organization (2013). *Global Alert and Response (GAR). Hepatitis B*. Available online at: http://www.who.int/csr/disease/hepatitis/whocdscsrlyo20022/en/index1.html (accessed May 29, 2019).

World Health Organization (2017). *Global Hepatitis Report*. Geneva: World Health Organization.

Wu, C.-Y., Lin, J.-T., Ho, H. J., Su, C.-W., Lee, T.-Y., Wang, S.-Y., et al. (2014). Association of Nucleos(t)ide analogue therapy with reduced risk of hepatocellular carcinoma in patients with chronic hepatitis B—A Nationwide cohort study. *Gastroenterology* 147, 143–151.e5. doi: 10.1053/j.gastro.2014.03.048

Xia, L., Tian, D., Huang, W., Zhu, H., Wang, J., Zhang, Y., et al. (2012). Upregulation of IL-23 expression in patients with chronic hepatitis B is mediated by the HBx/ERK/NF-κB pathway. *J. Immunol.* 188, 753–764. doi: 10.4049/jimmunol.1101652

Xiang, X. G., and Xie, Q. (2015). IL-35 a potential therapeutic target for controlling hepatitis B virus infection. *J. Dig. Dis.* 16, 1–6. doi: 10.1111/1751-2980.12218

Xu, R., Zhang, Z., and Wang, F. S. (2012). Liver fibrosis: mechanisms of immune-mediated liver injury. *Cell. Mol. Immunol.* 9, 296–301. doi: 10.1038/cmi.2011.53

Xue, W., Yan, D., and Kan, Q. (2019). Interleukin-35 as an emerging player in tumor microenvironment. *J. Cancer* 10, 2074–2082. doi: 10.7150/jca.29170

Yang, L., Jia, S., Shao, X., Liu, S., Zhang, Q., Song, J., et al. (2019). Interleukin-35 modulates the balance between viral specific CD4(+)CD25(+)CD127(dim/-) regulatory T cells and T helper 17 cells in chronic hepatitis B virus infection. *Virol. J.* 16:48. doi: 10.1186/s12985-019-1158-0

Yang, Z., Tang, T., Wei, X., Yang, S., and Tian, Z. (2015). Type 1 innate lymphoid cells contribute to the pathogenesis of chronic hepatitis B. *Innate Immun.* 21, 665–673. doi: 10.1177/1753425915586074

Ye, B., Liu, X., Li, X., Kong, H., Tian, L., and Chen, Y. (2015). T-cell exhaustion in chronic hepatitis B infection: current knowledge and clinical significance. *Cell Death Dis.* 6:e1694. doi: 10.1038/cddis.2015.42

Yoshimoto, N., Togo, S., Kubota, T., Kamimukai, N., Saito, S., Nagano, Y., et al. (2005). Role of transforming growth factor-beta1 (TGF-beta1) in endotoxin-induced hepatic failure after extensive hepatectomy in rats. *J. Endotoxin Res.* 11, 33–39. doi: 10.1179/096805105225006650

Yu, X., Guo, R., Ming, D., Su, M., Lin, C., Deng, Y., et al. (2014). Ratios of regulatory T cells/T-helper 17 cells and transforming growth factor-beta1/interleukin-17 to be associated with the development of hepatitis B virus-associated liver cirrhosis. *J. Gastroenterol. Hepatol.* 29, 1065–1072. doi: 10.1111/jgh.12459

Yuen, M. F., Elkashab, M., Chen, C. Y., Coffin, C., Fung, S., Greenbloom, S., et al. (2018). Dose response and safety of the daily, oral RIG-I agonist Inarigivir (SB 9200) in treatment naïve patients with chronic hepatitis B: results from the 25mg and 50mg cohorts in the ACHIEVE trial. *J. Hepatol.* 68, S509–S510. doi: 10.1016/s0168-8278(18)31267-4

Zhang, J., Zhang, Y., Wang, Q., Li, C., Deng, H., Si, C., et al. (2019). Interleukin-35 in immune-related diseases: protection or destruction. *Immunology* 157, 13–20. doi: 10.1111/imm.13044

Zhang, Y., Cobleigh, M. A., Lian, J. Q., Huang, C. X., Booth, C. J., Bai, X. F., et al. (2011). A proinflammatory role for interleukin-22 in the immune response to hepatitis B virus. *Gastroenterology* 141, 1897–1906. doi: 10.1053/j.gastro.2011.06.051

Zhao, J., Zhang, Z., Luan, Y., Zou, Z., Sun, Y., Li, Y., et al. (2014). Pathological functions of interleukin-22 in chronic liver inflammation and fibrosis with hepatitis B virus infection by promoting T helper 17 cell recruitment. *Hepatology* 59, 1331–1342. doi: 10.1002/hep.26916

Zhou, Y., Zhang, H., and Li, Y. (2015). IL-35 expression in peripheral blood CD4(+) T cells from chronic hepatitis B virus-infected patients directly correlates with virus load. *Cytokine* 73, 169–175. doi: 10.1016/j.cyto.2015.02.003

Zúñiga, L. A., Jain, R., Haines, C., and Cua, D. J. (2013). Th17 cell development: from the cradle to the grave. *Immunol. Rev.* 252, 78–88. doi: 10.1111/imr.12036

Conflict of Interest: The authors declare that the research was conducted in the absence of any commercial or financial relationships that could be construed as a potential conflict of interest.

frontiers in Cell and Developmental Biology

REVIEW
published: 27 April 2021
doi: 10.3389/fcell.2021.578825

The Mechanisms and Animal Models of SARS-CoV-2 Infection

Wenrui Jia[1†], Juan Wang[1†], Bao Sun[2], Jiecan Zhou[3], Yamin Shi[1] and Zheng Zhou[1*]*

[1] Department of Chinese Medicine, The First Affiliated Hospital of Zhengzhou University, Zhengzhou, China, [2] Department of Pharmacy, The Second Xiangya Hospital, Central South University, Changsha, China, [3] Institute of Clinical Medicine, The First Affiliated Hospital, University of South China, Hengyang, China

Coronavirus disease 2019 (COVID-19) is a highly contagious disease caused by severe acute respiratory syndrome coronavirus 2 (SARS-CoV-2), which has aroused great public health concern worldwide. Currently, COVID-19 epidemic is spreading in many countries and regions around the world. However, the study of SARS-CoV-2 is still in its infancy, and there is no specific therapeutics. Here, we summarize the genomic characteristics of SARS-CoV-2. In addition, we focus on the mechanisms of SARS-CoV-2 infection, including the roles of angiotensin converting enzyme II (ACE2) in cell entry, COVID-19 susceptibility and COVID-19 symptoms, as well as immunopathology such as antibody responses, lymphocyte dysregulation, and cytokine storm. Finally, we introduce the research progress of animal models of COVID-19, aiming at a better understanding of the pathogenesis of COVID-19 and providing new ideas for the treatment of this contagious disease.

Keywords: angiotensin converting enzyme II, animal models, immunopathology, pathogenesis, severe acute respiratory syndrome coronavirus 2

OPEN ACCESS

Edited by:
Giulia De Falco,
Queen Mary University of London, United Kingdom

Reviewed by:
Dengke Bao,
Henan University, China
Roberto Bruzzone,
Institut Pasteur, France

****Correspondence:***
Yamin Shi
shiyamin06@163.com
Zheng Zhou
zhouzheng037@163.com

[†] These authors have contributed equally to this work

Specialty section:
This article was submitted to Molecular Medicine, a section of the journal Frontiers in Cell and Developmental Biology

Received: *01 July 2020*
Accepted: *12 April 2021*
Published: *27 April 2021*

Citation:
Jia W, Wang J, Sun B, Zhou J, Shi Y and Zhou Z (2021) The Mechanisms and Animal Models of SARS-CoV-2 Infection. Front. Cell Dev. Biol. 9:578825. doi: 10.3389/fcell.2021.578825

INTRODUCTION

Coronavirus disease 2019 (COVID-19), caused by severe acute respiratory syndrome coronavirus 2 (SARS-CoV-2), is a highly contagious disease (Wu F. et al., 2020; Zhou P. et al., 2020; Zhu N. et al., 2020). Its most common symptoms are fever, cough, and fatigue, while other symptoms include sputum production, headache, gastrointestinal symptoms, liver injury, and even olfactory and gustatory dysfunctions (Guan et al., 2020; Lechien et al., 2020; Lin et al., 2020; Zhang C. et al., 2020). Meanwhile, the typical chest computerized tomography (CT) imaging features are ground glass opacities in bilateral multiple lobular, consolidation, adjacent pleura thickening and combined linear opacities (Xu et al., 2020). Unlike previously infected coronaviruses, SARS-CoV-2 is identified as the seventh member of the coronavirus family that infects humans (Zhu N. et al., 2020). COVID-19 has spread to many countries and regions and was judged as the sixth public health emergency of international concern (PHEIC) by the World Health Organization (WHO) (Eurosurveillance Editorial Team, 2020). As of March 2021, more than 120 million cases of COVID-19 have been reported worldwide, including 2.7 million deaths (European Centre for Disease Prevention and Control, 2021).

The bat was considered to be a probable natural reservoir host of SARS-CoV-2, whose whole genome was highly similar to a bat coronavirus RaTG13, with a genome sequence identity of 96.2% (Zhou P. et al., 2020). Considering that SARS-CoV is transmitted to humans through masked palm civets and middle east respiratory syndrome coronavirus (MERS-CoV) through

dromedary camels, it is also possible that SARS-CoV-2 has intermediate hosts that mediate its transmission (Guan et al., 2003; Alagaili et al., 2014). The latest study discovered that multiple lineages of pangolin coronavirus were similar to SARS-CoV-2, suggesting that pangolin might be a potential intermediate host for the new coronavirus (Lam et al., 2020; Zhang T. et al., 2020). Epidemiologically, the prevalence of COVID-19 is high and the population is generally susceptible, but people with chronic underlying diseases such as diabetes, hypertension, and heart disease are more susceptible to this virus (Wang D. et al., 2020). So far, the study of SARS-CoV-2 is still in its infancy. In this paper, we focus on the mechanisms and animal models of SARS-CoV-2 infection, in order to provide a theoretical basis for understanding the pathogenesis of COVID-19 and the prevention and treatment of the disease.

GENOMIC CHARACTERIZATION OF SARS-CoV-2

Phylogenetic analysis showed that SARS-CoV-2 was a new betacoronavirus belonging to the sarbecovirus subgenus of Coronaviridae family, which had the typical features of betacoronavirus, such as 5′ untranslated region (UTR), replicase complex (orf1ab) gene, Spike (S) gene, Envelope (E) gene, Membrane (M) gene, Nucleocapsid (N) gene, and 3′ UTR (Zhu N. et al., 2020). The nucleotide sequence of the S gene of SARS-CoV-2 was less than 75% identical to the nucleotide sequence of all the previously described SARS-related coronaviruses, except for a 93.1% identity to the bat coronavirus RaTG13 (Zhou P. et al., 2020). Compared to SARS-CoV, the SARS-CoV-2 S gene had three short insertions in the N-terminal domain and changes in four of the key residues in the receptor-binding motif. Furthermore, the SARS-CoV-2 orf8 was distant from the conserved orf8 or orf8b of SARS-CoV, and this new orf8 might encode a protein with an alpha-helix, following with a beta-sheet(s) (Chan and Kok, 2020). During the SARS epidemic, a common genetic change in SARS-CoV genome was the major deletions in the orf8 region (Chinese SARS Molecular Epidemiology Consortium, 2004; Muth and Corman, 2018). Interestingly, orf8 deletion SARS-CoV-2 variants seem to be associated with mild infections (Su and Anderson, 2020; Young et al., 2020a). In mammals, the zinc finger antiviral protein (ZAP) mediated the degradation of the RNA genome by specifically binding to the CpG dinucleotide in the viral RNA genome (Takata et al., 2017). Notably, among all known betacoronavirus, the CpG defect in the SARS-CoV-2 genome was the most severe, indicating that SARS-CoV-2 might have evolved in a host with high ZAP expression (Xia, 2020). Yang and Chen (2020) discovered that the composition of human-specific slow codons and two consecutive slow codons in SARS-CoV-2 and SARS-CoV was lower than that of other coronaviruses, indicating that these two coronaviruses might have faster protein synthesis. In addition, compared with SARS, bat SARS and MERS-CoV, SARS-CoV-2 had higher codon bias and gene expression efficiency (Kandeel et al., 2020). Specifically, most high frequency codons ended in A or T, while low frequency codons ended in G or C. Meanwhile, the effective number of codon (ENc) values of the SARS-CoV-2 structural proteins was 5–20 lower. These unique genomic features provide the basis for understanding the source and pathogenicity of this novel coronavirus.

PATHOGENICITY OF SARS-CoV-2

Roles of Angiotensin Converting Enzyme II (ACE2) in SARS-CoV-2 Infection

Receptor Interactions and Cell Entry

Coronavirus infection depends on the binding of its own S glycoprotein to cellular receptors and on the priming of S glycoprotein by cellular proteases. Preliminary studies found that SARS-CoV-2 entered host cells through the same receptor angiotensin converting enzyme II (ACE2) as SARS-CoV (Zhou P. et al., 2020). Moreover, VeroE6 cells with high expression of transmembrane protease serine 2 (TMPRSS2) were very susceptible to SARS-CoV-2 infection, suggesting that TMPRSS2 might be a key protease for SARS-CoV-2 cell entry and replication (Matsuyama et al., 2020). Consistently, Hoffmann et al. (2020b) demonstrated that ACE2 mediated the cell entry of SARS-CoV-2, while the serine protease TMPRSS2 was used for S protein priming. Meanwhile, camostat mesylate, a TMPRSS2 inhibitor, could block SARS-CoV-2 infection of lung cells, indicating that TMPRSS2 inhibitors might be a potential strategy for the treatment of COVID-19. Furthermore, TMPRSS2 was highly expressed in secretory cells, ciliated cells and type I alveolar epithelial cells (AT1), and SARS-CoV-2 RNA could be detected in these cells, indicating that SARS-CoV-2 mainly infected the secretory cells, ciliated cells and AT1 in lung epithelium (Schuler et al., 2021). Importantly, the expression of TMPRSS2 in cells increased with aging in mice and humans, which might partly explain the rarity of severe respiratory disease in children. Cryo–electron microscopy showed that the main state of the SARS-CoV-2 S trimer has one of the three receptor-binding domains (RBDs) rotated up in an accessible conformation of the receptor (Wrapp and Wang, 2020). Furthermore, the overall interface between the RBD of S glycoprotein and peptidase domain (PD) of ACE2 mediated mainly through the interactions of polar residues (Yan and Zhang, 2020). Specifically, an extended loop region of the RBD crossed the arch-shaped α1 helix of the PD, and the α2 helix and the loop connecting the β3 and β4 antiparallel chains of the PD also contributed to the coordination of RBD.

Noteworthily, SARS-CoV-2 mainly entered 293/hACE2 cells through endocytosis, and phosphatidylinositol 3-phosphate 5-kinase (PIKfyve) and two pore channel subtype 2 (TPC2) played an important role in this process (Ou et al., 2020). Moreover, cathepsins in lysosome, especially cathepsin L, were involved in the priming of SARS-CoV-2 S protein. In particular, the S glycoprotein of SARS-CoV-2 contained a furin-like cleavage site within the S1/S2 domain, which was potentially involved in the priming of S protein (Wang Q. et al., 2020). Hoffmann et al. (2020a) discovered that furin could cleave the S glycoprotein at the S1/S2 site, and this cleavage promoted the S protein-mediated virus-cell fusion and cell-cell fusion. Collectively, these

endogenous molecules such as ACE2, TMPRSS2, and furin were essential for SARS-CoV-2 infection, which could serve as potential targets for the treatment of COVID-19.

ACE2 and COVID-19 Susceptibility

Angiotensin converting enzyme II is the receptor for the entry of SARS-CoV-2 into host cells. Therefore, it is easy to think that its high expression may increase the susceptibility to infection. Based on this, the researchers found that many factors, including population, cancer, lupus, smoking, obesity and diabetes, all may increase the risk of COVID-19.

The genetic analysis of ACE2 in different populations showed that the East Asian populations had higher allele frequencies (AFs) of the expression quantitative trait loci (eQTL) variants than European populations, and these variants were associated with high ACE2 expression in tissues, indicating that different populations might have different susceptibility to SARS-CoV-2 (Cao et al., 2020a). Chai et al. (2020) discovered that ACE2 was overexpressed in certain cancers, such as colon adenocarcinoma, rectal adenocarcinoma, gastric adenocarcinoma, kidney renal papillary cell carcinoma, pancreatic adenocarcinoma, and lung adenocarcinoma. Meanwhile, ACE2 in tumors with high ACE2 expression usually showed hypomethylation. These results explain the higher risk of COVID-19 in cancer patients from the perspective of ACE2. Similarly, lupus patients also presented overexpression and hypomethylation of ACE2, suggesting that patients with such autoimmune diseases might have increased sensitivity COVID-19 (Sawalha et al., 2020). Meanwhile, the epigenetic dysregulation of interferon (IFN)-regulated genes in lupus patients might enhance the immune response to SARS-CoV-2, thereby increasing the severity of COVID-19. Of note, ACE2 expression was upregulated in the small airway epithelia of smokers and patients with chronic obstructive pulmonary disease (COPD), which partly explained the increased risk of SARS-CoV-2 infection in these people (Leung et al., 2020). Consistently, mice exposed to cigarette smoke showed a dose-dependent increase in ACE2 expression, while quitting smoking reduced ACE2 levels in cells (Smith et al., 2020). In-depth research found that ACE2 was mainly expressed in a subset of secretory cells of the lung epithelium, and cigarette smoke could increase the number of ACE2+ cells by stimulating the expansion of secretory cells. Interestingly, overweight COPD patients have higher expression levels of ACE2, indicating that obesity is also a risk factor for COVID-19 (Higham and Singh, 2020). Furthermore, a phenome-wide Mendelian randomization (MR) study showed that diabetes and its related traits were associated with increased expression of ACE2 in the lung, which in turn might mediate susceptibility to COVID-19 (Rao et al., 2020).

ACE2 and COVID-19 Symptoms

By analyzing the expression levels of ACE2 in 31 normal human tissues, Li M. Y. et al. (2020) found that small intestine, testis, kidney, heart, thyroid, and adipose tissue expressed high levels of ACE2, and lung, colon, liver, bladder, and adrenal gland expressed moderate levels of ACE2, while blood, spleen, bone marrow, brain, blood vessels, and muscle expressed low levels of ACE2. Importantly, ACE2 expression was related to the immune signatures of each tissue. For example, the expression of ACE2 in the lungs of the elderly was positively correlated with immune signatures, while the expression of ACE2 in the lungs of the young was negatively correlated with immune signatures.

Actually, the expression pattern and expression level of ACE2 in different organs and tissues to some extent determine the symptoms and outcome of COVID-19. Lukassen et al. (2020) observed that ACE2 and TMPRSS2 were primarily expressed in alveolar type II (AT2) cells in the lung and in transient secretory cells in subsegmental bronchial branches, suggesting that these cell types might be susceptible to SARS-CoV-2 infection. Electron microscopy showed that both bronchiole epithelial cells and AT2 cells showed obvious coronavirus particles, and immunohistochemical staining showed the presence of SARS-CoV-2 nucleocapsid in lung tissue, confirming lung injury secondary to SARS-CoV-2 infection (Yao et al., 2020). Usually, COVID-19 patients had some gastrointestinal symptoms, such as nausea, vomiting, and diarrhea (Jin et al., 2020; Song et al., 2020). ACE2 was highly expressed in enterocytes, and SARS-CoV-2 effectively infected enterocytes in human small intestinal organoids (hSIOs), indicating that the intestine might be a target organ of the new coronavirus (Lamers et al., 2020). Interestingly, although the expression levels of ACE2 in enterocytes were much higher than that in enterocyte-precursors, the infection rates of both were similar, suggesting that low ACE2 levels might be sufficient for SARS-CoV-2 to invade host cells. Consistently, Zhou J. et al. (2020) found that SARS-CoV-2 not only actively replicated in the human intestinal organoids, but also could infect bat intestinal cells. At the same time, they isolated infectious SARS-CoV-2 from the stool of a diarrheal COVID-19 patient. These findings suggest that the intestine may be a transmission route of SARS-CoV-2, which may lead to local and overall disease progression. Furthermore, acute kidney injury was one of the important complications of COVID-19 (Huang et al., 2020; Lescure et al., 2020). It was reported that there were coronavirus particles with distinctive spikes in the tubular epithelium and podocytes, and immunostaining with SARS-CoV nucleoprotein antibody was positive in tubules, which provided a basis for SARS-CoV-2 to directly infect kidney tissue (Su et al., 2020). Single-cell transcriptome analysis found that ACE2 and TMPRSSs were co-expressed in podocytes and proximal straight tubule cells, which might be candidate kidney host cells (Pan et al., 2020).

The latest autopsy findings showed that SARS-CoV-2 could be detected in multiple organs, such as heart, liver, brain, lungs, pharynx, and kidneys (Puelles et al., 2020). In addition, neurological tissue damage, pancreatic damage, heart injury and olfactory dysfunctions might also be related to ACE2 expression pattern in the corresponding tissues (Baig et al., 2020; Bilinska et al., 2020; Chen L. et al., 2020; Liu F. et al., 2020). However, these data are mainly from different tissues from healthy human donors, and more animal and cell experiments are needed to verify the pathological mechanism of COVID-19 symptoms. In short, receptor ACE2 mediates the entry of SARS-CoV-2 into host cells, and its expression pattern and level also play important roles in COVID-19 susceptibility and symptoms (**Figure 1**).

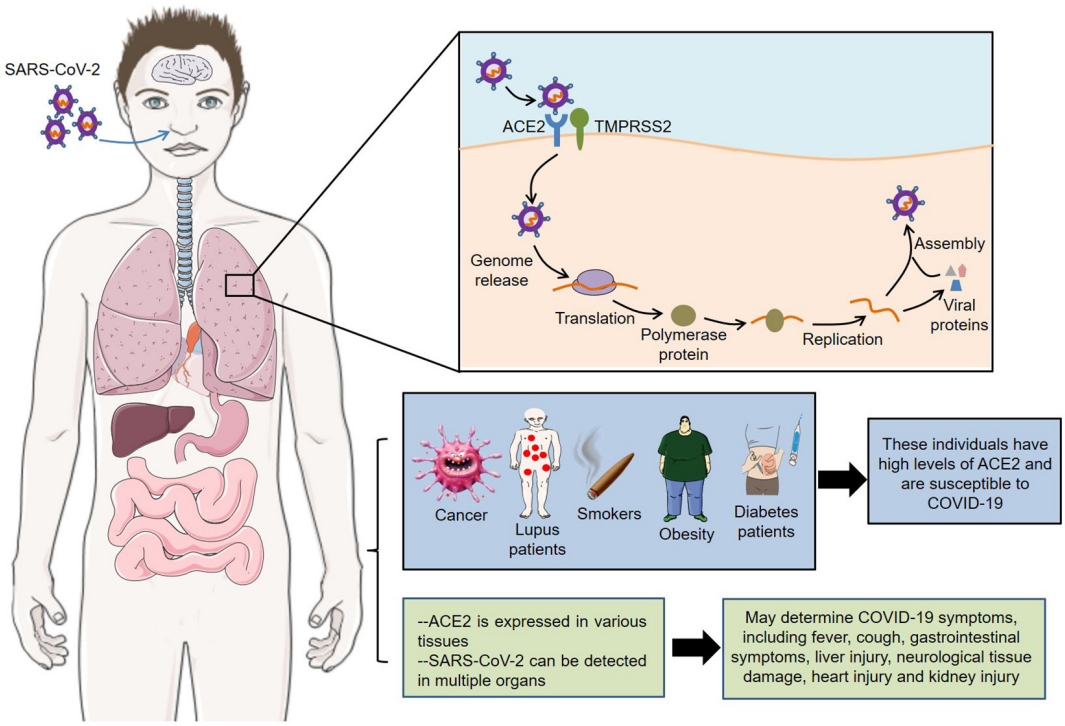

FIGURE 1 | Roles of ACE2 in SARS-CoV-2 infection. Receptor ACE2 mediates the entry of SARS-CoV-2 into host cells. Meanwhile, its expression pattern and level are closely related to the susceptibility and symptoms of COVID-19. SARS-CoV-2, severe acute respiratory syndrome coronavirus 2; ACE2, angiotensin converting enzyme II; COVID-19, coronavirus disease 2019; TMPRSS2, transmembrane protease serine 2.

Immunopathology of COVID-19

After infecting with SARS-CoV-2, macrophages and monocytes are recruited and subsequently release cytokines, thereby activating humoral and cellular immunity mediated by virus-specific B and T cells. However, impaired adaptive immune response and uncontrolled systemic inflammatory response may cause severe organ damage and even death (**Figure 2**).

Antibody Responses

Serum from COVID-19 patients cross-reacted with the nucleocapsid antigens of SARS-CoV, but showed no cross-binding with the S1 subunit of SARS-CoV peak antigen (Long et al., 2020). Within 19 days after symptom onset, the proportion of virus-specific immunoglobulin-G (IgG)-positive patients reached 100%, and within 22 days after symptom onset, the proportion of virus-specific IgM-positive patients reached a maximum of 94.1%. Moreover, IgM seroconversion increased rapidly from the 9th day after the onset of symptoms, while IgG seroconversion increased from the 11th day after the onset of symptoms (Xiang et al., 2020). Importantly, both specific IgM and IgG antibodies showed obvious specificity and positive predictive value, suggesting that antibody detection might help the diagnosis of COVID-19. Pediatric patients with COVID-19 could develop a protective humoral immunity (Zhang Y. et al., 2020). Specifically, compared with the uninfected controls, the percentage of IgG+ B cells were slightly higher in total B cells in infected children, while the percentage of IgG+ B cells in memory B cells was significantly higher. Meanwhile, total and IgG antibodies against the nucleocapsid protein and spike-RBD of SARS-CoV-2 were found in infected children around 2–3 weeks after the onset. Additionally, Wen et al. (2020) demonstrated that some new changes of B cell receptor (BCR) in the recovery stage of COVID-19 patients, especially IGHV3-23 and IGHV3-7, provided new ideas for the design of vaccines. Notably, Zeng F. et al. (2020) found that the mild and recovering patients with COVID-19 had no difference in the concentration of specific IgG antibody between sexes, while in severe conditions, there were higher serum IgG antibody concentrations in female patients, which might be related to the different outcomes between male and female COVID-19 patients.

Clinically, convalescent plasma has been used to treat critically ill patients with SARS-CoV-2 infection, which improved the clinical outcomes and showed good tolerance (Duan et al., 2020; Shen et al., 2020). At the same time, scientists are working to develop monoclonal antibodies that neutralize SARS-CoV-2. Wrapp et al. (2020) isolated two single-domain antibodies (VHHs), MERS VHH-55 and SARS VHH-72, from a llama immunized with prefusion-stabilized MERS-CoV and SARS-CoV S proteins. These VHHs could bind to the RBDs of the S proteins of MERS-CoV and SARS-CoV, and neutralize S pseudotyped viruses *in vitro*. Strikingly, the SARS VHH-72 cross-reacted with the SARS-CoV-2 RBD, and its bivalent IgG Fc-fusion VHH-72-Fc neutralized SARS-CoV-2 S pseudovirus, suggesting

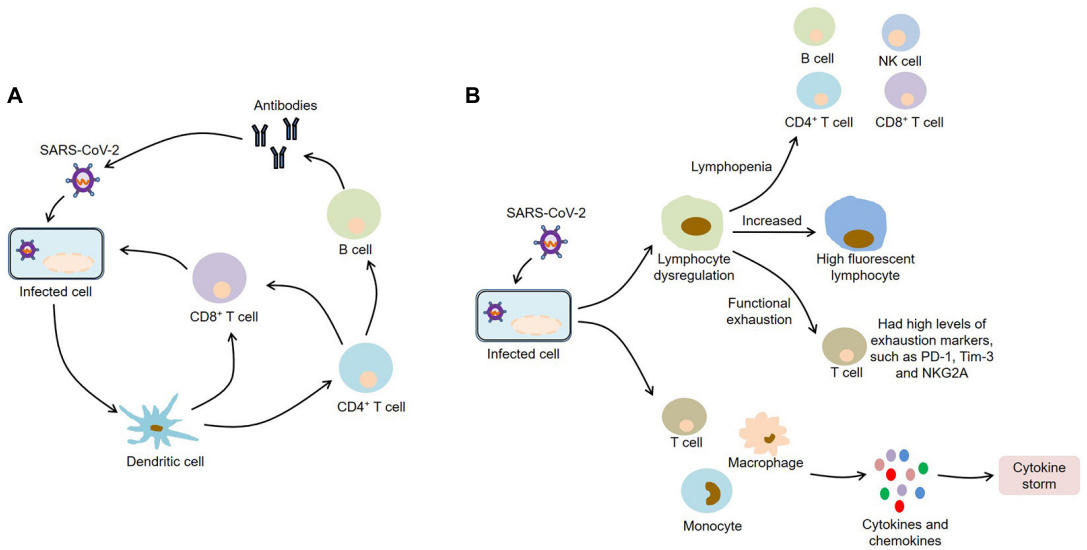

FIGURE 2 | Immunopathology of COVID-19. **(A)** SARS-CoV-2 infection activates humoral and cellular immunity mediated by virus-specific B and T cells; **(B)** SARS-CoV-2 infection causes lymphocyte dysregulation and cytokine storm, which contribute to the development of COVID-19. SARS-CoV-2, severe acute respiratory syndrome coronavirus 2; COVID-19, coronavirus disease 2019; NK, natural killer; PD-1, programmed death-1; Tim-3, T-cell immunoglobulin and mucin-domain containing-3; NKG2A, CD94/NK group 2 member A.

that VHH-72-Fc might act as a potential therapeutic candidate for COVID-19. CR3022, a neutralizing antibody isolated from a SARS patient, could effectively bind to the RBD of SARS-CoV-2 by recognizing an epitope that did not overlap with the ACE2 binding site (Tian et al., 2020). Further studies discovered that CR3022 targeted a conserved epitope distal from the receptor binding site, and the binding could only occur when at least two RBDs in the S trimer were in the up conformation and slightly rotated (Yuan and Wu, 2020). Unfortunately, CR3022 did not neutralize SARS-CoV-2 *in vitro*. Another research also found that cross-reactive binding to RBD and non-RBD regions was common between SARS-CoV and SARS-CoV-2, while the cross-neutralization of these two live viruses might be rare (Lv et al., 2020).

Of note, Chen X. et al. (2020) found that recovered COVID-19 patients produced the antibodies against S1 subunit, but only a small part could block the binding of RBD to ACE2 receptor. Subsequently, they cloned two monoclonal antibodies, 311mab-31B5 and 311mab-32D4, by using SARS-CoV-2 RBD-specific memory B cells isolated from recovered COVID-19 patients, which could block the binding of SARS-CoV-2 RBD to ACE2 receptor and effectively neutralize SARS-CoV-2 S protein pseudovirus. Similarly, Cao et al. (2020b) identified a neutralizing antibody BD-368-2 with strong ability to neutralize pseudotyped SARS-CoV-2 by high-throughput sequencing of antigen-binding single B cells, which could effectively treat and prevent SARS-CoV-2 infection in hACE2 transgenic mice. In fact, several cross-neutralizing antibodies, including COVA1-16, S309, H014, 47D11, ADI-56046, and 515-5, have been discovered, which provide a theoretical basis for the development of SARS-CoV-2 vaccines and therapies (Liu H. et al., 2020; Lv and Deng, 2020; Pinto et al., 2020; Wan et al., 2020; Wang and Li, 2020; Wec and Wrapp, 2020). COVA1-16 bound to SARS-CoV-2 RBD by a long complementarity-determining region H3, which blocked the interaction between ACE2 and RBD through steric hindrance rather than epitope overlap (Liu H. et al., 2020). Another human monoclonal antibody S309 were found from the memory B cells of SARS patients, which could not only neutralize SARS-CoV and SARS-CoV-2 pseudoviruses, but also neutralize live SARS-CoV-2 by binding to the RBD of the S glycoprotein (Pinto et al., 2020). It was worth noting that when other monoclonal antibodies were used in combination with S309, S309 further enhanced their neutralization, indicating that the antibody cocktails containing S309 might be an effective method for the treatment of COVID-19. Moreover, 47D11 could neutralize SARS-CoV and SARS-CoV-2 in cell culture (Wang and Li, 2020). Although this monoclonal antibody targeted a conserved epitope on the RBD of S protein, it did not compete with the S protein for interaction with the ACE2 receptor, suggesting that 47D11 blocked SARS-CoV-2 infection by a mechanism different from receptor binding-inhibition. In conclusion, these monoclonal antibodies may be an effective means of preventing and treating COVID-19.

Lymphocyte Dysregulation

Lymphocytes, such as B cells, $CD4^+$ T cells, $CD8^+$ T cells, and natural killer (NK) cells, are important components of the immune system. Strikingly, most COVID-19 patients usually show significant lymphopenia (Young et al., 2020b; Zhang J. J. et al., 2020). Specifically, total lymphocytes, B cells, $CD4^+$ T cells, $CD8^+$ T cells, and NK cells were decreased in COVID-19 patients, and severe patients were more severe than mild patients (Wang F. et al., 2020). Meanwhile, the $CD8^+$ T cells and $CD4^+/CD8^+$ ratio were significantly

related to the inflammation status of COVID-19, while the decrease in $CD8^+$ T cells and B cells and the increase in $CD4^+/CD8^+$ ratio were associated with poor efficacy after treatment, indicating that some peripheral lymphocyte subsets could be used as predictors of disease progression and treatment effect. Zhang and Tan (2020) confirmed that the decrease in lymphocyte counts in severe patients was negatively correlated with serum levels of interleukin-6 (IL-6) and IL-8. Moreover, the neutrophil to lymphocyte ratio (NLR) was often higher in severe COVID-19 patients and was an independent risk factor for mortality in hospitalized patients (Liu Y. et al., 2020). Notably, the reduced B cells were related to the prolongation of viral RNA shedding from respiratory tract in COVID-19 patients (Hao et al., 2020). Interestingly, high fluorescent lymphocytes (HFL) associated with activated B cells or plasma cells were elevated in COVID-19 patients (Wang Z. et al., 2020). HFL tended to increase as the disease progressed, which might promote the production of plasma cells and specific antibodies in patients. Ganji et al. (2020) found that the ratio of CD4 to CD8 was not significantly different between COVID-19 patients and healthy controls. However, COVID-19 patients had higher levels of CD8 expression, indicating that host T lymphocytes might increase their cytotoxic activity by upregulating CD8 during SARS-CoV-2 infection, thereby exerting antiviral effect.

In addition, the functional state of T cells in COVID-19 patients is also dysregulated. Compared with the healthy controls, T cells from COVID-19 patients had higher levels of the exhaustion markers, including programmed death-1 (PD-1) and T-cell immunoglobulin and mucin-domain containing-3 (Tim-3) (Diao et al., 2020). In the early stage of the disease, the proportions of $PD\text{-}1^+$ and $Tim\text{-}3^+$ on $CD8^+$ and $CD4^+$ T cells were low. As the disease progressed, the expression of PD-1 and Tim-3 in $CD8^+$ T cells has a tendency to increase, while the expression of Tim-3 was increased in $CD4^+$ T cells, but there is no significant change in PD-1 expression. These results indicate that T cells from COVID-19 patients have an exhaustion phenotype. Consistently, another study found that the levels of tumor necrosis factor-α (TNF-α) and IFN-γ in $CD4^+$ T cells of severe COVID-19 patients were lower than those of mild patients, while the levels of granzyme B and perforin in $CD8^+$ T cells of severe patients were higher than those of mild patients (Zheng H. Y. et al., 2020). Meanwhile, the levels of human leukocyte antigen D related (HLA-DR) and T cell Ig and ITIM domain (TIGIT) in $CD8^+$ T cells of severe patients were higher than those of mild patients. These findings suggest that SARS-CoV-2 infection can affect the functions of $CD4^+$ T cells and promote the excessive activation and exhaustion of $CD8^+$ T cells. Furthermore, the expression of CD94/NK group 2 member A (NKG2A) was increased on cytotoxic T lymphocytes (CTLs) and NK cells in COVID-19 patients, accompanied by low levels of CD107a, IFN-γ, IL-2, TNF-α, and granzyme B (Zheng M. et al., 2020). Importantly, effectively controlled COVID-19 patients had increased levels of NK cells and $CD8^+$ T cells, as well as decreased NKG2A expression, indicating that targeting NKG2A might prevent functional exhaustion of lymphocytes and thus contribute to COVID-19 recovery.

Actually, SARS-CoV-2 infected T lymphocytes through membrane fusion mediated by S protein, which could be inhibited by EK1 peptide (Wang X. et al., 2020). However, SARS-CoV-2 could not replicate in MT-2 cells. Furthermore, CD147 was another receptor that mediated SARS-CoV-2 infection (Ulrich and Pillat, 2020). Because CD147 existed on the surface of T lymphocytes, it might promote the SARS-CoV-2 infection of T cells. By transcriptome sequencing of the bronchoalveolar lavage fluid (BALF) and peripheral blood mononuclear cells (PBMCs) of COVID-19 patients, Xiong et al. (2020) found that some significantly altered genes were enriched in apoptosis and P53 pathway. These results may partially explain the cause of lymphopenia in patients with COVID-19.

Cytokine Storm

In response to infections, large amounts of cytokines released by immune cells may cause cytokine storm or macrophage activation syndrome (MAS), which is an excessive inflammation response to external stimuli. In this scenario, the immune system attacks normal organs and tissues, leading to acute respiratory distress syndrome (ARDS), multiple organ failure, and even death (Ye et al., 2020). Most patients with severe COVID-19 exhibited large amounts of pro-inflammatory cytokines and chemokines, such as IL-2, IL-6, IL-7, TNF-α, granulocyte colony stimulating factor (GCSF), CXC-chemokine ligand 10 (CXCL10), CC-chemokine ligand 2 (CCL2), and CCL3 (Chen N. et al., 2020; Huang et al., 2020). Consistently, the metatranscriptomic sequencing of the BALF discovered that COVID-19 patients showed marked hypercytokinemia and up-regulated IFN-stimulated genes, especially significantly elevated expression of chemokines, such as CXCL17, CXCL8, CCL2, and CCL7 (Zhou Z. et al., 2020). Interestingly, most cytokines were expressed after respiratory function nadir, whereas only IL-1 was induced before respiratory function nadir (Ong et al., 2020). Furthermore, inflammatory markers in blood, including C-reactive protein (CRP), ferritin, and D-dimer, were found to be abnormally up-regulated in patients (Tan et al., 2020; Zhou F. et al., 2020). Importantly, these cytokines and chemokines have been associated with disease severity and death. For example, IL-6, CRP, and hypertension were ideal predictors for the progression of COVID-19 (Zhu Z. et al., 2020), while older age, high Sequential Organ Failure Assessment (SOFA) score and D-dimer greater than 1 μg/L were risk factors for in-hospital death in COVID-19 patients (Zhou F. et al., 2020). Therefore, strategies to suppress inflammatory responses are particularly important in patients with COVID-19, especially in severe cases.

ANIMAL MODELS OF COVID-19

As can be seen from the above, current studies on COVID-19 pathogenesis are mainly focused on ACE2 and immunopathology. It is of great significance to further explore the molecular mechanisms. In this regard, effective animal models of COVID-19 are indispensable. So far, SARS-CoV-2

infection has been described in various animal models such as macaque, ferret, mouse, and hamster (**Figure 3**).

Non-human Primates, Including Cynomolgus Macaque and Rhesus Macaque

Rockx and Kuiken (2020) inoculated a SARS-CoV-2 strain into young and aged cynomolgus macaques by a combination of intratracheal and intranasal routes, causing a COVID-19-like disease. Specifically, none of these macaques showed obvious clinical symptoms and weight loss, except for one elderly who developed a serous nasal discharge on the 14th day after inoculation. The virus was mainly expelled from the nose and throat, and peaked early in the infection. Of note, one macaque showed shedding of viral RNA in rectal swabs on the 14th day. The autopsy of four macaques showed that SARS-CoV-2 RNA was detected in multiple tissues from the respiratory tract, ileum and tracheobronchial lymph nodes. Importantly, two out of four macaques had areas with acute or more advanced diffuse alveolar damage (DAD), whose histological features including alveolar edema, epithelial necrosis, hyaline membrane formation, and accumulation of neutrophils, macrophages, and lymphocytes.

Analogously, rhesus macaques inoculated with SARS-CoV-2 had a respiratory disease (Munster et al., 2020). The symptoms of infected animals included changes in respiratory pattern and piloerection, as well as loss of appetite, hunchback, pale complexion, dehydration and weight loss, and lung radiographs showed pulmonary infiltrates. Histologically, 3 out of 4 animals developed mild to moderate interstitial pneumonia with the features of thickening of alveolar septa, alveolar edema and hyaline membranes, indicating that the macaque model basically recapitulates the pathological features of COVID-19. Interestingly, Chandrashekar and Liu (2020) found that the rhesus macaques infected with SARS-CoV-2 were difficult to re-infect this virus, and the macaques showed anamnestic immune responses following rechallenge, indicating that protective immunity might play a role in this process. Furthermore, rhesus macaques vaccinated with DNA vaccines expressing different forms of S protein produced humoral and cellular immune responses (Yu and Tostanoski, 2020). Importantly, when the vaccinated animals were infected with SARS-CoV-2, their bronchoalveolar lavage and nasal mucosa showed reduced

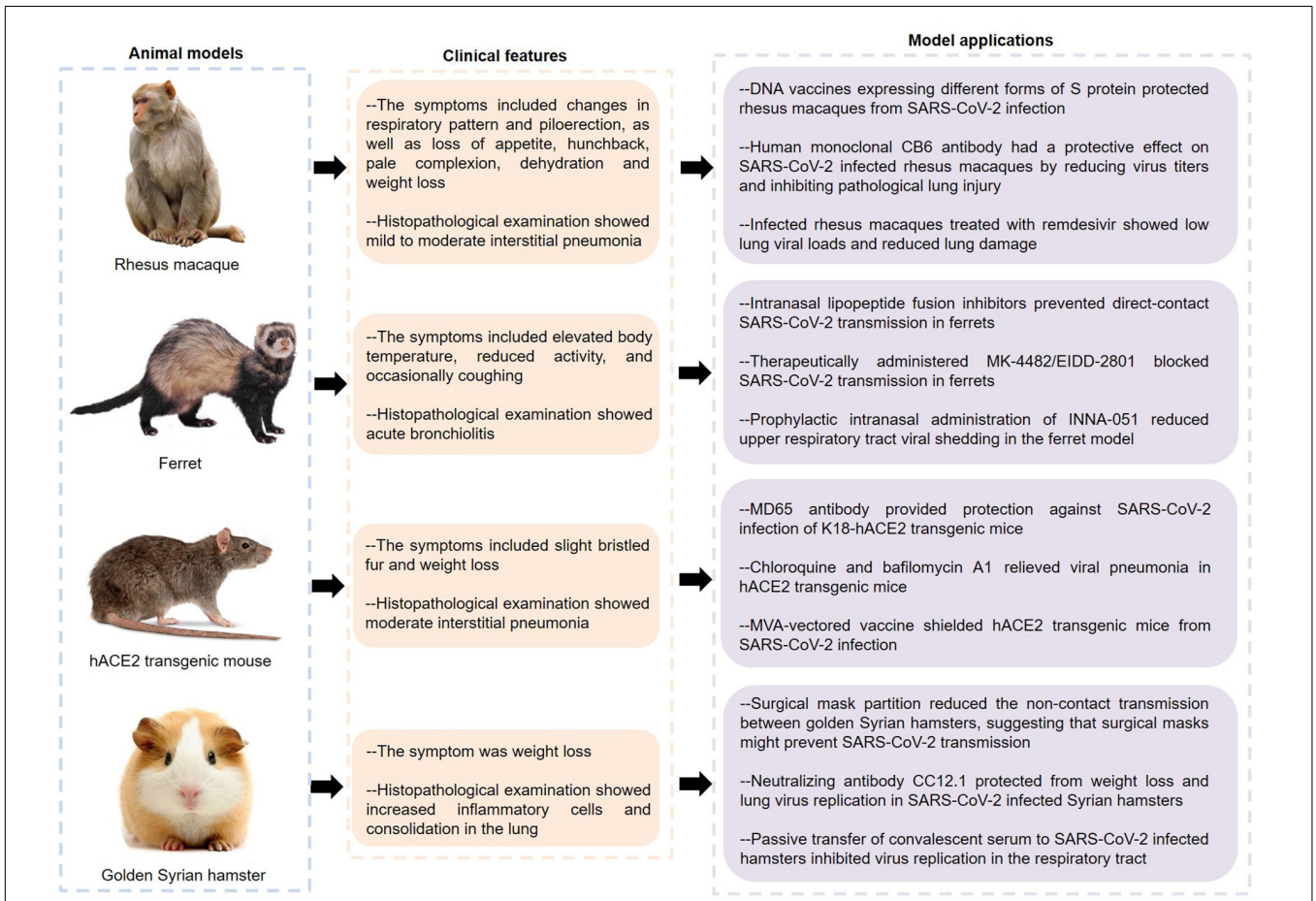

FIGURE 3 | Features and applications of animal models of COVID-19. SARS-CoV-2, severe acute respiratory syndrome coronavirus 2; hACE2, human angiotensin converting enzyme II; COVID-19, coronavirus disease 2019.

viral loads, indicating that these vaccines had protective effects on non-human primates. Notably, CB6, a human monoclonal antibody, had a protective effect on SARS-CoV-2 infected rhesus macaques by reducing virus titers and inhibiting pathological lung injury, indicating that CB6 might be a potential treatment for COVID-19 (Shi and Shan, 2020). Similarly, infected rhesus macaques treated with remdesivir showed low lung viral loads and reduced lung damage, which provided a basis for the clinical application of remdesivir (Williamson et al., 2020).

Ferret

Strikingly, ferrets were highly sensitive to SARS-CoV-2 infection and could transmit the virus to other ferrets in direct or indirect contact (Kim et al., 2020). The infected ferrets had elevated body temperature, reduced activity, and occasionally coughing. Meanwhile, viral RNA was detected in nasal turbinate, lung, trachea, intestine, and kidney tissues. Importantly, infected ferrets had more immune infiltration and cellular debris in the bronchial epithelium, bronchial lumen and alveolar wall, indicating that SARS-CoV-2 infection could cause acute bronchiolitis in ferrets. Additionally, many up-regulated cytokines and chemokines, such as IL-6, CCL2, CCL8, and CXCL9, were found in the nasal washes of ferrets infected with SARS-CoV-2, indicating that this animal model also showed an significant inflammatory response (Blanco-Melo et al., 2020). Interestingly, the newly designed lipoprotein fusion inhibitors inhibited the conformational changes of S protein and blocked the membrane fusion between the virus and host cell membrane by integrating into the host cell membranes, and their intranasal administration could effectively inhibit SARS-CoV-2 transmission in ferrets (de Vries and Schmitz, 2021). Similarly, the ribonucleoside analog inhibitor MK-4482/EIDD-2801 not only reduced the viral load in the upper respiratory tract, but also inhibited the viral transmission in ferrets, indicating that MK-4482/EIDD-2801 might become a potential drug to control the transmission of SARS-CoV-2 in the community (Cox et al., 2021). Recent studies found that preventive intranasal administration of TLR2/6 agonist INNA-051 could effectively reduce the virus levels in throat swabs and nasal washes of the ferrets infected with SARS-CoV-2 (Proud et al., 2021). Of note, although lopinavir-ritonavir, emtricitabine-tenofovir, and hydroxychloroquine sulfate slightly alleviated the clinical symptoms of SARS-CoV-2 infected ferrets, they did not significantly reduce the virus titers (Park et al., 2020). Therefore, more clinical studies are needed to evaluate the effects of these drugs on COVID-19.

Mouse

Bao et al. (2020a) generated hACE2 transgenic mice through microinjecting the mice ACE2 promoter driving the hACE2 coding sequence into the fertilized ova. Transgenic mice infected with SARS-CoV-2 showed slight bristled fur and weight loss. The lung tissues of infected mice showed moderate interstitial pneumonia characterized by thickened alveolar septa, accumulation of inflammatory cells in alveolar cavities, and fragmentation of bronchiolar epithelial cells. Importantly, the co-localization of ACE2 and S protein was found in alveolar epithelial cells. Similar to ferrets, SARS-CoV-2 could be spread in hACE2 transgenic mice through close contact and respiratory droplets (Bao et al., 2020b). These results indicate that the hACE2 transgenic mice can serve as valuable animal models for SARS-CoV-2 infection. Human monoclonal MD65 antibody showed high neutralization ability to SARS-CoV-2 *in vitro*, and it had a significant protective effect on SARS-CoV-2 infected K18-hACE2 transgenic mice (Rosenfeld and Noy-Porat, 2021). This protective effect is manifested in the improvement of lung inflammation and pathological processes, as well as the life-saving of infected mice. Furthermore, some endosomal acidification inhibitors, such as chloroquine, NH4CL, and bafilomycin A1, have been confirmed to have antiviral effects in SARS-CoV-2 infected cell or animal models (Shang et al., 2021). Among them, the lungs of infected mice treated with chloroquine and bafilomycin A1 showed reduced infiltration of inflammatory cells and improved alveolar structure. Liu et al. (2021) demonstrated that the recombinant modified vaccinia virus Ankaras (rMVAs) expressing modified forms of SARS-CoV-2 S proteins could not only suppress viral replication in the upper and lower respiratory tracts, but also reduce the expression of cytokines and chemokines in the lungs of hACE2 mice, suggesting that this vaccine had the potential to control COVID-19 during the current pandemic.

Besides hACE2 transgenic mice, hACE2 mice established by CRISPR/Cas9 knock-in technology, adeno-associated virus encoding for hACE2 (AAV-hACE2)-transduced mice, replication-deficient adenovirus encoding hACE2 (Ad5-hACE2)-transduced mice and wild-type mice infected with mouse-adapted SARS-CoV-2 have also been used in the pathological study of COVID-19 (Dinnon et al., 2020; Israelow et al., 2020; Sun J. et al., 2020; Sun S. H. et al., 2020). hACE2 mice established by CRISPR/Cas9 developed interstitial pneumonia with an increase in various cytokines after SARS-CoV-2 infection (Sun S. H. et al., 2020). Moreover, inoculation of SARS-CoV-2 in the stomach could cause a productive infection in hACE2 mice, indicating that SARS-CoV-2 might be transmitted through the fecal-oral route (Sun S. H. et al., 2020). Similarly, Ad5-hACE2-transduced mice showed some symptoms of pneumonia, and treatment with remdesivir or human convalescent plasma 1 day prior to infection could accelerate virus clearance and prevent weight loss and lung histological changes in mice, suggesting that this mouse model was very suitable for the evaluation of COVID-19 therapies (Sun J. et al., 2020). The SARS-CoV-2 variant containing the N501Y mutation could bind to mouse ACE2, causing wild-type mice to be infected with SARS-CoV-2 and develop interstitial pneumonia (Gu and Chen, 2020). Because the cost and practicality of this model are superior to other animal models, it has received great attention.

Golden Syrian Hamsters

In addition, SARS-CoV-2 could be highly transmitted among golden Syrian hamsters via direct contact and aerosols, and infected hamsters usually showed weight loss and increased inflammatory cells and consolidation in the lungs (Sia et al., 2020). The researchers discovered viral antigen in the bronchial epithelial cells, nasal epithelial cells and duodenum epithelial cells. At the same time, viral antigen was also detected in the

olfactory sensory neurons at the nasal mucosa, indicating that SARS-CoV-2 might have infected neurons and subsequently caused olfactory dysfunctions. Meaningfully, surgical mask partition could significantly reduce the non-contact transmission between golden Syrian hamsters, and the infected naïve hamsters showed milder clinical symptoms and histopathological changes, suggesting that surgical masks might play an important role in preventing SARS-CoV-2 transmission (Chan et al., 2020). Rogers and Zhao (2020) isolated a variety of neutralizing antibodies from recovered SARS-CoV-2 patients, which recognized the RBD or non-RBD epitopes of the S protein. Of these, the antibody CC12.1 targeting the RBD-A epitope could protect from weight loss and lung virus replication in SARS-CoV-2 infected Syrian hamsters, indicating that this monoclonal antibody had the potential to prevent and treat COVID-19. Moreover, passive transfer of convalescent serum from infected animals to SARS-CoV-2 infected hamsters could efficiently inhibit virus replication in the respiratory tract, indicating that convalescent plasma might serve as a potential therapy for COVID-19 (Imai et al., 2020). In addition, it was reported that certain animals such as dogs, cats and tigers could also be infected with SARS-CoV-2, which not only contributed to understanding the transmission of the virus, but also provided more possibilities for modeling (Halfmann et al., 2020; Sit et al., 2020; Wang L. et al., 2020).

CONCLUSION AND FUTURE PERSPECTIVE

All in all, the receptor ACE2 mediates the entry of SARS-CoV-2 into host cells, and its expression pattern and level are closely related to COVID-19 susceptibility and symptoms. Meanwhile, the knowledge of immunopathology related to COVID-19, such as antibody responses, lymphocyte dysregulation, and cytokine storms, is also crucial for understanding SARS-CoV-2 infection. Furthermore, COVID-19 animal models, including macaque, ferret, hamster and hACE2 transgenic mouse, not only help to explore the pathogenesis of COVID-19, but also provide useful tools for evaluating vaccines and therapeutics. However, some problems need to be solved in the future.

Firstly, since SARS-CoV-2 has obvious human-to-human transmission, it is of great significance to understand the transmission route for the prevention and control of the epidemic (Ghinai et al., 2020; Li Q. et al., 2020). Indeed, respiratory transmission is the main mode for SARS-CoV-2, while fecal-oral transmission, vertical maternal-fetal transmission, and transmission through the ocular surface are also potential transmission routes (Wu Y. et al., 2020; Zeng L. et al., 2020; Zhang X. et al., 2020). Secondly, there is no specific therapeutics for COVID-19. Although remdesivir and chloroquine could effectively inhibit SARS-CoV-2 *in vitro*, it was necessary to prove their effectiveness and safety through clinical trials (Wang M. et al., 2020). Interestingly, the cellular nanosponges composed of the plasma membranes of human lung epithelial type II cells or macrophages prevented virus infection by neutralizing SARS-CoV-2 (Zhang Q. et al., 2020). Furthermore, human recombinant soluble ACE2 (hrsACE2) could significantly inhibit the SARS-CoV-2 infection of human organoids, which might be a promising therapeutic (Monteil et al., 2020). Importantly, further research on molecular mechanisms is needed to provide new ideas for the prevention and treatment of COVID-19.

As the number of COVID-19 cases continues to increase globally, effective prevention and control measures are crucial. In addition to building a community prevention and control system to control the spread of the epidemic, achieving herd immunity through vaccination is also an indispensable means. Fortunately, nine vaccines against SARS-CoV-2 have been approved for use in humans, and more than 300 million people have been vaccinated worldwide. However, some complex situations, such as highly infectious SARS-CoV-2 variants, the evasion of viral variants from vaccine-induced humoral immunity, and the limited durability of humoral responses in coronavirus infections, pose severe challenges to the control of COVID-19 (Kaneko et al., 2020; Garcia-Beltran et al., 2021; Zhou and Thao, 2021). In this context, it is of great significance to develop broadly neutralizing antibodies and vaccine boosters that target these SARS-CoV-2 variants.

AUTHOR CONTRIBUTIONS

WJ and JW contributed toward the concept and manuscript writing. BS and JZ participated in the literature search and discussion. YS and ZZ revised and supervised overall project. All authors read and approved the final version of manuscript.

ACKNOWLEDGMENTS

The authors wish to acknowledge Xiaochuan Zhang from The First Affiliated Hospital of Zhengzhou University, China for editing of English grammar and syntax of the manuscript.

REFERENCES

Alagaili, A. N., Briese, T., Mishra, N., Kapoor, V., Sameroff, S. C., Burbelo, P. D., et al. (2014). Middle East respiratory syndrome coronavirus infection in dromedary camels in Saudi Arabia. *mBio* 5, e884–e814. doi: 10.1128/mBio.00884-14

Baig, A. M., Khaleeq, A., Ali, U., and Syeda, H. (2020). Evidence of the COVID-19 virus targeting the CNS: tissue distribution, host-virus interaction, and proposed neurotropic mechanisms. *ACS Chem. Neurosci.* 11, 995–998. doi: 10.1021/acschemneuro.0c00122

Bao, L., Deng, W., Huang, B., Gao, H., Liu, J., Ren, L., et al. (2020a). The pathogenicity of SARS-CoV-2 in hACE2 transgenic mice. *Nature* 583, 830–833. doi: 10.1038/s41586-020-2312-y

Bao, L., Gao, H., Deng, W., Lv, Q., Yu, H., Liu, M., et al. (2020b). Transmission of SARS-CoV-2 via close contact and respiratory droplets among hACE2 mice. *J. Infect. Dis.* 222, 551–555. doi: 10.1093/infdis/jiaa281

Bilinska, K., Jakubowska, P., Cs, V. O. N. B., and Butowt, R. (2020). Expression of the SARS-CoV-2 entry proteins, ACE2 and TMPRSS2, in cells of the olfactory epithelium: identification of cell types and trends with age. *ACS Chem. Neurosci.* 11, 1555–1562. doi: 10.1021/acschemneuro.0c00210

Blanco-Melo, D., Nilsson-Payant, B. E., Liu, W. C., Uhl, S., Hoagland, D., Moller, R., et al. (2020). Imbalanced host response to SARS-CoV-2 drives development of COVID-19. *Cell* 181, 1036–1045.e9. doi: 10.1016/j.cell.2020.04.026

Cao, Y., Li, L., Feng, Z., Wan, S., Huang, P., Sun, X., et al. (2020a). Comparative genetic analysis of the novel coronavirus (2019-nCoV/SARS-CoV-2) receptor ACE2 in different populations. *Cell Discov.* 6:11. doi: 10.1038/s41421-020-0147-1

Cao, Y., Su, B., Guo, X., Sun, W., Deng, Y., Bao, L., et al. (2020b). Potent neutralizing antibodies against SARS-CoV-2 identified by high-throughput single-cell sequencing of convalescent patients' B cells. *Cell* 182, 73–84.e16. doi: 10.1016/j.cell.2020.05.025

Chai, P., Yu, J., Ge, S., Jia, R., and Fan, X. (2020). Genetic alteration, RNA expression, and DNA methylation profiling of coronavirus disease 2019 (COVID-19) receptor ACE2 in malignancies: a pan-cancer analysis. *J. Hematol. Oncol.* 13:43. doi: 10.1186/s13045-020-00883-5

Chan, J. F., and Kok, K. H. (2020). Genomic characterization of the 2019 novel human-pathogenic coronavirus isolated from a patient with atypical pneumonia after visiting Wuhan. 9, 221–236. doi: 10.1080/22221751.2020.1719902

Chan, J. F., Yuan, S., Zhang, A. J., Poon, V. K., Chan, C. C., Lee, A. C., et al. (2020). Surgical mask partition reduces the risk of non-contact transmission in a golden Syrian hamster model for Coronavirus Disease 2019 (COVID-19). *Clin. Infect. Dis.* 71, 2139–2149. doi: 10.1093/cid/ciaa644

Chandrashekar, A., and Liu, J. (2020). SARS-CoV-2 infection protects against rechallenge in rhesus macaques. *Science* 369, 812–817. doi: 10.1126/science.abc4776

Chen, L., Li, X., Chen, M., Feng, Y., and Xiong, C. (2020). The ACE2 expression in human heart indicates new potential mechanism of heart injury among patients infected with SARS-CoV-2. *Cardiovasc. Res.* 116, 1097–1100. doi: 10.1093/cvr/cvaa078

Chen, N., Zhou, M., Dong, X., Qu, J., Gong, F., Han, Y., et al. (2020). Epidemiological and clinical characteristics of 99 cases of 2019 novel coronavirus pneumonia in Wuhan, China: a descriptive study. *Lancet* 395, 507–513. doi: 10.1016/s0140-6736(20)30211-7

Chen, X., Li, R., Pan, Z., Qian, C., Yang, Y., You, R., et al. (2020). Human monoclonal antibodies block the binding of SARS-CoV-2 spike protein to angiotensin converting enzyme 2 receptor. *Cell. Mol. Immunol.* 17, 647–649. doi: 10.1038/s41423-020-0426-7

Chinese SARS Molecular Epidemiology Consortium (2004). Molecular evolution of the SARS coronavirus during the course of the SARS epidemic in China. *Science* 303, 1666–1669. doi: 10.1126/science.1092002

Cox, R. M., Wolf, J. D., and Plemper, R. K. (2021). Therapeutically administered ribonucleoside analogue MK-4482/EIDD-2801 blocks SARS-CoV-2 transmission in ferrets. 6, 11–18. doi: 10.1038/s41564-020-00835-2

de Vries, R. D., and Schmitz, K. S. (2021). Intranasal fusion inhibitory lipopeptide prevents direct-contact SARS-CoV-2 transmission in ferrets. *Science* 371, 1379–1382. doi: 10.1126/science.abf4896

Diao, B., Wang, C., Tan, Y., Chen, X., Liu, Y., Ning, L., et al. (2020). Reduction and functional exhaustion of T cells in patients with Coronavirus Disease 2019 (COVID-19). *Front. Immunol.* 11:827. doi: 10.3389/fimmu.2020.00827

Dinnon, K. H. III, Leist, S. R., Schäfer, A., and Edwards, C. E. (2020). A mouse-adapted model of SARS-CoV-2 to test COVID-19 countermeasures. 586, 560–566. doi: 10.1038/s41586-020-2708-8

Duan, K., Liu, B., Li, C., and Zhang, H. (2020). Effectiveness of convalescent plasma therapy in severe COVID-19 patients. *Proc. Natl. Acad. Sci. U. S. A.* 117, 9490–9496. doi: 10.1073/pnas.2004168117

European Centre for Disease Prevention and Control (2021). *Situation Updates on COVID-19 [Online]*. Available online at: https://www.ecdc.europa.eu/en/covid-19/situation-updates (accessed April 5, 2021)

Eurosurveillance Editorial Team (2020). Note from the editors: World Health Organization declares novel coronavirus (2019-nCoV) sixth public health emergency of international concern. *Euro. Surveill.* 25:200131e. doi: 10.2807/1560-7917.ES.2020.25.5.200131e

Ganji, A., Farahani, I., Khansarinejad, B., Ghazavi, A., and Mosayebi, G. (2020). Increased expression of CD8 marker on T-cells in COVID-19 patients. *Blood Cells Mol. Dis.* 83:102437. doi: 10.1016/j.bcmd.2020.102437

Garcia-Beltran, W. F., Lam, E. C., St Denis, K., Nitido, A. D., Garcia, Z. H., Hauser, B. M., et al. (2021). Multiple SARS-CoV-2 variants escape neutralization by vaccine-induced humoral immunity. *Cell* doi: 10.1016/j.cell.2021.03.013 [Epub ahead of print].

Ghinai, I., McPherson, T. D., Hunter, J. C., Kirking, H. L., Christiansen, D., Joshi, K., et al. (2020). First known person-to-person transmission of severe acute respiratory syndrome coronavirus 2 (SARS-CoV-2) in the USA. *Lancet* 395, 1137–1144. doi: 10.1016/s0140-6736(20)30607-3

Gu, H., and Chen, Q. (2020). Adaptation of SARS-CoV-2 in BALB/c mice for testing vaccine efficacy. *Science* 369, 1603–1607. doi: 10.1126/science.abc4730

Guan, W. J., Ni, Z. Y., Hu, Y., Liang, W. H., Ou, C. Q., He, J. X., et al. (2020). Clinical characteristics of Coronavirus Disease 2019 in China. *N. Engl. J. Med.* 382, 1708–1720. doi: 10.1056/NEJMoa2002032

Guan, Y., Zheng, B. J., He, Y. Q., Liu, X. L., Zhuang, Z. X., Cheung, C. L., et al. (2003). Isolation and characterization of viruses related to the SARS coronavirus from animals in southern China. *Science* 302, 276–278. doi: 10.1126/science.1087139

Halfmann, P. J., Hatta, M., Chiba, S., Maemura, T., Fan, S., Takeda, M., et al. (2020). Transmission of SARS-CoV-2 in domestic cats. *N. Engl. J. Med.* 383, 592–594. doi: 10.1056/NEJMc2013400

Hao, S., Lian, J., Lu, Y., Jia, H., Hu, J., Yu, G., et al. (2020). Decreased B cells on admission was associated with prolonged viral RNA shedding from respiratory tract in Coronavirus Disease 2019: a case control study. *J. Infect. Dis.* 222, 367–371. doi: 10.1093/infdis/jiaa311

Higham, A., and Singh, D. (2020). Increased ACE2 expression in the bronchial epithelium of COPD patients who are overweight. *Obesity (Silver Spring)* 28, 1586–1589. doi: 10.1002/oby.22907

Hoffmann, M., Kleine-Weber, H., and Pohlmann, S. (2020a). A multibasic cleavage site in the spike protein of SARS-CoV-2 is essential for infection of human lung cells. *Mol. Cell* 78, 779–784.e5. doi: 10.1016/j.molcel.2020.04.022

Hoffmann, M., Kleine-Weber, H., Schroeder, S., Kruger, N., Herrler, T., Erichsen, S., et al. (2020b). SARS-CoV-2 cell entry depends on ACE2 and TMPRSS2 and is blocked by a clinically proven protease inhibitor. *Cell* 181, 271–280.e8. doi: 10.1016/j.cell.2020.02.052

Huang, C., Wang, Y., Li, X., Ren, L., Zhao, J., Hu, Y., et al. (2020). Clinical features of patients infected with 2019 novel coronavirus in Wuhan. China. *Lancet* 395, 497–506. doi: 10.1016/s0140-6736(20)30183-5

Imai, M., Iwatsuki-Horimoto, K., Hatta, M., and Loeber, S. (2020). Syrian hamsters as a small animal model for SARS-CoV-2 infection and countermeasure development. *Proc. Natl. Acad. Sci. U. S. A.* 117, 16587–16595. doi: 10.1073/pnas.2009799117

Israelow, B., Song, E., Mao, T., Lu, P., Meir, A., Liu, F., et al. (2020). Mouse model of SARS-CoV-2 reveals inflammatory role of type I interferon signaling. *J. Exp. Med.* 217:e20201241. doi: 10.1084/jem.20201241

Jin, X., Lian, J. S., Hu, J. H., Gao, J., Zheng, L., Zhang, Y. M., et al. (2020). Epidemiological, clinical and virological characteristics of 74 cases of coronavirus-infected disease 2019 (COVID-19) with gastrointestinal symptoms. *Gut* 69, 1002–1009. doi: 10.1136/gutjnl-2020-320926

Kandeel, M., Ibrahim, A., and Fayez, M. (2020). From SARS and MERS CoVs to SARS-CoV-2: moving toward more biased codon usage in viral structural and nonstructural genes. *J. Med. Virol.* 92, 660–666. doi: 10.1002/jmv.25754

Kaneko, N., Kuo, H. H., Boucau, J., Farmer, J. R., Allard-Chamard, H., Mahajan, V. S., et al. (2020). Loss of Bcl-6-expressing T follicular helper cells and germinal centers in COVID-19. *Cell* 183, 143–157.e13. doi: 10.1016/j.cell.2020.08.025

Kim, Y. I., Kim, S. G., Kim, S. M., Kim, E. H., Park, S. J., Yu, K. M., et al. (2020). Infection and rapid transmission of SARS-CoV-2 in ferrets. *Cell Host Microbe* 27, 704–709.e2. doi: 10.1016/j.chom.2020.03.023

Lam, T. T., Shum, M. H., Zhu, H. C., Tong, Y. G., Ni, X. B., Liao, Y. S., et al. (2020). Identifying SARS-CoV-2 related coronaviruses in Malayan pangolins. *Nature* 583, 282–285. doi: 10.1038/s41586-020-2169-0

Lamers, M. M., Beumer, J., van der Vaart, J., Knoops, K., Puschhof, J., Breugem, T. I., et al. (2020). SARS-CoV-2 productively infects human gut enterocytes. *Science* 369, 50–54. doi: 10.1126/science.abc1669

Lechien, J. R., Chiesa-Estomba, C. M., De Siati, D. R., Horoi, M., Le Bon, S. D., Rodriguez, A., et al. (2020). Olfactory and gustatory dysfunctions as a clinical presentation of mild-to-moderate forms of the coronavirus disease (COVID-19): a multicenter European study. *Eur. Arch. Otorhinolaryngol.* 277, 2251–2261. doi: 10.1007/s00405-020-05965-1

Lescure, F. X., Bouadma, L., Nguyen, D., Parisey, M., Wicky, P. H., Behillil, S., et al. (2020). Clinical and virological data of the first cases of COVID-19 in Europe:

a case series. *Lancet Infect. Dis.* 20, 697–706. doi: 10.1016/s1473-3099(20)30200-0

Leung, J. M., Yang, C. X., Tam, A., Shaipanich, T., Hackett, T. L., Singhera, G. K., et al. (2020). ACE-2 expression in the small airway epithelia of smokers and COPD patients: implications for COVID-19. *Eur. Respir. J.* 55:2000688. doi: 10.1183/13993003.00688-2020

Li, M. Y., Li, L., Zhang, Y., and Wang, X. S. (2020). Expression of the SARS-CoV-2 cell receptor gene ACE2 in a wide variety of human tissues. *Infect. Dis. Poverty* 9:45. doi: 10.1186/s40249-020-00662-x

Li, Q., Guan, X., Wu, P., Wang, X., Zhou, L., Tong, Y., et al. (2020). Early transmission dynamics in Wuhan, China, of novel coronavirus-infected pneumonia. *N. Engl. J. Med.* 382, 1199–1207. doi: 10.1056/NEJMoa2001316

Lin, L., Jiang, X., Zhang, Z., Huang, S., Zhang, Z., Fang, Z., et al. (2020). Gastrointestinal symptoms of 95 cases with SARS-CoV-2 infection. *Gut* 69, 997–1001. doi: 10.1136/gutjnl-2020-321013

Liu, F., Long, X., Zhang, B., Zhang, W., Chen, X., and Zhang, Z. (2020). ACE2 expression in pancreas may cause pancreatic damage after SARS-CoV-2 infection. *Clin. Gastroenterol. Hepatol.* 18, 2128–2130.e2. doi: 10.1016/j.cgh.2020.04.040

Liu, H., Wu, N. C., Yuan, M., Bangaru, S., Torres, J. L., Caniels, T. G., et al. (2020). Cross-neutralization of a SARS-CoV-2 antibody to a functionally conserved site is mediated by avidity. *Immunity* 53, 1272–1280.e5. doi: 10.1016/j.immuni.2020.10.023

Liu, R., Americo, J. L., and Cotter, C. A. (2021). One or two injections of MVA-vectored vaccine shields hACE2 transgenic mice from SARS-CoV-2 upper and lower respiratory tract infection. *Proc. Natl. Acad. Sci. U.S.A.* 118:e2026785118. doi: 10.1073/pnas.2026785118

Liu, Y., Du, X., Chen, J., Jin, Y., Peng, L., Wang, H. H. X., et al. (2020). Neutrophil-to-lymphocyte ratio as an independent risk factor for mortality in hospitalized patients with COVID-19. *J. Infect.* 81, e6–e12. doi: 10.1016/j.jinf.2020.04.002

Long, Q. X., Liu, B. Z., and Deng, H. J. (2020). Antibody responses to SARS-CoV-2 in patients with COVID-19. *Nat. Med.* 26, 845–848. doi: 10.1038/s41591-020-0897-1

Lukassen, S., Chua, R. L., Trefzer, T., Kahn, N. C., Schneider, M. A., Muley, T., et al. (2020). SARS-CoV-2 receptor ACE2 and TMPRSS2 are primarily expressed in bronchial transient secretory cells. *EMBO J.* 39:e105114. doi: 10.15252/embj.20105114

Lv, H., Wu, N. C., Tsang, O. T., Yuan, M., Perera, R., Leung, W. S., et al. (2020). Cross-reactive antibody response between SARS-CoV-2 and SARS-CoV infections. *Cell Rep.* 31:107725. doi: 10.1016/j.celrep.2020.107725

Lv, Z., and Deng, Y. Q. (2020). Structural basis for neutralization of SARS-CoV-2 and SARS-CoV by a potent therapeutic antibody. *Science* 369, 1505–1509. doi: 10.1126/science.abc5881

Matsuyama, S., Nao, N., Shirato, K., Kawase, M., Saito, S., Takayama, I., et al. (2020). Enhanced isolation of SARS-CoV-2 by TMPRSS2-expressing cells. *Proc. Natl. Acad. Sci. U. S. A.* 117, 7001–7003. doi: 10.1073/pnas.2002589117

Monteil, V., Kwon, H., Prado, P., Hagelkruys, A., Wimmer, R. A., Stahl, M., et al. (2020). Inhibition of SARS-CoV-2 infections in engineered human tissues using clinical-grade soluble human ACE2. *Cell* 181, 905–913.e7. doi: 10.1016/j.cell.2020.04.004

Munster, V. J., Feldmann, F., Williamson, B. N., van Doremalen, N., Perez-Perez, L., Schulz, J., et al. (2020). Respiratory disease in rhesus macaques inoculated with SARS-CoV-2. *Nature* 585, 268–272. doi: 10.1038/s41586-020-2324-7

Muth, D., and Corman, V. M. (2018). Attenuation of replication by a 29 nucleotide deletion in SARS-coronavirus acquired during the early stages of human-to-human transmission. *Sci. Rep.* 8:15177. doi: 10.1038/s41598-018-33487-8

Ong, E. Z., Chan, Y. F. Z., Leong, W. Y., Lee, N. M. Y., Kalimuddin, S., Haja Mohideen, S. M., et al. (2020). A dynamic immune response shapes COVID-19 progression. *Cell Host Microbe* 27, 879–882.e2. doi: 10.1016/j.chom.2020.03.021

Ou, X., Liu, Y., Lei, X., Li, P., Mi, D., Ren, L., et al. (2020). Characterization of spike glycoprotein of SARS-CoV-2 on virus entry and its immune cross-reactivity with SARS-CoV. *Nat. Commun.* 11:1620. doi: 10.1038/s41467-020-15562-9

Pan, X. W., Xu, D., Zhang, H., Zhou, W., Wang, L. H., and Cui, X. G. (2020). Identification of a potential mechanism of acute kidney injury during the COVID-19 outbreak: a study based on single-cell transcriptome analysis. *Intensive Care Med.* 46, 1114–1116. doi: 10.1007/s00134-020-06026-1

Park, S. J., Yu, K. M., Kim, Y. I., Kim, S. M., Kim, E. H., Kim, S. G., et al. (2020). Antiviral efficacies of FDA-approved drugs against SARS-CoV-2 infection in ferrets. *mBio*. 11:e01114-20. doi: 10.1128/mBio.01114-20

Pinto, D., Park, Y. J., Beltramello, M., Walls, A. C., and Tortorici, M. A. (2020). Cross-neutralization of SARS-CoV-2 by a human monoclonal SARS-CoV antibody. *Nature* 583, 290–295. doi: 10.1038/s41586-020-2349-y

Proud, P. C., Tsitoura, D., Watson, R. J., Chua, B. Y., Aram, M. J., Bewley, K. R., et al. (2021). Prophylactic intranasal administration of a TLR2/6 agonist reduces upper respiratory tract viral shedding in a SARS-CoV-2 challenge ferret model. *EBioMedicine* 63:103153. doi: 10.1016/j.ebiom.2020.103153

Puelles, V. G., Lutgehetmann, M., Lindenmeyer, M. T., Sperhake, J. P., Wong, M. N., Allweiss, L., et al. (2020). Multiorgan and renal tropism of SARS-CoV-2. *N. Engl. J. Med.* 383, 590–592. doi: 10.1056/NEJMc2011400

Rao, S., Lau, A., and So, H. C. (2020). Exploring diseases/traits and blood proteins causally related to expression of ACE2, the putative receptor of SARS-CoV-2: a mendelian randomization analysis highlights tentative relevance of diabetes-related traits. *Diabetes Care* 43, 1416–1426. doi: 10.2337/dc20-0643

Rockx, B., and Kuiken, T. (2020). Comparative pathogenesis of COVID-19, MERS, and SARS in a nonhuman primate model. *Science* 368, 1012–1015. doi: 10.1126/science.abb7314

Rogers, T. F., and Zhao, F. (2020). Isolation of potent SARS-CoV-2 neutralizing antibodies and protection from disease in a small animal model. *Science* 369, 956–963. doi: 10.1126/science.abc7520

Rosenfeld, R., and Noy-Porat, T. (2021). Post-exposure protection of SARS-CoV-2 lethal infected K18-hACE2 transgenic mice by neutralizing human monoclonal antibody. *Nat. Commun.* 12:944. doi: 10.1038/s41467-021-21239-8

Sawalha, A. H., Zhao, M., Coit, P., and Lu, Q. (2020). Epigenetic dysregulation of ACE2 and interferon-regulated genes might suggest increased COVID-19 susceptibility and severity in lupus patients. *Clin. Immunol.* 215:108410. doi: 10.1016/j.clim.2020.108410

Schuler, B. A., Habermann, A. C., Plosa, E. J., Taylor, C. J., Jetter, C., Negretti, N. M., et al. (2021). Age-determined expression of priming protease TMPRSS2 and localization of SARS-CoV-2 in lung epithelium. *J. Clin. Invest.* 131:e140766. doi: 10.1172/jci140766

Shang, C., Zhuang, X., Zhang, H., Li, Y., Zhu, Y., Lu, J., et al. (2021). Inhibitors of endosomal acidification suppress SARS-CoV-2 replication and relieve viral pneumonia in hACE2 transgenic mice. *Virol. J.* 18:46. doi: 10.1186/s12985-021-01515-1

Shen, C., Wang, Z., Zhao, F., Yang, Y., Li, J., Yuan, J., et al. (2020). Treatment of 5 critically ill patients with COVID-19 with convalescent plasma. *JAMA* 323, 1582–1589. doi: 10.1001/jama.2020.4783

Shi, R., and Shan, C. (2020). A human neutralizing antibody targets the receptor binding site of SARS-CoV-2. *Nature* 584, 120–124. doi: 10.1038/s41586-020-2381-y

Sia, S. F., Yan, L. M., Chin, A. W. H., Fung, K., Choy, K. T., Wong, A. Y. L., et al. (2020). Pathogenesis and transmission of SARS-CoV-2 in golden hamsters. *Nature* 583, 834–838. doi: 10.1038/s41586-020-2342-5

Sit, T. H. C., Brackman, C. J., Ip, S. M., Tam, K. W. S., Law, P. Y. T., and To, E. M. W. (2020). Infection of dogs with SARS-CoV-2. Nature 586, 776–778. doi: 10.1038/s41586-020-2334-5

Smith, J. C., Sausville, E. L., Girish, V., Yuan, M. L., Vasudevan, A., John, K. M., et al. (2020). Cigarette smoke exposure and inflammatory signaling increase the expression of the SARS-CoV-2 receptor ACE2 in the respiratory tract. *Dev. Cell* 53, 514–529.e3. doi: 10.1016/j.devcel.2020.05.012

Song, Y., Liu, P., Shi, X. L., Chu, Y. L., Zhang, J., Xia, J., et al. (2020). SARS-CoV-2 induced diarrhoea as onset symptom in patient with COVID-19. *Gut* 69, 1143–1144. doi: 10.1136/gutjnl-2020-320891

Su, H., Yang, M., Wan, C., Yi, L. X., Tang, F., Zhu, H. Y., et al. (2020). Renal histopathological analysis of 26 postmortem findings of patients with COVID-19 in China. *Kidney Int.* 98, 219–227. doi: 10.1016/j.kint.2020.04.003

Su, Y. C. F., and Anderson, D. E. (2020). Discovery and genomic characterization of a 382-nucleotide deletion in ORF7b and ORF8 during the early evolution of SARS-CoV-2. *mBio* 11:e01610-20. doi: 10.1128/mBio.01610-20

Sun, J., Zhuang, Z., Zheng, J., Li, K., Wong, R. L., Liu, D., et al. (2020). Generation of a broadly useful model for COVID-19 pathogenesis, vaccination, and treatment. *Cell* 182, 734–743.e5. doi: 10.1016/j.cell.2020.06.010

Sun, S. H., Chen, Q., Gu, H. J., Yang, G., Wang, Y. X., Huang, X. Y., et al. (2020). A mouse model of SARS-CoV-2 infection and pathogenesis. *Cell Host Microbe* 28, 124–133.e4. doi: 10.1016/j.chom.2020.05.020

Takata, M. A., Goncalves-Carneiro, D., Zang, T. M., Soll, S. J., York, A., Blanco-Melo, D., et al. (2017). CG dinucleotide suppression enables antiviral defence targeting non-self RNA. *Nature* 550, 124–127. doi: 10.1038/nature24039

Tan, M., Liu, Y., Zhou, R., Deng, X., Li, F., Liang, K., et al. (2020). Immunopathological characteristics of coronavirus disease 2019 cases in Guangzhou, China. *Immunology* 160, 261–268. doi: 10.1111/imm.13223

Tian, X., Li, C., Huang, A., Xia, S., Lu, S., and Shi, Z. (2020). Potent binding of 2019 novel coronavirus spike protein by a SARS coronavirus-specific human monoclonal antibody. *Emerg. Microbes Infect.* 9, 382–385. doi: 10.1080/22221751.2020.1729069

Ulrich, H., and Pillat, M. M. (2020). CD147 as a target for COVID-19 treatment: suggested effects of azithromycin and stem cell engagement. *Stem Cell Rev. Rep.* 16, 434–440. doi: 10.1007/s12015-020-09976-7

Wan, J., Xing, S., Ding, L., Wang, Y., Gu, C., Wu, Y., et al. (2020). Human-IgG-neutralizing monoclonal antibodies block the SARS-CoV-2 infection. *Cell Rep.* 32:107918. doi: 10.1016/j.celrep.2020.107918

Wang, C., and Li, W. (2020). A human monoclonal antibody blocking SARS-CoV-2 infection. *Nat. Commun.* 11:2251. doi: 10.1038/s41467-020-16256-y

Wang, D., Hu, B., Hu, C., Zhu, F., Liu, X., Zhang, J., et al. (2020). Clinical characteristics of 138 hospitalized patients with 2019 novel coronavirus-infected pneumonia in Wuhan, China. *JAMA* 323, 1061–1069. doi: 10.1001/jama.2020.1585

Wang, F., Nie, J., Wang, H., Zhao, Q., Xiong, Y., Deng, L., et al. (2020). Characteristics of peripheral lymphocyte subset alteration in COVID-19 pneumonia. *J. Infect. Dis.* 221, 1762–1769. doi: 10.1093/infdis/jiaa150

Wang, L., Mitchell, P. K., Calle, P. P., Bartlett, S. L., McAloose, D., Killian, M. L., et al. (2020). Complete genome sequence of SARS-CoV-2 in a tiger from a U.S. zoological collection. *Microbiol. Resour. Announc.* 9:e00468–20. doi: 10.1128/mra.00468-20

Wang, M., Cao, R., Zhang, L., Yang, X., Liu, J., Xu, M., et al. (2020). Remdesivir and chloroquine effectively inhibit the recently emerged novel coronavirus (2019-nCoV) in vitro. *Cell Res.* 30, 269–271. doi: 10.1038/s41422-020-0282-0

Wang, Q., Qiu, Y., Li, J. Y., Zhou, Z. J., Liao, C. H., and Ge, X. Y. (2020). A unique protease cleavage site predicted in the spike protein of the novel pneumonia coronavirus (2019-nCoV) potentially related to viral transmissibility. *Virol. Sin.* 35, 337–339. doi: 10.1007/s12250-020-00212-7

Wang, X., Xu, W., Hu, G., Xia, S., Sun, Z., Liu, Z., et al. (2020). SARS-CoV-2 infects T lymphocytes through its spike protein-mediated membrane fusion. *Cell Mol. Immunol.* doi: 10.1038/s41423-020-0424-9 [Epub ahead of print].

Wang, Z., He, Y., Shu, H., Wang, P., Xing, H., Zeng, X., et al. (2020). High fluorescent lymphocytes are increased in COVID-19 patients. *Br. J. Haematol.* 190, e76–e78. doi: 10.1111/bjh.16867

Wec, A. Z., and Wrapp, D. (2020). Broad neutralization of SARS-related viruses by human monoclonal antibodies. *Science* 369, 731–736. doi: 10.1126/science.abc7424

Wen, W., Su, W., Tang, H., Le, W., Zhang, X., Zheng, Y., et al. (2020). Immune cell profiling of COVID-19 patients in the recovery stage by single-cell sequencing. *Cell Discov.* 6:31. doi: 10.1038/s41421-020-0168-9

Williamson, B. N., Feldmann, F., Schwarz, B., Meade-White, K., Porter, D. P., Schulz, J., et al. (2020). Clinical benefit of remdesivir in rhesus macaques infected with SARS-CoV-2. Nature 585, 273–276. doi: 10.1038/s41586-020-2423-5

Wrapp, D., De Vlieger, D., Corbett, K. S., Torres, G. M., Wang, N., Van Breedam, W., et al. (2020). Structural basis for potent neutralization of betacoronaviruses by single-domain camelid antibodies. *Cell* 181, 1004–1015.e15. doi: 10.1016/j.cell.2020.04.031

Wrapp, D., and Wang, N. (2020). Cryo-EM structure of the 2019-nCoV spike in the prefusion conformation. *Science* 367, 1260–1263. doi: 10.1126/science.abb2507

Wu, F., Zhao, S., Yu, B., Chen, Y. M., Wang, W., Song, Z. G., et al. (2020). A new coronavirus associated with human respiratory disease in China. *Nature* 579, 265–269. doi: 10.1038/s41586-020-2008-3

Wu, Y., Guo, C., Tang, L., Hong, Z., Zhou, J., Dong, X., et al. (2020). Prolonged presence of SARS-CoV-2 viral RNA in faecal samples. *Lancet Gastroenterol. Hepatol.* 5, 434–435. doi: 10.1016/s2468-1253(20)30083-2

Xia, X. (2020). Extreme genomic CpG deficiency in SARS-CoV-2 and evasion of host antiviral defense. *Mol. Biol. Evol.* 37, 2699–2705. doi: 10.1093/molbev/msaa094

Xiang, F., Wang, X., He, X., Peng, Z., Yang, B., Zhang, J., et al. (2020). Antibody detection and dynamic characteristics in patients with COVID-19. *Clin. Infect. Dis.* 71, 1930–1934. doi: 10.1093/cid/ciaa461

Xiong, Y., Liu, Y., Cao, L., Wang, D., Guo, M., Jiang, A., et al. (2020). Transcriptomic characteristics of bronchoalveolar lavage fluid and peripheral blood mononuclear cells in COVID-19 patients. *Emerg. Microbes Infect.* 9, 761–770. doi: 10.1080/22221751.2020.1747363

Xu, X., Yu, C., Qu, J., Zhang, L., Jiang, S., Huang, D., et al. (2020). Imaging and clinical features of patients with 2019 novel coronavirus SARS-CoV-2. *Eur. J. Nucl. Med. Mol. Imaging* 47, 1275–1280. doi: 10.1007/s00259-020-04735-9

Yan, R., and Zhang, Y. (2020). Structural basis for the recognition of SARS-CoV-2 by full-length human ACE2. *Science* 367, 1444–1448. doi: 10.1126/science.abb2762

Yang, C. W., and Chen, M. F. (2020). Composition of human-specific slow codons and slow di-codons in SARS-CoV and 2019-nCoV are lower than other coronaviruses suggesting a faster protein synthesis rate of SARS-CoV and 2019-nCoV. *J. Microbiol. Immunol. Infect.* 53, 419–424. doi: 10.1016/j.jmii.2020.03.002

Yao, X. H., He, Z. C., Li, T. Y., Zhang, H. R., and Wang, Y. (2020). Pathological evidence for residual SARS-CoV-2 in pulmonary tissues of a ready-for-discharge patient. *Cell Res.* 30, 541–543. doi: 10.1038/s41422-020-0318-5

Ye, Q., Wang, B., and Mao, J. (2020). The pathogenesis and treatment of the 'Cytokine Storm' in COVID-19. *J. Infect.* 80, 607–613. doi: 10.1016/j.jinf.2020.03.037

Young, B. E., Fong, S. W., Chan, Y. H., Mak, T. M., Ang, L. W., Anderson, D. E., et al. (2020a). Effects of a major deletion in the SARS-CoV-2 genome on the severity of infection and the inflammatory response: an observational cohort study. *Lancet* 396, 603–611. doi: 10.1016/s0140-6736(20)31757-8

Young, B. E., Ong, S. W. X., Kalimuddin, S., Low, J. G., Tan, S. Y., Loh, J., et al. (2020b). Epidemiologic features and clinical course of patients infected with SARS-CoV-2 in Singapore. *JAMA* 323, 1488–1494. doi: 10.1001/jama.2020.3204

Yu, J., and Tostanoski, L. H. (2020). DNA vaccine protection against SARS-CoV-2 in rhesus macaques. *Science* 369, 806–811. doi: 10.1126/science.abc6284

Yuan, M., and Wu, N. C. (2020). A highly conserved cryptic epitope in the receptor binding domains of SARS-CoV-2 and SARS-CoV. *Science* 368, 630–633. doi: 10.1126/science.abb7269

Zeng, F., Dai, C., Cai, P., Wang, J., Xu, L., Li, J., et al. (2020). A comparison study of SARS-CoV-2 IgG antibody between male and female COVID-19 patients: a possible reason underlying different outcome between sex. *J. Med. Virol.* 92, 2050–2054. doi: 10.1002/jmv.25989

Zeng, L., Xia, S., Yuan, W., Yan, K., Xiao, F., Shao, J., et al. (2020). Neonatal early-onset infection with SARS-CoV-2 in 33 neonates born to mothers with COVID-19 in Wuhan, China. *JAMA Pediatr.* 174, 722–725. doi: 10.1001/jamapediatrics.2020.0878

Zhang, C., Shi, L., and Wang, F. S. (2020). Liver injury in COVID-19: management and challenges. *Lancet Gastroenterol. Hepatol.* 5, 428–430. doi: 10.1016/s2468-1253(20)30057-1

Zhang, J. J., Dong, X., Cao, Y. Y., Yuan, Y. D., Yang, Y. B., Yan, Y. Q., et al. (2020). Clinical characteristics of 140 patients infected with SARS-CoV-2 in Wuhan, China. *Allergy* 75, 1730–1741. doi: 10.1111/all.14238

Zhang, Q., Honko, A., Zhou, J., Gong, H., Downs, S. N., Vasquez, J. H., et al. (2020). Cellular nanosponges inhibit SARS-CoV-2 infectivity. *Nano Lett.* 20, 5570–5574. doi: 10.1021/acs.nanolett.0c02278

Zhang, T., Wu, Q., and Zhang, Z. (2020). Probable pangolin origin of SARS-CoV-2 associated with the COVID-19 outbreak. *Curr. Biol.* 30, 1346–1351.e2. doi: 10.1016/j.cub.2020.03.022

Zhang, X., Chen, X., Chen, L., Deng, C., Zou, X., Liu, W., et al. (2020). The evidence of SARS-CoV-2 infection on ocular surface. *Ocul. Surf.* 18, 360–362. doi: 10.1016/j.jtos.2020.03.010

Zhang, X., and Tan, Y. (2020). Viral and host factors related to the clinical outcome of COVID-19. *Nature* 583, 437–440. doi: 10.1038/s41586-020-2355-0

Zhang, Y., Xu, J., Jia, R., Yi, C., Gu, W., Liu, P., et al. (2020). Protective humoral immunity in SARS-CoV-2 infected pediatric patients. *Cell. Mol. Immunol.* 17, 768–770. doi: 10.1038/s41423-020-0438-3

Zheng, H. Y., Zhang, M., Yang, C. X., Zhang, N., Wang, X. C., Yang, X. P., et al. (2020). Elevated exhaustion levels and reduced functional diversity of T cells in peripheral blood may predict severe progression in COVID-19 patients. *Cell. Mol. Immunol.* 17, 541–543. doi: 10.1038/s41423-020-0401-3

Zheng, M., Gao, Y., Wang, G., Song, G., Liu, S., Sun, D., et al. (2020). Functional exhaustion of antiviral lymphocytes in COVID-19 patients. *Cell. Mol. Immunol.* 17, 533–535. doi: 10.1038/s41423-020-0402-2

Zhou, B., and Thao, T. T. N. (2021). SARS-CoV-2 spike D614G change enhances replication and transmission. *Nature* 592, 122–127. doi: 10.1038/s41586-021-03361-1

Zhou, F., Yu, T., Du, R., Fan, G., Liu, Y., Liu, Z., et al. (2020). Clinical course and risk factors for mortality of adult inpatients with COVID-19 in Wuhan, China: a retrospective cohort study. *Lancet* 395, 1054–1062. doi: 10.1016/s0140-6736(20)30566-3

Zhou, J., Li, C., Liu, X., and Chiu, M. C. (2020). Infection of bat and human intestinal organoids by SARS-CoV-2. *Nat. Med.* 26, 1077–1108. doi: 10.1038/s41591-020-0912-6

Zhou, P., Yang, X. L., Wang, X. G., Hu, B., Zhang, L., Zhang, W., et al. (2020). A pneumonia outbreak associated with a new coronavirus of probable bat origin. *Nature* 579, 270–273. doi: 10.1038/s41586-020-2012-7

Zhou, Z., Ren, L., Zhang, L., Zhong, J., Xiao, Y., Jia, Z., et al. (2020). Heightened innate immune responses in the respiratory tract of COVID-19 patients. *Cell Host Microbe* 27, 883–890.e2. doi: 10.1016/j.chom.2020.04.017

Zhu, N., Zhang, D., Wang, W., Li, X., Yang, B., Song, J., et al. (2020). A novel coronavirus from patients with pneumonia in China, 2019. *N. Engl. J. Med.* 382, 727–733. doi: 10.1056/NEJMoa2001017

Zhu, Z., Cai, T., Fan, L., Lou, K., Hua, X., Huang, Z., et al. (2020). Clinical value of immune-inflammatory parameters to assess the severity of coronavirus disease 2019. *Int. J. Infect. Dis.* 95, 332–339. doi: 10.1016/j.ijid.2020.04.041

Conflict of Interest: The authors declare that the research was conducted in the absence of any commercial or financial relationships that could be construed as a potential conflict of interest.

Advantages of publishing in Frontiers

OPEN ACCESS
Articles are free to read for greatest visibility and readership

FAST PUBLICATION
Around 90 days from submission to decision

HIGH QUALITY PEER-REVIEW
Rigorous, collaborative, and constructive peer-review

TRANSPARENT PEER-REVIEW
Editors and reviewers acknowledged by name on published articles

Frontiers
Avenue du Tribunal-Fédéral 34
1005 Lausanne | Switzerland

Visit us: www.frontiersin.org
Contact us: frontiersin.org/about/contact

REPRODUCIBILITY OF RESEARCH
Support open data and methods to enhance research reproducibility

DIGITAL PUBLISHING
Articles designed for optimal readership across devices

FOLLOW US
@frontiersin

IMPACT METRICS
Advanced article metrics track visibility across digital media

EXTENSIVE PROMOTION
Marketing and promotion of impactful research

LOOP RESEARCH NETWORK
Our network increases your article's readership